Rainer Behrisch
Wolfgang Eckstein
Editors

TOPICS IN APPLIED PHYSICS 110

Sputtering by Particle Bombardment

Experiments and Computer Calculations from Threshold to MeV Energies

Topics in Applied Physics
Volume 110

Available online at
SpringerLink.com

Topics in Applied Physics is part of the SpringerLink service. For all customers with standing orders for Topics in Applied Physics we offer the full text in electronic form via SpringerLink free of charge. Please contact your librarian.

Topics in Applied Physics

Topics in Applied Physics is a well-established series of review books, each of which presents a comprehensive survey of a selected topic within the broad area of applied physics. Edited and written by leading research scientists in the field concerned, each volume contains review contributions covering the various aspects of the topic. Together these provide an overview of the state of the art in the respective field, extending from an introduction to the subject right up to the frontiers of contemporary research.

Topics in Applied Physics is addressed to all scientists at universities and in industry who wish to obtain an overview and to keep abreast of advances in applied physics. The series also provides easy but comprehensive access to the fields for newcomers starting research.

Contributions are specially commissioned. The Managing Editors are open to any suggestions for topics coming from the community of applied physicists no matter what the field and encourage prospective editors to approach them with ideas.

Managing Editor

Dr. Claus E. Ascheron

Springer-Verlag GmbH
Tiergartenstr. 17
69121 Heidelberg
Germany
Email: claus.ascheron@springer.com

Assistant Editor

Dr. Werner Skolaut

Springer-Verlag GmbH
Tiergartenstr. 17
69121 Heidelberg
Germany
Email: werner.skolaut@springer.com

Rainer Behrisch, Wolfgang Eckstein (Eds.)

Sputtering by Particle Bombardment

Experiments and Computer Calculations from Threshold to MeV Energies

With 201 Figures

Rainer Behrisch
Max-Planck-Institut für Plasmaphysik,
Boltzmannstr. 2,
85748 Garching,
Germany
reb@ipp.mpg.de

Wolfgang Eckstein
Max-Planck-Institut für Plasmaphysik,
Boltzmannstr. 2,
85748 Garching,
Germany
wge@ipp.mpg.de

Library of Congress Control Number: 2007920813

Physics and Astronomy Classification Scheme (PACS):
02.70.-e,34.50.Bw,68.49.Sf,71.15.Pd,79.20.Rf

ISSN print edition: 0303-4216
ISSN electronic edition: 1437-0859
ISBN 987-3-540-44500-5 Springer Berlin Heidelberg New York

This work is subject to copyright. All rights are reserved, whether the whole or part of the material is concerned, specifically the rights of translation, reprinting, reuse of illustrations, recitation, broadcasting, reproduction on microfilm or in any other way, and storage in data banks. Duplication of this publication or parts thereof is permitted only under the provisions of the German Copyright Law of September 9, 1965, in its current version, and permission for use must always be obtained from Springer. Violations are liable for prosecution under the German Copyright Law.

Springer is a part of Springer Science+Business Media

springer.com

© Springer-Verlag Berlin Heidelberg 2007

The use of general descriptive names, registered names, trademarks, etc. in this publication does not imply, even in the absence of a specific statement, that such names are exempt from the relevant protective laws and regulations and therefore free for general use.

Typesetting: DA-TEX · Gerd Blumenstein · www.da-tex.de
Production: LE-TEX Jelonek, Schmidt & Vöckler GbR, Leipzig
Cover design: eStudio Calamar S. L., F. Steinen-Broo, Girona, Spain

Printed on acid-free paper 57/3180/YL 5 4 3 2 1 0

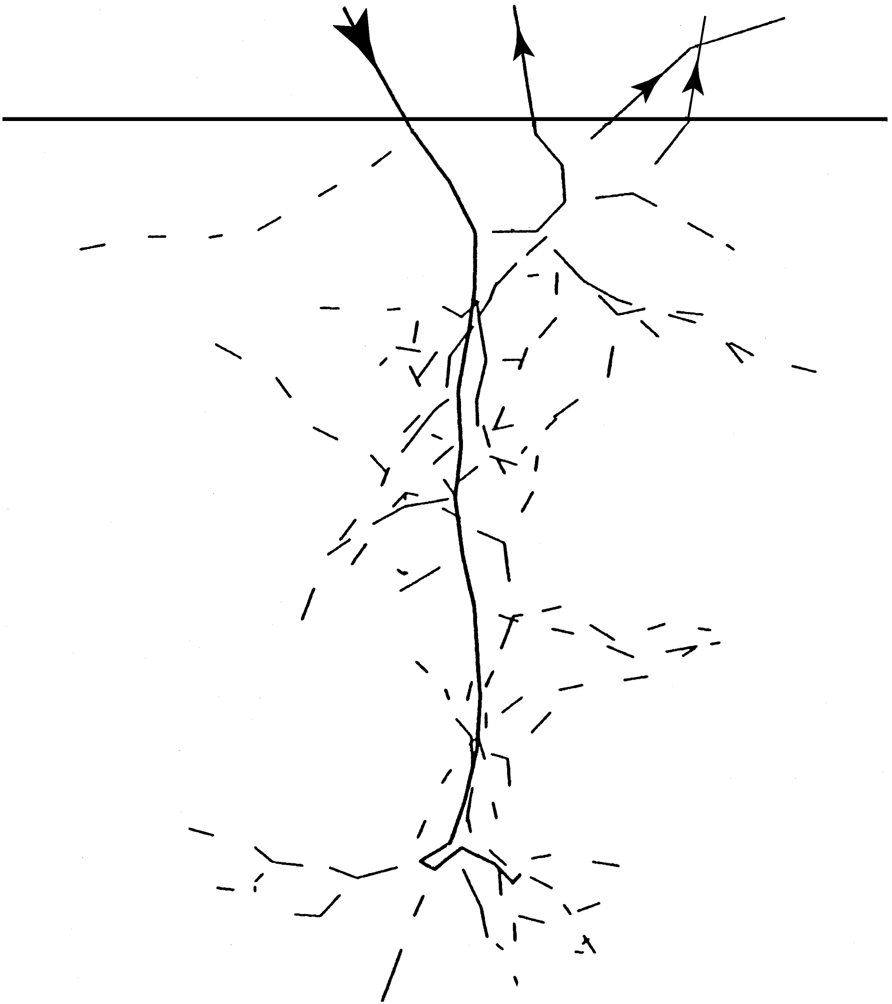

Collision cascade initiated by a 1 keV Ar at 30° incidence on Ni leading to three sputtered atoms as calculated by TRIM.SP

Preface

Within the last 15 years in the field of "sputtering by particle bombardment" several new and important results have been published in internal reports, in PhD thesis, as well as in the open literature. This relates especially to a more detailed understanding of the sputtering process by computational means such as molecular dynamics and binary collision approximation (BCA) programs. BCA programs allow confirmation of a large amount of measured data and predictions of sputtering yields and distributions. Progress has been achieved in chemical effects in sputtering, in sputtering by very high energy ions, in electronic sputtering, and in applications of sputtering for surface layer analysis and modifications of surfaces, such as machining, polishing and creation of surface structures such as dots and ripples. In this volume it is intended to summarise the new results by the experts in the fields. We hope that this will be of help for all colleagues who are working or plan to work in this interesting and important field of science and technology.

We like to thank especially our colleagues who accepted to contribute to this book by their experience in the different fields, Max-Plank-Institut für Plasmaphysik for the possibilities of using the Computer Centre and Springer Verlag for the good collaboration. Special thanks are given to our colleagues K. Ertl and U. von Toussaint for their help and B. Rauschenbach and S. Facsko for valuable information about nanostructuring of surfaces by ion bombardment.

Garching,
August 2006

Rainer Behrisch
Wolfgang Eckstein

Contents

Introduction and Overview
Rainer Behrisch and Wolfgang Eckstein 1
1 Overview 1
2 The Sputtering Yield 3
3 Distributions of Sputtered Particles 4
4 Surface Topography 4
5 Sputtering Calculations 7
5.1 Analytic Theory 7
5.2 Computer Calculations 8
6 Sputtering Measurements 9
7 Applications of Sputtering 11
8 Summary, Conclusions 12
References 12
Index 19

Computer Simulation of the Sputtering Process
Wolfgang Eckstein and Herbert M. Urbassek 21
1 Programs Based on the Binary Collision Approximation 21
1.1 The Binary Collision 22
1.2 The Interaction Potential for BCA 22
1.3 The Inelastic (Electronic) Energy Loss 23
1.4 The Surface Binding Energy 24
1.5 Problems of the Concept of BCA 24
1.6 Dynamic Monte Carlo Programs 24
1.7 Advantages of BCA Programs 25
2 Programs Based on Molecular Dynamics 25
2.1 Physics Input: Forces 25
2.1.1 Interatomic Potentials 25
2.1.2 Electrons 26
2.2 Technical Considerations 27
2.2.1 System Size 27
2.2.2 Boundary Conditions 27
2.2.3 Initial State 27
2.2.4 Sputtering 28
2.2.5 Simulation Time 28

2.3 Reliability ... 28
References ... 29
Index ... 31

Sputtering Yields
Wolfgang Eckstein ... 33
1 Experimental Methods ... 33
2 Calculational Methods ... 35
3 Mono-Atomic Targets ... 37
3.1 Energy Dependence of the Sputtering Yield at Normal Incidence ... 37
3.2 Fitting ... 38
3.3 Comparison of Calculated Values with Experimental Data ... 40
3.4 Angle of Incidence Dependence of the Sputtering Yield ... 101
3.5 Threshold Energy of Sputtering ... 125
4 Single Crystalline Materials ... 125
5 Multicomponent Targets ... 126
5.1 Fluence Dependence ... 127
5.2 Oscillations in the Partial Sputtering Yields ... 128
5.3 Sputtering of Compounds ... 129
5.4 Isotope Sputtering ... 130
6 Temperature Dependence of the Sputtering Yield ... 131
7 Yield Fluctuations ... 132
8 Time Evolution of the Sputtering Yield ... 133
9 Conclusions ... 133
References ... 171
Index ... 186

Results of Molecular Dynamics Calculations
Herbert M. Urbassek ... 189
1 Introduction ... 189
2 Linear-Cascade Regime ... 191
2.1 Low-Energy Sputtering ... 193
2.2 Preferential Sputtering ... 193
3 Ionic Crystals ... 196
4 Effect of Electronic Energy Loss and Electronic Excitations in Atomic Collision Cascades ... 197
4.1 Stopping ... 198
4.2 Excitation ... 198
5 High-Energy-Density (Spike) Phenomena ... 198
5.1 Sputtering from Fast-Ion-Induced Tracks ... 200
5.2 Cluster Impact ... 201
5.2.1 Small Cluster Impact ($n \leq 3$) ... 202
5.2.2 Larger Cluster Impact ($n > 3$) ... 202
5.2.3 Cluster-Induced Surface Smoothing ... 204

6 Cluster Emission . . . 204
7 Surface Topography Formation . . . 208
7.1 Surface Vacancy and Adatom Production . . . 209
7.2 Crater Production . . . 210
8 Effects of Surface Topography on Sputtering . . . 211
8.1 Effect of Surface Steps on Sputtering . . . 212
9 Fluence Dependence of Sputtering . . . 215
10 Sputtering of Molecular and Organic Solids . . . 216
10.1 Diatomic and Small Anorganic Molecular Solids . . . 216
10.2 Sputtering of Organic Solids . . . 217
10.3 Sputtering of Polymers . . . 217
11 Chemical Effects . . . 218
12 Conclusions . . . 219
References . . . 220
Index . . . 227

Energy and Angular Distributions of Sputtered Species
Hubert Gnaser . . . 231
1 Introduction . . . 231
2 Theoretical Concepts . . . 233
2.1 Energy Dissipation, Recoil Generation, and Sputtering . . . 233
2.2 Surface Binding Energy . . . 236
3 Experimental Techniques . . . 237
3.1 Post-Ionization of Sputtered Neutrals . . . 237
3.2 Methods for the Determination of Energy Spectra . . . 238
3.2.1 Electrostatic Energy Analysis . . . 238
3.2.2 Fluorescence Techniques . . . 239
3.2.3 Time-of-Flight Measurements . . . 240
3.3 Methods for Angular Distribution Measurements . . . 241
4 Energy and Angular Distributions in the Linear-Cascade Regime . . 244
4.1 Energy Spectra from Metals, Semiconductors, and Organic Materials . . . 245
4.1.1 Energy Spectra of Ground- and Excited-State Atoms, and of Ions . . . 245
4.1.2 Energy Distributions of Atoms Sputtered from Alloys . . 252
4.1.3 Energy Spectra of Sputtered Molecules . . . 254
4.2 Energy Spectra from Alkali Halides and Condensed Gases 269
4.2.1 Alkali Halides and Related Materials . . . 269
4.2.2 Condensed Gases . . . 271
4.3 Angular Distribution of Sputtered Species . . . 275
4.3.1 Angular Distributions from Amorphous and Polycrystalline Targets . . . 275
4.3.2 Angular Spectra from Single Crystals . . . 277
4.3.3 Angular Distributions from Multicomponent Targets . . . 280
5 Energy and Angular Distributions in the Single-Knockon Regime . . 283

5.1 Energy Spectra and Direct Recoils ... 285
5.1.1 Normal Incidence Bombardment ... 285
5.1.2 Oblique Incidence Bombardment ... 288
5.2 Angular Distributions at Low-Energy Irradiation ... 291
6 Energy and Angular Spectra from High-Density Cascades ... 293
6.1 Cluster-Ion Bombardment ... 293
6.2 Yield Enhancement under Cluster Impact ... 294
6.3 Energy Distributions under Cluster Bombardment ... 295
6.4 Angular Distributions under Cluster Irradiation ... 298
7 Summary ... 300
References ... 301
Index ... 323

Chemical Sputtering
Wolfgang Jacob and Joachim Roth ... 329
1 Introduction ... 329
2 Chemical Effects in Sputtering ... 330
3 Definitions ... 332
3.1 Physical Sputtering ... 332
3.2 Chemical Erosion ... 333
3.3 Chemical Sputtering ... 333
4 Experimental Methods ... 334
4.1 Weight Loss ... 335
4.2 Mass Spectrometry ... 335
4.3 Ellipsometry ... 339
4.4 Optical Emission Spectroscopy ... 339
4.5 Cavity Probes ... 340
4.6 Dedicated Multiple Beam Experiments ... 340
5 Chemical Erosion of Carbon by Atomic Hydrogen ... 342
5.1 Thermal Process ... 342
5.2 Species Released by Chemical Erosion ... 345
6 Chemical Sputtering ... 348
6.1 Chemical Sputtering with Reactive Ions ... 349
6.1.1 Temperature Dependence ... 349
6.1.2 Energy Dependence ... 350
6.1.3 Dependence on the Type of Graphite ... 354
6.1.4 Flux Dependence ... 355
6.1.5 Identification of Species Released by Chemical Sputtering ... 356
6.2 Combined Irradiation with Noble Gas Ions and Hydrogen Atoms ... 359
6.3 Effect of Doping ... 364
6.4 Chemical Sputtering with Molecular Ions at Low Energies ... 365
6.5 Summary of Experimental Results ... 367
7 Mechanisms and Modelling for Chemical Sputtering ... 369

7.1 Empirical Analytic Description . . . 369
7.1.1 Radiation Damage . . . 369
7.1.2 Low-temperature Near-surface Process, Y_{surf} . . . 370
7.1.3 Empirical Roth–García-Rosales Formula . . . 371
7.1.4 Comparison with Erosion Data . . . 372
7.1.5 Extrapolation to Thermal Energies . . . 373
7.2 Chemical Sputtering Model by Hopf . . . 374
7.3 Molecular Dynamics Simulations . . . 377
7.4 Isotope Effect . . . 380
7.5 Effects due to Out-diffusion of Hydrocarbons . . . 382
7.6 Summary . . . 383
8 Chemical Sputtering with Other Reactive Species . . . 384
8.1 Oxygen . . . 384
8.2 Nitrogen . . . 386
8.3 Fluorine . . . 389
References . . . 389
Index . . . 399

Electronic Sputtering with Swift Heavy Ions
Walter Assmann, Marcel Toulemonde, and Christina Trautmann . . . 401
1 Introduction . . . 401
2 Sputtering Experiments . . . 406
2.1 Special Problems in High-Energy Sputtering . . . 406
2.2 Measuring Techniques for Sputtering Yields . . . 407
2.3 Angular Distribution, Total Yield, and Fluence Effect . . . 410
2.4 Experimental Arrangements . . . 411
3 Experimental Results . . . 416
3.1 Dependence of Sputtering Yield on Charge State of Incoming Ions . . . 416
3.2 Dependence of Sputtering Yield on Angle of Beam Incidence . . . 416
3.3 Metallic Materials . . . 417
3.3.1 Angular Distribution of Sputtered Particles for Metallic Targets . . . 418
3.3.2 Total Sputtering Yields for Metallic Targets . . . 418
3.4 Insulating Oxides . . . 421
3.4.1 Angular Distributions of Sputtered Particles for Oxides . . . 421
3.4.2 Total Sputtering Yields for Oxides . . . 422
3.5 Ionic Insulators . . . 423
3.5.1 Angular Distributions of Sputtered Particles for Ionic Crystals . . . 423
3.5.2 Total Sputtering Yields for Ionic Crystals . . . 426
3.6 Summary of Experimental Sputtering Data of Different Materials . . . 426

4 Calculations Based on the Inelastic Thermal Spike Model 428
4.1 Application to Metals 434
4.2 Application to Insulators 437
4.3 Thermal Spike Conclusion 439
5 Concluding Remarks and Outlook 440
References 442
Index 449

Author Index 461

List of Symbols

Symbol	Meaning
A	ratio of target atom mass to projectile mass
$A(r,t)$	term in the equation of the i-TS model
A_θ	constant in the isotropic contribution to sputtering yield
a_B or a_0	Bohr radius
a_F	Firsov screening length
a_L	Lindhard screening length
α	exponent in the energy distribution of sputtered atoms
α_0	maximum possible angle of incidence if $E_{sp} \neq 0$
b	constant in the sputtering yield formula (angular dependence)
b_n	normalization factor
B_θ	constant in the jetlike contribution to sputtering yield
c_i	concentration of species i in the target
$C_\mathrm{a}(T_\mathrm{a}(r,t))$	specific heat coefficient of the lattice system
$C_\mathrm{e}(T_\mathrm{e}(r,t))$	specific heat coefficient of the electron system
C_m	constant in the analytic theory
c^{sp^x}	concentration of sp^x complexes
δ	preferentiality, fractionation
e	elementary charge
E_bb	C–C bond breaking energy
E, E_1	energy of sputtered atoms
E_0	energy of projectile
E_coh	cohesive energy
E_d	threshold energy for producing stable atomic displacements
E_des	activation energy for near surface desorption
E_F	Fermi energy
E_rel	activation energy for thermal hydrogen release
E_i, E_n	energy of a recoiling atom

Symbol	Meaning
E_{sb}	surface binding energy of target atoms, usually equal to U
E_{sp}	binding energy of a projectile to the target surface
E_{th}	threshold energy for sputtering
E_{vac}	vacancy formation energy
E_{therm}	activation energy for chemical erosion
ε	reduced energy
f	constant in the sputtering yield formula (angular dependence)
F	recoil density
$F_{\mathrm{D}}(E_0, \theta_0, x)$	depth profile of deposited energy
φ	azimuthal emission angle
Φ	fluence, also used for ion flux
$\Phi(r, t)$	evaporation rate
$g(T_{\mathrm{e}}(r, t))$	coupling constant from electrons to phonons
γ	energy transfer factor
$\Gamma, \Gamma_{\mathrm{m}}$	constants in the analytic theory
I	ionization potential
k_{B}	Boltzmann constant
$K_{\mathrm{a}}(T_{\mathrm{a}}(r, t))$	thermal conductivity of the lattice system
$K_{\mathrm{e}}(T_{\mathrm{e}}(r, t))$	thermal conductivity of the electron system
k_x, k_{h}	thermally activated rate coefficients
λ	constant in the sputtering yield formula
Λ	materials factor in the analytic theory
m	power exponent in the power interaction poential
m_{e}	electron mass
M	atom mass, molecular mass
M_1, M_2	mass of incident ion, of target atom
M_i	mass of target atoms in a multicomponent target
μ	constant in the sputtering yield formula
n_{e}	electron density
N, n_{a}	atomic density
N_0	Avogadro number
N_Y	number of deposited atoms per unit area
ν	speed of sound
ω, ω_0	excitation frequency of a moving atom
Ω	solid angle
p	impact parameter
P	clustering probability
q	proportionality factor in the sputtering yield formula
r	internuclear distance, radial distance
R	distance of closest approach
R	mean depth (range) of projectiles

Symbol	Meaning
R_{N}	particle (number) reflection coefficient
ρ	target density
$s_{\mathrm{n}}(\varepsilon)$	reduced nuclear stopping power
$S_{\mathrm{n}}(E_0)$	nuclear stopping cross-section
σ	width of jetlike sputtered components
$\sigma_{\mathrm{h}}, \sigma_{\mathrm{d}}$	cross-sections for hydrogenation and dehydrogenation
t, τ	time
t_0	time for electrons to reach thermal equilibrium
T	target temperature (K)
$T_{\mathrm{a}}(r.t)$	temperature of the lattice subsystem
T_{c}	transition temperature of superconductors
T_{D}	Debye temperature
$T_{\mathrm{e}}(r, t)$	temperature of the electron subsystem
$T_{\max}$	temperature of the maximum chemical sputtering yield
θ_0	angle of incidence (counted from the surface normal)
θ, θ_1	polar emission angle
θ_{m}	angle of incidence at maximum sputtering yield
Θ	recoil angle
ϑ	scattering angle in the center of mass system
U, U_{s}	surface binding energy (eV), heat of sublimation
x	depth or exponent in the angle of incidence dependence of Y
ξ_0	characteristic depth of origin of sputtered atoms
$V(r)$	interaction potential
y	exponent in the angular distribution of sputtered atoms
$Y_{\mathrm{diff}}(\theta, \phi) = d^2Y/d\Omega$	differential sputtering yield
$Y(E_0, \theta_0)$	sputtering yield, also called Y_{phys}
Y_{a}	adatom yield
$y_{\mathrm{bb}}^{C}(x, E)$	depth distribution of broken C–C bonds
Y_{dam}	radiation damage yield
$Y_i, Y_{\mathrm{m}}, Y_{\mathrm{n}}$	partial sputtering yield for multicomponent targets
Y_q	sputtering yield for atoms emitted in charge state q
Y_{surf}	near surface erosion yield
Y_{therm}	thermal erosion yield
Y_{tot}	sum of partial sputtering yields
Z_1, Z_2	atomic number of incident ion, of target atom
Z_i	atomic number of target atoms in a multicomponent target

Introduction and Overview

Rainer Behrisch and Wolfgang Eckstein

Max-Planck-Institut für Plasmaphysik,
Boltzmannstr. 2, 85748 Garching Germany
reb@ipp.mpg.de
wge@ipp.mpg.de

Abstract. The physics processes causing sputtering, i.e. the removal of atoms from the surface of solids or liquids at bombardment with particles having energies from the eV to the MeV range are today mostly understood. The erosion yields calculated with computer codes for different incident parameters agree reasonably well with experimentally measured yields; the same applies to energy and angular distributions. Sputtering is widely used for surface layer analysis, for removing surface atoms for thin film deposition and for surface machining.

1 Overview

If the surface of a solid is bombarded with energetic particles, it becomes eroded, surface atoms are removed, and the morphology of the surface gets modified. This phenomenon is usually named "Sputtering" in English and "Zerstäubung" in German. Sputtering was first discovered more than 150 years ago [1–7] as the erosion of the cathode in electric gas discharge tubes, and was named "cathode sputtering". Besides sputtering, several other effects are observed at particle bombardment of surfaces. A fraction of the incident ions is backscattered in collisions with target atoms [8–11], the others are implanted and come to rest in the solid in transferring their energy to electrons and lattice atoms [12]. After being slowed down they may diffuse further and finally be trapped in the solid or be desorbed at the surface [13, 14]. The ion bombardment further causes the emission of electrons [15–20] and of photons [21–25] and, finally radiation damage in the surface layers of the solid, i.e. a change of the surface structure and topography [26–29].

It took about 100 years until the physical processes involved in sputtering were clearly identified [30, 31] and about another 20 years until a quantitative description of the sputtering process for keV ions had been developed [32–39]. For energies in the 100 eV to the keV range sputtering is caused by atomic collisions between the incoming particles and the atoms in the surface layers of a solid, i.e. the incident particles initiate a collision cascade between the lattice atoms in the solid. For MeV ions also the energy deposited in electrons plays a major role for surface erosion. These processes are in principle the same as those causing radiation damage in the bulk of a solid [40–42]. The collisions take place far from thermal equilibrium, which means that

R. Behrisch, W. Eckstein (Eds.): Sputtering by Particle Bombardment,
Topics Appl. Physics **110**, 1–20 (2007)
© Springer-Verlag Berlin Heidelberg 2007

sputtering with keV ions is generally different from evaporation. However, evaporation contributes to sputtering for bombardment with MeV ions (see Chap by *Assmann*, *Toulemonde*, *Trautmann*). A target atom is sputtered, if it has received an energy component normal to the surface larger than the surface binding energy. This energy is generally approximated by the heat of sublimation, which is smaller than the displacement energy necessary for creating a stable displacement (radiation damage in the bulk of a solid) [32–63]. These processes are named *physical sputtering*. They take place for all particle solid combinations if the incident particles have an energy above a threshold energy in the 10 to few 100 eV range. Sputtering may be enhanced or reduced, if the incident ions form a chemical binding with the atoms of the solid material. This process is named *chemical sputtering* [30]. If gaseous molecules are formed, sputtering is enhanced (see Chap. by *Jacob*, *Roth*), while at the formation of a stronger binding at the surface of the material such as an oxide or carbide, sputtering is reduced. The very large chemical sputtering yields of about 0.2 of carbon at bombardment with hydrogen ions were shown to be reduced by doping the carbon with metal powder [64, 65] or fine grain carbide powder [66].

Depending on the energy of the incident particles and the collision cross-section between the incident particles and the atoms of the solid, for physical sputtering several collision regimes have been identified [48, 63]:

The *single knockon regime* for light ions and low energy heavier ions. Here the recoil atoms from the incident particle-target atom collisions receive a sufficient high energy that they may be sputtered, but not enough energy to generate a recoil cascade.

The *linear cascade regime*: Here recoil atoms from the incident particle-target atom collisions receive a sufficiently high energy to generate recoil cascades. But the density of recoil atoms is sufficiently low so that knock-on collisions with atoms of the solid at rest dominate and collisions between moving atoms are infrequent.

The *spike regime*: This applies for incidence of heavy ions having a large collision cross-section and for the incidence of molecules or atom clusters. Here the density of recoil atoms is so high that the majority of atoms in a certain volume (the spike volume) is set in motion.

For bombarding energies in the MeV range additional processes such as *electronic sputtering* contribute to surface erosion. A major part of the energy of incident heavy ions is transferred to electrons along the ion track. A coupling between the electrons and the phonons causes large local heating in a cylindrical volume. Surface atoms may be removed by evaporation in a jet from the heated volume (see Chap. by *Assmann*, *Toulemonde*, *Trautmann*). For insulators this erosion process is much larger than for metals. Electronic sputtering has also be reported for the incidence of slow, highly charged ions [67]. In this case the large potential energy of the bombarding ions is dissipated into the electronic subsystem causing large sputtering yields for semiconductors and insulating materials [68, 69].

For the different collision regimes the atoms sputtered have characteristic energy and angular distributions.

For crystalline targets, sputtering is largely influenced by the lattice structure. For ion incidence near close-packed crystal directions, the probability for collisions to create primary knockon atoms is reduced. Sputtering is lower than for other directions of ion incidence due to a higher transparency of the lattice and channeling [49, 52–56, 70, 71]. The maximum of the energy dependence of the sputtering yield is shifted towards lower energies [55, 58–62]. Furthermore, sputtered particles are preferentially emitted in close-packed crystal directions [50, 72]. This has been attributed to focusing collision sequences [73–79]. However, the details of the last collision between the subsurface layer and surface atoms can also play a major role [80].

In insulators, another energy transfer process is possible, which is also effective for low energy electrons and photons. The incident ions can produce a localized excitation which, after decay, creates a repulsive potential strong enough to replace lattice atoms [81]. The excitation in the bulk may diffuse to the surface and cause intense erosion [82].

2 The Sputtering Yield

The amount of erosion is measured by the sputtering yield, Y, which is defined as the mean number of atoms removed from the surface of a solid per incident particle:

$$Y = \frac{\text{average number of atoms removed}}{\text{incident particle}} \,. \tag{1}$$

The definition of the sputtering yield is meaningful only if the average number of atoms removed is proportional to the number of incident particles, which has indeed been found in most cases. Increased yields per atom are observed for heavy incident particles, such as molecular ions or atom clusters, at energies $\geq$ 10 keV, where spike effects [48, 83–92] can cause a nonlinear dependence of the yield on the number of atoms per incident molecule or cluster [93]. The number of atoms sputtered for one incident particle generally largely vary, as shown in computer calculations [94–96].

The incident particles may be energetic ions or neutral atoms, molecules, larger atom clusters, such as fullerenes, neutrons [97], electrons or energetic photons [81]. For bombardment with monoatomic molecular ions, each incident atom is generally counted separately. In sputtering experiments with other molecules it may be appropriate to define the yield per incident molecule. In counting the atoms removed, only those from the solid are included, while incident particles which become implanted and later reemitted are not taken into account. This is different for selfsputtering, i.e., for bombardment with the same ions as the solid where this distinction cannot be made in experiments, but in computer programs. A selfsputtering yield of

unity means that on average, one atom is removed or reemitted per incident ion.

3 Distributions of Sputtered Particles

The particles are emitted with a broad distribution in energy, E_1, in all polar exit angles, θ_1, measured relative to the surface normal [98]. They are emitted predominantly as neutral atoms in the ground state with energies of a few eV, some are excited and generally less than 5% are ions at different charge states, 'q' [99]. Y_q may be the total yield for atoms in state q with $Y = \sum Y_\mathrm{q}$. The distributions of the sputtered particles are described by the differential sputtering yields

$$\frac{\partial Y}{\partial E_1} \quad , \quad \frac{\partial^2 Y}{\partial^2 \Omega_1} \, . \tag{2}$$

In specific experiments, for example Secondary Ion Mass Spectroscopy (SIMS) [100], only sputtered ions within a given energy range and charge state emitted into a given angular range are measured, i.e.,

$$\frac{\partial^3 Y_\mathrm{q}}{\partial E_1 \partial^2 \Omega_1} \Delta E_1 \Delta \Omega_1 \tag{3}$$

is determined. The SIMS signal is generally proportional to the sputtering yield of the target species. However, the charge state q depends on the target composition and the bombardment conditions [99]. Therefore, calibration measurements are necessary.

The angular distribution of particles sputtered from single crystals shows maxima in close-packed crystal directions. For polycrystalline materials, the emission distribution is a superposition of the emission distributions of the differently oriented crystallites in the bombarded area. For normal incidence the angular distributions for amorphous and polycrystalline materials may be described in a first approximation by a cosine distribution. For heavy ions and low bombarding energies close to the threshold, more atoms are emitted at large angles, while for light ions and higher energies, more atoms leave the surface in the normal direction [98]. For oblique ion incidence the maximum of the emission distribution is shifted away from the incoming ion beam. In sputtering of compounds the different constituents may be sputtered with slightly different angular distributions [101, 102].

4 Surface Topography

Surface atom removal by sputtering, ion implantation, trapping of the incident ions, and radiation damage in the surface layers generally cause a

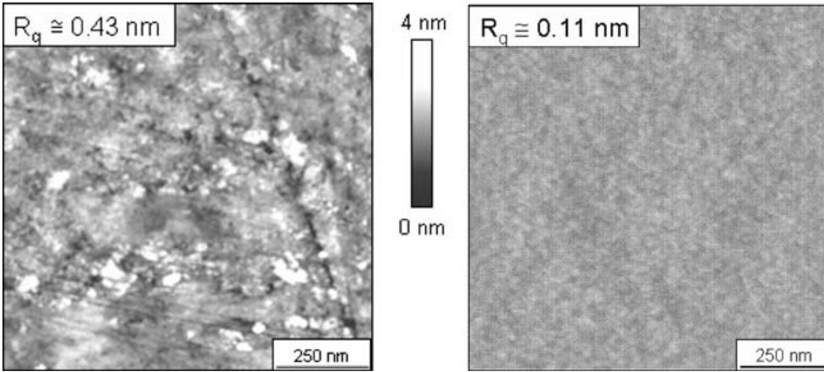

Fig. 1. Surface topography of fused silica; *left:* polished for optical purposes, *right:* after ion bombardment with 600 eV Ar at normal incidence, 300 nm material removed. The roughness has been reduced from 0.43 nm to 0.11 nm rms [111]

modification of the surface. This depends on the target material, its crystallinity and temperature as well as on the ion species and their energy and angle of incidence [26–28, 103, 104]. In sputtering the surface is generally not uniformly eroded, differently oriented crystallites are eroded at different rates and on the surfaces of the crystallites steps and pyramides may develop (Fig. 3) [105–107]. The surface roughness influences the sputtering yield. For bombardment with non-diffusing gaseous ions, blistering and flaking may occur at a fluence of 10^{17} to 10^{18} ions/cm^2, but will disappear at fluences of about ten times greater resulting in a very rough surface [27].

For bombardment with noble gas and reacting ions such as N_2^+ and O_2^+ in the energy range of 100 eV and a few keV besides nanostructuring also smoothing of the surface at an atomic scale is found [108]. Rough silver surfaces have been found to become polished by noble gas ion bombardment at normal incidence [109]. The surfaces of glasses and semiconductors may become polished at an atomic scale [108], as demonstrated in Fig. 1. Indium-containing III-V compound semiconductors, such as InAs, InP or InSb with initial rough surfaces get very smooth with a roughness of 0.2, 0.8 and 1.4 nm [110].

For low energy noble gas ions at normal or oblique incidence a regular ripple structure [112–114] and ordered nanoscale dots are observed. This has been explained by a competition of roughening due to sputtering and smoothing by surface diffusion [115]. An example is shown in Fig. 2.

If the target is rotated during the ion bombardment around an axis normal to the surface, also a periodic pattern of nanodots is formed [108, 116–118].

For bombardment with noble gas ions with energies above a few keV larger grain boundaries, etch pits, steps and pyramids are found [26, 105, 119–121], such as shown in Fig. 3 [106]. Pyramids are also found, if a small amount of

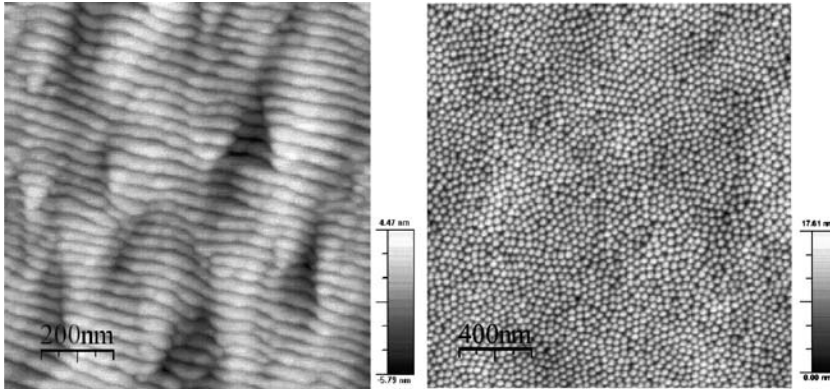

Fig. 2. Surface topography; *left:* ripple structure of Si bombarded with 500 eV Ar at an angle of incidence of 67° with respect to the surface normal after a dose of $1 \cdot 10^{18}\,\mathrm{cm}^{-2}$, *right:* dot structure after bombardment of GaSb with 500 eV Ar at normal incidence after a dose of $1 \cdot 10^{18}\,\mathrm{cm}^{-2}$ [114]

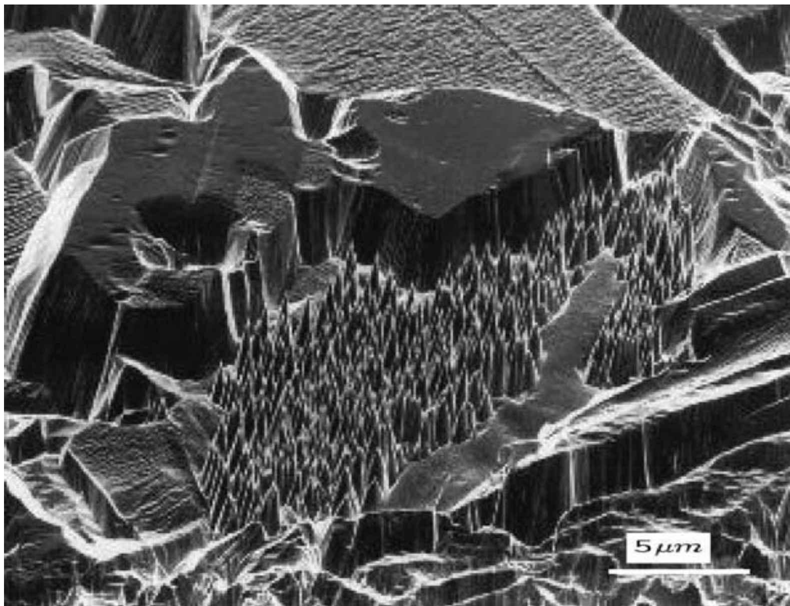

Fig. 3. Surface topography of polycrystalline Cu after 10 keV Kr bombardment at normal incidence and a fluence of 10^{18} atoms/cm^2 [106]

material with a low sputtering yield is evaporated onto the surface of a solid to be sputtered due to a shadowing effect [28, 122, 123].

5 Sputtering Calculations

5.1 Analytic Theory

A major step forward in understanding the sputtering process for amorphous solids in the linear cascade regime was the application of integral transport equations [32,33,35–37,124–127] and their approximate solutions for a special potential ($V(r) \propto r^{-1/m}$ with $0 \leq m < 0.5$) for the atom-atom collisions and neglecting the energy loss to electrons by *Sigmund* [32, 33, 48]. First-order asymptotic solutions achieved for some parameter ranges resulted in an approximate algebraic formula for the dependence of the sputtering yield and the distribution of the sputtered particles on the bombardment conditions for an amorphous solid target of one element [32, 33, 48].

$$Y(E_0, \theta_0) = \Lambda F_\mathrm{D}(E_0, \theta_0, 0) \tag{4}$$

Here E_0 is the incident energy and θ_0 the angle of incidence. $F_\mathrm{D}(E_0, \theta_0, x = 0)$ is the nuclear energy deposition function in an infinite medium at depth $x = 0$, which is proportional to the nuclear stopping power $S_\mathrm{n}(E_0)$ of the incident ion in the solid. Λ is a materials factor. For a planar surface barrier Λ is approximately given by:

$$\Lambda = \frac{\Gamma_\mathrm{m}}{8(1-2m)NC_\mathrm{m}U_\mathrm{s}^{1-2m}} \tag{5}$$

with Γ_m being a factor of about 0.4 and C_m a factor in the nuclear cross-section [32, 33, 48]. Λ was further approximated by $\Lambda = 0.04/NU_\mathrm{s}$ [128]. U_s is the surface binding energy, which is generally taken to be equal to the heat of sublimation. These equations show the dependencies of the sputtering yield on different parameters [32, 33]. To include the behaviour close to the threshold energy Bohdansky has derived a new formula for the sputtering yield at normal incidence onto mono-atomic solids [129]. However, in this formula a too stong interaction potential (Thomas-Fermi) was used, and the formula gave too large threshold energies according to later calculated values [130], and it did not allow to fit the calculated values in a reasonable way [131].

For these approximations the differential yield for atoms sputtered in an energy interval ΔE_1 and an angular interval $\Delta\Omega_1$, see (3), is given approximately by:

$$\frac{\partial^3 Y \Delta E_1 \Delta\Omega_1}{\partial E_1 \partial^2 \Omega_1} = Y(E_0, 0)\frac{2}{\pi}\left(1 - 3m + 2m^2\right)\frac{U_\mathrm{s}^{1-2m} E_1}{(E_1 + U_\mathrm{s})^{3-2m}} \left|\cos\theta_1\right| \Delta E_1 \Delta\Omega_1 \tag{6}$$

For $m = 0$ this reduces to

$$\frac{\partial^3 Y \Delta E_1 \Delta \Omega_1}{\partial E_1 \partial^2 \Omega_1} = Y(E_0, 0) \frac{2}{\pi} \frac{U_s E_1}{(E_1 + U_s)^3} |\cos \theta_1| \, \Delta E_1 \Delta \Omega_1 \,. \tag{7}$$

The energy distribution of the sputtered particles has a maximum at an energy $E_1 = U_s/(2 - 2m)$ or, for $m = 0$ at half the surface binding energy. At high emerging energies ($E_1 \gg U_s$), the number of sputtered particles decreases proportional to E_1^{-2}. Deviations are observed for incident energies close to the threshold energy for sputtering, for oblique angles of incidence and especially for the situation of spikes.

5.2 Computer Calculations

Another approach to calculate absolute values for sputtering yields and the distributions of sputtered particles is to follow the collisions and the trajectories of incident ions and recoil atoms in amorphous or single crystal solids with computer programs [95]. Two different approaches have been used:

1. The *binary collision approximation* (BCA) which is realized in several computer programs, such as MARLOWE [49, 132, 133], TRIM (= transport of ions in matter) [134], TRIM.SP [34], TRIM-CASCADE [135], TRIDYN [38, 39], and ACAT [136] (see Chap. by *Eckstein*, *Urbassek*).
2. *Molecular Dynamics programs* (MD) [137–139]. Here, after particle impact, the trajectories of all atoms in a solid are calculated taking into account the forces from all atoms on each other in some surrounding from their potentials (see Chap. by *Eckstein*, *Urbassek*). The advantage of the molecular dynamics method compared to the BCA approach is the possibility to calculate the formation of molecule and cluster emission. The disadvantage is the longer computational times and therefore a problem with good statistics.

Sputtering yields have been calculated for amorphous solids with TRIM.SP and ACAT for several incident energies and angles of incidence. The dependence of the sputtering yield on the incident energy as well as on the angle of incidence found in the calculations has been fitted with a new algebraic formula [131]. The sputtering yields measured by several authors are finally introduced into the new analytical curves (see Chap. by *Eckstein*).

Sputtering yields for polycrystalline solids with randomly oriented crystallites can be approximated to a first order by the yields calculated for amorphous solids. Thus the formulas derived for amorphous materials mostly give values in reasonable agreement with the sputtering yields measured for polycrystalline targets. For higher energies the binary collision approximation can be used, while for lower energies a molecular dynamics model may be more appropiate (see Chap. by *Urbassek*).

In the computer models it is possible to include an ideal or damaged surface and also damage in the solid. However, for these calculations a computer

with a large memory is needed (see Chap. by *Eckstein*, *Urbassek*). The computer calculations are, however, especially useful for comparing the details of the calculated distributions of cascades with the assumptions made to achieve analytical solutions.

6 Sputtering Measurements

For the sputtering yields a large amount of experimental data has been collected, which have been measured under continuously improved conditions, i.e., with beams of mass analyzed ions having a well defined energy, in high vacuum at well characterized materials with flat surfaces [128] (see Chap. by *Eckstein*). Most of the experimental investigations of sputtering have been performed for mono-atomic, polycrystalline, single crystal and amorphous targets, mainly metals, at bombardment with noble gas and hydrogen ions. The sputtering yields depend on the mass, the energy and angle of incidence of the bombarding ions and the mass of the target atoms, on the surface binding energies, on the crystallinity and the orientation of the crystallites of the solid, but for amorphous and polycrystalline targets they are nearly independent of the target temperature [140–142]. For single crystals the minima in the sputtering yield at incidence in close-packed crystal directions become less pronounced with increasing temperature [143, 144]. For magnetic materials the sputtering yield is modified according to the temperature dependence of the magnetization [145, 146]. Below a threshold energy of about 5 to 400 eV for normal incidence, no sputtering takes place. Above this threshold energy the yields increase with increasing incident energy and reach a broad maximum in the energy region of 0.2 to 150 keV. (see Chap by *Eckstein*). The decrease of the sputtering yields at higher energies is related to the larger penetration depth of the ions into the solid and a reduced energy deposition in the surface layers. Sputtering measurements with ions which react chemically with the atoms of the solid are still the field of many new investigations (see Chap. by *Jacob*, *Roth*) [147–150]. For bombardment with heavier ions of keV energies the yields are typically in the range of l to 10 atoms per incident particle, while for light ions the sputtering yields are well below 1. These results have been summarized and published in several review articles and books [22, 30, 43, 44, 46, 50, 63, 95, 97, 128, 151–165].

For ion bombardment at an oblique angle of incidence onto amorphous or polycrystalline solids, the sputtering yields increase monotonically with increasing angle of incidence up to a maximum around 50 to 80 deg., depending on the ion energy and the mass ratio between incident particles and target atoms, and it decreases again for lager angles of incidence. The location of the maximum depends further on the surface topography.

The sputtered particles are emitted predominantly as neutral atoms in the ground state and generally less than 5 % are ions [99]. A certain fraction can be emitted as atom clusters [138].

Sputtering can be observed in nature as well as in laboratory experiments. It occurs if matter in two extreme states, such as a hot plasma and a solid, interact with each other, or if a directed beam of energetic particles hits a surface. Such situations are found, for example, at the surface of the moon and other celestial bodies with no atmosphere, due to the impact of plasma particles from space such as the solar and the stellar winds [166–169]. Sputtering is also found at the surface of space crafts and satellites especially during the movement in the very upper part of the and atmosphere [170]. On earth energetic particles are produced by radioactive decay [171], in ion accelerators and at the boundary of plasmas. In laboratory experiments sputtering occurs, for example, at the cathode in electric gas discharges, where it was first observed. It is caused by energetic ions produced in the cathode fall [1, 3, 4]. Sputtering is also observed in the ion source of accelerators as well as at all diaphragms and targets hit by ion beams [172, 173]. The effort to understand the sputtering process was also stimulated by a broad application in surface analysis, surface etching, cleaning, thin film deposition and the wall problem in fusion research [161, 162, 174–178].

Sputtering of alloys and compounds is still a field of many detailed investigations [66, 148–150, 179–181]. Generally, one component is initially removed at a larger rate so that the surface layer is enriched in the other component. At low temperatures where diffusion is suppressed, a steady state condition is reached where the atoms are finally removed stoichiometrically. However, at high enough temperatures, a depletion up to large depths in the solid is possible. These effects can influence the sputter deposition of thin films and the results of depth profiling measurements when using sputtering.

In the case of bombardment with ions, which do not react chemically with the atoms of the solid, a surface layer corresponding to the ion range will be damaged and some ions become trapped [31, 52]. For bombardment with reactive ions, i.e. chemically enhanced or reduced sputtering, a compound surface layer generally builds up which has a different composition and structure than the material started with [147]. Sputtering effects will then correspond to those of the compound formed.

If the surface is contaminated such as by an oxide or carbide, these top atoms are predominantly removed and sputtering of bulk atoms can be largely reduced [52, 182, 183]. Generally, the effects involved with bombardment by species other than inert gas ions at different target temperatures are a field of more detailed studies.

The investigations of the differential sputtering yields are still very incomplete. However, these measurements, especially for atomically clean single crystal surfaces, allow to obtain detailed information about the sputtering process and the influence of the surface topography on the collision cascades.

7 Applications of Sputtering

Sputtering has long been regarded just as an undesired effect which destroys cathodes and grids in gas discharge tubes and ion sources. In high temperature plasma experiments with respect to controlled thermonuclear fusion, sputtering contributes to thinning of the vessel walls and a contamination of the hot hydrogen plasma with atoms of the vessel walls, which represents a major problem in fusion research [174–177, 184–188]. Sputtering is one of the causes for the destruction of diaphragms and targets in accelerators and in high-voltage electron microscopes [28]. In ion implantation the simultaneous removal of surface atoms by sputtering limits the achievable concentration in the implantation range [12].

However today, sputtering is used for many applications and has become an indispensable process in modern technology and physics [189]. Both the removal of atoms from a surface and the flux of atoms leaving the surface are successfully applied.

Sputtering allows a controlled removal of surface layers on a nearly atomic scale. It is applied for obtaining clean surfaces in field electron microscopy (FEM), field ion microscopy (FIM), low energy electron diffraction (LEED) and AUGER analysis of surfaces [189, 190]. An intense ion beam with a geometrical sharp edge is used for nearly destruction free cuts for analysis of thick films such as in ion beam slope cutting [28]. The controlled erosion with well-focussed ion beams is especially useful for optical components, lenses [191–193] and even large mirrors of glasses and some insulators such as SiC [108, 113, 194]. The topography of the mechanicly polished surface is analyzed with optical interferometry. The surface is finally machined and polished with a computer-controlled ion beam resulting in a submicron spatial resolution [195, 196]. With noble gas ion beams in the 100 eV range or gas clusters with noble gas atoms at energies in the 100 eV range, the surfaces are polished or nanostructured on an atomic scale [108, 195, 197, 198].

Sputtering is further applied for surface analysis and depth profiling of thin films. The ions removed by sputtering as well as the removed atoms after ionisation can be analysed in a mass spectrometer such as in SIMS or SNMS, and this gives very sensitive information about the surface concentrations, and a depth profile [199–202]. With rastered primary ion beams or imaging of the sputtered ions a high spatial resolution can be achieved [203–205]. If the surface is firstly smoothed by noble gas ion sputtering and sample rotation a very good depth resolution can be obtained [206, 207].

One of the largest applications of sputtering is, however, the deposition of thin films on a large variety of substrates [208], onto large areas of several m^2 [209–214] or onto extremely small areas such as in microelectronics. The composition and properties of the deposited films depend on the deposition process, such as short or long pused or continuous sputtering of the substrate and the residual gas pressure during deposition [213].

8 Summary, Conclusions

Because the investigation of sputtering phenomena dates back more than 100 years, the field has been covered by a large number of review articles in many languages. Those which have appeared within the last 30 years give a vital demonstration of the large advances made in understanding the sputtering process and its applications.

References

[1] W. R. Grove: Trans R. Soc. **142**, 87 (1852) 1, 10
[2] W. R. Grove: Philos. Mag. **5**, 203 (1853) 1
[3] J. P. Gassiot: Philos. Trans. R. Soc. **148**, 1 (1858) 1, 10
[4] J. Plücker: Pogg. Ann. Phys. **103**, 1858 (1858) 1, 10
[5] J. Stark: Z. Elektrochem. **14**, 752 (1908) 1
[6] J. Stark: Z. Elektrochem. **15**, 509 (1909) 1
[7] V. Kohlschütter: Jahrbuch Radioakt. Electron. **9**, 355 (1912) 1
[8] E. S. Mashkova, V. A. Molchanov: Radiat. Eff. **16**, 143 (1972) 1
[9] E. S. Mashkova, V. A. Molchanov: Radiat. Eff. **23**, 215 (1974) 1
[10] W. Eckstein, H. Verbeek: in R. A. Langley, et al. (Eds.): *Data Compendium for Plasma Surface Interactions*, NUCLEAR FUSION Special issue (IAEA, Vienna 1984) p. 12 1
[11] E. S. Mashkova, V. A. Molchanov: *Medium Energy Ion Reflection from Solids* (North Holland, Amsterdam, Oxford, New York, Tokyo 1985) 1
[12] G. Dearnaley, J. H. Freeman, R. S. Nelson, J. Stephen: *Ion Implantation* (North Holland, Amsterdam 1973) 1, 11
[13] G. M. McCracken: Rep. Prog. Phys. **38**, 241 (1975) 1
[14] E. Taglauer, W. Heiland: J. Nucl. Mater. **76/77**, 328 (1978) 1
[15] M. E. L. Oliphant: Proc. R. Soc. A **127**, 373 (1930) 1
[16] A. Güntherschulze: Z. Phys. **141**, 346 (1955) 1
[17] H. D. Hagstrum: Phys. Rev. **104**, 672 (1956) 1
[18] K. H. Krebs: Fortschr. Phys. **16**, 419 (1968) 1
[19] P. Sigmund, S. Tougard: in E. Taglauer, W. Heiland (Eds.): *Inelastic Particle Surface Collisions*, Springer Series in Chemical Physics **17** (Springer, Berlin, Heidelberg 1981) p. 2 1
[20] H. Rothard, B. Gervais: in P. Sigmund (Ed.): *Proc. ION06: Ion beam science: Solved and Unsolved Problems*, K. Dan. Vid. Selsk. Mat. Fys. Med. **52** (Copenhagen 2006) pp. 497–524 1
[21] C. Gerthsen: Ann. Phys. **65**, 881 (1928) 1
[22] N. H. Tolk, J. C. Tully, W. Heiland, C. W. White (Eds.): *Inelastic Ion Surface Collisions* (Academic, New York 1972) 1, 9
[23] J. C. Tully, N. H. Tolk, J. S. Kraus, C. Rau, R. C. Morris: in E. Taglauer, W. Heiland (Eds.): *Inelastic Particle Surface Collisions*, Springer Series in Chemical Physics **17** (Springer, Berlin, Heidelberg 1981) p. 196 1
[24] I. S. T. Tsong: in E. Taglauer, W. Heiland (Eds.): *Inelastic Particle Surface Collisions*, Springer Series in Chemical Physics (Springer, Berlin, Heidelberg 1981) p. 258 1

[25] S. A. E. Johannson, J. L. Campbell: *PIXE: A Novel Technique for Elemental Analysis* (Wiley, Chichester 1988) 1
[26] G. Carter, B. Navinšek, J. L. Whitton: in R. Behrisch (Ed.): *Sputtering by Particle Bombardment II*, Top. Appl. Phys. **52** (Springer, Berlin, Heidelberg 1983) p. 231, russ. translation: (MIR, Moscow 1986) 1, 5
[27] B. M. U. Scherzer: in R. Behrisch (Ed.): *Sputtering by Particle Bombardment II*, Top. Appl. Phys. **52** (Springer, Berlin, Heidelberg 1983) p. 271, russ. translation: (MIR, Moscow 1986) 1, 5
[28] W. Hauffe: in R. Behrisch, K. Wittmaack (Eds.): *Sputtering by Particle Bombardment III*, Top. Appl. Phys. **64** (Springer, Berlin, Heidelberg 1991) p. 305, russ. translation: (MIR, Moscow 1998) 1, 5, 7, 11
[29] D. Rosenberg, G. K. Wehner: J. Appl. Phys. **33**, 1842 (1962) 1
[30] A. Güntherschulze: J. Vac. Sci. Technol. **3**, 360 (1953) 1, 2, 9
[31] F. Keywell: Phys. Rev. **97**, 1611 (1955) 1, 10
[32] P. Sigmund: Phys. Rev. **184**, 383 (1969) 1, 2, 7
[33] P. Sigmund: Phys. Rev. **187**, 768 (1969) 1, 2, 7
[34] J. P. Biersack, W. Eckstein: Appl. Phys.A **34**, 73 (1984) 1, 2, 8
[35] D. E. Harrison, Jr.: Phys. Rev. **102**, 1473 (1956) 1, 2, 7
[36] D. E. Harrison, Jr.: Phys. Rev. **105**, 1202 (1957) 1, 2, 7
[37] D. E. Harrison, Jr.: J. Chem. Phys. **32**, 1336 (1960) 1, 2, 7
[38] W. Möller, W. Eckstein: Nucl. Instrum. Methods B **1**, 814 (1984) 1, 2, 8
[39] W. Möller, W. Eckstein, J. P. Biersack: Comput. Phys. Commun. **51**, 355 (1988) 1, 2, 8
[40] N. Bohr: K. Dan. Vid. Selsk. Mat. Fys. Medd. **18**, 8 (1948) 1, 2
[41] G. H. Kinchin, R. S. Pease: Rep. Prog. Phys. **18**, 1 (1955) 1, 2
[42] F. Seitz, J. S. Koehler: Phys. Stat. Solidi **2**, 307 (1956) 1, 2
[43] R. Behrisch: Ergeb. Exakt. Naturw. **35**, 295 (1964) 2, 9
[44] H. Oechsner: Appl. Phys. **8**, 185 (1975) 2, 9
[45] R. Behrisch (Ed.): *Sputtering by Particle Bombardment I*, Top. Appl. Phys. **47** (Springer, Berlin, Heidelberg 1981) russ. translation: (MIR, Moscow 1983) 2
[46] R. Behrisch (Ed.): *Sputtering by Particle Bombardment II*, Top. Appl. Phys. **52** (Springer, Berlin, Heidelberg 1983) russ. translation: (MIR, Moscow 1986) 2, 9
[47] R. Behrisch, K. Wittmaack (Eds.): *Sputtering by Particle Bombardment III*, Top. Appl. Phys. **64** (Springer, Berlin, Heidelberg 1991) russ. translation: (MIR, Moscow 1998) 2
[48] P. Sigmund: Sputtering by ion bombardment theoretical concepts, in R. Behrisch (Ed.): *Sputtering by Particle Bombardment I*, Top. Appl. Phys. **47** (Springer, Berlin, Heidelberg 1981) p. 9, russ. translation: (MIR, Moscow 1984) 2, 3, 7
[49] M. T. Robinson: Theoretical aspects of monocrystal sputtering, in R. Behrisch (Ed.): *Sputtering by Particle Bombardment I*, Top. Appl. Phys. **47** (Springer, Berlin, Heidelberg 1981) p. 73, russ. translation: (MIR, Moscow 1984) 2, 3, 8
[50] G. K. Wehner: Sputtering by ion bombardment, Adv. in Electronics and Electron Physics **7**, 239 (1955) 2, 3, 9
[51] G. K. Wehner, G. S. Anderson: in L.Maissel, R.Glang (Eds.): *The Nature of Physical Sputtering: Handbook of Thin Film Technology* (McGraw Hill, New York, St. Louis, San Francisco, Sydney, Toronto 1970) Chap. 3 2

[52] O. Almén, G. Bruce: Nucl. Instrum. Methods **11**, 257 (1961) 2, 3, 10
[53] V. A. Molchanov, V. G. Tel'kovskii: Sov. Phys. Doklady **6**, 137 (1961) 2, 3
[54] P. K. Rol, J. M. Fluit, J. Kistemaker: Symp. Sep. Radioact. Isot. (1960) 2, 3
[55] H. E. Roosendaal: Sputtering yields of single crystalline targets, in R. Behrisch (Ed.): *Sputtering by Particle Bombardment I*, Top. Appl. Phys. **47** (Springer, Berlin, Heidelberg 1981) p. 219, russ. translation: (MIR, Moscow 1984) 2, 3
[56] N. Winograd: in P. Sigmund (Ed.): *Fundamental Processes in Sputtering of Atoms and Molecules (SPUT92)*, K. Dan. Vidensk. Selsk. Mat. Fys. Medd. **43** (1993) p. 223 2, 3
[57] J. Stark, G. Wendt: Ann. Phys. **38**, 921 and 941 (1912) 2
[58] P. K. Rol, J. M. Fluit, F. P. Viehböck, M. de Jong: in Nielson (Ed.): *Proc. 4th Int. Conf. Phenom. Ion. Gases* (North Holland, Amsterdam 1959) 2, 3
[59] V. A. Molchanov, V. G. Tel'kovskii, V. M. Chicherov: Sov. Phys. Doklady **6**, 222 (1961) 2, 3
[60] O. Almén, G. Bruce: Nucl. Instrum. Methods **11**, 275 and 279 (1961) 2, 3
[61] G. S. Anderson, G. K. Wehner: J. Appl. Phys. **31**, 2305 (1960) 2, 3
[62] A. L. Southern, W. R. Willis, M. T. Robinson: J. Appl. Phys. **34**, 153 (1963) 2, 3
[63] P. Sigmund: *Fundamental Processes in Sputtering of Atoms and Molecules (SPUT92)*, K. Dan. Vidensk. Selsk. Mat. Fys. Medd. **43** (1993) 2, 9
[64] T. A. Burtseva, O. K. Chugunov, E. F. Dovguchits, V. L. Komarov, I. V. Mazul, A. A. Mitrofansky, M. I. Persin: J. Nucl. Mater. **191–194**, 309 (1992) 2
[65] C. García-Rosales, J. Roth, R. Behrisch: J. Nucl. Mater. **212–215**, 1211 (1994) 2
[66] C. García-Rosales, M. Balden: J. Nucl. Mater. **290-293**, 173 (2001) 2, 10
[67] T. Schenkel, M. A. Briere, H. Schmidt-Böcking, K. Bethge, D. H. Schneider: Phys. Rev. Lett. **78**, 2481 (1997) 2
[68] T. Schenkel, M. W. Newman, T. R. Niedermayr, T. A. Machicoane, J. W. MacDonald, A. V. Barnes, A. V. Hamza, J. C. Banks, B. L. Doyle, K. J. Wu: Nucl. Instrum. Methods B **161-163**, 65 (2000) 2
[69] G. Hayderer, S. Cernusca, V. Hoffmann, D. Niemann, N. Stolterfoht, M. Schmid, P. Varga, H. P. Winter, F. Aumayr: Nucl. Instrum. Methods B **182**, 143 (2001) 2
[70] J. Lindhard: K. Dan. Vidensk. Selsk. Mat. Fys. Medd. **34** (1965) 3
[71] D. Onderdelinden: Can. J. Phys. **46**, 739 (1968) 3
[72] G. K. Wehner: Phys. Rev. **102**, 690 (1956) 3
[73] R. H. Silsbee: J. Appl. Phys. **28**, 1246 (1957) 3
[74] G. Leibfried: J. Appl. Phys. **30**, 1388 (1959) 3
[75] M. Koedam: Physica **25**, 692 (1959) 3
[76] M. Koedam: Physica **26**, 351 (1960) 3
[77] M. Koedam: Ph.D. thesis, Utrecht (1961) 3
[78] R. S. Nelson, M. W. Thompson, H. Montgomery: Phil. Mag. **7**, 1385 (1963) 3
[79] V. E. Yurasova, W. M. Buchanov: Kristallographia **7**, 2 (1962) 3
[80] C. Lehmann, G. Leibfried: Z. Physik **162**, 203 (1961) 3

[81] P. D. Townsend: in R. Behrisch (Ed.): *Sputtering by Particle Bombardment II*, Top. Appl. Phys. **52** (Springer, Berlin, Heidelberg 1983) p. 147, russ. translation: (MIR, Moscow 1986) 3
[82] D. Fink, J. P. Biersack: Radiat. Eff. **64**, 89 (1982) 3
[83] M. W. Thompson: in J. J. Trillard (Ed.): *Le Bombardement Ionique*, Coll. Int. Centre Nat. Rech. Sci. (Bellevue, Paris 1961) 3
[84] H. H. Andersen, H. L. Bay: Radiat. Eff. **18**, 63 (1973) 3
[85] H. H. Andersen, H. L. Bay: in R. Behrisch, W. Heiland, W. Poschenrieder, P. Staib, H. Verbeek (Eds.): *Ion Surface Interactions, Sputtering and Related Phenomena* (Gordon and Breach, London, New York, Paris 1973) 3
[86] H. H. Andersen, H. L. Bay: Radiat. Eff. **19**, 139 (1973) 3
[87] P. Sigmund: Appl. Phys. Lett. **24**, 169 (1974) 3
[88] P. Sigmund: Appl. Phys. Lett. **27**, 768 (1975) 3
[89] H. H. Andersen, H. L. Bay: J. Appl. Phys. **45**, 953 (1974) 3
[90] H. H. Andersen, H. L. Bay: J. Appl. Phys. **46**, 2416 (1975) 3
[91] H. L. Bay, H. H. Andersen, W. O. Hofer, O. Nielsen: Nucl. Instrum. Methods **133**, 301 (1976) 3
[92] H. H. Andersen: in P. Sigmund (Ed.): *Fundamental Processes in Sputtering of Atoms and Molecules (SPUT92)*, K. Dan. Vidensk. Selsk. Mat. Fys. Medd. **43** (1993) p. 127 3
[93] L. Dutkiewicz, R. Pedrys, J. Schou, K. Kremer: Phys. Rev. Lett. **75**, 1407 (1995) 3
[94] W. Eckstein: Nucl. Instrum. Methods B **33**, 489 (1988) 3
[95] W. Eckstein: *Computer Simulation of Ion Solid Interactions*, Springer Series in Materials Science **10** (Springer, Berlin, Heidelberg 1991) russ. translation: (MIR, Moscow 1995) 3, 8, 9
[96] W. Eckstein: Nucl. Instrum. Methods **232**, 108 (2005) 3
[97] R. Behrisch: in R. Behrisch (Ed.): *Sputtering by Particle Bombardment II*, Top. Appl. Phys. **52** (Springer, Berlin, Heidelberg 1983) p. 179, russ. translation: (MIR, Moscow 1986) 3, 9
[98] W. O. Hofer: in R. Behrisch (Ed.): *Sputtering by Particle Bombardment II*, Top. Appl. Phys. **52** (Springer, Berlin, Heidelberg 1983) p. 15, russ. translation: (MIR, Moscow 1986) 4
[99] M. L. Yu: in R. Behrisch, K. Wittmaack (Eds.): *Sputtering by Particle Bombardment III*, Top. Appl. Phys. (Springer, Berlin, Heidelberg 1983) p. 91, russ. translation: (MIR, Moscow 1998) 4, 9
[100] K. Wittmaack: in R. Behrisch, K. Wittmaack (Eds.): *Sputtering by Particle Bombardment III*, Top. Appl. Phys. **64** (Springer, Berlin, Heidelberg 1983) p. 161, russ. translation: (MIR, Moscow 1998) 4
[101] W. Eckstein, J. P. Biersack: Appl. Phys. A **37**, 95 (1985) 4
[102] W. Eckstein, W. Möller: Nucl. Instrum. Methods B **7/8**, 727 (1985) 4
[103] R. S. Nelson, D. J. Mazey: Radiat. Eff. **18**, 199 (1973) 5
[104] I. H. Wilson: Radiat. Eff. **18**, 217 (1973) 5
[105] A. Güntherschulze, W. Tolmien: Z. Phys. A **119**, 685 (1942) 5
[106] W. Hauffe: *Ph.D.Theses A and B, Techn. Univ. Dresden* (Dresden 1971) 5, 6
[107] T. Michely, G. Comsa: Surf. Sci. **256**, 217 (1991) 5
[108] F. Frost, B. Rauschenbach: Appl. Phys. A **77**, 1 (2003) 5, 11
[109] G. J. Ogilvie, M. J. Ridge: J. Phys. Chem. Sol. **10**, 217 (1959) 5

[110] F. Frost, A. Schindler, F. Bigl: Appl. Phys. A **66**, 663 (1998) 5
[111] A. Schindler, F. Frost, A. Nickel, T. Hänsel, B. Rauschenbach: in *Proc. 1st Intern. Conf. On Micro- and Nano-Technology Vienna* (2005) p. 367 5
[112] S. Habenicht, W. Golse, H. Feldermann, U. Geyer, H. Hofsäss, K. L. Lieb, F. Roccaforte: Europhys. Lett. **50**, 209 (2000) 5
[113] S. Facsko: *Ph.D. Thesis D82, Techn. Univ. Aachen* (Shaker, Aachen 2001) 5, 11
[114] S. Facsko: FZ Rossendorf, priv. commun. 5, 6
[115] R. M. Bradley, J. M. E. Harper: J. Vac. Sci. Technol. A **6**, 2390 (1988) 5
[116] S. Facsko, T. Dekorsky, C. Koert, C. Trappe, H. Kunz, A. Vogt, H. L. Hartnagel: Science **285**, 1551 (1999) 5
[117] F. Frost, B. Ziberi, T. Höche, B. Rauschenbach: Nucl. Instrum. Methods B **216**, 9 (2004) 5
[118] S. Facsko, T. Bobek, A. Stahl, H. Kurz, T. Dekorsky: Phys. Rev. B **69**, 154312 (2004) 5
[119] G. K. Wehner: J. Appl. Phys. **29**, 217 (1958) 5
[120] P. Haymann: J. Chim. Phys. **57**, 572 (1960) 5
[121] W. Hauffe: Phys. Stat. Solidi A **4**, 11 (1971) 5
[122] A. D. G. Stewart: Ph.D. thesis, Univ. Cambridge (1962) 7
[123] G. K. Wehner, D. J. Haijeck: J. Appl. Phys. **42**, 1145 (1971) 7
[124] J. Lindhard, M. Scharff: Phys. Rev. **24**, 128 (1961) 7
[125] J. Lindhard, V. Nielsen, M. Scharff, P. V. Thompsen: K. Dan. Vid. Selsk. Mat. Fys. Medd. **33** (1963) 7
[126] G. Leibfried, K. Mika: Nucleonik **7**, 309 (1965) 7
[127] K. B. Winterbon, P. Sigmund, J. B. Sanders: K. Dan. Vid. Selsk. Mat. Fys. Medd. **37**, 14 (1970) 7
[128] H. H. Andersen, H. L. Bay: in R. Behrisch (Ed.): *Sputtering by Particle Bombardment I*, Top. Appl. Phys. **47** (Springer, Berlin, Heidelberg 1981) p. 145, russ. translation: (MIR, Moscow 1984) 7, 9
[129] J. Bohdansky: Nucl. Instrum. Methods B **2**, 587 (1984) 7
[130] C. García-Rosales, W. Eckstein, J. Roth: Nucl. Instrum. Methods B **218**, 8 (1994) 7
[131] W. Eckstein, R. Preuss: J. Nucl. Mater. **320**, 209 (2003) 7, 8
[132] M. T. Robinson, I. M. Torrens: Phys. Rev. B **9**, 5008 (1974) 8
[133] M. T. Robinson: *Fundamental Processes in Sputtering of Atoms and Molecules (SPUT92)*, K. Dan. Vidensk. Selsk. Mat. Fys. Medd. **43** (1993) 8
[134] J. P. Biersack, L. G. Haggmark: Nucl. Instrum. Methods **174**, 257 (1980) 8
[135] J. P. Biersack: Nucl. Instrum. Methods B **27**, 21 (1987) 8
[136] W. Takeuchi, Y. Yamamura: Radiat. Effects **71**, 53 (1983) 8
[137] R. M. Nieminen: in P. Sigmund (Ed.): *Fundamental Processes in Sputtering of Atoms and Molecules (SPUT92)*, K. Dan. Vidensk. Selsk. Mat. Fys. Medd. **43** (1993) p. 81 8
[138] H. M. Urbassek, W. O. Hofer: in P. Sigmund (Ed.): *Fundamental Processes in Sputtering of Atoms and Molecules (SPUT92)*, K. Dan. Vidensk. Selsk. Mat. Fys. Medd. **43** (1993) p. 97 8, 9
[139] H. M. Urbassek: Nucl. Instrum. Methods B **122**, 427 (1997) 8
[140] R. S. Nelson: Phil. Mag. **11**, 219 (1965) 9

[141] J. Bohdansky, H. Lindner, E. Hechtl, A. P. Martinelli, J. Roth: Nucl. Instrum. Methods B **18**, 509 (1985) 9
[142] R. Behrisch, W. Eckstein: Nucl. Instrum. Methods B **82**, 255 (1993) 9
[143] H. Sommerfeldt, E. S. Mashkova, V. A. Molchanov: Radiat. Eff. **9**, 267 (1971) 9
[144] H. Sommerfeldt, E. S. Mashkova, V. A. Molchanov: Phys. Lett. **38A**, 237 (1972) 9
[145] V. E. Yurasova, V. S. Chernysh, M. V. Kuvakin, L. B. Shelyakin: JETP Lett. **21**, 88 (1975) 9
[146] D. A. Konov, A. S. Mosunov, G. V. Adamov, L. B. Shelyakin, V. E. Yurasova: Vacuum **64**, 47 (2002) 9
[147] J. Roth: in R. Behrisch (Ed.): *Sputtering by Particle Bombardment II*, Top. Appl. Phys. **52** (Springer, Berlin, Heidelberg 1983) p. 91, russ. translation: (MIR, Moscow 1986) 9, 10
[148] E. de Juan Pardo, M. Balden, B. Cieciwa, C. García-Rosales, J. Roth: Physica Scripta T **11**, 62 (2004) 9, 10
[149] M. Balden, E. de Juan Pardo, H. Maier, P. Starke, U. Fantz: Physica Scripta T **11**, 123 (2004) 9, 10
[150] E. de Juan Pardo: Ph.D. thesis, Techn. Univ. München (2004) 9, 10
[151] M. Kaminsky: *Atomic and Ionic Impact Phenomena on Metal Surfaces*, Struktur und Eigenschaften der Materie in Einzeldarstellungen (Springer, Berlin, Heidelberg 1965) 9
[152] G. Carter, J. S. Colligon: *Ion Bombardment of Solids* (Heinemann, London 1968) 9
[153] N. V. Pleshivtsev: *Cathode Sputtering* (Atomisdat, Moscow 1968) in Russian 9
[154] R. S. Nelson: *The Observation of Atomic Collisions in Crystalline Solids* (North Holland, Amsterdam 1968) 9
[155] M. W. Thompson: *Defects and Radiation Damage in Metals* (Cambridge Univ. Press, Cambridge 1969) 9
[156] R. Behrisch, W. Heiland, W. Poschenrieder, P. Staib, H. Verbeek (Eds.): *Ion Surface Interaction, Sputtering and related Phenomena* (Gordon and Breach, London, New York, Paris 1973) 9
[157] P. Varga, G. Betz, F. P. Viehböck (Eds.): *Proc. Symp. on Sputtering (SOS 80)* (Institut für Allgemeine Physik, TU Wien 1980) 9
[158] E. Taglauer, E. W. Heiland (Eds.): *Inelastic Particle-Surface Collisions*, Springer Series in Chemical Physics **17** (Springer, Berlin, Heidelberg 1981) 9
[159] D. Briggs, M. P. Seah (Eds.): *Ion and Neutral Spectrometry*, vol. 2 (John Whiley & Sons, Chichester, New York, Brisbane, Toronto, Singapore) 9
[160] V. S. Smentkowski: Progr. Surf. Sci. **64**, 1 (2000) 9
[161] C. García-Rosales: J. Nucl. Mater. **211**, 202 (1994) 9, 10
[162] C. García-Rosales: J. Nucl. Mater. **212-215**, 97 (1995) 9, 10
[163] J. Roth, C. García-Rosales, R. Behrisch, W. Eckstein: J. Nucl. Mater. **191-194**, 45 (1992) 9
[164] W. Eckstein, C. García-Rosales, J. Roth: *IPP Report 9/82* (MPG, Garching 1993) 9
[165] M. Balden, J. Roth, E. de Juan Pardo, A. Wiltner: J. Nucl. Mater. **313-316**, 348 (2003) 9

[166] G. K. Wehner, C. E. Kenknight, D. Rosenberg: Planet. Space Sci. **11**, 885 (1963) 10
[167] T. A. Tombrello: in *Proc. 7th Intern. Conf. Atomic Collisions in Solids*, vol. II (Moscow State Univ. Publ. House, Moscow 1980) p. 35 10
[168] K. Thiel, U. Sassmannshausen, H. Külzer, W. Herr: Radiat. Eff. **64**, 83 (1982) 10
[169] T. A. Tombrello: in P. Sigmund (Ed.): *Fundamental Processes in Sputtering of Atoms and Molecules (SPUT92)*, K. Dan. Vidensk. Selsk. Mat. Fys. Medd. **43** (1993) p. 659 10
[170] D. McKoewn: Rev. Sci. Instrum. **32**, 133 (1961) 10
[171] R. Sizmann: Phys. Verh. **12**, 78 (1961) 10
[172] E. Goldstein: Verh. Dtsch. Phys. Ges. **4**, 228 (1902) 10
[173] E. Goldstein: Verh. Dtsch. Phys. Ges. **4**, 237 (1902) 10
[174] R. Behrisch: Nucl. Fusion **12**, 695 (1972) 10, 11
[175] J. Bohdansky: J .Nucl. Mater. **93 & 94**, 44 (1980) 10, 11
[176] J. Roth: in D. Post, R. Behrisch (Eds.): *Physics of Plasma-Wall Interactions in Controlled Fusion*, NATO ASI series B Physics **131** (Plenum Press, New York, London 1984) p. 351 10, 11
[177] R. Behrisch: Contrib. Plasmaphysics **42**, 431 (2002) 10, 11
[178] W. Eckstein: *IPP report 9/132* (MPG, Garching 2002) 10
[179] W. M. Wang, J. Roth, R. Behrisch: Nucl. Instrum. Methods B **42**, 29 (1989) 10
[180] P. Sigmund, N. Q. Lam: in P. Sigmund (Ed.): *Fundamental Processes in Sputtering of Atoms and Molecules (SPUT92)*, K. Dan. Vidensk. Selsk. Mat. Fys. Medd. **43** (1993) p. 255 10
[181] G. Betz, G. K. Wehner: in R. Behrisch (Ed.): *Sputtering by Particle Bombardment II*, Top. Appl. Phys. **52** (Springer, Berlin, Heidelberg 1983) p. 11, russ. translation: (MIR, Moscow 1986) 10
[182] H. Schirrwitz: Beitr. Plasmaphysik **2**, 188 (1962) 10
[183] R. Behrisch, J. Roth, J. Bohdansky, A. P. Martinelli, B. Schweer, D. Rusbüldt, E. Hintz: J. Nucl. Mater. **93 & 94**, 645 (1980) 10
[184] F. Engelmann: in D. Post, R. Behrisch (Eds.): *Physics of Plasma-Wall Interactions in Controlled Fusion*, NATO ASI series B Physics **131** (Plenum Press, New York, London 1984) p. 15 11
[185] J. Cecchi: J. Nucl. Mater. **93 & 94**, 30 (1980) 11
[186] R. Behrisch, E. Federici, A. Kukushkin, D. Reiter: J. Nucl. Mater. **313 - 316**, 388 (2003) 11
[187] R. Behrisch: Isvest. Acad. Nauk. **68**, 427 (2004) 11
[188] D. Naujoks: *Plasma Material Interaction in Controlled Fusion*, Springer Series on Atomic, Optical and Plasma Physics (Springer, Berlin, Heidelberg 2006) 11
[189] E. Taglauer: in P. Sigmund (Ed.): *Fundamental Processes in Sputtering of Atoms and Molecules (SPUT92)*, K. Dan. Vidensk. Selsk. Mat. Fys. Medd. **43** (1993) p. 643 11
[190] E. Taglauer: Appl. Phys. A **51**, 238 (1990) 11
[191] H. Bach: J. Noncryst. Solids **3**, 1 (1970) 11
[192] H. Bach: Z. Naturf. **27a**, 333 (1972) 11
[193] H. Bach: Beitr. Elektronenmikros. Direktabbildung Oberflächen **5**, 479 (1972) 11

[194] F. Frost, R. Fechner, B. Ziberi, D. Flamm, A. Schindler: Thin Solid Films **459**, 100 (2004) 11
[195] M. Fruit, A. Schindler, T. Hänsel: in R. Geyl, J. Maxwell (Eds.): *Optical Fabrication and Testing*, Proc. SPIE **3739** (1999) 11
[196] L. Aschke, F. Schubert, J. Kegeler, A. Schindler, T. Hänsel, K. Knapp: in , Proc. SPIE **4343** (2001) 11
[197] F. Frost, R. Fechner, D. Flamm, B. Ziberi, W. Frank, A. Schindler: Appl. Phys. A **78** (2004) 11
[198] I. Yamada, N. Toyoda: Nucl. Instrum. Methods B **232** (2005) 11
[199] R. E. Honig: *Adv. Mass Spectrometry* (Pergamon Press 1959) 11
[200] A. Benninghoven: Z. Naturf. **22a** (1967) 11
[201] A. Benninghoven: Z. Phys. **230** (1970) 11
[202] A. Benninghoven, A. M. Huber, H. W. Werner (Eds.): *Secondary Ion Mass Spectrometry (SIMS VI)* (Wiley, Chichester 1987) see also previous conferences in this row 11
[203] R. Castaing, G. Slodzian: J. Microscopie **1** (1962) 11
[204] H. Liebl: J. Appl. Phys. **38** (1967) 11
[205] H. Liebl: Anal. Chem. **46** (1975) 11
[206] A. Zalar: Thin Solid Films **124** (1985) 11
[207] E. H. Cirlin: Thin Solid Films **220** (1992) 11
[208] V. Kohlschütter, A. Noll: Z. Elektrochemie **11** (1912) 11
[209] E. D. McClanaham, N. Laegreid: in L. I. Maissel, R. Glang (Eds.): *Handbook of Thin Film Technology* (McGraw-Hill, New York 1967) 11
[210] S. Schiller, K. Goedicke, V. Kirchhoff, T. Kopte: in *38th Annual Technical Conf.* (Proc. Society of Vacuum Coaters 1995) p. 293 11
[211] S. Schiller, V. Kirchhoff, T. Kopte, M. Schulze: in *40th Annual Technical Conf.* (Proc. Society of Vacuum Coaters 1997) p. 168 11
[212] L. Maissel: in L. I. Maissel, R. Glang (Eds.): *Handbook of Thin Film Technology* (McGraw-Hill, New York 1970) Chap. 4 11
[213] O. Treichel, V. Kirchhoff: Surf. Coat. Technol. **123** (2000) 11
[214] A. Schindler, T. Hänsel, F. Frost, R. Fechner, A. Nickel, H.-J. Thomas, H. Neumann, D. Hirsch, R. Schwabe, G. Seidenkranz, K. Barucki: *OSA Technical Digest,* (Optical Society of America, Washington DC 2002) 11
[215] F. Frach, D. Glöß, K. Gödeke, M. Fahland, W. M. Gnehr: Thin Solid Films **445** (2003)

Index

angular distribution, 3, 4
  cosine, 4

BCA program
  ACAT, 8
  MARLOWE, 8
  TRIDYN, 8
  TRIM, 8
  TRIM-CASCADE, 8
  TRIM.SP, 8
binary collision approximation (BCA), 8
blistering, 5

channeling, 3
cluster, 2, 3, 9, 11
  impact
    fullerene, 3

collision cascade, 1, 10

depth resolution, 11
diffusion, 10
displacement energy, 2

electron microscopy, 11
energy loss
  electronic, 7
evaporation, 2

field ion microscopy (FIM), 11
fluence, 5, 6
focusing collision sequence, 3

heat of sublimation, 2, 7

implantation, 11
insulator, 3

low energy electron (LEED), 11

molecule, 2, 3

neutron sputtering, 3

radiation damage, 1, 2
recoil
  atom, 2, 8
regime
  linear cascade, 2, 7
  single knockon, 2
  spike, 2

secondary ion mass spectrometry (SIMS), 4
selfsputtering, 3
sputtering yield, 3–5, 7–10
state
  charge, 4
  ground, 4, 9
surface
  roughening, 4
  smoothing, 5
surface binding energy, 2, 7
surface topography, 4–6

target
  alloy, 10
  compound, 4, 10
  glass, 5
  semiconductor, 5
    InAs, 5
    InP, 5
    InSb, 5
  single crystal, 4, 9
target structure
  crystalline, 3
target temperature, 9, 10
thermal equilibrium, 1
thin film deposition, 11
threshold energy, 2, 4, 8, 9

Computer Simulation of the Sputtering Process

Wolfgang Eckstein[1] and Herbert M. Urbassek[2]

[1] Max-Planck-Institut für Plasmaphysik,
Boltzmannstr. 2, 85748 Garching, Germany
wge@ipp.mpg.de

[2] Fachbereich Physik, Universität Kaiserslautern,
Erwin-Schrödinger-Straße, 67663 Kaiserslautern, Germany
urbassek@rhrk.uni-kl.de

Abstract. Sputtering is caused by a series of atomic collisions between the incident projectiles and target atoms and between the target atoms themselves. These collision cascades can be followed with computer programs and with the Boltzmann transport equation. The two main approaches with computer programs are the binary collision approximation (BCA) and molecular dynamics (MD); they are both based on classical dynamics. Programs based on BCA describe sputtering by a sequence of independent binary collisions between atoms, whereas MD simulates the time evolution of the multiple interaction of each moving atom with all the atoms in some surrounding. The BCA approach can be regarded to be based on 'sequential event logic', whereas the MD approach is based on 'multiple interaction logic' according to *Harrison* [1]. Both approaches have advantages and disadvantages [2, 3].

1 Programs Based on the Binary Collision Approximation

Monte Carlo Programs based on the binary collision approximation were already developed at the end of the 6th decade of the 20th century. *Bredov* et al. [4] used such a program to investigate the penetration of ions in solids, and *Goldman* et al. [5] applied such a program to sputtering. Robinson's program MARLOWE [6] was intended to investigate ranges of energetic atoms in solids, which led to the discovery of channeling in single crystals [7, 8]. This success increased the understanding of energetic ions in solids and made the computing approach more trustworthy. Another widely distributed program is TRIM, which was also devised for the study of ranges of ions in solids by *Biersack* [9]. An extension of this program, TRIM.SP, allowed the investigation of sputtering [10]. Many other programs have been written at several places [2].

In these programs it is assumed that the collisions between atoms can be approximated by elastic binary collisions described by an interaction potential. It is further assumed that the energy loss to electrons can be handled separately as an inelastic energy loss.

R. Behrisch, W. Eckstein (Eds.): Sputtering by Particle Bombardment,
Topics Appl. Physics **110**, 21–31 (2007)
© Springer-Verlag Berlin Heidelberg 2007

1.1 The Binary Collision

In a binary collision between a moving atom with a single atom at rest the conservation of energy and momentum determines the elastic energy loss of the moving atom and the energy transferred to the recoil. The conservation of angular momentum allows to determine the scattering angle of the moving atom and the recoil angle of the atom set in motion. The scattering angle, ϑ, in the center-of-mass system is determined by an integral, if the impact parameter, p, and the interaction potential, $V(r)$, between the two colliding atoms is known:

$$\vartheta = \pi - 2p \int_R^\infty \left(r^2 \Big/ \sqrt{1 - \frac{V(r)}{E_\mathrm{r}} - \frac{p^2}{r^2}} \right) \mathrm{d}r \,. \tag{1}$$

r is the distance between the two colliding atoms, and R is the apsis (closest distance) of the collision [2,11]. Collisions are regarded for impact parameters smaller than a maximum value. The BCA procedure implies that the trajectories are approximated by their asymptotes between collisions. In principle, the collision between two moving atoms can be handled, too, but it is not used in most computer programs because it takes much more effort in the mathematical formulation with minor consequences.

In an actual program a sequence of binary collisions is considered. For sputtering the incident projectiles and the recoils generated in collisions are followed threedimensionally until their energy falls below some threshold. A target atom is sputtered, if its energy normal to the surface is larger than the surface binding energy, and if its distance from the surface is large enough, that it will not interact with other target atoms. For the development of the cascade the structure of the solid, crystalline, polycrystalline, and amorphous (randomized or structureless), is important. This leads to the distinction between Monte Carlo (MC) and lattice codes. In the case of a crystalline target the impact position on the target surface has to be chosen randomly; after this choice the cascade is completely determined. In an amorphous target the next collision is chosen randomly after a given mean free path. A crystal program has the advantage, that it can choose all three kinds of target structures by appropiate changes of the sequence of crystal cells. In contrast to crystal codes, where only the impact point is chosen randomly, the programs using an amorphous target are often called Monte Carlo programs because every collision (the impact parameter, azimuthal angle etc.) is chosen randomly. MARLOWE [6] is the best known example for a lattice code (using a crystalline target), TRIM.SP [10] for a Monte Carlo program (using an amorphous target).

1.2 The Interaction Potential for BCA

One important problem is the use of an appropiate interaction potential. These potentials are generally screened Coulomb potentials, i.e. the Coulomb

potential multiplied by a screening function, which is mostly represented as a sum of exponentials. These potentials are purely repulsive, and they depend only on the internuclear distance. For screened Coulomb potentials the determination of the scattering angle affords a numerical integration, which is the most time consuming part of a program based on the binary collision approximation. The mostly applied potentials are the Molière potential [12], the WHB (*Wilson-Haggmark-Biersack*) or KrC potential [13], and the ZBL (*Ziegler-Biersack-Littmark*) potential [14]. These potentials are adjusted to the different collision partners by the screening length, which depends on the nuclear charge of the individual atoms. The WHB and ZBL potentials are mean potentials determined from a number of individual potentials based on *Hartree-Fock-Slater* (HFS) atoms in the ground state. Therefore, these mean potentials have not the same quality for all different atom-atom combinations. The application of the Moliere potential often asks for a correction factor to the screening length for several ion-target combinations in order to get better agreement with experimental data. *Nakagawa* and *Yamamura* used a different screening function; their interaction potential is based on relativistic *Dirac-Hartree-Fock-Slater* (DHFS) atomic charge distributions. The individual constants for this potential are tabulated in [2, 15]. The use of screened Coulomb potentials is convenient, because it can be applied to all atomic species, on the other hand it does not care about the shell structure of the atomic element or changes due to the collision.

1.3 The Inelastic (Electronic) Energy Loss

The energy loss of a moving atom to target electrons can be dealt with as an inelastic energy loss, which has to be applied additively to the nuclear energy loss. This effect is smaller than the elastic energy loss at low energies but becomes dominant at high energies. This energy loss process reduces the energy of the moving atom, but does not change the direction of a moving atom. At low energies two theoretical models are applied: the *Lindhard-Scharff* model [16] and the *Oen-Robinson* model [17]. The *Lindhard-Scharff* proposal is a friction model, in which the energy loss depends on the atom velocity, an idea already proposed by *Fermi* and *Teller* [18]. In contrast to this continuous energy loss between collisions, the *Oen-Robinson* energy loss is a local model based on a model proposed by *Firsov* [19]. It is dependent on the impact parameter of the collision, and it also depends on the velocity of the moving atom. The *Oen-Robinson* energy loss is smaller than the *Lindhard-Scharff* loss in the keV range and below, but is adjusted to the Lindhard-Scharff loss at higher energies. At high energies, where the electronic energy loss has a maximum and then decreases according to the *Bethe-Bloch* formula [20, 21], the data tables for hydrogen and helium by *Andersen* and *Ziegler* [22, 23] are the best choice.

1.4 The Surface Binding Energy

The surface binding energy U describes the binding strength of surface atoms to the target. For sputtered atoms a planar surface potential is assumed, which causes an energy loss normal to the surface and a refraction towards the surface. The reason is, that the planar surface potential results in an energy distribution of sputtered atoms with a maximum at about half the surface binding energy in agreement with experimental data; for an isotropic surface potential the maximum would be at zero energy. The most common choice is to use the heat of sublimation for the surface binding energy. This value varies between 0.72 eV for Cs and 8.68 eV for W. It should be mentioned, that projectiles may experience a binding to the surface as for example hydrogen on C or in the case of selfbombardment. The surface binding energy should depend on the surface structure. To remove a target atom from a flat surface should need more energy, for example, than to remove it from an extended position above the surface. The application of the heat of sublimation is a good mean value for the surface binding energy, because these heats have been determined experimentally although for a not well-defined surface. In compound targets the surface binding energy is usually not known; therefore, an interpolation according to the composition is assumed.

1.5 Problems of the Concept of BCA

The binary collision approximation is based on some critical assumptions. A serious point is the assumption that at low energies a moving atom collides only with one single target atom. In TRIM.SP this problem is mitigated by including simultaneous weak collisions, but strictly in the binary collision approximation. Another problem is the concept of asymptotic trajectories, which is not a good description at low energies. This does not mean a sudden breakdown of the concept, but it worsens with decreasing energy. As discussed in [2] it starts at about 30 eV for the most unlikely process of a head-on collision; the energy depends also on the species of the colliding atoms. Both of these weaknesses seem not to be very serious, because otherwise the reasonable agreement between calculated and experimental results would be hard to explain.

1.6 Dynamic Monte Carlo Programs

In many cases projectiles are implanted in a target leading to a composition change with depth, and this composition changes with the incident fluence. The implanted atoms modify the cascade and as a consequence sputtering and backscattering. Similar effects occur in bombardment of multi-component targets. This problem is taken care of by dynamic programs, which make an update of the target composition after each fluence step. Then the bombardment proceeds until some maximum fluence or equilibrium is reached.

An example of such a program is TRIDYN [2, 24] and its newest version SDTrimSP [25], which combines TRIM.SP and TRIDYN. SDTrimSP is devised to run on all platforms (sequential and parallel).

1.7 Advantages of BCA Programs

BCA programs allow besides sputtering also the determination of backscattering, transmission, and radiation damage. This includes yields, reflection coefficients, their dependence on incident energy and angle of incidence as well as energy and angular distributions of sputtered and reflected atoms and even more detailed information. A big advantage of programs based on the binary collision approximation is the speed of calculations, which is about four to five orders of magnitude faster than for molecular dynamics programs.

2 Programs Based on Molecular Dynamics

The method of molecular dynamics simulation is based on the simple strategy of following the time evolution of a system of particles by solving Newton's equations of motion for the system. It has been used early when the calculation power of computers has been introduced to solve physics problems [26]. Indeed, one of the first applications of molecular dynamics in physics was a radiation damage problem [27]. Since then, the method has been used in many areas of science, such as the physics of liquids, of materials, of biomolecules, etc. Both the method and its applications are described in textbooks [28–33]; and also the issues of ion-solid interaction, radiation effects and, in particular, sputtering have been made accessible in monograph or review form [3, 34, 35].

2.1 Physics Input: Forces

The task of solving Newton's equations of motion needs as physical input the knowledge of the forces acting on the particles. For the issue of ion-solid interaction, and sputtering physics, one needs to know the interatomic forces between the projectile and the target atoms and between the target atoms themselves. These are assumed to be given by the interatomic potentials, and by the coupling of the atoms to the electronic system.

The role of quantum-mechanical phenomena in the field of sputtering physics appears to be small; it hence appears justified to use classical molecular dynamics simulation to study this phenomenon.

2.1.1 Interatomic Potentials

The calculation of appropriate interatomic potentials is a fundamental issue in solid-state physics [36]. During ion bombardment, however, the atom positions, and hence also the electronic states, deviate strongly from equilibrium;

hence interatomic potentials far away from equilibrium are needed. In principle, these potentials can be calculated by quantum chemistry or density functional theory. Due to the quick time evolution of a collision cascade, such an 'ab initio' potential calculation would best be performed at each time step of a molecular dynamics simulation; however, this solution is computationally too complex in large-scale simulations. Instead, as a rule, approximate parametrizations of the potential are used; their regimes of applicability have been assessed over the years.

At high interaction energies, above 100 eV relative energy, say, a collision between two atoms can be assumed to be binary. Then the repulsive potentials described in Sect. 1.2 above can be used. At small interaction energy, kinetic energies corresponding to < 1 eV, say, potentials taken to describe the equilibrium structure of solids or liquids at moderate temperatures can be used. These potentials differ for each class of materials – and the corresponding chemical bonding type – studied. Thus, for condensed rare gases, binary potentials of the *Lennard-Jones* type are appropriate. For metals, many-body potentials are necessary which are often used as parametrized in the embedded-atom-method (EAM) potentials [37, 38]. Covalent bonds need three-body potentials to describe the bonding geometry correctly [39–41]. In ionic solids the long-ranged Coulomb forces between anions and cations need to be included. The energy gap between the high- and low-energy regimes described above is usually filled by interpolation. Ideas of how to include physical knowledge – e.g. on displacement energies – to fill this gap are non-trivial to implement [42].

These few words may suffice to point out that the inclusion of appropriate interatomic potentials is a non-trivial task. However, as a benefit for sputtering and other radiation damage calculations, the appropriate binding energies (surface binding, adatom binding, etc.) and defect formation energies are directly included in the potentials.

2.1.2 Electrons

By the interaction with target electrons, swift atoms may be slowed down. This stopping force is implemented as an external force in the molecular dynamics routine. The schemes used are analogous to those described in Sect. 1.3 above.

At lower energies, the electron-atom interaction is better described as the electron-phonon interaction in a material. Several recipes exist of how to include this interaction into a molecular dynamics study [43–48]. A number of issues are still unsolved here: How to describe the electron-atom interaction in a 'hot' strongly disordered configuration such as in the centre of a collision cascade or a spike; how the band structure of the material (insulator or metal) enters; how to describe the interaction with hot, possibly non-thermal electrons.

2.2 Technical Considerations

In spite of the conceptual simplicity of a molecular dynamics algorithm, a number of more or less technical issues need be considered in order to perform reliable simulations [3].

2.2.1 System Size

The number N of target atoms to be included in a simulation cannot be arbitrarily large – simulations with several million atoms are considered big nowadays. This constraint essentially limits the impact energy for which sputtering can be calculated to the order of several 100 keV at the most [49].

2.2.2 Boundary Conditions

In order not to study the entire target material used in experiment (containing of the order of $N = 10^{23}$ atoms) only that subvolume is studied by molecular dynamics simulation in which the phenomena of interest occur. This subvolume – containing between 10^3 and 10^7 atoms, say – needs to be given the adequate boundary conditions to mimic the interaction with the surrounding material (energy and momentum exchange). This issue is particularly important for longer (> 1 ps, say) simulations, such as they are relevant under thermal-spike conditions or for cluster impact [50]. In the most refined simulations, the environment of the simulation volume is modelled by a finite-element-method (FEM) algorithm, which solves the elastic and heat conduction equations in the surrounding [51]. Simpler approaches employ energy-damping boundaries or provide for Langevin dynamics at the boundaries [52]. In cases where the question of how the surrounding material reacts is considered irrelevant, free boundary conditions (the simulation volume is considered as a free cluster in vacuum), fixed boundaries (in which in particular the bottommost target atom layer is kept at fixed positions), or laterally periodic boundary conditions (where in reality an infinite multitude of simultaneous projectile impacts are considered) are used.

2.2.3 Initial State

Ion-surface interaction presents an example of chaotic dynamics in the sense that slight variations in the initial conditions lead to large variations in the results, i.e., the sputtering yield [3, 53]. In experiment, it is unknown at which exact position (on a femtometer scale) the projectile impinges on the surface. Rather, the typical experiment measures the average over many projectile impacts at random positions. In the simulation, this average is analogously calculated, i.e., by considering a large number of trajectories which are randomly distributed over a representative surface zone (a surface elementary cell in the case of a crystalline target). The simulation results then allow

to provide besides the average quantities detected also an estimate of the statistical error of this quantity.

In the case where temperature effects in the target are considered important (e.g. where projectile channeling is an issue), statistics need to include impacts upon the target in different micro-realisations at this temperature.

2.2.4 Sputtering

The seemingly trivial question of when a target atom can be considered sputtered has to be approached carefully, in particular for cases where the surface is rough or becomes rough during sputtering (e.g. by crater formation). The sputtered-particle detector implemented in the code must make sure that atoms have no chance of being redeposited on the surface. More trivial questions include the detection of sputtered clusters as such, and to exclude atoms which are emitted sideways from the simulation volume (this may happen for free boundary conditions).

2.2.5 Simulation Time

While in a BCA code the simulation may terminate when no atom has a kinetic energy larger than the surface binding energy, the situation is more complex in molecular dynamics, since here moving atoms collide. In cases of high energy densities, i.e. in a thermal spike where part of the simulation volume is highly above the melting temperature, sputtering may proceed until 100 ps after projectile impact, or longer [54, 55]. Here a definite criterion of when to terminate the simulation is hard to find, and one may resort to analyzing the time dependence of sputtering instead.

2.3 Reliability

Let us assume that the technical issues discussed above – and those not discussed like the numerics of the ordinary differential equation solving routine applied – have been adequately mastered. Research on the influence of these technical issues on sputtering calculations continues until today, e.g., on the influence of the system size [56] or on strategies of how to choose the ion impact points [53]. Then, the simulation results will be as realistic as the physics input is – the interatomic potential and the electron-atom coupling. The experience attained from molecular dynamics simulations of sputtering in the last two decades gives us an optimistic picture. In many cases of disagreement between experimental and simulational results, the origin may be surmised to lie in the incomplete understanding of the experimental conditions, such as the geometric and stoichiometric characterization of the surface. However, the two caveats mentioned above – the role of the electron-atom interaction and the complexities of the interatomic potential in the energy regime important for sputtering – remain an important field of investigation for the future.

References

[1] D. E. Harrison, Jr.: *CRC Critical Reviews in Solid State and Material Sciences*, vol. 14, Supplement 1 (CRC Boca Raton 1988) 21
[2] W. Eckstein: *Computer Simulation of Ion Solid Interaction*, Springer Ser. Mater. Sci. **10** (Springer, Berlin, Heidelberg 1991) Russ. translation: (MIR, Moscow 1995) 21, 22, 23, 24, 25
[3] H. M. Urbassek: Nucl. Instrum. Methods B **122**, 427 (1997) 21, 25, 27
[4] M. M. Bredov, I. G. Lang, N. M. Okuneva: Zh. Tekh. Fiz. **28**, 252 (1958) Sov. Phys.-Tech. Phys. **3**, 228 (1958) 21
[5] D. T. Goldman, D. E. Harrison, Jr, R. R. Coveyou: *Tech. Rep. ORNL 2729*, Technical report, Oak Ridge (1959) 21
[6] M. T. Robinson, I. M. Torrens: Phys. Rev. B **9**, 5008 (1974) 21, 22
[7] M. T. Robinson, D. K. Holmes, O. S. Oen: *Le Bombardement Ionique: discussion* (CRNS, Paris 1962) p. 105 21
[8] M. T. Robinson, O. S. Oen: Appl. Phys. Lett. **2**, 30 (1963) 21
[9] J. P. Biersack, L. G. Haggmark: Nucl. Instrum. Methods **174**, 257 (1980) 21
[10] J. P. Biersack, W. Eckstein: Appl. Phys. A **34**, 73 (1984) 21, 22
[11] H. Goldstein: *Classical Mechanics*, 2nd ed. (Addison-Wesley, Reading 1980) Chap. 3 22
[12] G. Molière: Z. Naturforsch. A **2**, 133 (1947) 23
[13] W. D. Wilson, L. G. Haggmark, J. P. Biersack: Phys. Rev. B **15**, 2458 (1977) 23
[14] J. F. Ziegler, J. P. Biersack, U. Littmark: The stopping and range of ions in solids, in J. F. Ziegler (Ed.): *The Stopping and Range of Ions in Matter*, vol. 1 (Pergamon, New York 1985) 23
[15] S. T. Nakagawa, Y. Yamamura: Radiat. Eff. **105**, 239 (1988) 23
[16] J. Lindhard, M. Scharff: Phys. Rev. **124**, 128 (1961) 23
[17] O. S. Oen, M. T. Robinson: Nucl. Instrum. Methods **132**, 647 (1976) 23
[18] E. Fermi, E. Teller: Phys. Rev. **72**, 399 (1947) 23
[19] O. B. Firsov: Zh. Eksp. Teor. Fiz. **36**, 1517 (1959) Sov. Phys.-JETP **36**, 1076 (1959) 23
[20] H. A. Bethe: Z. Phys. **76**, 193 (1932) 23
[21] F. Bloch: Z. Phys. **81**, 363 (1933) 23
[22] H. H. Andersen, J. F. Ziegler: Hydrogen stopping powers and ranges in all elements, in J. F. Ziegler (Ed.): *The Stopping and Range of Ions in Matter*, vol. 3 (Pergamon, New York 1985) 23
[23] J. F. Ziegler: Helium stopping powers and ranges in all elements, in J. F. Ziegler (Ed.): *The Stopping and Range of Ions in Matter*, vol. 4 (Pergamon, New York 1977) 23
[24] W. Möller, W. Eckstein, J. P. Biersack: Comput. Phys. Commun. **51**, 355 (1988) 25
[25] W. Eckstein, R. Dohmen, A. Mutzke, R. Schneider: *Report IPP 12/3*, Technical report, Garching (2007) 25
[26] B. J. Alder, T. E. Wainwright: J. Chem. Phys. **27**, 1208 (1957) 25
[27] J. B. Gibson, A. N. G. M. Milgram, G. H. Vineyard: Phys. Rev. **120**, 1229 (1960) 25
[28] M. P. Allen, D. J. Tildesley (Eds.): *Computer Simulation of Liquids* (Clarendon, Oxford 1987) 25

[29] J. M. Haile: *Molecular Dynamics Simulation: Elementary Methods* (Wiley, New York 1992) 25
[30] M. P. Allen, D. J. Tildesley: *Computer Simulation in Chemical Physics*, NATO ASI E: Applied Sciences **397** (Kluwer, Dordrecht 1993) 25
[31] D. Raabe: *Computational Materials Science* (Wiley-VCH, Weinheim 1998) 25
[32] A. R. Leach: *Molecular Modelling – Principles and Applications*, 2nd ed. (Pearson Education, Harlow 2001) 25
[33] D. Frenkel, B. Smit: *Understanding Molecular Simulation*, 2nd ed. (Academic, San Diego 2002) 25
[34] J. R. Beeler, Jr.: *Radiation Effects Computer Experiments* (North-Holland, Amsterdam 1983) 25
[35] R. Smith (Ed.): *Atomic and Ion Collisions in Solids and at Surfaces* (Cambridge Univ. Press, Cambridge 1997) 25
[36] M. Finnis: *Interatomic Forces in Condensed Matter* (Oxford Univ. Press, Oxford 2003) 25
[37] M. S. Daw, S. M. Foiles, M. Baskes: Mater. Sci. Rep. **9**, 251 (1993) 26
[38] S. M. Foiles: MRS Bull. **21**, 24 (1996) 26
[39] F. H. Stillinger, T. A. Weber: Phys. Rev. B **31**, 5262 (1985) 26
[40] J. Tersoff: Phys. Rev. Lett. **56**, 632 (1986) 26
[41] D. W. Brenner: MRS Bull. **21**, 36 (1996) 26
[42] M. Jentschel, K. H. Heinig, H. G. Börner, J. Jolie, E. G. Kessler: Nucl. Instrum. Methods B **115**, 446 (1996) 26
[43] R. M. Nieminen: K. Dan. Vidensk. Selsk. Mat. Fys. Medd. **43**, 81 (1993) 26
[44] C. P. Flynn, R. S. Averback: Phys. Rev. B **38**, 7118 (1988) 26
[45] A. Caro, M. Victoria: Phys. Rev. A **40**, 2287 (1989) 26
[46] M. W. Finnis, P. Agnew, A. J. E. Foreman: Phys. Rev. B **44**, 567 (1991) 26
[47] I. Koponen: J. Appl. Phys. **72**, 1194 (1992) 26
[48] A. Caro: Radiat. Eff. Defects Solids **130-131**, 187 (1994) 26
[49] E. M. Bringa, K. Nordlund, J. Keinonen: Phys. Rev. B **64**, 235426 (2001) 27
[50] H. M. Urbassek, K. T. Waldeer: Phys. Rev. Lett. **67**, 105 (1991) 27
[51] M. Moseler, J. Nordiek, H. Haberland: Phys. Rev. B **56**, 15439 (1997) 27
[52] H. Haberland, Z. Insepov, M. Moseler: Phys. Rev. B **51**, 11061 (1995) 27
[53] T. J. Colla, B. Briehl, H. M. Urbassek: Radiat. Eff. Defects Solids **142**, 415 (1997) 27, 28
[54] K. Nordlund, J. Tarus, J. Keinonen, S. E. Donnelly, R. C. Birtcher: Nucl. Instrum. Methods B **206**, 189 (2003) 28
[55] S. Zimmermann, H. M. Urbassek: Nucl. Instrum. Methods B **228**, 75 (2005) 28
[56] M. A. Karolewski: Nucl. Instrum. Methods B **211**, 190 (2003) 28

Index

angular distribution, 25
asymptotic trajectory, 24

backscattering, 24, 25
band structure, 26
BCA program
  MARLOWE, 21, 22
  Monte Carlo (MC), 22
  SDTrimSP, 24
  TRIDYN, 24
  TRIM, 21
  TRIM.SP, 21, 22, 24, 25
binary collision approximation (BCA), 21, 23–25
Boltzmann transport equation, 21
boundary condition, 27
  free, 28
  periodic, 27

channeling, 28
collision cascade, 21, 26
composition, 24
compound target, 24

Dirac-Hartree-Fock-Slater (DHFS), 23
displacement energy, 26

electron-atom coupling, 28
electron-atom interaction, 26, 28
electron-phonon interaction, 26
energy loss, 24
  electronic, 21, 23
    Lindhard-Scharff model, 23
    Oen-Robinson model, 23
  nuclear, 23
energy spectra, 24, 25

finite-element-method, 27
friction, 23

Hartree-Fock-Slater (HFS), 23
heat of sublimation, 24

impact parameter, 22
interaction potential, 22, 25, 26, 28
  Coulomb, 23
  embedded-atom-method (EAM), 26
  Lennard-Jones, 26
  screened Coulomb, 22, 23
    KrC (WHB), 23
    Molière, 23
    ZBL, 23
  screening function, 23
  three-body, 26
ion-solid interaction, 25
isotropic surface potential, 24

Langevin dynamics, 27
lattice code, 22

molecular dynamics, 21, 25–28

Newton's equations of motion, 25

planar surface potential, 24

radiation damage, 25, 26
recoil
  angle, 22
reflection coefficient, 25
refraction, 24

scattering angle, 22, 23
screening length, 23
selfsputtering, 24
simultaneous weak collision, 24
spike
  thermal, 27, 28
surface binding energy, 22, 24, 28

target
  liquid, 25
  multicomponent, 24
target structure
  amorphous, 22
  crystalline, 22, 27
  polycrystalline, 22
trajectory, 22
transmission, 25

Sputtering Yields

Wolfgang Eckstein

Max-Planck-Institut für Plasmaphysik,
Boltzmannstr.2, 85748 Garching, Germany
wge@ipp.mpg.de

Abstract. Sputtering is caused by collision cascades initiated by energetic ions or neutrals incident on a solid or liquid target. The sputtering yield, Y, i.e., the average number of atoms removed from a target per incident particle (atom or ion), is the most global value in sputtering. It depends on the target material, on the species of bombarding particles and their energy and the angle of incidence. Most experimental and calculated results have been determined for amorphous and polycrystalline targets but also values for single crystal targets are available. An extensive comparison of experimental and calculated yield values are provided and the accuracies of these values are discussed. The sputtering yields of multicomponent systems depend on the bombarding fluence and show sometimes a complicated behaviour.

1 Experimental Methods

Several conditions have to be fulfilled for achieving reliable and reproducible results [1, 2]:

a) The beam of incident particles (ions or neutrals) should have a well defined energy with a small energy width (important especially at low energies) and a small angular divergence (important at grazing incidence). The beam should be mass-analyzed, especially for light ions, in order to separate different species such as molecular ions from atomic ions and especially particles with very different masses. The incident fluence should be measured accurately, which affords the knowledge of the ion current.
b) For elemental targets the impurity content in the target should be negligible, especially if impurities have masses very different from the investigated element. Due to the dependence of the yield on the angle of incidence the target should be flat. An initially polished surface will, however, generally become rough during particle bombardment [3, 4]. Implantation of the bombarding species into the target will also modify the yield; therefore a measurement of the yield versus the incident fluence is valuable to show the difference between low fluence and steady state (saturation). Most targets are not amorphous and the crystal grains are not randomly oriented. The target structure, if not a single crystal, should be checked to have an idea about any texture of the target. For a sputtering

R. Behrisch, W. Eckstein (Eds.): Sputtering by Particle Bombardment,
Topics Appl. Physics **110**, 33–187 (2007)
© Springer-Verlag Berlin Heidelberg 2007

measurement at a target consisting of a thin film on a substrate, the film should be thick enough, that the underlying substrate does not modify the collision cascade in the film.

c) The vacuum conditions should be good enough, that adsorption of residual gas species on the target during bombardment is negligible. This is of special importance if the yields are low such as for light incident ions and for oxide and nitride forming elements. The general condition is, that the arrival number and the sticking probability of these rest gas species per unit time must be smaller than the corresponding arrival of beam species times the sputtering yield of the gas species.

For the determination the sputtering yield the incident fluence and the removed target material have to be measured. The incident fluence is usually determined by the incident charge, the removed material by several methods [2]:

a) Mass change.
The amount of material removed from an elemental target can be determined by the measured mass change, Δm, giving for the sputtering yield

$$Y = \frac{\Delta m}{M_2 n_1} N_0 \,, \tag{1}$$

where M_2 is the target atomic mass, n_1 is the number of incident projectile ions (atoms), and N_0 is the Avogadro number. This formula is only correct, if implantation and trapping of bombarding projectiles [4,5] into the target is negligible. This is justified for light ions implanted into a target of heavy atoms, if their concentration stays low during bombardment and if the light ions do not accumulate in the target, i.e., diffusion into the bulk can be neglected. The mass change of a thin film evaporated on a quartz crystal oscillator can be determined by a frequency change of the oscillator [6–8]. Other problems are the weighing of the bombarded target outside the bombarding vacuum chamber due to adsorption of water or oxygen at the surface, adsorption of gaseous species inside the vacuum chamber, and surface roughness.

b) Thickness change.
The amount of material removed can be determined by the measurement of the thickness change of a thin film, for example, with Rutherford backscattering [9, 10]. The measured areal density before and after bombardment give the yield. Other methods are X-ray analysis, nuclear reaction analysis, methods using electrons such as an electron microprobe or transmission electron microscopy, mechanical methods such as the measurement of crater depth, and changes in interference colours. Changes in electrical resistivity have been applied to thin metal films and wires [11, 12]. Thin metal films have been sputtered until a hole appeared [13]. Possible errors are forward sputtering and a nonuniform current density distribution.

c) Collection of sputtered material.
Another procedure to determine the amount of atoms removed is a measurement of the sputtered material by collecting it on catcher foils. Possible errors are an incomplete collection of sputtered material due to a limited solid angle (smaller than half space), incomplete sticking, backscattering and sputtering of the deposited films. This is especially important for high energy sputtered atoms at oblique incidence bombardment. Another very sensitive technique is neutron activation of the collected material or of the target [14, 15].
d) Field ion microscopy.
This method allows counting of the atoms sputtered from a tip, but a problem appears for the determination of the incident ion fluence [16, 17]. An array of tips was used.
e) Spectroscopy method.
A plasma column in front of the target may be used for exciting the sputtered neutrals. Specific emission lines are observed [18]. The method needs knowledge about the plasma, and for the calculation of the excitation rate it relies on an atomic data base as ADAS [19]. The method is fast and very sensitive.
With these techniques a large amount of sputtering yield data have been accumulated for many ion–target combinations, mostly for polycrystalline targets.

2 Calculational Methods

Several efforts have been made to calculate sputtering yields for amorphous, polycrystalline and single crystal targets [20–23]. Besides the analytic approach by *Sigmund* [20, 21] many sputtering yields have been calculated with computer programs based on the binary collision approximation, see Chap. by Eckstein and Urbassek. A large number of yields have been provided mainly by *Yamamura* [24, 25] with his program ACAT [26] and by *Eckstein* [27] with the program TRIM.SP [28, 29]. These authors use different interaction potentials, *Yamamura* the Nakagawa-Yamamura potential [30], *Eckstein* the KrC (WHB) potential [31]. For the surface binding energy [29] the heat of sublimation is applied. A comparison for the energy dependence of the sputtering yield of silver bombarded with Ar calculated with different interaction potentials is shown in Fig. 1. Whereas the KrC, ZBL, and Moliere (correction factor to the screening length, ca=0.8) potentials give nearly the same results, however, Moliere (with ca = 1) and Nakagawa-Yamamura potentials show larger yields at higher bombarding energies. For comparison also sputtering yields determined by the analytic theory are given; these values are generally higher than the yields obtained by computer programs. In the threshold region the differences in the yield calculated with the different po-

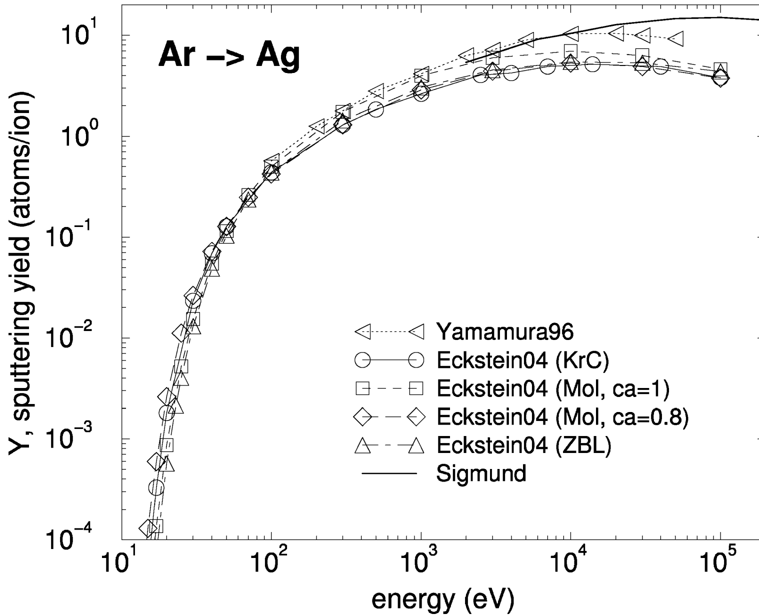

Fig. 1. Calculated energy dependence of the sputtering yield at normal incidence for the bombardment of Ag with Ar for different interaction potentials (ca is a correction factor to the screening length) calculated by *Yamamura* [24, 25] and by *Eckstein* [32]. The curve from the analytic theory (Sigmund) is taken from [2]. Lines are drawn to guide the eye

tentials are more pronounced due to the differences of the potentials at large interatomic distances.

For the inelastic energy loss an equipartition of the Lindhard-Scharff and the Oen-Robinson models is used in some computer simulations (see chapter by *Eckstein* and *Urbassek*). The influence of inelastic energy losses in the calculated sputtering yields is shown in Fig. 2. As expected the effect of the inelastic energy loss is smallest in the keV energy range and increases with higher and lower incident energies. The relative small effect may be a justification for the neglect of the inelastic energy loss in the analytic theory.

No assumptions are made to improve agreement with experimental data. Only for light ions *Yamamura* introduced small corrections in the screening length [24, 25] in the interaction potential, which he supported by theoretical arguments [33].

The static BCA programs allow the determination of sputtering yields under the assumption that the target composition is not changed during bombardment. This applies for selfbombardment, hydrogen and noble gas bombardment, as long as trapping of these species can be regarded as negligible. In most other cases, such as, for example, for metal atom bombardment of carbon the target composition is changed in the implantation range. Then

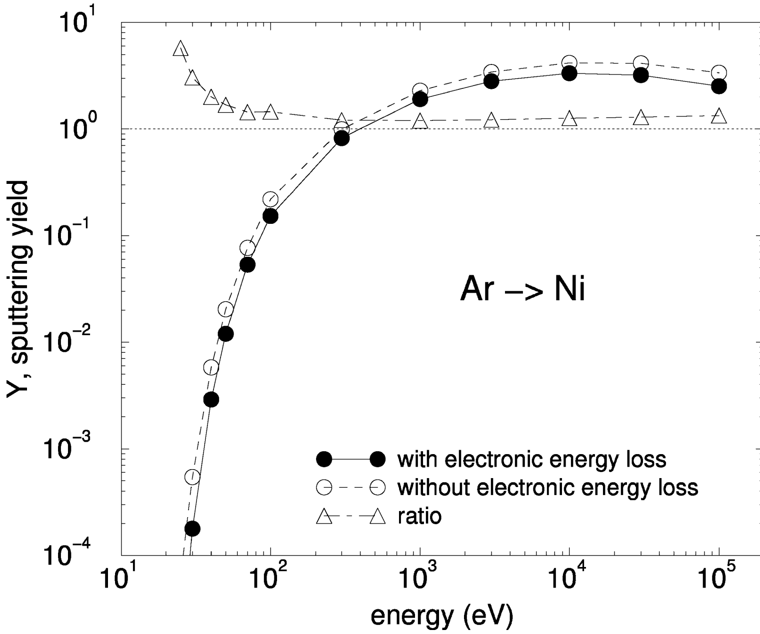

Fig. 2. Calculated energy dependence of the sputtering yield at normal incidence for the bombardment of Ni with Ar with and without inelastic energy loss calculated with TRIM.SP [32]. Lines are drawn to guide the eye

the yield will change with bombarding time or ion fluence. In these cases a dynamic program such as TRIDYN [29, 34, 35] has to be applied. An exception is the bombardment with a low fluence (negligible target change).

3 Mono-Atomic Targets

As bombarding particles mainly hydrogen isotopes and noble gases have been used. The implicit assumption is, that target composition changes due to bombardment as for example by implantation are negligible. All other examples are discussed in Sects. 4 to 8. Experimental data up to 1981 were presented in the review by *Andersen* and *Bay* [2]. Since that time computer simulation has provided many values [24, 25, 36]. Collection of sputtering yields for special materials for the nuclear fusion community can be found in [37–41].

3.1 Energy Dependence of the Sputtering Yield at Normal Incidence

For the survey of the many experimental and calculated sputtering yields at normal incidence the following procedure has been adopted. The calcu-

lated values have been fitted by an empirical formula and will be compared with experimental data, see Sect. 3.3. The reasoning for this procedure is the following: The experimental data often cover only a limited energy range between the threshold energy and at least 10 keV, whereas missing values can be obtained by calculations. Another point is, possible systematic deviations between calculated and experimental data will show up more clearly. In experiments the target surface roughness (which may change even with ion fluence) is usually not known, whereas in calculations a nearly flat surface is assumed. Due to the increase of the sputtering yield with an increasing angle of incidence (with respect to the surface normal) the experimental data at normal incidence should generally give a somewhat higher value than the calculated values (up to a factor of two). On the other side, simulations may suffer from insufficiently accurate interaction potentials or inelastic energy losses.

The procedure applied here is different from the fitting by *Yamamura* [24, 25] and *Janev* [42], who used all the experimental data for the fitting. In the last mentioned paper the authors derived a unified analytic representation for the sputtering yields, which is not convenient for practical purposes.

3.2 Fitting

Many formulae have been proposed to describe the energy dependence of the sputtering yield at normal incidence, see [43] and the literature in this paper. In this book the energy dependence of sputtering yields calculated for normal incidence has been fitted with the formula proposed by *Eckstein* and *Preuss* [44], which gives generally a better description of the available yield values; it was also used in [41]:

$$Y(E_0) = q\, s_{\mathrm{n}}^{\mathrm{KrC}}(\varepsilon) \frac{\left(\frac{E_0}{E_{\mathrm{th}}} - 1\right)^{\mu}}{\lambda + \left(\frac{E_0}{E_{\mathrm{th}}} - 1\right)^{\mu}} \tag{2}$$

with the nuclear stopping power for the KrC (WHB) potential [43]

$$s_{\mathrm{n}}^{\mathrm{KrC}} = \frac{0.5 \ln(1 + 1.2288\varepsilon)}{\varepsilon + 0.1728\sqrt{\varepsilon} + 0.008\varepsilon^{0.1504}}\,, \tag{3}$$

the reduced energy

$$\varepsilon = E_0 \frac{M_2}{M_1 + M_2} \frac{a_{\mathrm{L}}}{Z_1 Z_2 \mathrm{e}^2} \tag{4}$$

and the *Lindhard* screening length [45]

$$a_{\mathrm{L}} = \left(\frac{9\pi^2}{128}\right)^{1/3} a_{\mathrm{B}} \left(Z_1^{2/3} + Z_2^{2/3}\right)^{-1/2}, \quad a_{\mathrm{B}} = 0.0529177\,\mathrm{nm} \tag{5}$$

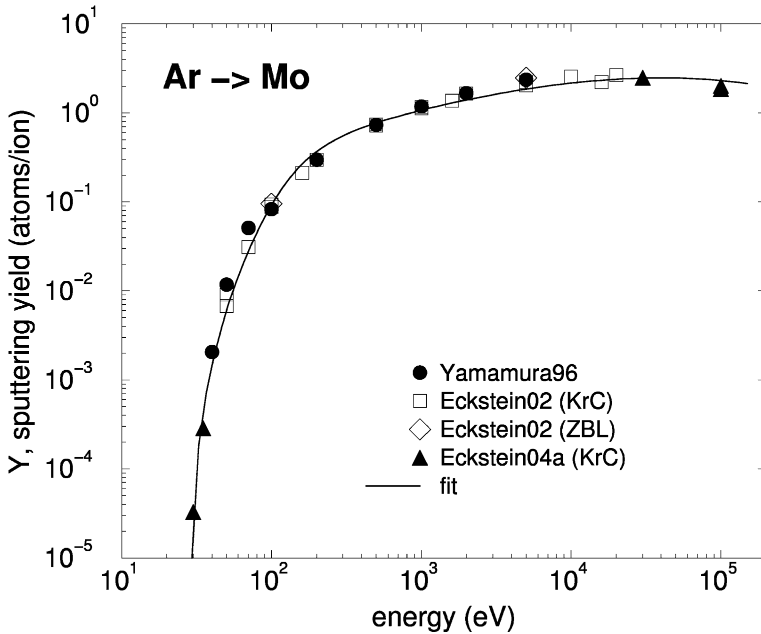

Fig. 3. Energy dependence of the sputtering yield at normal incidence for the bombardment of Mo with Ar calculated by *Yamamura* [24,25] and by *Eckstein* [32,36]

where a_B is the Bohr radius. Z_1, Z_2, and M_1, M_2 are the atomic numbers and the atomic masses of the projectile and target atom, respectively. The threshold energy E_{th} and the values q, λ and μ are fitting parameters.

The proportionality of the yield, Y, to the nuclear stopping power is adopted from analytic theory [20,21]. q describes the absolute yield, λ triggers the onset of the decrease of the sputtering yield at low energies towards the threshold, and μ is assigned in order to describe the strength of this decrease. The fitting parameters λ, q, μ and E_{th} are obtained by a procedure based on Bayesian statistics, which provides a region of confidence and the corresponding errors [44].

For the fitting of the calculated sputtering yields mainly the values by *Yamamura* [24,25] and *Eckstein* [32,36] are used. Both datasets agree mostly reasonably well, see Fig. 3, but in some cases deviations up to a factor of two occur. In many cases additional values of the sputtering yield have been calculated [32] to get a reasonable fit to lower energies or to extend the fit to higher energies, where experimental data were available.

The fitting parameters for the calculated values are given in Tables 1–9 (Appendix) together with ε, E_{sb} and E_{sb}/γ. E_{sb} is the surface binding energy, and $\gamma = 4M_1M_2/(M_1+M_2)^2$ is the energy transfer factor, M_1 and M_2 are the atomic masses of the projectile and target atom, respectively. Tables 25–

28 give a list of sputtering yields and the corresponding references not shown in the figures.

3.3 Comparison of Calculated Values with Experimental Data

For each ion–target combination, where experimental data are available, figures were produced as shown in Figs. 4–63. Each figure shows the algebraic fit for the energy dependence of the calculated sputtering yield values and the experimental data points measured by different authors at normal incidence for polycrystalline or amorphous materials. In cases, where only calculated values are available, fit curves for several incident ions are shown in one figure. The different plots have not always the same energy and yield scales. Usually, the energy scale for the light ions, hydrogen and helium, reaches up to 20 keV, whereas for the heavy ions the energy scale reaches up to 200 keV. In some cases the energy scale has been extended, if measured data at higher energies are available. The yield scale has a lower limit of 10^{-4}, the upper limit depends on the data. Experimental data for single crystals have not been included in these plots because of possible channeling effects; the same applies for bombardment with nonvolatile ion species due to fluence dependent results (Tables 29 to 31), and to ion species which form stable compounds with target atoms such as oxides.

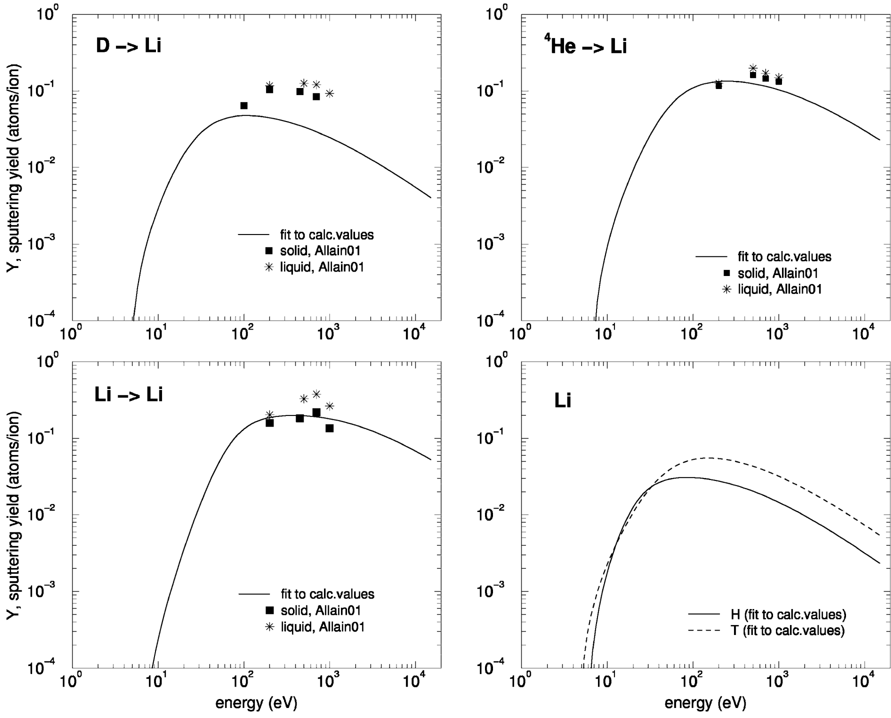

Fig. 4. Energy dependence of sputtering yields of Li for bombardment at normal incidence with D, ^{4}He, Li [46] and H and T

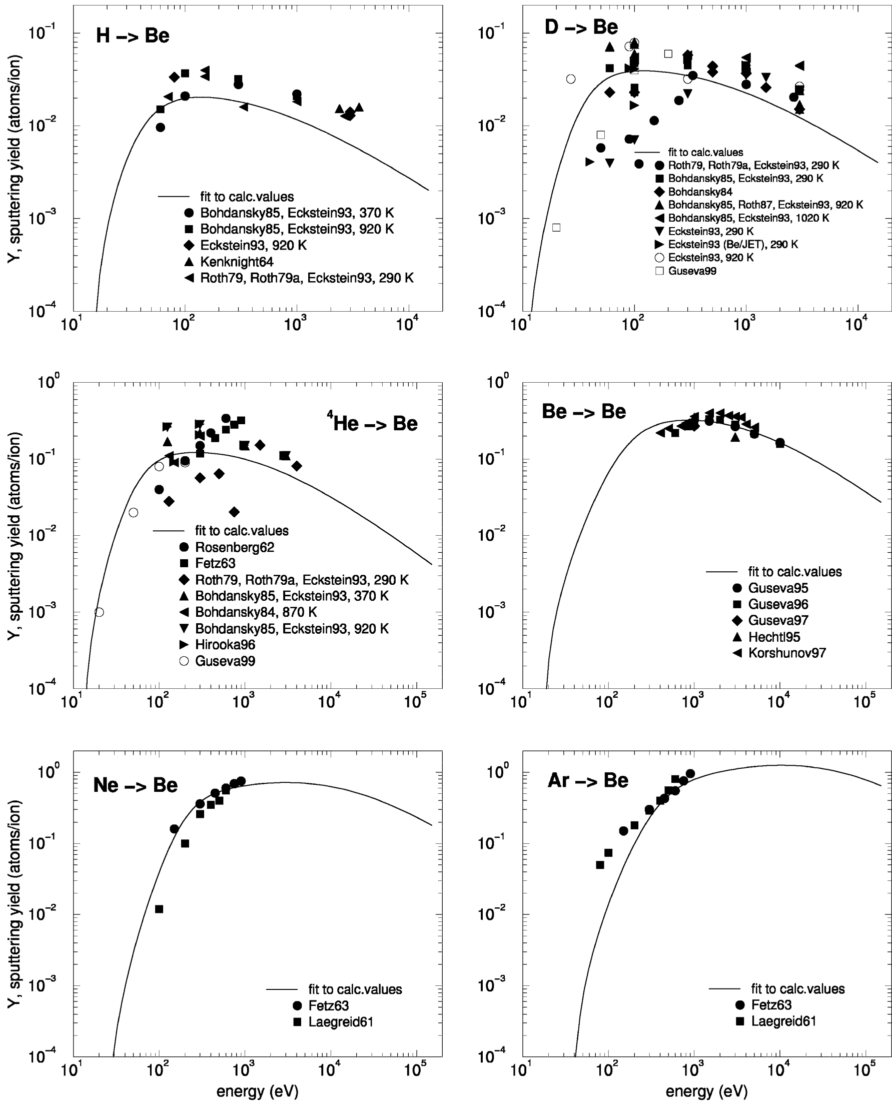

Fig. 5. Energy dependence of sputtering yields of Be for bombardment at normal incidence [47] with H [27, 48–51], D [16, 27, 48, 50–53], ^{4}He [16, 17, 48, 50, 51, 54–57], Be [58–62], Ne [55, 63] and Ar [55, 63]. Several authors in one line mean the same data in different publications

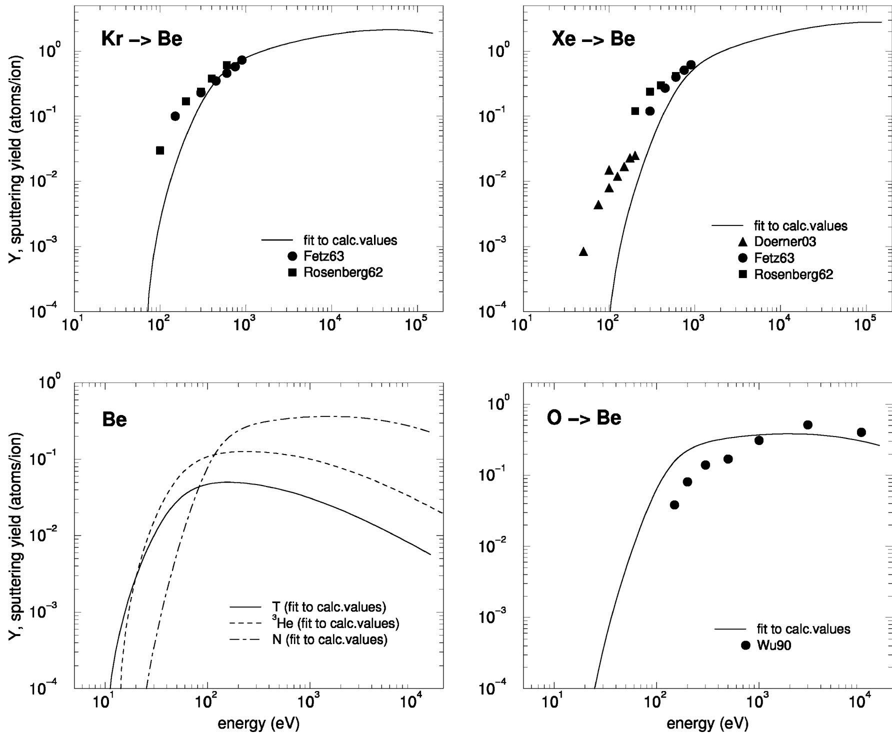

Fig. 6. Energy dependence of sputtering yields of Be for bombardment at normal incidence with Kr [54, 55], Xe [18, 54, 55], T and ^{3}He and N, and O [64]

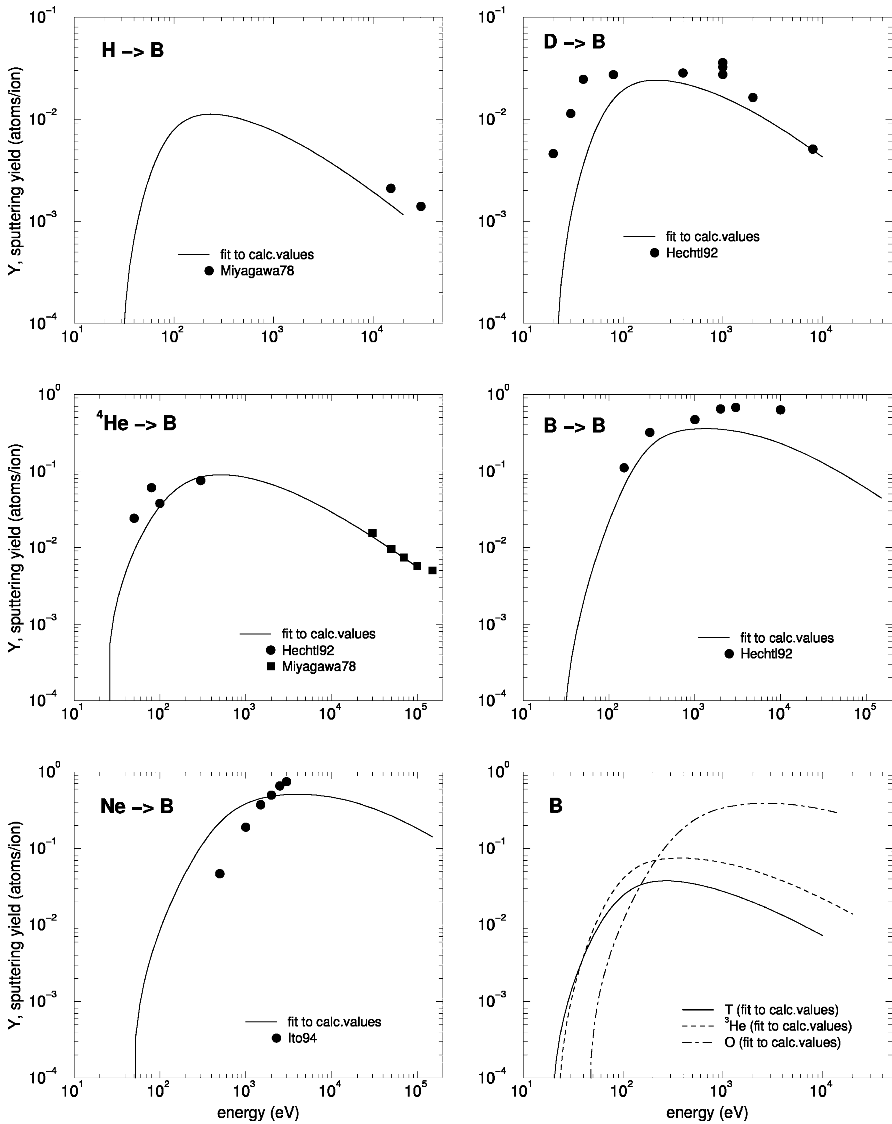

Fig. 7. Energy dependence of sputtering yields of B for bombardment at normal incidence with H [65], D [27, 66], ^{4}He [27, 65, 66], B [27, 66], Ne [67], and T, ^{3}He, O (only low fluence)

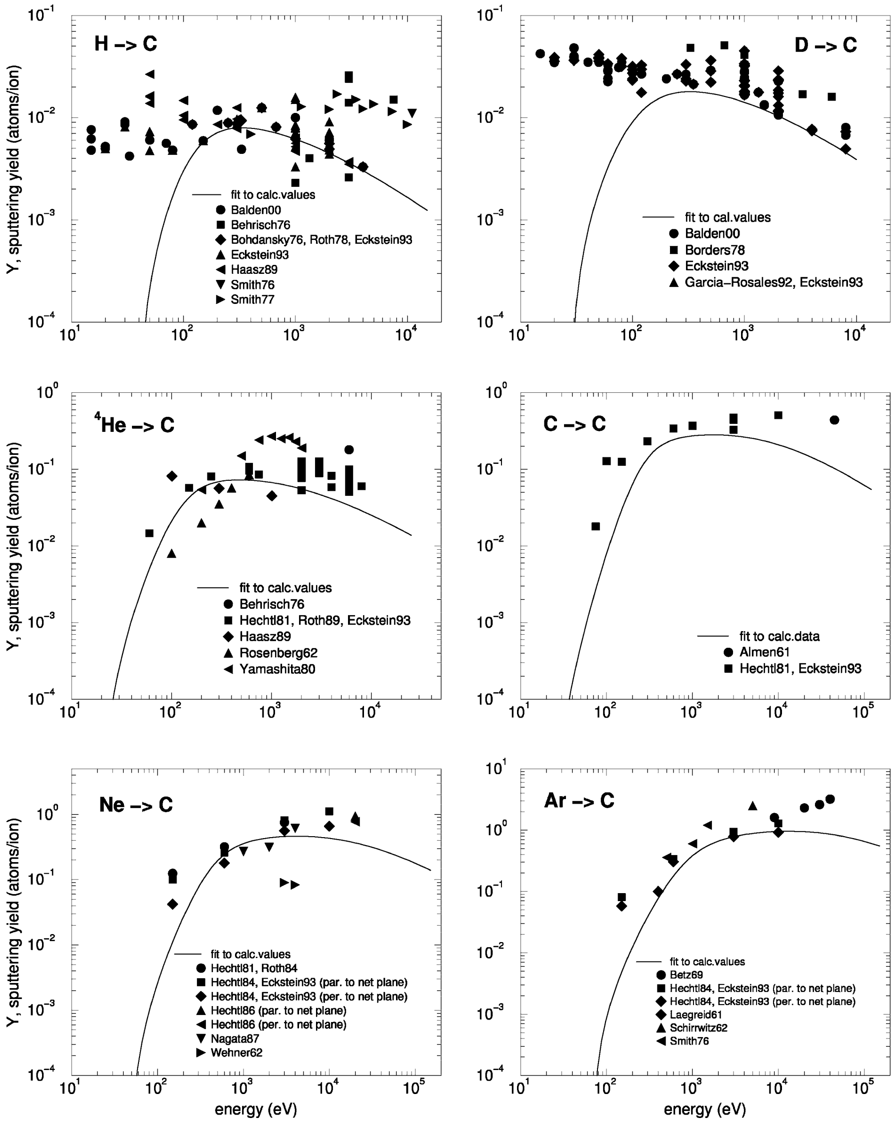

Fig. 8. Energy dependence of sputtering yields of C for bombardment at normal incidence with H [27,68–74], D [27,74–76], ^{4}He [27,54,68,72,73,77,78], C [27,78–83], Ne [27,78,80,84–87], and Ar [27,63,70,85,88,89]

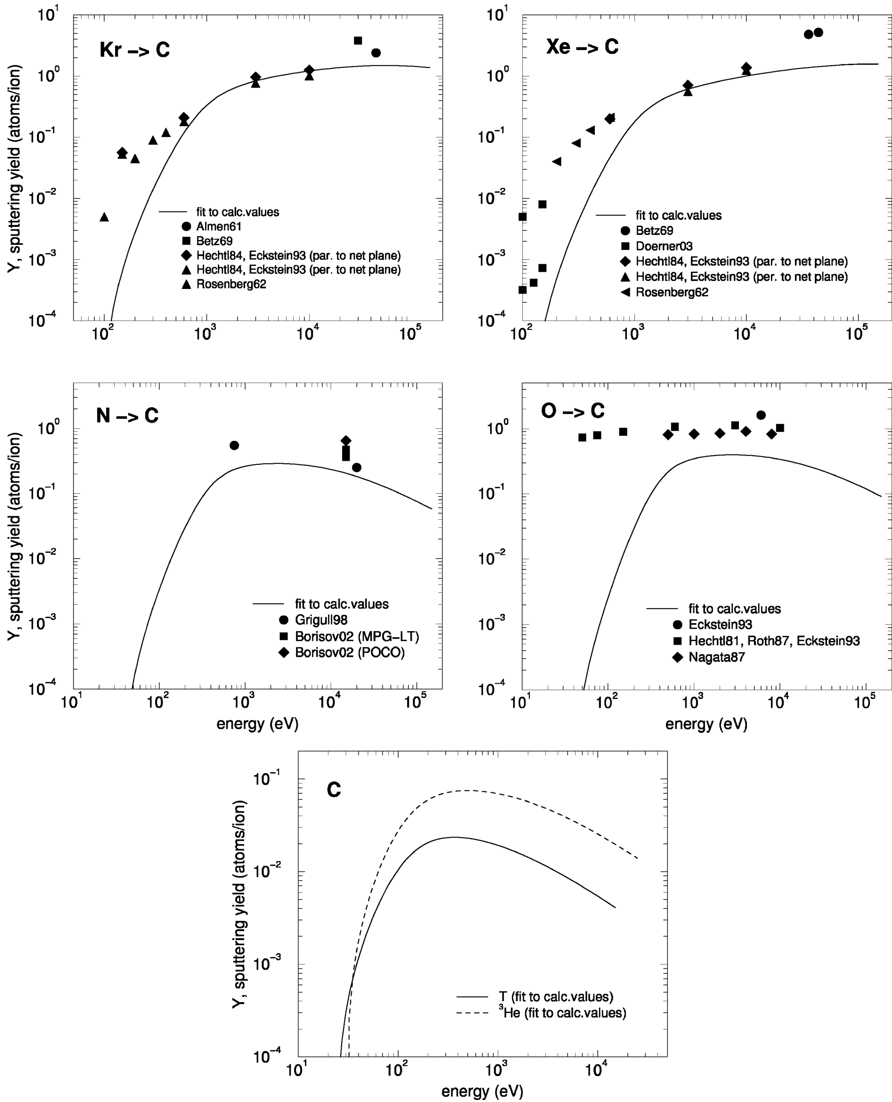

Fig. 9. Energy dependence of sputtering yields of C for bombardment at normal incidence with Kr [27, 54, 85, 89, 90], Xe [18, 27, 54, 85, 89], N [91–93], O [27, 53, 78, 80, 87], and T, ^{3}He

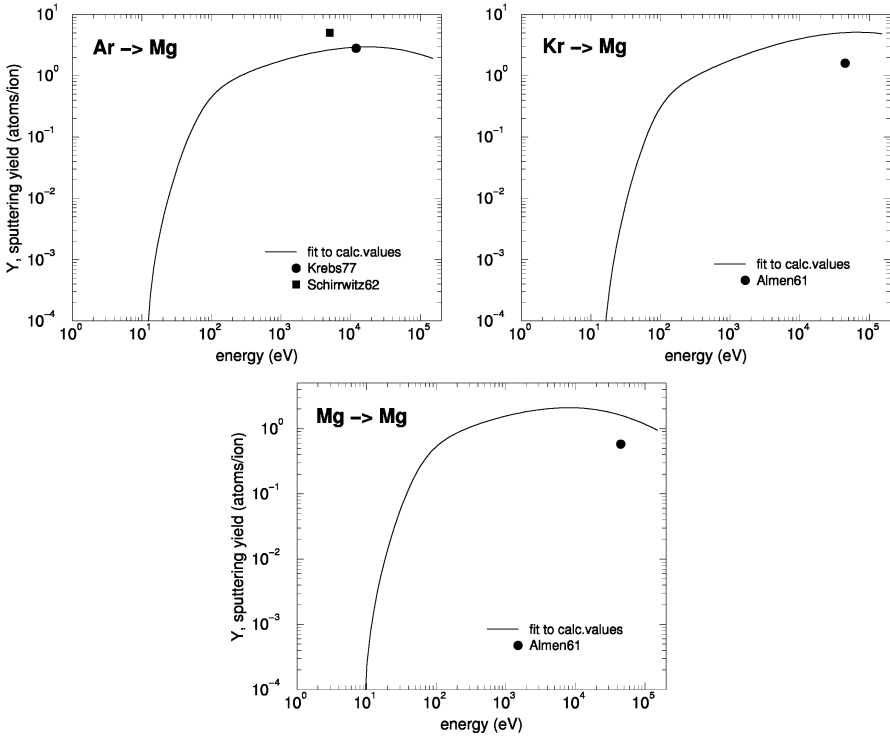

Fig. 10. Energy dependence of sputtering yields of Mg for bombardment at normal incidence with Ar [88, 94], Kr [90], and Mg [79]

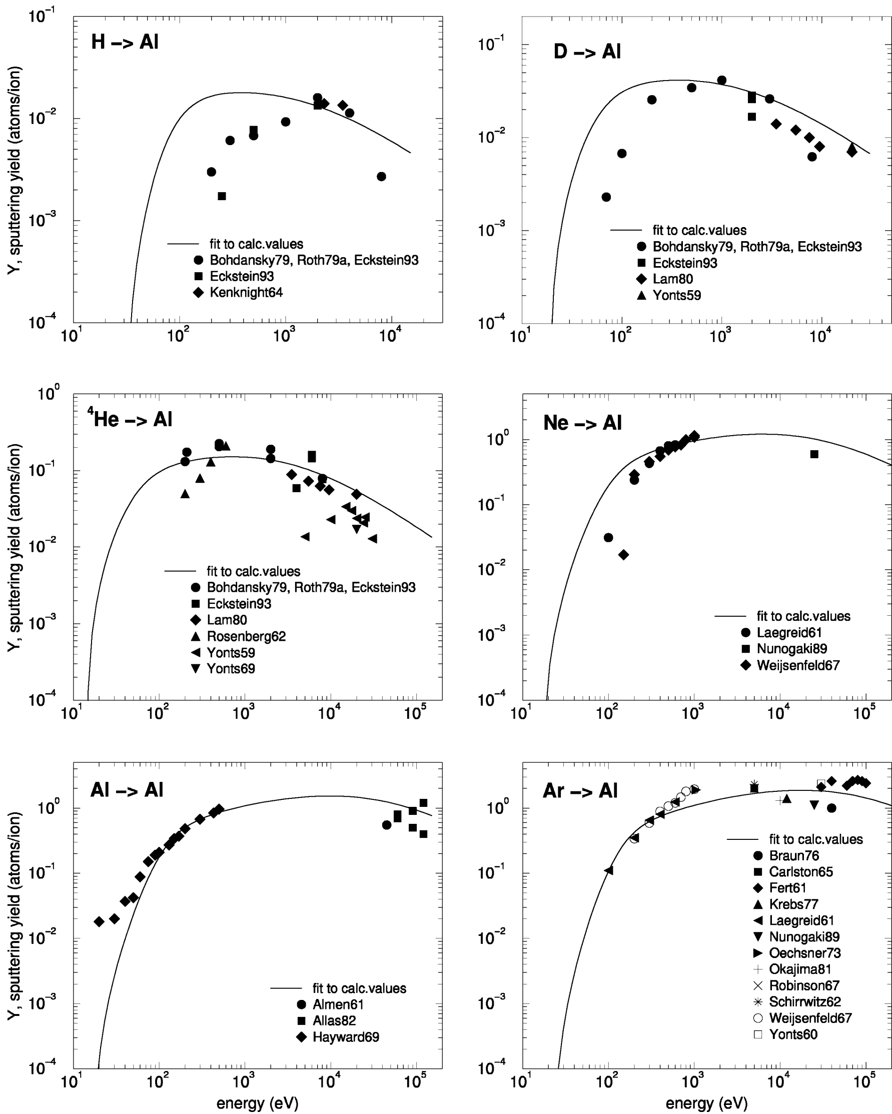

Fig. 11. Energy dependence of sputtering yields of Al for bombardment at normal incidence with H [27,49–51], D [27,51,95,96], ^{4}He [27,50,51,54,95–97], Ne [63,98,99], Al [79, 100, 101] and Ar [63, 88, 94, 98, 99, 102–108]

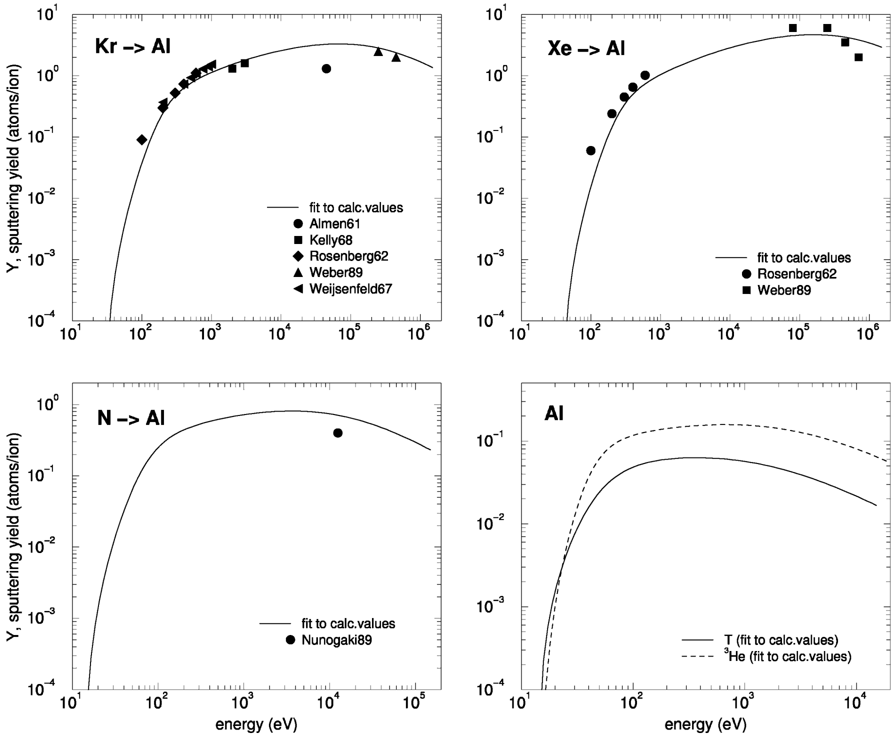

Fig. 12. Energy dependence of sputtering yields of Al for bombardment at normal incidence with Kr [54, 90, 98, 109, 110], Xe [54, 110], N [99] and T, ^{3}He

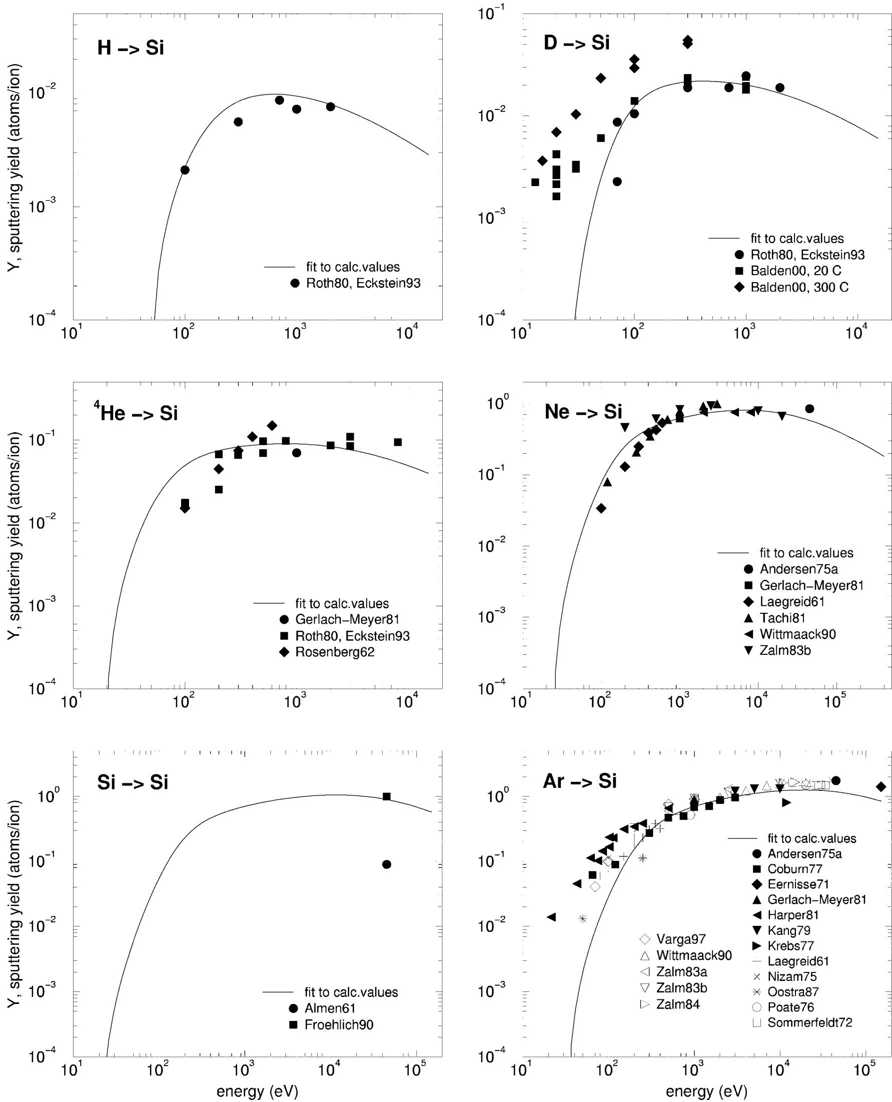

Fig. 13. Energy dependence of sputtering yields of Si for bombardment at normal incidence with H [27, 111], D [27, 111, 112], ^{4}He [27, 54, 111, 113], Ne [63, 113–117], Si [79, 118] and Ar [63, 94, 113, 114, 116, 117, 119–129]

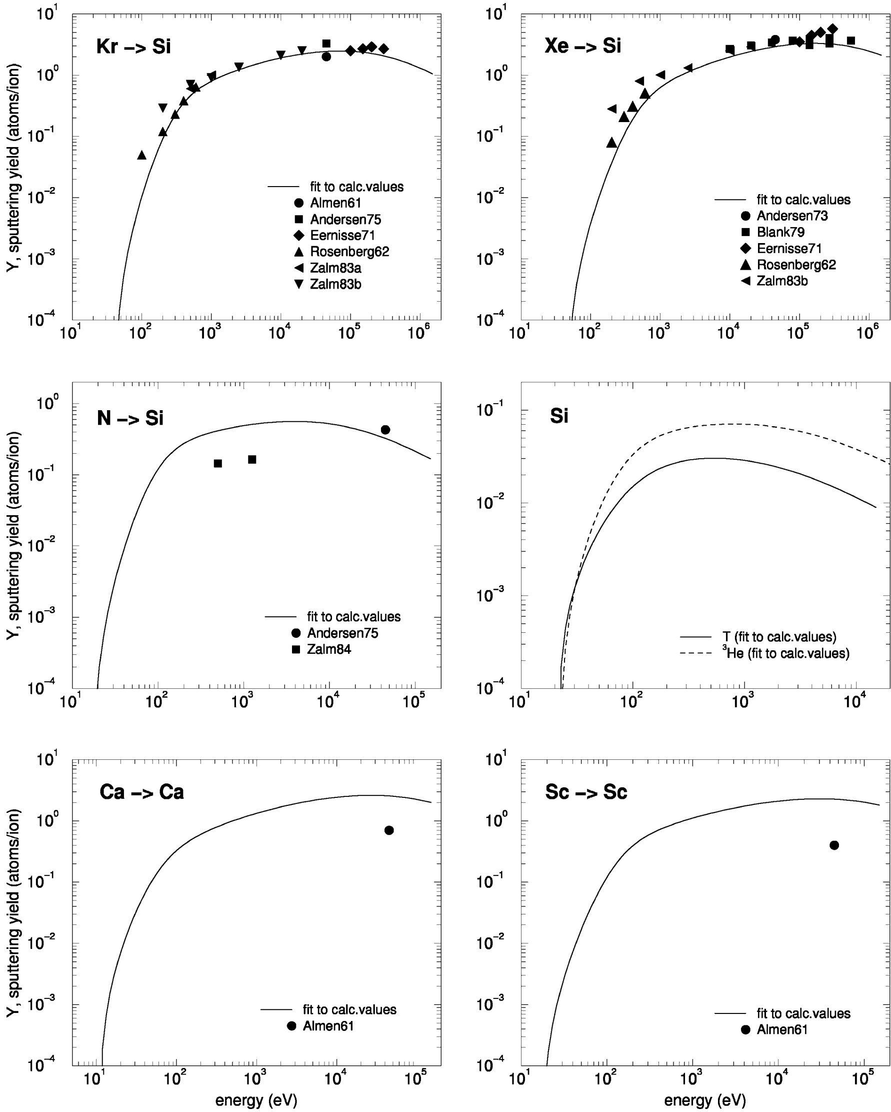

Fig. 14. Energy dependence of sputtering yields of Si for bombardment at normal incidence with Kr [54, 90, 114, 116, 120, 126], Xe [54, 114, 116, 120, 130], N [114, 127], and T, ^{3}He and Ca [79] and Sc [79] selfsputtering

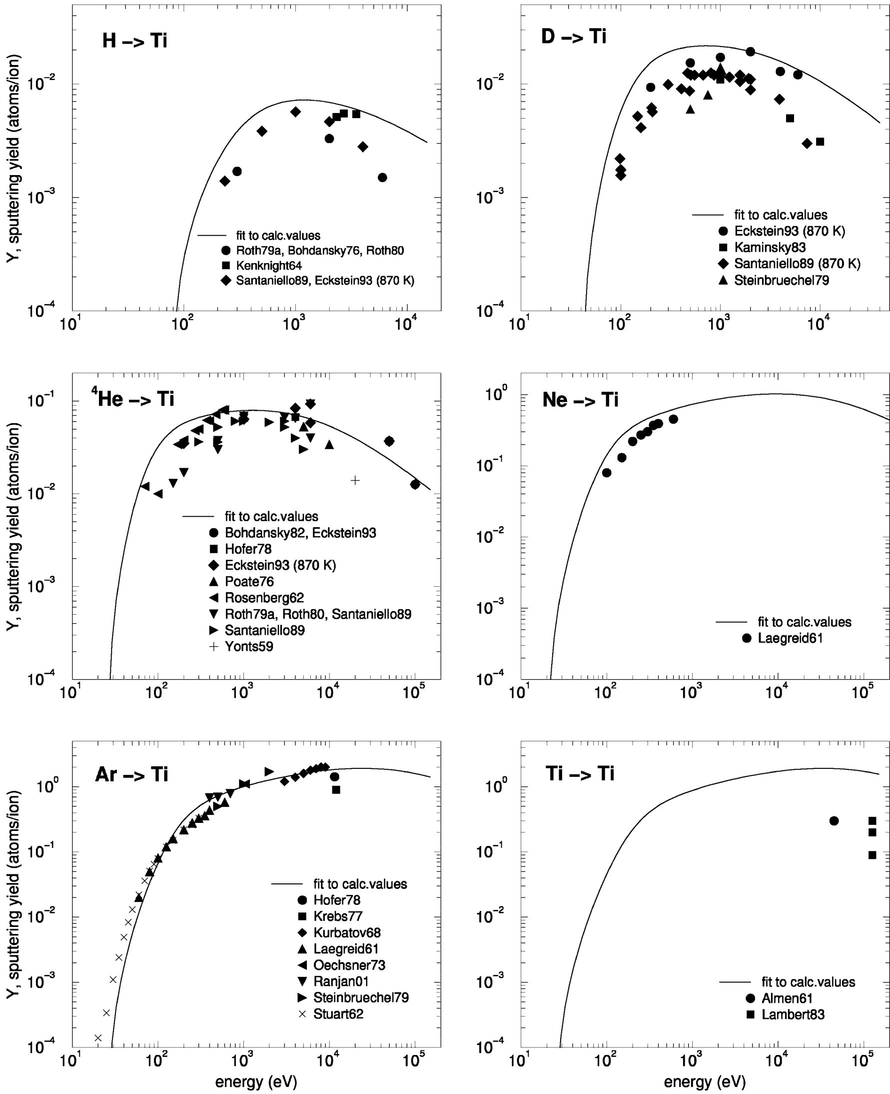

Fig. 15. Energy dependence of sputtering yields of Ti for bombardment at normal incidence with H [27, 49, 51, 69, 111, 131], D [27, 131–133], ^{4}He [27, 54, 123, 131, 134, 135], Ne [63], Ar [63, 94, 105, 133, 134, 136–138] and Ti [79, 139]

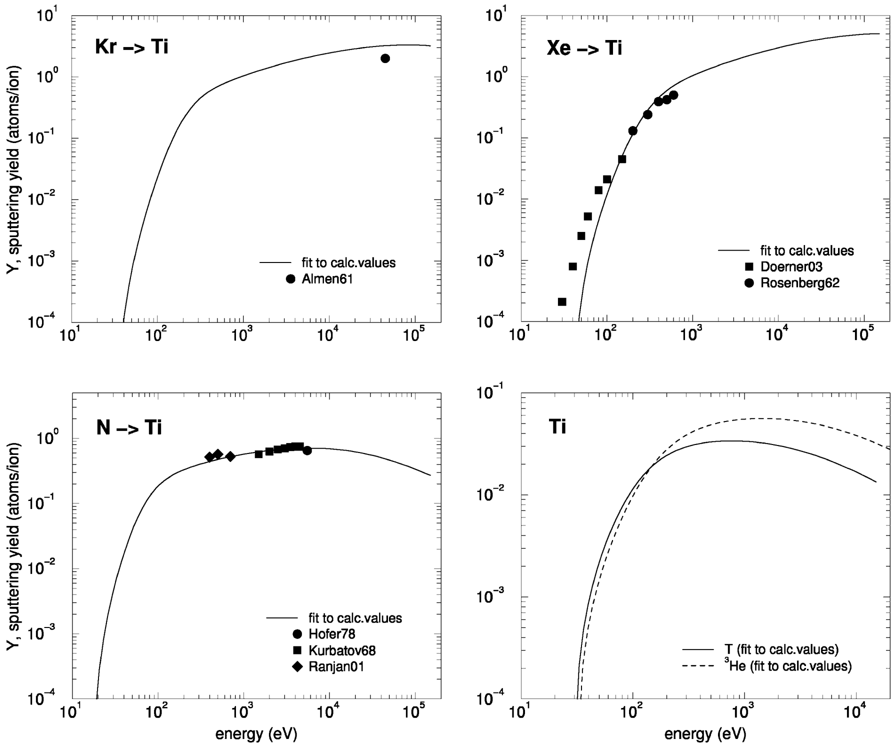

Fig. 16. Energy dependence of sputtering yields of Ti for bombardment at normal incidence with Kr [90], Xe [18, 54], N [134, 137, 138] and T, ^{3}He

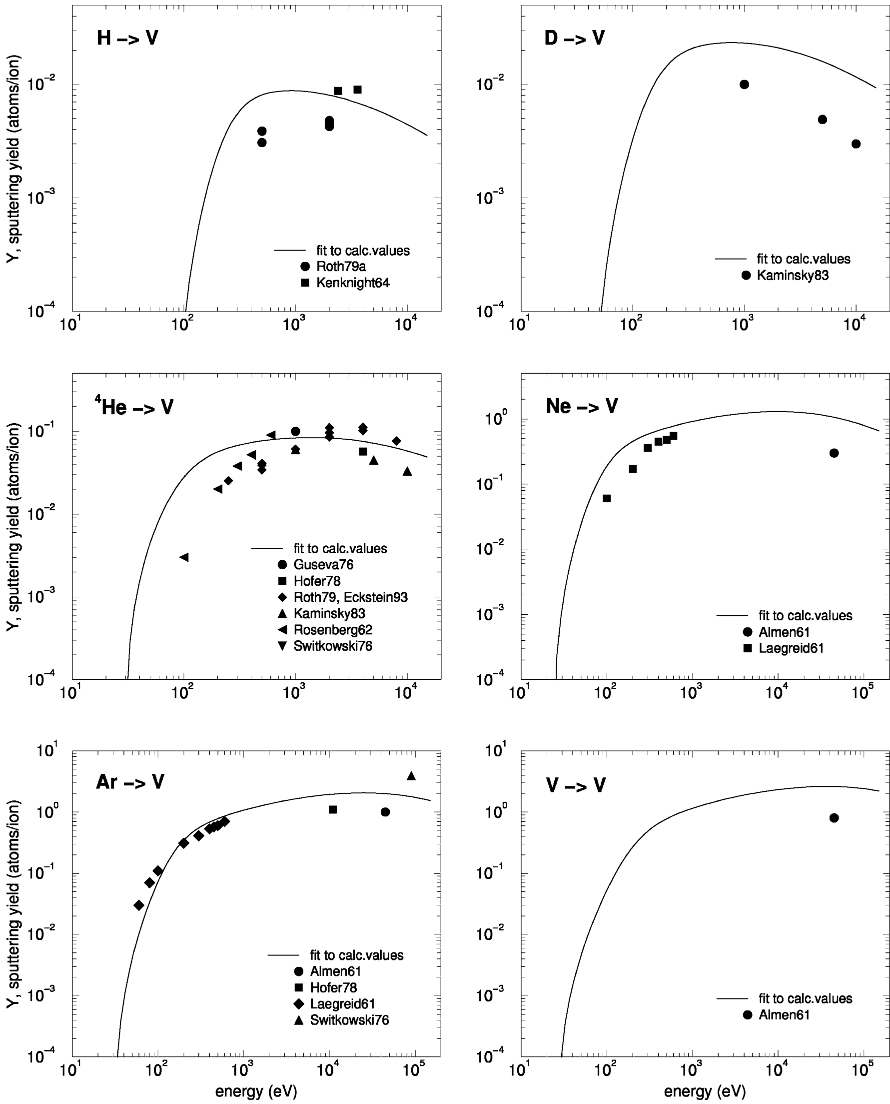

Fig. 17. Energy dependence of sputtering yields of V for bombardment at normal incidence with H [49, 51], D [132], ^{4}He [27, 51, 54, 132, 134, 140, 141], Ne [63, 90], Ar [63, 90, 134, 141] and V [79]

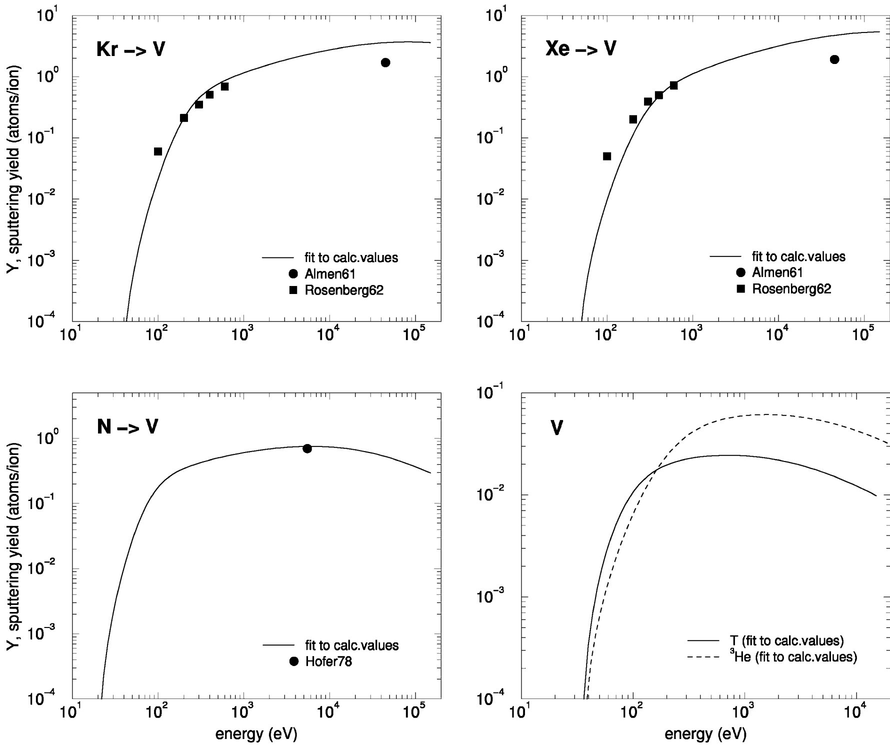

Fig. 18. Energy dependence of sputtering yields of V for bombardment at normal incidence with Kr [54, 90], Xe [54, 90], N [134] and T, ^{3}He

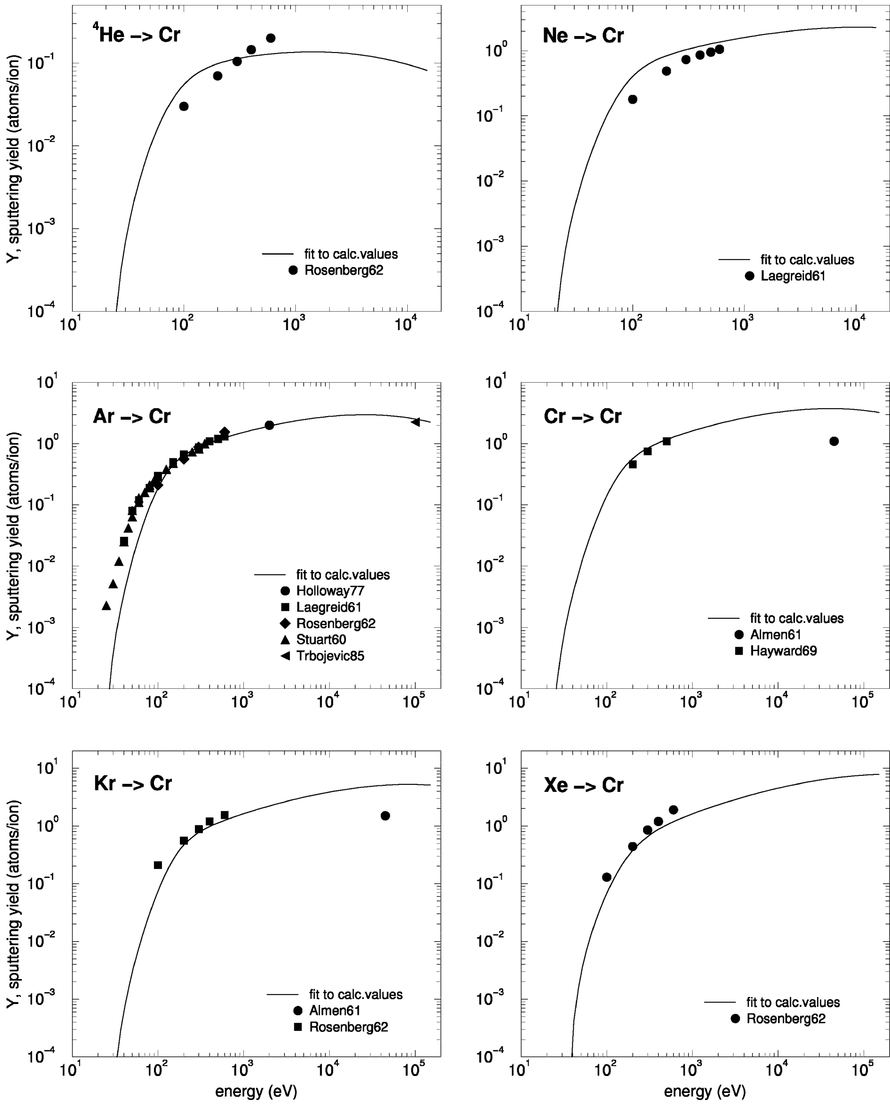

Fig. 19. Energy dependence of sputtering yields of Cr for bombardment at normal incidence with ^{4}He [54], Ne [63], Ar [54,63,142–144], Cr [79,101], Kr [54,90], Xe [54]

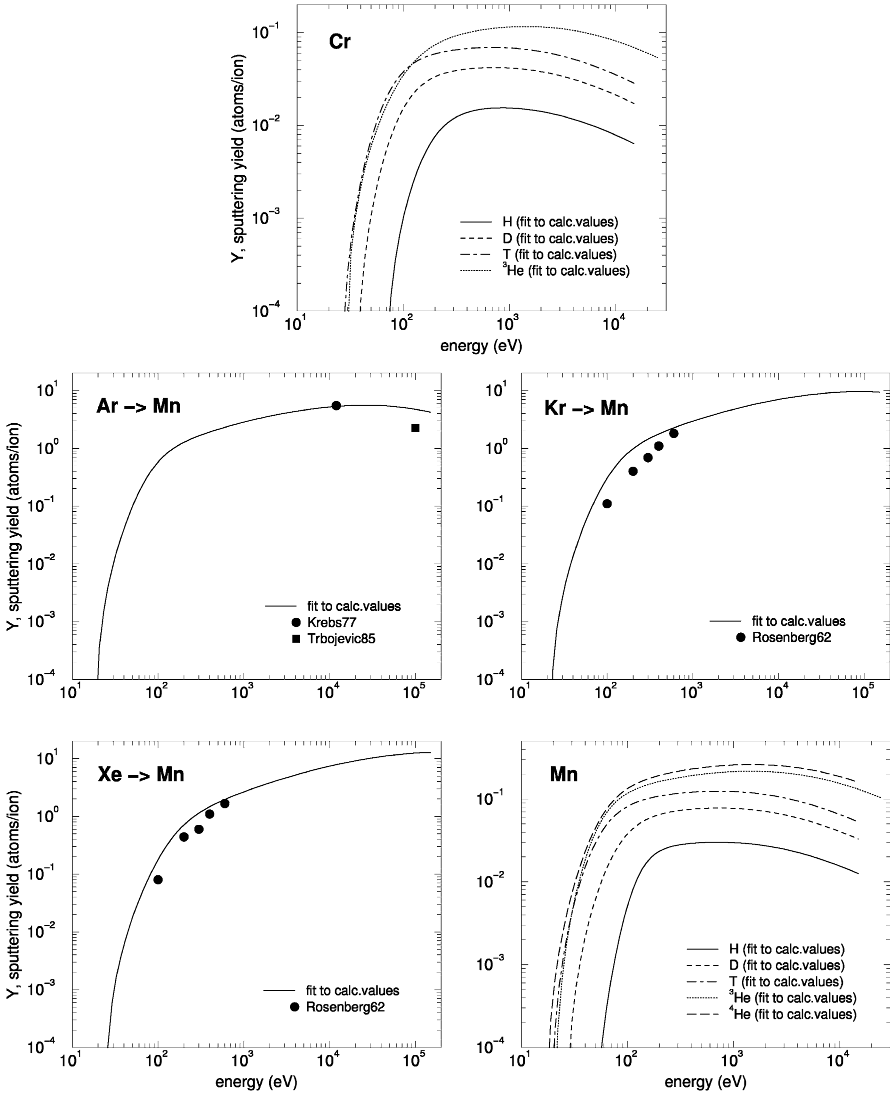

Fig. 20. Energy dependence of sputtering yields of Cr for bombardment at normal incidence with H, D, T, ^{3}He, and energy dependence of sputtering yields of Mn for bombardment at normal incidence with Ar [94, 144], Kr [54], Xe [54], and H, D, T, ^{3}He, ^{4}He

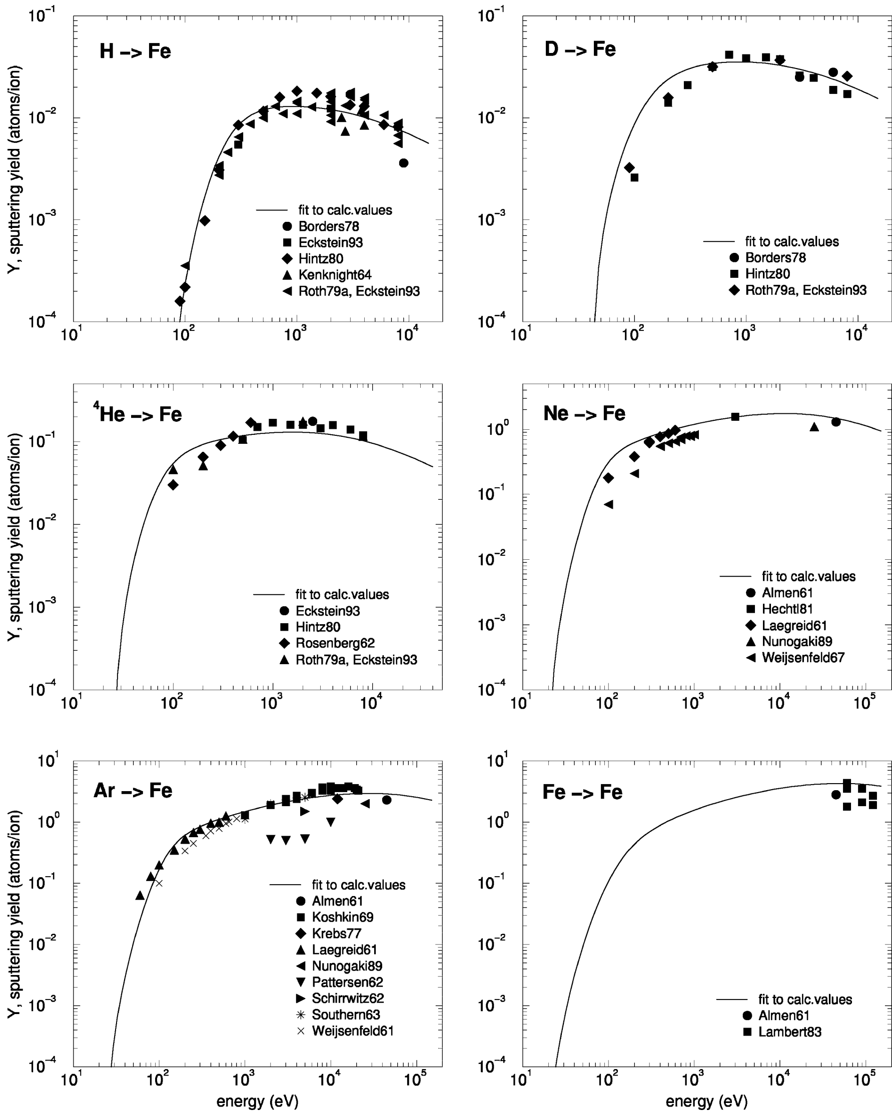

Fig. 21. Energy dependence of sputtering yields of Fe for bombardment at normal incidence with H [27, 49, 51, 75, 145], D [27, 51, 75, 145], ^{4}He [27, 51, 54], Ne [63, 78, 90, 98, 99], Ar [15, 63, 88, 90, 94, 98, 99, 146, 147], Fe [79, 139]

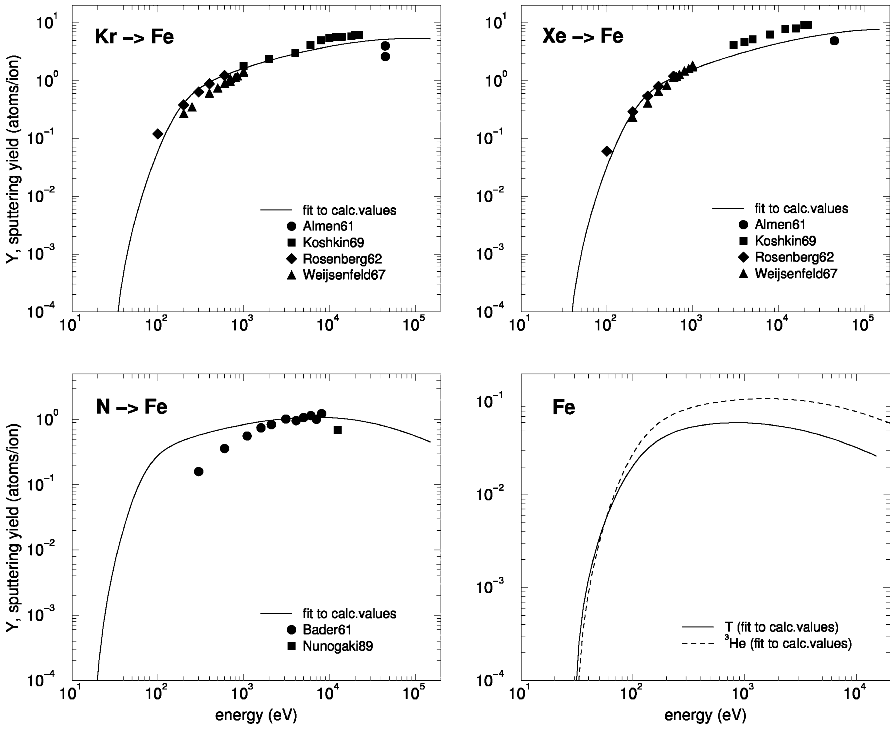

Fig. 22. Energy dependence of sputtering yields of Fe for bombardment at normal incidence with Kr [54, 90, 98, 147], Xe [54, 90, 98, 147], N [99, 148], and T, ^{3}He

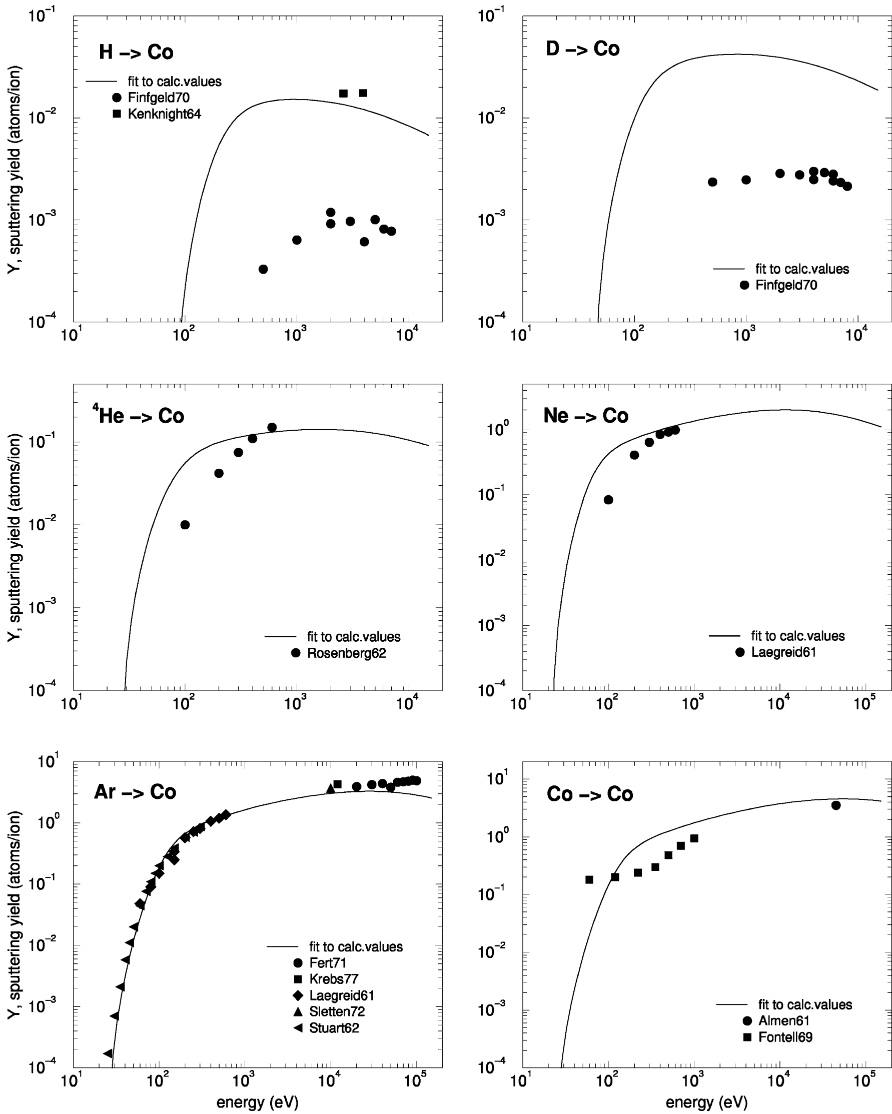

Fig. 23. Energy dependence of sputtering yields of Co for bombardment at normal incidence with H [49, 149], D [149], ^{4}He [54], Ne [63], Ar [63, 94, 104, 136, 150] and Co [79, 151]

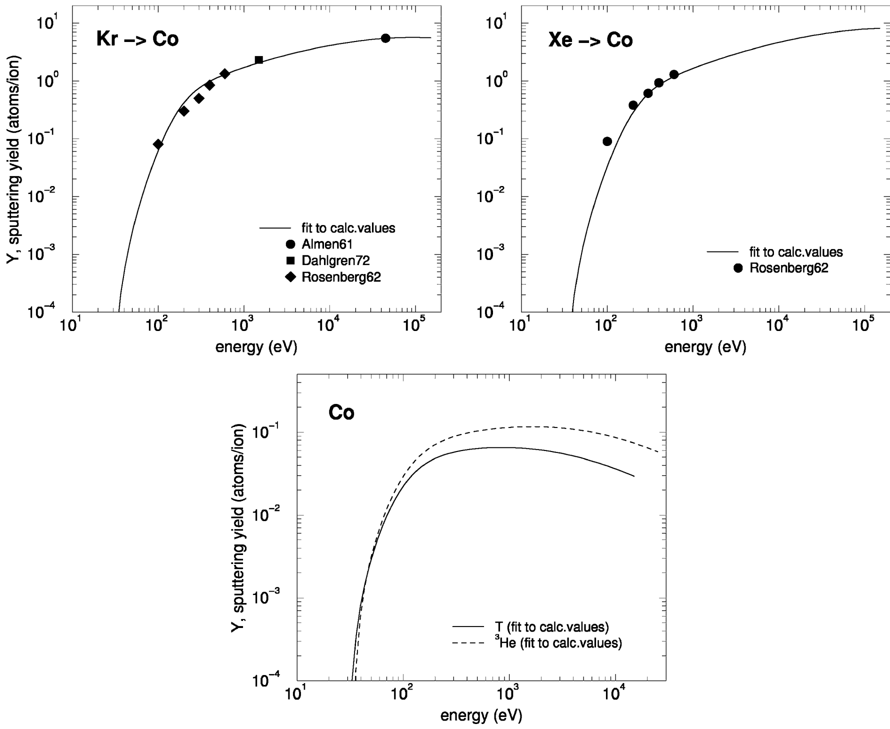

Fig. 24. Energy dependence of sputtering yields of Co for bombardment at normal incidence with Kr [54, 90, 152], Xe [54], and T, ^{3}He

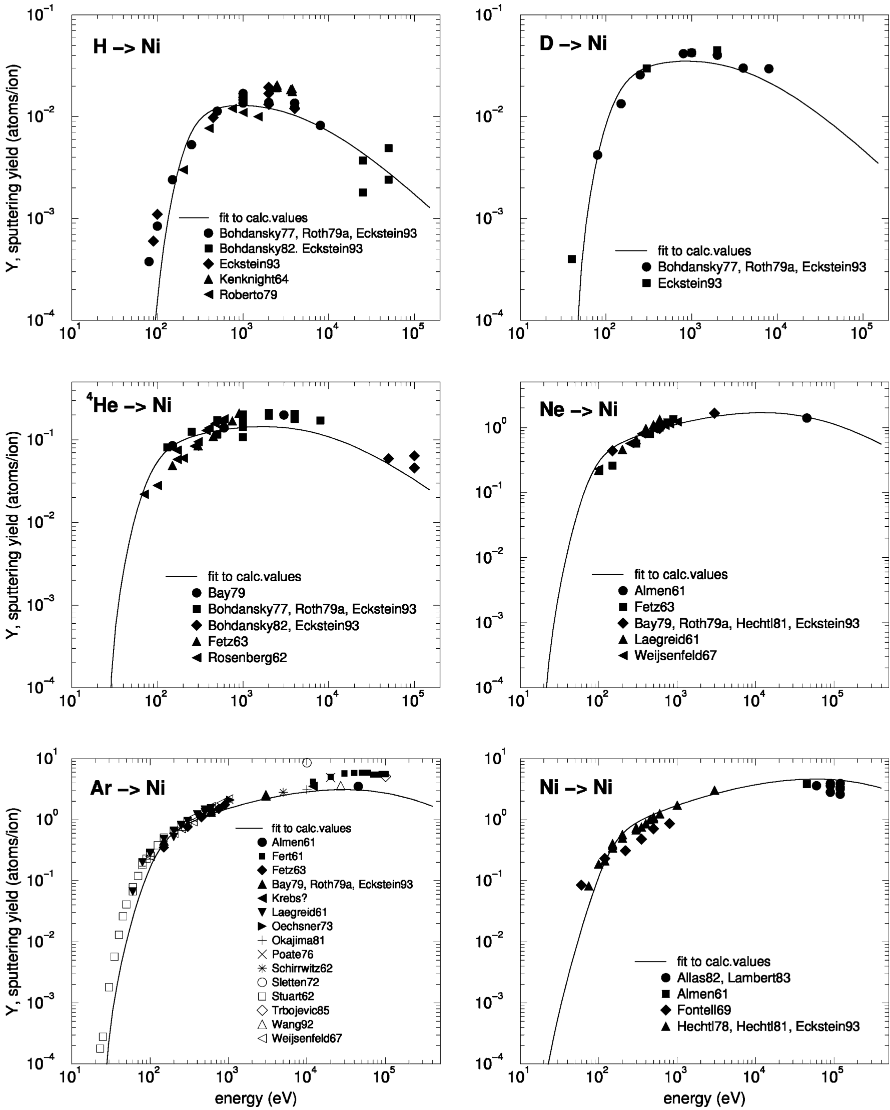

Fig. 25. Energy dependence of sputtering yields of Ni for bombardment at normal incidence with H [27,49,51,135,153,154], D [27,153], ^{4}He [27,51,54,55,135,153,155], Ne [27, 51, 55, 63, 78, 90, 98, 155], Ar [27, 51, 55, 63, 88, 90, 94, 98, 104–106, 123, 136, 144, 150, 155, 156] and Ni [27, 78, 79, 100, 139, 151, 157]

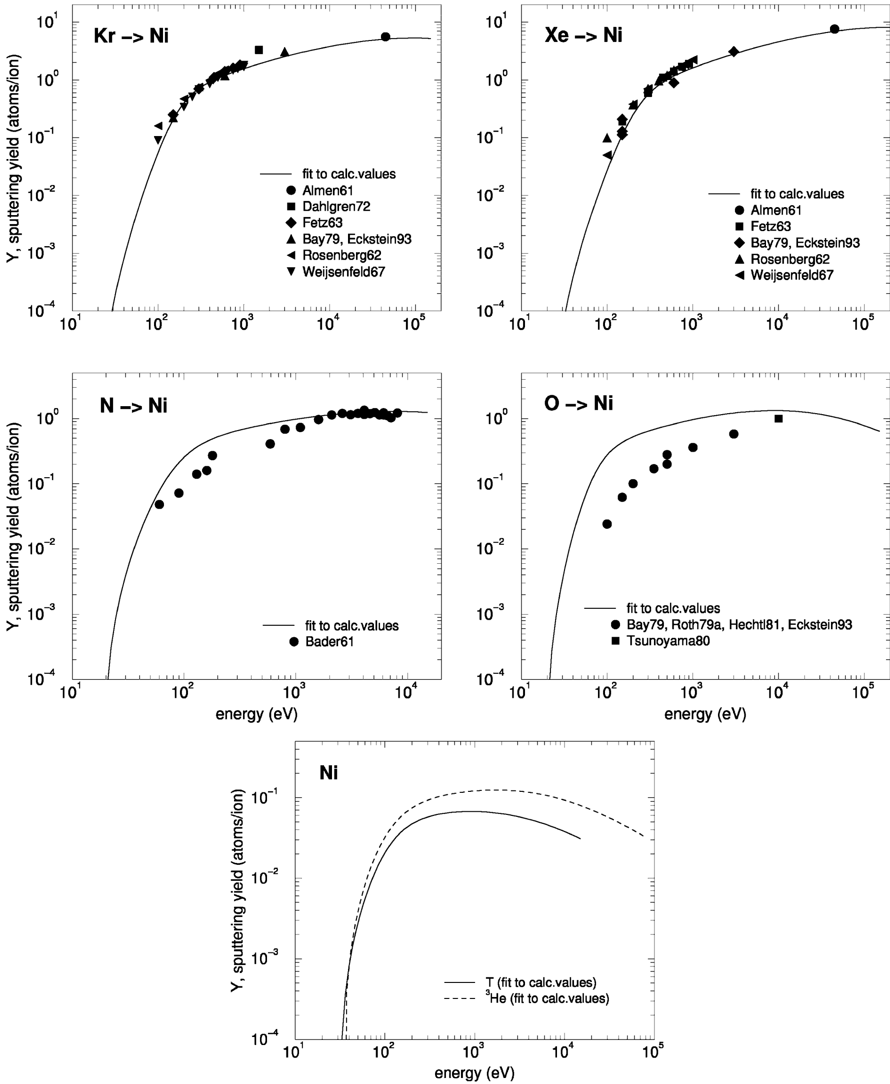

Fig. 26. Energy dependence of sputtering yields of Ni for bombardment at normal incidence with Kr [27, 54, 55, 90, 98, 152, 155], Xe [27, 54, 55, 90, 98, 155], N [148], O [27, 51, 78, 155, 158] and T, ^{3}He

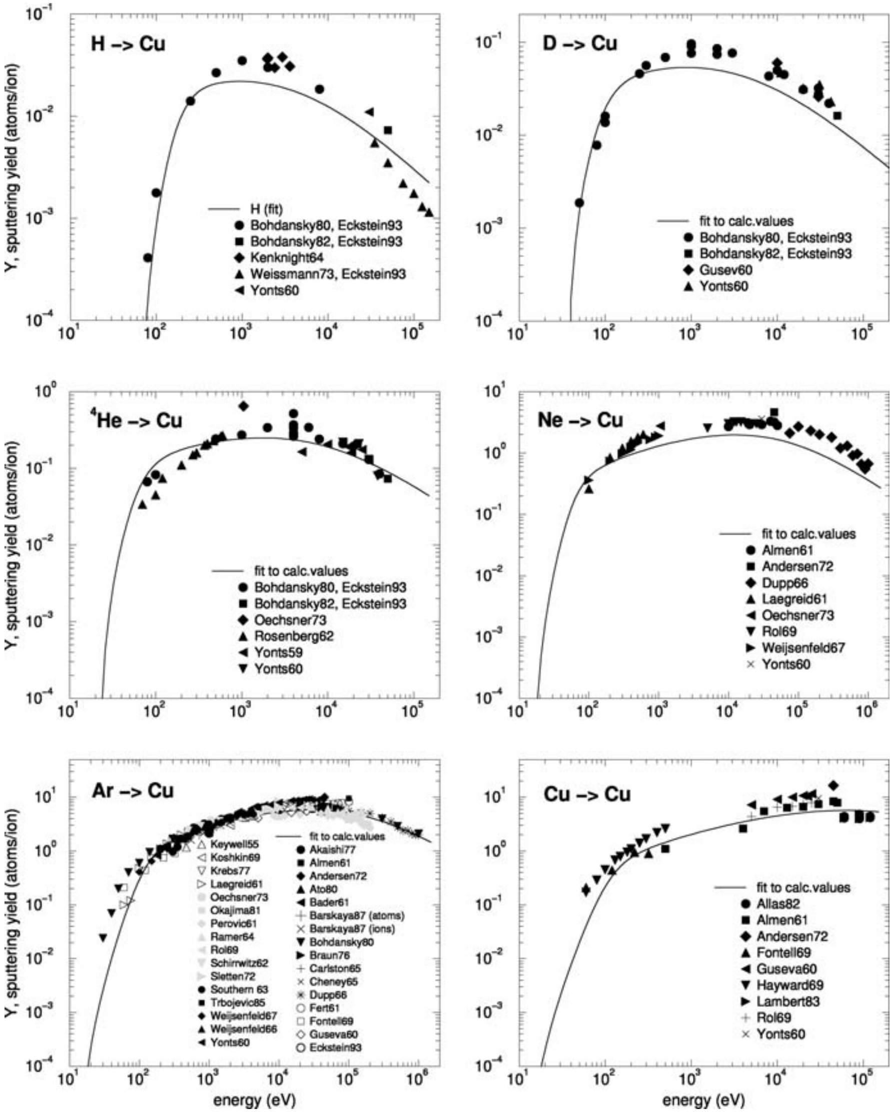

Fig. 27. Energy dependence of sputtering yields of Cu for bombardment at normal incidence with H [27, 49, 108, 135, 159, 160], D [27, 108, 135, 159, 161], ^{4}He [27, 54, 96, 105, 108, 135, 159], Ne [63, 90, 98, 105, 108, 162–164], Ar [27, 63, 88, 90, 94, 98, 102–106, 108, 144, 146–148, 150, 151, 159, 161–172], Cu [79, 100, 101, 108, 139, 151, 161, 162, 164]

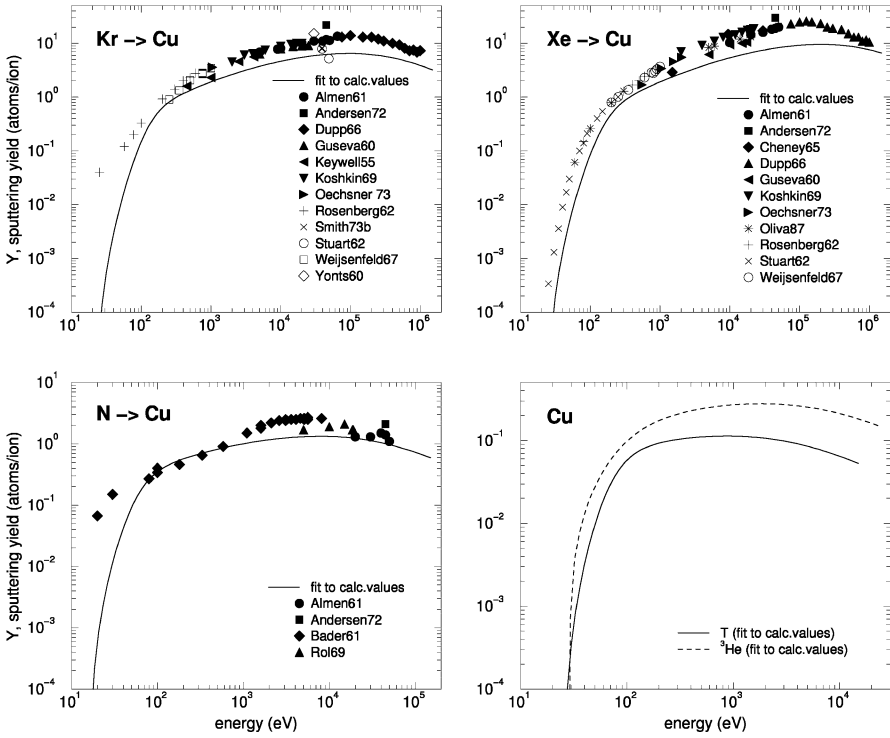

Fig. 28. Energy dependence of sputtering yields of Cu for bombardment at normal incidence with Kr [54, 90, 98, 105, 108, 136, 147, 161–163, 165, 173], Xe [54, 90, 98, 105, 136, 147, 161–163, 168, 174], N [90, 148, 162, 164], and T, ^{3}He

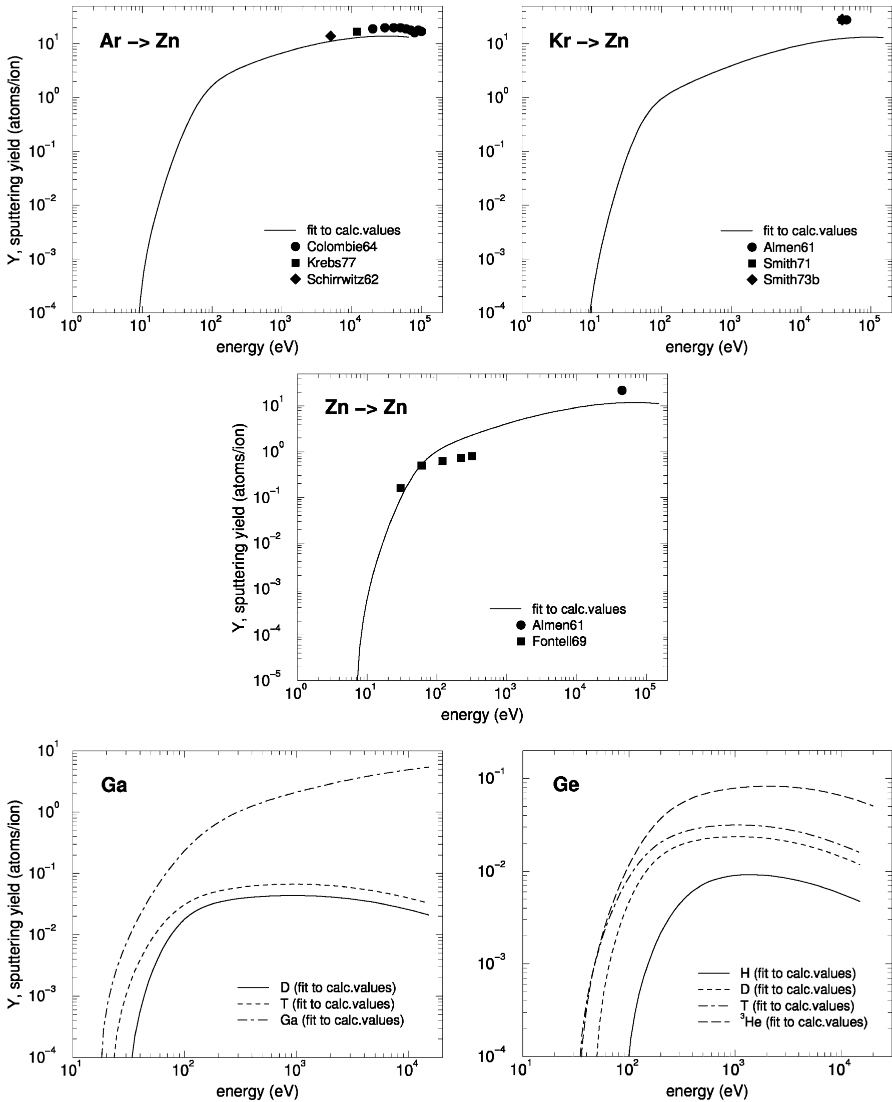

Fig. 29. Energy dependence of sputtering yields of Zn for bombardment at normal incidence with Ar [88,94,175], Kr [90,173,176], Zn [79,151], and energy dependence of sputtering yields of Ga for the bombardment at normal incidence with D, T, Ga, and energy dependence of sputtering yields of Ge for the bombardment at normal incidence with H, D, T, ^{3}He

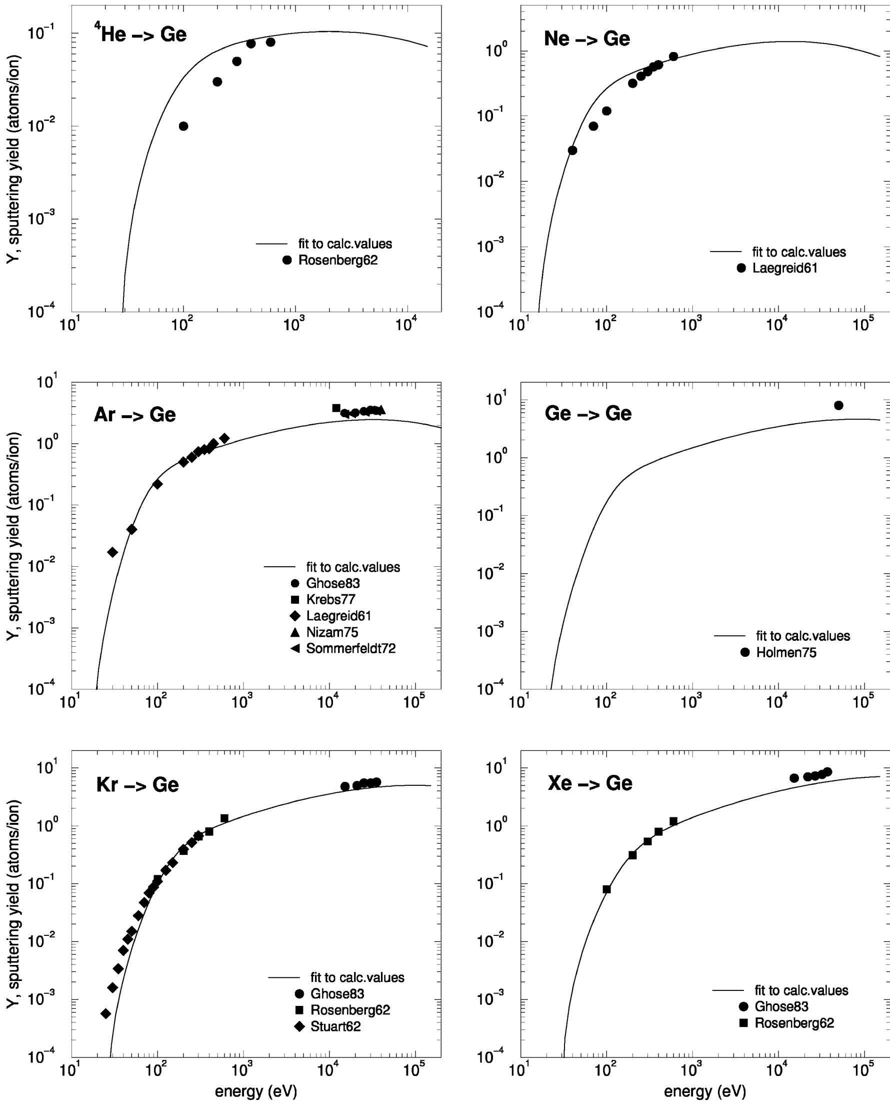

Fig. 30. Energy dependence of sputtering yields of Ge for bombardment at normal incidence with ^{4}He [54], Ne [63], Ar [63, 94, 121, 122, 177], Ge [178], Kr [54, 136, 177], Xe [54, 177]

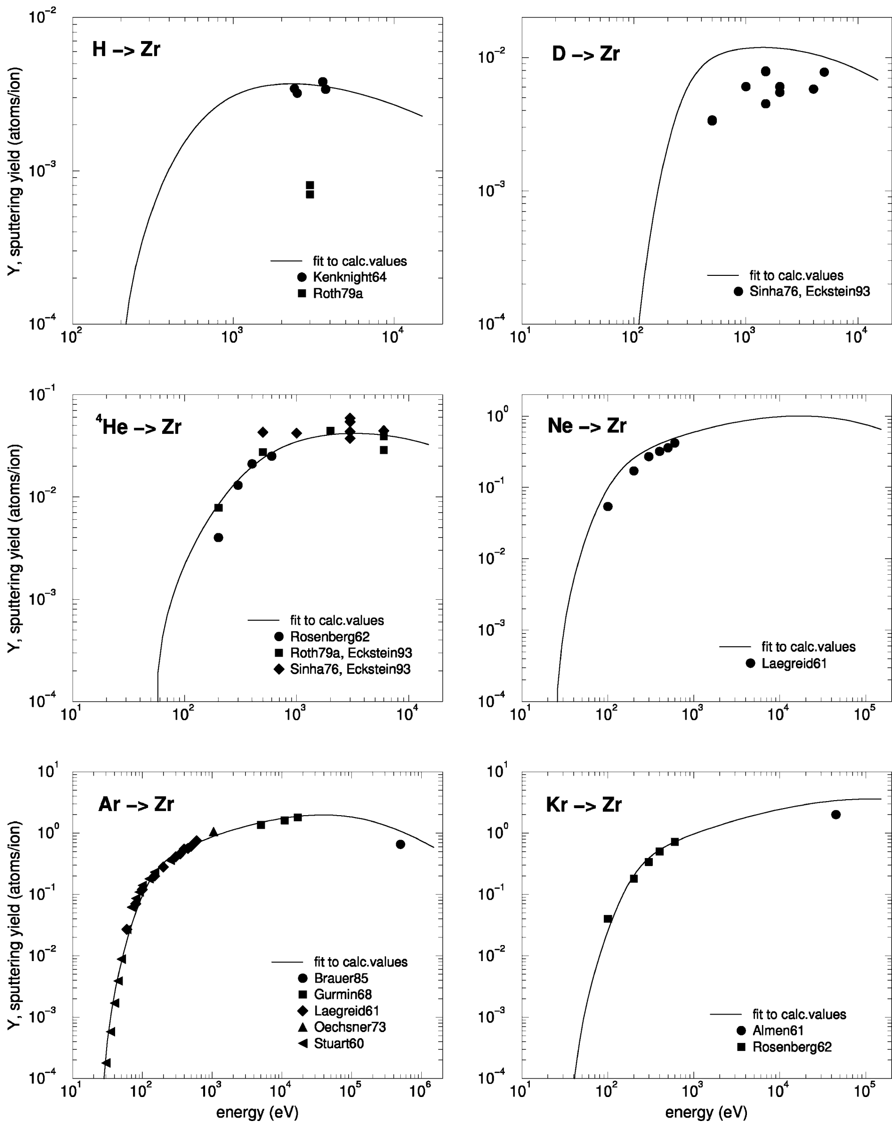

Fig. 31. Energy dependence of sputtering yields of Zr for bombardment at normal incidence with H [49, 51], D [27, 179], ^{4}He [27, 51, 54, 179], Ne [63], Ar [63, 105, 180–182], Kr [54, 90]

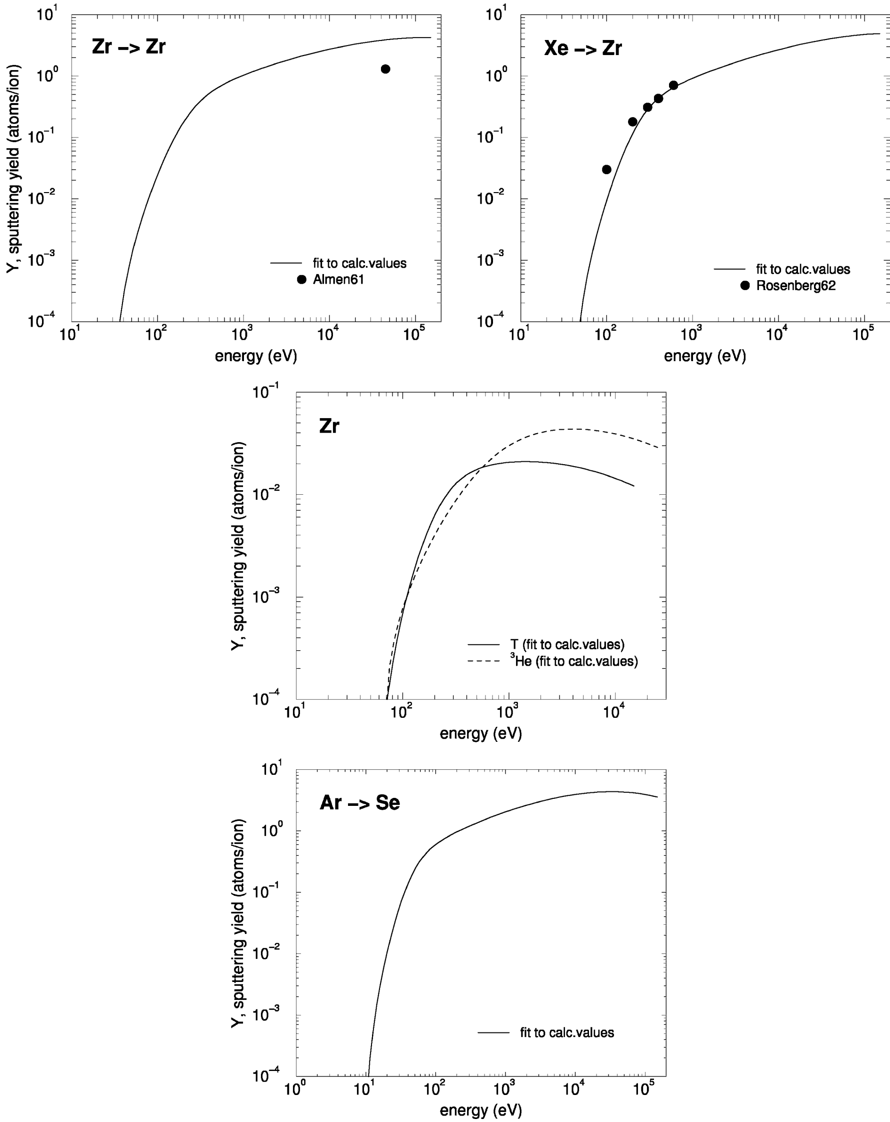

Fig. 32. Energy dependence of sputtering yields of Zr for bombardment at normal incidence with Zr [79], Xe [54], and T, ^{3}He, and for bombardment at normal incidence of Se with Ar

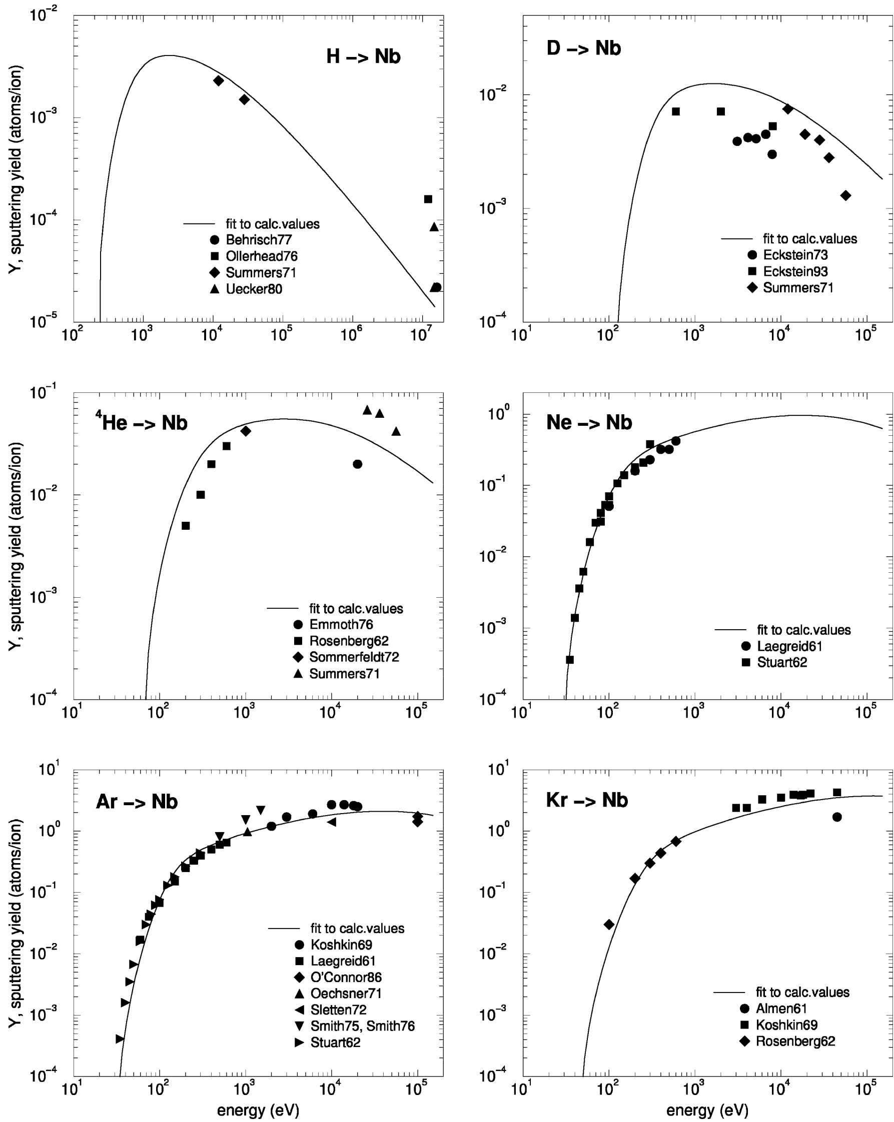

Fig. 33. Energy dependence of sputtering yields of Nb for bombardment at normal incidence with H [183–186], D [185, 187, 188], ^{4}He [54, 121, 185, 189], Ne [63, 136], Ar [63, 70, 136, 147, 150, 190–192], Kr [54, 90, 147]

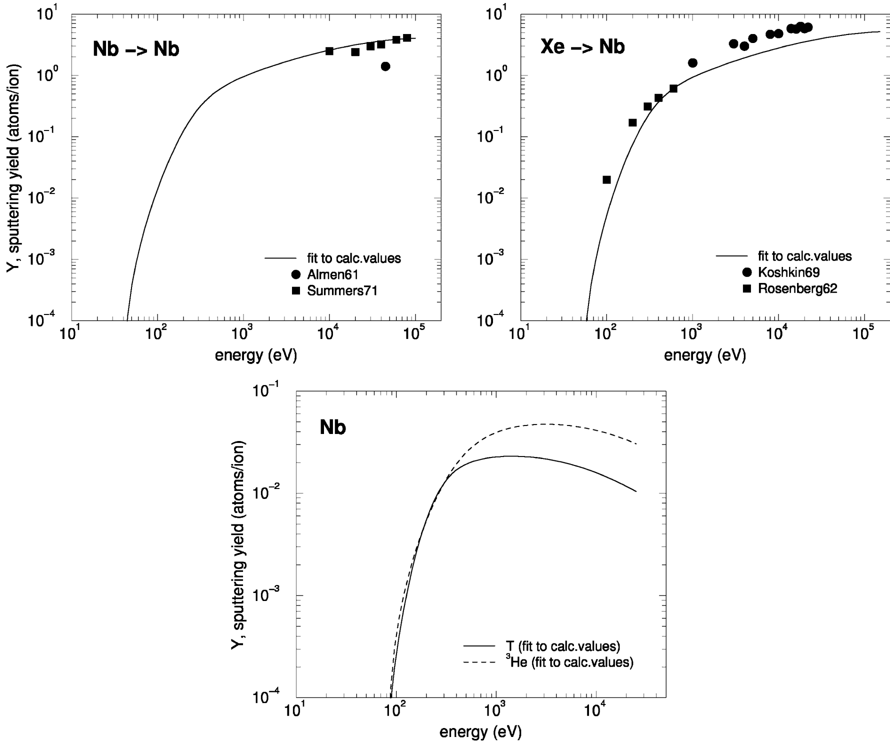

Fig. 34. Energy dependence of sputtering yields of Nb for bombardment at normal incidence with Nb [79, 185, 193], Xe [54, 147], and T, ^{3}He

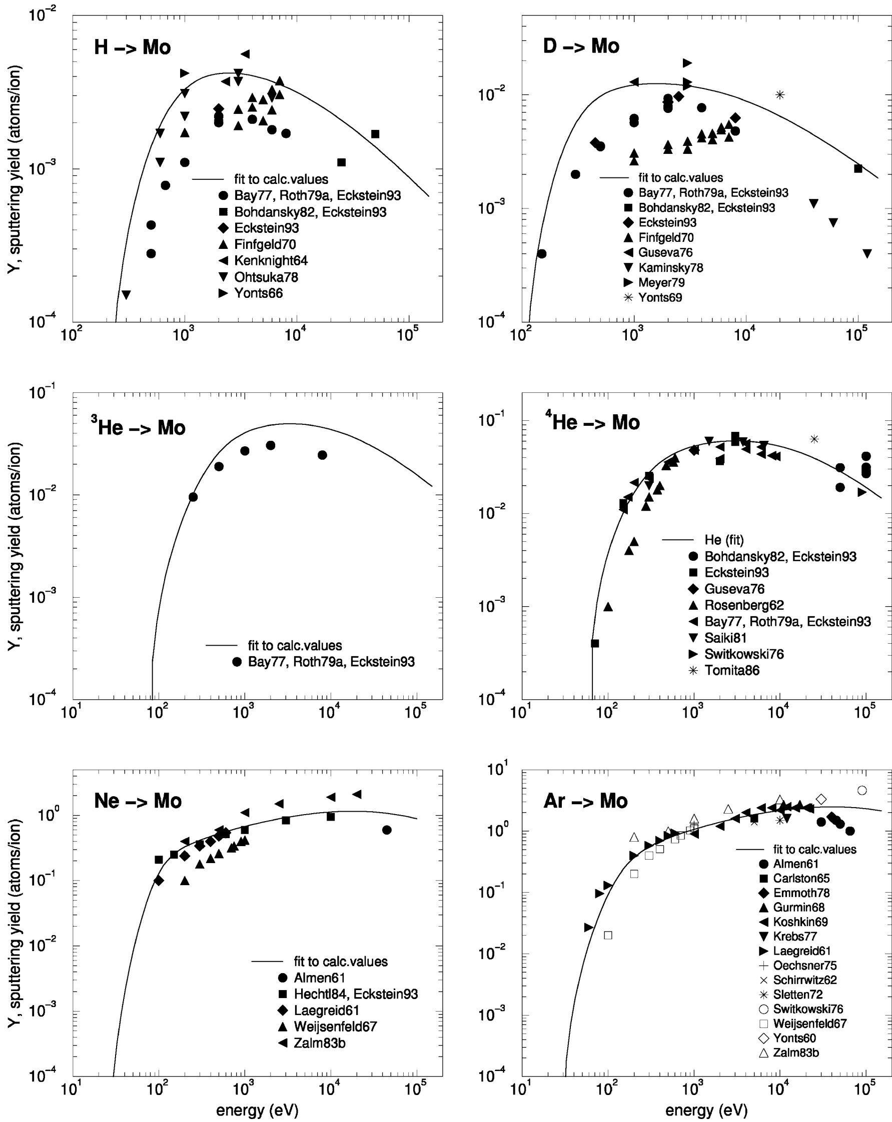

Fig. 35. Energy dependence of sputtering yields of Mo for bombardment at normal incidence with H [27, 49, 51, 108, 135, 149, 194, 195], D [27, 51, 97, 135, 140, 149, 194, 196, 197], ^{3}He [27, 51, 194], ^{4}He [27, 51, 54, 135, 140, 141, 194, 198, 199], Ne [27, 63, 90, 98, 116], Ar [63, 88, 90, 94, 98, 103, 108, 116, 141, 147, 150, 181, 200, 201]

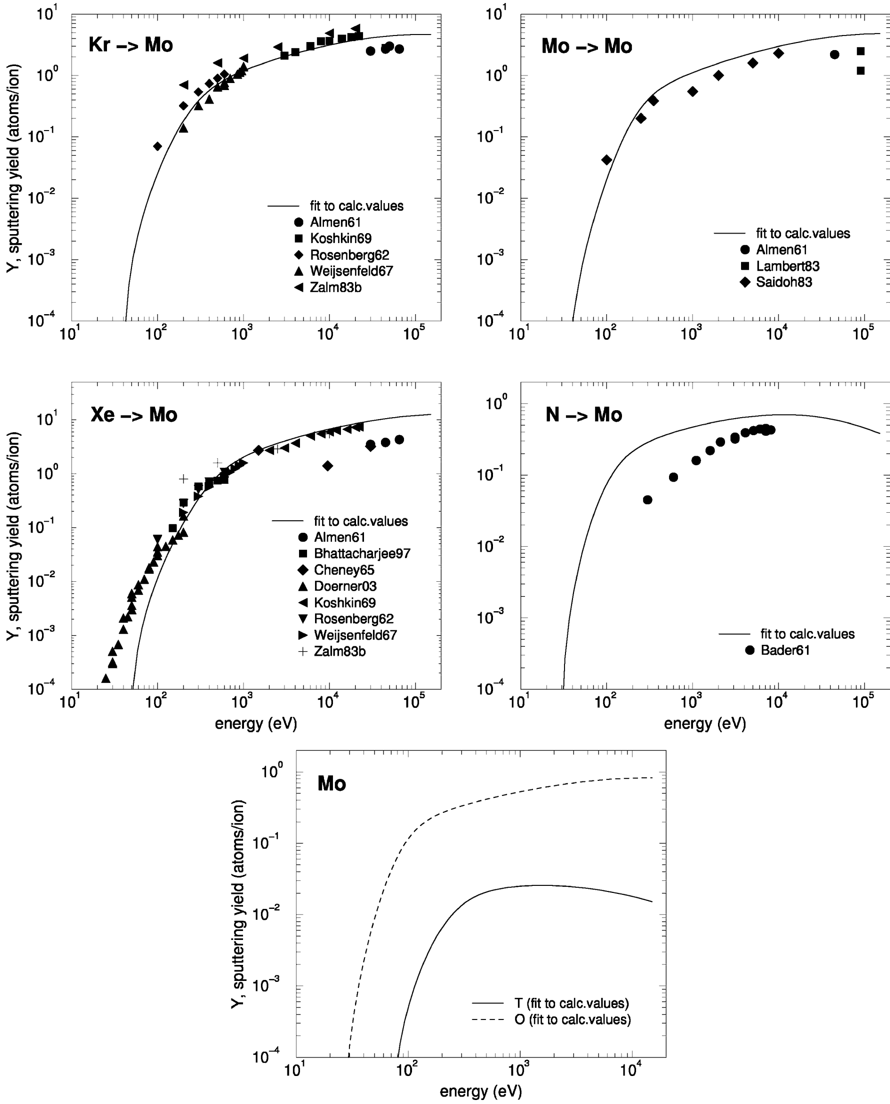

Fig. 36. Energy dependence of sputtering yields of Mo for bombardment at normal incidence with Kr [54, 90, 98, 116, 147], Mo [79, 139, 202, 203], Xe [18, 54, 90, 98, 116, 147, 168, 204], N [148] and T, O

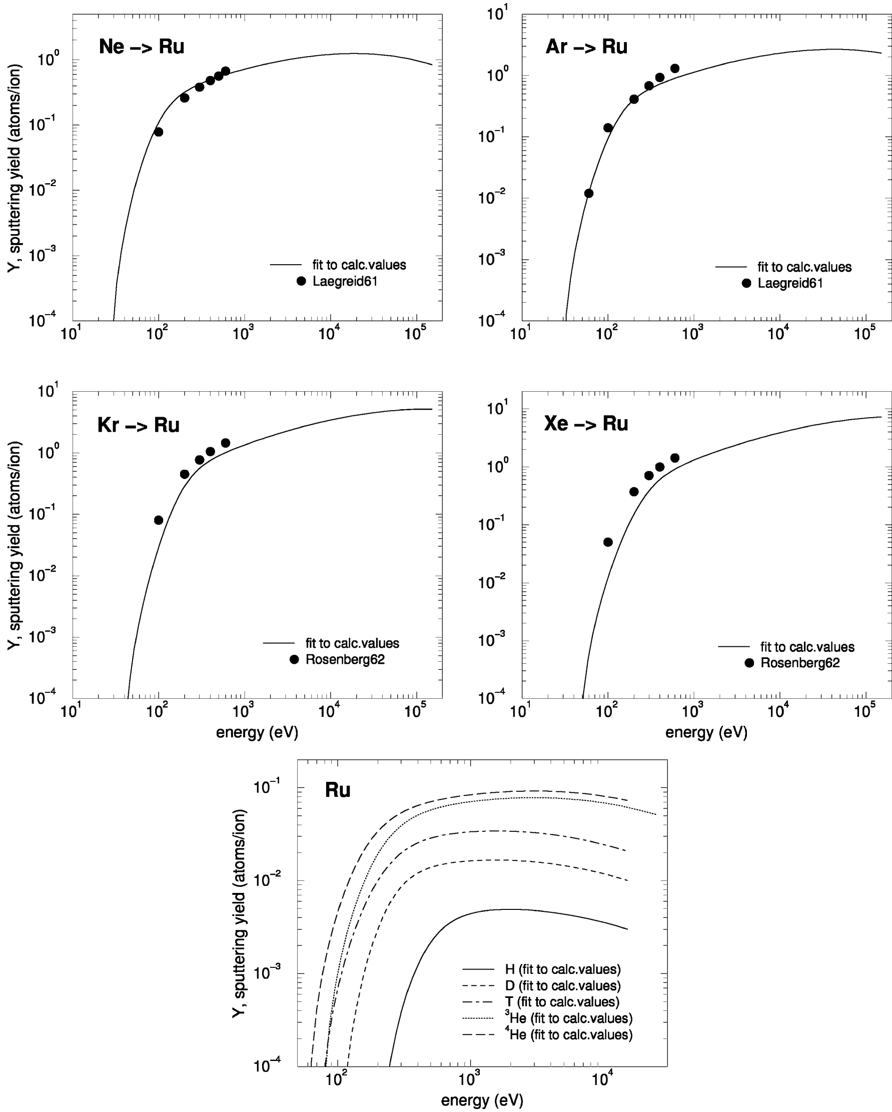

Fig. 37. Energy dependence of sputtering yields of Ru for bombardment at normal incidence with Ne [54], Ar [63], Kr [54], Xe [54] and H, D, T, ^{3}He, ^{4}He

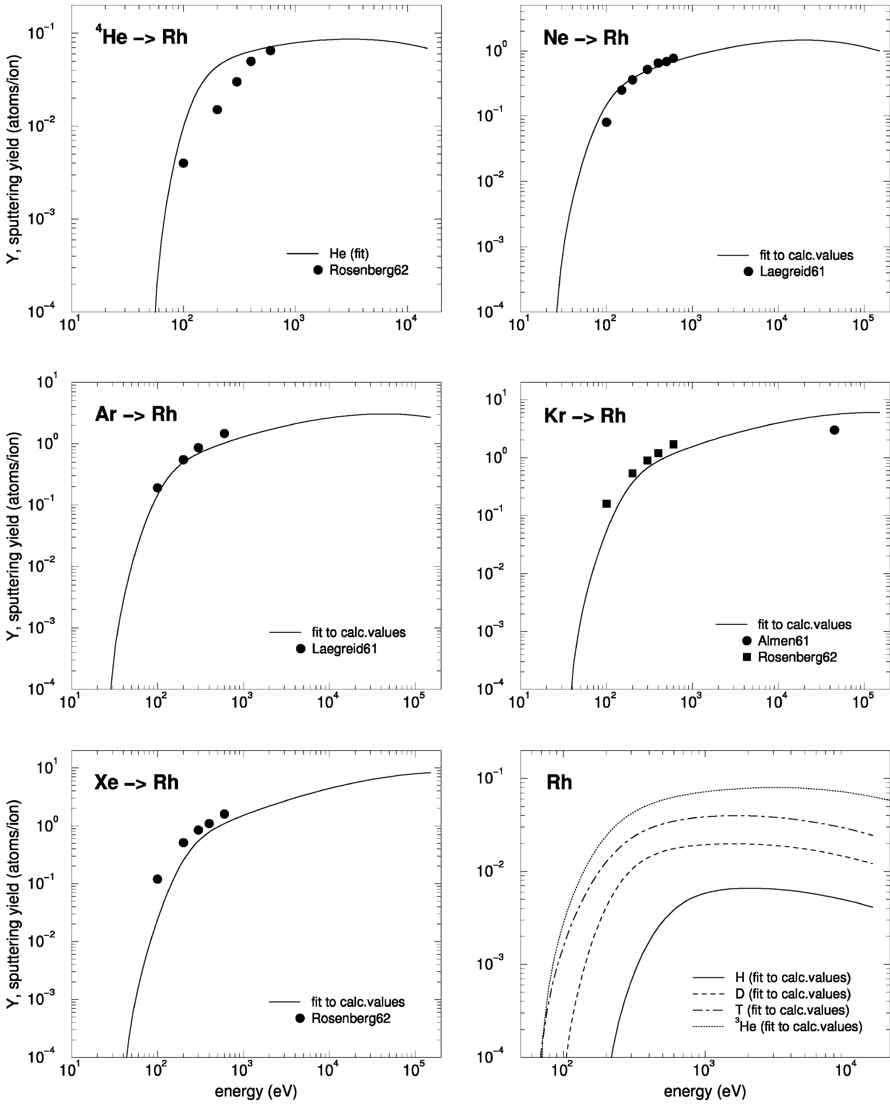

Fig. 38. Energy dependence of sputtering yields of Rh for bombardment at normal incidence with ^{4}He [54], Ne [63], Ar [63], Kr [54, 90], Xe [54], and H, D, T, ^{3}He

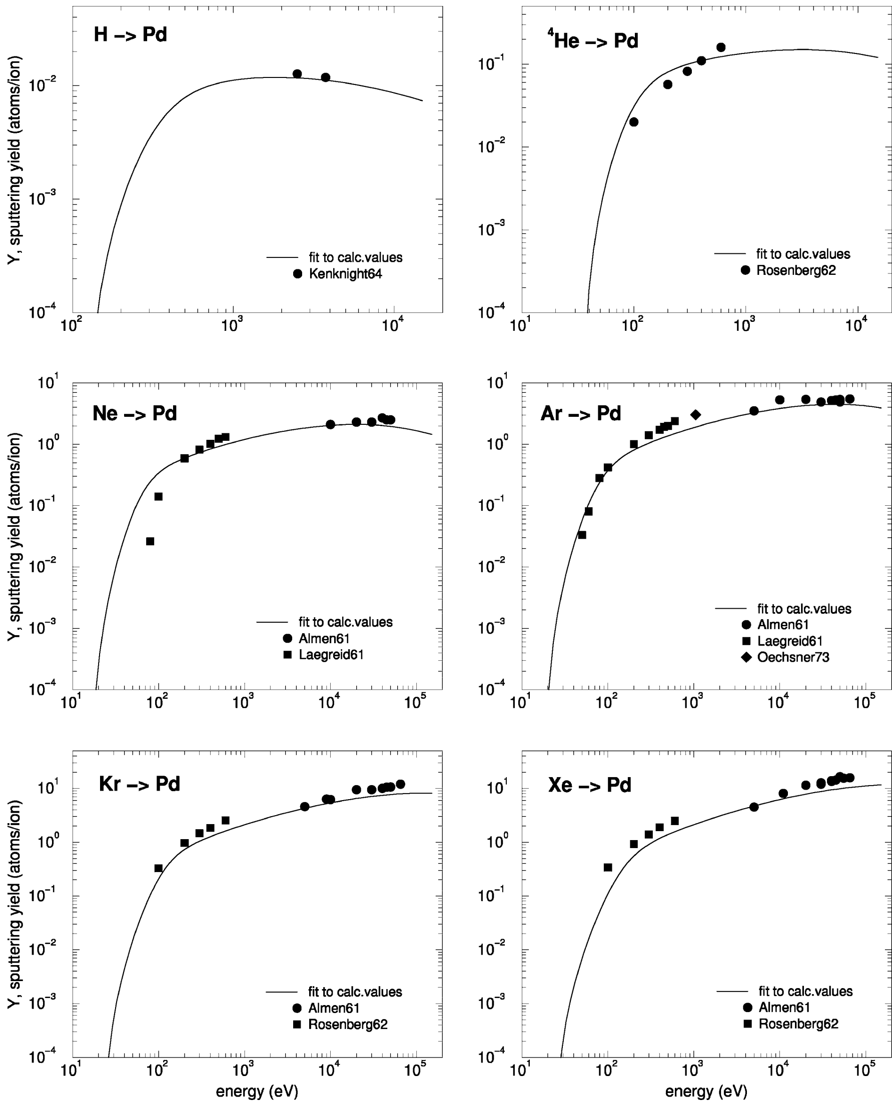

Fig. 39. Energy dependence of sputtering yields of Pd for bombardment at normal incidence with H [49], ^{4}He [54], Ne [63, 90], Ar [63, 90, 105], Kr [54, 90], Xe [54, 90]

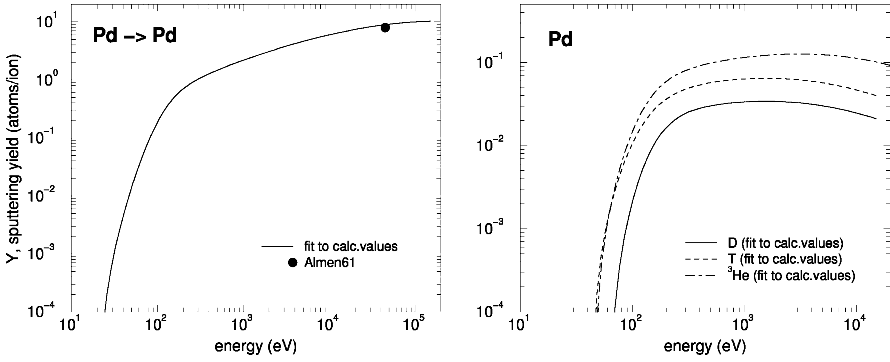

Fig. 40. Energy dependence of sputtering yields of Pd for bombardment at normal incidence with Pd [79], and D, T, ^{3}He

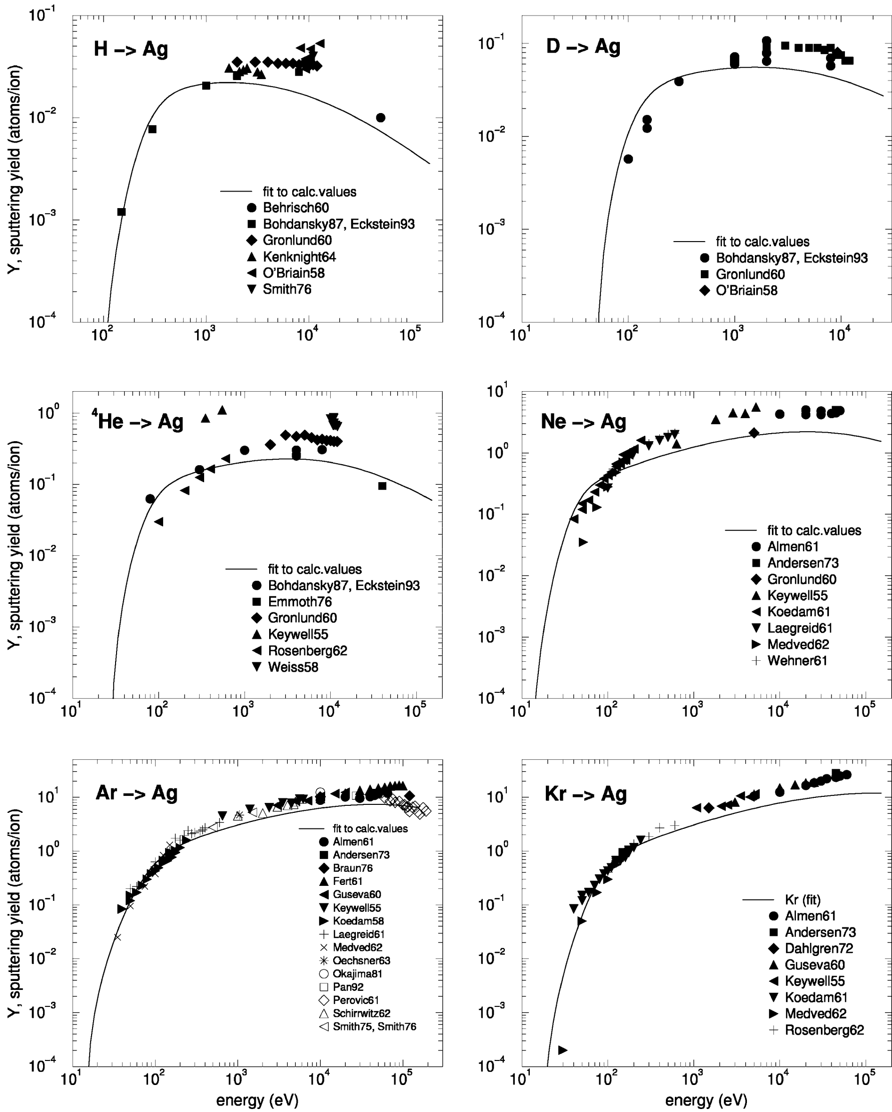

Fig. 41. Energy dependence of sputtering yields of Ag for bombardment at normal incidence with H [27, 49, 70, 205–208], D [27, 205, 206, 208], ^{4}He [27, 54, 165, 189, 205, 208–210], Ne [63, 90, 165, 205, 211–214], Ar [63, 70, 88, 90, 102, 104–106, 161, 165, 166, 190, 209, 212–215], Kr [54, 90, 152, 161, 165, 212–214]

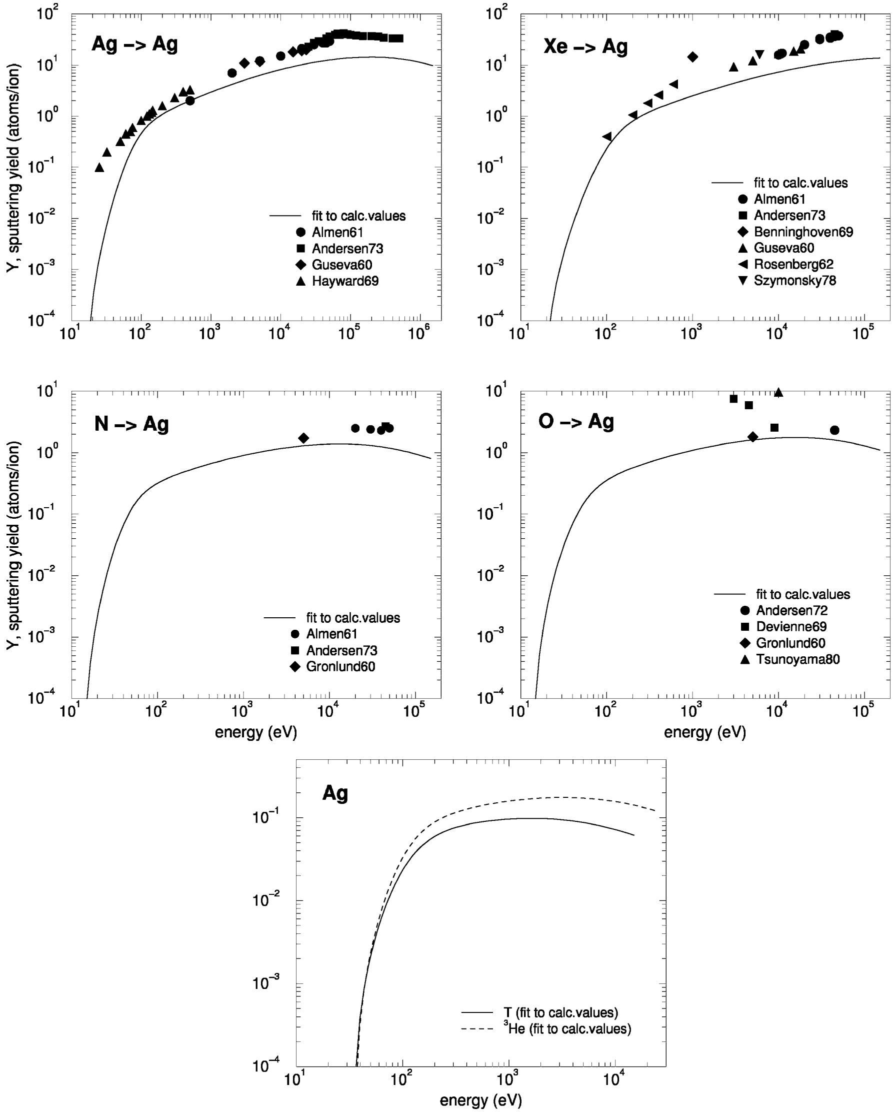

Fig. 42. Energy dependence of sputtering yields of Ag for bombardment at normal incidence with Ag [79, 101, 161, 214], Xe [54, 90, 161, 209, 214, 216], N [90, 205, 214], O [158, 162, 205, 217] and T, ^{3}He

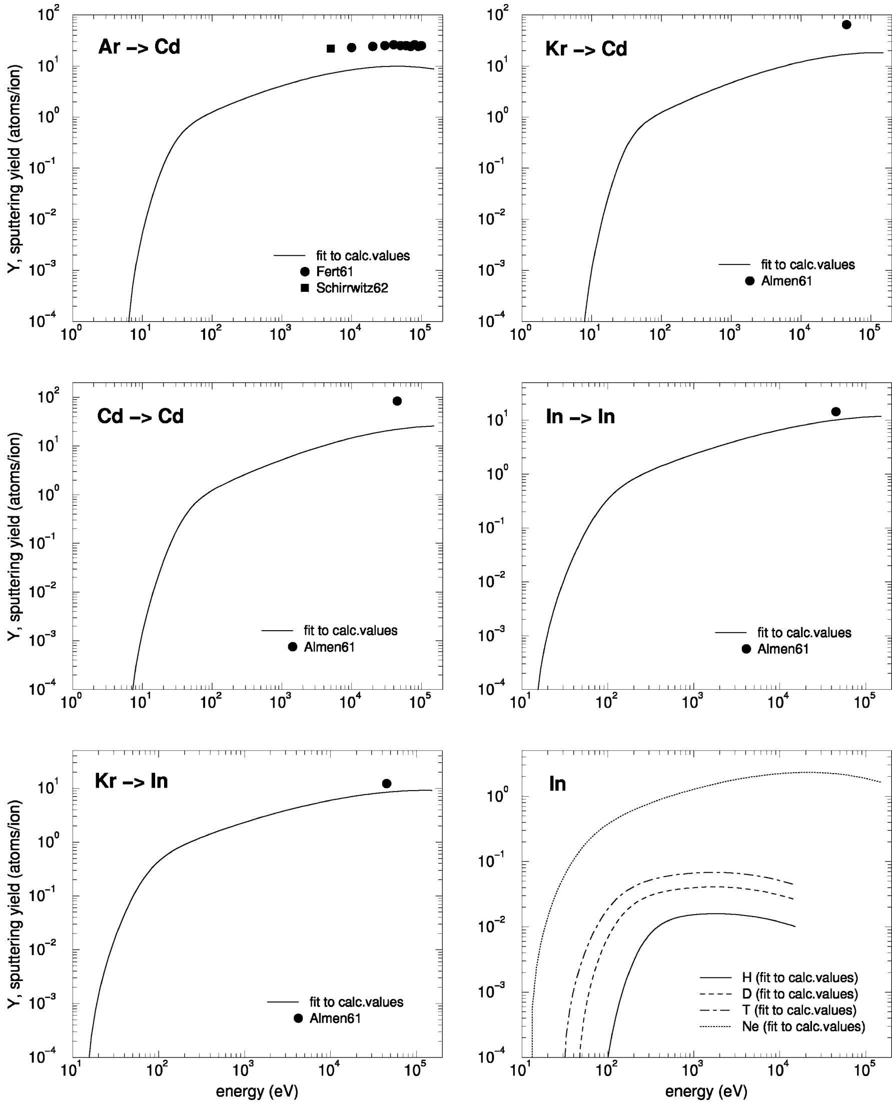

Fig. 43. Energy dependence of sputtering yields of Cd for bombardment at normal incidence with Ar[88, 104], Kr [90], Cd [79], and for bombardment at normal incidence of rIn with Kr [90], In [79], and H, D, T, Ne

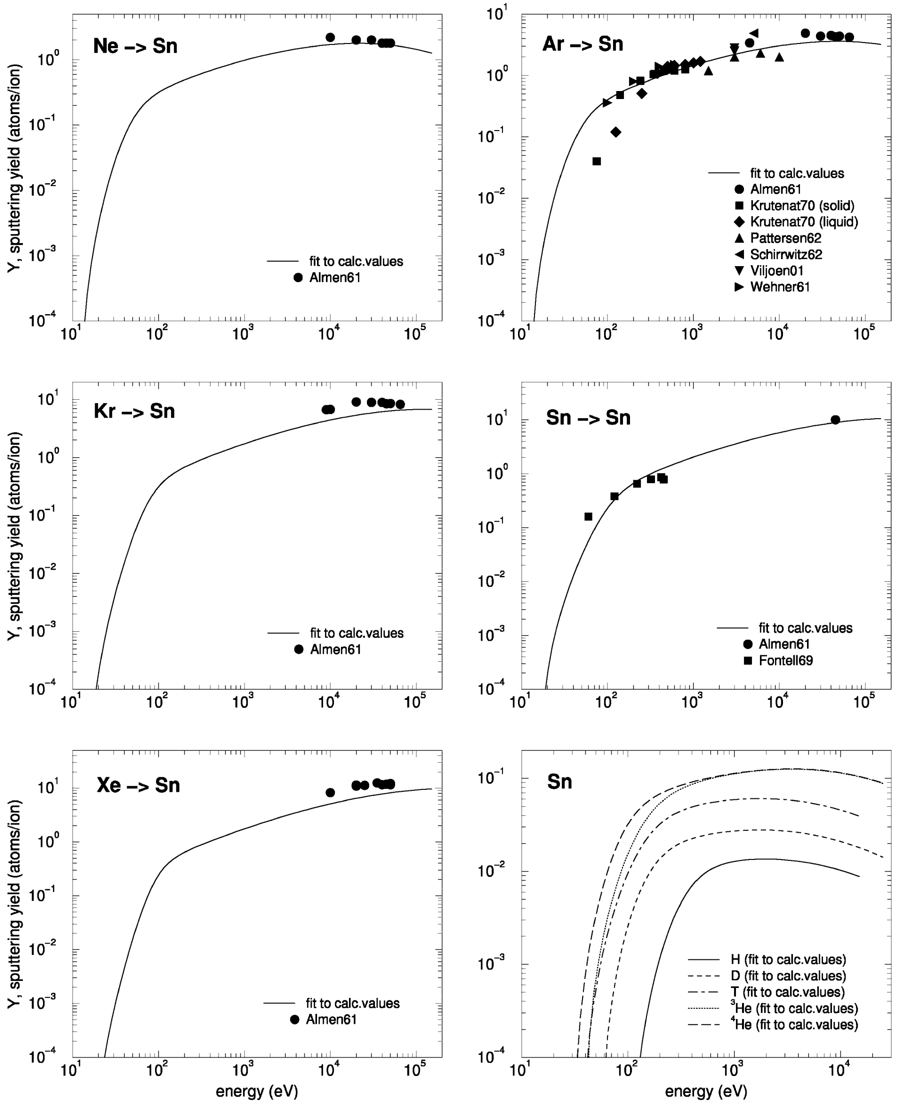

Fig. 44. Energy dependence of sputtering yields of Sn for bombardment at normal incidence with Ne [90], Ar [15, 88, 90, 211, 218, 219], Kr [90], Sn [79, 151], Xe [90], and H, D, T, ^{3}He, ^{4}He

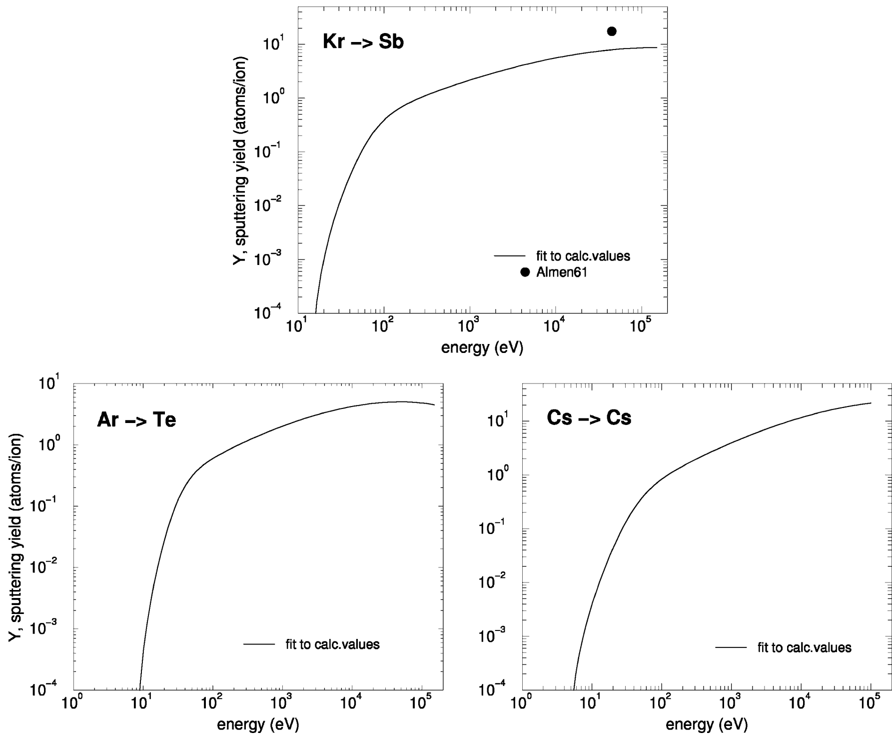

Fig. 45. Energy dependence of sputtering yields of Sb for bombardment at normal incidence with Kr [90], and for bombardment at normal incidence of Te with Ar and Cs with Cs

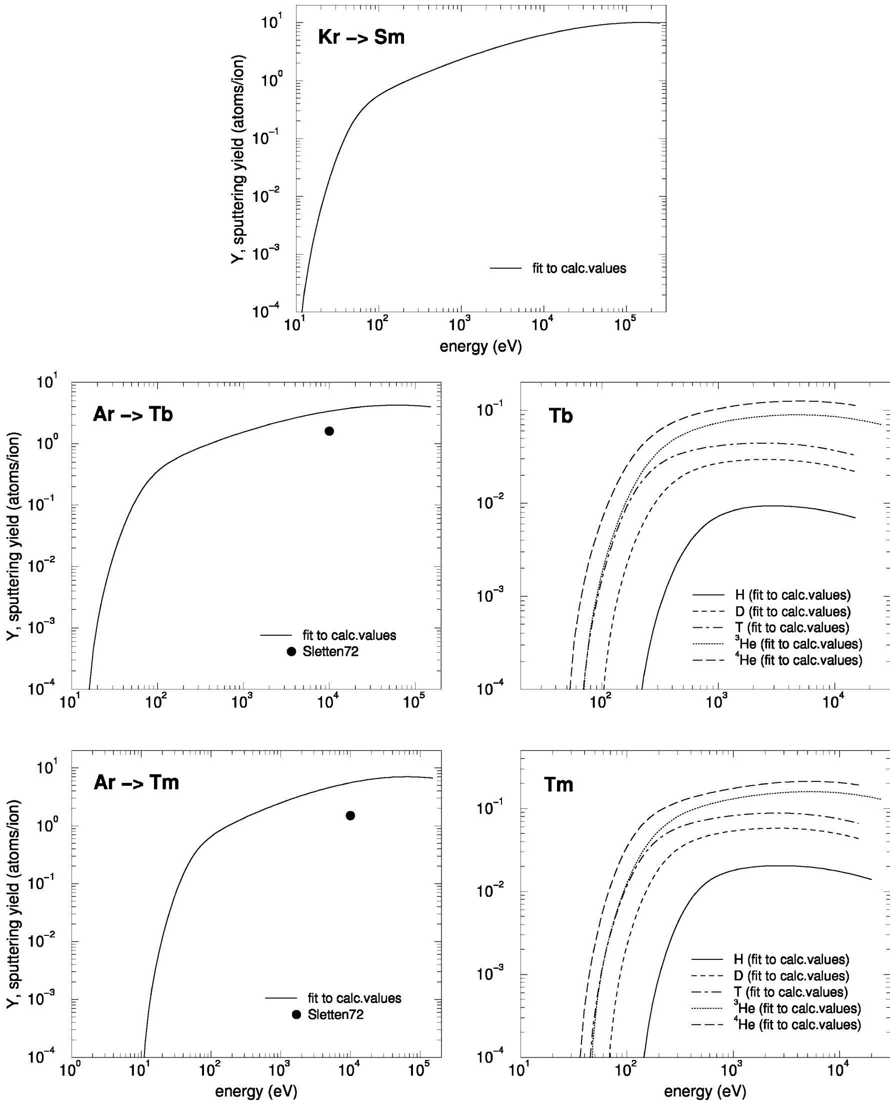

Fig. 46. Energy dependence of sputtering yields of Sm for bombardment at normal incidence with Kr, the bombardment at normal incidence of Tb with Ar [150] and H, D, T, ^{3}He, ^{4}He, and for bombardment at normal incidence of Tm with Ar [150] and H, D, T, ^{3}He, ^{4}He

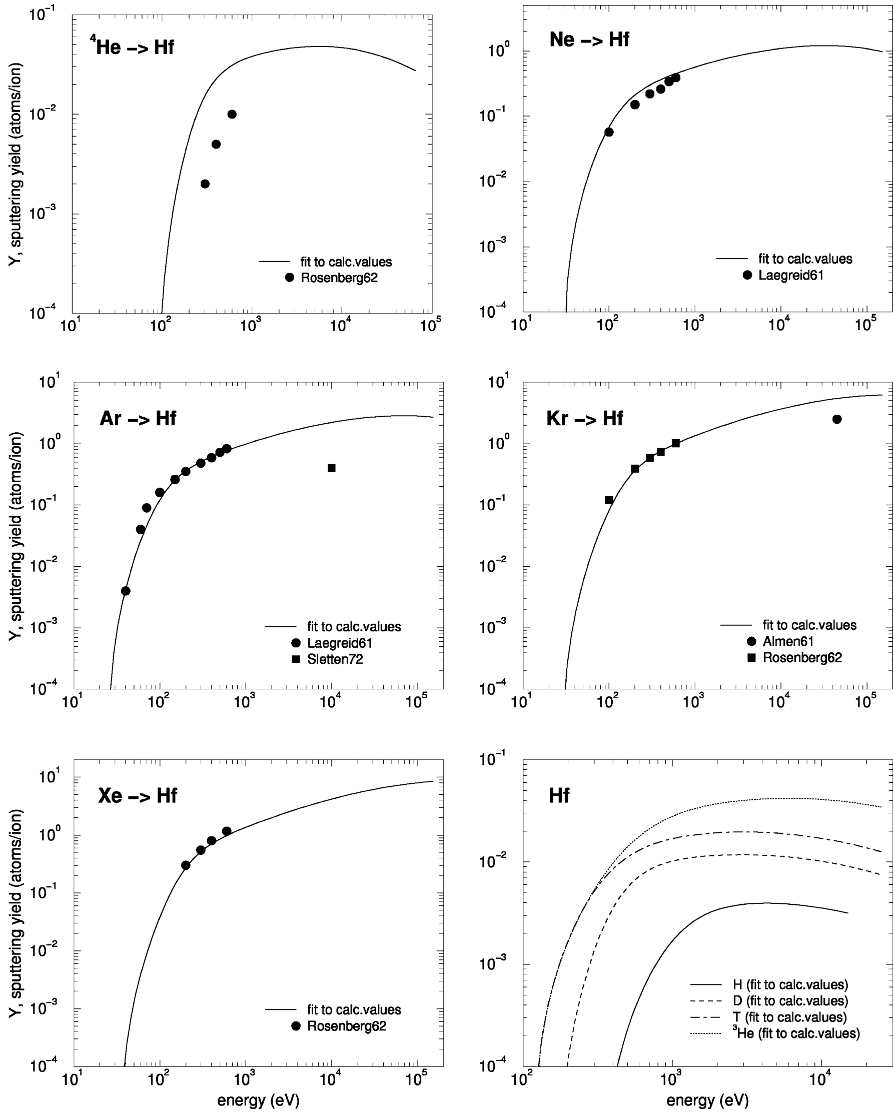

Fig. 47. Energy dependence of sputtering yields of Hf for bombardment at normal incidence with ^{4}He [54], Ne [63], Ar [63, 150], Kr [54, 90], Xe [54], and H, D, T and ^{3}He

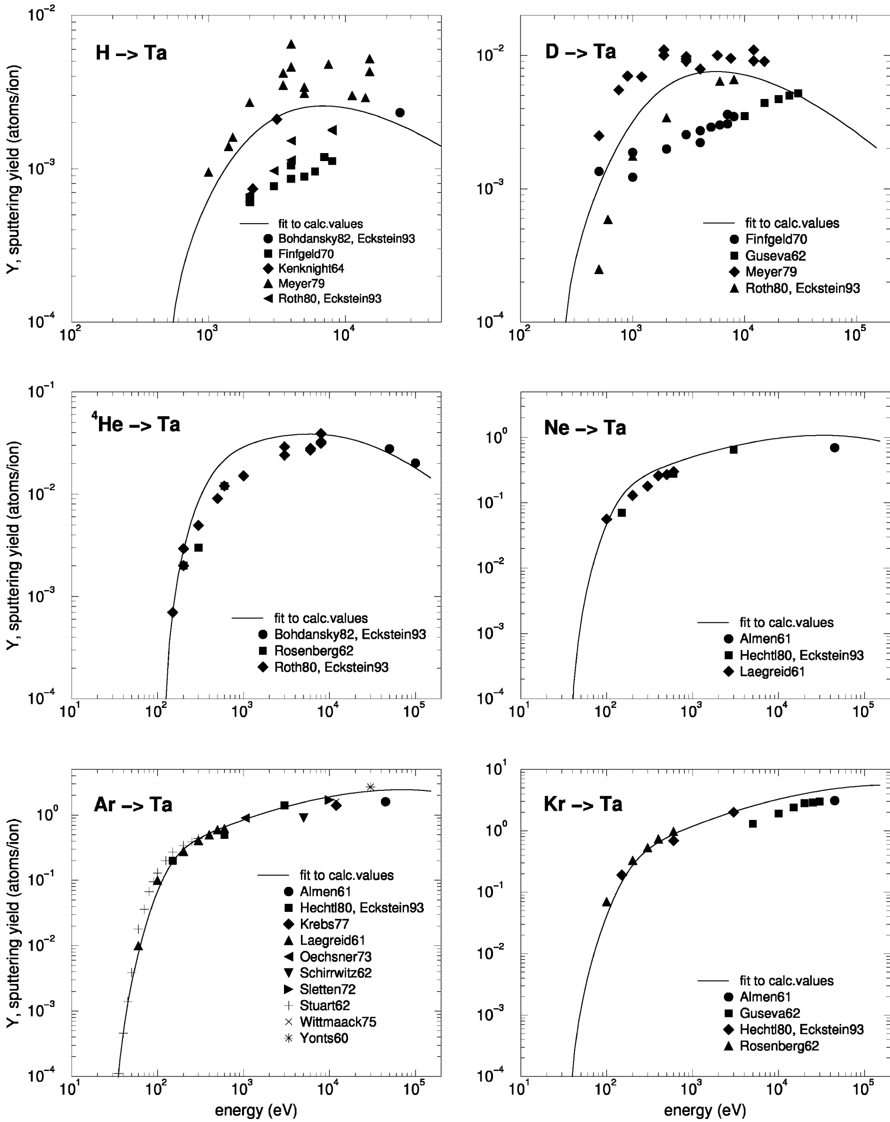

Fig. 48. Energy dependence of sputtering yields of Ta for bombardment at normal incidence with H [27, 49, 111, 135, 149, 197], D [27, 111, 149, 197, 220], ^{4}He [27, 54, 111, 135], Ne [27, 63, 90, 221], Ar [27, 63, 88, 90, 94, 105, 108, 136, 150, 221, 222], Kr [27, 54, 90, 220, 221]

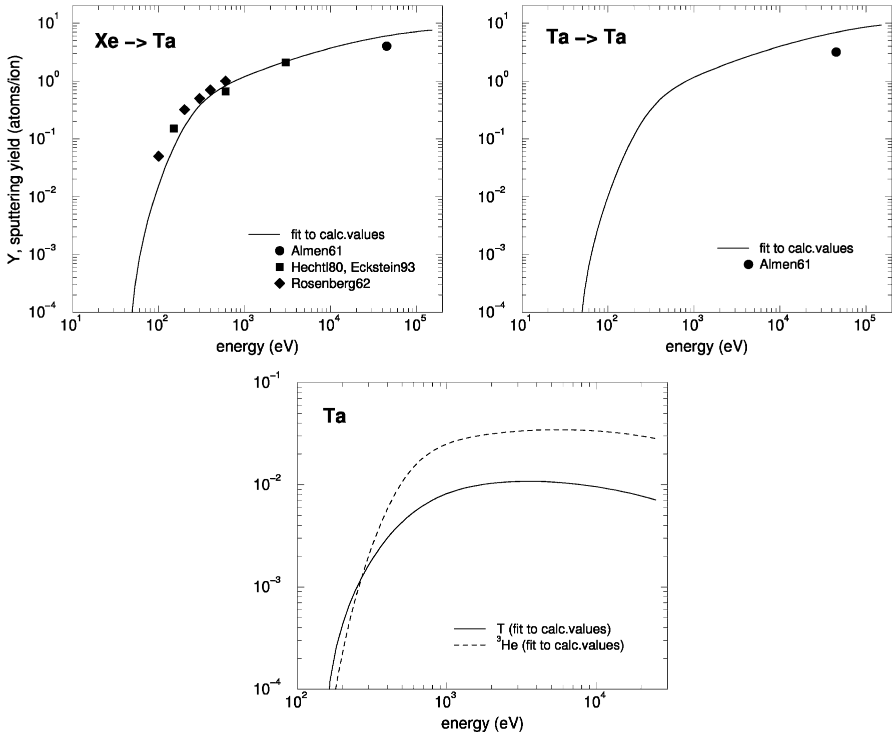

Fig. 49. Energy dependence of sputtering yields of Ta for bombardment at normal incidence with Xe [27, 54, 90, 221], Ta [79], and T, ^{3}He

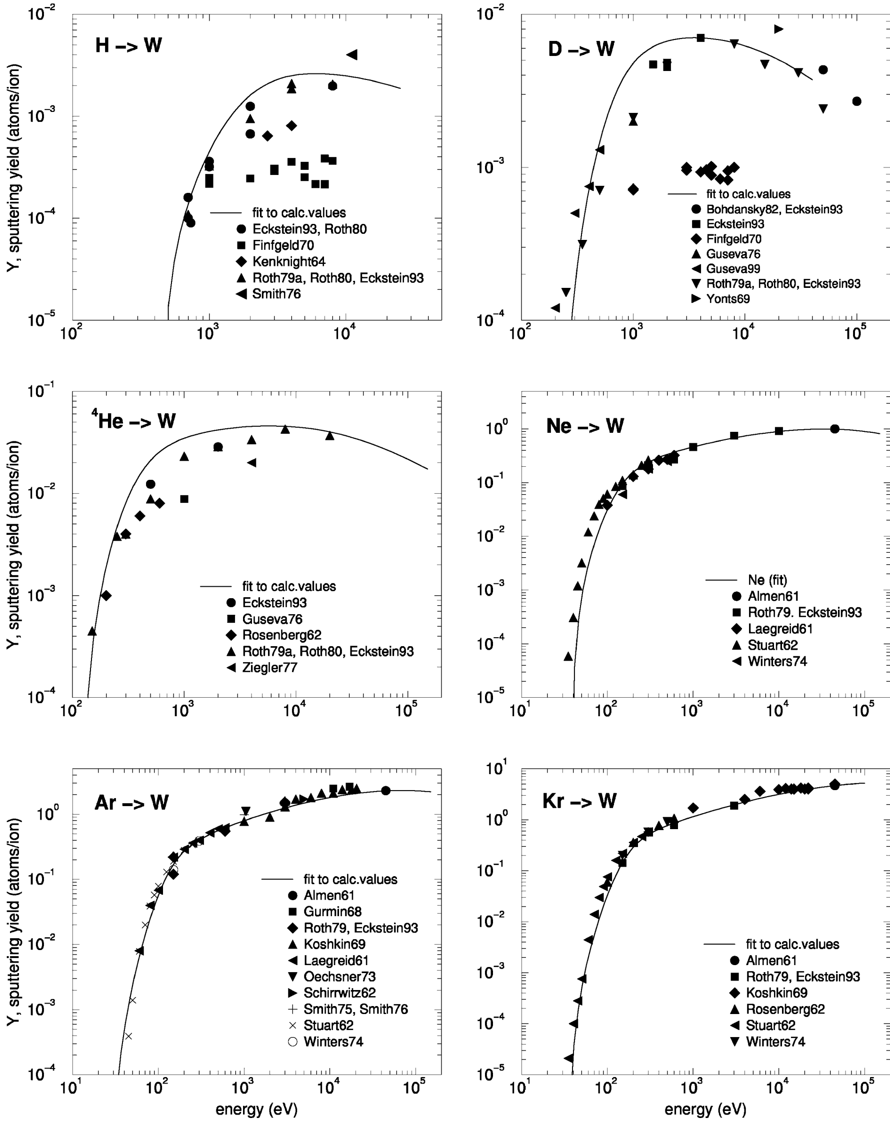

Fig. 50. Energy dependence of sputtering yields of W for bombardment at normal incidence with H [27, 49, 51, 70, 111, 149], D [17, 27, 51, 97, 111, 135, 140, 149], ^{4}He [27, 51, 54, 111, 140, 223], Ne [27, 50, 63, 90, 136, 224], Ar [27, 50, 63, 70, 88, 90, 105, 136, 147, 181, 190, 224], Kr [27, 50, 54, 90, 136, 147, 224]

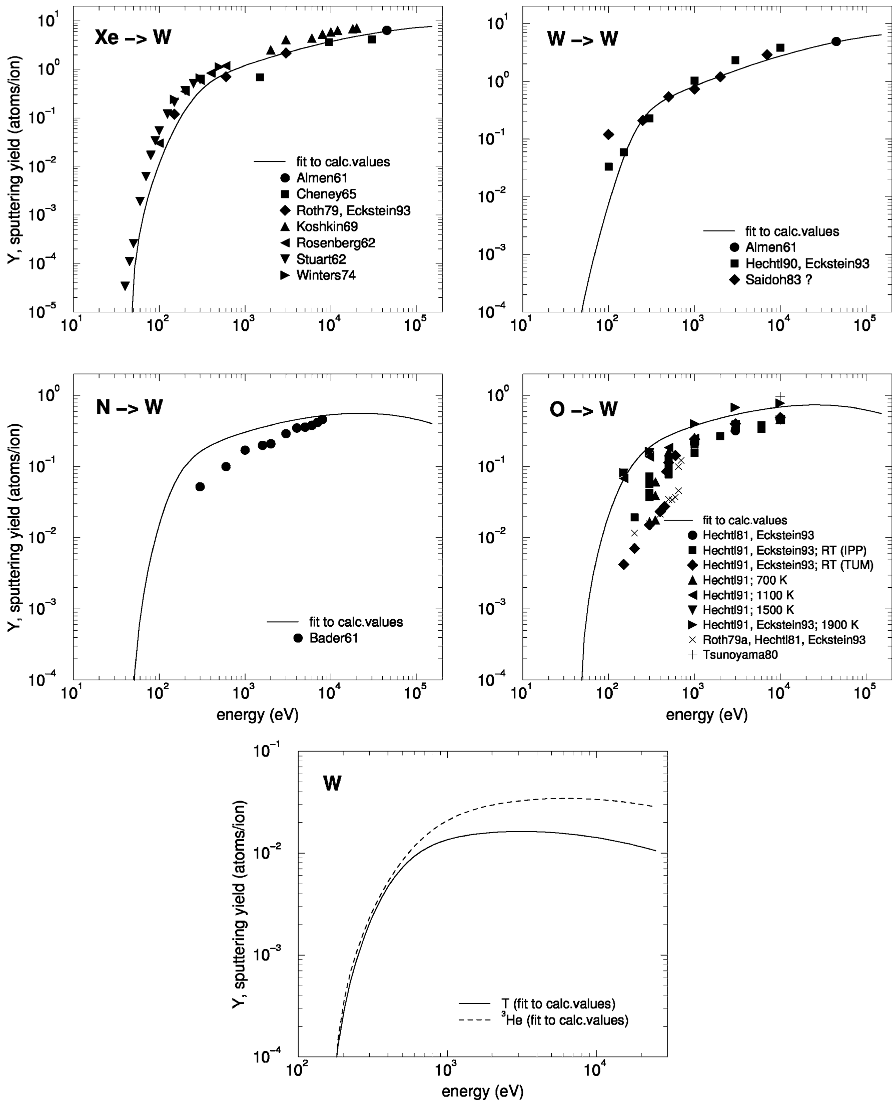

Fig. 51. Energy dependence of sputtering yields of W for bombardment at normal incidence with Xe [27, 50, 54, 90, 136, 147, 168, 224], W [27, 79, 202, 203, 225], N [148], O [27, 51, 78, 158, 225] and T, ^{3}He

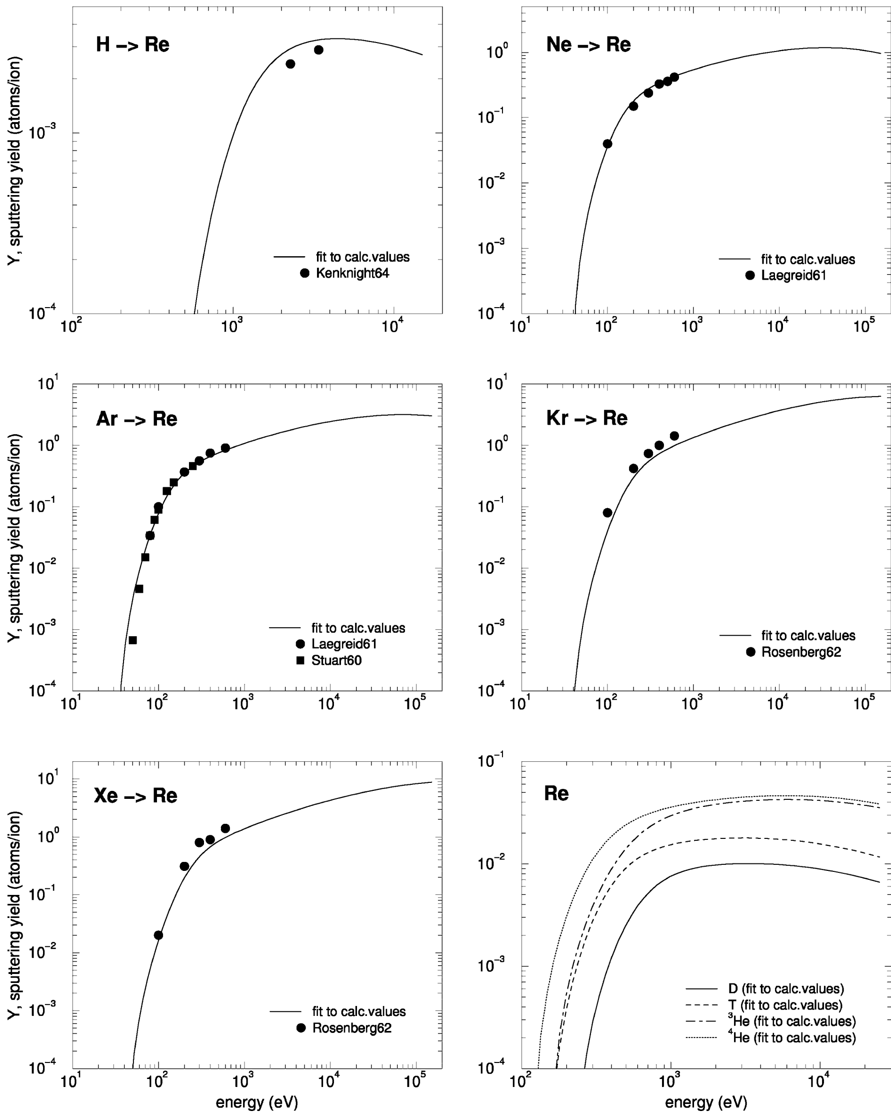

Fig. 52. Energy dependence of sputtering yields of Re for bombardment at normal incidence with H [49], Ne [63], Ar [63, 182], Kr [54], Xe [54] and D, T, ^{3}He, ^{4}He

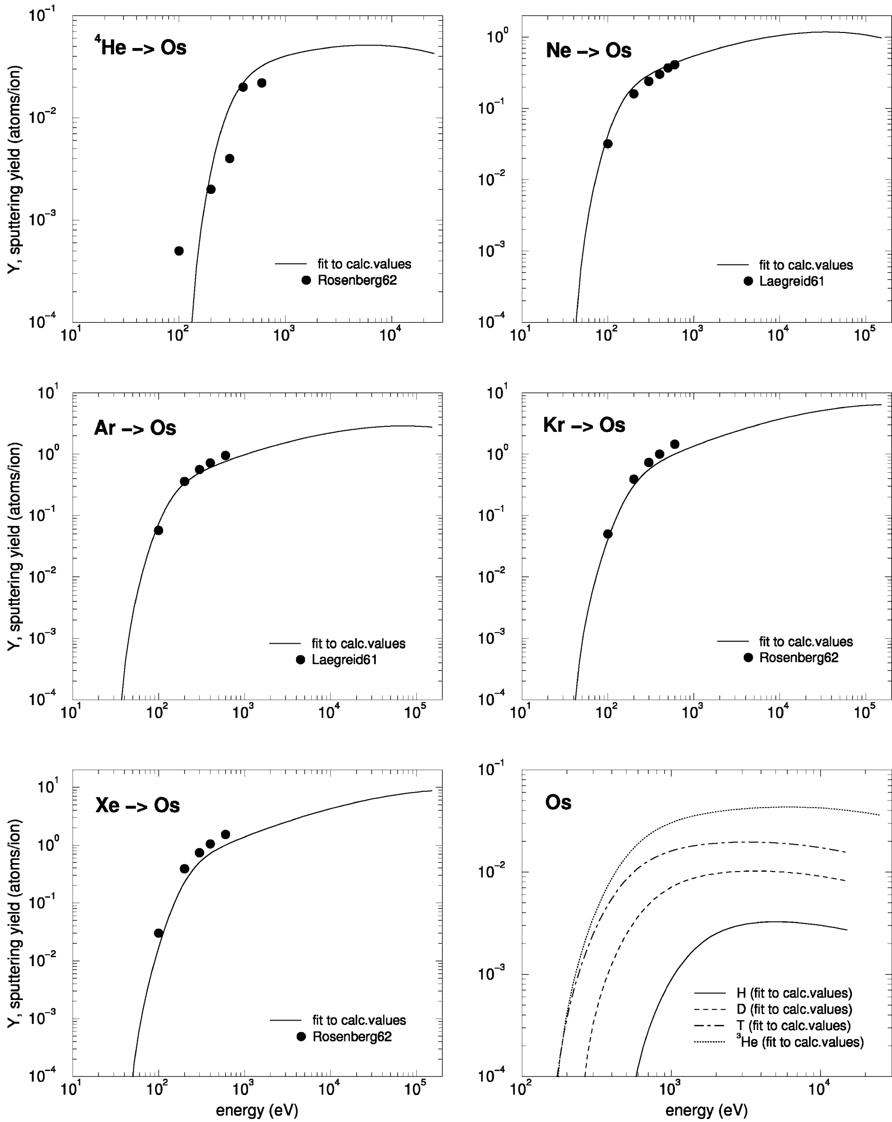

Fig. 53. Energy dependence of sputtering yields of Os for bombardment at normal incidence with ^{4}He [54], Ne [63], Ar [63], Kr [54], Xe [54], and H, D, T, ^{3}He

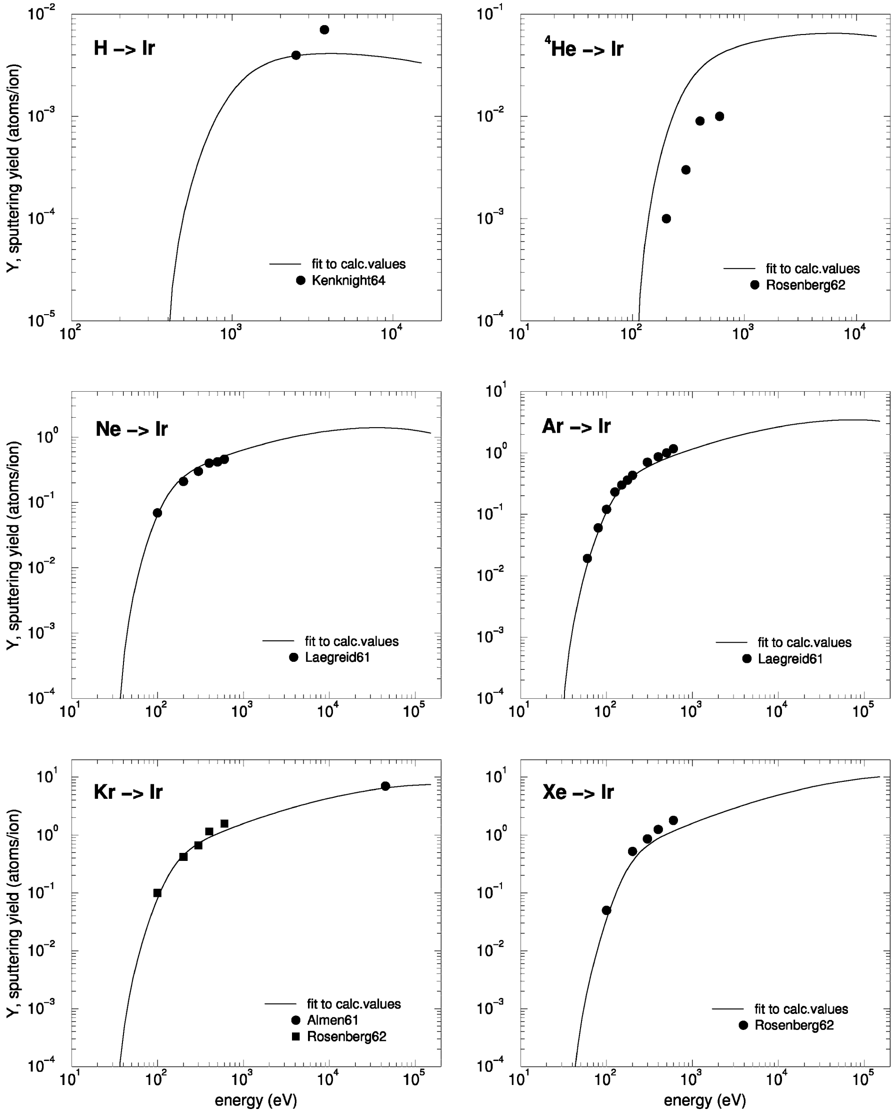

Fig. 54. Energy dependence of sputtering yields of Ir for bombardment at normal incidence with H [49], ^{4}He [54], Ne [63], Ar [63], Kr [54, 90], Xe [54]

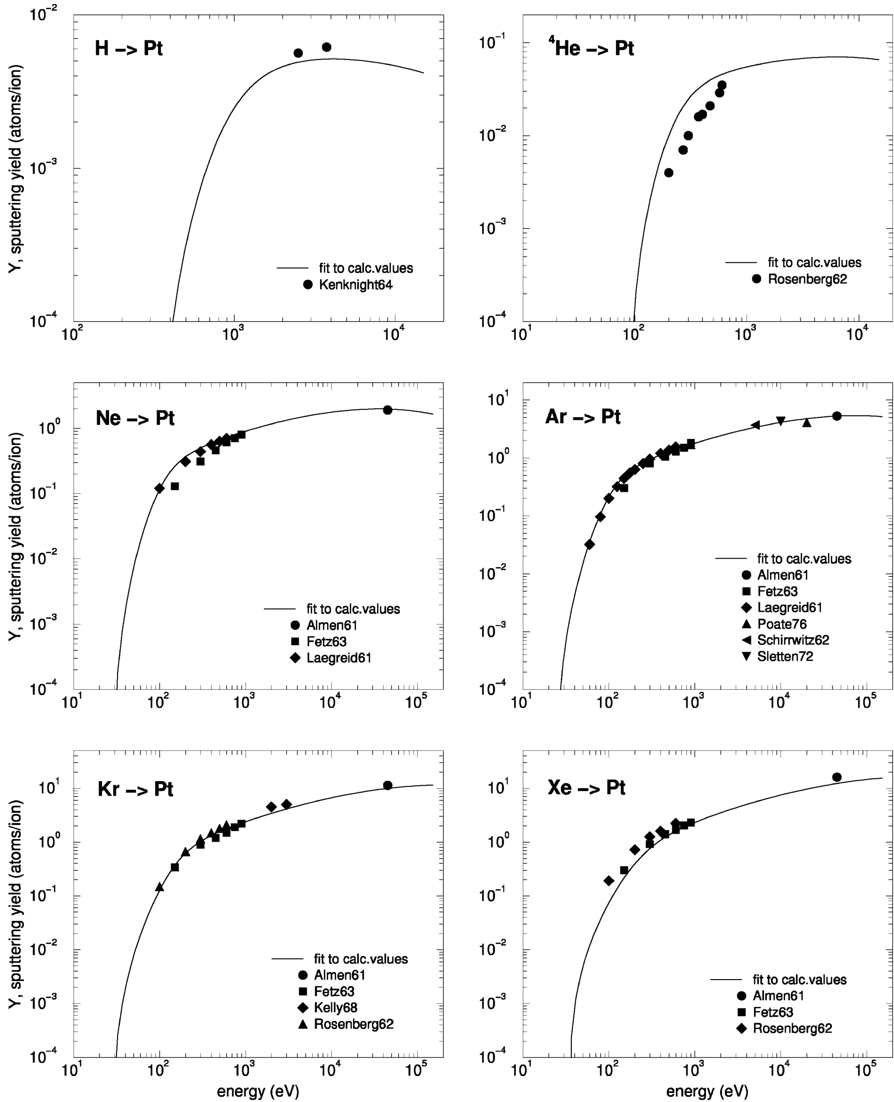

Fig. 55. Energy dependence of sputtering yields of Pt for bombardment at normal incidence with H [49], ^{4}He [54], Ne [55, 63, 90], Ar [55, 63, 88, 90, 123, 150], Kr [54, 55, 90, 109], Xe [54, 55, 90]

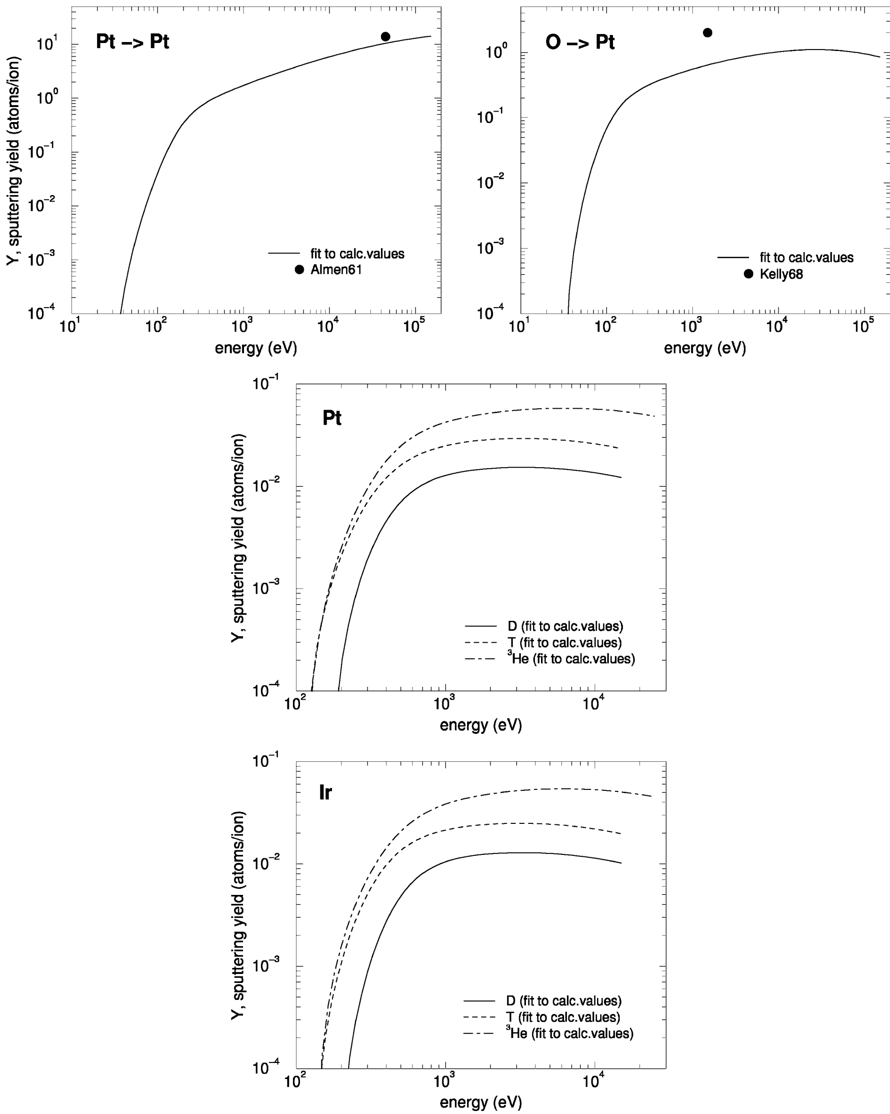

Fig. 56. Energy dependence of sputtering yields of Pt for bombardment at normal incidence with Pt [79], O [109] and D, T, and ^{3}He, and of Ir for bombardment at normal incidence with D, T, and ^{3}He

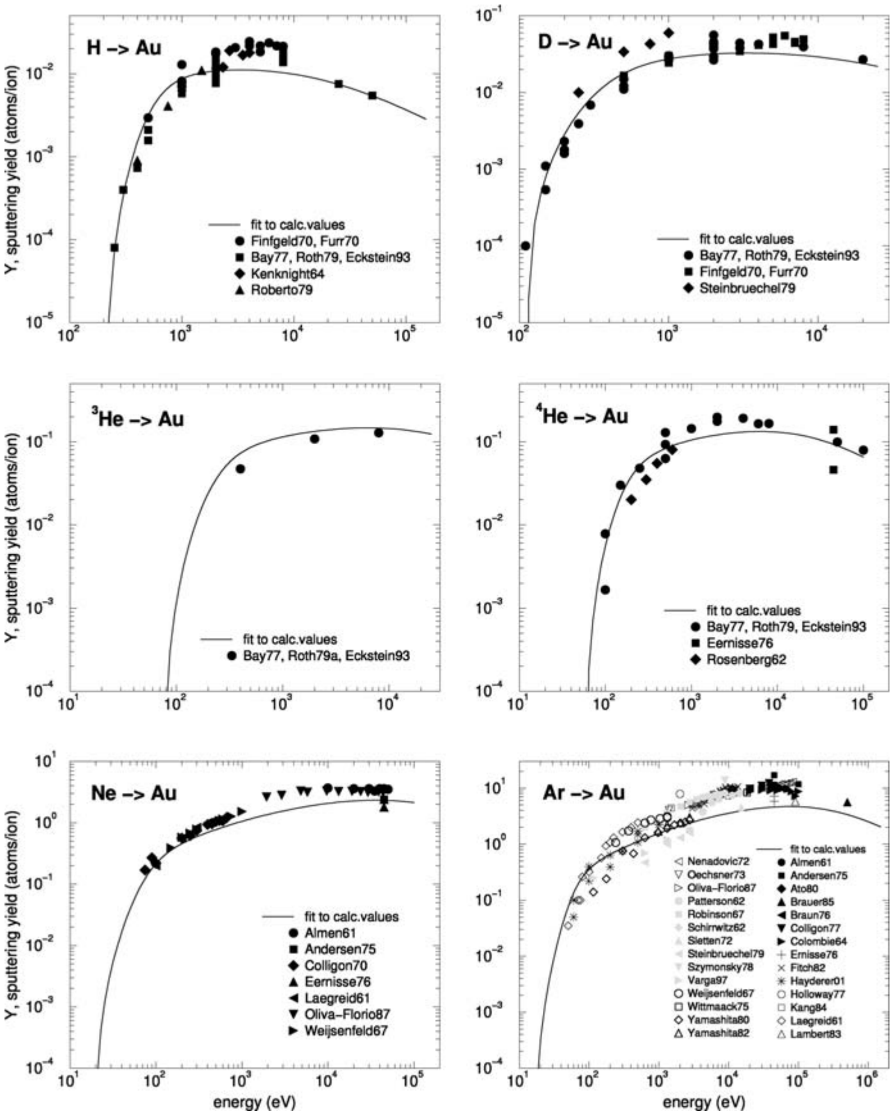

Fig. 57. Energy dependence of sputtering yields of Au for bombardment at normal incidence with H [27, 49, 50, 149, 154, 194, 226], D [27, 50, 133, 149, 194, 226], ^{3}He [27, 51, 194], ^{4}He [27, 50, 54, 194, 227], Ne [63, 90, 98, 174, 227–229], Ar [15, 63, 77, 88, 90, 98, 102, 105, 107, 129, 133, 139, 143, 150, 171, 174, 175, 180, 209, 216, 222, 227, 229–234]

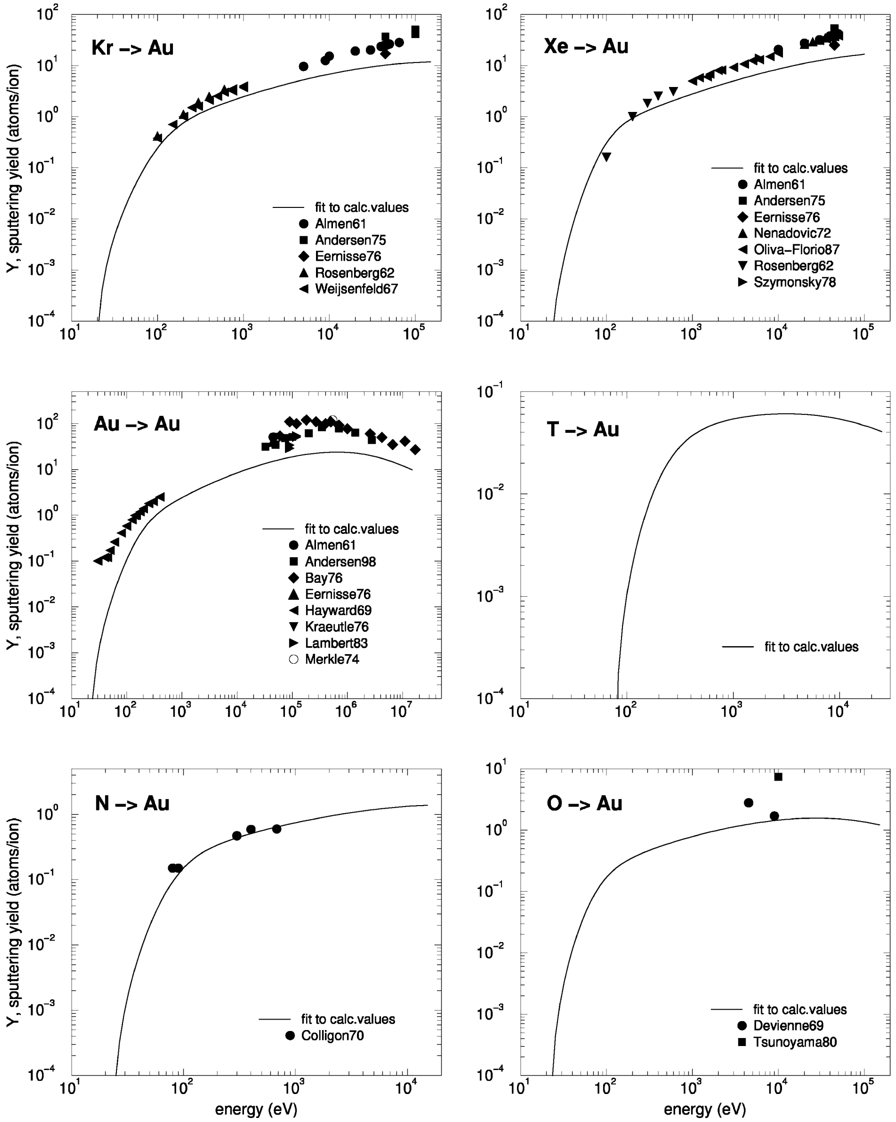

Fig. 58. Energy dependence of sputtering yields of Au for bombardment at normal incidence with Kr [54, 90, 98, 227, 229], Xe [54, 90, 174, 216, 227, 229, 230], Au [79, 101, 139, 227, 235–238], T, N [228], O [158, 217]

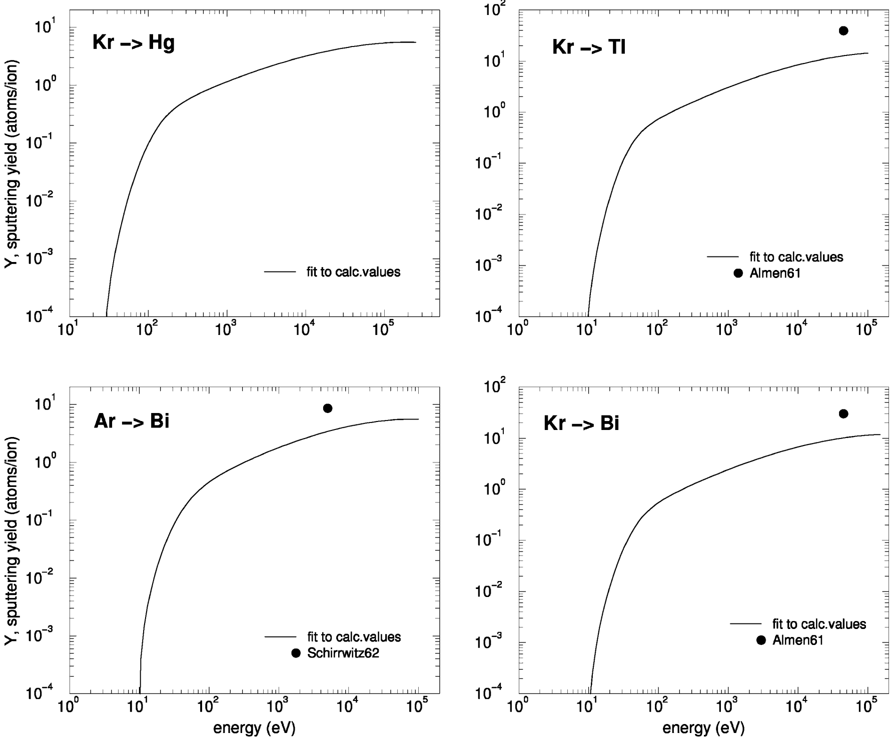

Fig. 59. Energy dependence of sputtering yields of Hg and Tl for bombardment at normal incidence with Kr [90] and of Bi bombardment at normal incidence with Ar [88], Kr [90]

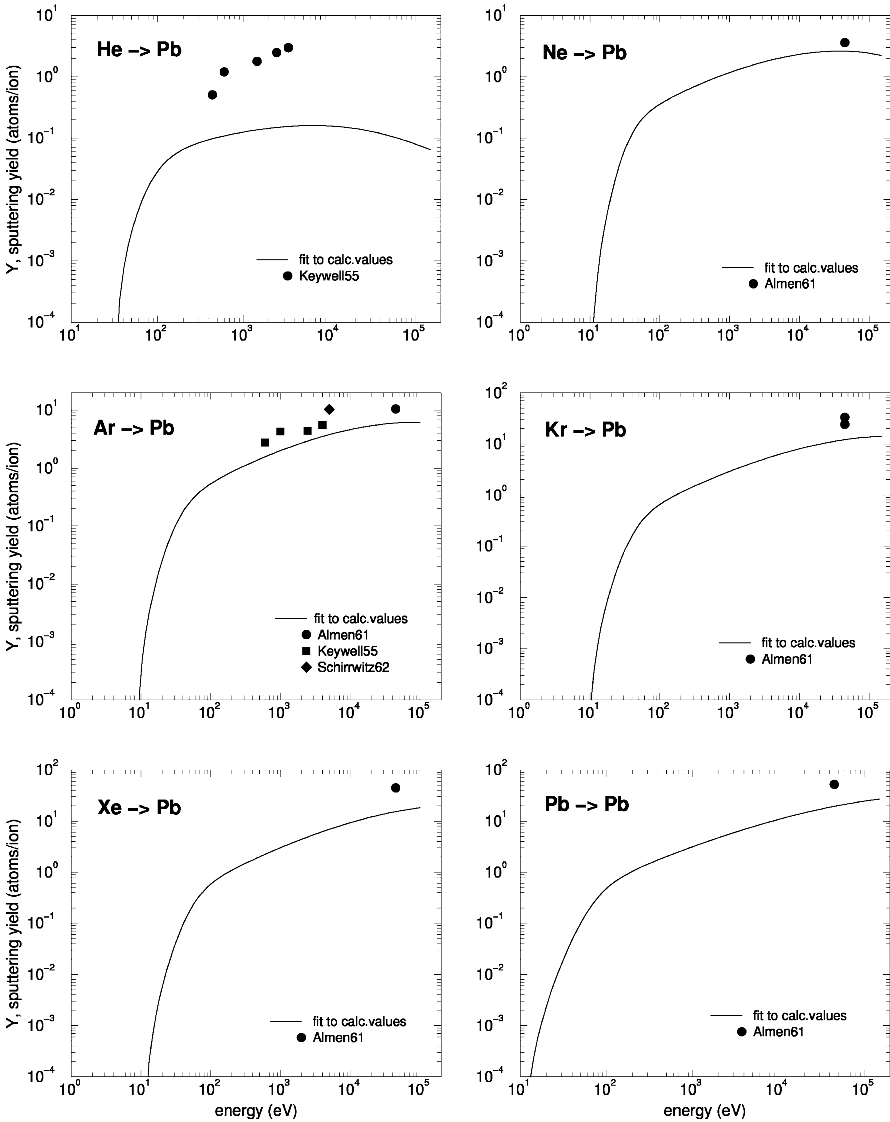

Fig. 60. Energy dependence of sputtering yields of Pb for bombardment at normal incidence with He [165], Ne [90], Ar [88, 90, 165], Kr [90], Xe [90], Pb [79]

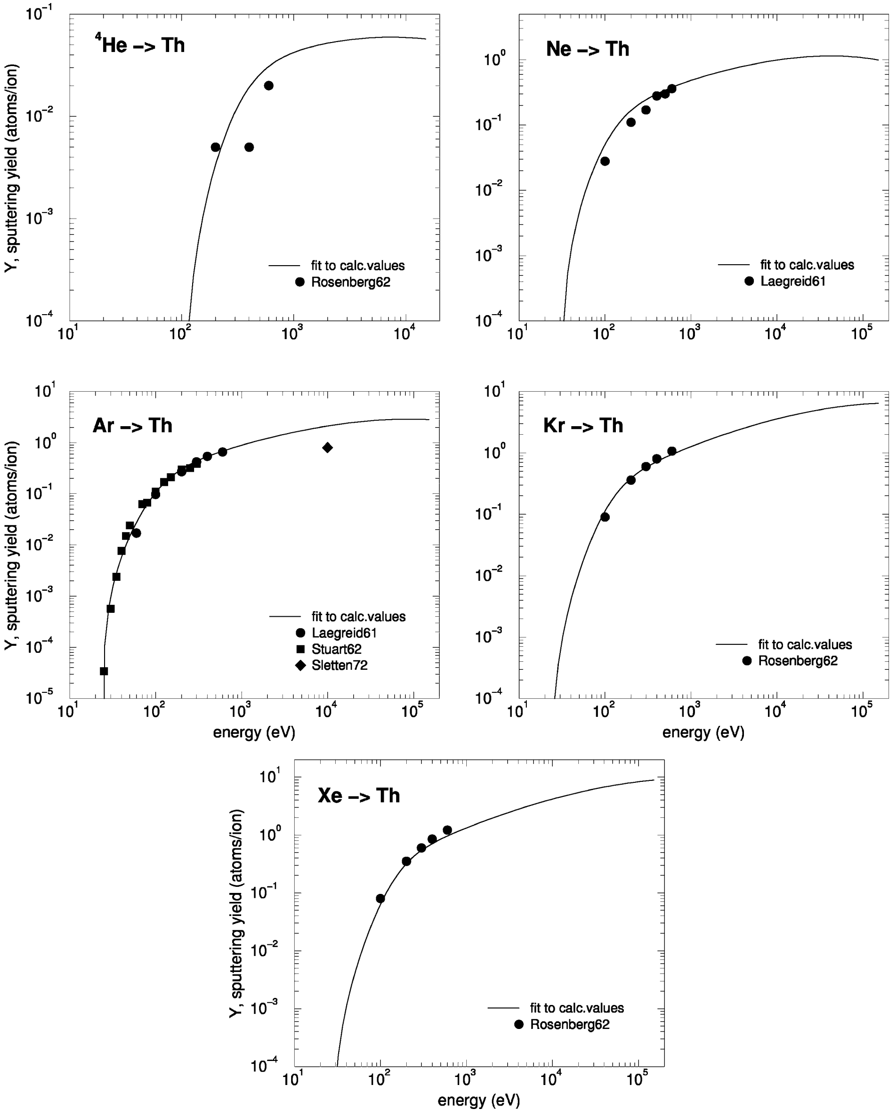

Fig. 61. Energy dependence of sputtering yields of Th for bombardment at normal incidence with ^{4}He [54], Ne [63], Ar [63, 136, 150], Kr [54], Xe [54]

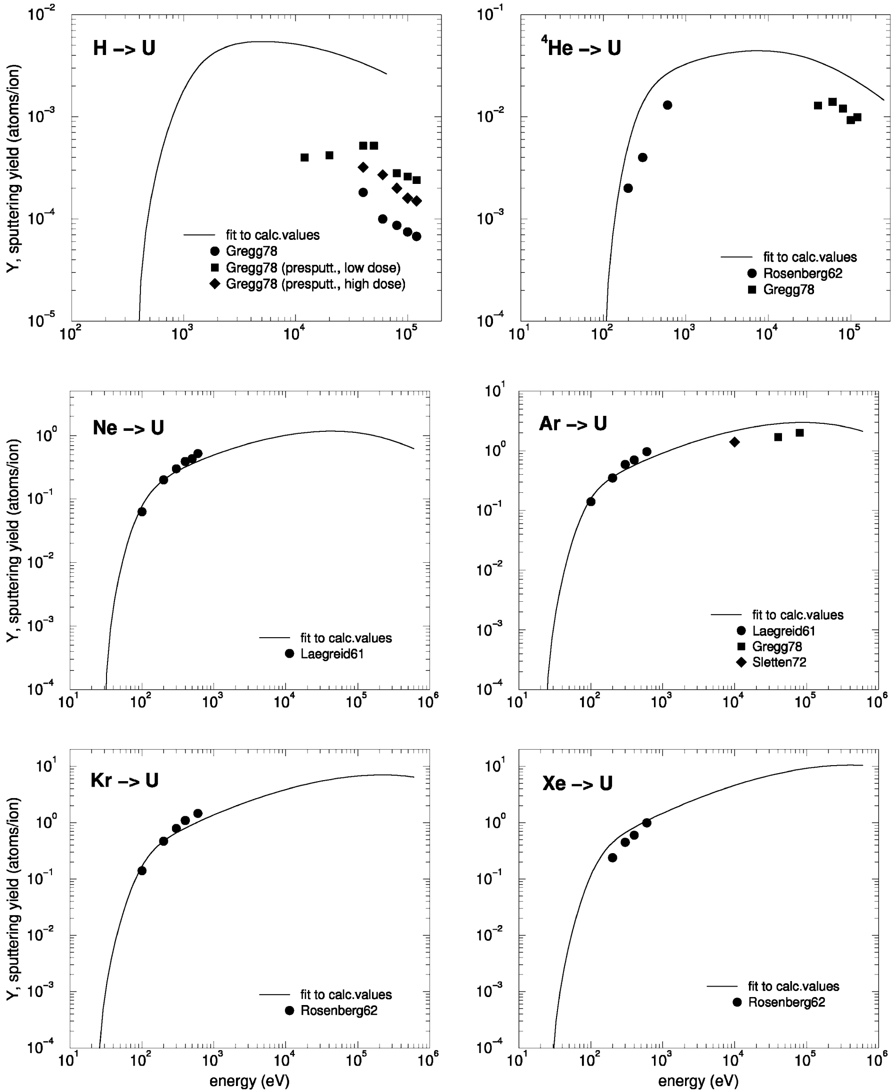

Fig. 62. Energy dependence of sputtering yields of U for bombardment at normal incidence with H [239], ^{4}He [54, 239], Ne [63], Ar [63, 150, 239], Kr [54], Xe [54]

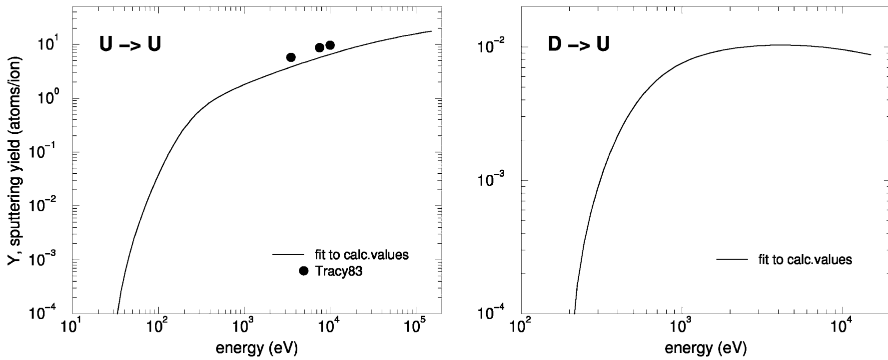

Fig. 63. Energy dependence of sputtering yields of U for bombardment at normal incidence with U [240], D

The agreement of the experimentally determined sputtering yields at normal incidence with the fit to the calculated values is generally reasonable. This gives confidence to the calculated and measured values. Deviations of up to a factor of two are likely due to uncertainties in the different experiments. Even for noble gases implanted into targets the measured sputtering yield can change by up to 30 % [130].

There are some obvious deviations:

For carbon bombardment by hydrogen isotopes and oxygen the measured sputtering yields are definitely larger than the calculated curves, especially at low energies. This is an indication for a different mechanism contributing to sputtering, which is named chemical sputtering (see chapter by *Jacob* and *Roth*). For materials which form oxides with a strong binding the measured sputtering yields are lower as in the case of beryllium, aluminum and tantalum [88]. The influence of an residual oxygen pressure in the vacuum system on the measured yield has been investigated systematically confirming lower yields of oxides on the surface [101, 134, 241, 242]. For some targets, as for example beryllium, the target had to be heated to an elevated temperature so that Be diffuses through the oxide layer resulting in a clean Be surface [48]. Experimental data below 100 eV may be too large due to the energy width and the angular divergence of the incident beam [243], energetic neutrals in the ion beam, surface roughness and adatoms. Also implantation of heavy noble gases in low Z targets can increase the yield and may shift the threshold to lower energies [18]. Experimental data deviating by an order of magnitude from the calculated curves are probably erroneous as in the case of hydrogen isotope bombardment of cobalt, see Fig. 23.

For Cu, Ag, and Au there is a general tendency, that the measured yields are systematically higher at energies above about 1 keV than the calculated curves. The reason could be a problem of the interaction potential, the surface binding energy, or the inelastic energy loss. An experimental reason could be a large fraction of sputtered molecular species. But the most likely reason

for the observed discrepancy is the occurrence of collisional spikes, which give a larger contribution to the yield than for neighbour elements (such as Pt in the case of Au) [244], see also chapter by *Assmann*, *Toulemonde*, and *Trautmann*.

Extraordinarily high sputtering yields of the order of 10^5 are reported for the sputtering of sulfur with He ions [245, 246]. These results cannot be understood by collisional effects; they are explained by the implantation of charge into the insulating material by the incoming ions and electrostatic repulsion.

In some experiments such as in fusion plasma devices the incident flux (of hydrogen) has a distribution in energy and angle of incidence [247]. Calculated yields for a Maxwellian distribution of hydrogen isotopes on several targets are provided in [36, 248].

The dependence of the sputtering yield on the target density has been studied by *Shulga* [249, 250] with computer simulation showing a slight increase in the yield with increasing target density.

3.4 Angle of Incidence Dependence of the Sputtering Yield

The sputtering yield depends on the angle of incidence of the bombarding particle. Yields have been calculated with TRIM.SP for different angles of incidence at various energies for several ion–target combinations Analoguously to the energy dependence of the sputtering yield, the angular dependence of calulated values is fitted with an algebraic formula [44] and subsequently compared to experimental data

$$\frac{Y(E_0,\theta_0)}{Y(E_0,0)} = \left\{\cos\left[\left(\frac{\theta_0}{\theta_0^*}\frac{\pi}{2}\right)^c\right]\right\}^{-f} \exp\left(b\left\{1-1\Big/\cos\left[\left(\frac{\theta_0}{\theta_0^*}\frac{\pi}{2}\right)^c\right]\right\}\right) \tag{6}$$

$$\theta_0^* = \pi - \arccos\sqrt{\frac{1}{1+E_0/E_{\mathrm{sp}}}} \quad \geq \quad \frac{\pi}{2}\,; \tag{7}$$

θ_0^* takes care of the effect, that an angle of incidence of 90° cannot be reached, if the projectile experience a binding energy E_{sp} (to simulate a chemical binding). $E_{\mathrm{sp}} = E_{\mathrm{sb}}$ for selfbombardment with E_{sb} being the surface binding energy (heat of sublimation), $E_{\mathrm{sp}} = 1\,\mathrm{eV}$ is assumed for hydrogen isotopes and nitrogen, $E_{\mathrm{sp}} = 0$ for nobel gases. This projectile binding effect is only important at low energies and especially for selfbombardment. If $E_{\mathrm{sp}} = 0$, θ_0^* becomes $\pi/2$ and formula (6) is close to the Yamamura formula [251] besides the parameter c. If $E_{\mathrm{sp}} > 0$ the projectile experiences an acceleration and a refraction (decrease of the angle of incidence). The angle θ_{0m}, at which the angular dependence reaches its maximum, is determined by

$$\theta_{0m} = \frac{2}{\pi}\theta_0^*\left[\arccos\left(b/f\right)\right]^{1/c}\,. \tag{8}$$

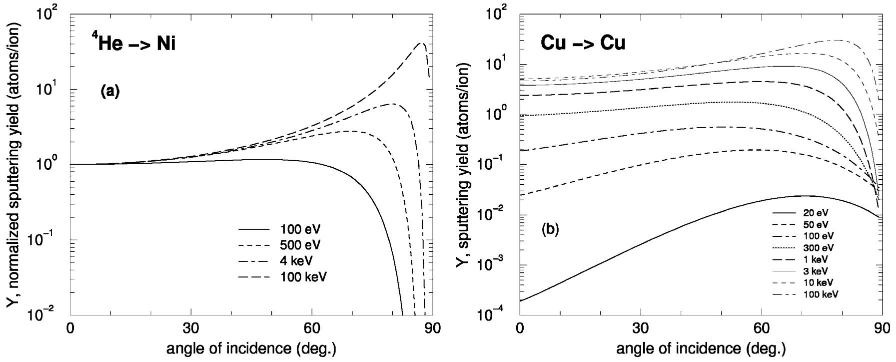

Fig. 64. Fit curves to the calculated angular dependence of sputtering yields at different incident energies for bombardment of nickel with helium (normalized at normal incidence) (**a**) and for selfsputtering of copper (**b**)

The values of the parameters f, c, b obtained by fitting the calculated yields (with TRIM.SP) with Bayesian statistics are provided in Tables 10 to 24 together with values $Y(E_0, 0), E_{\mathrm{sp}}, \theta_0^*, \theta_{0m}$. Figures are only given, if experimental data for more than three angles of incidence are available.

The general behaviour of the angular dependence of the calculated sputtering yields is shown in Fig. 64. As an example for noble gas ions Fig. 64a shows for ^{4}He on nickel, that the maximum of the angular dependence shifts to larger angles of incidence with increasing projectile energy, and that the ratio of maximum yield to the yield at normal incidence increases also with the incident energy. Close to threshold of sputtering the maximum of the dependence moves towards normal incidence. The situation is different for a case, where the binding of the projectile to the target becomes important such as for selfsputtering. Figure 64b shows the angular dependence for copper selfbombardment. Close to the threshold energy of sputtering the maximum occurs at large angles of incidence, moves then to smaller angles of incidence with increasing projectile energy. It shows the same behaviour as for noble gas ions at higher energies, where the influence of the projectile binding energy, E_{sp}, becomes negligible.

Plots of the angular dependence of the fits to the calculated sputtering yields are given in Figs. 65–86. In these plots the yields measured by many authors are introduced. In some figures the yield is normalized to the yield at normal incidence, because the experimental data were available in this form.

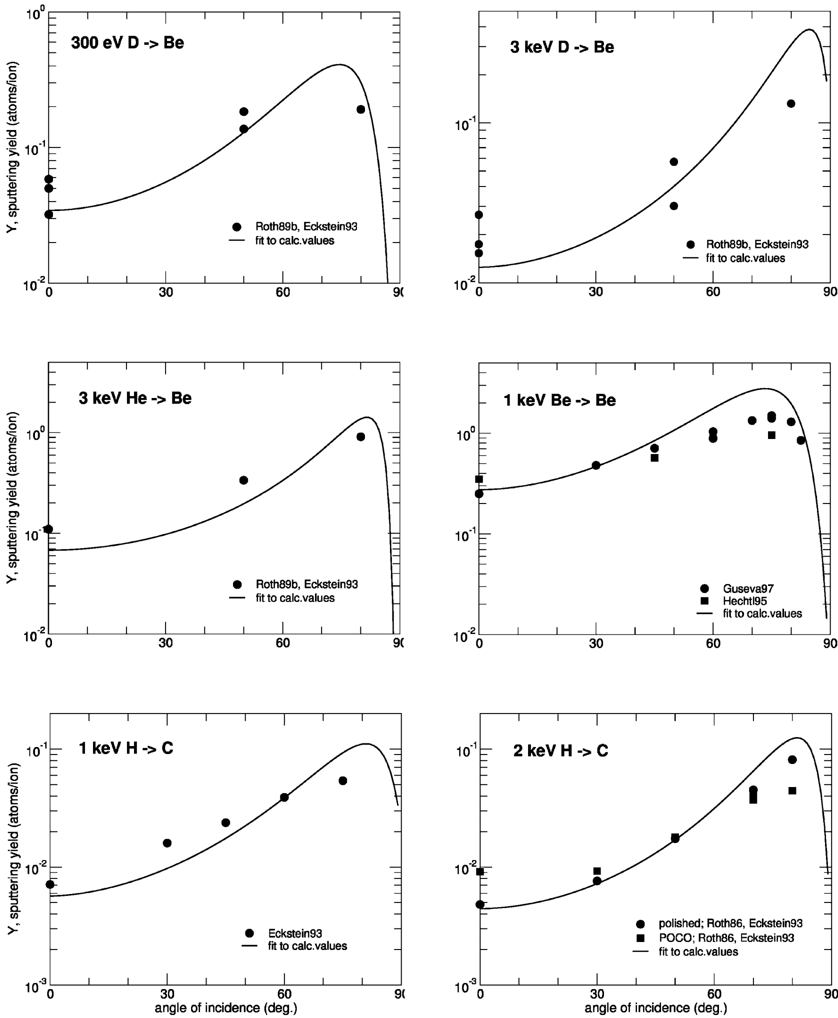

Fig. 65. Comparison of measured and calculated angular dependence of sputtering yields at different energies for different ion–target combinations: 0.3 keV D on Be [27, 252], 3 keV D on Be [27, 252], 3 keV ^{4}He on Be [27, 252], 1 keV Be on Be [60, 61], 1 keV H on C [27], 2 keV H on C [27, 253]

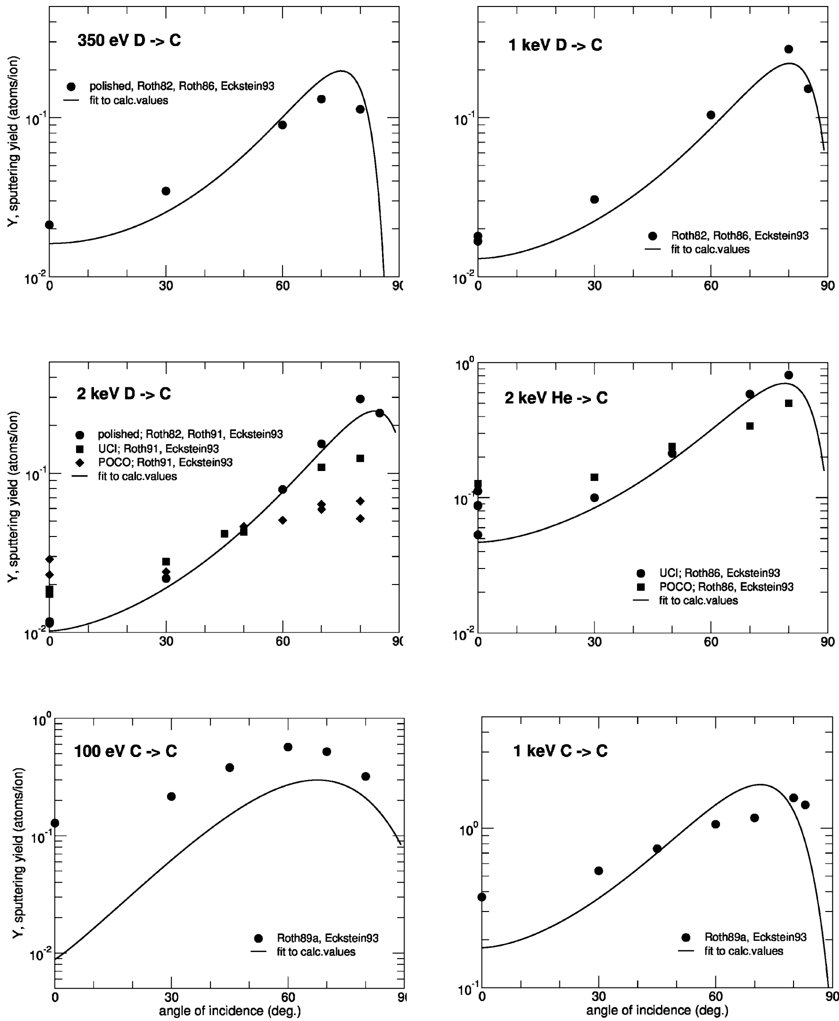

Fig. 66. Comparison of measured and calculated angular dependence of sputtering yields at different energies for different ion–target combinations: 0.35 keV D on C [27, 253, 254], 1 keV D on C [27, 253, 254], 2 keV D on C [27, 254, 255], 2 keV ^{4}He on C [27, 253], 100 eV C on C [27, 83], 1 keV C on C [27, 83]

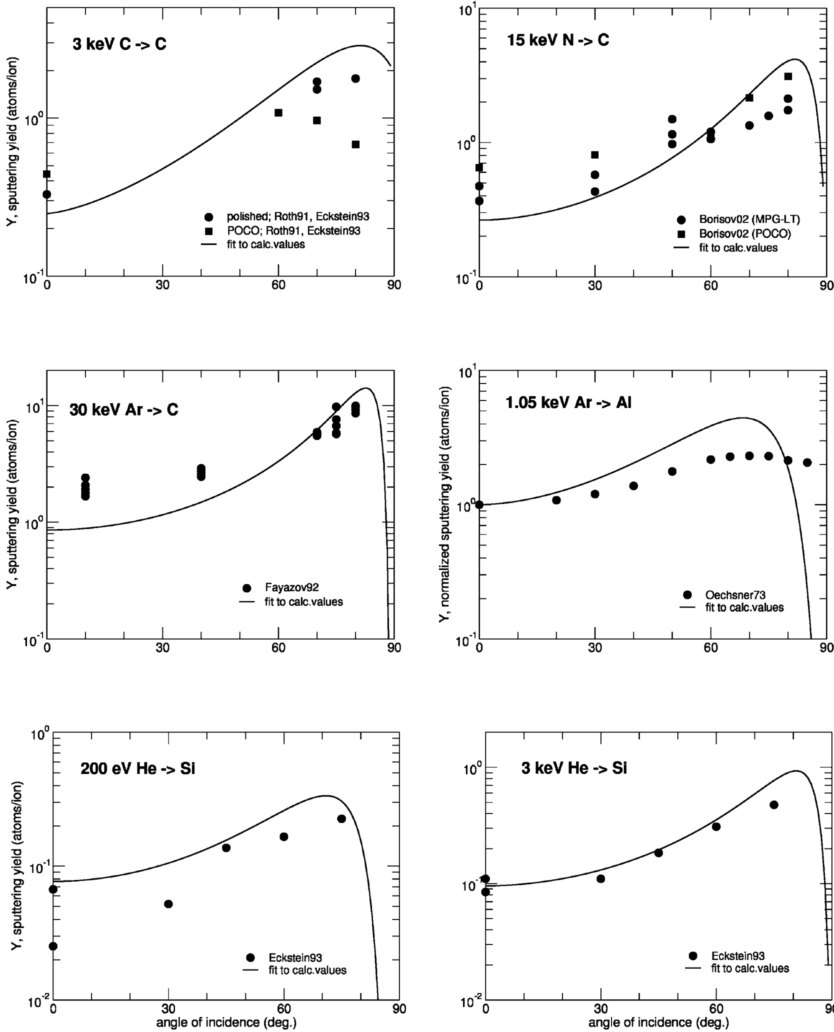

Fig. 67. Comparison of measured and calculated angular dependence of sputtering yields at different energies for different ion–target combinations: 3 keV C on C [27, 255], 15 keV N on C [93], 30 keV Ar on C [256], 1.05 keV Ar on Al [105], 0.2 keV ^{4}He on Si [27], 3 keV ^{4}He on Si [27]

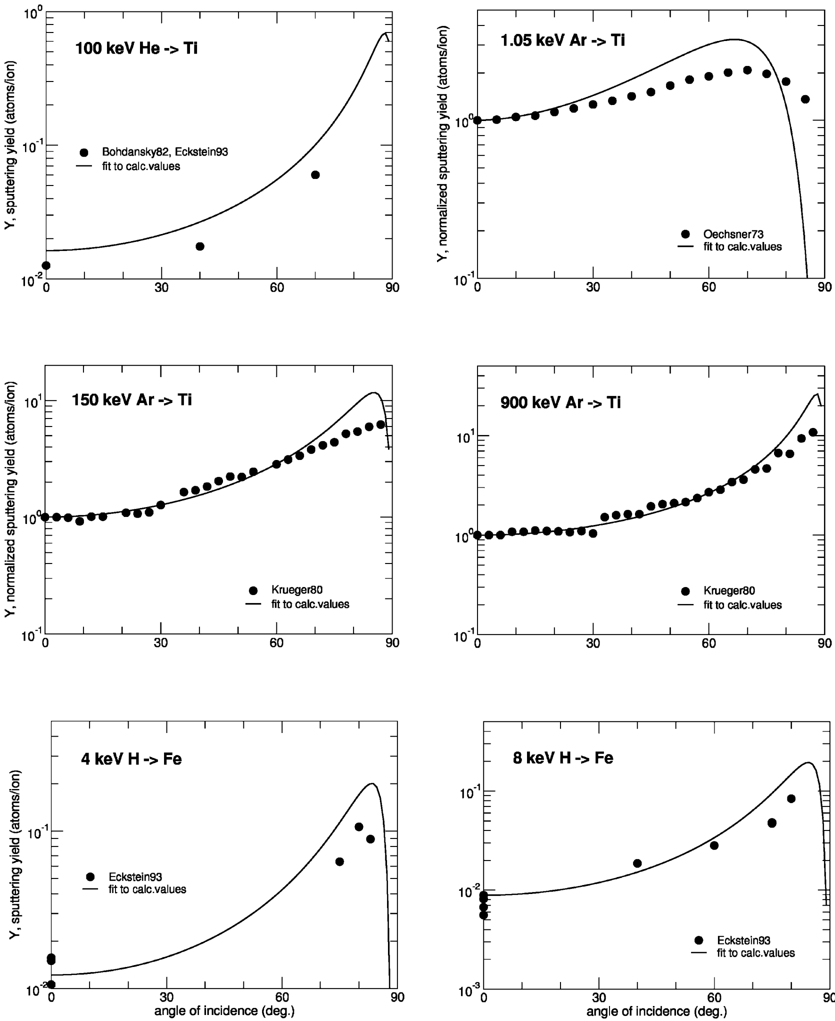

Fig. 68. Comparison of measured and calculated angular dependence of sputtering yields at different energies for different ion–target combinations: 100 keV ^{4}He on Ti [27, 135], 1.05 keV Ar on Ti [105], 150 keV Ar on Ti [257], 900 keV Ar on Ti [257], 4 keV H on Fe [27], 8 keV H on Fe [27]

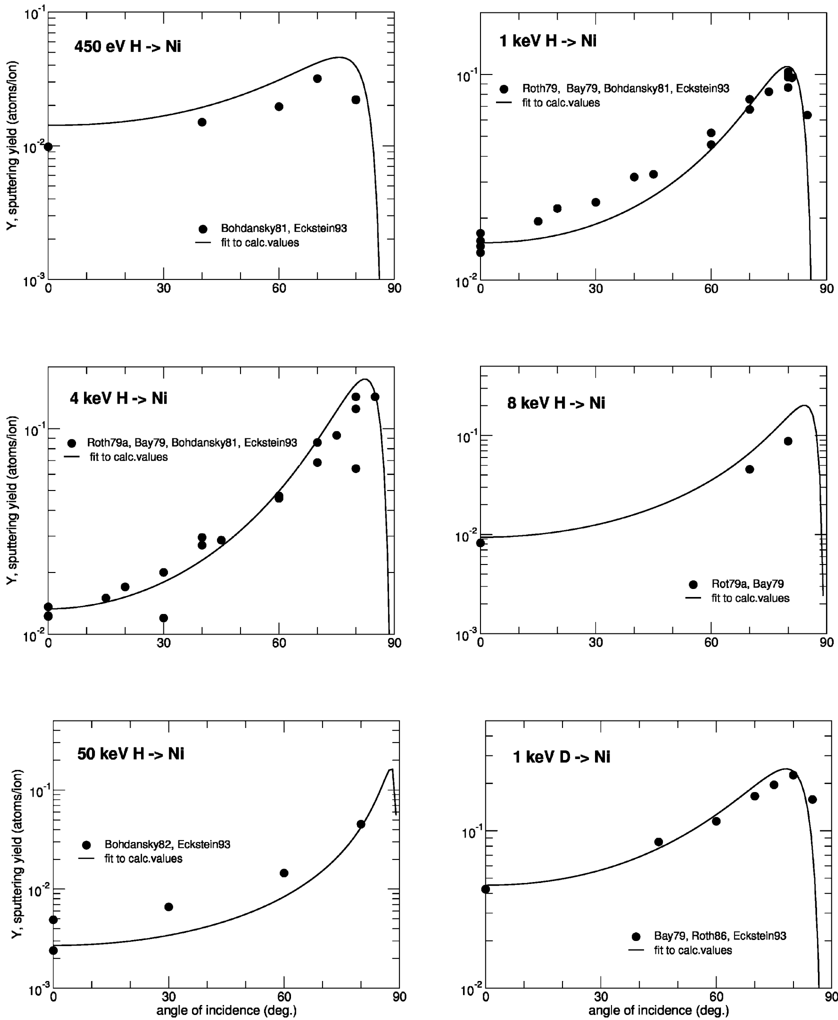

Fig. 69. Comparison of measured and calculated angular dependence of sputtering yields at different energies for different ion–target combinations: 0.45 keV H on Ni [27, 258], 1 keV H on Ni [27, 51, 258, 259], 4 keV H on Ni [27, 51, 258, 259], 8 keV H on Ni [51, 259], 50 keV H on Ni [27, 135], 1 keV D on Ni [27, 253, 259]

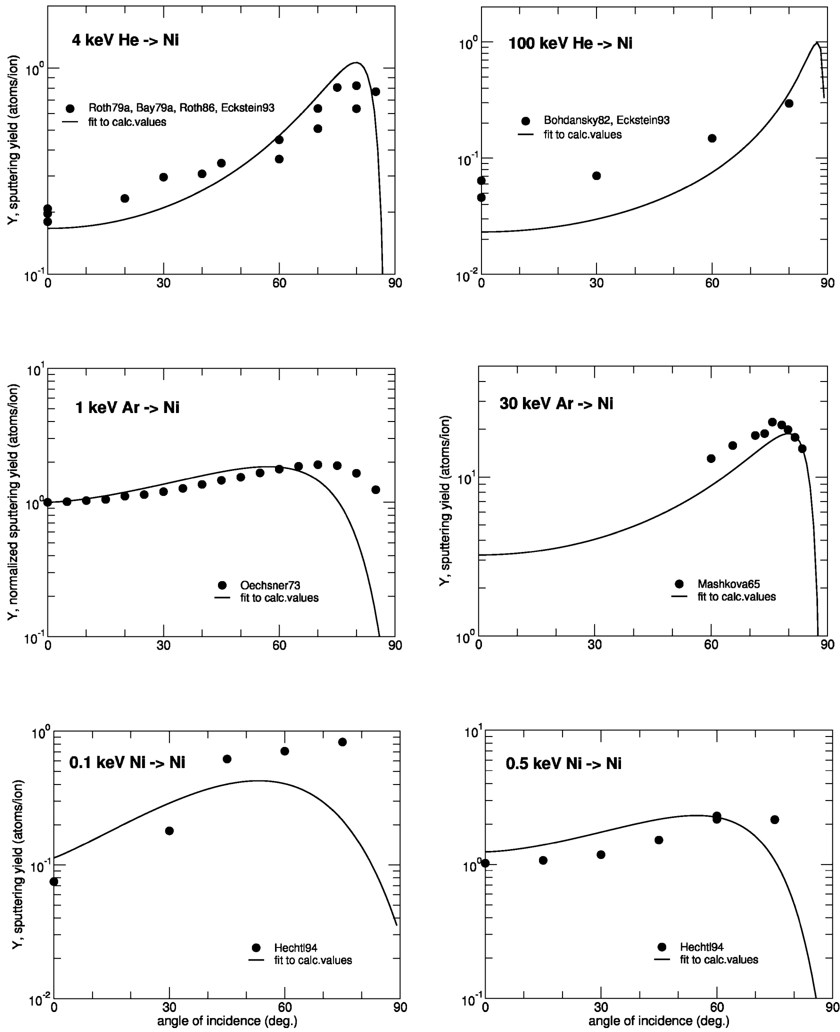

Fig. 70. Comparison of measured and calculated angular dependence of sputtering yields at different energies for different ion–target combinations: 4 keV He on Ni [27, 51, 253, 259], 100 keV He on Ni [27, 135], 1.05 keV Ar on Ni [105], 30 keV Ar on Ni [260], 0.1 keV Ni on Ni [261], 0.5 keV Ni on Ni [261]

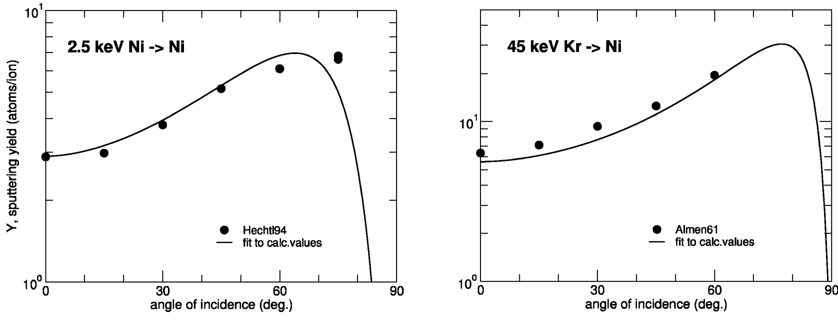

Fig. 71. Comparison of measured and calculated angular dependence of sputtering yields at different energies for different ion–target combinations: 2.5 keV Ni on Ni [261], 45 keV Kr on Ni [90]

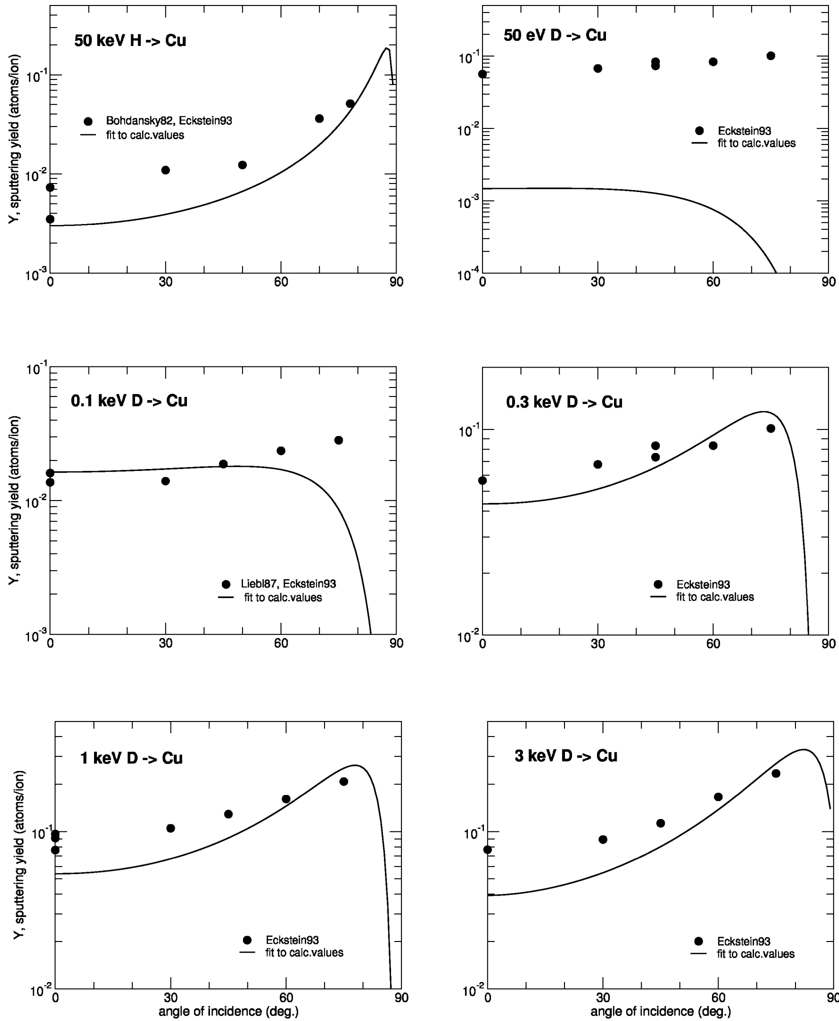

Fig. 72. Comparison of measured and calculated angular dependence of sputtering yields at different energies for different ion–target combinations: 50 keV H on Cu [27, 135], 0.05 keV D on Cu [27], 0.1 keV D on Cu [27, 262], 0.3 keV D on Cu [27], 1 keV D on Cu [27], 3 keV D on Cu [27]

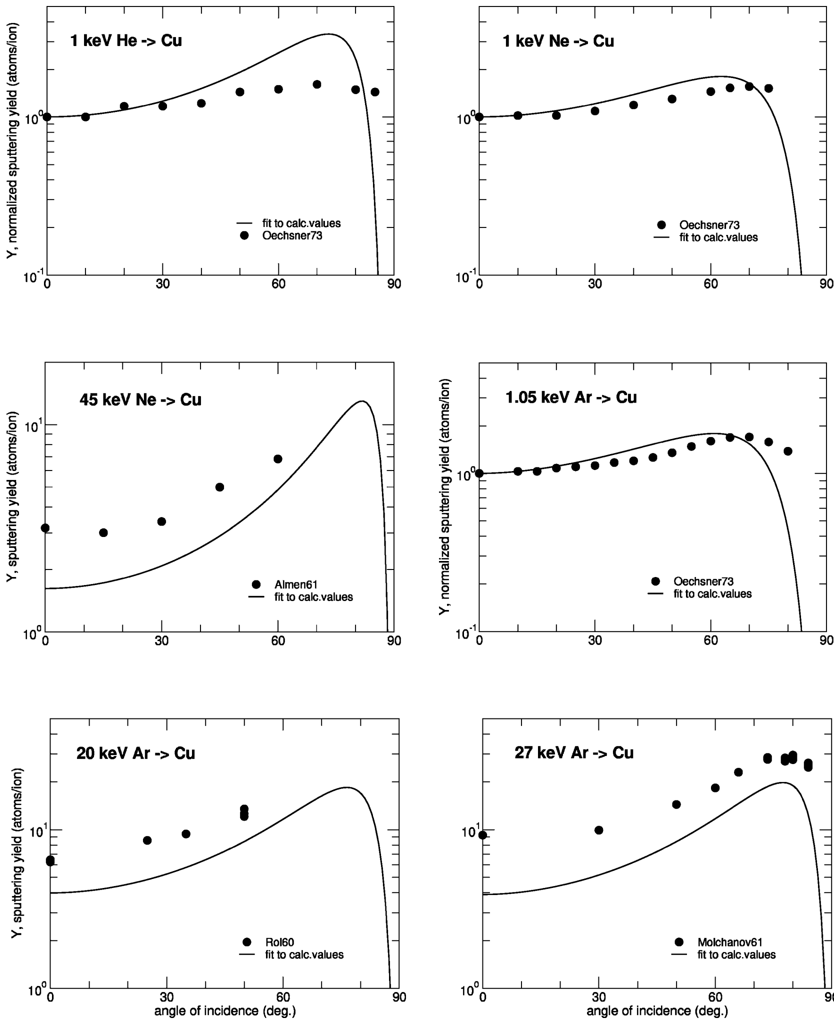

Fig. 73. Comparison of measured and calculated angular dependence of sputtering yields at different energies for different ion–target combinations: 1 keV He on Cu [105], 1 keV Ne on Cu [105], 45 keV Ne on Cu [90], 1.05 keV Ar on Cu [105], 20 keV Ar on Cu [263], 27 keV Ar on Cu [264]

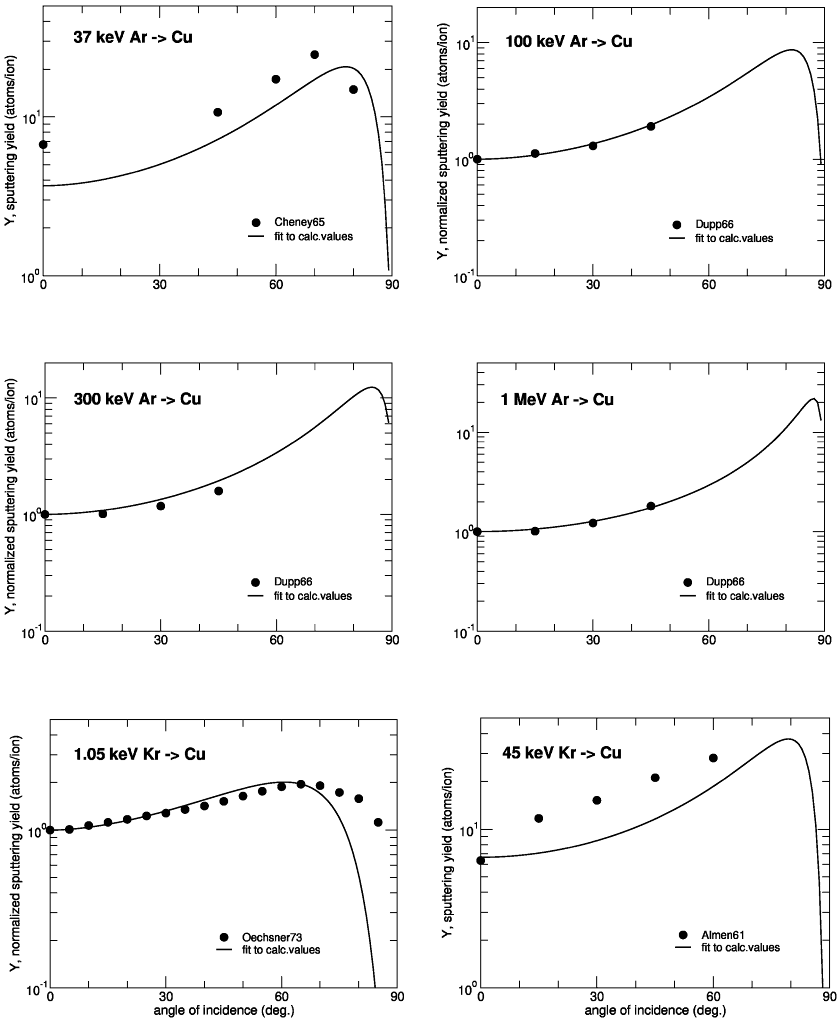

Fig. 74. Comparison of measured and calculated angular dependence of sputtering yields at different energies for different ion–target combinations: 37 keV Ar on Cu [168], 100 keV Ar on Cu [163], 300 keV Ar on Cu [163], 1 MeV Ar on Cu [163], 1.05 keV Kr on Cu [105], 45 keV Kr on Cu [90]

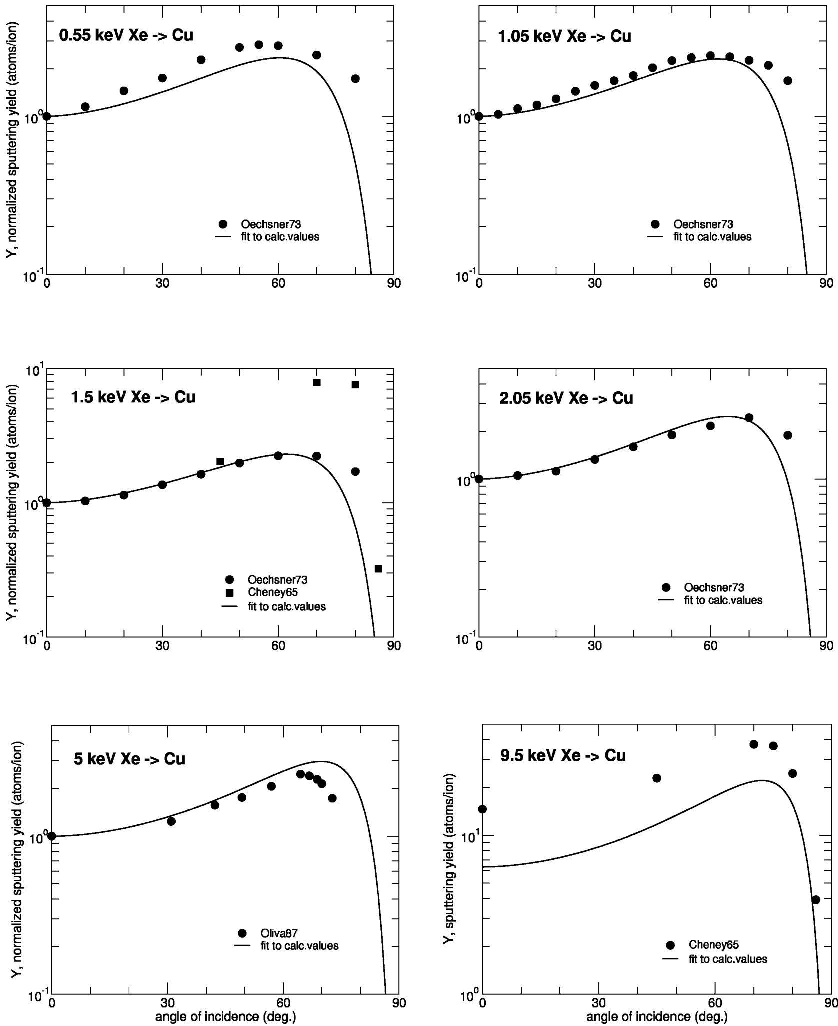

Fig. 75. Comparison of measured and calculated angular dependence of sputtering yields at different energies for different ion–target combinations: 0.55 keV Xe on Cu [105], 1.05 keV Xe on Cu [105], 1.5 keV Xe on Cu [105, 168], 2.05 keV Xe on Cu [105], 5 keV Xe on Cu [174], 9.5 keV Xe on Cu [168]

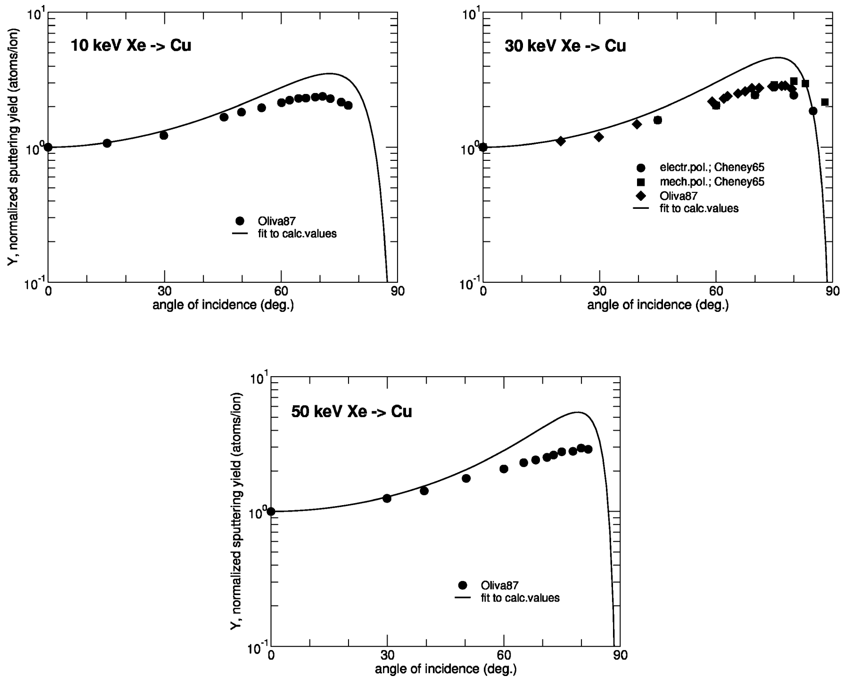

Fig. 76. Comparison of measured and calculated angular dependence of sputtering yields at different energies for different ion–target combinations: 10 keV Xe on Cu [174], 30 keV Xe on Cu [168, 174], 50 keV Xe on Cu [174]

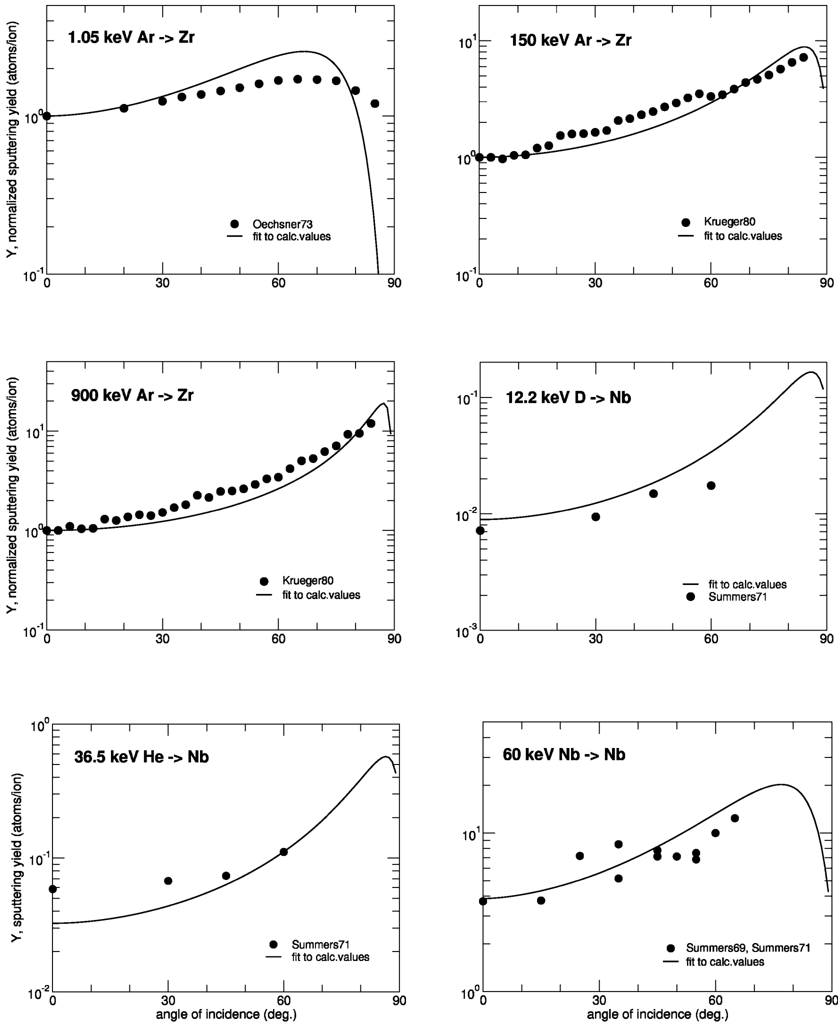

Fig. 77. Comparison of measured and calculated angular dependence of sputtering yields at different energies for different ion–target combinations: 1.05 keV Ar on Zr [105], 150 keV Ar on Zr [257], 900 keV Ar on Zr [257], 12.2 keV D on Nb [185], 36.5 keV He on Nb [185], 60 keV Nb on Nb [185, 193]

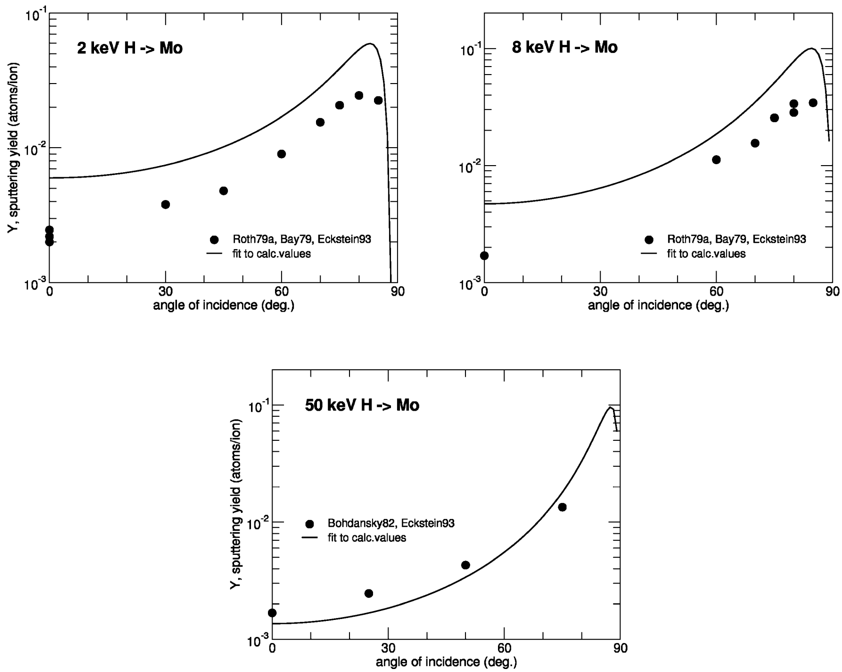

Fig. 78. Comparison of measured and calculated angular dependence of sputtering yields at different energies for different ion–target combinations: 2 keV H on Mo [27, 51, 259], 8 keV H on Mo [27, 51, 259], 50 keV H on Mo [27, 135]

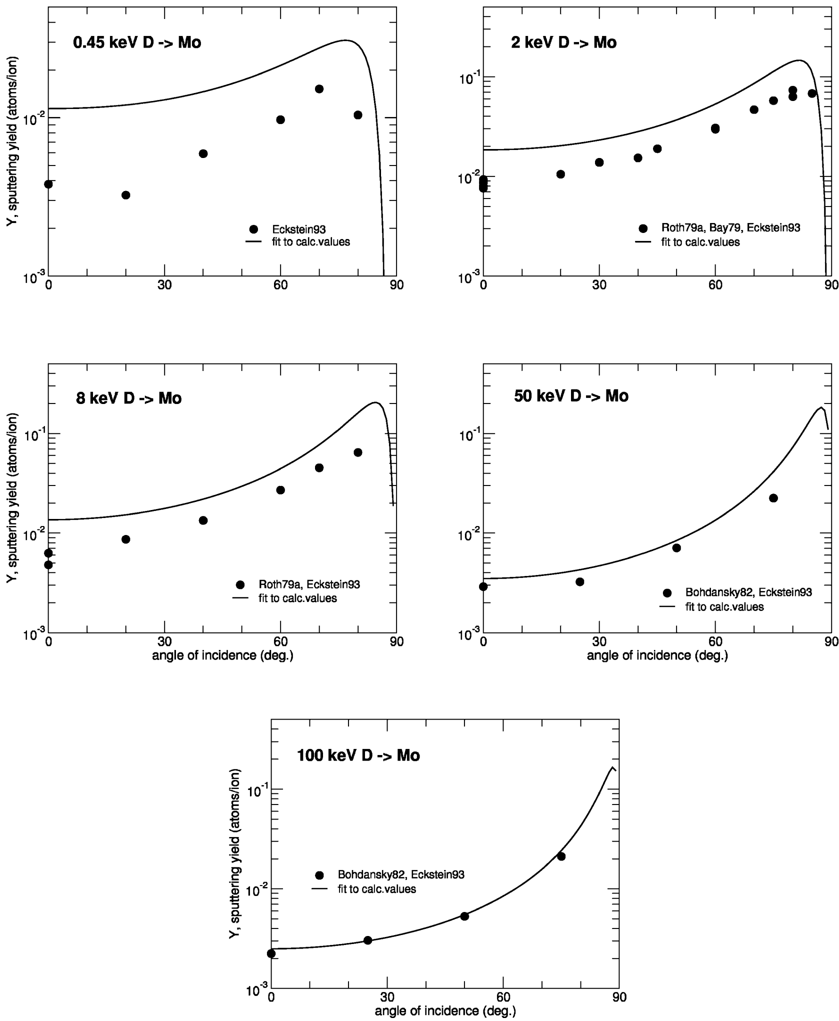

Fig. 79. Comparison of measured and calculated angular dependence of sputtering yields at different energies for different ion–target combinations: 0.45 keV D on Mo [27], 2 keV D on Mo [27, 51, 259], 8 keV D on Mo [27, 51], 50 keV D on Mo [27, 135], 100 keV D on Mo [27, 135]

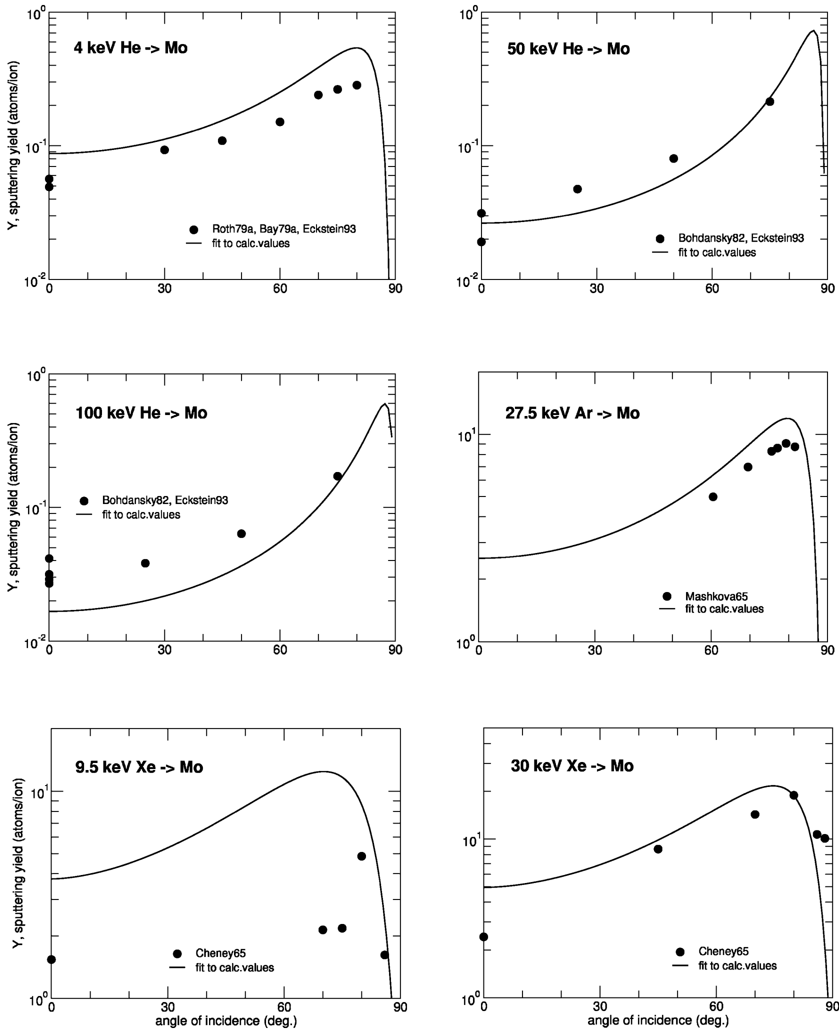

Fig. 80. Comparison of measured and calculated angular dependence of sputtering yields at different energies for different ion–target combinations: 4 keV He on Mo [27, 51, 259], 50 keV He on Mo [27, 135], 100 keV He on Mo [27, 135], 27.5 keV Ar on Mo [260], 9.5 keV Xe on Mo [168], 30 keV Xe on Mo [168]

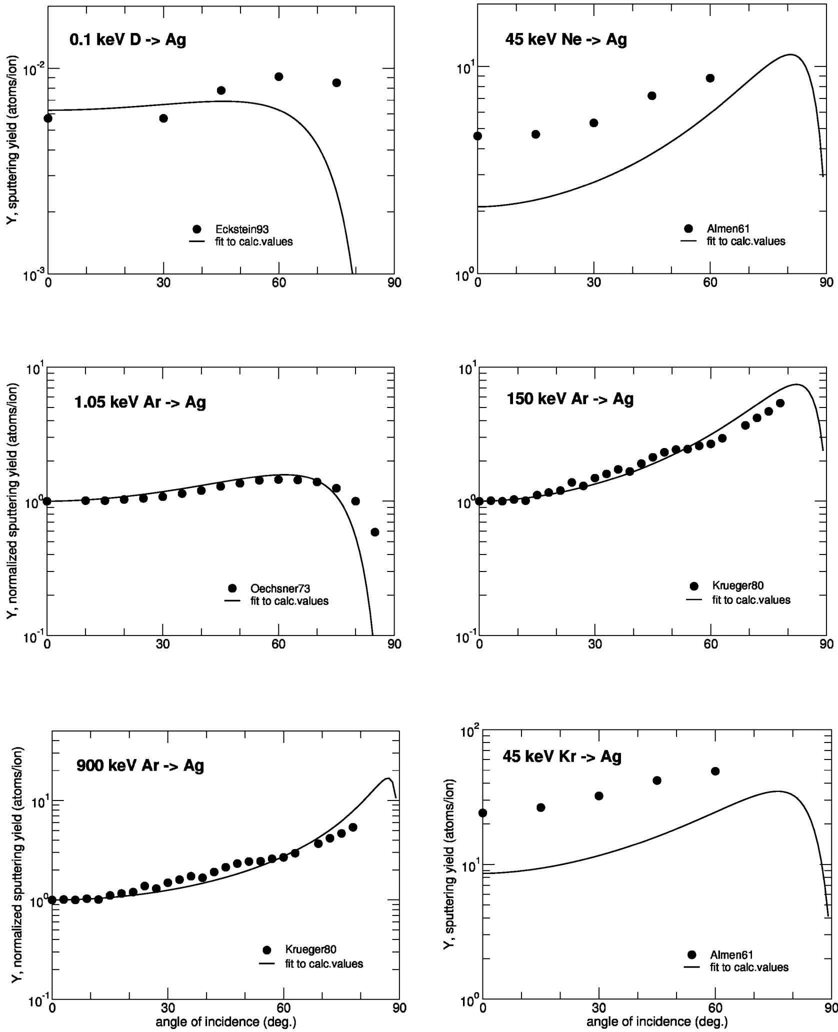

Fig. 81. Comparison of measured and calculated angular dependence of sputtering yields at different energies for different ion–target combinations: 0.1 keV D on Ag [27], 45 keV Ne on Ag [90], 1.5 keV Ar on Ag [105], 150 keV Ar on Ag [257], 900 keV Ar on Ag [257], 45 keV Kr on Ag [90]

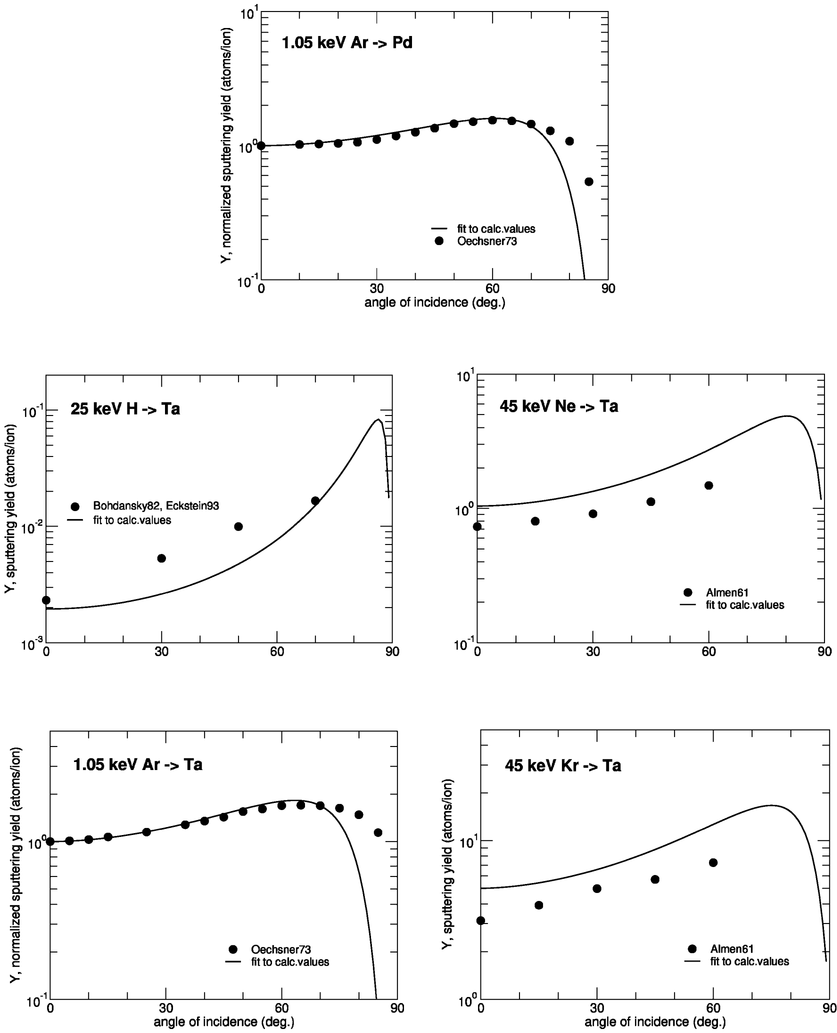

Fig. 82. Comparison of measured and calculated angular dependence of sputtering yields at different energies for different ion–target combinations: 1.05 keV Ar on Pd [105], 25 keV H on Ta [27, 135], 45 keV Ne on Ta [90], 1.5 keV Ar on Ta [105], 45 keV Kr on Ta [90]

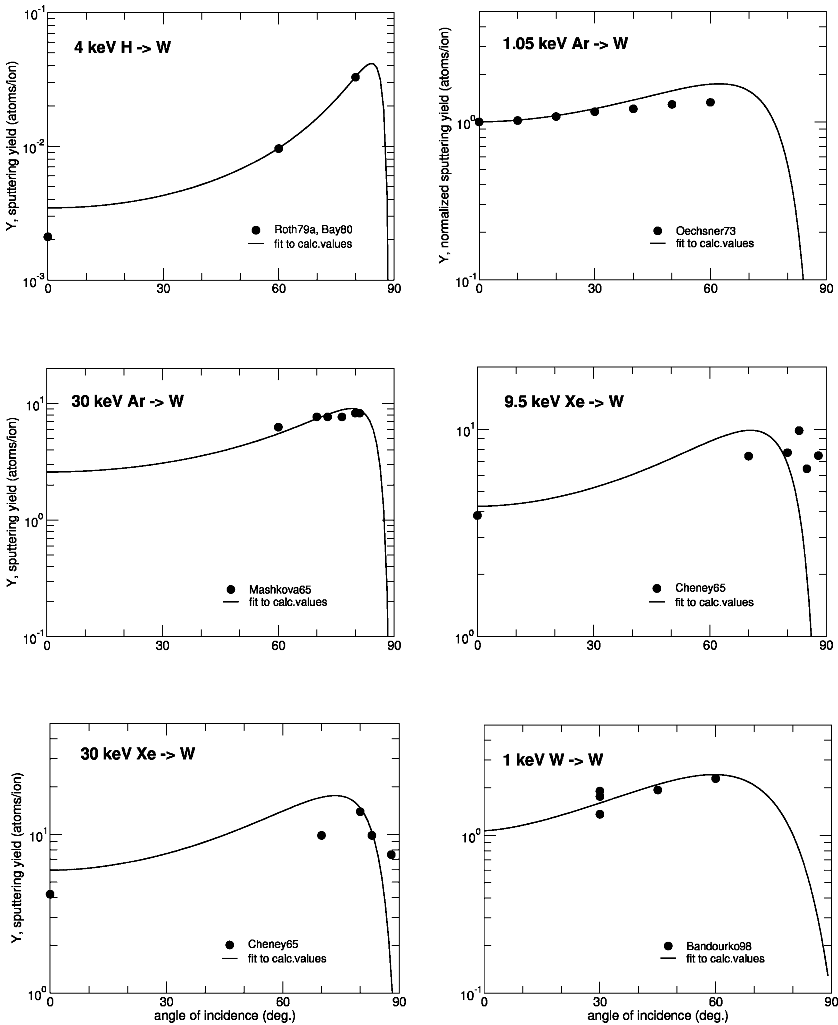

Fig. 83. Comparison of measured and calculated angular dependence of sputtering yields at different energies for different ion–target combinations: 4 keV H on W [51, 265], 1.05 keV Ar on W [105], 30 keV Ar on W [260] 9.5 keV Xe on W [168], 30 keV Xe on W [168], 1 keV W on W [266]

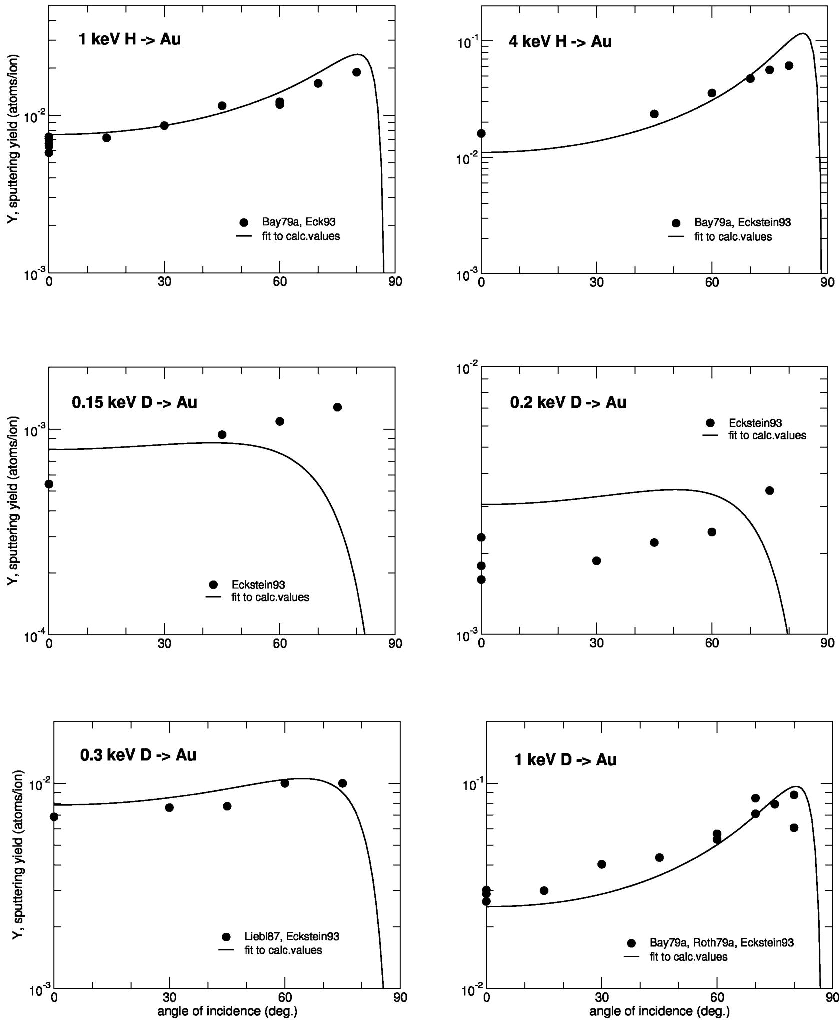

Fig. 84. Comparison of measured and calculated angular dependence of sputtering yields at different energies for different ion–target combinations: 1 keV H on Au [27, 259], 4 keV H on Au [27, 259], 0.15 keV D on Au [27], 0.2 keV D on Au [27], 0.3 keV D on Au [27, 262], 1 keV D on Au [27, 51, 259]

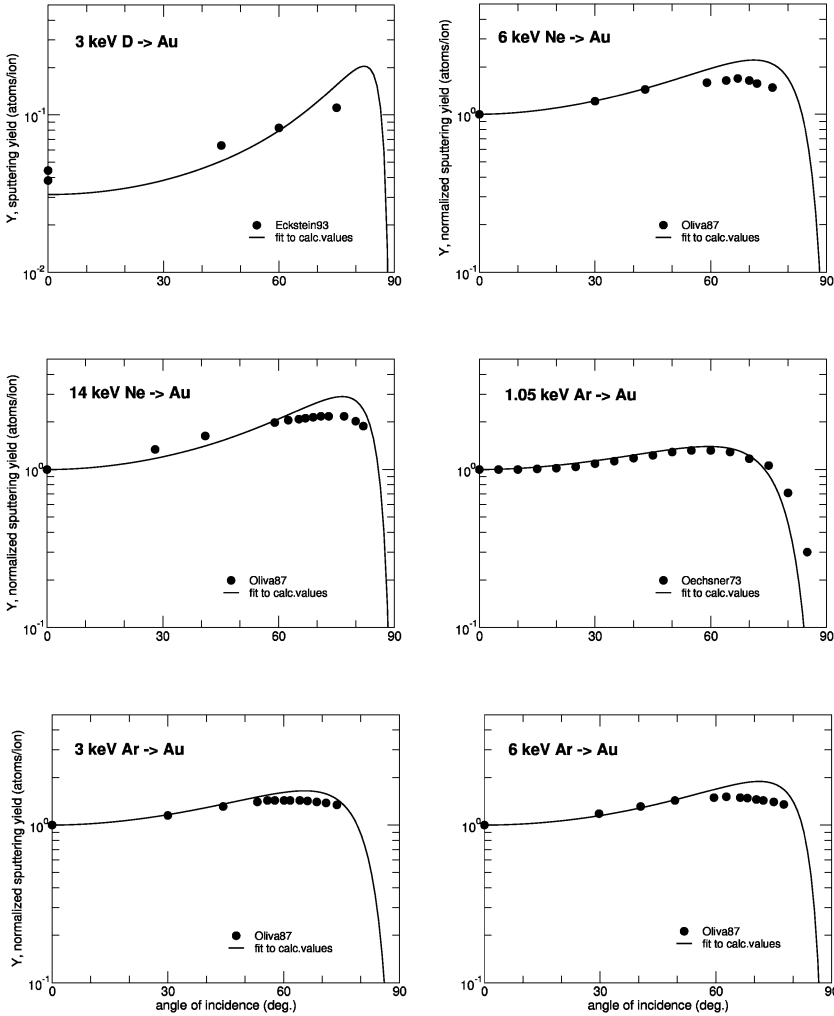

Fig. 85. Comparison of measured and calculated angular dependence of sputtering yields at different energies for different ion–target combinations: 3 keV D on Au [27], 6 keV Ne on Au [174], 14 keV Ne on Au [174], 1.05 keV Ar on Au [105], 3 keV Ar on Au [174], 6 keV Ar on Au [174]

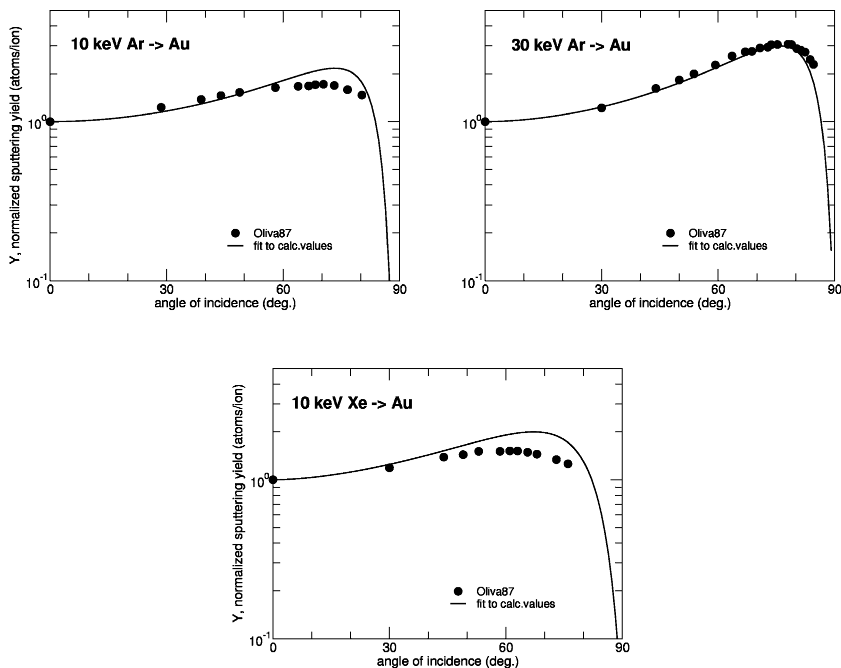

Fig. 86. Comparison of measured and calculated angular dependence of sputtering yields at different energies for different ion–target combinations: 10 keV Ar on Au [174], 30 keV Ar on Au [174], 10 keV Xe on Au [174]

The reasonable agreement of the experimental and calculated yields give again confidence to the calculated values. The angular dependence of the measured sputtering yield is dependent on the roughness of the target. There is a general tendency, that the yield at normal incidence is somewhat higher for rough surfaces than for flat ones and the opposite is true for large angles of incidence. At about 45° the values for flat and rough surfaces are approximately the same. *Küstner* et al. [267, 268] determined the surface roughness with a tunneling microscope and produced from that a distribution of angles of incidence. Using this distribution as input to a Monte Carlo calculation provided a much better agreement of the calculated values with the experimental data. Also the assumption of simple geometrical surface structures in simulation codes gives better agreement with experimental data [269]. For very rough surfaces the experimental yield at the maximum of the angular dependence can be a factor of five lower compared to a polished surface [255].

Citations of experimental data and static calculations of sputtering yields at normal and oblique incidence for elemental targets not included in fits and figures due to limited values. They are summerized in Tables 25–28.

3.5 Threshold Energy of Sputtering

The threshold energy, $E_{\rm th}$, must meet the condition, that the maximum transferable energy in a collision is larger than the surface binding energy. This means, that $E_{\rm th} + E_{\rm sp} > E_{\rm sb}/\gamma$, where $E_{\rm sp}$ is the binding energy of a projectile to the target surface ($E_{\rm sp} = 0$ for noble gas ions), $E_{\rm sb}$ is the surface binding energy (heat of sublimation), and $\gamma = 4M_1M_2/(M_1 + M_2)^2$ is the energy transfer factor in a binary collision. M_1 and M_2 are the masses of the projectile and target atom, respectively. This minimum energy is only an energy consideration, but does not take into account the necessary change in momentum.

The threshold energy cannot be determined directly. It can be obtained by extrapolating the sputtering yields to low energies [52, 188] using a formula such as (2). The threshold energies determined from the calculated sputtering yields by this fitting are shown in Tables 1 to 9. The resulting threshold energies obtained from the data fitting are presented in Fig. 87 in the form of $\gamma(E_{\rm th} + E_{\rm sp})/E_{\rm sb} = E_{\rm th}^{\rm red}$ versus the mass ratio M_2/M_1, because then $E_{\rm th}^{\rm red}$ should approach unity for large mass ratios. At low mass ratios the uncertainty in the threshold energy becomes rather large. Besides the above mentioned energy consideration the momentum reversal for an incident projectile is important. For a light projectile the momentum reversal occurs mainly in one collision of an incident light ion with a heavy target atom [270]. For smaller mass ratios several collisions are necessary for the momentum reversal thus increasing $E_{\rm th}^{\rm red}$ [271]. The scatter of the values shows, that the threshold energies at low mass ratios are not well defined.

The threshold energy depends also on the angle of incidence. It has been shown by simulations, that this dependence is stronger for heavy projectiles than for light incident ions [272].

4 Single Crystalline Materials

The sputtering yields are largely influenced by the crystallinity and the orientation of the crystal relative to the incident ion beam. For incidence parallel to crystal planes and/or low index crystal axes the sputtering yields show pronounced minima [90, 273–276]. In these directions the crystal looks more transparent and the sputtering is reduced. The probability of energy transfer from the incident atoms to lattice atoms in these open directions is reduced. The angular distributions of sputtered atoms are highly anisotropic and the atoms are emitted in closely packed directions. This was first observed experimentally by *Wehner* (Wehner spots) [277] and also established in computer simulations [278]. Surveys of these investigations are given in [1, 276] and in Tables 32 and 33. An example is shown in Fig. 88, where the sputtering yield is presented for the bombardment of Cu(001) with argon for two incident energies and two incident azimuthal angles [279]. At 5 keV incidence the yield

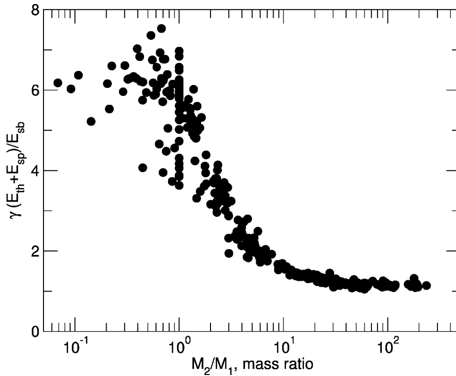

Fig. 87. Threshold energy, $E_{\rm th}$, of the sputtering yield at normal incidence determined by the fitting procedure in the form of $\gamma(E_{\rm th} + E_{\rm sp})/E_{\rm sb}$ versus the mass ratio of target mass divided by ion mass. $E_{\rm sb}$ is the surface binding energy, $E_{\rm sp}$ the binding energy of a projectile to the target surface

shows clear evidence of the open directions, in which the incident ions have a larger penetration depth and show a lower sputtering yield. The experimental data [280] agree nicely with the curves calculated with MARLOWE, although the surface region is damaged in the experiment by the incident beam. Some crystallinity must, therefore, remain after bombardment, at least for metals. It is interesting to note, that at lower energies (0.5 keV) the crystalline behaviour in the sputtering yield has disappeared in the results of the MARLOWE calculations.

5 Multicomponent Targets

Sputtering becomes more complex, if the target consists of two or more different atomic species [281]. This is generally the case, because some of the projectiles are implanted and trapped even in a mono-atomic target (species which form solids as metals, for example). The topic of preferential sputtering belongs to tis section. The complication arises, because the energy transfer from the projectile to the various target species is different and lighter elements have longer ranges. This leads to a target composition change with depth, and consequently to a change of the particle reflection coefficient and the partial sputtering yields, Y_i. In a multicomponent target Y_i is defined in the usual way as the ratio of the sputtered atoms of species (component) i per projectile. The composition changes proceed with bombardment until at some incident fluence a steady state or equilibrium is reached. The situation may become even more complex by compound formation (for example oxides, carbides, etc.), possible diffusion and segregation effects; surface roughness may also change with fluence. Diffusion may be suppressed if the target temperature is low enough.

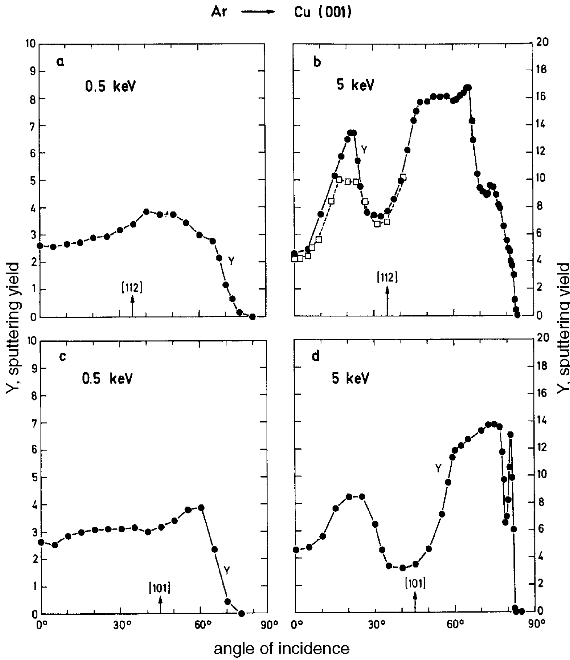

Fig. 88. Dependence of the sputtering yield, Y, on the angle of incidence for the bombardment of a Cu single crystal with a (001) surface. (**a**,**b**) the plane of incidence is parallel to the [110] surface direction. (**c**,**d**) the plane of incidence is parallel to the [100] surface direction (from [279]). *Open squares* in (**b**) are experimental data [280], all *other points* values calculated with MARLOWE

5.1 Fluence Dependence

It is known for a long time, that sputtering depends on fluence, especially for systems such as O bombardment of Al or Si [282] because of a compound formation (oxide). Computer simulations have been performed for a better understanding of these processes. Considering only collisional effects, a distinction can be made between a deposition and an erosion regime in the case of a bombardment with nonvolatile projectiles. If more atoms are implanted than atoms are sputtered, deposition dominates and the situation is that of a deposition regime. The border between the two regimes is given by [283]

$$1 - R_{\mathrm{N}} = \Sigma Y_i = Y_{\mathrm{tot}} \qquad \text{or} \qquad R_{\mathrm{N}} + \Sigma Y_i = 1 \,, \tag{9}$$

where R_{N} is the particle reflection coefficient and Y_i are the partial sputtering yields forming the total sputtering yield, Y_{tot}. Because R_{N} and Y_i depend on the angle of incidence, the border between the two regimes shift with the incident angle. In both regimes steady state is reached, if the partial yields become constant with increasing fluence. In the deposition regime this will

happen, if a layer of the projectile species on top of the original target reaches some thickness, so that backscattered particles and sputtered atoms must come from this layer. The thickness of this layer will still increase with further bombardment, but no other changes will occur due to the selfbombardment. In the erosion case, a final depth distribution of the different species will form at steady state at a sufficiently high fluence. This depth profile will not change anymore with increasing fluence although the target thickness will decrease. Steady state is generally reached for an incident particle fluence, f_{eq}, at which a layer corresponding to the range R of the implanted ions is removed by sputtering, i.e., $f_{\mathrm{eq}} Y_{\mathrm{tot}} = \rho R$, where ρ is the atomic density of the sputtered layer. This gives for the fluence, f_{eq}, to reach steady state or equilibrium [284, 285]

$$f_{\mathrm{eq}} = \rho R / Y_{\mathrm{tot}} \, . \tag{10}$$

The values, R and Y_{tot}, depend on the projectile energy and the angle of incidence. R increases monotonically with energy, whereas Y_{tot} has a maximum at some energy. This means, that f_{eq} has a minimum close to the energy, where the yield has its maximum. For heavy ions, f_{eq} is of the order of 10^{17} atoms/cm^2, whereas for light ions the equilibrium fluence can be much higher. Analoguously, f_{eq} decreases with an increasing angle of incidence until Y_{tot} reaches a maximum.

Impurities of heavy mass atoms or implantation of heavy ions in a target of light elements will increase the sputtering yield due to the larger scattering and larger scattering cross-section. The opposite effect will occur by light atom impurities in a matrix of heavy mass atoms. The first effect has been demonstrated experimentally by the implantation of Xe into Si [130]. Also TRIDYN computer simulation can reproduce this effect in good agreement with the experimental data [286]. This sputtering yield amplification is also called the SYA effect; it has been demonstrated for example by computer calculations with the program T-DYN [287] for the bombardment of thin layers of Al on several metallic substrates with noble gas ions [288].

5.2 Oscillations in the Partial Sputtering Yields

At bombardment of a polycrystalline target consisting of low Z atoms with heavy projectiles in the erosion regime oscillations in the partial sputtering yields have been found [289], see Fig. 89. At the beginning of the bombardment the implanted projectiles built up a profile at a depth corresponding to the mean range, R. Further bombardment broadens and increases the implanted profile. Due to the simultaneous erosion of the surface, the profile moves toward the surface. When the profile reaches the surface, the implanted atoms are removed effectively by selfsputtering. After removal of the implanted layer the partial sputtering yield of implanted atoms is reduced. Further bombardment builds up a new profile of implanted atoms, which

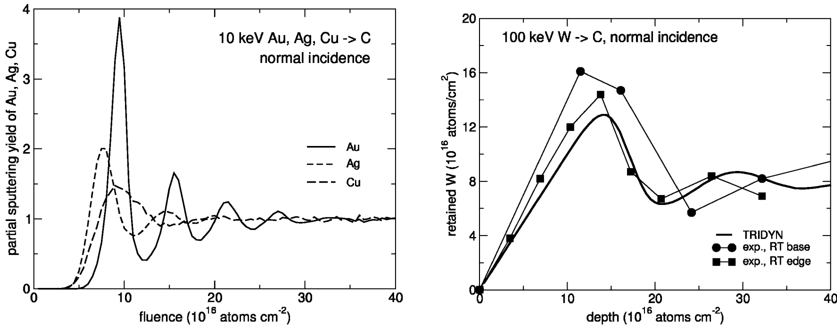

Fig. 89. Fluence dependence of partial sputtering yields for normal incidence bombardment. *Left*: Calculated partial yields due to the bombardment of C with 10 keV Au, Ag, Cu atoms [289]. *Right*: Comparison of measured and calculated retained W in C due to the bombardment od C with 100 keV W atoms [290]

is broader and less pronounced than the first one. This process may repeat a few times until a steady state profile is reached and oscillations die out. The partial sputtering yield of the heavy atoms reach a maximum, when the maximum of the depth profile appears at the surface. The minimum of the profile occurs, when the atomic fraction of the heavy atoms at the surface is lowest. These oscillations have been predicted with TRIDYN computer simulations [289] and have been confirmed by experiment [290]. The oscillatory behaviour will show up only for large mass ratios ($M_2/M_1 > 5$) and not too oblique angles of incidence, and if diffusion and/or segregation can be neglected. A similar example of In implantation into Si [291] can be explained in the same way by collisional effects, although the fluence in this experiment was not large enough to measure oscillations but only the first maximum. In such cases (10) does not apply. Calculated dynamic behaviour of Be and C targets by Cs bombardment has been reported by *Sielanko* and coworkers [292].

5.3 Sputtering of Compounds

Sputtering of compound targets by noble gas ions is always in the erosion regime, if retention of noble gases in the target is neglected. Due to the different energy transfer of the ion to the components of the compound target preferential sputtering will occur, causing different partial yields. The original stoichiometry will be modified in the projectile range. Usually one species is depleted in the target with increasing fluence until some steady state condition is established and the target is sputtered stoichiometrically. In these cases the fluence at which the yields have been measured should be always given. In many experimental results steady state conditions prevail due to the large fluences needed for example in weight change measurements. In Fig. 90 the partial yields of C and Ta due to the bombardment of TaC with 1 keV

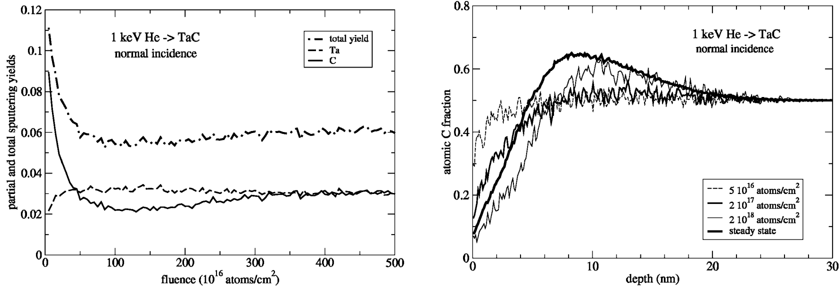

Fig. 90. Calculation of the bombardment of TaC with 1 keV He at normal incidence. *Left*: fluence dependence of partial sputtering yields of C and Ta. *Right*: depth distribution of the C atomic fraction for several fluences and steady state

He at normal incidence are shown versus the incident He fluence. The fluence at which steady state conditions are reached is about 3×10^{18} atoms/cm^2. For hydrogen bombardment this steady state fluence will be even higher, for heavier noble gases it will be lower. The target composition close to the surface resembles more a Ta target than a TaC target as can be seen in Fig. 90 from the C atomic fraction versus depth. The C depletion will be larger for hydrogen bombardment, but smaller for heavy atom incidence. For the bombardment of TiC the preferential sputtering effect is smaller due to the lower mass of Ti compared to Ta and due to the lower surface binding energy of Ti compared to Ta. The experimental equilibrium surface concentrations are close to those calculated [293, 294]. The following compound targets which have been investigated experimentally and by calculations (static calculations which means low fluence) are summarized in Tables 34 to 36.

Another topic in this field is the simultaneous bombardment with two or more species. This occurs for example in fusion plasmas, where the dominant wall bombarding species is hydrogen but with impurities of helium, carbon, oxygen, and heavier ions. All the incident particles have an energy and angular distribution, and due to a sheath potential in front of the vessel wall ions in different charge states are accelerated towards the vessel wall. Such kind of problems have been discussed in [295, 296] for a D influx with C impurity on Be, Si, C, Mo, and W, and in [297] for D and ^{4}He bombardment of carbon material.

5.4 Isotope Sputtering

The sputtering of isotope mixtures is also nonstoichiometric at low fluence. In most cases the lighter isotope is sputtered preferentially. This is usually described by the value of fractionation, which is defined as

$$\delta = \frac{Y(M_i)}{Y(M_j)} \frac{N_j}{N_i} - 1 \,, \tag{11}$$

where $Y(M_i)$ and $Y(M_j)$ are the partial sputtering yields of mass M_i and M_j, respectively, and N_i and N_j are the normalized abundances ($\sum N_k = 1$) of species i and j, respectively. The first theoretical prediction for the partial sputtering yield ratio has been given by analytic theory [298] and has been reviewed in [299]

$$\frac{Y(M_i)}{Y(M_j)} = \frac{N_i}{N_j} \left(\frac{M_j}{M_i}\right)^{2m} . \tag{12}$$

This gives a value for the fractionation, which is only dependent on the mass ratio:

$$\delta = \left(\frac{M_j}{M_i}\right)^{2m} - 1 . \tag{13}$$

The value m is the parameter in the power potential. It should be smaller than unity and has been chosen between 0.05 and 0.3. BCA computer simulations found a value of about 1/6 from the high energy slope of energy distributions of sputtered atoms [28, 300]. Because of the similar masses and the small value of m, the value of δ is of the order of a few percent. Measurements and computer simulations have shown, that isotope sputtering is more complex than predicted by the analytic theory. Measurements found, that the fractionation depends on the polar emission angle of sputtered atoms [301]. This was also found by molecular dynamics [302] and by Monte Carlo calculations [272]. The main result of these newer investigations are, that the fractionation is generally larger than expected from formula (13), see also [303–305]. Further computer simulation studies have shown, that the fractionation shows an energy and a weak incident angular dependence [285]. The main reason for the discrepancy between the theoretical result and the computed finding is the neglect of PKA in the theoretical approach. The simulations show clearly, that the energy and angular dependence originate predominantly from PKAs. Their contribution becomes dominant at low energies, especially near the threshold. The SKAs, which are only regarded in the analytic theory, show also in the simulations nearly no energy or angular dependence. Isotope sputtering is an important subject in planetary science [306].

6 Temperature Dependence of the Sputtering Yield

The collisional sputtering should not depend on temperature, at least for randomized target structures as long as the surface binding energy is constant. However, the surface binding energy (heat of sublimation) shows a small step at the solid–liquid transition. This step is of the order of 0.1 eV and the effect on the sputtering yield is very small and in experiments it is obscured by the onset of vaporization [307]. For single crystals lattice vibrations and

annealing of lattice damage influence the Wehner spots or channeling dips in the sputtering yield [276]. In the case of multicomponent targets diffusion and segregation can change the collisional results largely as found experimentally [308, 309] and modelled by simulations. For temperatures close to the melting point an exponential increase of the erosion yield is found experimentally. This can be attributed to evaporation [208, 310].

The influence of the magnetic state has been investigated for Fe and Ni single crystals by [311, 312] with MD; the effect is a consequence of slight changes in the interaction potential for the paramagnetic and the ferromagnetic state.

New experiments found subthreshold sputtering at high temperatures in the case of sputtering of tungsten at 1470 K [313] and at higher temperatures (2500 to 3400 K) [314]. The measured yield is reported to be about 10^{-4} for 5 eV D bombardment. The effect is explained by sputtering of weakly bound adsorbed W atoms at the surface due to damage and the near surface implantation of gaseous atoms below the surface. Similar effects have been reported for Li [315] and Sn [316].

7 Yield Fluctuations

The sputtering yield shows fluctuations, i.e., a different yield for every incident ion, due to the stochastic slowing down process of projectiles and recoils in the target. These fluctuations are not accessible experimentally but theoretically and by computer simulation. *Harrison* [22] called them ASI distributions (for "atoms per single ion"). A theoretical approach [317] did not give any distributions but predicted large fluctuations. In a more detailed investigation [318,319] the probability distributions of the sputtering yield were calculated by Monte Carlo simulations for Nickel bombarded with several ions at different incident energies and angles of incidence. The distributions were fitted with the two-parametric negative binomial distribution

$$L_{\zeta\eta} = \frac{\Gamma(n+\zeta\eta)\phi^{\zeta\eta}}{n!\Gamma(\zeta\eta)(1+\eta)^{n+\zeta\eta}}\,, \tag{14}$$

where n is an integer and ζ, η are parameters. The negative binomial distribution is broader than a Poisson distribution with the same yield (mean value of the distribution). Only at low energies and normal incidence the distributions were close to a Poisson distribution. At higher energies and oblique angles of incidence up to 100 atoms per single ion can be sputtered, see Fig. 91. This may explain the surface roughening by ion bombardment.

In another investigation the r^{-m} power potential was used in a Monte Carlo program [320]. The calculated distributions could not be fitted by a negative binomial distribution.

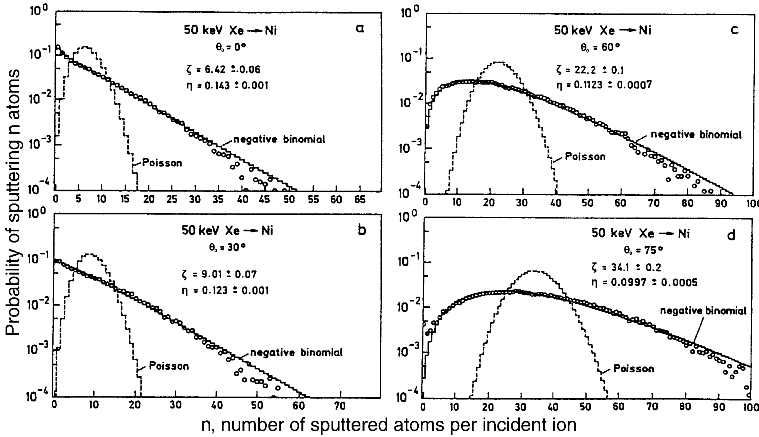

Fig. 91. Probability of sputtering n atoms versus the number, n, of sputtered atoms per single projectile. Ni is bombarded with 50 keV Xe at four angles of incidence, θ_0. The open circles show the distributions calculated with TRIM.SP [318]. The values ζ and η are the parameters of the negative binomial distribution, where $\zeta = Y$ and η is a measure of the width of the distribution. The corresponding Poisson distribution is given for comparison

8 Time Evolution of the Sputtering Yield

The sputtered atoms need time to leave the target from their original site. According to their depth of origin, their path to the surface and their energy, a distribution of escape times will develop. Whereas time is naturally included in MD programs, it is not necessary in BCA programs. But time has been incorporated, in MARLOWE [321], ACAT [322] and in TRIM [323–325]. Simulations have shown [22, 325–327], that the escape times of sputtered atoms are typically less than one ps. Light sputtered atoms show a shorter escape time than heavy atoms as demonstrated in Fig. 92.

The maximum of the escape time dependence of the yield exhibit a shorter time for oblique incidence than for normal incidence. Also the energy and angular distributions of sputtered atoms show a time dependence [325, 327].

9 Conclusions

The sputtering process of ion bombardment with energies from the threshold to the MeV range can be well described by BCA computer programs. The sputtering yields for many ion–target combinations agree in most cases very well with experimental yields. For practical use the constants in the algebraic formulae for the energy and angular dependence of the sputtering yield for mono-atomic targets have been determined and summarized in tables.

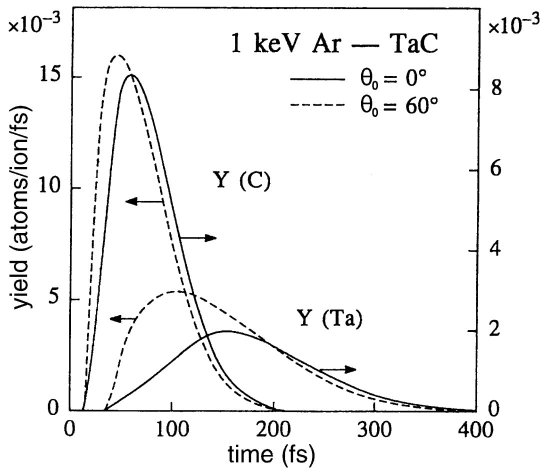

Fig. 92. Sputtering yield versus time for the bombardment of TaC with 1 keV Ar at two angles of incidence, θ_0, Fig. 1b of [325]

Table 1. Fitting values λ, q, μ for the energy dependence of the sputtering yield $Y(E_0)$ at normal incidence in (2). In addition, the threshold energy, E_{th}, the reduced energy, ε, the surface binding energy, E_{sb}, and E_{sb}/γ are given

Ion	Target	λ	q	μ	E_{th} (eV)	ε	E_{sb} (eV)	E_{sb}/γ
H	Li	0.9540	0.0833	1.4705	5.6499	1.85375e+2	1.67	3.76
D	Li	1.4358	0.1321	1.2091	4.6359	2.08692e+2	1.67	2.40
T	Li	1.8839	0.1629	0.9741	4.8558	2.32243e+2	1.67	1.98
^{4}He	Li	1.9370	0.3617	1.2501	6.5037	5.56715e+2	1.67	1.80
Li	Li	8.2237	0.5159	1.7546	5.5264	1.12841e+3	1.67	1.67
H	Be	0.8007	0.0564	1.5147	14.340	2.56510e+2	3.38	9.32
D	Be	1.7575	0.1044	1.9906	9.5059	2.82110e+2	3.38	5.67
T	Be	2.0794	0.1379	1.5660	9.4345	3.07966e+2	3.38	4.49
^{3}He	Be	0.7725	0.3310	1.6036	12.8963	6.65344e+2	3.38	4.49
^{4}He	Be	1.4745	0.3193	1.6989	12.3288	7.19545e+2	3.38	3.97
Be	Be	2.0334	0.8241	1.3437	16.9689	2.20796e+3	3.38	3.38
N	Be	5.2833	0.9334	2.5368	16.5425	5.46566e+3	3.38	3.55
O	Be	1.2209	1.2024	1.6881	22.6648	6.97104e+3	3.38	3.67
Ne	Be	2.5474	1.8309	1.9400	22.7750	1.06588e+4	3.38	3.96
Ar	Be	0.8082	3.2032	1.5058	37.1816	3.68450e+4	3.38	5.63
Kr	Be	0.3844	5.3588	1.9600	61.452	1.67028e+5	3.38	9.64
Xe	Be	0.4779	8.1740	1.8350	86.942	4.23834e+5	3.38	14.06
H	B	0.8989	0.0329	1.3689	28.5753	3.32864e+2	5.73	18.33
D	B	1.0068	0.0686	1.4105	20.255	3.61025e+2	5.73	10.84
T	B	2.0179	0.1107	1.3317	18.2282	3.89468e+2	5.73	8.39
^{3}He	B	1.2373	0.2013	1.5394	20.829	8.35205e+2	5.73	8.39
^{4}He	B	0.9493	0.2551	0.9796	23.533	8.94388e+2	5.73	7.27
B	B	3.1629	0.9355	1.5939	26.7860	3.71634e+3	5.73	5.73
O	B	0.8342	1.0128	1.1909	44.783	8.02325e+3	5.73	5.95
Ne	B	0.8654	1.3272	1.1180	47.0718	1.21179e+4	5.73	6.31
H	C	1.3533	0.0241	1.4103	38.630	4.14659e+2	7.41	25.89
D	C	1.2848	0.0539	1.1977	27.770	4.46507e+2	7.41	15.08
T	C	1.9050	0.0718	1.1512	23.617	4.78673e+2	7.41	11.54
^{3}He	C	0.7341	0.2058	1.1956	29.883	1.02061e+3	7.41	11.54
^{4}He	C	4.5910	0.1951	1.7852	19.124	1.08716e+3	7.41	9.88
C	C	13.9666	0.7015	2.0947	21.4457	5.68684e+3	7.41	7.41
N	C	5.4288	0.7481	1.7701	34.9372	7.37899e+3	7.41	7.45
O	C	9.6110	1.0171	2.0102	34.1293	9.29758e+3	7.41	7.56
Ne	C	2.5015	1.1912	1.6551	46.6904	1.39308e+4	7.41	7.92
Ar	C	1.2622	2.4576	1.3952	68.8460	4.57989e+4	7.41	10.42
Kr	C	1.3628	3.4372	2.2366	88.2918	1.99609e+5	7.41	16.90
Xe	C	0.4408	4.3004	1.7734	145.4236	4.98349e+5	7.41	24.13
Mg	Mg	0.2574	5.3651	1.6993	8.5706	2.86599e+4	1.54	1.54
Ar	Mg	0.2522	7.5660	1.8294	10.7751	6.10685e+4	1.54	1.64
Kr	Mg	0.2655	13.1219	2.1498	13.1728	2.37254e+5	1.54	2.21

Table 2. Fitting values λ, q, μ for the energy dependence of the sputtering yield $Y(E_0)$ at normal incidence in (2). In addition, the threshold energy, E_{th}, the reduced energy, ε, the surface binding energy, E_{sb}, and E_{sb}/γ are given

Ion	Target	λ	q	μ	E_{th} (eV)	ε	E_{sb} (eV)	E_{sb}/γ
H	Al	0.4138	0.0469	1.6177	30.2224	1.05916e+3	3.36	24.15
D	Al	0.2912	0.1076	1.3913	18.4706	1.09700e+3	3.36	13.02
T	Al	0.3384	0.1628	1.3777	14.067	1.13522e+3	3.36	9.28
^{3}He	Al	0.2670	0.4034	2.2720	14.217	1.37037e+3	3.36	9.28
^{4}He	Al	0.2072	0.3889	1.3234	14.0994	2.44780e+3	3.36	7.47
N	Al	0.3513	2.0764	1.7955	13.6115	1.28804e+4	3.36	3.73
Ne	Al	0.3813	3.0949	1.7394	16.904	2.22732e+4	3.36	3.43
Al	Al	0.6008	3.9180	1.9550	16.0955	3.45451e+4	3.36	3.36
Ar	Al	0.4713	4.7928	2.0810	21.5497	6.28194e+4	3.36	3.49
Kr	Al	0.3085	8.4547	1.9648	28.6055	2.39411e+5	3.36	4.56
Xe	Al	0.2200	11.9561	1.9797	37.3796	5.63459e+5	3.36	5.94
H	Si	0.4819	0.0276	0.9951	49.792	1.16317e+3	4.70	35.07
D	Si	0.5326	0.0569	1.6537	24.543	1.20314e+3	4.70	18.85
T	Si	0.4112	0.0816	0.9325	21.298	1.24352e+3	4.70	13.41
^{3}He	Si	0.3065	0.1823	1.3953	21.405	2.59209e+3	4.70	13.41
^{4}He	Si	0.2524	0.2319	1.4732	18.899	2.67374e+3	4.70	10.77
N	Si	0.4888	1.4367	1.7970	16.6977	1.38909e+4	4.70	5.29
Ne	Si	0.2995	2.0693	1.5152	23.412	2.39034e+4	4.70	4.83
Si	Si	0.6726	2.6951	1.7584	20.035	4.10661e+4	4.70	4.70
Ar	Si	0.2770	3.2299	1.5284	32.8380	6.67979e+4	4.70	4.85
Kr	Si	0.3000	6.3659	1.7639	39.5819	2.52242e+5	4.70	6.25
Xe	Si	0.3076	8.4521	1.6342	45.1518	5.91044e+5	4.70	8.09
Ca	Ca	0.0968	6.6980	1.5276	10.679	9.43891e+4	1.83	1.83
Sc	Sc	0.3163	5.8720	1.7448	16.804	1.05770e+5	3.49	3.49
H	Ti	0.6214	0.0207	0.9427	77.1765	2.05415e+3	4.89	60.45
D	Ti	0.3491	0.0565	1.3957	39.259	2.09615e+3	4.89	31.63
T	Ti	0.3469	0.0887	1.1426	29.3389	2.13856e+3	4.89	21.91
^{3}He	Ti	0.3632	0.1456	1.1171	31.303	4.41677e+3	4.89	21.91
^{4}He	Ti	0.2053	0.2036	1.6310	24.5359	4.50177e+3	4.89	17.19
N	Ti	0.2321	1.8168	2.0297	16.5403	2.07557e+4	4.89	6.98
Ne	Ti	0.2317	2.6253	1.8113	19.564	3.39688e+4	4.89	5.86
Ar	Ti	0.3152	4.8957	1.8291	25.019	8.56428e+4	4.89	4.93
Ti	Ti	0.3217	4.9010	1.6929	24.356	1.17898e+5	4.89	4.89
Kr	Ti	0.4445	8.4878	2.2691	30.9784	2.89844e+5	4.89	5.28
Xe	Ti	0.2234	12.9890	1.8943	39.6382	6.42730e+5	4.89	6.24
H	V	0.7528	0.0234	1.7703	79.7078	2.17329e+3	5.33	69.90
D	V	0.6688	0.0606	1.6983	42.766	2.21513e+3	5.33	36.49
T	V	0.1885	0.0630	1.4064	33.343	2.25738e+3	5.33	25.22
^{3}He	V	0.5942	0.1590	1.2342	34.402	4.65839e+3	5.33	25.22
^{4}He	V	0.1705	0.2146	1.4230	29.0921	4.74299e+3	5.33	19.74
N	V	0.2801	1.9363	2.1837	18.4653	2.16246e+4	5.33	7.88
Ne	V	0.1444	3.3295	1.8660	23.1560	3.52128e+4	5.33	6.56
Ar	V	0.2139	5.2774	1.9274	29.797	8.78018e+4	5.33	5.41
V	V	0.3015	6.7315	1.6807	25.9840	1.30783e+5	5.33	5.33
Kr	V	0.3500	9.4796	2.2023	34.6199	2.93342e+5	5.33	5.67
Xe	V	0.2601	13.9197	2.0005	41.6428	6.45981e+5	5.33	6.62

Table 3. Fitting values λ, q, μ for the energy dependence of the sputtering yield $Y(E_0)$ at normal incidence in (2). In addition, the threshold energy, $E_{\rm th}$, the reduced energy, ε, the surface binding energy, $E_{\rm sb}$, and $E_{\rm sb}/\gamma$ are given

Ion	Target	λ	q	μ	$E_{\rm th}$ (eV)	ε	$E_{\rm sb}$ (eV)	$E_{\rm sb}/\gamma$
H	Cr	0.3673	0.0405	1.4998	65.8795	2.29573e+3	4.12	55.11
D	Cr	0.2899	0.1084	1.7152	35.024	2.33904e+3	4.12	28.75
T	Cr	0.2663	0.1776	1.8134	25.074	2.38278e+3	4.12	19.85
^{3}He	Cr	0.1869	0.2985	1.3060	28.803	4.91344e+3	4.12	19.85
^{4}He	Cr	0.3120	0.3508	1.8564	21.611	5.00096e+3	4.12	15.53
Ne	Cr	0.2550	5.8847	2.2414	18.550	3.68638e+4	4.12	5.11
Ar	Cr	0.3285	7.6222	2.3546	22.3536	9.15022e+4	4.12	4.19
Cr	Cr	0.3472	9.6358	2.1501	21.4357	1.44437e+5	4.12	4.12
Kr	Cr	0.3681	13.4719	2.4061	26.2860	3.04062e+5	4.12	4.36
Xe	Cr	0.0642	20.0590	1.7830	35.7764	6.67613e+5	4.12	5.07
H	Mn	0.5704	0.0774	2.5497	43.501	2.41819e+3	2.92	41.18
D	Mn	0.3203	0.2007	1.7627	25.5675	2.46141e+3	2.92	21.44
T	Mn	0.2140	0.3193	1.8198	18.5434	2.50506e+3	2.92	14.78
^{3}He	Mn	0.1201	0.5548	1.9758	19.7689	5.16191e+3	2.92	14.78
^{4}He	Mn	0.2061	0.6680	1.8364	16.4824	5.24919e+3	2.92	11.54
Ar	Mn	0.1275	14.2168	1.9572	17.9964	9.37995e+4	2.92	2.99
Kr	Mn	0.1164	24.5351	1.8377	21.0972	3.08095e+5	2.92	3.05
Xe	Mn	0.0978	32.8089	1.7796	23.9217	6.72160e+5	2.92	3.51
H	Fe	0.8696	0.0339	1.8635	67.2578	2.54382e+3	4.34	62.19
D	Fe	0.2743	0.0919	1.3489	40.8547	2.58856e+3	4.34	32.36
T	Fe	0.3131	0.1545	1.3250	28.9747	2.67374e+3	4.34	22.29
^{3}He	Fe	0.2630	0.2780	1.5947	29.6538	5.42342e+3	4.34	22.29
^{4}He	Fe	0.1836	0.3347	1.8574	24.2208	5.51371e+3	4.34	17.40
N	Fe	0.2590	2.7806	2.3278	16.6110	2.46747e+4	4.34	6.77
Ne	Fe	0.2608	4.4877	2.3857	18.7098	3.98491e+4	4.34	5.56
Ar	Fe	0.3517	7.5705	2.3822	22.5719	9.75914e+4	4.34	4.46
Fe	Fe	0.3409	11.0481	1.8048	13.7676	1.74096e+5	4.34	4.34
Kr	Fe	0.3296	13.8062	2.2461	27.8579	3.19107e+5	4.34	4.52
Xe	Fe	0.2492	19.8866	2.1631	32.2100	6.94435e+5	4.34	5.18
H	Co	0.4456	0.0396	1.7711	77.3535	2.66922e+3	4.43	66.85
D	Co	0.2832	0.1085	1.6859	42.1606	2.71375e+3	4.43	34.72
T	Co	0.3065	0.1689	1.4653	30.5090	2.75873e+3	4.43	23.88
^{3}He	Co	0.1762	0.3000	1.4515	33.4129	5.67719e+3	4.43	23.88
^{4}He	Co	0.1652	0.3649	1.8250	25.9871	5.76700e+3	4.43	18.61
Ne	Co	0.0828	5.1602	2.2943	20.8124	4.11463e+4	4.43	5.83
Ar	Co	0.2709	8.4019	2.3291	23.8571	9.98420e+4	4.43	4.60
Co	Co	0.3615	11.6517	2.3889	22.5211	1.90123e+5	4.43	4.43
Kr	Co	0.3021	14.5284	2.2207	28.5342	3.22806e+5	4.43	4.57
Xe	Co	0.2561	20.8948	2.1435	32.0848	6.98061e+5	4.43	5.18

Table 4. Fitting values λ, q, μ for the energy dependence of the sputtering yield $Y(E_0)$ at normal incidence in (2). In addition, the threshold energy, E_{th}, the reduced energy, ε, the surface binding energy, E_{sb}, and E_{sb}/γ are given

Ion	Target	λ	q	μ	E_{th} (eV)	ε	E_{sb} (eV)	E_{sb}/γ
H	Ni	0.6039	0.0334	2.0121	72.9013	2.79866e+3	4.46	67.06
D	Ni	0.2649	0.0904	1.6534	42.0439	2.84552e+3	4.46	34.84
T	Ni	0.3185	0.1734	1.3881	30.7743	2.89285e+3	4.46	23.96
^{3}He	Ni	0.1421	0.3183	1.3582	33.9111	5.94964e+3	4.46	23.96
^{4}He	Ni	0.2024	0.3704	1.9128	25.3764	6.04409e+3	4.46	18.67
N	Ni	0.1941	2.9510	2.0380	18.4448	2.67793e+4	4.46	7.17
O	Ni	0.2107	3.4027	2.2297	18.3954	3.18555e+4	4.46	6.63
Ne	Ni	0.2478	4.5041	2.4046	18.7208	4.30554e+4	4.46	5.86
Ar	Ni	0.3068	7.9565	2.3102	23.3069	1.04416e+5	4.46	4.63
Ni	Ni	6.5700	11.8130	2.7875	11.7462	2.06960e+5	4.46	4.46
Kr	Ni	1.9541	13.5535	2.5909	18.1503	3.37355e+5	4.46	4.60
Xe	Ni	1.3490	20.8734	2.3649	21.2671	7.29221e+5	4.46	5.22
H	Cu	0.5015	0.0566	1.9914	61.7219	2.92563e+3	3.52	57.14
D	Cu	0.1989	0.1374	1.6642	35.5599	2.97095e+3	3.52	29.61
T	Cu	0.2904	0.2899	1.9648	24.2892	3.01673e+3	3.52	20.32
^{3}He	Cu	0.0750	0.7126	1.0303	28.4759	6.20088e+3	3.52	20.32
^{4}He	Cu	0.1639	0.6376	1.9937	21.5232	6.29218e+3	3.52	15.79
N	Cu	0.1595	3.4102	2.1567	15.6557	2.75601e+4	3.52	5.95
Ne	Cu	0.2009	5.0380	2.4014	15.5801	4.40689e+4	3.52	4.81
Ar	Cu	1.9417	14.8712	2.3907	12.9166	1.05525e+5	3.52	3.71
Cu	Cu	2.6044	14.5469	2.5577	10.7777	2.24619e+5	3.52	3.52
Kr	Cu	0.3072	16.6183	2.3257	21.3482	3.35590e+5	3.52	3.59
Xe	Cu	0.2781	24.4581	2.2393	23.6265	7.18907e+5	3.52	4.00
Ar	Zn	0.5168	35.7476	2.0349	7.6061	1.08696e+5	1.35	1.43
Zn	Zn	0.3077	30.3139	2.1318	6.5831	2.43109e+5	1.35	1.35
Kr	Zn	0.4951	34.1270	2.4413	6.9161	3.43442e+5	1.35	1.37
D	Ga	0.2292	0.1113	1.7674	29.5602	3.23166e+3	2.82	25.88
T	Ga	0.2369	0.1706	1.4510	21.3773	3.27716e+3	2.82	17.72
Ga	Ga	0.1105	16.5357	1.4877	16.8456	2.62439e+5	2.82	2.82
H	Ge	0.3938	0.0245	1.1582	88.3539	3.31932e+3	3.88	71.67
D	Ge	0.2327	0.0609	1.4101	44.6555	3.36441e+3	3.88	37.00
T	Ge	0.2998	0.0815	1.3007	30.8678	3.40997e+3	3.88	25.30
^{3}He	Ge	0.3206	0.2127	1.3195	32.3887	6.99838e+3	3.88	25.30
^{4}He	Ge	0.1446	0.2673	1.5062	26.2298	7.08909e+3	3.88	19.60
Ne	Ge	0.1485	3.5700	2.0064	14.1111	4.82268e+4	3.88	5.70
Ar	Ge	0.2357	6.2991	2.3935	15.5675	1.12992e+5	3.88	4.24
Ge	Ge	0.3535	11.8041	2.3480	17.2208	2.82619e+5	3.88	3.88
Kr	Ge	0.1769	12.8791	2.0150	23.9964	3.49421e+5	3.88	3.90
Xe	Ge	0.0838	18.2164	1.7290	28.5395	7.36368e+5	3.88	4.23
Ar	Se	0.1608	11.1577	2.2076	9.0783	1.18037e+5	2.14	2.40

Table 5. Fitting values λ, q, μ for the energy dependence of the sputtering yield $Y(E_0)$ at normal incidence in (2). In addition, the threshold energy, E_{th}, the reduced energy, ε, the surface binding energy, E_{sb}, and E_{sb}/γ are given

Ion	Target	λ	q	μ	E_{th} (eV)	ε	E_{sb} (eV)	E_{sb}/γ
H	Zr	0.4518	0.0103	1.0406	182.7468	4.42211e+3	6.33	146.11
D	Zr	0.6485	0.0306	1.9944	80.1168	4.47714e+3	6.33	75.02
T	Zr	0.7209	0.0542	1.6586	54.9858	4.52564e+3	6.33	51.02
^{3}He	Zr	0.5744	0.1184	0.7719	66.7939	9.25829e+3	6.33	51.02
^{4}He	Zr	0.2633	0.1371	0.9538	53.1725	9.35457e+3	6.33	39.32
Ne	Zr	0.1101	2.5721	1.6851	23.4583	6.06862e+4	6.33	10.67
Ar	Zr	0.1601	5.0472	2.0223	24.0260	1.37106e+5	6.33	7.47
Kr	Zr	0.2163	9.2238	2.1484	33.5793	4.03685e+5	6.33	6.34
Zr	Zr	0.2699	10.8645	1.9248	29.9208	4.75691e+5	6.33	6.33
Xe	Zr	0.2943	12.8431	2.2275	37.8291	8.25496e+5	6.33	6.54
H	Nb	0.6259	0.0112	1.3327	210.8697	4.57351e+3	7.59	178.37
D	Nb	0.3858	0.0328	1.5253	106.8707	4.62220e+3	7.59	91.55
T	Nb	0.6475	0.0593	1.8826	68.8233	4.67139e+3	7.59	62.23
^{3}He	Nb	0.3872	0.1233	1.1568	79.8178	9.55327e+3	7.59	62.23
^{4}He	Nb	0.2626	0.1418	1.3089	62.2687	9.65087e+3	7.59	47.95
Ne	Nb	0.1307	2.4654	1.8441	28.0914	6.23657e+4	7.59	12.94
Ar	Nb	0.1913	5.3954	2.3033	28.6038	1.40484e+5	7.59	9.02
Kr	Nb	0.1964	9.5591	1.9919	42.3615	4.11932e+5	7.59	7.61
Nb	Nb	0.2284	10.4521	1.8885	37.3983	5.03904e+5	7.59	7.59
Xe	Nb	0.1998	13.4775	2.0015	49.0697	8.40173e+5	7.59	7.82
H	Mo	0.5124	0.0114	1.1469	201.4886	4.71832e+3	6.83	165.63
D	Mo	0.3241	0.0326	1.5410	97.7738	4.76698e+3	6.83	84.95
T	Mo	0.5078	0.0661	1.5955	67.1475	4.81614e+3	6.83	57.71
^{3}He	Mo	0.3541	0.1373	0.9926	75.3995	9.84614e+3	6.83	57.71
^{4}He	Mo	0.1537	0.1563	0.9989	59.3088	9.94365e+3	6.83	44.44
N	Mo	0.1157	1.7900	1.8032	28.2561	4.10879e+4	6.83	15.36
O	Mo	0.1762	2.1069	2.4821	23.9169	4.83320e+4	6.83	13.94
Ne	Mo	0.2205	2.8995	2.6514	23.6170	6.38956e+4	6.83	11.89
Ar	Mo	0.1339	6.3606	1.9562	28.2149	1.43274e+5	6.83	8.23
Kr	Mo	0.1412	11.9419	1.6911	38.6337	4.17411e+5	6.83	6.86
Mo	Mo	0.3580	12.2715	2.1844	31.4737	5.33049e+5	6.83	6.83
Xe	Mo	0.2401	32.5719	1.6694	47.4030	8.47848e+5	6.83	7.00
H	Ru	0.3912	0.0129	1.6744	194.6779	5.01173e+3	6.69	170.73
D	Ru	0.2887	0.0428	1.9612	97.5326	5.06083e+3	6.69	87.48
T	Ru	0.3922	0.0882	1.7061	68.6863	5.11042e+3	6.69	59.37
^{3}He	Ru	0.1990	0.1998	1.7831	72.7607	1.04414e+4	6.69	59.37
^{4}He	Ru	0.1617	0.2364	1.7290	57.4279	1.05397e+4	6.69	45.67
Ne	Ru	0.1389	3.1882	2.1092	26.1200	6.70985e+4	6.69	12.06
Ar	Ru	0.1872	6.8381	2.2039	27.4779	1.49334e+5	6.69	8.24
Kr	Ru	0.2419	13.1833	2.3683	35.6820	4.30460e+5	6.69	6.75
Xe	Ru	0.1828	18.9085	2.0945	43.4787	6.68372e+5	6.69	6.81

Table 6. Fitting values λ, q, μ for the energy dependence of the sputtering yield $Y(E_0)$ at normal incidence in (2). In addition, the threshold energy, E_{th}, the reduced energy, ε, the surface binding energy, E_{sb}, and E_{sb}/γ are given

Ion	Target	λ	q	μ	E_{th} (eV)	ε	E_{sb} (eV)	E_{sb}/γ
H	Rh	0.4883	0.0174	1.5635	173.8870	5.16041e+3	5.78	150.14
D	Rh	0.3593	0.0511	1.8715	85.5661	5.21007e+3	5.78	76.90
T	Rh	0.3510	0.1026	1.4508	61.9159	5.26022e+3	5.78	52.17
^{3}He	Rh	0.1514	0.2049	1.5288	64.9824	1.07444e+4	5.78	52.17
^{4}He	Rh	0.1038	0.2212	2.0736	49.0159	1.08438e+4	5.78	40.12
Ne	Rh	0.1310	3.7410	2.0601	23.2979	6.87945e+4	5.78	10.54
Ar	Rh	0.1519	7.8385	2.1666	24.8932	1.52692e+5	5.78	7.17
Kr	Rh	0.1467	15.4269	2.1139	33.6867	4.38429e+5	5.78	5.84
Xe	Rh	0.2480	21.6042	2.3157	34.9750	8.82222e+5	5.78	5.87
H	Pd	0.3805	0.0307	1.5679	119.3501	5.30935e+3	3.91	104.94
D	Pd	0.1879	0.0875	1.7784	61.2249	5.35878e+3	3.91	53.72
T	Pd	0.2011	0.1654	1.5686	42.9267	5.40870e+3	3.91	36.42
^{3}He	Pd	0.1429	0.3249	1.7971	44.0328	1.10446e+4	3.91	36.42
^{4}He	Pd	0.1312	0.3839	1.8906	34.3297	1.11435e+4	3.91	27.99
Ne	Pd	0.1449	5.3982	2.3415	15.9494	7.03218e+4	3.91	7.29
Ar	Pd	0.1147	11.4507	2.1538	18.1505	1.55391e+5	3.91	4.93
Kr	Pd	0.1636	20.9141	2.3051	22.0273	4.43321e+5	3.91	3.97
Pd	Pd	0.2531	26.4367	2.3402	19.4305	6.59103e+5	3.91	3.91
Xe	Pd	0.1879	30.3470	2.1409	23.6613	8.88306e+5	3.91	3.95
H	Ag	0.4315	0.0568	1.9568	88.4899	5.46029e+3	2.97	80.79
D	Ag	0.1118	0.1421	1.7562	48.1788	5.51044e+3	2.97	41.35
T	Ag	0.2015	0.2513	1.5178	33.7714	5.56109e+3	2.97	28.03
^{3}He	Ag	0.1344	0.4479	1.6924	34.1484	1.13527e+4	2.97	28.03
^{4}He	Ag	0.1136	0.5817	1.9719	26.4533	1.14531e+4	2.97	21.54
N	Ag	0.1020	3.5600	2.2635	13.0433	4.66664e+4	2.97	7.30
O	Ag	0.0839	4.5394	2.0010	13.4494	5.47544e+4	2.97	6.60
O(Mol)	Ag	0.1711	5.6305	2.5908	13.4489	5.47544e+4	2.97	6.60
Ne	Ag	0.0995	5.5124	2.7313	11.8829	7.20736e+4	2.97	5.59
Ar	Ag	0.1650	18.8203	1.9424	13.9098	1.58921e+5	2.97	3.76
Ar(KrC)	Ag	0.1178	13.6070	2.1743	13.5876	1.58921e+5	2.97	3.76
Ar(Mol)	Ag	0.2320	16.4201	2.4019	13.6547	1.58921e+5	2.97	3.76
Ar(Mola)	Ag	0.1673	12.4010	2.3562	12.0571	1.58921e+5	2.97	3.76
Ar(ZBL)	Ag	0.2100	13.9829	2.4962	14.0709	1.58921e+5	2.97	3.76
Kr	Ag	0.1801	30.5548	2.4713	16.2072	4.51993e+5	2.97	3.02
Ag	Ag	0.1687	36.6162	2.4091	15.2340	6.93021e+5	2.97	2.97
Xe	Ag	0.2236	35.8737	2.2844	17.5897	9.03858e+5	2.97	3.00
Ar	Cd	0.1235	25.3480	2.2793	5.4146	1.61276e+5	1.16	1.50
Kr	Cd	0.1779	46.8071	2.6365	6.1572	4.55218e+5	1.16	1.19
Cd	Cd	0.1861	66.4019	2.2778	5.7795	7.27916e+5	1.16	1.16
H	In	0.4760	0.0408	1.7747	77.6070	5.76339e+3	2.49	72.02
D	In	0.1803	0.1049	1.4528	42.4095	5.81315e+3	2.49	36.82
T	In	0.1745	0.1751	1.3489	29.0900	5.86340e+3	2.49	24.93
Ne	In	0.0348	5.9422	1.3768	12.1811	7.51927e+4	2.49	4.90
Kr	In	0.0996	23.4774	2.0666	13.4197	4.62260e+5	2.49	2.55
In	In	0.1224	30.7665	1.9472	13.0986	7.63793e+5	2.49	2.49

Table 7. Fitting values λ, q, μ for the energy dependence of the sputtering yield $Y(E_0)$ at normal incidence in (2). In addition, the threshold energy, E_{th}, the reduced energy, ε, the surface binding energy, E_{sb}, and E_{sb}/γ are given

Ion	Target	λ	q	μ	E_{th} (eV)	ε	E_{sb} (eV)	E_{sb}/γ
H	Sn	0.4702	0.0352	1.6669	104.1095	5.91631e+3	3.12	93.23
D	Sn	0.1829	0.0715	1.6497	53.8847	5.96574e+3	3.12	47.63
T	Sn	0.2917	0.1556	1.5871	36.4853	6.01566e+3	3.12	32.23
^{3}He	Sn	0.1558	0.3227	1.5754	38.8436	1.22714e+4	3.12	32.23
^{4}He	Sn	0.1102	0.3244	1.8523	29.6119	1.23702e+4	3.12	24.73
Ne	Sn	0.1152	4.5687	2.2682	11.5544	7.67367e+4	3.12	6.28
Ar	Sn	0.0746	9.2172	2.1869	11.9822	1.67157e+5	3.12	4.14
Kr	Sn	0.3289	17.5340	2.6550	13.6369	4.66941e+5	3.12	3.22
Sn	Sn	0.1494	27.3600	2.0140	15.7681	8.00660e+5	3.12	3.12
Xe	Sn	0.9767	25.3092	3.2145	14.2636	9.22556e+5	3.12	3.13
Kr	Sb	0.1171	22.1319	2.0888	13.5706	4.73059e+5	2.72	2.82
Ar	Te	0.0993	12.8971	2.2723	7.4376	1.72282e+5	2.02	2.78
Cs	Cs	0.1310	59.8329	1.7733	4.4983	1.00007e+6	0.82	0.82
Kr	Sm	0.1279	25.7558	2.4453	9.2611	5.50683e+5	2.16	2.35
H	Tb	0.4151	0.0245	1.4450	180.8106	8.32995e+3	3.89	154.97
D	Tb	0.2514	0.0764	1.4668	92.1545	8.38203e+3	3.89	78.85
T	Tb	0.2675	0.1140	1.7383	58.8710	8.43464e+3	3.89	53.14
^{3}He	Tb	0.1970	0.2290	1.5498	62.3825	1.71555e+4	3.89	53.14
^{4}He	Tb	0.1613	0.3219	1.5186	48.4940	1.72593e+4	3.89	40.61
Ar	Tb	0.0825	10.8668	2.0502	14.1521	2.15976e+5	3.89	6.06
H	Tm	0.3646	0.0525	1.6677	119.3908	9.00672e+3	2.52	106.64
D	Tm	0.1931	0.1483	1.5930	61.7026	9.05971e+3	2.52	54.22
T	Tm	0.2005	0.2252	1.7487	39.5783	9.11324e+3	2.52	36.51
^{3}He	Tm	0.1329	0.4083	1.5808	42.9760	1.85244e+4	2.52	36.51
^{4}He	Tm	0.1182	0.5425	1.8624	32.4379	1.86300e+4	2.52	27.88
Ar	Tm	0.1010	18.0207	2.1079	9.4852	2.29744e+5	2.52	4.07
H	Hf	0.6050	0.0106	1.3803	320.9804	9.52208e+3	6.31	281.94
D	Hf	0.2980	0.0303	1.8401	157.1012	9.57512e+3	6.31	143.26
T	Hf	0.2352	0.0507	1.3451	112.2792	9.62870e+3	6.31	96.42
^{3}He	Hf	0.2596	0.1083	1.1964	115.5387	1.95639e+4	6.31	96.42
^{4}He	Hf	0.1695	0.1230	1.7304	84.5645	1.96695e+4	6.31	73.58
Ne	Hf	0.0698	3.0827	1.6671	28.7970	1.15397e+5	6.31	17.29
Ar	Hf	0.0841	7.2844	1.9088	23.6839	2.39690e+5	6.31	10.56
Kr	Hf	0.0969	15.8759	1.9090	27.1771	6.21788e+5	6.31	7.26
Xe	Hf	0.1218	22.7796	2.0536	32.7651	1.16579e+6	6.31	6.46
H	Ta	0.5966	0.0078	0.7141	483.1426	9.69565e+3	8.10	366.86
D	Ta	0.6251	0.0218	0.7705	225.5901	9.74893e+3	8.10	186.37
T	Ta	0.2642	0.0284	1.0425	147.2448	9.80275e+3	8.10	125.42
^{3}He	Ta	0.5951	0.0885	2.0793	131.9549	1.99149e+4	8.10	125.42
^{4}He	Ta	0.1193	0.0989	1.3173	116.3022	2.00210e+4	8.10	95.70
Ne	Ta	0.0675	2.7626	2.0170	36.3551	1.17263e+5	8.10	22.43
Ar	Ta	0.1468	6.2661	2.3669	28.6179	2.43215e+5	8.10	13.67
Kr	Ta	0.1074	14.2018	2.0456	34.5045	6.29462e+5	8.10	9.36
Xe	Ta	0.1175	20.2166	2.0128	42.5105	1.17814e+6	8.10	8.31
Ta	Ta	0.1583	26.6919	1.9785	41.4906	1,93615e+6	8.10	8.10

Table 8. Fitting values λ, q, μ for the energy dependence of the sputtering yield $Y(E_0)$ at normal incidence in (2). In addition, the threshold energy, E_{th}, the reduced energy, ε, the surface binding energy, E_{sb}, and E_{sb}/γ are given

Ion	Target	λ	q	μ	E_{th} (eV)	ε	E_{sb} (eV)	E_{sb}/γ
H	W	1.0087	0.0075	1.2046	457.42	9.86986e+3	8.68	399.36
D	W	0.3583	0.0183	1.4410	228.84	9.92326e+3	8.68	202.85
T	W	0.2870	0.0419	1.5802	153.8842	9.97718e+3	8.68	136.48
^{3}He	W	0.2424	0.0884	1.2439	164.3474	2.02666e+4	8.68	136.48
^{4}He	W	0.1692	0.1151	1.7121	120.56	2.03728e+4	8.68	104.13
N	W	0.0921	1.4389	2.0225	45.3362	7.90505e+4	8.68	32.98
O	W	0.0777	1.8824	1.7536	44.2135	9.19794e+4	8.68	29.46
Ne	W	0.0828	2.5520	1.9534	38.6389	1.19107e+5	8.68	24.35
Ar	W	0.2113	5.9479	2.3857	27.0503	2.46646e+5	8.68	14.80
Kr	W	0.1747	13.6917	2.5161	34.7592	6.36677e+5	8.68	10.09
Xe	W	0.1385	20.5321	2.0952	44.8701	1.18932e+6	8.68	8.93
W	W	2.2697	18.6006	3.1273	24.9885	1.99860e+6	8.68	8.68
H	Re	0.6547	0.0089	1.5919	410.7532	1.00450e+4	8.09	376.92
D	Re	0.3445	0.0262	1.6638	214.3341	1.00987e+4	8.09	191.42
T	Re	0.2667	0.0460	1.7325	143.8798	1.01529e+4	8.09	128.78
^{3}He	Re	0.2026	0.1092	1.5099	151.8603	2.06207e+4	8.09	128.78
^{4}He	Re	0.1179	0.1189	1.6235	115.5715	2.07275e+4	8.09	98.24
Ne	Re	0.0871	3.0197	1.9011	37.8276	1.20995e+5	8.09	22.93
Ar	Re	0.0922	8.1299	2.0957	32.2292	2.50221e+5	8.09	13.91
Kr	Re	0.1159	16.1742	2.1166	35.8918	6.44513e+5	8.09	9.45
Xe	Re	0.1345	23.6228	2.1797	42.6697	1.20203e+6	8.09	8.34
H	Os	0.5133	0.0089	1.3016	458.5624	1.02204e+4	8.13	386.83
D	Os	0.2692	0.0267	1.3190	232.7884	1.02739e+4	8.13	196.42
T	Os	0.3100	0.0507	1.5438	148.1225	1.03279e+4	8.13	132.10
^{3}He	Os	0.2226	0.1111	1.6367	152.6164	2.09735e+4	8.13	132.10
^{4}He	Os	0.1207	0.1315	1.9064	115.7747	2.10799e+4	8.13	100.75
Ne	Os	0.0816	3.0236	2.1827	37.7170	1.22785e+5	8.13	23.44
Ar	Os	0.0985	7.4153	2.2543	32.1090	2.53422e+5	8.13	14.17
Kr	Os	0.1140	16.3882	2.1619	36.1888	6.50625e+5	8.13	9.57
Xe	Os	0.1751	23.5196	2.4600	40.4010	1.21043e+6	8.13	8.41
H	Ir	0.4857	0.0108	1.7106	367.3325	1.03972e+4	6.90	331.72
D	Ir	0.2445	0.0332	1.6722	188.7811	1.04510e+4	6.90	168.42
T	Ir	0.2550	0.0640	1.6312	127.4106	1.05053e+4	6.90	113.26
^{3}He	Ir	0.1693	0.1387	1.4318	134.4943	2.13313e+4	6.90	113.26
^{4}He	Ir	0.1057	0.1664	1.6693	102.6618	2.14384e+4	6.90	86.37
Ne	Ir	0.0847	3.5828	2.0777	32.7658	1.24708e+5	6.90	20.06
Ar	Ir	0.1070	8.8295	2.2049	27.7592	2.57103e+5	6.90	12.11
Kr	Ir	0.1117	19.1063	2.2947	31.0366	6.58875e+5	6.90	8.16
Xe	Ir	0.1933	27.1913	2.5754	34.0523	1.22412e+6	6.90	7.15

Table 9. Fitting values λ, q, μ for the energy dependence of the sputtering yield $Y(E_0)$ at normal incidence in (2). In addition, the threshold energy, E_{th}, the reduced energy, ε, the surface binding energy, E_{sb}, and E_{sb}/γ are given

Ion	Target	λ	q	μ	E_{th} (eV)	ε	E_{sb} (eV)	E_{sb}/γ
H	Pt	0.4428	0.0136	1.4981	325.0317	1.05744e+4	5.86	285.91
D	Pt	0.2020	0.0395	1.5601	166.7835	1.06283e+4	5.86	145.14
T	Pt	0.2492	0.0756	1.4307	112.6259	1.06828e+4	5.86	97.59
^{3}He	Pt	0.1998	0.1482	1.5445	113.4769	2.16890e+4	5.86	97.59
^{4}He	Pt	0.1214	0.1802	1.8192	85.5658	2.17963e+4	5.86	74.41
O	Pt	0.0785	2.8246	2.0224	31.5095	9,78987e+4	5.86	20.91
Ne	Pt	0.0949	5.0805	2.1232	28.0853	1.26583e+5	5.86	17.24
Ar	Pt	0.1380	13.7922	2.2949	23.3808	2.60590e+5	5.86	10.38
Kr	Pt	0.1087	29.4816	1.9534	27.9365	6.66218e+5	5.86	6.97
Xe	Pt	0.0658	41.7055	1.5076	34.0986	1.23553e+6	5.86	6.09
Pt	Pt	0.2616	42.2193	2.4689	28.0416	2.25981e+6	5.86	5.86
H	Au	0.3117	0.0286	1.8415	206.4074	1.07527e+4	3.80	187.17
D	Au	0.2082	0.0843	1.2739	112.9565	1.08070e+4	3.80	95.00
T	Au	0.1680	0.1560	1.4421	74.8582	1.08618e+4	3.80	63.88
^{3}He	Au	0.1346	0.3759	1.6028	75.1673	2.20499e+4	3.80	63.88
^{4}He	Au	0.0928	0.3406	1.6773	57.2732	2.21579e+4	3.80	48.70
N	Au	0.0934	3.6067	2.0278	22.0847	8.55290e+4	3.80	15.32
O	Au	0.0634	4.0269	1.9029	21.3321	9,94281e+4	3.80	13.67
Ne	Au	0.0758	5.9707	1.8885	19.0757	2.18526e+5	3.80	11.27
Ar	Au	0.0906	12.0104	2.3969	15.6192	2.64318e+5	3.80	6.78
Kr	Au	0.0940	30.2381	1.7709	18.7951	6.74618e+5	3.80	4.54
Xe	Au	0.1371	47.6103	2.5053	19.7602	1.24955e+6	3.80	3.96
Au	Au	0.1126	61.2607	1.7156	21.4123	2.32799e+6	3.80	3.80
Kr	Hg	0.0964	14.1592	2.1495	24.7454	6.81273e+5	6.36	7.65
Kr	Tl	0.0707	37.5934	2.3358	8.2027	6.87823e+5	1.88	2.28
He	Pb	0.0686	0.4081	1.6658	31.7654	2.32414e+4	2.03	27.31
Ne	Pb	0.0569	6.7337	2.1626	9.6887	1.34122e+5	2.03	6.27
Ar	Pb	0.0462	15.7003	1.9270	8.4298	2.74555e+5	2.03	3.74
Kr	Pb	0.0551	35.9566	2.0207	9.1375	6.95357e+5	2.03	2.48
Xe	Pb	0.0637	52.3584	2.0982	10.8209	1.28038e+6	2.03	2.14
Pb	Pb	0.1461	81.3238	2.1946	10.3121	2.53951e+6	2.03	2.03
Ar	Bi	0.0289	14.2020	1.5639	9.4013	2.78342e+5	2.17	4.03
Kr	Bi	0.0578	30.2017	2.0562	9.1764	7.03904e+5	2.17	2.66
^{4}He	Th	0.1680	0.1524	1.5450	103.5217	2.61980e+4	5.93	88.99
Ne	Th	0.0592	2.9258	1.6073	30.7814	1.49508e+5	5.93	20.14
Ar	Th	0.0543	7.3739	1.6067	23.7676	3.02995e+5	5.93	11.83
Kr	Th	0.0767	16.5776	1.8831	22.9040	7.54519e+5	5.93	7.61
Xe	Th	0.1059	24.2490	1.9981	26.4766	1.37124e+6	5.93	6.42
H	U	0.5069	0.0144	1.4948	365.5917	1.31300e+4	5.42	322.05
D	U	0.1807	0.0266	1.2763	189.3173	1.31849e+4	5.42	163.18
^{4}He	U	0.0839	0.1136	1.6784	95.3598	2.69513e+4	5.42	83.37
Ne	U	0.0449	3.0029	1.8839	28.5107	1.53434e+5	5.42	18.81
Ar	U	0.0584	7.6218	2.1314	21.6010	3.10275e+5	5.42	11.01
Kr	U	0.0592	18.0929	2.0957	22.5283	7.69792e+5	5.42	7.04
Xe	U	0.0694	26.9596	2.2075	25.9587	1.39494e+6	5.42	5.91
Rn	U	0.1709	40.4320	2.3889	30.1936	2.96732e+6	5.42	5.43
U	U	0.1932	56.2825	2.0420	26.7960	3.32167e+6	5.42	5.42

Table 10. Fitting values f, b, c for the angular dependence of the sputtering yield in (6). Furthermore, the values for the yield at normal incidence, $Y(E_0, 0)$, the binding energy, E_{sp}, for the projectiles, the value θ_0^* (deg.), (7), and the angular position, θ_{0m} (deg.), of the maximum yield, (8), are given

Ion	Target	E_0 (eV)	f	b	c	Y(E_0,0)	E_{sp} (eV)	θ_0^*	θ_{0m}
T	Li	100	7.2592	2.6907	0.8685	4.20e-2	1.00	95.71	74.53
T	Li	300	5.3765	1.5393	0.9380	4.52e-2	1.00	93.30	77.31
Li	Li	100	10.9922	5.1816	0.7382	9.48e-2	1.67	97.36	68.79
Li	Li	200	8.0198	3.3011	0.8089	1.50e-1	1.67	95.22	71.79
Li	Li	1000	4.8470	1.4003	0.8167	2.07e-1	1.67	92.34	79.36
H	Be	15	11.1512	10.4683	1.1501	2.39e-5	1.00	104.48	25.75
H	Be	17	16.2828	13.6595	0.5330	1.80e-4	1.00	103.63	23.40
H	Be	20	11.8530	9.7870	0.6069	8.03e-4	1.00	102.60	28.10
H	Be	22	9.9611	8.0685	0.6398	1.45e-3	1.00	102.04	31.29
H	Be	25	8.5822	6.5543	0.6820	2.57e-3	1.00	101.31	38.37
H	Be	30	6.2386	4.3193	0.8005	4.68e-3	1.00	100.35	48.80
H	Be	40	6.1156	3.5415	0.8961	8.46e-3	1.00	98.98	59.73
H	Be	50	5.9126	3.0661	0.9447	1.15e-2	1.00	98.05	64.11
H	Be	70	5.7275	2.5808	0.9899	1.54e-2	1.00	96.82	68.08
H	Be	100	5.3523	2.1181	1.0194	1.85e-2	1.00	95.71	70.71
H	Be	140	5.2036	1.8698	1.0226	1.98e-2	1.00	94.83	72.34
H	Be	200	4.9195	1.5975	1.0221	2.02e-2	1.00	94.04	73.90
H	Be	300	4.7651	1.4198	1.0017	1.93e-2	1.00	93.30	75.30
H	Be	500	4.5468	1.2312	0.9622	1.69e-2	1.00	92.56	77.19
H	Be	1000	4.3749	1.0536	0.8651	1.26e-2	1.00	91.81	81.10
D	Be	11	15.1382	12.5716	0.5871	2.61e-5	1.00	106.78	27.74
D	Be	12	12.2769	9.7520	0.4890	9.29e-5	1.00	106.10	28.24
D	Be	13	11.8349	9.1246	0.5030	2.32e-4	1.00	105.50	32.16
D	Be	14	11.1728	8.4156	0.5234	4.65e-4	1.00	104.96	35.47
D	Be	15	10.3229	7.5816	0.5573	8.10e-4	1.00	104.48	39.31
D	Be	17	9.3601	6.5239	0.6180	1.73e-3	1.00	103.63	45.94
D	Be	20	8.6777	5.6452	0.7059	3.64e-3	1.00	102.60	52.97
D	Be	25	8.5752	5.1717	0.7833	7.30e-3	1.00	101.31	58.26
D	Be	30	8.6869	4.9678	0.8221	1.08e-2	1.00	100.35	60.94
D	Be	40	8.3485	4.4220	0.8753	1.68e-2	1.00	98.98	63.92
D	Be	50	8.4098	4.2438	0.8948	2.09e-2	1.00	98.05	65.35
D	Be	70	7.8175	3.6199	0.9330	2.63e-2	1.00	96.82	67.56
D	Be	100	7.1106	3.0041	0.9611	3.10e-2	1.00	95.71	69.49
D	Be	140	6.6162	2.5702	0.9727	3.32e-2	1.00	94.83	71.06
D	Be	200	5.8071	2.0229	0.9890	3.51e-2	1.00	94.04	72.90
D	Be	300	5.3019	1.6773	0.9801	3.44e-2	1.00	93.30	74.52
D	Be	500	4.7090	1.3205	0.9559	3.24e-2	1.00	92.56	76.70
D	Be	1000	4.2992	1.0429	0.8839	2.53e-2	1.00	91.81	80.41
D	Be	3000	3.2495	0.4832	0.9270	1.25e-2	1.00	91.05	84.71
T	Be	10	11.3143	7.1581	0.5161	1.75e-5	1.00	107.55	54.13
T	Be	11	10.9347	6.8942	0.5346	7.08e-5	1.00	106.78	54.50
T	Be	12	11.3517	7.0538	0.5714	1.77e-4	1.00	106.10	56.20
T	Be	13	11.3297	6.9311	0.5920	3.49e-4	1.00	105.50	57.54
T	Be	15	11.8958	7.0949	0.6393	9.03e-4	1.00	104.48	59.55
T	Be	17	12.0355	7.0598	0.6734	1.74e-3	1.00	103.73	60.62
T	Be	20	12.3549	7.1299	0.7128	3.43e-3	1.00	102.60	61.29
T	Be	25	12.2645	6.9111	0.7510	6.83e-3	1.00	101.31	62.12

Table 11. Fitting values f, b, c for the angular dependence of the sputtering yield in (6). Furthermore, the values for the yield at normal incidence, $Y(E_0, 0)$, the binding energy, E_{sp}, for the projectiles, the value θ_0^* (deg.), (7), and the angular position, θ_{0m} (deg.), of the maximum yield, (8), are given

Ion	Target	E_0 (eV)	f	b	c	Y(E_0,0)	E_{sp} (eV)	θ_0^*	θ_{0m}
T	Be	30	11.9180	6.5619	0.7738	1.03e-2	1.00	100.35	62.87
T	Be	50	10.7247	5.4280	0.8473	2.11e-2	1.00	98.05	65.39
T	Be	100	8.7843	3.8375	0.9167	3.27e-2	1.00	95.71	68.86
T	Be	200	6.8472	2.5074	0.9558	4.00e-2	1.00	94.04	72.19
T	Be	300	6.0145	1.9963	0.9542	4.14e-2	1.00	93.30	73.94
T	Be	500	5.1690	1.5181	0.9354	4.05e-2	1.00	92.56	76.25
T	Be	1000	4.4884	1.1230	0.8709	3.38e-2	1.00	91.81	80.25
^{4}He	Be	11	13.3115	7.4762	0.6483	1.59e-5	0.00	90.00	55.05
^{4}He	Be	12	11.3837	5.9236	0.7450	4.18e-5	0.00	90.00	59.11
^{4}He	Be	13	11.0954	5.5450	0.8004	8.92e-5	0.00	90.00	60.71
^{4}He	Be	15	12.0126	6.1657	0.7756	3.08e-4	0.00	90.00	59.66
^{4}He	Be	17	11.0765	5.5593	0.8258	8.21e-4	0.00	90.00	60.43
^{4}He	Be	20	11.1672	5.7241	0.8209	2.27e-3	0.00	90.00	59.58
^{4}He	Be	25	10.8794	5.6025	0.8297	6.28e-3	0.00	90.00	59.36
^{4}He	Be	30	10.6545	5.4832	0.8281	1.16e-2	0.00	90.00	59.39
^{4}He	Be	40	9.8918	4.9831	0.8487	2.35e-2	0.00	90.00	60.20
^{4}He	Be	50	9.3707	4.6041	0.8623	3.42e-2	0.00	90.00	61.11
^{4}He	Be	70	8.5526	3.9849	0.8863	5.03e-2	0.00	90.00	62.89
^{4}He	Be	100	7.7207	3.3762	0.9077	6.76e-2	0.00	90.00	64.80
^{4}He	Be	140	6.8183	2.7618	0.9309	8.31e-2	0.00	90.00	66.81
^{4}He	Be	200	6.1209	2.2840	0.9469	9.60e-2	0.00	90.00	68.75
^{4}He	Be	300	5.4354	1.8381	0.9580	1.06e-1	0.00	90.00	70.86
^{4}He	Be	400	5.1109	1.6232	0.9604	1.09e-1	0.00	90.00	72.14
^{4}He	Be	500	4.7756	1.4360	0.9609	1.10e-1	0.00	90.00	73.20
^{4}He	Be	700	4.6688	1.3495	0.9432	1.09e-1	0.00	90.00	74.29
^{4}He	Be	1000	4.5214	1.2552	0.9168	1.04e-1	0.00	90.00	75.61
^{4}He	Be	2000	3.9996	0.9553	0.8655	8.70e-2	0.00	90.00	79.63
^{4}He	Be	3000	2.9548	0.4527	0.9860	6.80e-2	0.00	90.00	81.59
^{4}He	Be	5000	2.3689	0.2360	1.0133	5.93e-2	0.00	90.00	83.86
^{4}He	Be	10000	2.3184	0.2110	0.9873	4.08e-2	0.00	90.00	85.21
Be	Be	12	35.8412	18.6635	0.4936	1.26e-5	3.38	117.96	78.65
Be	Be	13	36.3925	19.1900	0.5105	2.14e-5	3.38	117.02	76.76
Be	Be	15	36.6304	19.6402	0.5253	5.23e-5	3.38	115.39	74.15
Be	Be	17	35.6814	19.3245	0.5289	1.15e-4	3.38	114.03	72.38
Be	Be	20	33.7964	18.4992	0.5227	3.05e-4	3.38	112.35	70.38
Be	Be	25	30.3372	16.8120	0.5223	1.09e-3	3.38	110.19	67.94
Be	Be	30	27.7102	15.5065	0.5251	2.68e-3	3.38	108.55	66.10
Be	Be	40	24.3009	13.7865	0.5368	8.41e-3	3.38	106.21	63.58
Be	Be	50	22.2057	12.6890	0.5547	1.68e-2	3.38	104.57	62.14
Be	Be	70	19.4611	11.1466	0.5914	3.77e-2	3.38	102.39	60.93
Be	Be	100	16.6662	9.3775	0.6469	7.00e-2	3.38	100.42	61.30
Be	Be	200	12.0795	6.2040	0.7708	1.43e-1	3.38	97.41	64.55
Be	Be	300	9.7816	4.6056	0.8401	1.86e-1	3.38	96.06	67.06
Be	Be	500	7.6374	3.1692	0.8981	2.33e-1	3.38	94.70	69.96
Be	Be	700	6.6434	2.5351	0.9168	2.57e-1	3.38	93.97	71.61
Be	Be	1000	5.7378	1.9957	0.9261	2.74e-1	3.38	93.33	73.36
Be	Be	3000	4.1459	1.0784	0.8930	2.63e-1	3.38	91.92	79.02
Be	Be	5000	3.7580	0.8504	0.8638	2.27e-1	3.38	91.49	81.91

Table 12. Fitting values f, b, c for the angular dependence of the sputtering yield in (6). Furthermore, the values for the yield at normal incidence, $Y(E_0, 0)$, the binding energy, E_{sp}, for the projectiles, the value θ_0^* (deg.), (7), and the angular position, θ_{0m} (deg.), of the maximum yield, (8), are given

Ion	Target	E_0 (eV)	f	b	c	Y(E_0,0)	E_{sp} (eV)	θ_0^*	θ_{0m}
N	Be	20	48.9385	26.5720	0.5034	1.30e-5	1.00	102.60	64.91
N	Be	25	40.8964	22.5484	0.5362	1.32e-4	1.00	101.31	62.92
N	Be	27	39.8702	22.1580	0.5309	2.23e-4	1.00	100.89	62.01
N	Be	30	37.4299	20.9914	0.5363	4.97e-4	1.00	100.35	60.99
N	Be	40	32.2237	18.4203	0.5534	2.72e-3	1.00	98.98	58.78
N	Be	50	27.1013	15.5100	0.5983	7.94e-3	1.00	98.05	58.46
N	Be	70	23.2661	13.3500	0.6312	2.53e-2	1.00	96.82	56.99
N	Be	100	18.5794	10.4007	0.6958	6.02e-2	1.00	95.71	58.90
N	Be	140	14.9483	8.0322	0.7602	1.08e-1	1.00	94.83	60.25
N	Be	200	11.8204	5.9812	0.8224	1.72e-1	1.00	94.04	62.81
N	Be	500	7.1837	2.9571	0.9262	3.38e-1	1.00	92.56	68.30
N	Be	1000	5.3902	1.8661	0.9559	4.48e-1	1.00	91.81	71.80
Ne	Be	22	37.8307	19.0105	0.6044	1.54e-5	0.00	90.00	61.56
Ne	Be	25	35.8007	18.1513	0.6087	4.73e-5	0.00	90.00	61.02
Ne	Be	30	32.6599	16.7384	0.6188	1.99e-4	0.00	90.00	60.35
Ne	Be	35	30.1281	15.5617	0.6274	5.66e-4	0.00	90.00	59.88
Ne	Be	40	27.8302	14.4241	0.6390	1.28e-3	0.00	90.00	59.64
Ne	Be	45	25.8448	13.4144	0.6510	2.44e-3	0.00	90.00	59.52
Ne	Be	50	24.3632	12.6735	0.6597	4.08e-3	0.00	90.00	59.37
Ne	Be	60	21.5727	11.1858	0.6815	9.11e-3	0.00	90.00	59.47
Ne	Be	70	19.3093	9.9345	0.7037	1.63e-2	0.00	90.00	59.79
Ne	Be	100	15.1087	7.5705	0.7520	4.51e-2	0.00	90.00	60.82
Ne	Be	150	12.1657	5.8694	0.7943	9.80e-2	0.00	90.00	62.20
Ne	Be	200	10.3791	4.8187	0.8263	1.50e-1	0.00	90.00	63.45
Ne	Be	300	8.4375	3.6736	0.8644	2.40e-1	0.00	90.00	65.34
Ne	Be	500	6.6629	2.6321	0.9027	3.72e-1	0.00	90.00	67.84
Ne	Be	700	5.8331	2.1425	0.9218	4.58e-1	0.00	90.00	69.49
Ne	Be	1000	5.1859	1.7686	0.9333	5.44e-1	0.00	90.00	71.07
Ar	Be	30	35.7128	17.2562	0.6278	1.18e-5	0.00	90.00	63.48
Ar	Be	35	32.4561	15.7178	0.6419	5.22e-5	0.00	90.00	63.23
Ar	Be	40	30.6583	14.9605	0.6464	1.48e-4	0.00	90.00	62.79
Ar	Be	45	28.8311	14.1259	0.6530	3.43e-4	0.00	90.00	62.53
Ar	Be	50	27.0273	13.2560	0.6634	6.98e-4	0.00	90.00	62.39
Ar	Be	60	24.1964	11.8526	0.6801	2.02e-3	0.00	90.00	62.32
Ar	Be	70	21.9850	10.7572	0.6948	4.36e-3	0.00	90.00	62.27
Ar	Be	100	17.3823	8.3702	0.7353	1.83e-2	0.00	90.00	62.69
Ar	Be	150	13.3017	6.1743	0.7841	5.72e-2	0.00	90.00	63.81
Ar	Be	200	11.1755	4.9841	0.8183	1.01e-1	0.00	90.00	64.98
Ar	Be	300	9.0871	3.8726	0.8510	1.91e-1	0.00	90.00	66.18
Ar	Be	500	7.1160	2.7974	0.8891	3.49e-1	0.00	90.00	68.15
Ar	Be	700	6.1626	2.2693	0.9109	4.71e-1	0.00	90.00	69.59
Ar	Be	1000	5.3790	1.8371	0.9295	6.07e-1	0.00	90.00	71.10

Table 13. Fitting values f, b, c for the angular dependence of the sputtering yield in (6). Furthermore, the values for the yield at normal incidence, $Y(E_0, 0)$, the binding energy, E_{sp}, for the projectiles, the value θ_0^* (deg.), (7), and the angular position, θ_{0m} (deg.), of the maximum yield, (8), are given

Ion	Target	E_0 (eV)	f	b	c	Y(E_0,0)	E_{sp} (eV)	θ_0^*	θ_{0m}
D	B	30	9.8225	6.6573	0.7286	1.17e-3	1.00	100.35	49.15
D	B	50	7.3199	3.8871	0.9134	6.66e-3	1.00	98.05	63.17
D	B	100	6.5102	2.7189	0.9959	1.46e-2	1.00	95.71	69.50
D	B	400	5.0009	1.4855	0.9885	2.05e-2	1.00	92.86	75.34
D	B	500	5.0131	1.4255	0.9687	1.87e-2	1.00	92.56	76.18
D	B	8000	2.9214	0.3459	0.9361	5.43e-3	1.00	90.64	85.95
B	B	1000	7.1514	2.8161	0.8867	2.12e-1	5.73	94.33	71.41
B	B	2000	5.4626	1.8079	0.9049	2.50e-1	5.73	93.06	74.71
H	C	40	19.9809	13.5817	0.8381	9.00e-6	1.00	98.98	49.97
H	C	50	12.0758	8.1489	0.7350	1.75e-4	1.00	98.05	48.45
H	C	70	5.4383	3.1284	0.9195	1.23e-3	1.00	96.82	58.82
H	C	100	3.9021	1.5976	1.0451	2.92e-3	1.00	95.71	69.59
H	C	140	4.0027	1.3367	1.0590	4.42e-3	1.00	94.83	73.42
H	C	200	3.8151	1.0804	1.0649	5.84e-3	1.00	94.04	75.69
H	C	300	3.8086	0.9751	1.0455	7.05e-3	1.00	93.30	77.01
H	C	500	4.1077	1.0059	0.9884	6.76e-3	1.00	92.56	78.24
H	C	1000	4.4299	1.0578	0.8756	5.68e-3	1.00	91.81	80.93
H	C	2000	4.1024	0.8166	0.9397	4.44e-3	1.00	91.28	81.26
D	C	30	18.7533	13.3928	0.6303	8.58e-5	1.00	102.60	43.62
D	C	40	10.5178	6.5616	0.7465	7.35e-4	1.00	98.98	54.48
D	C	50	7.5874	4.1326	0.8655	1.96e-3	1.00	98.05	62.05
D	C	70	6.1109	2.7764	0.9695	4.79e-3	1.00	96.82	67.95
D	C	100	5.4981	2.1396	1.0110	8.18e-3	1.00	95.71	71.23
D	C	140	5.1852	1.8064	1.0205	1.10e-2	1.00	94.83	73.06
D	C	200	5.1235	1.6777	1.0074	1.32e-2	1.00	94.04	73.95
D	C	300	4.9019	1.4719	0.9931	1.47e-2	1.00	93.30	75.31
D	C	350	4.9419	1.4793	0.9963	1.62e-2	1.00	93.06	75.12
D	C	500	4.9952	1.4436	0.9320	1.44e-2	1.00	92.56	76.64
D	C	1000	4.4895	1.1320	0.8660	1.30e-2	1.00	91.81	80.25
D	C	2000	4.5151	1.0312	0.8022	1.02e-1	1.00	91.28	83.72
T	C	25	19.6619	13.0973	0.5723	4.70e-5	1.00	101.31	47.74
T	C	30	14.1788	8.6868	0.6507	2.44e-4	1.00	100.35	55.39
T	C	35	12.8594	7.3628	0.7278	6.90e-4	1.00	99.59	60.04
T	C	40	10.8275	5.8369	0.7969	1.23e-3	1.00	98.98	63.13
T	C	50	9.4042	4.6780	0.8682	2.76e-3	1.00	98.05	66.04
T	C	70	7.8716	3.4803	0.9388	6.05e-3	1.00	96.82	69.07
T	C	100	7.3284	2.9473	0.9618	9.44e-3	1.00	95.71	70.90
T	C	140	6.5713	2.4171	0.9798	1.28e-2	1.00	94.83	72.35
T	C	200	6.2607	2.1538	0.9746	1.54e-2	1.00	94.04	73.39
T	C	300	5.9195	1.9209	0.9502	1.75e-2	1.00	93.30	74.51
T	C	500	5.4224	1.6330	0.9126	1.87e-2	1.00	92.56	76.23
T	C	1000	5.0328	1.3613	0.8358	1.68e-2	1.00	91.81	79.77

Table 14. Fitting values f, b, c for the angular dependence of the sputtering yield in (6). Furthermore, the values for the yield at normal incidence, $Y(E_0, 0)$, the binding energy, E_{sp}, for the projectiles, the value θ_0^* (deg.), (7), and the angular position, θ_{0m} (deg.), of the maximum yield, (8), are given

Ion	Target	E_0 (eV)	f	b	c	Y(E_0,0)	E_{sp} (eV)	θ_0^*	θ_{0m}
^{4}He	C	25	14.6404	8.8559	0.6282	4.20e-5	0.00	90.00	50.27
^{4}He	C	27	12.0307	6.8705	0.7074	1.00e-4	0.00	90.00	54.32
^{4}He	C	30	13.1803	7.2609	0.7109	2.40e-4	0.00	90.00	56.28
^{4}He	C	35	10.6979	5.5485	0.7917	7.20e-4	0.00	90.00	59.15
^{4}He	C	40	9.2954	4.4707	0.8724	1.50e-3	0.00	90.00	61.85
^{4}He	C	50	8.8544	4.1314	0.8858	3.83e-3	0.00	90.00	62.85
^{4}He	C	60	8.2705	3.7475	0.8993	6.84e-3	0.00	90.00	63.74
^{4}He	C	70	7.7165	3.3800	0.9141	1.01e-2	0.00	90.00	64.69
^{4}He	C	100	7.0586	2.8816	0.9323	1.83e-2	0.00	90.00	66.58
^{4}He	C	140	6.5107	2.4872	0.9451	2.63e-2	0.00	90.00	68.19
^{4}He	C	200	6.0474	2.1599	0.9522	3.45e-2	0.00	90.00	69.73
^{4}He	C	300	5.5877	1.8616	0.9536	4.28e-2	0.00	90.00	71.26
^{4}He	C	400	5.2835	1.6741	0.9516	4.75e-2	0.00	90.00	72.34
^{4}He	C	500	5.0843	1.5587	0.9464	5.05e-2	0.00	90.00	73.10
^{4}He	C	700	5.0583	1.5204	0.9217	5.17e-2	0.00	90.00	73.97
^{4}He	C	1000	4.6895	1.3191	0.9059	5.19e-2	0.00	90.00	75.61
^{4}He	C	2000	4.5101	1.1834	0.8292	4.69e-2	0.00	90.00	79.01
^{4}He	C	3000	4.0905	0.9440	0.8126	4.24e-2	0.00	90.00	81.98
^{4}He	C	5000	3.7153	0.7059	0.7928	3.40e-2	0.00	90.00	85.98
^{4}He	C	10000	2.6820	0.2986	0.9802	2.43e-2	0.00	90.00	91.35
^{4}He	C	20000	2.0022	0.1082	1.0128	1.66e-2	0.00	90.00	86.45
C	C	30	42.3520	22.5877	0.5107	1.83e-5	7.41	116.43	75.33
C	C	40	37.6060	20.3491	0.5157	1.35e-4	7.41	113.29	71.99
C	C	50	32.0236	17.1592	0.5118	5.21e-4	7.41	111.06	71.44
C	C	70	26.5068	14.2187	0.5267	2.57e-3	7.41	108.02	69.37
C	C	100	22.0310	11.8066	0.5552	8.84e-3	7.41	105.23	67.62
C	C	140	18.7261	9.9820	0.5946	2.13e-2	7.41	102.96	66.50
C	C	200	15.8273	8.2671	0.6395	4.14e-2	7.41	100.90	66.38
C	C	300	13.1991	6.6409	0.6938	7.16e-2	7.41	98.93	66.97
C	C	500	10.5675	4.9405	0.7630	1.16e-1	7.41	96.94	68.62
C	C	1000	7.7788	3.1823	0.8291	1.78e-1	7.41	94.92	71.47
C	C	300	13.0293	6.6396	0.7021	8.05e-2	7.40	98.93	66.24
C	C	1000	8.0328	3.4041	0.7226	1.79e-1	7.40	94.92	71.84
C	C	3000	4.9485	1.5045	0.7311	2.49e-1	7.40	92.85	81.25
N	C	40	46.4143	25.1992	0.5238	1.81e-5	1.00	98.98	62.64
N	C	50	41.1533	22.6413	0.5434	1.23e-4	1.00	98.05	61.08
N	C	70	33.5042	18.5624	0.5864	1.11e-3	1.00	96.82	59.92
N	C	100	26.2400	14.2958	0.6513	5.53e-3	1.00	95.71	60.43
N	C	140	20.3476	10.7156	0.7195	1.63e-2	1.00	94.83	61.73
N	C	200	15.5449	7.7646	0.7867	3.68e-2	1.00	94.04	63.53
N	C	300	11.9070	5.5403	0.8432	6.94e-2	1.00	93.30	65.56
N	C	500	8.9090	3.7472	0.8908	1.21e-1	1.00	92.56	68.04
N	C	1000	6.7186	2.4884	0.9106	1.96e-1	1.00	91.81	70.84
N	C	15000	3.1017	0.5614	0.9345	2.64e-1	1.00	90.47	81.85
N	C	30000	2.4599	0.3007	0.9258	2.15e-1	1.00	90.33	85.79

Table 15. Fitting values f, b, c for the angular dependence of the sputtering yield in (6). Furthermore, the values for the yield at normal incidence, $Y(E_0, 0)$, the binding energy, E_{sp}, for the projectiles, the value θ_0^* (deg.), (7), and the angular position, θ_{0m} (deg.), of the maximum yield, (8), are given

Ion	Target	E_0 (eV)	f	b	c	Y(E_0,0)	E_{sp} (eV)	θ_0^*	θ_{0m}
Ne	C	45	42.4911	21.3692	0.6065	1.07e-5	0.00	90.00	61.50
Ne	C	50	39.2571	19.9517	0.6096	3.41e-5	0.00	90.00	60.88
Ne	C	60	34.9544	17.7437	0.6312	1.48e-4	0.00	90.00	60.82
Ne	C	70	30.5197	15.4178	0.6536	4.59e-4	0.00	90.00	60.95
Ne	C	100	23.0552	11.4059	0.7070	3.25e-3	0.00	90.00	61.66
Ne	C	140	17.8207	8.5421	0.7551	1.18e-2	0.00	90.00	62.74
Ne	C	200	13.9445	6.4094	0.7992	3.03e-2	0.00	90.00	64.05
Ne	C	300	10.9291	4.7545	0.8387	6.50e-2	0.00	90.00	65.64
Ne	C	500	8.4196	3.3744	0.8761	1.26e-1	0.00	90.00	67.77
Ne	C	1000	6.3131	2.2510	0.9033	2.32e-1	0.00	90.00	70.51
Ne	C	2000	5.1757	1.6622	0.9003	3.36e-1	0.00	90.00	73.01
Ne	C	5000	4.3556	1.2290	0.8572	4.16e-1	0.00	90.00	76.75
Ne	C	10000	3.6410	0.8456	0.8528	4.21e-1	0.00	90.00	80.50
Ne	C	20000	2.8697	0.4814	0.8953	3.81e-1	0.00	90.00	83.58
Ar	C	70	33.8798	16.4564	0.6471	6.64e-5	0.00	90.00	63.02
Ar	C	100	26.2324	12.6103	0.6901	8.27e-4	0.00	90.00	63.14
Ar	C	140	20.3486	9.5425	0.7354	4.62e-3	0.00	90.00	63.83
Ar	C	200	15.8749	7.1967	0.7784	1.66e-2	0.00	90.00	64.78
Ar	C	300	12.3051	5.3108	0.8200	4.54e-2	0.00	90.00	66.11
Ar	C	500	9.2928	3.7250	0.8616	1.09e-1	0.00	90.00	67.95
Ar	C	1000	6.6196	2.3464	0.9035	2.47e-1	0.00	90.00	70.65
Ar	C	30000	2.4175	0.3179	0.9919	8.57e-1	0.00	90.00	82.69
Xe	C	150	30.7260	13.6835	0.6070	4.50e-5	0.00	90.00	67.97
Xe	C	170	29.2745	12.9894	0.6384	1.24e-4	0.00	90.00	67.57
Xe	C	200	25.3437	11.1859	0.6259	4.15e-4	0.00	90.00	68.05
Xe	C	250	22.4002	9.7749	0.6740	1.70e-3	0.00	90.00	67.72
Xe	C	300	19.5075	8.3043	0.7070	4.24e-3	0.00	90.00	68.20
Xe	C	500	13.2878	5.3847	0.7239	2.76e-2	0.00	90.00	69.80
Xe	C	1000	8.5390	3.0860	0.7752	1.27e-1	0.00	90.00	72.57
Xe	C	3000	5.1292	1.4472	0.7645	4.66e-1	0.00	90.00	79.52
Xe	C	10000	3.8051	0.8756	0.9244	1.02e-0	0.00	90.00	78.55
Xe	C	30000	2.4297	0.3057	1.0023	1.46e-0	0.00	90.00	82.70
Xe	C	100000	1.9300	0.1564	1.0042	1.69e-0	0.00	90.00	85.21
Ar	Al	100	14.7601	8.5471	0.6703	1.17e-1	0.00	90.00	53.34
Ar	Al	500	6.7055	3.4612	0.8024	9.10e-1	0.00	90.00	59.33
Ar	Al	1000	5.4733	2.5849	0.8298	1.37e-0	0.00	90.00	62.79
Ar	Al	1050	4.4893	1.7504	0.8913	1.17e-0	0.00	90.00	68.35
Ar	Al	10000	3.3890	1.0004	0.8667	2.39e-0	0.00	90.00	75.57
D	Si	30	44.6047	26.3734	0.3164	1.52e-4	1.00	100.35	52.21
D	Si	50	25.2643	14.1721	0.5693	3.09e-3	1.00	98.05	59.73
D	Si	100	12.7099	6.0832	0.6848	1.15e-2	1.00	95.71	67.42
D	Si	500	6.3060	2.0569	0.8725	2.48e-2	1.00	92.56	75.30
D	Si	1000	4.6790	1.2020	0.8521	2.36e-2	1.00	91.81	80.31
^{4}He	Si	200	3.3626	1.1091	0.9879	7.68e-2	0.00	90.00	70.92
^{4}He	Si	2000	2.3967	0.4284	0.9844	1.08e-1	0.00	90.00	80.12
^{4}He	Si	3000	2.5727	0.4683	0.9532	9.56e-2	0.00	90.00	80.80
Ar	Si	4500	3.1385	0.8328	0.9440	1.28e-0	0.00	90.00	75.79

Table 16. Fitting values f, b, c for the angular dependence of the sputtering yield in (6). Furthermore, the values for the yield at normal incidence, $Y(E_0, 0)$, the binding energy, E_{sp}, for the projectiles, the value θ_0^* (deg.), (7), and the angular position, θ_{0m} (deg.), of the maximum yield, (8), are given

Ion	Target	E_0 (eV)	f	b	c	Y(E_0,0)	E_{sp} (eV)	θ_0^*	θ_{0m}
Si	Si(KrC)	200	11.0479	6.1405	0.6299	2.13e-1	4.70	98.72	61.01
Si	Si(Mol)	200	10.5874	6.1453	0.6210	2.86e-1	4.70	98.72	58.02
Si	Si(ZBL)	200	11.0834	5.9494	0.6393	1.73e-1	4.70	98.72	63.26
Si	Si(SiSi)	200	7.9001	3.8139	0.6017	1.70e-1	4.70	98.72	65.35
Si	Si	500	7.4656	3.6011	0.8032	4.40e-1	4.70	95.54	65.97
Si	Si	2000	4.7498	1.8181	0.8645	8.96e-1	4.70	92.78	71.39
He	Ti	100000	1.9229	0.1065	0.9665	1.63e-2	0.00	90.00	88.09
Ne	Ti	38	7.8592	4.0707	0.8577	1.12e-2	0.00	90.00	59.06
Ne	Ti	380	4.1989	1.9114	0.9136	5.33e-1	0.00	90.00	63.48
Ne	Ti	3800	3.3212	1.1093	0.8712	1.08e-0	0.00	90.00	72.68
Ar	Ti	1050	3.9753	1.6427	0.8942	1.12e-0	0.00	90.00	66.65
Ar	Ti	150000	1.7921	0.1849	0.9639	1.24e-0	0.00	90.00	85.29
Ar	Ti	900000	1.4988	0.0650	0.9866	6.30e-1	0.00	90.00	88.02
H	V	100	4.3828	3.2190	0.8990	1.01e-4	1.00	95.71	43.98
H	V	120	3.3311	2.2723	0.9700	4.49e-4	1.00	95.22	49.41
H	V	140	2.8610	1.8516	0.9921	1.03e-3	1.00	94.83	52.28
H	V	200	2.1946	1.0807	1.0293	3.09e-3	1.00	94.04	63.12
H	V	400	2.0664	0.5226	1.0687	7.87e-3	1.00	92.86	76.39
H	V	1000	2.3097	0.3954	1.0493	1.04e-2	1.00	91.81	80.48
H	V	3000	2.3607	0.2866	1.0250	8.30e-3	1.00	91.05	83.24
H	V	10000	2.6833	0.3268	0.9415	4.88e-3	1.00	90.57	85.48
D	V	55	5.1320	4.2287	0.8769	2.54e-4	1.00	97.68	34.89
D	V	60	4.7591	3.8345	0.8881	5.51e-4	1.00	97.36	37.10
D	V	70	4.0378	3.1247	0.9217	1.47e-3	1.00	96.82	40.94
D	V	100	2.8895	1.8739	0.9819	5.49e-3	1.00	95.71	52.57
D	V	200	1.9899	0.6708	1.0998	1.70e-2	1.00	94.04	72.10
D	V	500	2.4386	0.5933	1.0536	2.68e-2	1.00	92.56	76.97
D	V	1000	2.3231	0.4408	1.0423	2.85e-2	1.00	91.81	79.60
D	V	3000	2.3990	0.3768	0.9870	2.31e-2	1.00	91.05	82.28
D	V	10000	2.3706	0.2715	0.9614	1.24e-2	1.00	90.57	85.23
T	V	40	6.3376	5.3953	0.8382	3.49e-4	1.00	98.98	31.03
T	V	50	4.7448	3.8690	0.8969	1.79e-3	1.00	98.05	36.46
T	V	70	3.5720	2.5052	0.9398	6.60e-3	1.00	96.82	48.19
T	V	100	2.4950	1.3038	1.0454	1.43e-2	1.00	95.71	62.15
T	V	300	2.7891	0.8677	1.0445	3.78e-2	1.00	93.30	73.79
T	V	1000	2.3834	0.4768	1.0372	4.53e-2	1.00	91.81	79.14
T	V	3000	2.3246	0.3700	0.9891	3.71e-2	1.00	91.05	82.10
T	V	10000	2.2078	0.2396	0.9737	2.03e-2	1.00	90.57	85.17
^{4}He	V	35	1.7453	2.6763	0.9355	5.04e-4	0.00	90.00	0.00
^{4}He	V	40	2.1705	2.6154	0.9342	1.63e-3	0.00	90.00	0.00
^{4}He	V	50	2.5628	2.4407	0.9078	5.65e-3	0.00	90.00	15.76
^{4}He	V	70	1.9394	1.4203	0.9787	1.68e-2	0.00	90.00	42.65
^{4}He	V	100	2.2659	1.2170	1.0013	3.35e-2	0.00	90.00	57.51
^{4}He	V	300	2.6903	0.9304	1.0086	8.98e-2	0.00	90.00	69.65
^{4}He	V	1000	2.2475	0.5217	1.0161	1.24e-1	0.00	90.00	76.23
^{4}He	V	3000	2.1180	0.3668	1.0015	1.17e-1	0.00	90.00	79.99
^{4}He	V	10000	1.9835	0.2272	0.9958	7.55e-2	0.00	90.00	83.55

Table 17. Fitting values f, b, c for the angular dependence of the sputtering yield in (6). Furthermore, the values for the yield at normal incidence, $Y(E_0, 0)$, the binding energy, E_{sp}, for the projectiles, the value θ_0^* (deg.), (7), and the angular position, θ_{0m} (deg.), of the maximum yield, (8), are given

Ion	Target	E_0 (eV)	f	b	c	Y(E_0,0)	E_{sp} (eV)	θ_0^*	θ_{0m}
H	Fe	4000	2.2066	0.2560	1.0265	1.22e-2	1.00	90.49	82.98
H	Fe	8000	2.3317	0.2544	0.9961	8.87e-3	1.00	90.64	84.46
H	Ni	150	3.2117	2.2893	0.9835	2.00e-3	1.00	94.67	46.65
H	Ni	200	2.7207	1.6060	1.0171	4.30e-3	1.00	94.04	56.30
H	Ni	400	2.1098	0.6960	0.9564	1.16e-2	1.00	92.86	73.69
H	Ni	450	1.8895	0.4824	1.0956	1.42e-2	1.00	92.70	75.64
H	Ni	1000	2.0731	0.3479	1.0856	1.52e-2	1.00	91.81	79.80
H	Ni	4000	2.5028	0.3836	0.9871	1.33e-2	1.00	90.91	82.38
H	Ni	8000	2.3038	0.2492	1.0029	9.39e-3	1.00	90.64	84.29
H	Ni	50000	1.7324	0.0610	1.0093	2.70e-3	1.00	90.26	87.89
D	Ni	1000	2.2389	0.4761	1.0506	4.51e-2	1.00	91.81	78.13
D	Ni	4000	1.9552	0.2335	1.0325	3.34e-2	1.00	90.91	83.00
D	Ni	8000	2.0430	0.2136	1.0102	2.37e-2	1.00	90.64	84.27
^{4}He	Ni	100	2.0241	1.3441	0.9916	5.47e-2	0.00	90.00	48.32
^{4}He	Ni	500	2.5267	0.8794	1.0066	1.68e-1	0.00	90.00	69.54
^{4}He	Ni	1000	2.4668	0.7284	0.9950	1.90e-1	0.00	90.00	72.91
^{4}He	Ni	4000	1.9873	0.3420	1.0072	1.67e-1	0.00	90.00	79.90
^{4}He	Ni	8000	2.0723	0.3149	0.9841	1.32e-1	0.00	90.00	81.72
^{4}He	Ni	100000	1.8360	0.0921	0.9937	2.23e-2	0.00	90.00	87.36
Ne	Ni	1000	4.7811	2.7093	0.7414	1.47e-0	0.00	90.00	54.86
Ar	Ni	40	20.4675	11.2697	0.6240	2.88e-3	0.00	90.00	56.17
Ar	Ni	50	14.8926	8.1426	0.7142	1.20e-2	0.00	90.00	56.68
Ar	Ni	70	10.5289	5.9310	0.7567	5.35e-2	0.00	90.00	55.22
Ar	Ni	100	7.6304	4.4032	0.7971	1.53e-1	0.00	90.00	54.13
Ar	Ni	290	5.5978	3.4646	0.7233	7.65e-1	0.00	90.00	49.79
Ar	Ni(ZBL)	290	5.1631	3.2541	0.7388	7.80e-1	0.00	90.00	48.85
Ar	Ni	300	5.0306	2.9919	0.8059	7.78e-1	0.00	90.00	52.63
Ar	Ni	1000	3.9887	2.1644	0.7780	1.97e-0	0.00	90.00	57.09
Ar	Ni	3000	2.8656	1.1258	0.9315	2.81e-0	0.00	90.00	67.63
Ar	Ni	30000	1.9547	0.3494	0.9924	3.23e-0	0.00	90.00	79.90
Ni	Ni	100	14.1078	8.8411	0.5677	1.13e-1	4.46	101.92	53.21
Ni	Ni	500	5.8343	3.5339	0.8012	1.24e-0	4.46	95.40	54.74
Ni	Ni	1000	4.8757	2.7113	0.8474	2.03e-0	4.46	93.82	58.40
Ni	Ni	2500	3.9820	1.8894	0.8896	2.90e-0	4.46	92.42	63.91
Ni	Ni	5000	3.4691	1.4129	0.9121	3.74e-0	4.46	91.71	68.14
Ni	Ni	10000	2.6717	0.8456	0.9678	4.34e-0	4.46	91.21	73.05
Kr	Ni	45000	2.7039	0.6843	0.9179	5.61e-0	0.00	90.00	77.21

Table 18. Fitting values f, b, c for the angular dependence of the sputtering yield in (6). Furthermore, the values for the yield at normal incidence, $Y(E_0, 0)$, the binding energy, E_{sp}, for the projectiles, the value θ_0^* (deg.), (7), and the angular position, θ_{0m} (deg.), of the maximum yield, (8), are given

Ion	Target	E_0 (eV)	f	b	c	Y(E_0,0)	E_{sp} (eV)	θ_0^*	θ_{0m}
H	Cu	50000	1.9195	0.0855	1.0004	3.01e-3	1.00	90.26	87.68
D	Cu	50	4.4937	4.2207	0.8591	1.47e-3	1.00	98.05	18.41
D	Cu	100	1.7910	1.2622	1.0565	1.64e-2	1.00	95.71	48.67
D	Cu	300	2.1337	0.6577	1.1002	4.34e-2	1.00	93.30	70.56
D	Cu	1000	2.1945	0.4894	1.0319	5.39e-2	1.00	91.81	76.41
D	Cu	3000	2.6275	0.5238	0.9010	3.93e-2	1.00	91.05	81.26
D	Cu	10000	2.2766	0.2868	0.9299	2.47e-2	1.00	90.57	85.09
^{4}He	Cu	1000	2.3431	0.6903	0.9933	2.30e-1	0.00	90.00	72.98
Ne	Cu	1000	2.5361	1.1735	0.9540	1.84e-0	0.00	90.00	62.70
Ne	Cu	45000	2.0420	0.3165	0.9773	1.62e-0	0.00	90.00	81.74
Ar	Cu	16	23.7198	11.9382	0.6384	2.12e-5	0.00	90.00	61.24
Ar	Cu	18	22.1882	11.3333	0.6891	7.78e-5	0.00	90.00	60.20
Ar	Cu	20	21.4383	11.0751	0.6527	1.80e-4	0.00	90.00	59.76
Ar	Cu	25	19.9619	10.5883	0.6529	8,40e-4	0.00	90.00	58.33
Ar	Cu	30	17.3814	9.4935	0.6603	3.12e-3	0.00	90.00	56.69
Ar	Cu	40	14.1287	8.0673	0.6709	1.54e-2	0.00	90.00	54.17
Ar	Cu	50	11.7916	6.8970	0.6891	3.96e-2	0.00	90.00	52.86
Ar	Cu	100	5.8601	3.5052	0.8223	2.71e-1	0.00	90.00	52.43
Ar	Cu	300	3.4966	2.0419	0.8881	1.05e-0	0.00	90.00	53.90
Ar	Cu	1050	2.8705	1.4081	0.9193	2.45e-0	0.00	90.00	60.93
Ar	Cu	20000	2.4430	0.6188	0.9469	3.99e-0	0.00	90.00	76.49
Ar	Cu	27000	2.4527	0.5926	0.9391	3.90e-0	0.00	90.00	77.43
Ar	Cu	30000	2.5535	0.6295	0.9259	3.84e-0	0.00	90.00	77.44
Ar	Cu	37000	2.6151	0.6326	0.9153	3.68e-0	0.00	90.00	78.01
Ar	Cu	100000	2.3985	0.4287	0.9369	2.93e-0	0.00	90.00	81.47
Ar	Cu	300000	2.1945	0.2936	0.9252	2.05e-0	0.00	90.00	84.76
Ar	Cu	1000000	1.7152	0.1116	0.9744	1.17e-0	0.00	90.00	87.20
Cu	Cu	20	32.1005	17.5504	0.5452	1.90e-4	3.52	112.76	70.78
Cu	Cu	50	18.4043	10.9887	0.5362	2.45e-2	3.52	104.86	58.42
Cu	Cu	100	12.6246	8.0725	0.5792	1.87e-1	3.52	100.63	51.08
Cu	Cu	300	6.5005	4.0702	0.7677	9.47e-1	3.52	96.18	52.93
Cu	Cu	1000	4.0103	2.1565	0.8836	2.40e-0	3.52	93.40	59.67
Cu	Cu	3000	3.4447	1.5309	0.9067	3.80e-0	3.52	91.96	65.70
Cu	Cu	10000	3.1653	1.1604	0.8892	5.14e-0	3.52	91.07	70.87
Cu	Cu	100000	2.7838	0.6638	0.9178	4.66e-0	3.52	90.34	78.47
Kr	Cu	1050	3.5413	1.7566	0.8719	2.50e-0	0.00	90.00	60.71
Kr	Cu	45000	2.0693	0.4034	0.9762	6.65e-0	0.00	90.00	79.37
Xe	Cu	550	4.4365	2.2223	0.8477	1.37e-0	0.00	90.00	60.43
Xe	Cu	1050	3.9040	1.8736	0.8561	2.31e-0	0.00	90.00	62.02
Xe	Cu	1500	3.8896	1.8648	0.8579	2.32e-0	0.00	90.00	62.05
Xe	Cu	2050	3.5977	1.6054	0.8667	3.48e-0	0.00	90.00	64.51
Xe	Cu	5000	2.8734	1.0386	0.9247	5.17e-0	0.00	90.00	69.84
Xe	Cu	9500	2.8168	0.9214	0.9274	6.33e-0	0.00	90.00	72.10
Xe	Cu	30000	2.6217	0.7036	0.9293	8.10e-0	0.00	90.00	75.93
Xe	Cu	50000	2.1291	0.4332	0.9697	8.70e-0	0.00	90.00	79.03

Table 19. Fitting values f, b, c for the angular dependence of the sputtering yield in (6). Furthermore, the values for the yield at normal incidence, $Y(E_0, 0)$, the binding energy, $E_{\rm sp}$, for the projectiles, the value θ_0^* (deg.), (7), and the angular position, θ_{0m} (deg.), of the maximum yield, (8), are given

Ion	Target	E_0 (eV)	f	b	c	Y(E_0,0)	$E_{\rm sp}$ (eV)	θ_0^*	θ_{0m}
Ga	Ga	100	11.5816	7.0037	0.6206	2.37e-1	2.97	99.78	55.67
Ga	Ga	150	9.1207	5.4708	0.6617	4.43e-1	2.97	98.01	55.69
Ga	Ga	200	7.9098	4.6934	0.6991	6.33e-1	2.97	96.95	56.11
Ga	Ga	300	6.5454	3.7692	0.7209	9.46e-1	2.97	95.68	57.32
Ga	Ga	900	4.6037	2.3725	0.7691	2.08e-0	2.97	93.29	61.67
Ga	Ga	1000	4.4426	2.2574	0.7917	2.22e-0	2.97	93.12	62.13
Ar	Zr	1050	3.1470	1.2965	0.9014	1.00e-0	0.00	90.00	66.66
Ar	Zr	150000	1.9591	0.2715	0.9305	1.28e-0	0.00	90.00	84.26
Ar	Zr	900000	1.5211	0.0854	0.9871	6.60e-1	0.00	90.00	87.25
D	Nb	12200	2.3944	0.2938	0.9234	8.91e-3	1.00	90.52	86.03
He	Nb	36500	2.1121	0.2220	0.9265	3.25e-2	0.00	90.00	86.55
Nb	Nb	60000	3.1234	0.9023	0.8518	3.86e-0	7.59	90.64	76.94
H	Mo	230	2.5308	1.5589	0.9749	6.45e-5	1.00	93.77	54.02
H	Mo	250	2.4814	1.4465	0.9794	1.36e-4	1.00	93.62	56.47
H	Mo	300	1.9363	1.0499	1.0147	4.51e-4	1.00	93.30	59.26
H	Mo	400	1.7189	0.7725	1.0282	1.32e-3	1.00	92.86	65.13
H	Mo	700	1.4682	0.3142	1.0664	3.72e-3	1.00	92.16	78.02
H	Mo	1400	1.8628	0.2690	1.0462	5.79e-3	1.00	91.53	81.76
H	Mo	2000	1.8885	0.2330	1.0410	5.99e-3	1.00	91.28	82.88
H	Mo	3000	2.0833	0.2444	1.0274	6.04e-3	1.00	91.05	83.28
H	Mo	4000	2.2339	0.2605	1.0147	5.55e-3	1.00	90.91	83.69
H	Mo	7000	2.4427	0.2922	0.9822	4.82e-3	1.00	90.68	84.32
H	Mo	8000	2.4361	0.2873	0.9759	4.70e-3	1.00	90.64	84.78
H	Mo	50000	2.2285	0.1283	0.9825	1.36e-3	1.00	90.26	87.59

Table 20. Fitting values f, b, c for the angular dependence of the sputtering yield in (6). Furthermore, the values for the yield at normal incidence, $Y(E_0, 0)$, the binding energy, E_{sp}, for the projectiles, the value θ_0^* (deg.), (7), and the angular position, θ_{0m} (deg.), of the maximum yield, (8), are given

Ion	Target	E_0 (eV)	f	b	c	Y(E_0,0)	E_{sp} (eV)	θ_0^*	θ_{0m}
D	Mo	110	3.6499	2.6095	0.9457	4.86e-5	1.00	95.45	46.36
D	Mo	120	3.2952	2.3286	0.9466	1.57e-4	1.00	95.22	47.01
D	Mo	200	1.9634	1.1456	1.0224	2.83e-4	1.00	94.04	56.81
D	Mo	300	1.4416	0.5467	1.0712	6.97e-3	1.00	93.30	69.42
D	Mo	450	1.4557	0.3418	1.0933	1.14e-2	1.00	92.70	76.80
D	Mo	2000	2.0337	0.3153	1.0220	1.84e-2	1.00	91.28	81.62
D	Mo	8000	2.0631	0.2276	0.9909	1.36e-2	1.00	90.64	84.55
D	Mo	50000	2.1611	0.1359	0.9794	3.50e-3	1.00	90.26	87.40
D	Mo	100000	1.8823	0.0773	0.9826	2.50e-3	1.00	90.18	88.49
T	Mo	75	5.7190	4.3244	0.8477	4.99e-5	1.00	96.59	41.28
T	Mo	80	4.4191	3.3686	0.8953	1.40e-4	1.00	96.38	41.46
T	Mo	90	3.7017	2.7864	0.9114	4.73e-4	1.00	96.02	42.54
T	Mo	100	3.0735	2.2637	0.9516	1.00e-3	1.00	95.71	44.59
T	Mo	170	1.9057	1.0592	1.0260	6.88e-3	1.00	94.39	59.00
T	Mo	300	1.5224	0.4495	1.0976	1.66e-2	1.00	93.30	73.90
T	Mo	1000	1.9541	0.3696	1.0454	3.03e-2	1.00	91.81	79.57
T	Mo	3000	1.8690	0.2429	1.0270	3.03e-2	1.00	91.05	82.70
T	Mo	10000	1.9745	0.2106	0.9852	2.09e-2	1.00	90.57	84.89
^{3}He	Mo	90	2.2907	2.0843	0.9297	4.75e-4	0.00	90.00	22.98
^{3}He	Mo	100	2.2428	1.9581	0.9243	1.12e-3	0.00	90.00	27.62
^{3}He	Mo	140	1.6236	1.2028	0.9934	5.50e-3	0.00	90.00	42.11
^{3}He	Mo	300	1.4534	0.5258	1.0395	2.59e-2	0.00	90.00	68.31
^{3}He	Mo	1000	1.8915	0.4184	1.0215	5.66e-2	0.00	90.00	76.74
^{3}He	Mo	3000	1.9766	0.3390	1.0012	6.41e-2	0.00	90.00	80.09
^{3}He	Mo	10000	1.8416	0.2120	0.9975	5.29e-2	0.00	90.00	83.47
^{4}He	Mo	70	2.1772	2.1982	0.9302	4.82e-4	0.00	90.00	0.00
^{4}He	Mo	80	2.3636	2.1575	0.9161	1.44e-3	0.00	90.00	22.26
^{4}He	Mo	100	1.6240	1.4009	0.9877	4.56e-3	0.00	90.00	30.15
^{4}He	Mo	140	1.4173	0.9332	1.0098	1.28e-2	0.00	90.00	48.90
^{4}He	Mo	1500	1.9254	0.3901	1.0151	8.56e-2	0.00	90.00	77.95
^{4}He	Mo	4000	2.0918	0.3877	0.9785	8.73e-2	0.00	90.00	79.89
^{4}He	Mo	8000	2.0587	0.3226	0.9598	7.73e-2	0.00	90.00	82.17
^{4}He	Mo	50000	1.8652	0.1239	0.9958	2.64e-2	0.00	90.00	86.34
^{4}He	Mo	100000	1.9021	0.1135	0.9788	1.67e-2	0.00	90.00	87.36
Ar	Mo	160	4.8275	2.6130	0.8934	2.12e-1	0.00	90.00	57.22
Ar	Mo	1601	3.1027	1.3279	0.9136	1.37e-0	0.00	90.00	65.40
Ar	Mo	16010	2.9182	0.9421	0.8367	2.23e-0	0.00	90.00	74.24
Ar	Mo	27500	1.7967	0.3351	0.9851	2.52e-0	0.00	90.00	79.64
Mo	Mo	300	10.1673	5.9485	0.6592	3.15e-1	6.83	98.58	57.67
Mo	Mo	350	9.4843	5.5342	0.6670	3.90e-1	6.83	97.95	57.34
Mo	Mo	1000	5.9822	3.2443	0.7442	1.12e-0	6.83	94.72	60.11
Mo	Mo	2000	4.7935	2.4008	0.7783	1.76e-0	6.83	93.34	62.97
Xe	Mo	9500	3.3127	1.2332	0.8500	3.77e-0	0.00	90.00	70.26
Xe	Mo	30000	2.9323	0.8811	0.8899	4.96e-0	0.00	90.00	74.66

Table 21. Fitting values f, b, c for the angular dependence of the sputtering yield in (6). Furthermore, the values for the yield at normal incidence, $Y(E_0, 0)$, the binding energy, E_{sp}, for the projectiles, the value θ_0^* (deg.), (7), and the angular position, θ_{0m} (deg.), of the maximum yield, (8), are given

Ion	Target	E_0 (eV)	f	b	c	Y(E_0,0)	E_{sp} (eV)	θ_0^*	θ_{0m}
Ar	Pd	1050	2.3568	1.1640	0.9286	2.32e-0	0.00	90.00	60.65
D	Ag	100	1.6699	1.1575	0.9596	6.25e-3	0.00	90.00	45.70
Ne	Ag	45000	2.1511	0.4426	0.9044	2.10e-0	0.00	90.00	80.73
Na	Ag	30000	2.2411	0.4338	0.7345	2.34e-0	0.00	90.00	88.48
Ar	Ag	1050	2.1556	1.0385	0.9298	2.82e-0	0.00	90.00	61.50
Ar	Ag	150000	2.2567	0.4090	0.9091	3.50e-0	0.00	90.00	82.21
Ar	Ag	900000	1.6226	0.1125	0.9708	1.56e-0	0.00	90.00	87.08
K	Ag	30000	2.5838	0.7509	0.8372	4.76e-0	0.00	90.00	76.65
Kr	Ag	45000	2.6001	0.7415	0.8747	8.56e-0	0.00	90.00	76.09
H	In	2000	2.1191	0.3247	0.9816	1.65e-2	1.00	91.28	82.88
In	In	100	9.7358	5.6869	0.6304	2.97e-1	2.52	99.02	57.82
In	In	200	6.8624	3.9483	0.6930	7.49e-1	2.52	96.40	57.66
In	In	1000	3.8772	1.9659	0.7756	2.76e-0	2.52	92.87	62.12
H	Ta	25000	2.2410	0.1662	0.9913	1.95e-3	1.00	90.36	86.39
^{4}He	Ta	100000	1.8527	0.1291	0.9751	2.05e-2	0.00	90.00	86.90
Ne	Ta	45000	2.0106	0.4231	0.9077	1.04e-0	0.00	90.00	80.32
Ar	Ta	1050	2.4778	1.1269	0.9297	9.69e-1	0.00	90.00	63.40
Kr	Ta	45000	2.3799	0.7121	0.8775	5.01e-0	0.00	90.00	75.03
H	W	500	2.5871	1.3240	0.9573	1.18e-5	1.00	92.56	60.99
H	W	550	2.0951	1.0881	0.9637	4.25e-5	1.00	92.44	60.36
H	W	600	2.1147	1.0569	0.9534	8.88e-5	1.00	92.34	61.71
H	W	700	1.5690	0.7245	0.9963	2.42e-4	1.00	92.16	64.02
H	W	800	1.9786	0.8800	0.9555	4.18e-4	1.00	92.02	65.34
H	W	900	1.3549	0.5469	0.9980	6.72e-4	1.00	91.91	67.62
H	W	1000	1.3708	0.4824	1.0067	8.64e-4	1.00	91.81	70.70
H	W	2000	1.3195	0.1490	1.0566	2.42e-3	1.00	91.28	83.01
H	W	4000	1.7762	0.1779	1.0283	3.46e-3	1.00	90.91	84.21
D	W	250	4.2860	2.9471	0.7250	2.34e-5	1.00	93.62	44.77
D	W	270	2.6708	1.6256	0.9398	7.63e-5	1.00	93.48	54.23
D	W	300	2.0195	1.1760	0.9927	2.08e-4	1.00	93.30	56.36
D	W	350	1.9721	1.1169	0.9762	5.98e-4	1.00	93.06	57.35
D	W	400	1.6044	0.8545	1.0054	1.11e-3	1.00	92.86	59.65
D	W	500	1.3909	0.6348	1.0216	2.20e-3	1.00	92.56	64.51
D	W	600	0.9409	0.3319	1.0655	3.39e-3	1.00	92.34	70.32
D	W	700	1.1523	0.3351	1.0523	4.22e-3	1.00	92.16	73.95
D	W	1000	1.1544	0.1901	1.0824	6.55e-3	1.00	91.81	80.04
T	W	170	4.0524	2.7547	0.8673	3.77e-5	1.00	94.39	48.03
T	W	180	2.0906	1.4464	0.9946	9.81e-5	1.00	94.26	48.35
T	W	200	2.1916	1.4650	0.9693	3.03e-4	1.00	94.04	49.93
T	W	250	1.6394	1.0231	1.0104	1.23e-3	1.00	93.62	53.51
T	W	300	1.5437	0.8764	1.0206	2.41e-3	1.00	93.30	57.48
T	W	400	1.2873	0.5691	1.0391	4.89e-3	1.00	92.86	65.52
T	W	500	1.1505	0.3777	1.0626	7.22e-3	1.00	92.56	71.95
T	W	700	1.0887	0.2120	1.0927	1.11e-2	1.00	92.16	78.51
T	W	1000	1.1499	0.1573	1.1050	1.49e-2	1.00	91.81	80.97

Table 22. Fitting values f, b, c for the angular dependence of the sputtering yield in (6). Furthermore, the values for the yield at normal incidence, $Y(E_0, 0)$, the binding energy, E_{sp}, for the projectiles, the value θ_0^* (deg.), (7), and the angular position, θ_{0m} (deg.), of the maximum yield, (8), are given

Ion	Target	E_0 (eV)	f	b	c	Y(E_0,0)	E_{sp} (eV)	θ_0^*	θ_{0m}
^{4}He	W	130	3.9913	3.1578	0.8285	3.21e-5	0.00	90.00	34.58
^{4}He	W	140	3.2148	2.5337	0.8598	1.32e-4	0.00	90.00	35.53
^{4}He	W	150	2.0005	1.6150	0.9398	3.10e-4	0.00	90.00	35.12
^{4}He	W	170	2.0656	1.6420	0.9004	9.50e-4	0.00	90.00	35.63
^{4}He	W	200	1.2584	0.9604	0.9999	2.33e-3	0.00	90.00	40.25
^{4}He	W	250	1.1950	0.8161	1.0037	5.42e-3	0.00	90.00	49.96
^{4}He	W	300	1.1907	0.6873	1.0087	8.61e-3	0.00	90.00	54.77
^{4}He	W	350	0.9696	0.4845	1.0304	1.21e-2	0.00	90.00	59.94
^{4}He	W	400	1.2471	0.5171	1.0235	1.47e-2	0.00	90.00	65.30
^{4}He	W	500	1.1760	0.3783	1.0397	2.03e-2	0.00	90.00	70.65
^{4}He	W	600	1.3199	0.3561	1.0396	2.42e-2	0.00	90.00	73.61
^{4}He	W	700	1.2670	0.3010	1.0461	2.88e-2	0.00	90.00	75.30
^{4}He	W	1000	1.4993	0.3257	1.0302	3.78e-2	0.00	90.00	76.77
^{4}He	W	1400	1.6342	0.3388	1.0143	4.57e-2	0.00	90.00	77.70
^{4}He	W	2000	1.7995	0.3688	0.9903	5.15e-2	0.00	90.00	78.41
^{4}He	W	5000	2.0005	0.3776	0.9353	5.91e-2	0.00	90.00	80.91
^{4}He	W	10000	2.0468	0.3395	0.8989	5.63e-2	0.00	90.00	83.58
^{4}He	W	20000	1.5332	0.1238	1.0084	4.78e-2	0.00	90.00	85.08
^{4}He	W	50000	1.6774	0.1195	0.9966	3.23e-2	0.00	90.00	86.03
N	W	48	2.9557	5.8879	0.9465	1.82e-5	1.00	98.21	0.00
N	W	50	1.7735	4.3144	0.9468	5.70e-5	1.00	98.05	0.00
N	W	52	1.2707	3.6458	0.8840	1.35e-4	1.00	97.90	0.00
N	W	55	1.1002	3.3751	0.9604	3.60e-4	1.00	97.68	0.00
N	W	60	0.4622	2.5095	1.0118	9.73e-4	1.00	97.36	0.00
N	W	70	3.5011	4.1573	0.8630	3.26e-3	1.00	96.82	0.00
N	W	80	2.7960	3.4029	0.8841	7.00e-3	1.00	96.38	0.00
N	W	90	2.1152	2.6541	0.9226	1.17e-2	1.00	96.02	0.00
N	W	100	1.7312	2.1735	0.9489	1.72e-2	1.00	95.71	0.00
N	W	120	1.6230	1.6737	1.0004	2.77e-2	1.00	95.22	0.00
N	W	140	1.7195	1.5092	1.0176	3.99e-2	1.00	94.83	30.54
N	W	200	2.0738	1.3460	1.0316	7.57e-2	1.00	94.04	51.98
N	W	300	2.2531	1.2151	1.0310	1.32e-1	1.00	93.30	59.47
N	W	500	2.4324	1.1313	1.0171	2.13e-1	1.00	92.56	62.20
N	W	1000	2.4383	0.9940	0.9936	3.39e-1	1.00	91.81	66.00
Ne	W	45	1.4835	3.8004	0.8094	1.64e-5	0.00	90.00	0.00
Ne	W	50	0.2818	2.3919	0.9244	7.38e-5	0.00	90.00	0.00
Ne	W	60	0.1490	1.7027	0.9423	3.61e-4	0.00	90.00	0.00
Ne	W	70	1.0487	1.9268	0.8972	8.44e-3	0.00	90.00	0.00
Ne	W	80	0.4630	1.3150	0.9399	1.58e-2	0.00	90.00	0.00
Ne	W	100	0.7008	1.0256	0.9957	3.15e-2	0.00	90.00	0.00
Ne	W	140	1.3407	1.0746	0.9942	6.97e-2	0.00	90.00	36.63
Ne	W	200	1.9700	1.1784	0.9844	1.23e-1	0.00	90.00	53.20
Ne	W	300	2.1649	1.1382	0.9810	2.02e-1	0.00	90.00	58.30
Ne	W	400	2.3287	1.1413	0.9754	2.67e-1	0.00	90.00	60.74
Ne	W	500	2.4225	1.1426	0.9688	3.24e-1	0.00	90.00	62.01
Ne	W	700	2.2943	1.0333	0.9668	4.25e-1	0.00	90.00	63.45
Ne	W	1000	2.2664	0.9602	0.9638	5.33e-1	0.00	90.00	65.24

Table 23. Fitting values f, b, c for the angular dependence of the sputtering yield in (6). Furthermore, the values for the yield at normal incidence, $Y(E_0, 0)$, the binding energy, E_{sp}, for the projectiles, the value θ_0^* (deg.), (7), and the angular position, θ_{0m} (deg.), of the maximum yield, (8), are given

Ion	Target	E_0 (eV)	f	b	c	Y(E_0,0)	E_{sp} (eV)	θ_0^*	θ_{0m}
Ar	W	30	18.8008	14.3233	0.5298	1.03e-5	0.00	90.00	29.59
Ar	W	35	6.8215	6.2803	0.5504	1.17e-4	0.00	90.00	10.89
Ar	W	40	0.0399	1.2328	0.8651	4.63e-4	0.00	90.00	0.00
Ar	W	45	0.0200	0.9444	0.9324	1.26e-3	0.00	90.00	0.00
Ar	W	50	0.0092	0.7256	1.0034	2.85e-3	0.00	90.00	0.00
Ar	W	55	0.0177	0.5887	1.0523	5.23e-3	0.00	90.00	0.00
Ar	W	60	0.4625	0.7963	1.0148	8.40e-3	0.00	90.00	0.00
Ar	W	70	1.1976	1.1420	0.9778	1.75e-2	0.00	90.00	17.06
Ar	W	80	1.5694	1.2543	0.9772	2.86e-2	0.00	90.00	36.57
Ar	W	100	1.9354	1.3595	0.9674	5.60e-2	0.00	90.00	45.02
Ar	W	140	2.4932	1.5322	0.9542	1.16e-1	0.00	90.00	51.84
Ar	W	200	2.8464	1.6178	0.9437	2.01e-1	0.00	90.00	55.25
Ar	W	300	2.7481	1.4845	0.9442	3.36e-1	0.00	90.00	57.30
Ar	W	500	2.6042	1.3461	0.9401	5.62e-1	0.00	90.00	58.98
Ar	W	700	2.6193	1.3056	0.9333	7.25e-1	0.00	90.00	60.31
Ar	W	1000	2.4763	1.1745	0.9366	9.26e-1	0.00	90.00	62.00
Ar	W	1005	2.4753	1.1700	0.9371	9.39e-1	0.00	90.00	62.11
Ar	W	1050	2.4911	1.1739	0.9341	9.61e-1	0.00	90.00	62.22
Ar	W	30000	1.5166	0.2967	0.9875	2.59e-0	0.00	90.00	79.04
Xe	W	9500	2.1148	0.7406	0.9329	4.25e-0	0.00	90.00	70.47
Xe	W	30000	2.2644	0.7036	0.9115	5.94e-0	0.00	90.00	73.50
W	W	35	32.1495	16.2298	0.4627	2.13e-5	8.68	116.47	80.98
W	W	40	31.5560	16.1944	0.4990	5.60e-5	8.68	114.98	77.95
W	W	50	31.1720	16.3715	0.5115	1.92e-4	8.68	112.62	74.22
W	W	50	29.1892	14.9454	0.4922	1.77e-4	8.68	112.62	76.62
W	W	50	31.1660	16.1845	0.5159	1.92e-4	8.68	112.62	75.18
W	W	60	28.4556	15.0978	0.5159	5.89e-4	8.68	110.82	72.13
W	W	70	25.7454	13.7699	0.5175	1.51e-3	8.68	109.40	70.52
W	W	80	23.3907	12.5813	0.5156	3.15e-3	8.68	108.23	69.29
W	W	100	19.8712	10.8397	0.5208	9.54e-3	8.68	106.42	66.95
W	W	100	20.1422	10.9606	0.5241	9.26e-3	8.68	106.42	67.16
W	W	120	17.5207	9.6863	0.5251	2.04e-2	8.68	105.05	64.98
W	W	140	15.8372	8.8582	0.5403	3.58e-2	8.68	103.98	63.43
W	W	200	12.9717	7.4152	0.5705	9.68e-2	8.68	101.77	60.57
W	W	300	10.2481	5.9264	0.6168	2.28e-1	8.68	99.65	58.79
W	W	350	9.5022	5.4740	0.6363	2.92e-1	8.68	98.95	58.78
W	W	400	8.9966	5.1930	0.6532	3.59e-1	8.68	98.38	58.41
W	W	500	8.1383	4.6991	0.6674	4.97e-1	8.68	97.51	60.21
W	W	800	6.1837	3.4586	0.7349	8.47e-1	8.68	95.95	59.20
W	W	1000	5.6049	3.0949	0.7587	1.07e-0	8.68	95.32	59.35
W	W	1000	5.8226	3.2309	0.7429	1.04e-0	8.68	95.32	59.26
W	W	2000	4.4556	2.3233	0.7594	1.81e-0	8.68	93.77	61.45
W	W	2500	4.0991	2.0502	0.8270	2.10e-0	8.68	93.37	62.84
W	W	5000	3.6732	1.7278	0.8289	3.11e-0	8.68	92.39	64.62

Table 24. Fitting values f, b, c for the angular dependence of the sputtering yield in (6). Furthermore, the values for the yield at normal incidence, $Y(E_0, 0)$, the binding energy, E_{sp}, for the projectiles, the value θ_0^* (deg.), (7), and the angular position, θ_{0m} (deg.), of the maximum yield, (8), are given

Ion	Target	E_0 (eV)	f	b	c	Y(E_0,0)	E_{sp} (eV)	θ_0^*	θ_{0m}
H	Au	1000	1.1436	0.1758	1.0340	7.55e-3	0.00	90.00	80.23
H	Au	4000	1.7553	0.1874	1.0068	1.10e-2	0.00	90.00	83.65
D	Au	130	2.8168	2.1780	0.8276	2.44e-4	1.00	95.01	38.42
D	Au	140	2.1529	1.6150	0.9556	4.92e-4	1.00	94.83	42.96
D	Au	150	2.0274	1.5209	0.9366	7.96e-4	1.00	94.67	42.59
D	Au	160	1.9649	1.3976	0.9776	1.14e-3	1.00	94.52	46.64
D	Au	200	1.7254	1.1440	0.9847	3.05e-3	1.00	94.04	50.51
D	Au	250	1.9522	1.1324	0.9057	5.45e-3	1.00	93.62	56.45
D	Au	300	1.2658	0.5848	1.0421	7.84e-3	1.00	93.30	64.55
D	Au	500	0.9402	0.1928	1.1191	1.60e-2	1.00	92.56	77.78
D	Au	1000	1.3545	0.2159	1.0734	2.51e-2	1.00	91.81	80.27
D	Au	3000	1.6865	0.2338	0.9943	3.12e-2	0.00	90.00	82.20
Na	Au	30000	2.2786	0.6106	0.8236	2.20e-0	1.00	90.33	79.04
Ne	Au	6000	1.9240	0.6608	0.9121	2.18e-0	0.00	90.00	71.27
Ne	Au	14000	1.6611	0.4130	0.9587	2.31e-0	0.00	90.00	76.51
Ar	Au	1050	1.8345	0.9363	0.9395	2.24e-0	0.00	90.00	59.44
Ar	Au	3000	1.7776	0.7560	0.9330	3.52e-0	0.00	90.00	65.41
Ar	Au	6000	1.4391	0.4722	0.9762	4.28e-0	0.00	90.00	71.21
Ar	Au	10000	1.5072	0.4461	0.9697	4.74e-0	0.00	90.00	73.33
Ar	Au	30000	1.8818	0.5059	0.9221	5.11e-0	0.00	90.00	76.07
K	Au	30000	2.2529	0.3512	0.8527	4.72e-0	1.00	90.33	86.35
Xe	Au	10000	2.3259	0.9589	0.8569	8.88e-0	0.00	90.00	67.16
Kr	Hg	762	3.0516	1.4476	0.8695	1.06e-0	0.00	90.00	62.37
H	U	2000	1.2788	0.1275	1.0504	4.13e-3	1.00	91.28	82.73
Kr	U	17900	1.6156	0.4821	0.9436	5.76e-0	0.00	90.00	73.68

Table 25. Elemental targets for which measurements and static calculations (low fluence), not included in fits and figures, have been performed

Target	Ion	Energy (keV)	Angle (deg.)	Meas.	Calc.
Li	D,Li	0.075,0.125,0.2	0–89		[328]
Li	D,T,Li	0.01–10	0–85		[329]
Li	D,^{4}He,Li	0.1–1	45	[46]	[46]
Li	D,^{4}He,Li	0.7	45	[330]	[330]
Li	T	0.01–1	0–85		[331]
Li	Li	0.05–50	0		[332]
Be	D	0.01–0.7	45	[333]	[333]
Be	T	0.015–1	0–85		[331]
Be	Be	0.05–50	0		[332]
Be	Be	1, 3	0–85		[334]
B	B	1	0–85		[334]
C	H	0.3	0, 60		[335]
C	H,D,T	0.05–10	0		[336]
C	H,D,T,^{3}He,^{4}He	0.02–10	0–85		[331]
C	H, Xe	0.4,1,10,40	0,60,80		[28]
C	^{4}He	0.1–9	0		[337]
C	C	0.03–10	0–85		[332, 338]
C	C	0.1, 0.3	0–75		[335]
C	Ar	0.4, 10, 40	0, 60		[339]
C	Ar	1	0–85		[340]
C	Ar_n	0.1/atom	0		[341]
C	C + Pt	0.3–1	0		[342]
Al	O	10	0	[158]	
Al	O	5	0	[343]	
Al	Ne,Al,Ar,Kr,Xe	10–50	0		[344]
Al	Al	0.025–0.09	0–90		[345]
Al	Ar	40	0–85		[346]
Al	Ar	3	0		[347]
Si	O	10	0	[158]	
Si	O	5	0	[343]	
Si	O,Ar	4.5,9	0–60	[242]	
Si	Ne	0.2–0.62	0		[348]
Si	Ne,Ar,Xe	0.5,1,5	60	[349]	[349]
Si	Si	0.05–100	0		[332]
Si	Si	0.5–5	0		[350]
Si	Si	0.03–10	0–89		[351]
Si	Si,Ar,Kr	0.04, 0.6	0		[348]
Si	Ar	3,5,10	0,45,60		[124]
Si	Ar	0.4,1	0		[339]
Si	Ar	0.2–100	0		[352]
Si	Ar	3	51		[353, 354]
Si	Ar	0.15–3	0		[355]
Si	Ar	1.05	0–85		[356, 357]
Si	Ar	5,10	0		[358, 359]
Si	Ar	0.05–2			[360]
Si	Ar,Kr	1	0		[361]
Si	Xe	2–12	0	[362]	

Table 26. Elemental targets for which measurements and static calculations (low fluence), not included in fits and figures, have been performed

Target	Ion	Energy (keV)	Angle (deg.)	Meas.	Calc.
Ti	O	10	0	[158]	
Ti	^{4}He	0.15–10	0		[337]
V	O	10	0	[158]	
V	^{4}He	0.2–10	0		[363]
Cr	O	10	0	[158]	
Mn	O	10	0	[158]	
Fe	H,D,T,^{4}He	0.6–10	0		[270, 364]
Fe	D	0.06–200	0		[365]
Fe	D	50,100,200	60,75,85		[365]
Fe	O	10	0	[158]	
Fe	Ar	0.3–5	0		[366]
Co	O	10	0	[158]	
Co	Ar	0.2–10			[367]
Co	Ar	1	0–85		[368]
Ni	H	50	0–85		[135]
Ni	H	0.45,1,4	0–80		[258]
Ni	H	0.1,0.2,0.45,1	0–85		[369, 370]
Ni	H	1	0–80		[318]
Ni	H	4	80		[371]
Ni	H,D,T,^{4}He	0.1–10	0–85		[372]
Ni	H,D,T,^{4}He	0.05–8	0		[336]
Ni	H,D,^{4}He,Ne,Ar	0.15–100	0–87.5		[28, 373]
Ni	D	0.08–50	0		[28, 373]
Ni	D	1	0–85		[365]
Ni	^{4}He	100	0–80		[135]
Ni	^{4}He	0.03,0.1,1	0		[370]
Ni	^{4}He	4	0–85		[374]
Ni	^{4}He,Ne	1	0–80		[318]
Ni	^{4}He,Ne	0.1–100	0		[318]
Ni	Li,B,N,Ne,Al	0.15	0		[375, 376]
Ni	O	10	0	[158]	
Ni	Ca,Ni,Ga,Kr,Xe	0.15	0		[375, 376]
Ni	Ne	1	0–87.5		[28]
Ni	Ne	0.1–100	0–85		[377]
Ni	Ar	40	0–85		[346]
Ni	Ar	0.1–0.5	0		[134]
Ni	Ar	0.2	0	[378, 379]	
Ni	Ar	0.5, 1	0–85		[340]
Ni	Ni	0.03–100	0–80		[332, 380]
Ni	Ni	0.03,0.1,1	0		[370]
Ni	Xe	0.07–100	0–87.5		[28, 318]

Table 27. Elemental targets for which measurements and static calculations (low fluence), not included in fits and figures, have been performed

Target	Ion	Energy (keV)	Angle (deg.)	Meas.	Calc.
Cu	H	50	0–78		[135]
Cu	D	30–300	0		[381]
Cu	^{4}He	0.08–50	0		[337]
Cu	^{4}He,Ne,Xe	3	0		[382, 383]
Cu	^{4}He,Ne,Kr,Xe	1	0		[352, 358]
Cu	^{4}He,N,Ne,Ar,Kr,Xe	0.5–2	0–70		[384]
Cu	O	10	0	[158]	
Cu	Ne	10	0		[385]
Cu	Ne, Xe	3	0		[382]
Cu	Ar	1–30	0		[383]
Cu	Ar	1.05	0–85		[356]
Cu	Ar	0.01–1	0–85		[370]
Cu	Ar	0.1–1.4	0		[352]
Cu	Ar	40	0–85		[346]
Cu	Ar	3,30,300	0		[382]
Cu	Ar	5	0		[386]
Cu	Ar	5	0		[387]
Cu	Ar	1	0–85		[368]
Cu	Ar	0.3	0–60		[388]
Cu	Ar, Cu	0.5–10	0		[389]
Cu	Ar, Xe	0.4,10,40	0,60		[339]
Cu	Cu	1	0		[358]
Zn	O,Ar	1	70	[209]	
Ga	D,T,Ga	0.02–10	0–80		[329]
Ga	D,Ga	0.075,0.125,0.2	0–89		[328]
Ga	O	5	0	[343]	
Ge	O a	10	0	[158]	
Ge	O	5	0	[343]	
Ge	Ar	0.4,1	0		[339]
Ge	Ar	1.05	0–85		[356, 357]
Ge	Ge,Kr	0.1–0.62	0		[348]
Nb	H	16400	0		[186, 390]
Nb	O	10	0	[158]	
Nb	Ar	20	0,45,77,85		[391]
Mo	H,^{4}He	0.1 – 10	0		[270]
Mo	H,D,^{4}He	50,100	0–75		[135]
Mo	H, D, T	2	0–85		[365, 372]
Mo	D	0.06–200	0,60,75,85		[365]
Mo	D,T,^{4}He	0.15–9	0		[336]
Mo	D,T,Mo	0.03–100	0–85		[392]
Mo	O	10	0	[158]	
Mo	Mo	0.05–100	0		[332]
Ag	^{4}He,O,Ar,Xe	1	70	[209]	
Ag	O	10	0	[158]	
Ag	Ar	0.015,0.1,1	0		[370]
Ag	Ar	1.05	0–85		[356]
Ag	Xe	0.4,10	0		[339]

Table 28. Elemental targets for which measurements and static calculations (low fluence), not included in fits and figures, have been performed

Target	Ion	Energy (keV)	Angle (deg.)	Meas.	Calc.
Cd	O	5	0	[343]	
Cd	Ar, Xe	0.4,10,40	0		[339]
In	D,T,In	0.02–10	0–80		[329]
In	Ar	1	70	[209]	
Sn	H,D,^{4}He	0.3–1	45	[393]	[393]
Sn	O	10	0	[158]	
Sn	O	5	0	[343]	
Ta	H	25	0–70		[135]
Ta	Ar	1.05	0–85		[356, 357]
Ta	Li,B,N,Ne,Al	0.15	0		[375, 376]
Ta	Ca,Ni,Ga,Kr,Xe	0.15	0		[375, 376]
W	D	0.06–200	0,60,75,85		[365]
W	D,T,W	0.03–50	0–85		[392]
W	O	10	0	[158]	
W	W	0.03 -100	0–80		[332]
W	W	10	70		[358]
W	W	0.15–1	0, 20		[394]
Pt	Ne	0.03,0.1,1	0		[370]
Pt	Ar	0.2–50	0		[395]
Au	H, D, T	1	0–83		[372]
Au	D	0.15–20	0		[337]
Au	D,T,^{4}He	0.1–8	0		[336]
Au	^{4}He	0.15–9	0		[337]
Au	O	10	0	[158]	
Au	Ar	1	70	[209]	
Au	Ar	0.4,10	0,60		[339]
Au	Ar	0.02,0.1,1	0		[370]
Au	Xe	0.4,10	0,60		[339]
Au	Au	100	0		[396]
Au	Au	10–10000	0		[397]
U	U	0.05–9	0–85		[300]
U	U	0.1–10	0		[398]
U	U	0.05–100	0		[332]

Table 29. Elemental targets bombarded with metal ions for which experiments and/or static calculations (low fluence) have been performed

Target	Ion	Energy (keV)	Angle (deg.)	Exp.	Calc.
Be	C	3	0–70		[334]
Be	Hg	1	0	[399]	
C	Cd	0.1–0.5	0	[400]	
C	W	100	0	[290]	[290]
C	Hg	0.05–0.5	0	[401]	
C	Hg	5–100	0–60	[402]	
C	Hg	10–25	0	[403]	
C	Hg	0.4–10	0		[25, 370]
Al	Au	50	0	[237]	
Al	Hg	0.5–3	0	[399]	
Al	Hg	0.125–0.35	0	[401, 404]	
Al	Hg	0.4	0	[63]	
Al	Hg	20	0	[403]	
Al	Hg	0.07,0.2,1	0		[370]
Si	B	20,40,60	0		[405]
Si	Al	25,50,100,150	0		[405]
Si	P	25,50,100,150	0		[405]
Si	Ge	0.04–0.2	0		[348]
Si	As	25,50,100,150	0		[405]
Si	Cs	2–12	0–60	[362]	
Si	Au	50	0	[237]	
Si	Hg	1	0	[399]	
Si	Hg	0.125–0.35	0	[401]	
Si	Hg	0.4	0	[63]	
Si	Pb	25–500	0	[114]	
Si	Pb	0.03–20	0		[25, 370]
Ti	Cd	0.1–0.5	0	[400, 406]	
Ti	Hg	0.1–0.5	0	[401, 404]	
Ti	Hg	4–14	0	[211]	
Ti	Hg	0.4	0	[63]	
Ti	Hg	0.04–0.28	0	[407]	
Ti	Hg	15,20,25	0	[403]	
V	Hg	0.125–0.35	0	[401]	
V	Hg	4–15	0	[211]	
V	Hg	0.4	0	[63]	
Cr	Hg	1	0	[399]	
Cr	Hg	0.1–0.3	0	[401, 404]	
Cr	Hg	0.025–0.35	0	[142]	
Cr	Hg	0.05–0.23	0	[407]	
Mn	Hg	1	0	[399]	
Fe	Ti	110	0	[408]	
Fe	Ni	90	0	[139]	
Fe	Hg	0.5–4	0	[399]	
Fe	Hg	0.4,0.8	0–75	[409]	
Fe	Hg	1–100	0–60	[402]	
Fe	Hg	0.1–0.4	0	[401, 404]	
Fe	Hg	4–15	0	[211]	
Fe	Hg	0.04–0.3	0	[407]	
Fe	Hg	20	0	[403]	

Table 30. Elemental targets bombarded with metal ions for which experiments and/or static calculations (low fluence) have been performed

Target	Ion	Energy (keV)	Angle (deg.)	Exp.	Calc.
Ni	Cu	90	0	[139]	
Ni	Hg	0.5–4	0	[399]	
Ni	Hg	0.07–0.4	0	[401]	
Ni	Hg	0.2,0.8	0–62	[409]	
Ni	Hg	4–15	0	[211]	
Ni	Hg	0.02–0.25	0	[407]	
Ni	Hg	10–25	0	[403]	
Ni	Hg	0.03–0.1	0–85		[369, 370]
Co	Hg	1	0	[399]	
Co	Hg	0.125–0.35	0	[401]	
Co	Hg	4–15	0	[211]	
Co	Hg	0.04–0.25	0	[407]	
Cu	Be	0.5, 1	0		[384]
Cu	Na,Si,P,S,Cl,K	5–20	0	[263]	
Cu	V,Bi	45	0	[410]	
Cu	Ni	90	0	[139]	
Cu	Zn,Cd,I,Hg,Tl	5–20	0–53	[263]	
Cu	Co,Ni,Cd	39	0	[173, 411]	
Cu	Cd, Hg	0.1–0.5	0	[400]	
Cu	Ag	0.5, 1	0		[384]
Cu	Hg	1	0	[399]	
Cu	Hg	0.06–0.3	0	[401]	
Cu	Hg	4–15	0	[211]	
Cu	Hg	0.03–0.25	0	[407]	
Cu	Hg	10–25	0–45	[403]	
Cu	U	30	0	[108]	
Zn	Ni,Co,Cu,Cd	39	0	[173, 176, 411]	
Ge	Hg	0.125–0.4	0	[401]	
As	Ag	45,90	0	[139]	
Zr	Cd	0.1–0.5	0	[400, 406]	
Zr	Hg	1	0	[399]	
Zr	Hg	0.1–0.4	0	[401]	
Zr	Hg	0.04–0.28	0	[407]	
Nb	Br	100,70000	0	[192]	
Nb	Hg	0.2–0.4	0	[401]	
Nb	Hg	0.05–0.25	0	[407]	
Mo	Cd	0.1–0.5	0	[400]	
Mo	Hg	0.5–4	0	[399]	
Mo	Hg	0.15–0.8	0–65	[401, 409]	
Mo	Hg	4–15	0	[211]	
Mo	Hg	0.04–0.26	0	[407]	
Mo	Hg	15,20,25	0	[403]	
Rh	Hg	0.075–0.3	0	[401]	
Rh	Hg	4–15	0	[211]	
Pd	Hg	1	0	[399]	
Pd	Hg	0.075–0.3	0	[401]	
Pd	Hg	4–15	0	[211]	

Table 31. Elemental targets bombarded with metal ions for which experiments and/or static calculations (low fluence) have been performed

Target	Ion	Energy (keV)	Angle (deg.)	Exp.	Calc.
Ag	Hg	1	0	[399]	
Ag	Hg	0.05–0.25	0–60	[401]	
Ag	Hg	0.125	0–60	[409]	
Ag	Hg	4–15	0	[211]	
Ag	Hg	0.03–0.2	0	[407]	
Ag	Hg	10–25	0	[403]	
Ag	Bi	30	0		[397]
Cd	Ni	39	0	[411]	
In	Hg	20	0	[403]	
Sn	Co,Cu,Cd	39	0	[411]	
Ho	Hg	20	0	[403]	
Hf	Hg	0.12–0.4	0	[401]	
Ta	Cd	0.1–0.5	0	[400]	
Ta	Hg	1	0	[399]	
Ta	Hg	0.11–0.35	0	[401]	
Ta	Hg	0.4	0–70	[409]	
Ta	Hg	4–15	0	[211]	
Ta	Hg	0.04–0.26	0	[407]	
Ta	Hg	10–25	0	[403]	
W	C	1, 6	0–70		[412]
W	C	2.4	0	[413]	
W	CH_3	3.0	0	[413]	
W	Cd	0.1–0.5	0	[400]	
W	Hg	0.5–2	0	[399]	
W	Hg	0.04–0.4	0	[401]	
W	Hg	0.2–0.8	0–65	[409]	
W	Hg	4–15	0	[211]	
W	Hg	0.05–0.29	0	[407]	
Re	Hg	0.125–0.35	0	[401]	
Ir	Hg	0.1–0.3	0	[401]	
Pt	Hg	1	0	[399]	
Pt	Hg	0.2	0–70	[409]	
Pt	Hg	4–15	0	[211]	
Pt	Hg	0.03–0.29	0	[407]	
Au	Al	50	0	[237]	
Au	S	80000	0	[414]	
Au	Ni	69000	0	[414]	
Au	I	99000,198000	0	[414]	
Au	Hg	0.05–0.25	0	[401]	
Au	Hg	4–15	0	[211]	
Au	Hg	0.02–0.19	0	[407]	
Au	Bi	30	0		[397]
Pb	Ni	39	0	[411]	
Th	Hg	0.1–0.42	0	[401]	
U	Hg	0.075–0.35	0	[401]	

Table 32. Crystalline targets for which experiments and/or static calculations (low fluence) have been performed

Single crystal target	Ion	Energy (keV)	Angle (deg.)	Exp.	Calc.
Be(001),(010),(110)	D,^{4}He	0.1	0–80		[415]
Bn(0001)	Ar,Xe	0.3–3	0	[416]	[416]
Al(100)	Al	0.1–1.3	0		[417]
Al(111)	Al	0.025–0.15	0–90		[345]
Al(111)	Ar	3	0		[347]
Si	Ar	1	0–50	[418]	
Si(100)	Ar	0.5	45		[419]
Si(100),(110),(111)	Ar	40	0	[122]	
Si(111)	Ar	0.04–8	0		[420]
Si(111)	Ar	0.05–0.8	0	[421]	
Si(111)	Ar	1–5	0	[146]	
Si(111)	V,Co,Ni,Er	40	0	[422]	
Fe(001)	Ar	1	65		[311]
Ni(100)	Ar	0.2	0		[423]
Ni(100)	Ar	0.2	0		[424]
Ni(100)	Ar	1	0		[425]
Ni(100)	Ar	0.02–0.04	0		[426]
Ni(001)	Ar	1	0–75		[311]
Ni(001)	Ne	10	0–85		[312]
Ni(110)	Ar	15	30	[379, 427]	
Ni(111)	Al	0.025–0.15	0–90		[345]
Ni_3Al(100)	Al	0.5,1.3	0		[417]
$Ni_{0.35}Fe_{0.65}$(111)	Ne	10	45	[428]	
minerals(001)	^{4}He,N,Ne,Ar,Xe	50	0–60	[429]	

Table 33. Crystalline targets for which experiments and/or static calculations (low fluence) have been performed

Single crystal target	Ion	Energy (keV)	Angle (deg.)	Exp.	Calc.
Cu(111)	^{4}He,B,Ne,Ar,Xe	3	0		[347, 430]
Cu(111)	Ne,Ar	0.6, 5	0		[431]
Cu(100),(110),(111)	Ar	1–20	0		[432]
Cu(100)	Ar	5	0		[433]
Cu(100)	Ar	20	29–61		[433]
Cu(100),(110),(111)	Ar	0.6	0		[434]
Cu(100)	Ar	0.6	0		[435]
Cu(100),(111)	Ar	0.6–20	0		[436, 437]
Cu(100)	Ar	5	0		[438]
Cu(100)	Ar	0.6	0–60		[439]
Cu(100),(111)	Ar,Kr,Xe	0.6,5	0		[440]
Cu(111)	Ar	1–10	0		[358]
Cu(100)	Ar	40	1–8		[441]
Cu(100)	Ar	27	0–75		[442]
Cu(100)	Ar	1.05,5	0–85		[443]
Cu(100)	Ar	0.1,0.5	0		[444]
Cu(100)	Ar	27	0–87		[445, 446]
Cu(100),(110),(111)	Ar	0.2,5	0		[447]
Cu(100)	Ar	0.5,5	0–85		[279]
Cu(001)	Ar	0.05–0.6	0		[448]
Cu(100)	Ar	0.05–1	0		[449]
Cu(100),(110).(111)	Ar	0.5–5	0		[278]
Cu(122)	Ar	0.5–5	0		[278]
Cu(001)	Ar	0.06–0.6	0		[450]
Cu(111),(113),(122)	Ar	0.5–5	0	[146]	
Cu(123),(011),)001)	Ar	0.5–5	0	[146]	
Cu(012)	Ar	0.5–5	0	[146]	
Cu(111)	Ar,Cu	0–0.25	0–85		[451]
Cu(001)	Ar	20, 30	0–41		[452, 453]
Cu(001)	Ar	0.01–2.5	0		[454]
Cu(100)	Ar,Kr,Xe	5	60–70		[455]
Cu(100)	Ar	5	0–48		[456]
Zn(1000),(1010),(1120)	Ar	3	0		[278]
Ge(100),(110),(111)	Ar	1–5	0	[146]	
Ge(100),(110),(111)	Ar	40	0	[122]	
Ge(100),(110),(111)	Ge	50	0	[402]	
Gd(0001)	Ne	20	30	[379, 457]	
Pt(111)	Ne,Ar,Xe	0.04–5	0		[458]
Pt(111)	Xe	5	0–85		[459]
Pt(100)	Pt	0.1–200	0		[460]
Pt(111)	Pt	0.1–200	0		[461]
Au(100)	Be,N,Ne,Cu	0.1–2	0		[462]
Au(111)	Ar	3	0		[347]
Au(100)	Mo,Xe,Er,Au	0.1–2	0		[462]
Au(111),(001)	Au	0.5–500/nucl.	0		[463]
Pb/CU(100)	Ar	3	0		[464]

Table 34. Compound targets for which experiments and/or static calculations (low fluence) have been performed

Compound	Ion	Energy (keV)	Angle (deg.)	Exp.	Calc.
LiF	Ar	0.01–5	0	[129, 465]	[466]
Be_4B	H,D,^{4}He	0.05–4	0	[27, 467]	
Be_2C	D	0.02–2	0		[47]
Be-C	Be	0.3–5	0	[62]	
Be-W	Be	0.3–5	0	[62]	
$^{10}B_{0.2}{}^{11}B_{0.8}$	^{4}He,Ar,Kr,Xe	0.07–2	60		[293]
B_4C	H	0.06–8	0	[69]	
B_4C	H,D,^{4}He	0.1–4	0	[27, 72]	[27]
B_4C	H,D,^{4}He	0.06–8	0–75	[27, 51, 111]	
B_4C	H,D,^{4}He	0.025–8	0–85		[27, 36]
B_4C	D,^{4}He	0.03–10	0		[468]
B_4C	Ne	0.15–10	0	[27, 66]	
B_4C	C,O, Ne	0.015–3	0–80		[27, 36]
B_4C	Cd	0.1–0.5	0	[400]	
BN	Ar	0.3–5	0,45	[469]	[469]
BN	Ar	0.3–10	0,45		[470, 471]
BN	B,N,Ne,Ar,Kr,Xe	0.15–10	0,45	[472]	[472]
BN	Li,B,N,Ne,Al	0.2–2	0		[375, 376]
BN	Ca,Ni,Ga,Kr,Xe	0.2–2	0		[375, 376]
BeO	H,D,^{4}He	0.05–4	0	[27, 50, 51, 252]	
BeO	D	0.33–3.33	0	[75]	
BeO	O	0.1–10	0–85		[27, 36]
B_2O_3	O	0.15–3	0		[27, 36]
$B(OH)_3$	O	0.15–3	0		[36]
C/USB15	D	0.01–3	0–80	[27]	[27]
SAP	H,D,^{4}He	0.25–8	0	[51, 473]	
MgO	Ar	3–25	0	[474]	
MgO	Ar	0.05–1	0	[129]	
AlN	Ar	0.3–5	0,45	[469]	[469]
AlN	Ar	0.3–10	0,45		[470, 471]
Al_2O_3	H,D,^{4}He	0.10–8	0	[27, 51, 473]	
Al_2O_3	Ar	3–25	0	[474]	
Al_2O_3	Xe^{q+}	0.1–1.5	0	[475]	
SiC	H	0.6–20	0	[69]	
SiC	H	5, 7.5	0	[68]	
SiC	H,D,^{4}He	0.10–8	0–80	[27, 51, 72, 111]	
SiC	H,D,^{4}He	0.10–8	0	[52]	
SiC	D,^{4}He	0.02–10	0		[468]
SiC	O,Ne	0.15–10	0	[27, 78]	
SiC	Ar,Xe	0.5–5	60,80	[349]	[349]
Si_3N_4	H	0.1–1	0	[127]	
Si_3N_4	Ar,Kr	0.5–2.5	0?	[126]	
SiO_2	H,D,^{4}He	0.06–8	0	[27, 51]	
SiO_2	Ar	3–40	0–70	[474]	
SiO_2	Ar	0.06–1	0	[129]	
SiO_2	Ar,CF_4	0.07–1.5	0	[125]	
SiO_2	Ar,Kr	0.5–2.5	0?	[126]	

Table 35. Compound targets for which experiments and/or static calculations (low fluence) have been performed

Compound	Ion	Energy (keV)	Angle (deg.)	Exp.	Calc.
TiH_2	H	0.1	0		[476]
TiB_2	H,D,^{4}He	0.20–8	0	[27]	
TiB_2	^{4}He	3–20	0	[477]	
TiB_2	^{4}He	0.02–25	0		[468]
TiB_2	Cd	0.1–0.5	0	[406]	
TiC	H,D,^{4}He	0.10–8	0	[27, 72]	
TiC	H,D,^{4}He	0.10–8	0–80	[27, 51, 111]	
TiC	D	0.02–40	0		[398]
TiC	D	0.4–10	0	[478]	
TiC	D	2	0	[131]	
TiC	D,^{4}He	1.5–60	0	[477]	
TiC	D,^{4}He	0.02–80	0		[468]
TiC	O,Ne	0.15–10	0	[27, 78]	
TiC	Cd	0.1–0.5	0	[400]	
Ti_xC_y	H	0.5,6	0,30		[36]
TiN	N,Ar	0.4–0.7	0	[138]	[138]
TiN	Cd	0.1–0.5	0	[406]	
Ti_xAl_y	O	9.25	0	[479]	
VC	Cd	0.1–0.5	0	[400]	
VN	Cd	0.1–0.5	0	[406]	
VSi_2	Kr	0.2	0		[480]
Cr_3C_2	Cd	0.1–0.5	0	[400]	
FeH, FeH_2, FeT	H	0.1, 0.5	0		[476]
SS	H	0.6–20	0	[69]	
SS	H	0.5–7.5	0	[68]	
SS	H	0.4–1	0	[154]	
SS	H,D,^{4}He	0.10–8	0	[27, 51, 153]	
SS	D	0.33–10	0	[75]	
SS	D	5–30	0	[220]	
SS	O	0.10–10	0	[27, 78]	
SS	H,D,^{4}He	0.08–10	0	[145]	
SS304	H,D,^{4}He,Ne,Ar	1–20	0	[481]	
SS	N,Ne,Ar	25	0	[99]	
SS	Ar	1–5	0	[146]	
Inconel	H,D,^{4}He	0.07–8	0	[51, 153]	
Inconel	D,^{4}He	0.10–10	0	[145]	
Inconel	Hg	0.1–0.3	0	[404]	
K-Monel	Hg	0.15–0.3	0	[404]	
S-Monel	Hg	0.1–0.3	0	[404]	
NiCroFer	H,D,^{4}He	0.07–8	0	[51, 153]	
$B_{20}Fe_{40}Ni_{40}$	^{4}He	2–20	0	[482]	
Cu/Li	D,^{4}He,Ne,Ar	0.1–8	0	[483, 484]	[483, 484]

Table 36. Compound targets for which experiments and/or static calculations (low fluence) have been performed

Compound	Ion	Energy (keV)	Angle (deg.)	Exp.	Calc.
GaN	Ar	0.15–0.6	0	[485]	
GaN	Ar	0.3–10	0,45		[470]
GaN	Ar	0.3–3	0,45	[471]	[471]
GaN	Li,B,N,Ne,Al	0.2–2	0		[376]
GaN	Ca,Ni,Ga,Kr,Xe	0.2–2	0		[376]
GaP	Ar	0.15–0.6	0	[485]	
GaAs	Ar	0.15–0.6	0	[485]	
GaAs	Ar	0.03–1	0	[129]	
GaAs	Ar	0.3	0–85		[355]
GaAs	Cs	8	0–60	[362]	
GaSb	Ar	0.15–0.6	0	[485]	
ZrB_2	Cd	0.1–0.5	0	[406]	
ZrC	H,D,^{4}He	0.12–8	0	[27, 51]	
ZrC	Cd	0.1–0.5	0	[400]	
ZrN	Cd	0.1–0.5	0	[406]	
NbB_2	D	0.40–8	0–70	[258]	[258]
NbC	Cd	0.1–0.5	0	[400]	
$MoSi_2$	Cd	0.1–0.5	0	[406]	
$^{92}Mo^{100}Mo$	Ar,Xe	5,10	0–85		[188]
MoW	Cd	0.1–0.5	0	[406]	
InP	Ar	0.15–0.6	0	[485]	
InAs	Ar	0.15–0.6	0	[485]	
Sn-Li	D, He,Li	0.2–1	45	[486]	[486]
$Sn_{0.8}Li_{0.2}$	D	0.5	0		[487]
LaB_6	Cd	0.1–0.5	0	[406]	
TaC	H,D,^{4}He	0.40–8	0	[27, 51, 111]	
TaC	^{4}He	0.15–10	0,30		[34]
TaC	^{4}He	1	0		[294]
TaC	Ne	0.07–50	0–90		[293, 488]
TaC	Cd	0.1–0.5	0	[400]	
Ta_2O_5	H,D,^{4}He	0.50–8	0	[27, 51]	
Ta_2O_5	H,D,^{4}He,Ne	2–15	0	[10]	
WC	H,D,^{4}He	0.20–8	0	[27, 51, 111]	
WC	^{4}He	0.02–15	0		[293, 468]
W_xC_{1-x}	^{4}He	1	30		[293]
WC	^{4}He	0.20–15	0		[27]
WC	^{4}He,Xe	0.07–15	30		[293]
W_xC_{1-x}	D	0.07–0.2	0		[489]
W_xC_{1-x}	^{4}He	1	30		[293]
WN	N	10	0,45,70		[490]
WO_3	O,Ne,Kr	0.05–10	0–85		[36]
WO_3	O	0.50–6	0		[36]
W_xO_y	O	0.10–5	0		[36]
UF_4	O,F,Ne	100,1.2–3 MeV	0	[491]	
glasses	^{4}He,N,Ne,Ar,Xe	50, 70, 100	0–60	[429]	
minerals	^{4}He,N,Ne,Ar,Xe	50	0–60	[429]	

References

[1] R. Behrisch: Ergeb. Exakt. Naturw. **35**, 295 (1964) 33, 125
[2] H. H. Andersen, H. L. Bay: in R. Behrisch (Ed.): *Sputtering by Particle Bombardment I*, Top. Appl. Phys. **47** (Springer, Berlin, Heidelberg 1981) p. 145, russ. translation: (MIR, Moscow 1984) 33, 34, 36, 37
[3] G. Carter: in R. Behrisch (Ed.): *Sputtering by Particle Bombardment II*, Top. Appl. Phys. **52** (Springer, Berlin, Heidelberg 1983) p. 213, russ. translation: (MIR, Moscow 1986) 33
[4] B. M. U. Scherzer: in R. Behrisch (Ed.): *Sputtering by Particle Bombardment II*, Top. Appl. Phys. **52** (Springer, Berlin, Heidelberg 1983) p. 271, russ. translation: (MIR, Moscow 1986) 33, 34
[5] G. M. McCracken: Rep. Prog. Phys. **38**, 241 (1975) 34
[6] G. Sauerbrey: Z. Phys. **155**, 206 (1959) 34
[7] D. McCown: Rev. Sci. Instrum. **32**, 133 (1961) 34
[8] E. P. Eernisse: J. Vac. Sci. Technol. **12**, 564 (1975) 34
[9] R. Weissmann, R. Behrisch: Radiat. Eff. **18**, 55 (1973) 34
[10] H. von Seefeld, R. Behrisch, B. M. U. Scherzer, P. Staib, H. Schmidl: in *Proc. 7th Intern. Conf. Atomic Collisions in Solids*, vol. II (Moscow State Univ. Publ. House, Moscow 1980) p. 327 34, 170
[11] H. Fetz: Z. Phys. **119**, 590 (1942) 34
[12] H. G. Scott: J. Appl. Phys. **33**, 2011 (1962) 34
[13] G. K. Wehner, D. Rosenberg: J. Appl. Phys. **32**, 887 (1960) 34
[14] R. S. Nelson, B. W. Farmery, M. W. Thompson: Proc. R. Soc. **259**, 458 (1961) 35
[15] H. Pattersen, D. H. Tomlin: Proc. R. Soc. London A **265**, 474 (1962) 35, 58, 81, 94
[16] M. I. Guseva, A. L. Suvorov, S. N. Korshunov, N. E. Lazarev: J. Nucl. Mater. **266–269**, 222 (1999) 35, 42
[17] M. I. Guseva, A. L. Suvorov, S. N. Korshunov, N. E. Lazarev: J. Techn. Phis. **69**, 69 (1999) 35, 42, 87
[18] R. P. Doerner, D. Whyte, D. M. Goebel: J. Appl. Phys. **93**, 5816 (2003) 35, 43, 46, 53, 73, 100
[19] H. P. Summers: *Atomic Data and Analysis Structure - User Manual*, Rep. JET-IR(94) (JET Joint Undertaking, Abingdon 1994) 35
[20] P. Sigmund: Phys. Rev. **184**, 383 (1969) 35, 39
[21] P. Sigmund: Phys. Rev. **187**, 768 (1969) 35, 39
[22] D. E. Harrison, Jr.: *CRC Critical Reviews in Solid State and Material Sciences*, vol. 14, Supplement 1 (CRC Press 1988) 35, 132, 133
[23] M. T. Robinson: in *Fundamental Processes in Sputtering of Atoms and Molecules (SPUT92)*, K. Dan. Videns. Selsk. Mat. Fys. Medd. **33** (1993) p. 27 35
[24] Y. Yamamura, H. Tawara: *NIFS-DATA-23* (NIFS, Nagoya 1995) 35, 36, 37, 38, 39
[25] Y. Yamamura, H. Tawara: Atomic Data and Nucl. Data Tables **62**, 149–253 (1996) 35, 36, 37, 38, 39, 163
[26] W. Takeuchi, Y. Yamamura: Radiat. Eff. **71**, 53 (1983) 35

[27] W. Eckstein, C. García-Rosales, J. Roth, W. Ottenberger: *Sputtering Data, Report IPP 9/82* (MPG, Garching 1993) 35, 42, 44, 45, 46, 48, 50, 52, 54, 58, 62, 63, 64, 68, 72, 78, 85, 86, 87, 88, 94, 103, 104, 105, 106, 107, 108, 110, 116, 117, 118, 119, 120, 122, 123, 168, 169, 170

[28] J. P. Biersack, W. Eckstein: Appl. Phys. **34**, 73 (1984) 35, 131, 159, 160

[29] W. Eckstein: *Computer Simulation of Ion-Solid Interactions*, Springer Series in Material Science **10** (Springer, Berlin, Heidelberg) russ. translation: (MIR, Moscow 1995) 35, 37

[30] S. T. Nakagawa, Y. Yamamura: Radiat. Eff. **105**, 239 (1988) 35

[31] W. D. Wilson, L. G. Haggmark, J. P. Biersack: Phys. Rev. B **15**, 2458 (1977) 35

[32] W. Eckstein: unpublished results, can be retrieved from ftp://ftp.rzg.mpg.de/ftp/pub/ipp/eckstein/rep05 36, 37, 39

[33] Y. Yamamura, W. Takeuchi, T. Kawamura: *NIFS-DATA-45* (NIFS, Nagoya 1998) 36

[34] W. Möller, W. Eckstein: Nucl. Instrum. Methodsds B **2**, 814 (1984) 37, 170

[35] W. Möller, W. Eckstein, J. P. Biersack: Comput. Phys. Commun. **51**, 355 (1988) 37

[36] W. Eckstein: *Report IPP 9/132* (MPG, Garching 2002) 37, 39, 101, 168, 169, 170

[37] W. Eckstein, J. Bohdansky, J. Roth: Physical sputtering, in *Nucl. Fusion*, vol. 1 (Supplement) (IAEA, Vienna) p. 51 37

[38] W. Eckstein, E. S. Mashkova, V. A. Molchanov, A. I. Tolmachev: Nucl. Instrum. Methods B **115**, 482 (1996) 37

[39] W. Eckstein: J. Nucl. Mater. **248**, 1 (1997) 37

[40] W. Eckstein: Sputtering, reflection and range values for plasma edge codes, in *Report IPP 9/117* (MPG, Garching 1998) 37

[41] W. Eckstein, J. A. Stephens, R. E. H. Clark, J. W. Davis, A. A. Haasz, E. Vietzke, Y. Hirooka: Particle Induced Erosion of Be, C and W in Fusion Plasmas, Part B: Physical Sputtering and Radiation-Enhanced Sublimation, in *Atomic and Plasma-Material Interaction Data for Fusion* (IAEA, Vienna 2001) 37, 38

[42] R. K. Janev, Yu. V. Ralchenko, T. Kenmotsu, K. Hosaka: J. Nucl. Mater. **290–293**, 104 (2001) 38

[43] C. Garcia-Rosales, W. Eckstein, J. Roth: J. Nucl. Mater. **218**, 8 (1994) 38

[44] W. Eckstein, R. Preuss: J. Nucl. Mater. **320**, 209 (2003) 38, 39, 101

[45] J. Lindhard, V. Nielsen, M. Scharff: K. Dan. Vidensk. Selsk. Mat. Fys. Medd. (1968) 38

[46] J. P. Allain, D. N. Ruzic, M. R. Hendricks: J. Nucl. Mater. **290–293**, 180 (2001) 41, 159

[47] J. Roth, W. Eckstein, M. Guseva: Fusion Engineering Design **37**, 465 (1997) 42, 168

[48] J. Bohdansky, J. Roth, W. Ottenberger: *IPP-JET Report 31* (MPG, Garching 1985) 42, 100

[49] C. E. Kenknight, G. K. Wehner: J. Appl. Phys. **35**, 322 (1964) 42, 48, 52, 54, 58, 60, 62, 64, 68, 72, 76, 78, 85, 87, 89, 91, 92, 94

[50] J. Roth, J. Bohdansky, R. S. Blewer, W. Ottenberger: J. Nucl. Mater. **85 & 86**, 1077 (1979) 42, 48, 87, 88, 94, 168

[51] J. Roth, J. Bohdansky, W. Ottenberger: *Report IPP 9/26* (MPG, Garching 1979) 42, 48, 52, 54, 58, 62, 63, 68, 72, 87, 88, 94, 107, 108, 116, 117, 118, 121, 122, 168, 169, 170

[52] J. Bohdansky, J. Roth: J. Nucl. Mater. **122 & 123**, 1417 (1984) 42, 125, 168

[53] J. Roth: J. Nucl. Mater. **145–147**, 87 (1987) 42, 46

[54] D. Rosenberg, G. K. Wehner: J. Appl. Phys. **33**, 1842 (1962) 42, 43, 45, 46, 48, 49, 50, 51, 52, 53, 54, 55, 56, 57, 58, 59, 60, 61, 62, 63, 64, 65, 67, 68, 69, 70, 71, 72, 73, 74, 75, 76, 78, 79, 84, 85, 86, 87, 88, 89, 90, 91, 92, 94, 95, 98, 99

[55] H. Fetz, H. Oechsner: in *Proc. 6ieme Int. Conf. Phènomène dans les Gaz* (1963) p. 39 42, 43, 62, 63, 92

[56] Y. Hirooka, J. Won, R. Boivin, D. Sze, V. Neumoin: J. Nucl. Mater. **228**, 148 (1996) 42

[57] Y. Hirooka, J. Won, R. Boivin, D. Sze, V. Neumoin: J. Nucl. Mater. **230**, 173 (1996) 42

[58] M. I. Guseva, V. M. Gureev, S. N. Korshunov, V. E. Neumoin, Yu. A. Sokolov, V. G. Stolyarova, V. I. Vasiliev, S. V. Rylov, V. M. Strunnikov: J. Nucl. Mater. **220–222**, 957 (1995) 42

[59] M. I. Guseva, A. Y. Birukov, V. M. Gureev, L. S. Daneljan, S. N. Korshunov, Yu. V. Martynenko, P. S. Moskovkin, Yu. A. Sokolov, V. G. Stolyarova, V. V. Z. V. S. Kulikauskas: J. Nucl. Mater. **233–237**, 681 (1996) 42

[60] E. Hechtl, J. Roth, W. Eckstein, C. H. Wu: J. Nucl. Mater. **220–222**, 883 (1995) 42, 103

[61] M. I. Guseva, S. N. Korshunov, V. M. Gureev, Yu. V. Martynenko, V. E. Neumoin, V. G. Stolyarova: J. Nucl. Mater. **241–243**, 1117 (1997) 42, 103

[62] S. N. Korshunov, M. I. Guseva, V. M. Gureev, V. E. Neumoin, V. G. Stolyarova: in H. Kawamura, M. Okamoto (Eds.): JAERI-Conf. **98-001** (1997) p. 216 42, 168

[63] N. Laegreid, G. K. Wehner: J. Appl. Phys. **32**, 365 (1961) 42, 45, 48, 50, 52, 54, 56, 58, 60, 62, 64, 67, 68, 70, 72, 74, 75, 76, 78, 84, 85, 87, 89, 90, 91, 92, 94, 98, 99, 163

[64] C. H. Wu, E. Hechtl, H. R. Yang, W. Eckstein: J. Nucl. Mater. **176–177**, 845 (1990) 43

[65] S. Miyagawa, Y. Ato, Y. Moriya: J. Appl. Phys. **49**, 6194 (1978) 44

[66] E. Hechtl, A. Mazanec, W. Eckstein, J. Roth, C. García-Rosales: J. Nucl. Mater. **196–198**, 713 (1992) 44, 168

[67] Y. Ito, S. Kuriki, M. Saidoh, M. Nishikawa: Jpn. J. Appl. Phys. **33**, 5959 (1994) 44

[68] R. Behrisch, J. Bohdansky, G. H. Oetjen, J. Roth, G. Schilling, H. Verbeek: J. Nucl. Mater. **60**, 321 (1976) 45, 168, 169

[69] J. Bohdansky, J. Roth, M. K. Sinha: in *Proc. 9th Symp. on Fusion Technology* (Pergamon, London 1976) p. 541 45, 52, 168, 169

[70] J. N. Smith, Jr., C. H. Meyer, Jr., J. K. Layton: Nucl. Technol. **29**, 318 (1976) 45, 70, 78, 87

[71] J. N. Smith, Jr., C. H. Meyer, Jr., J. K. Layton: J. Nucl. Mater. **67**, 234 (1977) 45

[72] J. Bohdansky, H. L. Bay, W. Ottenberger: J. Nucl. Mater. **76 & 77**, 163 (1978) 45, 168, 169

[73] A. A. Haasz, J. W. Davis, C. H. Wu: J. Nucl. Mater. **162–164**, 915 (1989) 45
[74] M. Balden, J. Roth: J. Nucl. Mater. **280**, 39 (2000) 45
[75] J. A. Borders, R. A. Langley, K. L. Wilson: J. Nucl. Mater. **76**, 168 (1978) 45, 58, 168, 169
[76] C. García-Rosales, J. Roth: J. Nucl. Mater. **196–198**, 573 (1992) 45
[77] M. Yamashita: in *Proc. 4th Symp. on Ion Sources and Appl. Technology* (1980) p. 311 45, 94
[78] E. Hechtl, J. Bohdansky, J. Roth: J. Nucl. Mater. **103 & 104**, 333 (1981) 45, 46, 58, 62, 63, 88, 168, 169
[79] O. Almén, G. Bruce: Nucl. Instrum. Methods **11**, 279 (1961) 45, 47, 48, 50, 51, 52, 54, 56, 58, 60, 62, 64, 66, 69, 71, 73, 77, 79, 80, 81, 86, 88, 93, 95, 97
[80] R. A. Langley, J. Bohdansky, W. Eckstein, P. Mioduszewski, J. Roth, E. Taglauer, E. W. Thomas, H. Verbeek, K. L. Wilson: in *Nuclear Fusion*, Special Issue 1984 (IAEA, Vienna 1984) p. 72 45, 46
[81] U. Mayerhofer: Diploma thesis, Technical University of Munich (1986) 45
[82] H. Bergsaker, S. Nagata, B. Emmoth: J. Nucl. Mater. **145–147**, 364 (1987) 45
[83] J. Roth, J. Bohdansky, W. Ottenberger: J. Nucl. Mater. **165**, 193 (1989) 45, 104
[84] G. K. Wehner: General Mills Report **2309** (1962) 45
[85] E. Hechtl, J. Bohdansky: J. Nucl. Mater. **122 & 123**, 1431 (1984) 45, 46
[86] E. Hechtl, J. Bohdansky: J. Nucl. Mater. **141–143**, 139 (1986) 45
[87] S. Nagata, H. Bergsaker, B. Emmoth, L. Ilyinsky: Nucl. Instrum. Methods B **18**, 515 (1987) 45, 46
[88] H. Schirrwitz: Beitr. Plasmaphys. **2**, 188 (1962) 45, 47, 48, 58, 62, 64, 66, 72, 78, 80, 81, 85, 87, 92, 94, 96, 97, 100
[89] G. Betz, R. Dobrozemsky, F. P. Viehböck, H. Wottke: in *Proc. 9th Int. Conf. Phenomenon Ionized. Gases* (1969) p. 91 45, 46
[90] O. Almén, G. Bruce: Nucl. Instrum. Methods **11**, 257 (1961) 46, 47, 49, 51, 53, 54, 55, 56, 58, 59, 61, 62, 63, 64, 65, 66, 68, 70, 72, 73, 75, 76, 78, 79, 80, 81, 82, 84, 85, 86, 87, 88, 91, 92, 94, 95, 96, 97, 109, 111, 112, 119, 120, 125
[91] S. Grigull, W. Jacob, D. Henke, C. Spaeth, L. Sümmchen, W. Sigle: J. Appl. Phys. **83**, 5185 (1998) 46
[92] S. Grigull, R. Behrisch, S. Parascandola: J. Nucl. Mater. **275**, 158 (1999) 46
[93] A. M. Borisov, W. Eckstein, E. S. Mashkova: J. Nucl. Mater. **304**, 15 (2002) 46, 105
[94] K. H. Krebs: in *Atomic and Molecular Data for Fusion* (IANA, Vienna 1977) p. 185 47, 48, 50, 52, 57, 58, 60, 62, 64, 66, 67, 72, 85
[95] S. K. Lam, M. Kaminsky: J. Nucl. Mater. **89**, 205 (1980) 48
[96] O. C. Yonts, D. E. Robinson: ORNL **2802** (1959) 48, 64
[97] O. C. Yonts: in *BNS Nucl. Fusion Reactor Conf.* (Culham 1969) p. 424 48, 72, 87
[98] C. H. Weijsenfeld: *Philips Research Reports Supplements No.2* (1967) see also thesis (1966) 48, 49, 58, 59, 62, 63, 64, 65, 72, 73, 94, 95
[99] M. Nunogaki, M. Uchida, Y. Kuratomi, K. Miyazaki: Nucl. Instrum. Methods B **37/38**, 325 (1989) 48, 49, 58, 59, 169
[100] R. G. Allas, A. R. Knudson, J. M. Lambert, P. A. Treado, G. W. Reynolds: Nucl. Instrum. Methods **194**, 615 (1982) 48, 62, 64

[101] W. H. Hayward, A. R. Wolter: J. Appl. Phys. **40**, 2911 (1969) 48, 56, 64, 79, 95, 100
[102] M. Braun, B. Emmoth, R. Buchta: Radiat. Eff. **28**, 77 (1976) 48, 64, 78, 94
[103] C. E. Carlston, C. D. Magnuson, A. Comeaux, P. Mahavedan: Phys. Rev. **138**, A759 (1965) 48, 64, 72
[104] C. Fert, N. Colombie, B. Fagot, P. van Chuong: in *Le Bombardment Ionique* (CRNS, Paris 1961) p. 67 48, 60, 62, 64, 78, 80
[105] H. Oechsner: Z. Phys. **261**, 37 (1973) 48, 52, 62, 64, 65, 68, 76, 78, 85, 87, 94, 105, 106, 108, 111, 112, 113, 115, 119, 120, 121, 123
[106] Y. Okajima: Jpn. J. Appl. Phys. **20**, 2313 (1981) 48, 62, 64, 78
[107] M. T. Robinson, A. L. Southern: J. Appl. Phys. **38**, 2969 (1967) 48, 94
[108] O. C. Yonts, C. E. Normand, D. E. Harrison: J. Appl. Phys. **31**, 447 (1960) 48, 64, 65, 72, 85, 164
[109] R. Kelly: J. Appl. Phys. **39**, 5298 (1968) 49, 92, 93
[110] T. Weber, K.-P. Lieb: Nucl. Instrum. Methods B **44**, 54 (1989) 49
[111] J. Roth, J. Bohdansky, A. P. Martinelli: Radiat. Eff. **48**, 213 (1980) 50, 52, 85, 87, 168, 169, 170
[112] M. Balden, J. Roth: J. Nucl. Mater **279**, 351 (2000) 50
[113] U. Gerlach-Meyer, J. W. Coburn, E. Kay: Surf. Sci. **103**, 177 (1981) 50
[114] H. H. Andersen, H. L. Bay: J. Appl. Phys. **46**, 1919 (1975) 50, 51, 163
[115] S. Tachi, K. Miyake, T. Tokuyama: Jpn. J. Appl. Phys. **20**, L411 (1981) 50
[116] P. C. Zalm: J. Appl. Phys. **54**, 2660 (1983) 50, 51, 72, 73
[117] K. Wittmaack, D. B. Poker: Nucl. Instrum. Methods B **47**, 224 (1990) 50
[118] O. Frölich, H. Baumann, K. Bethge: Nucl. Instrum. Methods B **50**, 436 (1990) 50
[119] J. W. Coburn, H. F. Winters, T. J. Chuang: J. Appl. Phys. **48**, 3532 (1977) 50
[120] E. P. Eernisse: J. Appl. Phys. **42**, 4774 (1971) 50, 51
[121] H. Sommerfeldt, E. S. Mashkova, V. A. Molchanov: Phys. Lett. A **38**, 237 (1972) 50, 67, 70
[122] J. Nizam, N. Benazeth-Colombie: Revue de Physique Appl. **10**, 183 (1975) 50, 67, 166, 167
[123] J. M. Poate, W. L. Brown, R. Homer, W. M. Augustyniak, J. W. Mayer, K. N. Tu, W. F. van der Weg: Nucl. Instrum. Methods **132**, 345 (1976) 50, 52, 62, 92
[124] S. T. Kang, R. Shimizu, T. Okutani: Jpn. J. Appl. Phys. **18**, 1717 (1979) 50, 159
[125] J. M. E. Harper, J. J. Cuomo, P. A. Leary, G. M. Summa, H. R. Kaufman, F. J. Bresnock: J. Electrochem. Soc.: Solid-State Sci. Technol. **128**, 1077 (1981) 50, 168
[126] P. C. Zalm, L. J. Beckers, F. H. M. Sanders: Nucl. Instrum. Methods **209–210**, 561 (1983) 50, 51, 168
[127] P. C. Zalm, L. J. Beckers: J. Appl. Phys. **56**, 220 (1984) 50, 51, 168
[128] D. J. Oostra, R. P. van Ingen, A. E. de Vries, G. N. A. van Veen: Appl. Phys. Lett. **50**, 1506 (1987) 50
[129] P. Varga, T. Neidhart, M. Sporn, G. Libiseller, M. Schmid, F. Aumayr, H. P. Winter: Physica Scripta T **73**, 307 (1997) 50, 94, 168, 170
[130] P. Blank, K. Wittmaack: J. Appl. Phys. **50**, 1519 (1979) 51, 100, 128

[131] A. Santaniello, J. Appelt, J. Bohdansky, J. Roth: J. Nucl. Mater. **162–164**, 951 (1989) 52, 169
[132] M. Kaminsky: private communication 52, 54
[133] C. Steinbrüchel, D. M. Gruen, J. Dawson: J. Vac. Sci. Technol. **16**, 251 (1979) 52, 94
[134] W. O. Hofer, H. L. Bay, P. J. Martin: J. Nucl. Mater. **76 & 77**, 156 (1978) 52, 53, 54, 55, 100, 160
[135] J. Bohdansky, G. L. Chen, W. Eckstein, J. Roth, B. M. U. Scherzer, R. Behrisch: J. Nucl. Mater. **111 & 112**, 717 (1982) 52, 62, 64, 72, 85, 87, 106, 107, 108, 110, 116, 117, 118, 120, 160, 161, 162
[136] R. V. Stuart, G. K. Wehner: J. Appl. Phys. **33**, 2345 (1962) 52, 60, 62, 65, 67, 70, 85, 87, 88, 98
[137] O. V. Kurbatov: Sov. Phys. Techn. Phys. **12**, 1328 (1968) 52, 53
[138] R. Ranjan, J. P. Allain, M. R. Hendricks, D. N. Ruzic: J. Vac. Sci. Technol. A **19**, 1004 (2001) 52, 53, 169
[139] J. M. Lambert, P. A. Treado, D. Trbojevic, R. G. Allas, A. R. Knudson, G. W. Reynolds, F. R. Vozzo: IEEE Trans. Nucl. Sci. **NS-30**, 1285 (1983) 52, 58, 62, 64, 73, 94, 95, 163, 164
[140] M. I. Guseva, Yu. V. Martynenko: Fiz. Plas. (USSR) **2**, 593 (1976) 54, 72, 87
[141] Z. E. Switkowski, F. M. Mann, D. W. Kneff, R. W. Ollerhead, T. A. Tombrello: Radiat. Eff. **29**, 65 (1976) 54, 72
[142] R. V. Stuart, G. K. Wehner: Phys. Rev. Lett. **4**, 409 (1960) 56, 163
[143] P. H. Holloway: Surf. Sci. **66**, 479 (1977) 56, 94
[144] D. Trbojevic, P. A. Treado, G. S. Daniel: Nucl. Instrum. Methods B **10–11**, 743 (1985) 56, 57, 62, 64
[145] E. Hintz, D. Rusbüldt, B. Schweer, J. Bohdansky, J. Roth, A. P. Martinelli: J. Nucl. Mater. **93 & 94**, 656 (1980) 58, 169
[146] A. L. Southern, W. R. Willis, M. T. Robinson: J. Appl. Phys. **34**, 153 (1963) 58, 64, 166, 167, 169
[147] V. K. Koshkin: in *Phenom. Ioniz. Gases* (Bucharest 1969) p. 92 58, 59, 64, 65, 70, 71, 72, 73, 87, 88
[148] M. Bader, F. C. Witteborn, T. W. Snouse: *NASA Techn. Report R-105*, Technical report, NASA (1961) 59, 63, 64, 65, 73, 88
[149] C. R. Finfgeld: *Report ORO-3557-15*, Technical report, Salem (1970) 60, 72, 85, 87, 94
[150] G. Sletten, P. Knudsen: Nucl. Instrum. Methods **102**, 459 (1972) 60, 62, 64, 70, 72, 83, 84, 85, 92, 94, 98, 99
[151] A. Fontell, E. Arminen: Can. J. Phys. **47**, 2405 (1969) 60, 62, 64, 66, 81
[152] S. D. Dahlgren, E. C. McClanahan: J. Appl. Phys. **43**, 1514 (1972) 61, 63, 78
[153] J. Bohdansky, H. L. Bay, J. Roth: in R. Dobrozemsky, F. Rüdenauer, F. P. Viehböck, A. Breth (Eds.): *Prog. 7th Int. Vac. Congr. and 3rd Int. Conf. on Solid Surfaces* (Techn. Univ., Vienna 1977) p. 1509 62, 169
[154] J. B. Roberto, R. A. Zuhr, J. L. Moore, G. D. Alton: J. Nucl. Mater. **85 & 86**, 1073 (1979) 62, 94, 169
[155] H. L. Bay, J. Bohdansky, E. Hechtl: Radiat. Eff. **41**, 77 (1979) 62, 63
[156] Z. Wang, J. Zhang, J. Pan, Z. Tao: Phys. Lett. A **164**, 227 (1992) 62
[157] E. Hechtl, H. L. Bay, J. Bohdansky: Appl. Phys. **16**, 147 (1978) 62

[158] K. Tsunoyama, T. Suzuki, Y. Ohashi, H. Kishidaka: Surf. Interf. Anal. **2**, 212 (1980) 63, 79, 88, 95, 159, 160, 161, 162
[159] J. Bohdansky: J. Nucl. Mater. **93 & 94**, 44 (1980) 64
[160] R. Weissmann, R. Behrisch: Radiat. Eff. **19**, 69 (1973) 64
[161] M. I. Guseva: Fiz. Tverd. Tela **1**, 1540 (1959) engl. transl.: Sov. Phys. Solid State **1**, 1410 (1960) 64, 65, 78, 79
[162] H. H. Andersen, H. L. Bay: Radiat. Eff. **13**, 67 (1972) 64, 65, 79
[163] G. Dupp, A. Scharmann: Z. Phys. **192**, 284 (1966) 64, 65, 112
[164] P. K. Rol: Physica **26**, 1000 (1969) 64, 65
[165] F. Keywell: Phys. Rev. **97**, 1611 (1955) 64, 65, 78, 97
[166] B. Perovic, B. Cobic: in *Ioniz. Phenom. Gases* (Munich 1961) p. 1165 64, 78
[167] C. E. Ramer, N. A. Narasinham, H. K. Reynolds, J. C. Alldred: J. Appl. Phys. **35**, 1673 (1964) 64
[168] K. B. Cheney, E. T. Pitkin: J. Appl. Phys. **36**, 3542 (1965) 64, 65, 73, 88, 112, 113, 114, 118, 121
[169] K. Akaishi, A. Kiyahara, Z. Kabeya, M. Komizo, T. Gotoh: J. Vac. Soc. Japan **20**, 161 (1977) 64
[170] K. Akaishi, A. Kiyahara, Z. Kabeya, M. Komizo, T. Gotoh: in R. Dobrozemsky, F. Rüdenauer, F. P. Viehböck, A. Breth (Eds.): *Prog. 7th Int. Vac. Congr. and 3rd Int. Conf. on Solid Surfaces* (Techn. Univ., Vienna 1977) p. 1477 64
[171] Y. Ato: J. Vac. Soc. Japan **23**, 339 (1980) 64, 94
[172] A. Y. Barskaya, S. P. Varshavskii, O. Ryazantseva, L. A. Sena: Zh. Tekh. Fiz. **57**, 1223 (1987) 64
[173] H. J. Smith: Radiat. Eff. **18**, 73 (1973) 65, 66, 164
[174] A. Oliva-Florio, R. A. Baragiola, M. M. Jakas, E. V. Alonso, J. Ferrón: Phys. Rev. B **35**, 2198 (1987) 65, 94, 95, 113, 114, 123, 124
[175] N. Colombie: Thesis, Univ. Toulouse (1964) 66, 94
[176] H. J. Smith: Phys. Lett. **37A**, 289 (1971) 66, 164
[177] D. Ghose, D. Basu, S. B. Karmohapatro: Phys. Stat. Solidi A **77**, 121 (1983) 67
[178] G. Holmen: Radiat.Eff. **24**, 7 (1975) 67
[179] M. K. Sinha, J. Roth, J. Bohdansky: in *Proc. 9th Symp. Fusion Technol.* (Pergamon, New York 1976) p. 41 68
[180] G. Bräuer, D. Hasselkamp, W. Krüger, A. Scharmann: Nucl. Instrum. Methods B **12**, 458 (1985) 68, 94
[181] B. M. Gurmin: Sov. Phys. Solid State **10**, 324 (1968) 68, 72, 87
[182] R. V. Stuart, G. K. Wehner: in *Trans. 7th Natl. Vac. Symp.* (Pergamon, New York 1960) p. 290 68, 89
[183] R. Behrisch, O. K. Harling, M. T. Thomas, R. L. Brodzinski, L. H. Jenkins, G. J. Smith, J. F. Wedelking, M. J. Saltmarsh, M. Kaminsky, S. K. Das, C. M. Logan, R. Meiseneimer, J. E. Robinson, M. Shimotomai, D. A. Thompson: J. Appl. Phys. **48**, 3914 (1977) 70
[184] R. W. Ollerhead, F. M. Mann, D. W. Kneff, Z. E. Switkowski, T. A. Tombrello: Phys. Rev. Lett. **36**, 439 (1976) 70
[185] A. J. Summers, N. J. Freeman, N. R. Daly: J. Appl. Phys. **42**, 4774 (1971) 70, 71, 115
[186] H. Uecker, A. Riccato, G. R. Thacker, J. Ney, J. P. Biersack: J. Nucl. Mater. **93 & 94**, 670 (1980) 70, 161
[187] W. Eckstein, B. M. U. Scherzer, H. Verbeek: Radiat. Eff. **18**, 135 (1973) 70

[188] W. Eckstein: Nucl. Instrum. Methods B **83**, 329 (1993) 70, 125, 170
[189] B. Emmoth, M. Braun, H. P. Palenius: J. Nucl. Mater. **63**, 482 (1976) 70, 78
[190] J. N. Smith, Jr.: Trans. Am. Nucl. Soc. **22**, 29 (1975) 70, 78, 87
[191] H. Oechsner: Habil. schrift, Würzburg (1971) 70
[192] J. P. O'Connor, L. M. Baumel, P. G. Blauner, K. M. Hubbard, M. R. Weller, R. A. Weller: Nucl. Instrum. Methods B **13**, 365 (1986) 70, 164
[193] A. J. Summers, N. J. Freeman, N. R. Daly: in *Proc. Brit. Nucl. Soc.* (1969) p. 347 71, 115
[194] H. L. Bay, J. Roth, J. Bohdansky: J. Appl. Phys. **48**, 4722 (1977) 72, 94
[195] H. Ohtsuka, R. Yamada, K. Sone, M. Saidoh, T. Abe: J. Nucl. Mater. **76 & 77**, 188 (1978) 72
[196] M. Kaminsky, S. K. Das, P. Busza, J. Cecchi: in *Int. Symp. Fusion Technology* (Euratom, Padova 1978) p. 112 72
[197] C. H. Meyer, Jr., J. N. Smith, Jr.: J. Vac. Sci. Technol. **16**, 248 (1979) 72, 85
[198] K. Saiki, H. Tanaka, S. Tanaka, A. Koma: J. Nucl. Mater. **97**, 173 (1981) 72
[199] M. Tomita, T. Nate, S. Miyagi, M. Sakisaka: J. Nucl. Mater. **138**, 248 (1986) 72
[200] H. Oechsner: Appl. Phys. **8**, 185 (1975) 72
[201] B. Emmoth, T. Fried, M. Braun: J. Nucl. Mater. **76 & 77**, 129 (1978) 72
[202] M. Saidoh, K. Sone: Jpn. J. Appl. Phys. **22**, 1361 (1983) 73, 88
[203] M. Saidoh, K. Sone: in , JAERI-M **58** (1983) 73, 88
[204] S. Bhattacharjee, J. Zhang, V. Shutthanandan, P. K. Ray, N. R. Shivaparan, R. J. Smith: Nucl. Instrum. Methods B **129**, 123 (1997) 73
[205] F. Grønlund, W. J. Moore: J. Chem. Phys. **32**, 1540 (1960) 78, 79
[206] C. D. O'Briain, A. Lindner, W. J. Moore: J. Chem. Phys. **29**, 3 (1958) 78
[207] R. Behrisch: Diploma thesis, University of Munich (1960) 78
[208] J. Bohdansky, H. Lindner, E. Hechtl, A. P. Martinelli, J. Roth: Nucl. Instrum. Methods B **18**, 509 (1987) 78, 132
[209] A. Benninghoven: Z. Angew. Phys. **27**, 51 (1969) 78, 79, 94, 161, 162
[210] A. Weiss, L. Heldt, W. J. Moore: J. Chem. Phys. **29**, 7 (1958) 78
[211] G. K. Wehner: *General Mills Report No. 2243* (1961) 78, 81, 163, 164, 165
[212] M. Koedam: Physica **24**, 692 (1962) 78
[213] D. B. Medved, H. Poppa: J. Appl. Phys. **33**, 1759 (1962) 78
[214] H. H. Andersen, H. L. Bay: Radiat. Eff. **19**, 139 (1973) 78, 79
[215] J. Pan, Z. Wang, Z. Tao, J. Zhang: Nucl. Instrum. Methods B **67**, 514 (1992) 78
[216] M. Szymonski, R. S. Bhattacharya, H. Overeijnder, A. E. de Vries: J. Phys. D **11**, 751 (1978) 79, 94, 95
[217] F.-M. Devienne, A. Roustan: C. R. Acad. Sc. Paris **268**, 1362 (1969) 79, 95
[218] R. C. Krutenat, C. Panzera: J. Appl. Phys. **41**, 4953 (1970) 81
[219] E. C. Viljoen, E. Taglauer, J. du Plessis: Nucl. Instrum. Methods B **179**, 515 (2001) 81
[220] M. I. Guseva: Radiotekh. Elektron. **7**, 1680 (1962) engl. translation: Radio Eng. Electron Phys. USSR **7**, 1563 (1962) 85, 169
[221] E. Hechtl: in *Proc. Symp. on Sputtering* (Techn. Univ., Vienna 1980) p. 834 85, 86
[222] K. Wittmaack: Surf. Sci. **51**, 626 (1975) 85, 94
[223] J. F. Ziegler, J. J. Cuomo, J. Roth: Appl. Phys. Lett. **30**, 328 (1977) 87
[224] H. F. Winters, D. Horne: Phys. Rev. B **10**, 55 (1974) 87, 88

[225] E. Hechtl, H. R. Yang, C. H. Wu, W. Eckstein: J. Nucl. Mater. **176–177**, 874 (1990) 88
[226] A. K. Furr, C. R. Finfgeld: J. Appl. Phys. **41**, 1739 (1970) 94
[227] E. P. Eernisse: Appl. Phys. Lett. **29**, 14 (1976) 94, 95
[228] J. S. Colligon, R. W. Bramham: in *Proc. Atomic Coll. in Solids* (1970) p. 258 94, 95
[229] H. H. Andersen, H. L. Bay: J. Appl. Phys. **46**, 2416 (1975) 94, 95
[230] T. M. Nenadovic, Z. B. Fotric, D. S. Dimitrijevic: Surf. Sci. **33**, 607 (1972) 94, 95
[231] J. S. Colligon, M. H. Patel: Radiat. Eff. **32**, 193 (1977) 94
[232] R. K. Fitch, E. A. Mahmoud: Thin Solid Films **87**, 379 (1982) 94
[233] M. Yamashita, S. Baba, A. Kinbara: J. Vac. Soc. Japan **25**, 249 (1982) 94
[234] H. J. Kang, E. Kawatoh, R. Shimizu: Surf. Sci. **144**, 541 (1984) 94
[235] K. L. Merkle, P. P. Pronko: J. Nucl. Mater. **53**, 231 (1974) 95
[236] H. L. Bay, H. H. Andersen, W. O. Hofer, O. Nielsen: Nucl. Instrum. Methods **132**, 301 (1976) 95
[237] H. Kräutle: Nucl. Instrum. Methods **137**, 553 (1976) 95, 163, 165
[238] H. H. Andersen, A. Brunelle, S. Della-Negra, J. Depauw, D. Jacquet, , Y. L. Beyec: Phys. Rev. Lett. **80**, 5433 (1998) 95
[239] R. Gregg, T. A. Tombrello: Radiat. Eff. **35**, 243 (1978) 99
[240] J. G. Tracy: ORNL private communication 100
[241] R. Behrisch, J. Roth, J. Bohdansky, A. P. Martinelli, B. Schweer, D. Rusbüldt, E. Hintz: J. Nucl. Mater. **93 & 94**, 645 (1980) 100
[242] A. E. Morgan, H. A. M. de Grefte, N. Warmoltz, H. A. Werner: Appl. Surf. Sci. **7**, 372 (1981) 100, 159
[243] P. C. Zalm: Radiat. Eff. Lett. **86**, 29 (1983) 100
[244] M. Toulemonde: private communication 101
[245] D. Fink, J. P. Biersack: Radiat. Eff. **64**, 89 (1982) 101
[246] D. Fink, J. P. Biersack, M. Städele, K. Tjan, R. A. Haring, A. E. de Vries: Nucl. Instrum. Methods B **1**, 275 (1984) 101
[247] R. Behrisch, G. Federici, A. Kukushkin, D. Reiter: J. Nucl. Mater. **313 - 316**, 388 (2003) 101
[248] T. Kawamura, T. Ono, Y. Yamamura: J. Nucl. Mater. **220–222**, 1010 (1995) 101
[249] V. I. Shulga: Nucl. Instrum. Methods B **174**, 77 (2001) 101
[250] V. I. Shulga: Nucl. Instrum. Methods B **187**, 178 (2002) 101
[251] Y. Yamamura, Y. Itikawa, N. Itoh: *IPPJ-AM-26* (Nagoya 1993) 101
[252] J. Roth, W. Eckstein, J. Bohdansky: J. Nucl. Mater. **165**, 199 (1989) 103, 168
[253] J. Roth: in D. E. Post, R. Behrisch (Eds.): *Physics of Plasma-Wall Interactions in Controlled Fusion* (Plenum, New York, London 1986) p. 351 103, 104, 107, 108
[254] J. Roth, J. Bohdansky, K. L. Wilson: J. Nucl. Mater. **111 & 112**, 775 (1982) 104
[255] J. Roth, W. Eckstein, E. Gauthier, J. László: J. Nucl. Mater. **179–181**, 34 (1991) 104, 105, 124
[256] I. M. Fayazov, E. S. Mashkova, V. A. Molchanov, A. V. Siderov, A. I. Tolmachev, W. Eckstein: Nucl. Instrum. Methods B **67**, 523 (1992) 105

[257] W. Krüger, A. Scharmann, H. Afridi, G. Bräuer: *SOS* (Vienna 1980) p. 125 106, 115, 119
[258] J. Bohdansky, G. L. Chen, W. Eckstein, J. Roth: J. Nucl. Mater. **103 & 104**, 339 (1981) 107, 160, 170
[259] H. L. Bay, J. Bohdansky: Appl. Phys. **19**, 421 (1979) 107, 108, 116, 117, 118, 122
[260] E. S. Mashkova, V. A. Molchanov: Sov. Phys. - Techn. Phys. **9**, 1601 (1965) 108, 118, 121
[261] E. Hechtl, A. Mazanec, W. Eckstein, J. Roth: Nucl. Instrum. Methods B **90**, 505 (1994) 108, 109
[262] H. Liebl, J. Bohdansky, J. Roth, V. Dose: Rev. Sci. Instrum. **58**, 1830 (1987) 110, 122
[263] P. K. Rol, J. M. Fluit, J. Kistemaker: Physica **26**, 1000 (1960) 111, 164
[264] V. A. Molchanov, V. G. Tel'kovskii: Dokl. Akad. Nauk SSSR **136**, 801 (1961) engl. transl.: Sov. Phys. - Doklady **6**, 137 (1961) 111
[265] H. L. Bay, J. Bohdansky, W. O. Hofer, J. Roth: Appl. Phys. **21**, 327 (1980) 121
[266] V. Bandourko, R. Jimbou, K. Nakamura, M. Akiba: J. Nucl. Mater. **258–263**, 917 (1998) 121
[267] M. Küstner, W. Eckstein, V. Dose, J. Roth: Nucl. Instrum. Methods B **145**, 320 (1998) 124
[268] M. Küstner, W. Eckstein, E. Hechtl, J. Roth: J. Nucl. Mater. **265**, 22 (1999) 124
[269] Yu. N. Zhukova, E. S. Mashkova, V. A. Molchanov, V. M. Sotnikov, W. Eckstein: Povern. Phys. Chem. Mek. **8-9**, 107 (1994) 124
[270] R. Behrisch, G. Maderlechner, B. M. U. Scherzer, M. T. Robinson: Appl. Phys. **18**, 391 (1979) 125, 160, 161
[271] W. Eckstein, J. Roth, W. Nagel, R. Dohmen: J. Nucl. Mater. **328**, 55 (2004) 125
[272] W. Eckstein, C. García-Rosales, J. Roth: Nucl. Instrum. Methods B **83**, 95 (1993) 125, 131
[273] G. J. Ogilvie, M. J. Ridge: J. Phys. Chem. Sol. **10**, 217 (1959) 125
[274] P. K. Rol, J. M. Fluit, F. P. Viehböck, M. de Jong: in N. R. Nilsson (Ed.): *Proc. 4th Int. Conf. Phen. Ion. Gases* (North-Holland, Amsterdam 1959) p. 257 125
[275] V. A. Molchanov, V. G. Tel'kovskii, V. M. Chicherov: Sov. Phys. - Doklady **6**, 222 (1961) 125
[276] H. E. Roosendaal: in R. Behrisch (Ed.): *Sputtering by Particle Bombardment I*, Top. Appl. Phys. **47** (Springer, Berlin, Heidelberg 1981) p. 219, russ. translation: (MIR, Moscow 1984) 125, 132
[277] G. K. Wehner: Phys. Rev. **102**, 690 (1956) 125
[278] Y. Yamamura, W. Takeuchi: Nucl. Instrum. Methods B **29**, 461 (1987) 125, 167
[279] M. Hou, W. Eckstein: Nucl. Instrum. Methods B **13**, 324 (1986) 125, 127, 167
[280] D. Onderdelinden: Can. J. Phys. **46**, 739 (1968) 126, 127
[281] G. Betz, G. K. Wehner: in R. Behrisch (Ed.): *Sputtering by Particle Bombardment II*, Top. Appl. Phys. **52** (Springer, Berlin, Heidelberg 1983) p. 11, russ. translation: (MIR, Moscow 1986) 126

[282] K. Wittmaack, W. Wach: Nucl. Instrum. Methods **191**, 327 (1981) 127
[283] W. Eckstein: J. Nucl. Mater. **281**, 195 (2000) 127
[284] W. Eckstein, M. Hou, V. I. Shulga: Nucl. Instrum. Methods B **119**, 477 (1996) 128
[285] W. Eckstein, R. Dohmen: Nucl. Instrum. Methods B **129**, 327 (1997) 128, 131
[286] W. Eckstein: unpublished results 128
[287] J. P. Biersack, S. Berg, C. Nender: Nucl. Instrum. Methods B **59/60**, 21 (1991) 128
[288] S. Berg, I. V. Katardjiev: J. Vac. Sci. Technol. A **17**, 1916 (1999) 128
[289] W. Eckstein: Nucl. Instrum. Methods B **171**, 435 (2000) 128, 129
[290] R. A. Zuhr, J. Roth, W. Eckstein, U. von Toussaint, J. Luthin: J. Nucl. Mater. **290**–**293**, 162 (2001) 129, 163
[291] V. S. Touboltsev, G. Dybkjaer, A. Johansen, E. Johnson, L. Sarholt, H. H. Andersen, M. Olsen: Phil. Mag. A **77**, 341 (1998) 129
[292] J. Sielanko, J. Filiks, J. Hereć: Vacuum **70**, 381 (2003) 129
[293] W. Eckstein, J. P. Biersack: Appl. Phys. A **37**, 95 (1985) 130, 168, 170
[294] W. Eckstein, W. Möller: Nucl. Instrum. Methods B **7/8**, 727 (1985) 130, 170
[295] D. Naujoks, W. Eckstein: J. Nucl. Mater. **220 - 222**, 993 (1995) 130
[296] D. Naujoks, W. Eckstein: J. Nucl. Mater. **220**, 93 (1996) 130
[297] V. Bandourko, R. Jimbou, K. Nakamura, M. Akiba, Y. Okumura: J. Nucl. Mater. **313**–**316**, 413 (2003) 130
[298] N. Andersen, P. Sigmund: K. Dan. Vidensk. Selsk. Mat. Fys. Medd. **39**, 1 (1979) 131
[299] P. Sigmund: K. Dan. Vidensk. Selsk. Mat. Fys. Medd. **93**, 255 (1993) 131
[300] M. T. Robinson: J. Appl. Phys. **54**, 2650 (1983) 131, 162
[301] D. L. Weathers, S. J. Spicklemire, T. A. Tombrello, I. D. Hutcheon, H. Gnaser: Nucl. Instrum. Methods B **73**, 135 (1993) 131
[302] D. Y. Lo, T. A. Tombrello, M. H. Shapiro: Nucl. Instrum. Methods B **40 & 41**, 270 (1989) 131
[303] H. M. Urbassek, U. Conrad: Nucl. Instrum. Methods B **73**, 151 (1993) 131
[304] V. I. Shulga, P. Sigmund: Nucl. Instrum. Methods B **103**, 383 (1995) 131
[305] V. I. Shulga, P. Sigmund: Nucl. Instrum. Methods B **119**, 359 (1996) 131
[306] T. A. Tombrello: K. Dan. Vidensk. Selsk. Mat. Fys. Medd. **93**, 659 (1993) 131
[307] R. Behrisch, W. Eckstein: Nucl. Instrum. Methods B **82**, 255 (1993) 131
[308] W. Eckstein, V. I. Shulga, J. Roth: Nucl. Instrum. Methods B **153**, 415 (1999) 132
[309] K. Schmid, J. Roth: J. Nucl. Mater. **313**–**316**, 302 (2003) 132
[310] R. S. Nelson: Phil. Mag. **11**, 219 (1965) 132
[311] V. E. Yurasova, A. S. Mosunov, A. A. Promokhov: Bull. Russian Acad. Sci. **62**, 1164 (1998) 132, 166
[312] D. A. Konov, A. S. Mosunov, G. V. Adamov, L. B. Shelyakin, V. E. Yurasova: Vacuum **64**, 47 (2002) 132, 166
[313] M. I. Guseva, V. M. Gureev, B. N. Kolbasov, S. N. Korshunov, Yu. V. Martynenko, V. B. Petrov, B. I. Khripunov: JETP Letters **77**, 430 (2003) 132
[314] K. Schmid, J. Roth: private communication 132

[315] R. P. Doerner, M. J. Baldwin, R. W. Conn, A. A. Grossman, S. C. Luckhardt, R. Seraydarian, G. R. Tynan, D. G. Whyte: J. Nucl. Mater. **290–293**, 166 (2001) 132
[316] M. D. Coventry, J. P. Allain, D. N. Ruzic: J. Nucl. Mater. **335**, 115 (2004) 132
[317] J. E. Westmoreland, P. Sigmund: Radiat. Eff. **6**, 187 (1970) 132
[318] W. Eckstein: Nucl. Instrum. Methods B **33**, 489 (1988) 132, 133, 160
[319] W. Eckstein: Radiat. Eff. Defects Solids **130–131**, 239 (1994) 132
[320] U. Conrad, H. M. Urbassek: Nucl. Instrum. Methods B **48**, 399 (1990) 132
[321] M. T. Robinson: Phys. Rev. B **40**, 10717 (1989) 133
[322] Y. Yamamura: Nucl. Instrum. Methods B **45**, 582 (1990) 133
[323] S. S. Todorov, I. R. Chakarov, D. S. Karpuzov: Vacuum **43**, 543 (1992) 133
[324] R. G. Vichev, D. S. Karpuzov: Nucl. Instrum. Methods B **83**, 345 (1993) 133
[325] R. G. Vichev, W. Eckstein: Nucl. Instrum. Methods B **102**, 272 (1995) 133, 134
[326] M. Hou, W. Eckstein, M. T. Robinson: Nucl. Instrum. Methods B **82**, 234 (1993) 133
[327] R. G. Vichev, W. Eckstein: Nucl. Instrum. Methods B **122**, 215 (1997) 133
[328] A. Grossman, R. P. Doerner, S. Luckhardt: J. Nucl. Mater. **290–293**, 80 (2001) 159, 161
[329] J. László, W. Eckstein: J. Nucl. Mater. **184**, 22 (1991) 159, 161, 162
[330] J. P. Allain, M. D. Coventry, D. N. Ruzic: J. Nucl. Mater. **313–316**, 641 (2003) 159
[331] W. Eckstein, A. Sagara, K. Kamada: J. Nucl. Mater. **150**, 266 (1987) 159
[332] W. Eckstein, J. P. Biersack: Z. Phys. B **63**, 109 (1986) 159, 160, 161, 162
[333] P. C. Smith, D. N. Ruzic: Nucl. Fusion **38**, 673 (1998) 159
[334] W. Eckstein, J. Roth, E. Gauthier, J. László: Fusion Technology **19**, 2076 (1991) 159, 163
[335] D. N. Ruzic: Nucl. Instrum. Methods B **47**, 118 (1990) 159
[336] L. G. Haggmark, W. D. Wilson: J. Nucl. Mater. **76 & 77**, 149 (1978) 159, 160, 161, 162
[337] P. S. Chou, N. M. Ghoniem: Nucl. Instrum. Methods B **28**, 175 (1987) 159, 160, 161, 162
[338] W. Eckstein: *IPP report 9/54*, Technical report, MPG, Garching (1985) 159
[339] G. Betz, R. Dobrozemsky, F. P. Viehböck: Int. J. Mass. Spectrom. Ion Phys. **6**, 671 (1971) 159, 161, 162
[340] A. Barna, M. Menyhard, L. Kotis, G. J. Kovacs, G. Radnoczi, A. Zalar, P. Panjan: J. Appl. Phys. **98**, 024901 (2005) 159, 160
[341] Y. Yamamura: Nucl. Instrum. Methods B **33**, 493 (1988) 159
[342] S. Berg, I. V. Katardjiev: J. Vac. Sci. Technol. A **13**, 831 (1995) 159
[343] A. E. Morgan, H. A. M. de Grefte, H. J. Tolle: J. Vac. Sci. Technol. **18**, 164 (1981) 159, 161, 162
[344] K. Ohya: Nucl. Instrum. Methods B **195**, 281 (2002) 159
[345] D. E. Hanson, B. C. Stephens, C. Saravanan, J. D. Kress: J. Vac. Sci. Technol. A **19**, 820 (2001) 159, 166
[346] D. S. Karpuzov: Nucl. Instrum. Methods B **19/20**, 109 (1987) 159, 160, 161
[347] M. M. Jakas, D. E. Harrison, Jr.: Phys. Rev. B **32**, 2752 (1985) 159, 166, 167
[348] N. Herbots, B. R. Appleton, T. S. Noggle, R. A. Zuhr, S. J. Pennycook: Nucl. Instrum. Methods B **13**, 250 (1986) 159, 161, 163

[349] G. Ecke, R. Kosiba, V. Kharmalov, Y. Trushin, J. Pezoldt: Nucl. Instrum. Methods B **196**, 39 (12002) 159, 168
[350] T. S. Pugacheva, M. S. Saidov, A. S. Lutovich: Radiat. Eff. **105**, 117 (1987) 159
[351] W. Eckstein, S. Hackel, D. Heinemann, B. Fricke: Z. Phys. D **24**, 171 (1992) 159
[352] J. Sielanko, W. Szyszko: Surf. Sci. **161**, 101 (1985) 159, 161
[353] M. L. Roush, T. D. Andreadis, F. Davarya, O. F. Goktepe: J. Nucl. Mater. **191**, 135 (1981) 159
[354] M. L. Roush, T. D. Andreadis, F. Davarya, O. F. Goktepe: Appl. Surf. Sci. **11/12**, 235 (1982) 159
[355] Y. Kido, A. Kawano, J. Kawamoto: (1988) private communication 159, 170
[356] Y. Yamamura, C. Mössner, H. Oechsner: Radiat. Eff. **103**, 25 (1987) 159, 161, 162
[357] Y. Yamamura, C. Mössner, H. Oechsner: Radiat. Eff. **105**, 31 (1987) 159, 161, 162
[358] M. L. Roush, T. D. Andreadis, F. Davarya, O. F. Goktepe: Radiat. Eff. **55**, 119 (1981) 159, 161, 162, 167
[359] T. Ishitani, R. Shimizu: Appl. Phys. **6**, 241 (1975) 159
[360] T. Aoki, S. Chiba, J. Matsuo, I. Yamada, J. P. Biersack: Nucl. Instrum. Methods B **180**, 312 (2001) 159
[361] J. Sielanko, W. Szyszko: Nucl. Instrum. Methods B **16**, 340 (1986) 159
[362] K. Wittmaack: J. Vac. Sci. Technol. **3**, 1350 (1985) 159, 163, 170
[363] A. M. Hassanein, D. L. Smith: Nucl. Instrum. Methods B **13**, 225 (1986) 160
[364] R. Behrisch, G. Maderlechner, B. M. U. Scherzer, M. T. Robinson: in W.Lindinger, F.Howorka, F.Egger (Eds.): *Proc. SASP 78* (Institut für Atomphysik, Universität Innsbruck, Innsbruck 1978) p. 33 160
[365] L. G. Haggmark, J. P. Biersack: J. Nucl. Mater. **103 & 104**, 345 (1981) 160, 161, 162
[366] Y. Yamamura, K. Muraoka: Nucl. Instrum. Methods B **42**, 175 (1989) 160
[367] V. M. Samoylov, A. H. Phillips, V. A. Eltekov, V. E. Yurasova: Nucl. Instrum. Methods B **18**, 243 (1987) 160
[368] A. Barna, M. Menyhard, G. Zsolt, N. Q. Khanh, A. Zalar, P. Panjan: J. Vac. Sci. Technol. A **21**, 196 (2003) 160, 161
[369] Y. Yamamura, Y. Mizuno: J. Nucl. Mater. **128/129**, 559 (1984) 160, 164
[370] Y. Yamamura, Y. Mizuno: *IPPJ-AM-40: Tech. Rpt* (Nagoya 1985) 160, 161, 162, 163, 164
[371] R. Becerra-Acevedo, J. Bohdansky, W. Eckstein, J. Roth: Nucl. Instrum. Methods B **2**, 631 (1984) 160
[372] L. G. Haggmark, J. P. Biersack: J. Nucl. Mater. **93 & 94**, 664 (1980) 160, 161, 162
[373] W. Eckstein, J. P. Biersack: Nucl. Instrum. Methods B **2**, 550 (1984) 160
[374] P. S. Chou, N. Ghoniem: J. Nucl. Mater. **117**, 55 (1983) 160
[375] A. S. Mosunov, E. Yu. Zhukova, D. S. Colligon, S. A. Postnikov, V. E. Yurasova: Isvestia Akad. Nauk. Ser. Fiz. **68**, 313 (2004) 160, 162, 168
[376] Yu. A. Ryzhov, A. A. Semyonov, I. I. Shkarban, A. S. Mosunov, V. E. Yurasova: Voproz Atom. Nauk. Tek. **2**, 54 (2004) 160, 162, 168, 170

[377] V. I. Nikiforov, V. I. Pavlenko, R. P. Slabopitskii, I. V. Khirnov: *KhFTI 87-58* (1987) 160
[378] L. B. Shelyakin, T. P. Martynenko, A. Bischoff, V. E. Yurasova, G. Shaarschmidt: Poverkhnost (USSR) **N 6**, 65 (1983) 160
[379] V. E. Yurasova: in A. Gras-Marti, H. M. Urbassek, N. R. Arista, F. Flores (Eds.): *Interaction of Charged Particles with Solids and Surfaces* (Plenum, New York, London 1991) p. 505 160, 166, 167
[380] W. Eckstein, H.-J. Barth, E. Mühling: Nucl. Instrum. Methods B **14**, 507 (1986) 160
[381] D. T. Goldman, D. E. Harrison, Jr., R. R. Coveyeau: *Tech. Rpt. ORNL 2729* (Oak Ridge 1959) 161
[382] D. E. Harrison, Jr., M. M. Jakas: Nucl. Instrum. Methods B **15**, 25 (1986) 161
[383] M. M. Jakas, D. E. Harrison, Jr.: Nucl. Instrum. Methods B **14**, 535 (1986) 161
[384] M. Hou, M. T. Robinson: Appl. Phys. **18**, 381 (1979) 161, 164
[385] C. Coudray, G. Slodzian: Nucl. Instrum. Methods B **15**, 29 (1986) 161
[386] M. H. Shapiro, D. Y. Lo, P. K. Haff, T. A. Tombrello: Nucl. Instrum. Methods B **13**, 348 (1986) 161
[387] J. Likonen, M. Hautala: J. Phys. B **1**, 4697 (1989) 161
[388] A. S. Mosunov, Yu. A. Ryzhov, A. A. Semenov, I. I. Shkarban, D. S. Colligon, V. E. Yurasova: Isvestia Akad. Nauk. Ser. Fiz. **68**, 1665 (2004) 161
[389] R. N. Schlaug: *Sputtering Calculations from a Realistic Model*, thesis, Univ. Calif., Berkeley (1965), published at (University Microfilms, Ann Arbor, MI 1966) 161
[390] J. P. Biersack, A. Riccato, W. Kaczerowski: in *Proc. of the Workshop on Sputtering Caused by Plasma (Neutral Beam) Surface Interaction* (CONF-790775, U.S.DOE, Washington DC 1979) pp. 16–1 161
[391] S. M. Sotnikov: Pover. Fiz. Khim. Mekh. **8**, 45 (1989) 161
[392] W. Eckstein, J. László: J. Nucl. Mater. **183**, 19 (1991) 161, 162
[393] M. D. Coventry, J. P. Allain, D. N. Ruzic: J. Nucl. Mater. **313–316**, 636 (2003) 162
[394] E. Salonen, K. Nordlund, J. Keinonen, C. H. Wu: J. Nucl. Mater. **313–316**, 404 (2003) 162
[395] V. I. Shulga: Nucl. Instrum. Methods B **174**, 423 (2001) 162
[396] Y. Yamamura, Y. Kitazoe: Radiat. Eff. **39**, 251 (1978) 162
[397] Y. Yamamura: Nucl. Instrum. Methods **194**, 515 (1982) 162, 165
[398] M. T. Robinson: Inst. Phys. Conf. Ser. **71**, 151 (1984) 162, 169
[399] V. K. Meyer, A. Güntherschulze: Z. Phys. **71**, 19 (1931) 163, 164, 165
[400] T. P. Martynenko: Sov. Phys. - Solid State **9**, 2232 (1968) 163, 164, 165, 168, 169, 170
[401] G. K. Wehner: Phys. Rev. **108**, 35 (1957) 163, 164, 165
[402] G. Holmén, O. Almén: Ark. Fys. **40**, 429 (1969) 163, 167
[403] H. Ismail: Rev. Phys. Appl. **5**, 759 (1970) 163, 164, 165
[404] G. K. Wehner: Phys. Rev. **112**, 1120 (1958) 163, 169
[405] P. V. Pavlov, D. I. Tetelbaum, E. I. Zorin, V. I. Alekseev: Fiz. Tverd. Tela **8**, 2679 (1966) 163
[406] T. P. Martynenko: Sov. Phys. - Solid State **9**, 2887 (1968) 163, 164, 169, 170

[407] S. G. Askerov, L. A. Sena: Sov. Phys. - Solid State **11**, 288 (1969) 163, 164, 165
[408] M. A. El Khakani, H. Jaffrezic, G. Marest, N. Montcoffre, J. Tousset: Nucl. Instrum. Methods B **50**, 406 (1990) 163
[409] G. K. Wehner: J. Appl. Phys. **30**, 1762 (1959) 163, 164, 165
[410] H. H. Andersen: Radiat. Eff. **19**, 257 (1973) 164
[411] H. J. Smith: Radiat. Eff. **18**, 55 (1973) 164, 165
[412] W. Eckstein, J. Roth: Nucl. Instrum. Methods B **53**, 279 (1991) 165
[413] K. Krieger, J. Roth: J. Nucl. Mater. **290–293**, 107 (2001) 165
[414] N. Matsunami, M. Sataka, A. Iwase, T. Inami, M. Kobiyama: J. Nucl. Mater. **302**, 206 (2002) 165
[415] S. Ueda, T. Ohsaka, S. Kuwajima: J. Nucl. Mater. **283–287**, 1100 (2000) 166
[416] S. S. Elovikov, V. A. Eltekov, N. N. Negrebetskaya, J. V. Sushkova, V. E. Yurasova, I. I. Shkarban, O. I. Buzhinskij, I. V. Opimach: J. Nucl. Mater. **212–215**, 1335 (1994) 166
[417] E. E. Zhurkin, A. S. Kolesnikov: Nucl. Instrum. Methods B **193**, 822 (2002) 166
[418] T. Mizutani, C. J. Dale, W. K. Chu, T. M. Mayer: Nucl. Instrum. Methods B **7/8**, 825 (1985) 166
[419] E. F. C. Haddeman, B. J. Thijsse: Nucl. Instrum. Methods B **202**, 161 (2003) 166
[420] V. A. Eltekov, V. E. Yurasova, N. N. Negrebetskaya, N. G. Vasichkina: Pover. Fiz. Khim. Mekh. **2**, 46 (1994) 166
[421] S. P. Wolsky, E. J. Zdanuk: J. Appl. Phys. **32**, 782 (1961) 166
[422] Y. Zhang, T. Zhang, Z. Xiao, H. J. Whitlow: Nucl. Instrum. Methods B **173**, 427 (2001) 166
[423] V. M. Samoylov, A. H. Phillips, V. A. Eltekov, V. E. Yurasova: Vestn. Mosk. Univ. **27**, 87 (1986) 166
[424] V. A. Eltekov, V. N. Samoylov, V. E. Yurasova, H. A. Motaweh: Nucl. Instrum. Methods B **13**, 443 (1986) 166
[425] B. J. Garrison: J. Am. Chem. Soc. **105**, 373 (1983) 166
[426] Z. B. Güvenc, Y. Hundur, R. Hippler: Nucl. Instrum. Methods B **164–165**, 854 (2000) 166
[427] V. E. Yurasova, V. S. Chernysh, M. V. Kuvakin, L. B. Shelyakin: JETP (USSR) **21**, 197 (1975) 166
[428] S. S. Elovikov, D. A. Konov, R. S. Gvosdover, L. B. Shelyakin, V. E. Yurasova: Poverknost **5**, 21 (2004) 166
[429] K. Thiel, U. Sassmannshausen, H. Külzer, W. Herr: Radiat. Eff. **64**, 83 (1982) 166, 170
[430] M. M. Jakas, D. E. Harrison, Jr.: Phys. Rev. B **30**, 3573 (1984) 167
[431] D. E. Harrison, Jr.: J. Appl. Phys. **52**, 4251 (1981) 167
[432] D. E. Harrison, Jr., N. S. Levy, J. P. J. III, D. E. Harrison, Jr., N. S. Levy, J. P. J. III, H. M. Effron: J. Appl. Phys. **39**, 3742 (1968) 167
[433] D. E. Harrison, Jr., W. L. Moore, Jr., H. T. Holcombe: Radiat. Eff. **17**, 167 (1973) 167
[434] D. E. Harrison, Jr., P. W. Kelly, B. J. Garrison, N. Winograd: Surf. Sci. **76**, 311 (1978) 167
[435] B. J. Garrison, N. Winograd, D. E. Harrison, Jr.: Phys. Rev. B **18**, 6000 (1978) 167

[436] N. Winograd, B. J. Garrison, T. Fleisch, W. N. Delgass, N. Winograd, B. J. Garrison, T. Fleisch, W. N. Delgass, D. E. Harrison, Jr.: J. Vac. Sci. Technol. **16**, 629 (1979) 167
[437] N. Winograd, K. E. Foley, B. J. Garrison, D. E. Harrison, Jr.: Phys. Lett. A **73**, 253 (1979) 167
[438] L. P. Razvina, V. A. Eltekov, V. E. Yurasova: in *Proc. 17th All-Union Conf. Emission Electronics* (Akad. NAUK SSSR, Moscow 1979) 167
[439] K. E. Foley, B. J. Garrison: J. Chem. Phys. **72**, 1018 (1980) 167
[440] D. E. Harrison, Jr.: J. Appl. Phys. **52**, 1499 (1981) 167
[441] V. A. Eltekov, V. N. Samoylov, V. E. Yurasova: Pover. Fiz. Khim. Mekh. **3**, 43 (1982) 167
[442] V. I. Shulga: Radiat. Eff. **70**, 65 (1983) 167
[443] J. Likonen, M. Hautala: Appl. Phys. A **45**, 137 (1988) 167
[444] B. J. Garrison, N. Winograd: Chem. Phys. Lett. **97**, 381 (1983) 167
[445] V. I. Shulga: Radiat. Eff. **82**, 169 (1984) 167
[446] V. I. Shulga: Radiat. Eff. **84**, 1 (1985) 167
[447] M. H. Shapiro, P. K. Haff, T. A. Tombrello, D. E. Harrison, Jr., R. P. Webb: Radiat. Eff. **89**, 243 (1985) 167
[448] S. C. Park, R. A. Stansfield, D. C. Clary: J. Phys. D **20**, 880 (1987) 167
[449] M. H. Shapiro, T. A. Tombrello: Nucl. Instrum. Methods B **18**, 355 (1987) 167
[450] K. Broomfield, R. A. Stansfield, D. C. Clary: Surf. Sci. **202**, 320 (1988) 167
[451] J. D. Kress, D. E. Hanson, A. F. Voter, C. L. Liu, X.-Y. Liu, D. G. Coronell: J. Vac. Sci. Technol. A **17**, 2819 (1999) 167
[452] I. N. Iwanov, D. W. Ledyakin, I. F. Urazgil'din, V. E. Yurasova: Fisika Tverd. - Solid State Phys. **33**, 924 (1991) 167
[453] V. E. Yurasova, I. F. Urazgil'din: Radiat. Eff. Defects Sol. **117**, 99 (1991) 167
[454] A. A. Promokhov, V. A. Eltekov, V. E. Yurasova, J. S. Colligon, A. S. Mosunov: Nucl. Instrum. Methods B **115**, 544 (1996) 167
[455] T. T. Nuver: Proefschrift (2202) 167
[456] M. H. Shapiro, T. A. Tombrello: Nucl. Instrum. Methods B **194**, 425 (2002) 167
[457] V. I. Bachurin, E. S. Kharlamochkin, M. V. Kuvakin, V. E. Yurasova: in *Proc. 15th ICPIG*, vol. 1 (1981) p. 465 167
[458] T. Michely, C. Teichert: Phys. Rev. B **50**, 11156 (2003) 167
[459] A. Friedrich, H. M. Urbassek: Surf. Sci. **547**, 315 (2003) 167
[460] Z.-Y. Ye, Q.-Y. Zhang: Chin. Phys. **10**, 329 (2001) 167
[461] H. F. Lu, C. Zhang, Q. Y. Zhang: Nucl. Instrum. Methods B **206**, 22 (2003) 167
[462] M. Hou: in F. P. V. P. Varga, G. Betz (Ed.): *Proc. Symp. on Sputtering* (Techn. Univ., Vienna 1980) p. 101 167
[463] M. M. Jakas, D. E. Harrison, Jr.: Phys. Rev. Lett. **55**, 1782 (1985) 167
[464] M. A. Karolewski: Nucl. Instrum. Methods B **194**, 26 (2002) 167
[465] T. Neidhart, Z. Toth, M. Hochhold, M. Schmid, P. Varga: Nucl. Instrum. Methods B **90**, 496 (1994) 168
[466] N. Seifert, W. Husinsky, G. Betz, Q. Yan, N. H. Tolk: Phys. Rev. B **51**, 12202 (1995) 168
[467] E. Gauthier, W. Eckstein, J. László, J. Roth: J. Nucl. Mater. **176 & 177**, 438 (1990) 168

[468] J. P. Biersack: Fusion Technol. **6**, 475 (1984) 168, 169, 170
[469] S. S. Elovikov, E. Yu. Zykova, A. A. Promokhov, V. E. Yurasova: in A. I. Melker (Ed.): *Nondestructive Testing and Computer Simulations in Science and Engineering*, vol. 3687 (SPIE - The International Society for Optical Engineering) 168
[470] A. A. Promokhov, A. S. Mosunov, S. S. Elovikov, V. E. Yurasova: Vacuum **56**, 247 (2000) 168, 170
[471] S. S. Elovikov, R. S. Gvosdover, E. Yu. Zykova, A. S. Mosunov, V. E. Yurasova: Poverknost Rent. Synk. Netr. **12**, 34 (2000) 168, 170
[472] S. S. Elovikov, E. Yu. Zykova, A. S. Mosunov, A. A. Semenov, I. I. Shkarban, V. E. Yurasova: Bull. Russian Acad. Sci. **66**, 608 (2002) 168
[473] J. Bohdansky, J. Roth, F. Brossa: J. Nucl. Mater. **85 & 86**, 1145 (1979) 168
[474] T. Nenadović, B. Perraillon, Z. Bogdanov, Z. Djordjević, M. Milić: Nucl. Instrum. Methods B **48**, 538 (1990) 168
[475] G. Hayderer, S. Cernusca, V. Hoffmann, D. Niemann, N. Stolterfoht, M. Schmid, P. Varga, H. P. Winter, F. Aumayr: Nucl. Instrum. Methods B **182**, 143 (2001) 168
[476] O. S. Oen, M. T. Robinson: J. Nucl. Mater. **76 & 77**, 370 (1978) 169
[477] M. Kaminsky, R. Nielsen, P. Zschack: J. Vac. Sci. Technol. **20**, 1304 (1982) 169
[478] J. A. Borders, G. C. Nelson: J. Nucl. Mater. **103 & 104**, 369 (1981) 169
[479] K. Inoue, Y. Taga: Surf. Sci. **140**, 491 (1984) 169
[480] B. Fritzsch, V. N. Samoylov, A. Zehe: Solid State Commun. **60**, 553 (1986) 169
[481] H. von Seefeld, H. Schmidl, R. Behrisch, B. M. U. Scherzer: J. Nucl. Mater. **63**, 215 (1976) 169
[482] B. Emmoth, M. Braun, T. Fried, J. Winter, F. Waelbroeck, P. Wienhold: J. Nucl. Mater. **103 & 104**, 393 (1981) 169
[483] R. P. Schorn, E. Hintz, B. Baretzky, J. Bohdansky, W. Eckstein, J. Roth, E. Taglauer: J. Nucl. Mater. **162–164**, 924 (1989) 169
[484] B. Baretzky, W. Eckstein, R. P. Schorn: J. Nucl. Mater. **224**, 50 (1995) 169
[485] I. P. Soshnikov, Yu. A. Kudriavtsev, A. V. Lunev, N. A. Bert: Nucl. Instrum. Methods B **127–128**, 115 (1997) 170
[486] J. P. Allain, D. N. Ruzic, M. R. Hendricks: J. Nucl. Mater. **290–293**, 33 (2001) 170
[487] R. Bastasz, W. Eckstein: J. Nucl. Mater. **290–293**, 19 (2001) 170
[488] W. Möller, W. Eckstein: *IPP-Report 9/64* (MPG, Garching 1988) 170
[489] M. Taniguchi, K. Sato, K. Ezato, K. Yokoyama, M. Dairaku, M. Akiba: J. Nucl. Mater. **313–316**, 360 (2003) 170
[490] O. F. Goktepe, T. D. Andreadis, M. L. Roush: (Univ. Maryland, College Park 1979) 170
[491] J. E. Griffith, R. A. Weller, L. E. Seiberling, T. A. Tombrello: Radiat. Eff. **51**, 223 (1980) 170

Index

adatom, 100
adsorption of
  oxygen, 34
  water, 34
angular dependence of the sputtering yield
  Ag, 119
  Al, 105
  Au, 122–124
  Be, 103
  C, 103–105
  Cu, 110–114, 127
  Fe, 106
  Mo, 116–118
  Nb, 115
  Ni, 107–109
  Pd, 120
  Si, 105
  Ta, 120
  Ti, 106
  W, 121
  Zr, 115
annealing, 131

backscattering, 35
Bayesian statistics, 39
BCA program
  ACAT, 35, 133
  MARLOWE, 126, 133
  Monte Carlo (MC), 124, 131, 132
  TRIDYN, 37, 128, 129
  TRIM, 133
  TRIM.SP, 35, 101, 133
binary collision approximation (BCA), 35

catcher foils, 35
channeling, 40, 131
composition
  change, 37, 126
compound formation, 126
crater
  depth, 34

depth
  distribution, 128, 129
depth of origin, 132
diffusion, 126, 129, 131

electrical resistivity, 34
electron microprobe, 34
energy dependence of the sputtering yield
  Ag, 35, 36, 78, 79
  Al, 48, 49
  Au, 94, 95
  B, 44
  Be, 42, 43
  Bi, 96
  C, 45, 46
  Ca, 51
  Cd, 80
  Co, 60, 61
  Cr, 56, 57
  Cs, 82
  Cu, 64, 65
  Fe, 58, 59
  Ga, 66
  Ge, 66, 67
  Hf, 84
  Hg, 96
  In, 80
  Ir, 91, 93
  Li, 41
  Mg, 47
  Mn, 57
  Mo, 39, 72, 73
  Nb, 70, 71
  Ni, 37, 62, 63
  Os, 90
  Pb, 97
  Pd, 76, 77
  Pt, 92, 93
  Re, 89
  Rh, 75
  Ru, 74
  Sb, 82
  Sc, 51
  Se, 69
  Si, 50
  Sm, 83
  Sn, 81
  Ta, 85, 86
  Tb, 83

Te, 82
Th, 98
Ti, 52, 53
Tl, 96
Tm, 83
U, 99, 100
V, 54, 55
W, 87, 88
Zr, 68, 69
energy loss
electronic, 36, 38, 100
Lindhard-Scharff model, 36
Oen-Robinson model, 36
escape time, 133
evaporation, 132

field ion microscopy (FIM), 35
fluctuation, 132
fluence, 36–38, 126–129
fractionation, 130, 131

heat of sublimation, 35, 125, 131

implantation, 128, 129
interaction potential, 35, 36, 38, 100, 132
Nakagawa-Yamamura, 35
power, 131, 132
screened Coulomb
KrC (WHB), 35, 38
Molière, 35
ZBL, 35
isotope sputtering, 130, 131

lattice vibration, 131

mass change, 34
molecular dynamics, 131

negative binomial distribution, 132
neutron activation, 35

oscillations, 129

partial sputtering yield, 126
planetary science, 131
Poisson distribution, 132
preferential sputtering, 129, 130
projectile binding energy, 102

reduced energy, 38
reflection coefficient, 126, 127
refraction, 101
regime
deposition, 127
erosion, 127–129

screening length, 35, 38
segregation, 126, 129, 131
selfsputtering, 101, 102, 128
sheath potential, 130
simultaneous bombardment, 130
solid–liquid transition, 131
spike
elastic collision, 101
sputtering yield, 34–36
sputtering yield oscillations, 128
state
charge, 130
ferromagnetic, 132
magnetic, 132
paramagnetic, 132
steady, 33, 126–130
sticking, 35
stoichiometry, 129
stopping power
nuclear, 38
surface
roughness, 34, 38, 100, 124, 126, 132
surface binding energy, 35, 100, 125, 130, 131

target
amorphous, 35, 40
composition, 130
compound, 129, 130
multicomponent, 126, 131
polycrystalline, 35, 40
randomized, 131
single crystal, 35, 40, 127, 132
target structure
amorphous, 33
crystalline, 33
polycrystalline, 33
threshold energy, 39, 102, 125, 126
tunneling microscope, 124

vaporization, 131

Wehner spot, 131

x-ray analysis, 34

Results of Molecular Dynamics Calculations

Herbert M. Urbassek

Fachbereich Physik, Universität Kaiserslautern,
Erwin-Schrödinger-Straße, 67663 Kaiserslautern, Germany
urbassek@rhrk.uni-kl.de

Abstract. In recent years, the method of molecular-dynamics computer simulation has increasingly been employed to investigate the mechanisms underlying sputtering of solids by ion and cluster impact. This review highlights the results obtained by this method. The topics covered include sputtering in the linear-cascade and the spike regime, cluster emission, the formation of surface topography by sputtering and its effects on sputtering, sputtering of molecular solids and chemical effects in sputtering.

1 Introduction

Sputtering [1–4] is the process of emission of (neutral or charged) atoms due to the bombardment of the surface of a material by energetic particles. Usually these projectiles are ions, but as well atoms, clusters or other particles (neutrons, electrons, etc.) may be employed.

The theoretical understanding of the sputter phenomenon is quite advanced. While the main progress in the theoretical description of the sputter phenomenon came by analytical theory [5], computer simulations were increasingly used throughout the last decades to investigate ion irradiation-induced phenomena. Simulation algorithms based on the so-called 'binary collision approximation' (BCA) as well as various Monte Carlo schemes were set up to study processes in structureless [6] and crystalline [7] targets; they are reviewed in [8] and elsewhere in this book.

Molecular dynamics simulations have been employed for a long time to obtain an atomistic understanding of irradiation-induced processes. Indeed one of the earliest applications of the method has been a seminal contribution by *Vineyard* et al. [9], who applied molecular dynamics to the study of primary knock-on processes in metals. This was only three years after this method was invented to study the equilibrium properties of a hard-sphere fluid [10].

There are good reasons to apply molecular dynamics to sputtering:

1. A complete description of the projectile-surface interaction process starts with the projectile slowing down in the target and ends with the dissipation and finally thermalization of the energy. The molecular dynamics

R. Behrisch, W. Eckstein (Eds.): Sputtering by Particle Bombardment,
Topics Appl. Physics **110**, 189–230 (2007)
© Springer-Verlag Berlin Heidelberg 2007

method is, in principle, able to follow this whole sequence of events without any further assumptions or approximations, once the interatomic interaction potentials and the electronic stopping have been specified.
2. Material dependent parameters – like surface binding energies, nuclear stopping powers, melting or boiling temperatures – are included naturally in the interatomic interaction potentials. Thus with a realistic specification of these potentials, no further ad hoc parameters need to be introduced.
3. The effects of bonding and reactions, which are particularly important for the sputtering of molecules and clusters, but also for the sputtering of non-elemental and in particular molecular solids, are included in a straightforward way, once the appropriate potentials have been formulated.
4. The effects of a nanoscopic structure of the surface – atomic roughness or surface topography – are easily included in the simulation.

A draw-back of the method of molecular dynamics is that it is able to study the processes only for a short period of time (roughly $< 1\,\mathrm{ns}$) and on small spatial scales (in target volumes comprising some millions of atoms, say). While these limits may change with the development of hard- and software, it is a difficult task to stretch the simulation to the time and space scales over which real experiments extend. The methods of analytical sputter theory (transport theory), and the binary-collision-approximation Monte-Carlo methods easily transgress these restrictions in time and space scales.

An advantage of the method is that it lends itself easily to the visualisation of the processes occurring and even to their animation. Thus the graphical presentation of the data obtained is often appealing to imagination and may provide for a deeper understanding of the processes occurring.

Since the early days of the application of molecular dynamics to ion-irradiation and sputtering processes, a number of reviews have appeared [8, 11–16]. These cover both the methods applied and the simulation results obtained. The aim of the present review is to delineate the lines of development of the method to show 1. where molecular dynamics has been used intensely in sputter physics; 2. where molecular dynamics has contributed to an understanding of sputter physics. While no complete coverage of the literature is possible, it is hoped that the main lines of development can be shown here.

The progress in this method is established both in the development of hardware and software. Trivially, progress in hardware capacities allows for the simulation of larger targets – this allows for an increase of the bombarding energy which can realistically be studied – and the simulation of a larger number of impact events, which increases the significance of the data obtained. The development in software leads to:

1. The formulation of better potentials, which describe the materials behaviour; these are in particular important for the description of chemical effects and the bombardment of molecular solids.

2. The formulation of better boundary conditions of the simulation crystallite which allow to better control the effects of the finite size of the simulation target in contrast to the experiment.
3. The inclusion of further effects in the molecular dynamics simulation, such as electronic effects in sputtering (excitation or ionization).

In this contribution, the impact of molecular dynamics simulations on the understanding of the physics underlying the sputter phenomenon is presented and discussed. While a complete coverage of all scientific contributions to this subject appears impossible, it has been attempted to sketch the various fields in which molecular dynamics simulations have proven fruitful to widen and deepen our understanding. Due to the atomistic nature of this simulation technique, as diverse aspects as cluster impact, chemical effects in sputtering, or the effect of surface topography on sputtering could benefit from this method.

2 Linear-Cascade Regime

A number of molecular dynamics studies have been performed in order to investigate basic issues in linear sputtering theory. The grouping of the results reported below under this heading may not appear fair in all cases. However, this section is meant to contain all those results that can be understood at least in a first approximation from the assumptions underlying linear-cascade theory, and refer to processes where neither atomic binding nor high energy densities play a strong role.

Single-crystalline targets are implemented with particular ease in molecular dynamics; hence several studies on clarifying the sputter mechanisms of single crystals have been performed. The evolution of this field until 1992 is described in [17]. A special impetus for performing these simulations is provided by experimental techniques which allow to measure energy-resolved angular distributions of sputtered particles for small irradiation fluences and hence under well defined surface conditions. Such an experimental situation lends itself in an ideal way to molecular dynamics simulations. In fact, it may be hoped that here it is only the interatomic interaction potential the knowledge of which limits the accuracy of the simulation. In this situation, a new potential – due to *DePristo* et al. [18, 19] – was incorporated into the simulation, which was believed to describe interatomic interaction in metals in a more accurate way, and the sputter calculations which were previously performed with the established embedded-atom-method (EAM) potential [20] were repeated. The new results appear to show a better agreement with experimental data [21].

Among further work on single-crystal sputtering we wish to mention [22], which aimed at identifying the mechanism of Wehner spot formation for low-energy sputtering, i.e., the preferential emission of sputtered atoms in

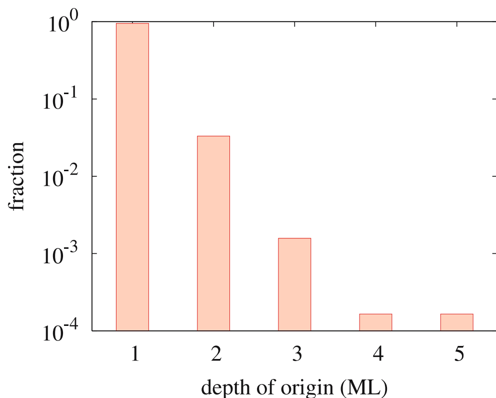

Fig. 1. Distribution of depth of origin of Cu atoms sputtered by 1 keV Ar ions from a Cu (100) surface. Molecular dynamics data from [30]

close-packed crystal directions. Also [23] and [24] investigated this subject with a particular interest in the temperature dependence of Wehner spots. Sputtering induced by hyperthermal rare-gas atoms bombarding different low-indexed surfaces of a Cu crystal was investigated in [25]. Other work tried to identify the differences between the sputtering of an amorphous in contrast to a single-crystal Si surface [26]; there also several discrepancies with previous simulation results of crystalline Si sputtering [27, 28] are discussed. The depth of origin of sputtered atoms was studied using molecular dynamics (and Monte Carlo) simulations in [29] for random target orientation. Figure 1 exemplifies the distribution of depth of origin for 1 keV Ar impact on a Cu (100) surface. It shows that some 95 % of the sputtered atoms originate from the topmost surface layer for impact on a (100) surface; on a (111) surface it is only 85 % [23].

Finally, some unusual work on linear-cascade sputtering should be mentioned. In condensed gases, very low-energy atoms – in the eV region – may give rise to so-called mini-cascades [31]. Such low energy atoms may be excited for instance by electronic excitation, and subsequent energy transfer to atomic motion. Molecular dynamics simulations of this phenomenon have been performed with the aim of describing electronic sputtering in condensed gases [32] and the transmission of atoms through thin rare-gas films, and the concomitant sputtering [33].

In summary, the method of molecular dynamics is well able to study sputtering in the linear-cascade regime. Since, however, the BCA method is readily applied to this regime, and with less expenses in computer time, molecular dynamics simulations are in general only performed in those cases where either the binding situation in the target needs to be accurately implemented (such as in compounds), the number of approximations introduced needs to be minimized in order to study a small effect (such as in prefer-

ential sputtering of isotopes) or simply advantage is drawn from the ready availability of the molecular dynamics program. Two specific areas where molecular dynamics simulations have been successfully used in this respect are discussed in the following.

2.1 Low-Energy Sputtering

The sputtering behaviour for low-energy impacts ($< 1000\,\mathrm{eV}$, say) lends itself readily to molecular-dynamics simulation. *Kress* et al. [34] investigate the low-energy off-normal Ar and copper bombardment of Cu (111). *Gades* and *Urbassek* [25] investigate energy deposition, reflection and sputtering of normal-incidence rare-gas atoms with energies of 5–400 eV off polycrystalline Cu, and compare to experimental measurements by *Winters* et al. [35, 36]. Good agreement is obtained for the energy dependence of the deposited energy. Light projectiles deposit less energy in the target due to their increased reflection probability; for heavy projectiles, sputtering is the dominant energy loss channel from the target. *Abrams* and *Graves* [37, 38] study sputtering of Cu by Ar and Cu low-energy impacts ($< 175\,\mathrm{eV}$). They discuss the sputtering and the sticking coefficient as a function of the incidence angle and state favourable agreement of their sputtering yields with the experimental data compiled in [39]. The same authors also study sputtering of rough SiO_2 surfaces by obliquely incident low-energy Ar atoms [40] and emphasize the angular and energy distributions of sputtered atoms and molecules. *Kubota* and *Economou* [41] investigate the growth of a thin oxide film on Si induced by thermal O atoms and sputtering by 100 eV Ar ions.

Several low-indexed surfaces of fcc and bcc crystal have been reinvestigated by *Shapiro* et al. [42]. *Güvenc* et al. [43] discuss the sputtering mechanism, including the effect of the projectile-target interaction potential, on the sputtering yield of the Ar $\rightarrow$ Ni (100) system for bombarding energies between 10 and 40 eV. They find the theoretical yields to be considerably higher than the experimental yields [44] and attribute this discrepancy to the incomplete knowlegde of the real interatomic potential functions.

2.2 Preferential Sputtering

The sputtering behaviour of compounds and alloys is of considerable practical interest [45]. In these materials, sputtering yields, but also the angular and energy distributions, will depend on the species that is ejected. In other words, the measurement of *partial* yields and distributions is of prime interest.

Let us concentrate in the following on the sputtering of a binary system of species i and j which are homogeneously mixed with concentrations c_i, c_j, where $c_i + c_j = 1$. While after irradiation with sufficiently high fluence, a steady state will be reached, in which the ratio of the sputtering yields is stoichiometric, i.e., equals the ratio of the bulk concentrations,

$$Y_i/Y_j = c_i/c_j\,, \tag{1}$$

this is in general not the case for small fluences. We shall call the normalized ratio

$$\delta = \frac{Y_i}{Y_j} \frac{c_j}{c_i} \tag{2}$$

the sputter preferentiality, since its deviation from the value 1 indicates over- or under-stoichiometric emission of a particular species. Note that in some papers, $(\delta - 1)$ is called the sputter preferentiality. Analytical sputter theory [46] predicts δ to depend on the masses $M_{i,j}$ and the surface binding energies $U_{i,j}$ of the respective species in the alloy as

$$\delta = \left(\frac{M_j}{M_i}\right)^{2m} \left(\frac{U_j}{U_i}\right)^{1-2m} . \tag{3}$$

Here m denotes the power exponent describing the interaction potential.

The sputtering of such a system is of considerable interest to SIMS. The static SIMS case corresponds to low fluences, $\Phi \to 0$, while the interpretation of dynamic SIMS data needs (among others) a knowledge of the dependence of the partial sputtering yields on fluence Φ. A wealth of experimental data as well as (dynamic) binary-collision simulations is reviewed in *Gnaser* [47], and elsewhere in this volume.

Molecular dynamics simulations on sputtering of multi-component materials are comparatively rare. In the following, only results on the static case ($\Phi \to 0$) will be reviewed. *Gades* and *Urbassek* [48] studied the preferential sputtering of a series of model alloys CuX. By choosing X as a pseudo-copper species which is more weakly (strongly) bound than natural copper, the dependence of the preferential sputtering on the surface binding could be explored. Here it was shown that – in particular for low bombarding energies of 1 keV – the simulated preferentiality is stronger than in the analytical estimates; with increasing bombarding energy the analytical estimate appears to describe the simulation data better.

A special case of particular interest is the sputtering of isotopic mixtures. Here sputtering is governed by the mass ratios of the different isotopes in the specimen. Equation (3) thus predicts a preferentiality

$$\delta = \left(\frac{M_j}{M_i}\right)^{2m} . \tag{4}$$

Since this effect is generally small, in the percentage range, in molecular dynamics simulations the mass differences are often artificially enhanced in order to increase the preferentiality, and hence improve the statistical significance of the results [49]. Early work was performed by *Shapiro* et al. [50, 51] who considered a variety of targets (both two- and three-isotope crystals and liquids) and compositions. The preferentiality showed a size compatible with the experimental findings. Large emission-angle-dependent effects were

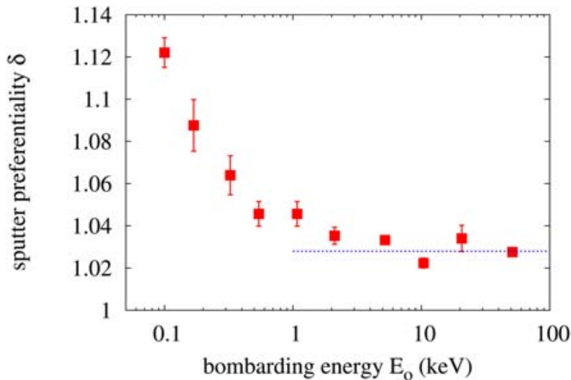

Fig. 2. Computer simulation data [54] for the sputter preferentiality δ in a 1:1 stoichiometric mixture of ^{92}Mo and ^{100}Mo, sputtered by Ar ions of energy E_0. δ shows a strong dependence on the ion impact energy; only for sufficiently high energy, $E_0 > 10\,\text{keV}$, the asymptotic result, (4), with $m = 1/6$ (*dotted line*) is retrieved

found, and a strong dependence on the target crystallinity, such that liquid samples, deviated strongly in their angular emission pattern from crystalline samples.

In their study of model CuX alloys, *Gades* and *Urbassek* [48] also chose X as a heavy copper atom with twice the natural mass. A sputter preferentiality of $\delta = 1.30 \pm 0.05$ was obtained, in good agreement with the theoretical value 2^{2m}, where $m = 0.19$ for the potential adopted.

Lam and *Johannessen* [52] studied the preferential sputtering of CuNi; this study was later repeated by *Gades* and *Urbassek* [48]. The resulting preferentialities of $\delta = 1.22$ and 1.25, respectively, of the two simulation studies coincide; in this case the preferentiality originates mainly from the different surface binding energies of copper and nickel in the specimen.

Shulga and *Sigmund* performed a series of simulations, where besides binary-collision simulations also molecular dynamics was employed [53, 54]. Molybdenum isotope samples with an artificially increased mass ratio were investigated. These authors studied in particular the dependence of the preferentiality on the bombarding ion energy, and showed that the theoretical result is only retrieved for high energies ($E_0 > 10\,\text{keV}$ in their case), cf. Fig. 2. At low bombarding energies, the sputter preferentiality strongly depends on the mass and energy of the bombarding species and varies considerably with the emission angle; this effect could be reduced to the collision kinematics of binary scattering.

3 Ionic Crystals

Sputtering of ionic crystals has been investigated experimentally; it is known to give rise to considerably larger sputtering yields than those expected from collisional theory [55]. This is believed to be due to 'electronic sputtering', i.e., long-lived electronic excitation states which are created by the bombardment, diffuse to the surface and induce sputtering there. This process has been studied in alkali halides with quite some detail [56].

Ionic bonding occurs in many materials of practical interest. Thus, e.g., alkali halides are used for radioactive waste storage. Other relevant materials, such as SiO_2, but also SiC, and many non-metallic compounds, exhibit at least partial ionic bonding. In molecular solids, the molecular constituents may be polar, possessing permanent dipole moments; the outstanding example is given here by water. In all these cases, the long-range nature of the Coulomb (or dipole) forces complicates the strict calculation of the attractive forces used for molecular dynamics. Usually, the Coulomb contribution to the forces is ignored or cut off, when calculating the effect of ion irradiation on these compounds. Thus, e.g., in a molecular dynamics simulation of Coulomb explosion from a fast-ion-induced ion track [57], the Coulomb forces enter the simulation with an exponential screening factor $\exp(-r/a)$ and are furthermore cut off at $r_c = 7a$. In a related case, the laser ablation of water, the dipole force is cut off at a relatively short distance [58].

Nordlund [59] studies radiation effects induced by keV Ga PKA's in the strongly ionic compound GaN. By comparing the simulation results of a non-ionic model to those of an ionic charge-transfer model, he can demonstrate that in this case, the inclusion of explicit ionicity shows no strong effect on collision cascade development. In agreement with experiments [60, 61], he finds an amorphisation dose which is considerably higher in this material than in Si or comparable semiconductors; based on his simulations he attributes this effect to a high threshold displacement energy and cascade-induced annealing of damage as well as to in-cascade annealing.

Only few investigations have been published in which the long-range electrostatic forces have been fully taken into account. A recent paper by *Ramasawmi* et al. [62] investigates the sputtering of NaCl by 1 keV Na impact. Technically, these authors consider the target as a free crystallite, with fixed lateral boundaries. In this way, all electrostatic forces are taken into account for the 2 ps during which the simulation is performed. The results show a relatively low sputtering yield of 0.36 attributed to a large amount of channeling. A large number of dimers, often neutral, are emitted. Recent studies by *Young* [63, 64] model the Coulomb explosion spike in KCl and LiF crystals containing 12,800 particles generated by a swift ion. While sputter processes are not considered here, this work gives insight into the dynamical effects associated with ion track formation in such a material, affecting in this case a cylindric region of 78 Å in diameter.

4 Effect of Electronic Energy Loss and Electronic Excitations in Atomic Collision Cascades

Another thread of work attempts to identify the role of electronic inelastic loss processes in a cascade, and of electron excitation [65–67]. Such a procedure requires an *ad hoc* introduction of electronic processes into the simulation. The results achieved were also used to assess the mechanisms by which core-excited atoms are sputtered [68].

Besides giving away their energy in elastic collisions with other atoms, atoms may be slowed down in the solid also by the so called electronic stopping, i.e., inelastic losses with target atoms or the ‘friction’ in the electron gas of the target. This electronic stopping can be described as a velocity-proportional friction; the proportionality coefficient has been calculated by *Lindhard* and *Scharff* [69] and *Firsov* [70] and also in later more recent work [71, 72]. Such a stopping process can be included as a friction force in molecular dynamics simulation. This friction dampens the motion of the projectile but also of each target atom in the collision cascade of the solid [73].

As a consequence, projectile ranges are shortened, but also the lifetime of thermal spikes is reduced [74–76]. Since for low atom velocities, the electronic stopping has to obey the same physics as, e.g., electron-atom scattering in electrical conduction, the low-energy stopping can alternatively be described by the electron-phonon interaction [77, 78]. The magnitude of the proportionality coefficient entering the velocity-proportional stopping at low velocities has been subject to considerable debate in the past [78]. Note that recent experiments [79] allow to measure directly the kinetic electron excitation in atomic collision cascades.

Several schemes have been employed to include electronic excitation processes into the molecular dynamic simulation of collision cascades.

1. Electron promotion in close binary encounters may form the basis of excitation [80–82]. This treatment has also been applied to describing the sputter emission of highly excited metastable atoms [83, 84].
2. Low-energy atom motion (below 1 eV, say) has been modelled to couple via the electron-phonon interaction to electrons. This approach has been used to describe effects like defect production and ion-beam mixing [85]; we note that the importance of including electron-phonon coupling for these phenomena is still under discussion [76]. Assuming thermalization of the electronic and the atomic systems separately, this regime can be described by a two-temperature model [86, 87].
3. At energies above 1 eV/atom, the coupling of atomic motion to the electronic subsystems may be described by the electronic stopping power of individual atoms [88].

4.1 Stopping

The consequences of the electronic stopping of the projectile on the sputtering process are considered small and are mostly connected to the reduction of the deposited nuclear energy density; as a consequence the sputtering yield may be somewhat reduced [89].

4.2 Excitation

An interesting consequence of the energy loss into the electronic system is that it may serve as input to models of atom excitation or ionisation; these processes are of immediate interest to sputtering of ions and hence to SIMS experiments. While this idea has been exploited by *Sroubek* in several papers in the past [90, 91], recently this model was also incorporated in molecular dynamics simulations of atomic collision cascades [92]. Since the parameters describing the electronic excitation – besides the proportionality constant of the velocity-proportional friction, also the electronic mean-free path enters the problem. which is itself dependent in particular on the structure (melting, amorphisation) of the irradiated crystal [85] – are not all precisely known, such simulations have at the time being model character and allow the prediction of qualitative features rather than of quantitative effects. Nevertheless, the simulation showed that transient electronic temperatures reaching several thousand Kelvin may be reached in the vicinity of the surface and can thus influence the ionization properties of sputtered atoms.

5 High-Energy-Density (Spike) Phenomena

As soon as the energy imparted per atom E_{atom} in a certain subvolume of the cascade becomes of the order of the cohesive energy E_{coh} of the solid, or above, the linear-cascade sputter regime is left, and a so-called high-energy-density zone, or a (thermal or elastic-collision) spike is created. If this high-energy-density zone is established close to the surface, intense sputtering may result. We note that the idea that regions of high energy density are relevant for sputtering is rather old [46].

Early research concentrated on the investigation of spikes in metals. Thus for example it was established experimentally that at energies around the maximum of the nuclear stopping power, spikes contribute substantially to the sputtering of Au by heavy projectiles [93, 94]. The molecular dynamics simulation study of *Ghaly* and *Averback* [95] could visualise the spike induced by 20 keV Au bombardment of a Au target; for the trajectory shown dramatic atom emission resulted (cf. also Fig. 3).

Clear evidence of spikes was presented in simulations of keV atom bombardment of condensed rare gases [96, 97]. More recently, also the transition from collision-cascade to spike (or from linear to nonlinear) sputtering was

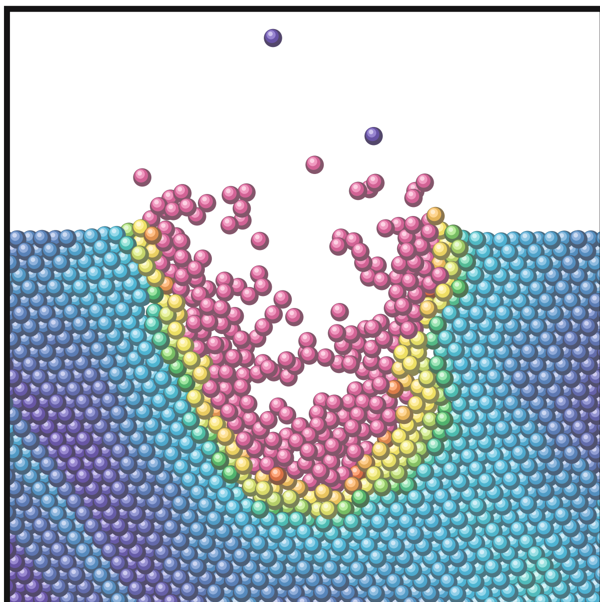

Fig. 3. Cross section through a Au crystal 1.5 ps after perpendicular impact of a Au_{13} cluster with 10 keV total energy on its (111) surface. Color denotes local 'temperature'; the *green zone* corresponds to the melting temperature, the *red zone* has reached double this temperature

investigated in such systems [98]. In the (nonlinear) spike regime, the molecular dynamics analysis of such events allowed to describe the phenomena occurring after atom impact using hydrodynamical and thermodynamical quantities:

1. a low particle density in the spike region, which has been created due to the high pressure established there;
2. an explosion-like velocity distribution leading to a radial expansion of the material around the 'centre of the spike'; this velocity distribution leads to the correlated outward emission of the surface of the energized cascade volume;
3. a huge sputtering yield, resulting in the formation of a crater;
4. the energy distribution of emitted atoms exhibits a $1/E^2$-tail for higher energies ($E > 0.2$ eV in the case of an Ar target) in agreement with linear-cascade theory. Below 0.1 eV an excess amount of low-energy particles are sputtered; these particles are associated with the thermal-spike character of the emission.

The last two features have been observed experimentally [99–101]. Spikes may be rather long lived – on the order of 1 to several ps –, whereas linear collision cascades have died several 100 fs after ion impact, when the energy of all

atoms has decreased below the cohesive energy, and hence no more collision-cascade sputtering can occur. The reason hereto is that in a spike, energy has more or less been equilibrated between all the atoms, and hence its lifetime is governed by energy diffusion (heat conduction) out of the spike volume, while in a linear collision cascade each moving atom loses energy when it collides with an atom at rest. Hence it is a question of major importance for the lifetime of spikes whether electrons can participate in energy dissipation. Various schemes have been proposed to include electrons into a molecular dynamics simulation in a phenomenological way [14, 73, 77, 85, 86, 88]. One result of these considerations is that for good electrical conductors – such as Cu or Ag – the coupling between electrons and atoms is too small to sensibly affect the lifetime of a spike; in other cases, however, – such as Ni or Pt – spikes may be efficiently quenched by electronic heat conduction [77, 86]. Even arguments were raised that in some cases energy may be imparted from the electrons to the phonon systems. Such a situation may be important for high-energy irradiation (in the MeV region) where a nonnegligible part of the projectile energy is given to the electronic system, and may be imparted from the electrons to the atoms [87].

In the following Sect. 5.1, results on sputtering from fast-ion-induced tracks will be presented, since these offer a situation in which high energy densities are imparted to the target. High energy densities also occur for cluster impact; the sputtering induced in this situation will be reviewed in Sect. 5.2. In cases where a spike has been formed due to ion or cluster impact, a crater may be produced at the surface, see Sect. 7.2. Finally, Sect. 10.2 reviews simulation results on the sputtering of molecular and organic solids, in which often – due to the low cohesive energy of the materials – a situation of a high-energy-density zone will be produced.

5.1 Sputtering from Fast-Ion-Induced Tracks

Sputter emission from fast-ion-induced tracks in the electronic-stopping regime, i.e., at energies, where the electronic stopping dominates the nuclear stopping, was analysed using molecular dynamics in the last decade. These tracks are produced by swift ions, typically fission fragments, which penetrate on a straight line deep into the material and deliver energy mainly in the form of electronic excitation. Close to the surface, the high energy deposition may induce sputtering from these tracks. Molecular dynamics simulations usually skip the details of how the electronic energy is converted into nuclear motion and immediately assume the excitation energy to be imparted as random kinetic energy of the atoms.

Often a model system has been chosen for simulation; it consists of a van-der-Waals bonded material, described by a Lennard-Jones potential. The initial excitation in the fast ion track is modelled as a cylindrical region extending into the target which is filled with excitation energy. The processes

occurring in the material after this initial energization are followed using molecular dynamics.

An early paper by *Fenyö* et al. [102, 103] showed that molecular dynamics simulation is able to analyze this process. Later *Kafemann* et al. [104] discussed the dependence of the sputtering yield on the radius of the cylindrical excitation region and on the energy density in this region. They showed the existence of two sputter regimes: A threshold or onset regime, in which the sputtering yield depends highly nonlinearly on the excitation energy density, and a higher-energy linear regime. In a series of papers, *Bringa* and *Johnson* analysed this scenario in greater detail. The following results could be obtained [105–108]: 1. A third regime was identified where at low densities of the energetic excitation events the yield is linear due to the sparse distribution of the excitations [109]. 2. The high-energy-density linear regime is connected to the formation of a melt and the removal of energy by a pressure pulse. In this regime the size of the yield increases with the initial radial extension of the track and is determined by the removal of energy radially by the pressure pulse and by the transport of energy from depth to the surface.

This analysis was later corroborated by comparison to fluid-dynamic calculations [110–113]. These ascribe the linear dependence of the yield on the excitation density by a competition of cooling of the cascade and mass ejection from the surface.

In [57] *Bringa* and *Johnson* analyse the Coulomb explosion of a cylindrical ionisation track using molecular dynamics and compare it to sputtering by a spike. They argue that Coulomb explosion and spike refer to the early and late aspects of the ionisation track produced in a solid by a fast incident ion.

Beuve et al. [114] study two further aspects of fast-ion-induced sputtering by including the dynamics of the electronic subsystem: 1. the energy transfer from the electronic to the atomic system is assumed not to occur instantaneously but to take a period of time Δt. For $\Delta t > 1\,\mathrm{ps}$ it is found that the sputtering yield becomes strongly nonlinear as a function of the stopping power. 2. The influence of a non-homogeneous spatial distribution of the electronic excitations is modelled. It is shown that such a spatial distribution also leads to a strongly non-linear dependence of the yield on the excitation density.

5.2 Cluster Impact

In recent years, the consequences of energetic cluster impact on solids have received increased attention. Thus, the consequences of bombarding surfaces with clusters have been investigated by molecular dynamics for the purpose of identifying the basic interaction mechanisms of clusters with solids [115–122], and to model cluster deposition [123–126]. Besides sputtering, the induced surface modification and defect formation [127, 128], cluster ranges [129, 130], surface growth (thin-film deposition) [123, 126] and surface smoothing [131–133] have been investigated.

Early investigations of molecular dynamics simulations of sputtering induced by cluster impact include [116, 134] and are reviewed in [94]. In terms of sputtering physics, cluster impact, in particular for large cluster sizes, represents a clear-cut example for spike sputtering. Figure 3 gives an atomistic view of the processes occurring in a crystal shortly after impact of a large cluster.

5.2.1 Small Cluster Impact ($n \leq 3$)

Lindenblatt et al. [135] performed a detailed study of Ag_n ($n = 1, 2, 3$) bombardment of the Ag (111) surface at 2 keV/atom. Besides the total sputtering yields, the cluster abundancies in the flux of sputtered particles were determined. For the case of Ag_2 and Ag_3 projectiles, a pronounced dependence of the yields on the orientation of the projectiles could be observed. The authors show that polyatomic projectiles produce colder sputtered clusters.

Medvedeva et al. [136] study similarly the sputtering of a Si (100) surface by Al_n and Au_n clusters with 1.5 keV/atom incidence energy for sizes $n = 1$ and 2. This study emphasizes the role of an oblique incidence angle in producing high sputtering yields and enhanced probability for producing clusters.

Shapiro and *Tombrello* [137–139] study the sputtering of a Au (111) surface with 100 keV/atom Au_n ions ($n = 1$, 2, 3). They restrict their attention to the first 3 ps after projectile impact and hence to the collision-cascade phase and the earliest phase of the thermal spike; angular and energy distributions of atoms sputtered during this time are discussed.

5.2.2 Larger Cluster Impact ($n > 3$)

Insepov and co-workers have published the results of a series of investigations performed over the years [127, 128, 131, 140–143]. They are interested in large cluster impacts with sizes between several 10 and 10^4 atoms. While their main interest is the modification of the target, also the results of sputtering have been published. In [140] *Insepov* and *Yamada* study Ar_n cluster impact with energies of between 10 and 100 eV/atom for sizes $n = 55-200$. They calculate the sputtering yields of a Au and a Si target and show that cluster bombardment induces sputtering of clusters more efficiently than atom bombardment. In [128] these studies are extended to applications such as surface-smoothing under cluster-beam irradiation, which is discussed in Sect. 5.2.3 below. In these studies as well as in [131] also the angular distribution of sputtered atoms is obtained which shows preferential ejection at rather oblique angles. In [142] besides sputtering yields also the scaling of the crater depth with the total cluster energy E for Ar_n impact on a Cu (100) surface is calculated and shown to obey a $E^{1/3}$ power law. In this study, the impact energies range between 6.4 and 20 keV and the cluster sizes between 236 and 736 atoms.

Betz and *Husinsky* [144] examine Al_n cluster impact on Cu (111) with energies between 0.1 and 30 eV/atom and cluster sizes between $n = 60$ and 1080.

They study the transition between cluster deposition and surface erosion, and emphasize the role of the local deposition ‘temperature’ on the eventual fate (melting, mixing with the surface, evaporation, ...) of the cluster.

Sputtering of the Au (111) surface induced by Au_n clusters ($n = 1 - 12$) at fixed total energy of 16 keV is discussed by *Colla* et al. [145] and *Colla* and *Urbassek* [146]. They obtain the following results:

1. Sputtering lasts a long time (> 8 ps) with the exception of monomer bombardment.
2. Pronounced craters are formed as a rule on initially flat surfaces.
3. Large clusters are emitted late from the crater rim and contribute substantially to the sputtering.
4. Sputter-yield fluctuations – originating from varying cluster orientations and impact points on the surface – decrease with increasing cluster size.

Colla and *Urbassek* [146] also study equi-velocity Au_n ($n = 1, 2, 4$) clusters at an energy $E/n = 16$ keV/atom. *Salonen* et al. [147] extend these studies to Au_n cluster impact with n up to 65600 at a total energy of 25 keV. They show that the cluster yield is more or less constant for cluster sizes $n = 2 - 7600$, giving evidence that the total energy determines the sputtering yield in this regime.

Yamaguchi and *Gspann* [148] study cluster impacts on the diamond (111) surface; both Ar_n and $(CO_2)_n$ clusters with a size of $n \cong 1000$ are used. Total impact energies between 10 and 100 keV are studied. Besides an analysis of the temporal evolution of kinetic and potential energies and the temperatures in the system, the dependence of the crater volumes on the bombarding energy is analysed. Furthermore this study shows a considerable enhancement of the sputtering by CO_2 clusters with respect to those of an Ar cluster impact and attribute it to chemical sputtering, i.e., the reactive enhancement of surface erosion by C-O chemistry.

Simulation of fullerene bombardment and the induced sputtering has early been attacked by molecular dynamics [149]. More recently, *Postawa* et al. [150] compare the consequences of a C_{60} cluster impact and a Ga atom impact, each with 15 keV (total) energy, on Ag (111). C_{60} bombardment leads to a yield enhancement by a factor 16 and the yield of Ag_3 is enhanced by a factor of 35. The reason hereto is assigned to the fact that C_{60} deposits its energy close to the surface, thus providing for an efficient means for sputtering.

Zhurkin and *Kolesnikov* [151] report on the sputtering of Al and Ni_3Al induced by Al_n equi-velocity clusters with energies of 100 and 500 eV/atom and sizes between $n = 1$ and 55. The authors discuss the dependence of the sputtering yield on the cluster size, and also give data on the preferential particle ejection from the compound target.

5.2.3 Cluster-Induced Surface Smoothing

Sputtering by cluster bombardment has been used to reduce the atomistic roughness of surfaces. This process, which has been termed 'ion-beam polishing'or 'ion-beam milling' when performed with obliquely incident ions bombarding a rotating target surface, has been found to proceed efficiently when using clusters to smoothen the surface [131].

Moseler et al. [132] give a detailed explanation of the cluster-induced smoothing process. Taking the typical case of a Cu_{2000} cluster at 5 eV/atom impinging on a Cu (001) surface they show how, immediately after the impact, a crater is produced by the enormous pressure of 80 GPa at the contact area between cluster and substrate. However, if the cluster impinges on an inclined surface, the crater rim becomes asymmetric: the 'uphill' motion is impeded, while in the 'downhill direction' the crater rim is free to develop. As a result, a net atom transport downhill exists. Since one can consider such an inclined surface as part of a rough surface, the net downhill atom motion serves to decrease the slope and hence the large-scale surface roughness. The same paper shows that good quantitative agreement with corresponding experiments exists.

[133] simulate the smoothing of a fractal rough surface by cluster impact and show that its fractal dimension decreases. [131] study Ar_n impacts ($n = 200 - 1000$) on a Cu target at 20 eV/atom. They show that these cluster impacts reduce surface roughness and propose that this is the effect of atoms sputtered 'sideways' from the cluster, i.e., having a high lateral momentum.

6 Cluster Emission

In the flux of sputtered particles, as a rule not only atoms, but also clusters are found. This applies in particular to the neutral species emitted. Thus in many experiments performed by keV bombardment of metals, a fraction of some 10 % of the sputtered atoms are bound as dimers; therefore quite a large body of information on sputtered dimers has been assembled in the past, and has been reviewed in [152].

The question of how dimers are emitted and what their fraction in the flux of sputtered particles is, has been investigated in several molecular dynamics simulations [23, 153–155]. The results have mostly been interpreted by comparison to the recombination model of cluster formation of *Können* et al. [156, 157].

Shapiro and *Tombrello* [154] study 5 keV Ar impact on Cu (100). They find three main mechanisms for dimer ejection: direct ejection of intact dimers, recombination of two atoms close to the surface (this mechanism has been proposed by *Können* et al. [156, 157]), and so-called 'push-stick' events, in which a cascade atom colliding with a surface atom is ejected together with it in a bound state [158]. At smaller bombarding energies, 300 eV Ar →

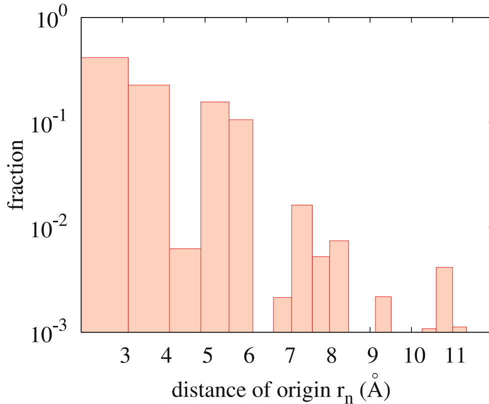

Fig. 4. Distribution of the 'distance of origin' of sputtered dimers: probability that the two atoms contained in a sputtered dimer were at a distance r_n in the solid before emission. Molecular dynamics results [30] for Cu_2 dimers sputtered by 1 keV Ar ions from a Cu target

Cu (100) bombardment, *Karetta* and *Urbassek* [153] find that the majority of sputtered dimers originate from second-nearest neighbour sites, while at higher bombarding energies, above around 1 keV, the majority of dimers stem from nearest-neighbour sites [23, 159]. Figure 4 displays detailed molecular dynamics data of the distribution of the distance that the two atoms contained in the dimer initially had in the target ('distance of origin'). For the specific case of 1 keV Ar → Cu bombardment simulated, some 70 % of the dimers were nearest or second-nearest neighbours in the solid, and have thus been tightly bound to each other before emission. We note that in this simulation the attractive potential extended out to 6.2 Å (5th-nearest-neighbour shell).

Gades and *Urbassek* [155] correlate the dimer sputtering yield Y_2 with the number of sputtered atom pairs, $N_{\text{pairs}} = Y(Y-1)/2$, where Y is the total sputtering yield:

$$Y_2 = p_{\text{clu}} N_{\text{pairs}} \,. \tag{5}$$

Here, the coefficient of proportionality p_{clu} denotes the clustering probability. It assumes a value of around $p_{\text{clu}} = 0.03 - 0.04$ in simulations of 1 keV Cu bombardment of Cu and model Cu alloys. *Gnaser* [47] applies these ideas to experimental data of 1 keV Ar → Cu bombardment and finds his data to be well described by $p_{\text{clu}} = 0.06$, a value comparable to those of the simulations.

A particularly fascinating feature of the sputter phenomenon is that quite large clusters may be emitted. Thus, in experiments of 15 keV Xe bombardment of Ag, Ag clusters up to Ag_{60} have been found [160]; and for the same projectiles bombarding In, even In_{200} has been detected [161]. In these and in

earlier experiments it could be shown that the cluster abundance distribution follows a power-law decay,

$$Y_n \propto n^{-\alpha} , \tag{6}$$

and that the exponent α decreases with increasing total sputtering yield. For keV bombardment of Ag, α varies from 8 to 4 [160], for an In target it even reaches the value of 2 [161]; $\alpha = 2$ has also been found by rare-gas-ion bombardment of Au with $400 - 500$ keV energy, where clusters Au_n with $n > 500$ were detected [162]. A transparent theoretical argument for the origin of the power law (6) is still missing. We note, however, that phenomenological models exist which predict power-law cluster-abundance distributions (6); these are the shock-wave model ($\alpha = 2$) [163] and the thermodynamic-equilibrium model ($\alpha = 7/3$) [164].

Wucher and *Garrison* [165] study sputtering of Ag by up to 5 keV Ar impact. At their highest bombarding energy, the power exponent α reaches a value of 5.3. Good quantitative agreement with experimental data of sputtered-cluster abundance distributions is observed; the authors attribute this fact to the use of a realistic Ag potential [18, 19].

Hartman et al. [166, 167] study cluster emission induced by sputtering of a liquid In-Ga sample by 3 keV Ar impact. The authors investigate the dependence of the cluster yield on the total sputtering yield of the individual ion impact and show a strong positive correlation in the sense that large clusters originate preferably from large-yield events. The power exponent $\alpha = 8.1$ is, however, based only on clusters containing at most 4 atoms. The authors relate their simulation results to a (generalized) recombination model of cluster formation in the spirit of *Können* et al. [156, 157].

In *Colla* et al. [168], simulations of three groups are combined to model the sputtering of a Cu (111) crystal by 5 keV Ar impact and to compare the simulation results to experimental data. Their results exemplify the power-law decay of the cluster-abundance distribution, (6), as shown in Fig. 5. The authors show that large clusters are emitted late after ion impact and originate from 'hot spots', i.e., surface regions with a temperature around or above the melting temperature of copper. A clear correlation of large-cluster emission with the individual sputtering yield could be found such that ion impact events leading to abundant sputtering give also rise to abundant cluster formation.

Muramoto et al. [169] study the cluster formation due to impact of Cu_n clusters on a Cu (111) surface for a cluster energy of 100 eV/atom and for cluster sizes n between 6 and 55. They find the abundance distribution of sputtered clusters to be described by a power law, (6), with an exponent α that decreases with the incident cluster size, and hence with the total sputtering yield. For large sputtering yields α is found to saturate at a value of around 3.

Colla et al. [145, 146] showed that the formation of large clusters (droplets) originating from cluster impact on Au surfaces is connected to the formation

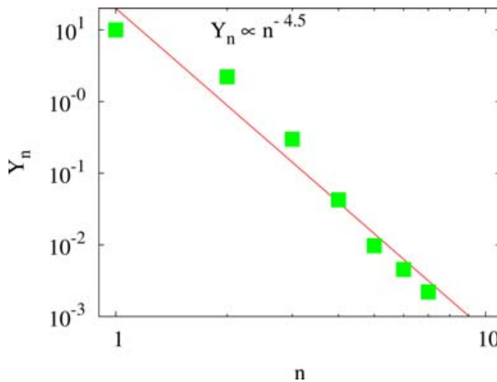

Fig. 5. Abundance distribution of sputtered clusters Y_n vs number of atoms contained in the cluster, n. *Symbols*: Results from molecular dynamics simulations of 5 keV Ar impact on a Cu (111) surface; fragmentation of metastable clusters after emission has been taken into account. *Line*: power-law decay, (6), with $\alpha = 4.5$. Data taken from [168]

of a crater in these events. Large clusters originate from the crater rims; they are emitted comparatively late after ion impact (≥ 10 ps). At this time, the rims are still molten, since they have only poor thermal contact to the bulk of the material. Furthermore, due to the high pressure which initially started the 'micro-explosion' that gave rise to crater formation, the crater rims still contain an outward-directed momentum. It is the balance between the kinetic energy in this outward-directed motion and the potential energy of surface tension that determines whether some part of the crater rim finally is emitted as a large droplet or remains bound to the surface. Figure 6 gives an example of the formation of large clusters late in the sputter process.

As molecular-dynamics simulations show, sputtered clusters as a rule contain a high amount of internal energy. As a consequence, many of them fragent very quickly, on a time scale of 1 ps to several 100 ps, depending on the internal excitation; clusters with an internal excitation just above the dissociation threshold can even live much longer, and can be detected experimentally as metastable clusters on a µs time scale [152]. By calculating the fragmentation process with molecular dynamics, the distribution of stable clusters could be determined. These results were then extrapolated towards larger clusters by a special MC routine built as a post-processor of the molecular-dynamics data; the MC routine incorporates cluster fragmentation via the RRK transition-state theory of unimolecular decay. The result of this simulation shows an astonishingly good overall agreement with the measured data.

Wucher et al. [170] compare experimentally measured and simulated data on the internal energy distributions and fragmentation rate constants of sputtered ${Fe_n}^+$ clusters. To this end, the dynamics of the sputtered clusters is followed by molecular-dynamic simulations until 1 ns; the experimental data

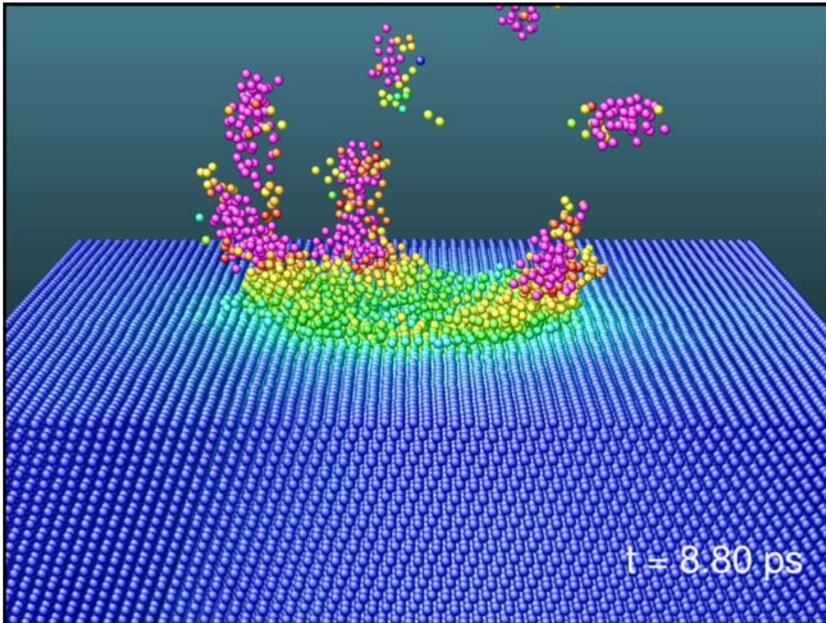

Fig. 6. Perspective view of a Au crystal 8.8 ps after perpendicular impact of a Au_4 cluster with 16 keV total energy on its (111) surface. *Color* denotes local 'temperature'; the *green zone* corresponds to the melting temperature, the *red zone* has reached double this temperature. Data taken from [145]

give information on the time scale of 1 ns and above. The authors obtain fair agreement between measured and simulated internal energies of clusters with sizes between $n = 2$ and 10. The measured internal energies are systematically smaller than the simulated data; the deviation increases with increasing cluster size n and reaches a value of about 50 % for $n = 10$. This deviation is discussed to be due to further ongoing evaporation and fragmentation processes occurring in the sputtered clusters after the end of the simulation time, 1 ns. The authors derive information on the fragmentation rates from their data and the comparison between simulation and experiment.

Another feature which has already been studied in some detail by molecular dynamics in the past was molecule sputtering; i.e., the emission of preformed molecules from the surface. Sputtering of adsorbed molecules and their fragmentation were investigated in [171, 172].

7 Surface Topography Formation

The energy deposited by the irradiating particle close to the surface leads, besides sputtering, to the formation of a variety of surface defects: isolated

adatoms and surface vacancies, and their clustered analogues, i.e., adatom islands and surface-vacancy islands. In extreme cases considerable craters may be created, with adjacent crater rims consisting of piled-up adatoms.

7.1 Surface Vacancy and Adatom Production

These phenomena are directly related, and relevant, to the sputtering process: 1. Adatoms may be viewed as atoms which have attempted to be ejected from the surface, but have not succeeded since their kinetic energy was too small with respect to the surface binding energy. 2. Due to the formation of surface topography, the next impinging ion will encounter an altered surface, and hence the sputtering behaviour may be changed.

The creation of adatoms on a surface induced by keV-atom impact has first been observed by *Harrison* and *Webb* in molecular-dynamics simulations [12, 173, 174].

Ghaly et al. [175] present an extended study of surface damage produced by $5-20$ keV self-ion bombardment in several metals and germanium. They identify three separate mechanisms:

1. ballistic damage created in the linear collision cascade
2. viscous flow due to local melting and the forced flow of liquid to the surface
3. micro-explosions induced by the high pressure in the cascade which lead to rupturing the nearby surface.

Gades and *Urbassek* [176] investigated the formation of adatoms on the Pt (111) surface, induced by the impact of rare-gas atoms with energies below 3 keV. For not too small bombarding energies, > 200 eV, they found for the ratio of the adatom yield Y_a to the sputtering yield Y_s:

$$Y_\mathrm{a}/Y_\mathrm{s} \cong 4\,, \tag{7}$$

in agreement with a simple model derived from analytical sputter theory [176]. This ratio is quite independent of the projectile species. For lower bombarding energies, the number of adatoms formed increases strongly with respect to the sputtering yield, cf. Fig. 7.

In later work, *Busse* et al. [177] investigated adatom production on the Al (111) surface and compared to experimental measurements. Excessive adatom production was found which leads to an experimentally observable irradiation-induced growth instead of the expected erosion for keV Xe impact. In contrast to the Pt (111) surface, the low melting temperature of aluminium emphasises the role of the molten zone induced by the ion impact. Rapid resolidification leaves amorphous parts in the bulk, thus separating surface adatoms from the bulk vacancies and inducing swelling.

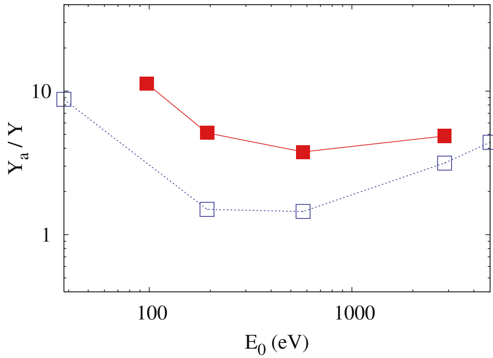

Fig. 7. Ratio of the yield of adatoms, Y_a, to the sputtering yield Y for Xe ion bombardment of a Pt (111) surface. *Open symbols*: molecular-dynamics simulation. *Full symbols*: experimental data. Lines to guide the eye. Data taken from [176]

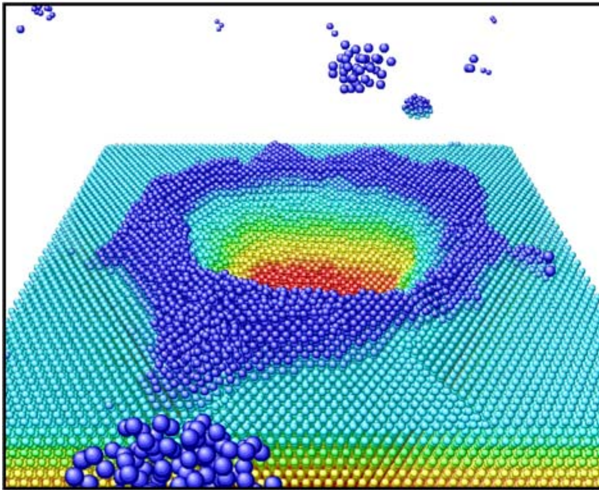

Fig. 8. Perspective view of the crater formed in a Au (111) crystal 40 ps after bombardment with a 64 keV Au_4 cluster. *Color* denotes height above the surface. Data taken from [146]

7.2 Crater Production

Ion bombardment may lead to individual craters at the surface. This phenomenon is quite ubiquitous in cases where a strong thermal spike is formed [178]. In [179], as well as in [180] and also earlier in [181], cratering induced by ions and small clusters is connected to cratering processes induced by hypervelocity projectiles, such as cosmic dust particle or meteorites. Figure 8 presents a view of a crater formed by the sputter process.

Aderjan and *Urbassek* [179] discussed crater formation by Cu_n clusters ($n = 13, 43$) impinging with total energies between 5 and 20 keV on a Cu (100) surface. They find craters to be formed above the threshold bombarding energy of around 5 keV. Then the crater volume increases linearly with the bombarding energy. By artificially varying the cohesive energy of their target, they find that the crater volume scales inversely proportional to the *square* of the target cohesive energy.

Nordlund et al. [182] re-investigate the dependence of the size of ion-induced craters on the materials properties of the target. For this end, they change parameters of the target-target atom interaction potential. In this way they show that the crater size scales inversely proportional to the cohesive energy and to the melting temperature of the material.

Bringa et al. [178] studied this phenomenon by considering Xe impacts on Au for energies between 0.4 and 100 keV. They find that in a low-energy regime (< 10 keV), the mechanism can be understood by considering the high energy density deposited by the projectile in the vicinity of the surface. They argue that at high impact energies (> 50 keV), the formation of craters can be attributed to the long lifetime of the induced heat spike.

Nordlund et al. [183] identify various macroscopic features connected to crater production by < 100 keV atom and cluster impact on heavy metals (Ag and Au). Similarly as in experiment [184, 185], they find the craters produced to be often of a highly asymmetric form, accompanied by adatom ridges extending far from the crater itself. The origin of these structures is reported to lie in atomic 'fingers' and 'bridges', which exist above the crater structure; these structures are propelled onto the surface, resulting in the features observed.

Bringa et al. investigate crater formation by fast-ion impact in the electronic stopping regime [186,187]. They find the threshold for crater formation to occur when the excitation density in the ion track approaches the cohesive energy density; indexcohesive energy a crater rim is formed at about 6 times that energy density. The crater length scales roughly as the square root of the electronic stopping power, and the crater width and depth seem to saturate for the largest energy densities considered. They also find the crater to be much larger than expected from the sputtering yield, and argue therefore that the crater size cannot easily be used to estimate the sputtering yield.

8 Effects of Surface Topography on Sputtering

In molecular-dynamics computer simulation, as a rule, sputtering onto a flat surface is considered. However, in experiment the surface is usually rough. Various forms of surface topography can be found on real surfaces: Atomic-scale roughness, surface steps, larger-scale structures like ripples etc.

The sputtering of surfaces with a large-scale topography, such as ripples, can be easily described, as long as the spatial extent of the collision cascade

is small compared to the curvature radius of the surface structure. Then, the main influence of the surface topography is to alter the incidence angle of the bombarding ion with respect to the local surface normal. In principle, also the surface curvature may influence the sputtering yield. The incorporation of such effects is well possible within analytical sputter theory [188, 189] and does not require modelling on a molecular-dynamics basis. Note, however, the study by *Moseler* et al. [132] discussed in Sect. 5.2.3 on surface smoothing of a rippled surface by cluster beams.

Atomistically rough surfaces, on the other hand, are well suited for a study by molecular-dynamics simulation. In one particular study [190], a Pt (111) surface was randomly covered with a definite coverage Θ of adatoms. Only a small effect, of the order of 10 %, on the sputtering yield was observed. This is reassuring in view of the fact that sputter theory employs a mean, site-independent value for the surface binding. In an earlier simulation [191], analogous results were obtained for pair-potential interaction and a surface covered with half a monolayer of adatoms.

The formation of surface topographical structures may affect the sputtering behavior of the surface. In craters, for instance, redeposition will act to lower the sputtering yield. Due to the general dependence of the sputtering yield on the incidence angle of the bombarding ion, any large-scale (i.e., on the length of a cascade dimension) surface structure will change the incidence angle of the bombarding ion with respect to the local surface normal. Calculations of the consequences of this feature on surface topography formation have been performed [188, 189], but not on a molecular-dynamics basis.

In the case of covalent materials with their directional bonding, the effect of surface topography may be considerably stronger. A detailed study of the effect of 225 eV Xe bombardment on the surface topography evolution of Si(111) and the influence of this topography on the sputtering mechanism has been performed in [192]; the results were shown to be consistent with the layer-by-layer sputter mode found in experiment [193].

8.1 Effect of Surface Steps on Sputtering

A basic irregularity occurring on crystalline surfaces are steps. These occur necessarily in a quite regular fashion on vicinal surfaces, i.e., surfaces that are cut under a small angle towards a low-indexed surface. Furthermore, steps form the boundary between adatom islands or vacancy islands on an otherwise flat terrace. Thus steps form an essential structure occurring on realistic surfaces.

With the advent of high-resolution surface-topography measurement techniques, such as in particular the scanning tunnelling microscope, the ion-induced damage on a surface can be directly observed. Using low fluences, the damage induced by individual ions can be observed experimentally. Including experimental knowledge on the diffusion behaviour of defects, such measurements also allow to deduce the individual sputtering yield from such

measurements. Thus, recently, molecular-dynamics investigations of sputtering of ions interacting with surface steps have been reported.

Early work on the application of molecular-dynamics simulation on stepped surfaces was concerned with ion-induced defect formation and interlayer mobility close to steps. Thus *Mazzone* [194] studied the effects of a primary knock-on atom (PKA) with energies below 10 eV in the vicinity of a step on a Si (100) surface, where the possiblilty of sputtering is also explored. In [195] this study is extended to low-energy ($5-30$ eV) irradiation by Ar and B atoms, where the effect of a step on the implantation and reflection probability is investigated. *Jacobsen* et al. [196] use molecular-dynamics simulation to study the energetic beam deposition of Ag $\to$ Ag (111), and Pt $\to$ Pt (111), for incoming energies up to 35 eV. They inquire in particular into the dependence of the impact-induced interlayer mobility as a function of the impact distance to a step on the surface.

Shapiro and *Tombrello* [197] study the impact of 5 keV Ar $\to$ Cu (111) surface in the vicinity of a step and compare to the values for a flat terrace. These authors restrict their bombarding angle to polar angles $\theta < 50°$ with respect to the surface normal. Around the surface normal, $\theta < 30°$, a slight reduction in the sputtering yield is found, while for $\theta > 30°$, the sputtering yield exceeds that of a flat terrace.

Friedrich and *Urbassek* [198] study more oblique and even glancing incidence angles for 5 keV Xe impact on a stepped Pt (111) surface. The sputtering yield shows a maximum around $\theta = 60°$ similar to ion impact on a flat (111) terrace; the influence of the existence of a step on the surface on the sputtering yield is in the 20 % range. For more glancing incidence, however, the presence of a step increases the sputtering yield dramatically. Thus, e.g., for 80° incidence angle, the sputtering yield from a flat terrace is 0 while it amounts to 20 if the ion impinges in the vicinity of a step. In the molecular-dynamics simulation, the influence of the exact ion impact point in the vicinity of the step could be explored. It was shown that the effect is maximum if the ion impinges on the lower terrace in front of the step with a direction towards the step, and the range of influence of the step on the yield could be determined and rationalized by a simple geometrical model. Figure 9a exemplifies the considerable sputtering induced by 5 keV Ar impact on a terraced Pt (111) surface at 83° incidence towards the surface normal. Note that for this impact angle, on a flat terrace the sputtering yield is almost zero. In a recent publication [199] such molecular-dynamics simulation data could be used to interprete experimental data on the fluence dependence of sputtering of Pt (111), where with increasing fluence the number of islands, and thus the effective step length, changes and influences the sputtering yield. Figure 9b exemplifies the change in surface topography induced by glancing-incidence keV-ion impact in the vicinity of a surface step.

Karolewski [200] studies 3 keV glancing Ar ion incidence on a stepped Cu (100) surface and shows that sputtered atoms originate preferentially from the vicinity of the steps.

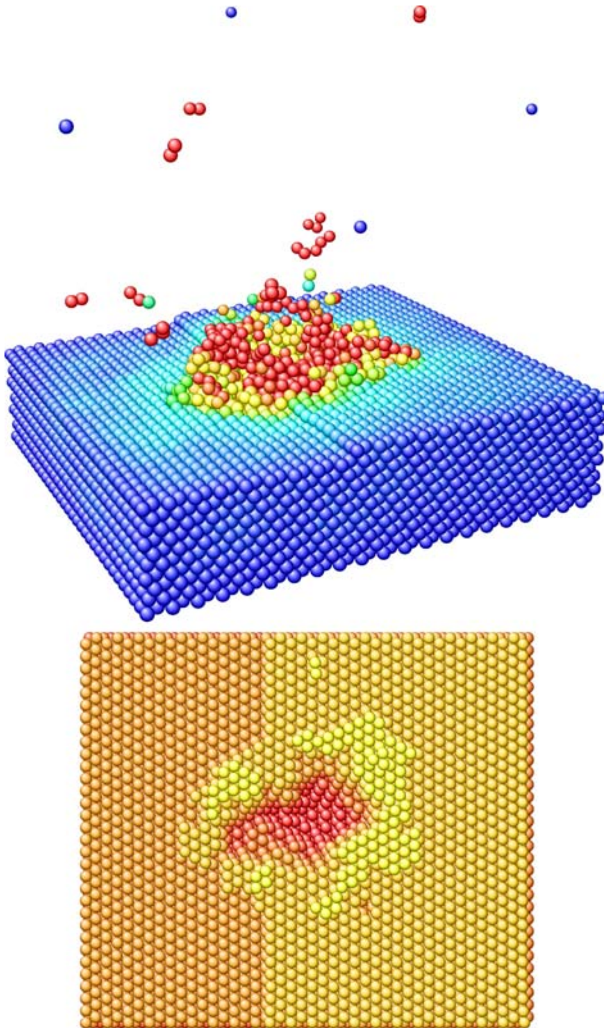

Fig. 9. Sputtering of a terraced Pt (111) surface induced by a 5 keV Ar ion. The ion impinges at an angle of $\theta_0 = 83^\circ$ towards the surface normal onto the lower terrace from the left in the direction of the ascending step. **a**) Perspective view at 2.5 ps after impact. *Color* denotes local 'temperature'; the *red zone* corresponds to the melting temperature. **b**) *Top view* of the damaged surface at 20 ps after impact. *Color* denotes height above the surface

9 Fluence Dependence of Sputtering

Solids change during the irradiation with energetic projectiles. This has several reasons:

1. Erosion (sputtering) changes the surface topography; thus surfaces may become atomically rough. They may also develop surface topography such as craters with adatom rims, or surface vacancy and adatom islands. After higher fluences, also mesoscopic structures may be formed such as ripples or nano-dots.
2. Furthermore, in the case of non-selfbombardment, the incorporation of the bombarding atoms into the surface will change the surface composition, and hence the sputtering behaviour.
3. In the case of a non-elemental target, further composition changes are brought about by preferential sputtering effects.

The molecular-dynamic simulation of fluence effects on sputtering is primarily hampered by the different time scales which enter this problem. While individual ion-induced processes, and hence sputtering, occur after 100 ps at most after ion impact, the advent of the next ion impinging on the same relevant surface area ($10-100\,\mathrm{nm}^2$, say) will occur after microseconds or seconds, depending on the ion current density. Finally, the entire sputter experiment may take minutes or hours until completion. Clearly such time scales are completely inaccessible to a molecular-dynamics treatment. Several hybrid approaches, combining molecular-dynamics techniques to describe the individual ion-induced phenomena with (kinetic) Monte Carlo simulations for assessing the phenomena occurring in between the individual ion impacts, have been devised, in particular in the areas of energetic beam deposition and thin-film growth processes [196, 201, 202].

However, several investigations on the fluence dependence of sputtering have also appeared which are purely based on molecular dynamics. This means that the activity of all processes occurring in between the individual ion impacts has been neglected. This approach thus describes the zero-temperature limit of dynamic sputtering: The substrate temperature must be so small that any atom migration is suppressed, at least at and in the vicinity of the surface.

Si (100) amorphisation under Ar bombardment was investigated by *Marqués* et al. [26, 203, 204] and by *Haddeman* and *Thijsse* [205]. *Zhong* et al. [206] investigated the ion-beam-induced smoothing of metal surfaces by 40 keV Xe ion impact. *Hanson* et al. [207] present a study of selfsputtering of nickel and aluminium (111) surfaces by low-energy projectiles. *Peltolta* et al. [208] study the fluence dependence of range profiles in Si. Most recently, *Karolewski* [209] investigates the sputtering of a Cu (100) crystallite surface by 2 keV copper ions up to a fluence of $1.25\times10^{14}\ \mathrm{cm}^{-2}$. He finds a broadening of the angular distribution and a rapid increase of the depth of origin of sputtered atoms. Both effects originate from the surface roughening induced

by sputtering on the copper surface. Other sputtered-particle properties such as the sputtering yield, and the sputtered-atom energy distribution, are quite insensitive to fluence.

10 Sputtering of Molecular and Organic Solids

The understanding of sputtering of molecular solids is of importance in a variety of applications ranging from SIMS of organic materials to desorption processes in matrix isolation spectroscopy. Also the sputtering of ice-covered surfaces, such as the moons in the outer solar system, comets or particles constituting the rings of the giant planets, provide motivation for studying ion-induced processes and sputtering in molecular solids. The simulation of these processes with molecular dynamics requires – besides the knowledge of the role that target electrons, which may become excited during ion bombardment, play for the ensuing processes – an understanding of the interatomic and intermolecular interaction potentials in these solids. Since in the last decade the description of these potentials has matured, more and more computer simulations of these systems have been performed.

10.1 Diatomic and Small Anorganic Molecular Solids

Diatomic molecular solids like O_2 and N_2 have been investigated in a variety of studies. Here simulations have been performed using site-site potentials in which each atom interacts with the other atoms in neighbouring molecules via a pair potential (typically the Lennard-Jones potential), while the intramolecular interaction is simulated by a Morse potential. This allows for vibrational and rotational excitation of the molecules and also dissociation. Recombination of dissociated atoms and further reactions have generally been excluded from consideration.

In an early study, *Kafemann* and *Urbassek* [210] investigated the sputtering of a condensed N_2 sample by 100 eV N atom impact. The temporal evolution of the heat spike in the sample, and of the sputtering, are investigated and data for the kinetic energy distribution of sputtered molecules as well as the partitioning of the sputtered energy into translational, rotational and vibrational energy are given in this case study.

The sputtering of other inorganic solids or ices has been studied only rarely using molecular dynamics. An exception is [211] where water ice has been modelled induced by O^+ ions at energies between 23 and 115 eV. Energy and angular distributions of ejected H_2O molecules are described and the emission of $(H_2O)_n$ clusters is reported.

Several simulations were performed that mainly aimed at understanding the electronic sputtering of molecular solids, induced by MeV light ions [106, 109, 212]. Vibrational and rotational excitation as well as dissociation were studied, and the dependence of the sputtering yield on the energy deposited

by the fast projectile in the ion track were investigated. In earlier studies, the vibrational to translational coupling of diatomic molecular model crystals was investigated [32, 213–216], where a reduced intramolecular well depth was employed to enhance the coupling.

10.2 Sputtering of Organic Solids

The sputtering of solids – or overlayer films – consisting of organic molecules, e.g., hydrocarbons, polymers, or more complex organic materials – has attracted considerable interest in the recent past, in particular due to applications in organic SIMS. Several reviews have been dedicated to the molecular-dynamic simulation of these events [217, 218].

Very early studies modelled organic molecules as single entities, in the sense of (soft) spheres and a simple intermolecular interaction potential [102]. While these early studies do not allow for molecule fragmentation and not even for internal excitation, the breathing sphere approach – which has been extensively used for studying laser ablation of organic films [219,220] – aims at including internal excitation via one internal degree of freedom, the breathing mode. Clearly, energetic atom irradiation may create more extensive internal excitation, and molecule fragmentation and dissociation, such that more refined interaction potentials need to be used to model the internal degrees of freedom. Ideally they also allow for the inclusion of reaction processes of the radicals created by ion bombardment. This has become possible through the invention of sophisticated classical interaction potentials of which we mention the hydrocarbon potential developed by *Brenner* [221,222] and the AIREBO potential by *Stuart* and *Harrison* [223]. This potential allows to improve the inter-molecular interaction while still maintaining the reactive nature of the potential. The latter potential has been used recently in [224,225] for studying the sputtering of benzene molecular crystals and multilayer films adsorbed on Ag (111) by 0.3 keV Xe and 4 keV Ar projectiles, respectively.

The following features in the sputtering of organic solids were demonstrated in the simulations:

- Formation of fragments.
- Reactions between fragments (radical-radical recombinations).
- Molecule emission by a collective mechanism called ‘molecule liftoff’ [217].
- Individual high-yield events have been reported and analyzed [226].
- Quantitative results on energy and angular distributions, e.g., for benzene molecules desorbed from the surface of a Ag (111) surface, have been reported [227].

10.3 Sputtering of Polymers

These simulations have also been extended to study the sputtering of polymers. The work of *Beardmore* and *Smith* on the ion bombardment of

polyethylene [228] gives an early example. More recently, *Delcorte* and co-workers [229] reported on simulations of the particle-induced fragmentation and sputtering of a 7.5 kDalton organic sample based on a polystyrene coil adsorbed on Ag (111). Using the AIREBO potential, the emission of recombined and rearranged fragments is reported, the existence of long-lived vibration excitations is demonstrated and delayed emission via vibration-induced bond scission is observed.

11 Chemical Effects

While chemical effects, i.e., reactions, may play some role in any bombardment of a non-elemental solid in which the two species present are not completely chemically inert, and in particular in the bombardment of molecular and organic samples, the term ‘chemical sputtering’ implies that the chemistry induced in the sample by the irradiation, and in particular by reactions between the projectile and target atoms, contributes by itself significantly to the sputter process. Chemical effects can only be modelled if potentials are available which include the chemistry at least in a qualitative way [230]. A prominent example of such a potential is the so-called Brenner potential [221, 222], an example of the class of bond-order potentials [231], which has been found to describe well the chemistry of hydrocarbons.

Nordlund et al. [232–234] describe the low-energy (< 100 eV) sputtering of an amorphous hydrogenated carbon (a-C:H) target by H atoms. By using the Brenner potential [221, 222], they allow for the inclusion of reactions in the simulation. Erosion yields far exceeding those expected for a physical sputtering process are observed in the simulation. This is attributed to a process termed ‘swift chemical sputtering’ by a C-C bond-breaking mechanism induced by the swift H ions.

The sputtering or reactive ion beam etching (RIBE) of Si by F and Cl has been investigated by *Garrison* and co-workers [235, 236] and by *Feil* [237]; these studies became possible after the availability of potentials for thermal surface reactions – such as the thermal etching of a Si surface by F atoms – was demonstrated [238]. The system studied was 200 eV Ar bombardment of Si in a Cl atmosphere. The simulations were used to interprete the synergetics of chemical sputtering, and the emission mechanisms of low-energy reaction products. In other work, the sputtering of a H-terminated Si-surface by low-energy ion irradiation was studied [239].

A possible pathway for Si etching was demonstrated to be the breaking of a Si-Si bond by an incoming F atom. *Barone* and *Graves* [240, 241] modelled Si sputtering by F or Cl atoms with energies between 10 and 50 eV, and also the sputtering of fluorinated Si samples by low-energy Ar atoms [242]. The potentials used are based on the Stillinger-Weber potential [243]. These authors also performed ‘high fluence’ simulations, in which the transformation of the original Si to a $SiCl_x$ layer was observed. Cl incorporation, Si etching

and the resulting surface roughness are reported. These simulations were extended by *Abrams* and *Graves* [244] to Si etching by energetic (100 eV) CF_3^+ bombardment.

Chiba et al. [245] study low-energy (< 30 eV) F etching of Si and emphasize the effect of the substrate temperature and the ion incidence angle. *Aoki* et al. [246] extend these studies to etching of Si by F cluster impact with clusters containing up to 6000 atoms.

12 Conclusions

The strength of the molecular-dynamics method is based on the simple physical picture behind it – the solution of Newton's equations of motion – and the small number of physical input required: The interatomic interaction potential, and (when appropriate) the coupling of the atoms to the electrons. In this sense, it is simple to judge whether a given application has been modelled adequately by a simulation.

In the actual implementation, besides these questions a number of more technical (or numerical) issues need be solved: System size and the connected question of the boundary conditions of the simulation cell, the duration of the simulation, and the question of sufficient statistics – usually the answer to a physical question is the average over many simulations in which the initial conditions are slightly varied.

Often molecular-dynamics simulations are undertaken in order to obtain insight on mechanisms at work in sputtering, to obtain a qualitative picture of the event, and to study exemplary cases. Here, the benefit of this atomistic simulation method to lend itself easily to visualization is often exploited. Nowadays the production of animated video sequences has become routine and helps to convey insight into the dynamics of the sputter processes investigated. However, in several of the research results presented in this chapter, it became also apparent that molecular-dynamics simulation is in selected research issues equally well suited to provide systematic information and quantitative results. Such studies include those on preferential sputtering of isotope systems, sputtering by cluster impact, or the influence of surface topography on the sputtering yield.

The research fields in which molecular dynamics is best applied are those, where simpler or faster methods, such as analytical theory, Monte-Carlo and BCA simulation, fail or where their assumptions need to be controlled. These include issues,

1. where many-body interactions are essential, such as sputtering from high-energy-density zones (spikes) or sputtering by cluster impact;
2. which are controlled by collective motion, such as cluster emission, the formation of surface topography and, in particular, craters;

3. where the bonding situation is complex, such as in molecular and organic targets, in compounds, in chemical sputtering and also for rough surfaces.

However, this method will also be used at advantage in those areas where the assumptions entering other simulation procedures or analytical theory need to be controlled by a more realistic simulation. This includes the areas of isotope sputtering, the effect of surface topography on sputtering, and the fluence dependence of sputtering.

Acknowledgements

Thanks are due to C. Anders, C. Engin, Y. Rosandi, and St. Zimmermann for help with the preparation of the figures.

References

[1] R. Behrisch (Ed.): *Sputtering by Particle Bombardment I*, Top. Appl. Phys. **47** (Springer, Berlin, Heidelberg 1981) russ. translation: (MIR, Moscow 1984) 189
[2] R. Behrisch (Ed.): *Sputtering by Particle Bombardment II*, Top. Appl. Phys. **52** (Springer, Berlin, Heidelberg 1983) russ. translation: (MIR, Moscow 1986) 189
[3] R. Behrisch, K. Wittmaack (Eds.): *Sputtering by Particle Bombardment III*, Top. Appl. Phys. **64** (Springer, Berlin, Heidelberg 1991) russ. translation: (MIR, Moscow 1998) 189
[4] P. Sigmund (Ed.): *Fundamental Processes in Sputtering of Atoms and Molecules (SPUT92)*, K. Dan. Vidensk. Selsk. Mat. Fys. Medd. **43** (1993) 189
[5] P. Sigmund: Phys. Rev. **184**, 383 (1969) 189
[6] J. P. Biersack, W. Eckstein: Appl. Phys. A **34**, 73 (1984) 189
[7] M. T. Robinson, I. M. Torrens: Phys. Rev. **9**, 5008 (1974) 189
[8] W. Eckstein: *Computer Simulation of Ion-Solid Interactions*, Springer Ser. Mater. Sci. **10** (Springer, Berlin, Heidelberg 1991) russ. translation: (MIR, Moscow 1995) 189, 190
[9] J. B. Gibson, A. N. Goland, M. Milgram, G. H. Vineyard: Phys. Rev. **120**, 1229 (1960) 189
[10] B. J. Alder, T. E. Wainwright: J. Chem. Phys. **27**, 1208 (1957) 189
[11] H. H. Andersen: Nucl. Instrum. Methods B **18**, 321 (1987) 190
[12] D. E. Harrison, Jr.: Crit. Rev. Solid State Mater. Sci. **14**, S1 (1988) 190, 209
[13] M. T. Robinson: K. Dan. Vidensk. Selsk. Mat. Fys. Medd. **43**, 27 (1993) 190
[14] R. M. Nieminen: K. Dan. Vidensk. Selsk. Mat. Fys. Medd. **43**, 81 (1993) 190, 200
[15] H. M. Urbassek: Nucl. Instrum. Methods B **122**, 427 (1997) 190
[16] R. Smith (Ed.): *Atomic and ion collisions in solids and at surfaces* (Cambridge Univ. Press, Cambridge 1997) 190
[17] N. Winograd: Mat. Fys. Medd. Dan. Vid. Selsk. **43**, 223 (1993) 191

[18] T. J. Raeker, A. E. DePristo: Int. Rev. Phys. Chem. **10**, 1 (1991) 191, 206
[19] M. S. Stave, D. E. Sanders, T. J. Raeker, A. E. DePristo: J. Chem. Phys. **93**, 4413 (1990) 191, 206
[20] R. Maboudian, Z. Postawa, M. El-Maazawi, B. J. Garrison, N. Winograd: Phys. Rev. B **42**, 7311 (1990) 191
[21] S. W. Rosencrance, J. S. Burnham, D. E. Sanders, C. He, B. J. Garrison, N. Winograd, Z. Postawa, A. E. DePristo: Phys. Rev. B **52**, 6006 (1995) 191
[22] K. Johannessen: Nucl. Instrum. Methods B **71**, 171 (1992) 191
[23] G. Betz, R. Kirchner, W. Husinsky, F. Rüdenauer, H. M. Urbassek: Radiat. Eff. Defects Solids **130–131**, 251 (1994) 192, 204, 205
[24] S. W. Rosencrance, N. Winograd, B. J. Garrison, Z. Postawa: Phys. Rev. B **53**, 2378 (1996) 192
[25] H. Gades, H. M. Urbassek: Appl. Phys. A **61**, 39 (1995) 192, 193
[26] J. E. Rubio, L. A. Marqués, M. Jaraíz, L. A. Bailón, J. Barbolla: Nucl. Instrum. Methods B **102**, 301 (1995) 192, 215
[27] R. Smith, D. E. Harrison, Jr., B. J. Garrison: Phys. Rev. B **40**, 93 (1989) 192
[28] R. A. Stansfield, K. Broomfield, D. C. Clary: Phys. Rev. B **39**, 7680 (1989) 192
[29] V. I. Shulga, W. Eckstein: Nucl. Instrum. Methods B **145**, 492 (1998) 192
[30] T. J. Colla, H. M. Urbassek: Nucl. Instrum. Methods B **152**, 459 (1999) 192, 205
[31] R. E. Johnson, J. Schou: K. Dan. Vidensk. Selsk. Mat. Fys. Medd. **43**, 403 (1993) 192
[32] R. E. Johnson, M. Liu: J. Chem. Phys. **104**, 6041 (1996) 192, 217
[33] P. Klein, H. M. Urbassek, M. Vicanek: Phys. Rev. B **51**, 4597 (1995) 192
[34] J. D. Kress, D. E. Hanson, A. F. Voter, C. L. Liu, X. Y. Liu, D. G. Coronell: J. Vac. Sci. Technol. A **17**, 2819 (1999) 193
[35] H. Coufal, H. F. Winters, H. L. Bay, W. Eckstein: Phys. Rev. B **B44**, 4747 (1991) 193
[36] H. L. Bay, H. F. Winters, H. J. Coufal, W. Eckstein: Appl. Phys. A **55**, 274 (1992) 193
[37] C. F. Abrams, D. B. Graves: J. Appl. Phys. **86**, 2263 (1999) 193
[38] C. F. Abrams, D. B. Graves: IEEE Trans. Plasma Sci. **27**, 1426 (1999) 193
[39] C. Steinbrüchel: Appl. Phys. Lett. **55**, 1960 (1989) 193
[40] C. F. Abrams, D. B. Graves: J. Vac. Sci. Technol. A **16**, 3006 (1998) 193
[41] A. Kubota, D. J. Economou: IEEE Trans. Plasma Sci. **27**, 1416 (1999) 193
[42] M. H. Shapiro, E. Trovato, T. A. Tombrello: Nucl. Instrum. Methods B **180**, 58 (2001) 193
[43] Z. B. Güvenc, Y. Hundur, R. Hippler: Nucl. Instrum. Methods B **164-165**, 854 (2000) 193
[44] R. V. Stuart, G. K. Wehner: J. Appl. Phys. **33**, 2345 (1962) 193
[45] P. Sigmund, N. Q. Lam: K. Dan. Vidensk. Selsk. Mat. Fys. Medd. **43**, 255 (1993) 193
[46] P. Sigmund: in R. Behrisch (Ed.): *Sputtering by Particle Bombardment I*, Top. Appl. Phys. **47** (Springer, Berlin, Heidelberg 1981) p. 9 194, 198
[47] H. Gnaser: *Low-Energy Ion Irradiation of Solid Surfaces*, Tr. Mod. Phys. **146** (Springer, Berlin, Heidelberg 1999) 194, 205
[48] H. Gades, H. M. Urbassek: Nucl. Instrum. Methods B **102**, 261 (1995) 194, 195

[49] M. H. Shapiro, P. K. Haff, T. A. Tombrello, D. E. Harrison, Jr.: Nucl. Instrum. Methods B **12**, 137 (1985) 194
[50] M. H. Shapiro, T. A. Tombrello, D. E. Harrison, Jr.: Nucl. Instrum. Methods B **30**, 152 (1988) 194
[51] D. Y. Lo, T. A. Tombrello, M. H. Shapiro: Nucl. Instrum. Methods B **40/41**, 270 (1989) 194
[52] N. Q. Lam, K. Johannessen: Nucl. Instrum. Methods B **71**, 371 (1992) 195
[53] V. I. Shulga, P. Sigmund: Nucl. Instrum. Methods B **103**, 383 (1995) 195
[54] V. I. Shulga, P. Sigmund: Nucl. Instrum. Methods B **119**, 359 (1996) 195
[55] R. Behrisch: in R. Behrisch (Ed.): *Sputtering by Particle Bombardment II*, Top. Appl. Phys. **52** (Springer, Berlin, Heidelberg 1983) p. 1 196
[56] M. Szymonski: K. Dan. Vidensk. Selsk. Mat. Fys. Medd. Dan. **43**, 495 (1993) 196
[57] E. M. Bringa, R. E. Johnson: Phys. Rev. Lett. **88**, 165501 (2002) 196, 201
[58] Y. S. Dou, L. V. Zhigilei, N. Winograd, B. J. Garrison: J. Phys. Chem. A **105**, 2748 (2001) 196
[59] K. Nordlund: Nucl. Instrum. Methods B **218**, 9 (2004) 196
[60] C. Liu, et al.: Nucl. Instrum. Methods B **178**, 200 (2001) 196
[61] W. Jiang, W. J. Weber, S. Thevuthasan: J. Appl. Phys. **87**, 7671 (2000) 196
[62] D. Ramasavmy, S. D. Kenny, R. Smith: Nucl. Instrum. Methods B **202**, 175 (2003) 196
[63] D. A. Young: Europhys. Lett. **59**, 540 (2002) 196
[64] D. A. Young: Nucl. Instrum. Methods B **225**, 231 (2004) 196
[65] M. H. Shapiro, T. A. Tombrello: Nucl. Instrum. Methods B **90**, 473 (1994) 197
[66] M. H. Shapiro, T. A. Tombrello: Nucl. Instrum. Methods B **94**, 186 (1994) 197
[67] M. H. Shapiro, T. A. Tombrello: Nucl. Instrum. Methods B **102**, 277 (1995) 197
[68] M. H. Shapiro, T. A. Tombrello: Nucl. Instrum. Methods B **66**, 317 (1992) 197
[69] J. Lindhard, M. Scharff: Phys. Rev. **124**, 128 (1961) 197
[70] O. B. Firsov: Sov. Phys. JETP **36**, 1076 (1959) 197
[71] I. S. Tilinin: Phys. Rev. A **51**, 3058 (1995) 197
[72] P. M. Echenique, R. M. Nieminen, J. C. Ashley, R. H. Ritchie: Phys. Rev. A **33**, 897 (1986) 197
[73] A. Caro: Radiat. Eff. Defects Solids **130-131**, 187 (1994) 197, 200
[74] S. Prönnecke, A. Caro, M. Victoria, T. Diaz de la Rubia, M. W. Guinan: J. Mater. Res. **6**, 483 (1991) 197
[75] V. G. Kapinos, D. J. Bacon: Phys. Rev. B **50**, 13194 (1994) 197
[76] K. Nordlund, L. Wei, Y. Zhong, R. S. Averback: Phys. Rev. B **57**, R13965 (1998) 197
[77] I. Koponen: J. Appl. Phys. **72**, 1194 (1992) 197, 200
[78] I. Koponen: Phys. Rev. B **47**, 14011 (1993) 197
[79] S. Meyer, D. Diesing, A. Wucher: Phys. Rev. Lett. **93**, 137601 (2004) 197
[80] M. H. Shapiro, J. Fine: Nucl. Instrum. Methods B **44**, 43 (1989) 197
[81] D. N. Bernardo, B. J. Garrison: J. Chem. Phys. **97**, 6910 (1992) 197
[82] M. H. Shapiro, T. A. Tombrello, J. Fine: Nucl. Instrum. Methods B **74**, 385 (1993) 197

[83] I. Wojciechowski, B. J. Garrison: Surf. Sci. **527**, 209 (2003) 197
[84] Z. Sroubek, F. Sroubek, A. Wucher, J. A. Yarmoff: Phys. Rev. B **68**, 115426 (2003) 197
[85] C. P. Flynn, R. S. Averback: Phys. Rev. B **38**, 7118 (1988) 197, 198, 200
[86] M. W. Finnis, P. Agnew, A. J. E. Foreman: Phys. Rev. B **44**, 567 (1991) 197, 200
[87] I. Koponen, M. Hautala: Nucl. Instrum. Methods B **93**, 374 (1994) 197, 200
[88] A. Caro, M. Victoria: Phys. Rev. A **40**, 2287 (1989) 197, 200
[89] D. E. Harrison, Jr., M. M. Jakas: Nucl. Instrum. Methods B **15**, 25 (1986) 198
[90] Z. Sroubek: Nucl. Instrum. Methods B **78**, 140 (1993) 198
[91] A. Wucher, Z. Sroubek: Phys. Rev. B **55**, 780 (1997) 198
[92] A. Duvenbeck, Z. Sroubek, F. Sroubek, A. Wucher: Nucl. Instrum. Methods B **225**, 464 (2004) 198
[93] H. L. Bay, H. H. Andersen, W. O. Hofer, O. Nielsen: Nucl. Instr. Methods **132**, 301 (1976) 198
[94] H. H. Andersen: K. Dan. Vidensk. Selsk. Mat. Fys. Medd. **43**, 127 (1993) 198, 202
[95] M. Ghaly, R. S. Averback: Phys. Rev. Lett. **72**, 364 (1994) 198
[96] H. M. Urbassek, K. T. Waldeer: Phys. Rev. Lett. **67**, 105 (1991) 198
[97] K. T. Waldeer, H. M. Urbassek: Nucl. Instrum. Methods B **73**, 14 (1993) 198
[98] L. Dutkiewicz, R. Pedrys, J. Schou, K. Kremer: Phys. Rev. Lett. **75**, 1407 (1995) 199
[99] J. Schou: Nucl. Instrum. Methods B **27**, 188 (1987) 199
[100] H. M. Urbassek, J. Michl: Nucl. Instrum. Methods B **22**, 480 (1987) 199
[101] D. E. David, J. Michl: Prog. Solid St. Chem. **19**, 283 (1989) 199
[102] D. Fenyö, B. U. R. Sundqvist, B. R. Karlsson, R. E. Johnson: Phys. Rev. B **42**, 1895 (1990) 201, 217
[103] D. Fenyö, R. E. Johnson: Phys. Rev. B **46**, 5090 (1992) 201
[104] H. M. Urbassek, H. Kafemann, R. E. Johnson: Phys. Rev. B **49**, 786 (1994) 201
[105] E. M. Bringa, R. E. Johnson: Nucl. Instrum. Methods B **143**, 513 (1998) 201
[106] E. M. Bringa, R. E. Johnson, L. Dutkiewicz: Nucl. Instrum. Methods B **152**, 267 (1999) 201, 216
[107] E. M. Bringa, R. E. Johnson, M. Jakas: Phys. Rev. B **60**, 15107 (1999) 201
[108] E. M. Bringa, M. Jakas, R. E. Johnson: Nucl. Instrum. Methods B **164-165**, 762 (2000) 201
[109] E. M. Bringa, R. E. Johnson: Surf. Sci. **451**, 108 (2000) 201, 216
[110] M. M. Jakas, E. M. Bringa: Phys. Rev. B **62**, 824 (2000) 201
[111] M. M. Jakas: Radiat. Eff. Defects Solids **152**, 157 (2000) 201
[112] M. M. Jakas, E. M. Bringa, R. E. Johnson: Phys. Rev. B **65**, 165425 (2002) 201
[113] M. M. Jakas: Nucl. Instrum. Methods B **193**, 727 (2002) 201
[114] M. Beuve, N. Stolterfoht, M. Toulemonde, C. Trautmann, H. M. Urbassek: Phys. Rev. B **68**, 125423 (2003) 201
[115] V. I. Shulga, M. Vicanek, P. Sigmund: Phys. Rev. A **39**, 3360 (1989) 201
[116] V. I. Shulga, P. Sigmund: Nucl. Instrum. Methods B **62**, 23 (1991) 201, 202
[117] R. S. Averback, T. Diaz de la Rubia, H. Hsieh, R. Benedek: Nucl. Instrum. Methods B **59/60**, 709 (1991) 201

[118] H. Hsieh, R. S. Averback, H. Sellers, C. P. Flynn: Phys. Rev. B **45**, 4417 (1992) 201
[119] Z. Pan: Nucl. Instrum. Methods B **66**, 325 (1992) 201
[120] R. S. Averback, M. Ghaly: Nucl. Instrum. Methods B **90**, 191 (1994) 201
[121] R. S. Averback, M. Ghaly, H. Zhu: Radiat. Eff. Defects Solids **130-131**, 211 (1994) 201
[122] Z. Y. Pan, M. Hou: Nucl. Instrum. Methods B **102**, 317 (1995) 201
[123] H. Haberland, Z. Insepov, M. Moseler: Phys. Rev. B **51**, 11061 (1995) 201
[124] H. Hsieh, R. S. Averback: Phys. Rev. B **42**, 5365 (1990) 201
[125] H. Hsieh, R. S. Averback: Nucl. Instrum. Methods B **59/60**, 203 (1991) 201
[126] H. Haberland, Z. Insepov, M. Moseler: Z. Phys. D **26**, 229 (1993) 201
[127] T. Aoki, J. Matsuo, Z. Insepov, I. Yamada: Nucl. Instrum. Methods B **121**, 49 (1997) 201, 202
[128] Z. Insepov, I. Yamada: Nucl. Instrum. Methods B **121**, 44 (1997) 201, 202
[129] M. Henkel, H. M. Urbassek: Nucl. Instrum. Methods B **145**, 503 (1998) 201
[130] C. F. Sanz-Navarro, R. Smith, D. J. Kenny, S. Pratontep, R. E. Palmer: Phys. Rev. B **65**, 165420 (2002) 201
[131] Z. Insepov, I. Yamada, M. Sosnowski: Mater. Chem. Phys. **54**, 234 (1998) 201, 202, 204
[132] M. Moseler, O. Rattunde, J. Nordiek, H. Haberland: Nucl. Instrum. Methods B **164-165**, 522 (2000) 201, 204, 212
[133] T. Muramoto, N. Hirotami, K. Itabasi, A. Harada, Y. Yamamura: Nucl. Instrum. Methods B **202**, 289 (2003) 201, 204
[134] K. Johannessen: Nucl. Instrum. Methods B **73**, 481 (1993) 202
[135] M. Lindenblatt, R. Heinrich, A. Wucher, B. J. Garrison: J. Chem. Phys. **115**, 8643 (2001) 202
[136] M. Medvedeva, I. Wojciechowski, B. J. Garrison: Surf. Sci. **505**, 349 (2002) 202
[137] M. H. Shapiro, T. A. Tombrello: Nucl. Instrum. Methods B **152**, 221 (1999) 202
[138] M. H. Shapiro, T. A. Tombrello: Surf. Sci. **453**, 143 (2000) 202
[139] M. H. Shapiro, T. A. Tombrello: Nucl. Instrum. Methods B **217**, 253 (2004) 202
[140] Z. Insepov, I. Yamada: Nucl. Instrum. Methods B **99**, 248 (1995) 202
[141] I. Yamada, J. Matsuo, Z. Insepov, D. Takeuchi, M. Akizuki, N. Toyoda: J. Vac. Sci. Technol. A **14**, 781 (1996) 202
[142] Z. Insepov, I. Yamada: Nucl. Instrum. Methods B **153**, 199 (1999) 202
[143] I. Yamada, J. Matsuo, Z. Insepov, T. Aoki, T. Seki, N. Toyoda: Nucl. Instrum. Methods B **164-165**, 944 (2000) 202
[144] G. Betz, W. Husinsky: Nucl. Instrum. Methods B **122**, 311 (1997) 202
[145] T. J. Colla, R. Aderjan, R. Kissel, H. M. Urbassek: Phys. Rev. B **62**, 8487 (2000) 203, 206, 208
[146] T. J. Colla, H. M. Urbassek: Nucl. Instrum. Methods B **164-165**, 687 (2000) 203, 206, 210
[147] E. Salonen, K. Nordlund, J. Keinonen: Nucl. Instrum. Methods B **212**, 286 (2003) 203
[148] Y. Yamaguchi, J. Gspann: Phys. Rev. B **66**, 155408 (2002) 203
[149] R. Smith, K. Beardmore, A. Gras-Marti, R. Kirchner, R. P. Webb: Nucl. Instrum. Methods B **102**, 211 (1995) 203

[150] Z. Postawa, B. Czerwinski, M. Szewczyk, E. J. Smiley, N. Winograd, B. J. Garrison: Anal. Chem. **75**, 4402 (2003) 203
[151] E. E. Z. Zhurkin, S. K. Kolesnikov: Nucl. Instrum. Methods B **193**, 822 (2002) 203
[152] H. M. Urbassek, W. O. Hofer: K. Dan. Vidensk. Selsk. Mat. Fys. Medd. **43**, 97 (1993) 204, 207
[153] F. Karetta, H. M. Urbassek: Appl. Phys. A **55**, 364 (1992) 204, 205
[154] M. H. Shapiro, T. A. Tombrello: Nucl. Instrum. Methods B **84**, 453 (1994) 204
[155] H. Gades, H. M. Urbassek: Nucl. Instrum. Methods B **103**, 131 (1995) 204, 205
[156] G. P. Können, A. Tip, A. E. de Vries: Radiat. Eff. **21**, 269 (1974) 204, 206
[157] G. P. Können, A. Tip, A. E. de Vries: Radiat. Eff. **26**, 23 (1975) 204, 206
[158] I. S. Bitensky, E. S. Parilis, I. A. Wojciechowski: Nucl. Instrum. Methods B **67**, 595 (1992) 204
[159] G. Betz, W. Husinsky: Nucl. Instrum. Methods B **102**, 281 (1995) 205
[160] C. Staudt, R. Heinrich, A. Wucher: Nucl. Instrum. Methods B **164-165**, 677 (2000) 205, 206
[161] C. Staudt, A. Wucher: Phys. Rev. B **66**, 075419 (2002) 205, 206
[162] L. E. Rehn, R. C. Birtcher, S. E. Donnelly, P. M. Baldo, L. Funk: Phys. Rev. Lett. **87**, 207601 (2001) 206
[163] I. S. Bitensky, E. S. Parilis: Nucl. Instrum. Methods B **21**, 26 (1987) 206
[164] H. M. Urbassek: Nucl. Instrum. Methods B **31**, 541 (1988) 206
[165] A. Wucher, B. J. Garrison: J. Chem. Phys. **105**, 5999 (1996) 206
[166] J. W. Hartman, M. H. Shapiro, T. A. Tombrello: Nucl. Instrum. Methods B **124**, 31 (1997) 206
[167] J. W. Hartman, M. H. Shapiro, T. A. Tombrello: Nucl. Instrum. Methods B **132**, 406 (1997) 206
[168] T. J. Colla, H. M. Urbassek, A. Wucher, C. Staudt, R. Heinrich, B. J. Garrison, C. Dandachi, G. Betz: Nucl. Instrum. Methods B **143**, 284 (1998) 206, 207
[169] T. Muramoto, M. Okai, Y. Yamashita, K. Yorizane, Y. Yamamura: Nucl. Instrum. Methods B **180**, 222 (2001) 206
[170] A. Wucher, N. K. Dzhemilev, I. V. Veryovkin, S. V. Verkhoturov: Nucl. Instrum. Methods B **149**, 285 (1999) 207
[171] R. S. Taylor, B. J. Garrison: Chem. Phys. Lett. **230**, 495 (1994) 208
[172] R. S. Taylor, C. L. Brummel, N. Winograd, B. J. Garrison, J. C. Vickerman: Chem. Phys. Lett. **233**, 575 (1995) 208
[173] R. P. Webb, D. E. Harrison, Jr.: Radiat. Eff. Lett. **86**, 15 (1983) 209
[174] D. E. Harrison, Jr., R. P. Webb: Nucl. Instr. Methods **218**, 727 (1983) 209
[175] M. Ghaly, K. Nordlund, R. S. Averback: Philos. Mag. A **79**, 795 (1999) 209
[176] H. Gades, H. M. Urbassek: Phys. Rev. B **50**, 11167 (1994) 209, 210
[177] C. Busse, C. Engin, H. Hansen, U. Linke, T. Michely, H. M. Urbassek: Surf. Sci. **488**, 346 (2001) 209
[178] E. M. Bringa, K. Nordlund, J. Keinonen: Phys. Rev. B **64**, 235426 (2001) 210, 211
[179] R. Aderjan, H. M. Urbassek: Nucl. Instrum. Methods B **164-165**, 697 (2000) 210, 211
[180] K. Nordlund: Phys. World **14**, 22 (2001) 210

[181] J. Gspann: in P. Jena, et al. (Eds.): *Physics and Chemistry of Finite Systems*, vol. II (Kluwer, Dordrecht 1992) p. 1115 210
[182] K. Nordlund, K. O. E. Henriksson, J. Keinonen: Appl. Phys. Lett. **79**, 3624 (2001) 211
[183] K. Nordlund, J. Tarus, J. Keinonen, S. E. Donnelly, R. C. Birtcher: Nucl. Instrum. Methods B **206**, 189 (2003) 211
[184] R. C. Birtcher, S. E. Donnelly: Phys. Rev. Lett. **77**, 4374 (1996) 211
[185] S. E. Donnelly, R. C. Birtcher: Phys. Rev. B **56**, 13599 (1997) 211
[186] E. M. Bringa, R. E. Johnson, R. Papaleo: Phys. Rev. B **65**, 094113 (2002) 211
[187] E. M. Bringa, E. Hall, R. E. Johnson, R. Papaleo: Nucl. Instrum. Methods B **193**, 734 (2002) 211
[188] P. Sigmund: J. Mater. Sci. **8**, 1545 (1973) 212
[189] U. Littmark, W. O. Hofer: J. Mater. Sci. **13**, 2577 (1978) 212
[190] T. J. Colla, H. M. Urbassek: Nucl. Instrum. Methods B **117**, 361 (1996) 212
[191] G. Betz, M. J. Pellin, J. W. Burnett, D. M. Gruen: Nucl. Instrum. Methods B **58**, 429 (1991) 212
[192] V. A. Zinovyev, L. N. Aleksandrov, A. V. Dvurechenskii, K.-H. Heinig, D. Stock: Thin Solid Films **241**, 167 (1994) 212
[193] P. Bedrossian, T. Klitsner: Phys. Rev. B **44**, 13783 (1991) 212
[194] A. M. Mazzone: Nucl. Instrum. Methods B **160**, 38 (2000) 213
[195] A. M. Mazzone: Nucl. Instrum. Methods B **183**, 251 (2001) 213
[196] J. Jacobsen, B. H. Cooper, J. P. Sethna: Phys. Rev. B **58**, 15847 (1998) 213, 215
[197] M. H. Shapiro, T. A. Tombrello: Nucl. Instrum. Methods B **194**, 425 (2002) 213
[198] A. Friedrich, H. M. Urbassek: Surf. Sci. **547**, 315 (2003) 213
[199] H. Hansen, C. Polop, T. Michely, A. Friedrich, H. M. Urbassek: Phys. Rev. Lett. **92**, 246106 (2004) 213
[200] M. A. Karolewski: Nucl. Instrum. Methods B **211**, 190 (2003) 213
[201] J. M. Pomeroy, A. Couture, J. Jacobsen, B. H. Cooper, J. P. Sethna, J. D. Brock: Mater. Res. Soc. Symp. Proc. **672**, O2.9.1 (2001) 215
[202] J. M. Pomeroy, A. Couture, J. Jacobsen, C. C. Hill, J. P. Sethna, B. H. Cooper, J. D. Brock: Mater. Res. Soc. Symp. Proc. **648**, P7.3.1 (2001) 215
[203] J. E. Rubio, L. A. Marqués, L. Pelaz, M. Jaraíz, J. Barbolla: Nucl. Instrum. Methods B **112**, 156 (1996) 215
[204] L. A. Marqués, J. E. Rubio, M. Jaraíz, L. A. Bailón, J. Barbolla: J. Appl. Phys. **81**, 1488 (1997) 215
[205] E. F. C. Haddeman, B. Thijsse: Nucl. Instrum. Methods B **202**, 161 (2003) 215
[206] Y. Zhong, Y. Ashkenazy, K. Albe, R. S. Averback: J. Appl. Phys. **94**, 4432 (2003) 215
[207] D. E. Hanson, B. C. Stephens, C. Saravanan, J. D. Kress: J. Vac. Sci. Technol. A **19**, 820 (2001) 215
[208] J. Peltola, K. Nordlund, J. Keinonen: Nucl. Instrum. Methods B **206**, 61 (2003) 215
[209] M. A. Karolewski: Nucl. Instrum. Methods B **225**, 217 (2004) 215
[210] H. Kafemann, H. M. Urbassek: Mod. Phys. Lett. B **7**, 857 (1993) 216

[211] D. W. Brenner, B. J. Garrison: Phys. Rev. B **34**, 5782 (1986) 216
[212] L. Dutkiewicz, R. E. Johnson, A. Vertes, R. Pedrys: J. Phys. Chem. **A 103**, 2925 (1999) 216
[213] S. T. Cui, R. E. Johnson: Int. J. Quantum Chem. **23**, 575 (1989) 217
[214] S. Banerjee, R. E. Johnson: Int. J. Quantum Chem. **41**, 383 (1992) erratum 217
[215] S. Banerjee, R. E. Johnson, S. Cui, P. T. Cummings: Phys. Rev. B **43**, 707 (1991) 217
[216] S. Banerjee, M. Liu, R. E. Johnson: Surf. Sci. Lett. **255**, L504 (1991) 217
[217] B. J. Garrison, A. Delcorte, K. D. Krantzman: Acc. Chem. Res. **33**, 69 (2000) 217
[218] B. J. Garrison: in J. C. Vickerman, D. Briggs (Eds.): *ToF-SIMS: Surface Analysis by Mass Spectrometry* (IM Publications, Chichester 2001) p. 223 217
[219] L. V. Zhigilei, P. B. S. Kodali, B. J. Garrison: J. Phys. Chem. **101**, 2028 (1997) 217
[220] L. V. Zhigilei, B. J. Garrison: J. Appl. Phys. **88**, 1281 (2000) 217
[221] D. W. Brenner: Phys. Rev. B **42**, 9458 (1990) 217, 218
[222] D. W. Brenner: Phys. Rev. B **46**, 1948 (1992) erratum 217, 218
[223] S. J. Stuart, A. B. Tutein, J. A. Harrison: J. Chem. Phys. **112**, 6472 (2000) 217
[224] K. D. Krantzman, Z. Postawa, B. J. Garrison, N. Winograd, S. J. Stuart, J. A. Harrison: Nucl. Instrum. Methods B **180**, 159 (2001) 217
[225] Z. Postawa, K. Ludwig, J. Piaskowy, K. Krantzman, N. Winograd, B. J. Garrison: Nucl. Instrum. Methods B **202**, 168 (2003) 217
[226] A. Delcorte, B. J. Garrison: J. Phys. Chem. B **104**, 6785 (2000) 217
[227] R. Chatterjee, Z. Postawa, N. Winograd, B. J. Garrison: J. Phys. Chem. B **103**, 151 (1999) 217
[228] K. Beardmore, R. Smith: Nucl. Instrum. Methods B **102**, 223 (1995) 218
[229] A. Delcorte, P. Bertrand, B. J. Garrison: J. Phys. Chem. B **105**, 9474 (2001) 218
[230] B. J. Garrison, D. Srivastava: Ann. Rev. Phys. Chem. **46**, 373 (1995) 218
[231] D. W. Brenner: MRS Bull. **21**, 36 (1996) 218
[232] E. Salonen, K. Nordlund, J. Keinonen, C. H. Wu: Europhys. Lett. **52**, 504 (2000) 218
[233] K. Nordlund, E. Salonen, J. Keinonen, C. H. Wu: Nucl. Instrum. Methods B **180**, 77 (2001) 218
[234] E. Salonen, K. Nordlund, J. Keinonen, C. H. Wu: Phys. Rev. B **63**, 195415 (2001) 218
[235] T. A. Schoolcraft, B. J. Garrison: J. Am. Chem. Soc. **113**, 8221 (1991) 218
[236] H. Feil, J. Dieleman, B. J. Garrison: J. Appl. Phys. **74**, 1303 (1993) 218
[237] H. Feil: Phys. Rev. Lett. **74**, 1879 (1995) 218
[238] P. C. Weakliem, C. J. Wu, W. A. Carter: Phys. Rev. Lett. **69**, 200 (1992) 218
[239] M. V. R. Murty, H. A. Atwater: Phys. Rev. B **51**, 4889 (1995) 218
[240] M. E. Barone, D. B. Graves: J. Appl. Phys. **78**, 6604 (1995) 218
[241] M. E. Barone, D. B. Graves: Plasma Sources Sci. Technol. **5**, 187 (1996) 218
[242] M. E. Barone, D. B. Graves: J. Appl. Phys. **77**, 1263 (1995) 218
[243] F. H. Stillinger, T. A. Weber: Phys. Rev. B **31**, 5262 (1985) 218
[244] C. F. Abrams, D. B. Graves: J. Appl. Phys. **86**, 5938 (1999) 219

[245] S. Chiba, T. Aoki, J. Matsuo: Nucl. Instrum. Methods B **180**, 317 (2001) 219
[246] T. Aoki, J. Matsuo, I. Yamada: Nucl. Instrum. Methods B **180**, 164 (2001) 219

Index

adatom, 208–212
  island, 208, 212, 213
  production, 210
amorphization, 198, 215
  dose, 196
annealing, 196

BCA program
  Monte Carlo (MC), 189, 190, 215, 219
binary collision approximation (BCA), 189
boundary condition, 191, 219
breathing sphere approach, 217
bulk
  vacancy, 210

channeling, 196
chemical sputtering, 203, 218
cluster, 189, 201, 207
  abundance distribution, 205
  deposition, 201
  dimer, 204, 205
  emission, 206, 219
    $(H_2O)_n$, 216
    Ag_{60}, 205
    Au_n, 206
    In_{200}, 205
  energy, 206
  formation, 204, 206
  fragmentation, 207, 208
  impact, 200–204, 206, 211, 218, 219
    $(CO)_2$, 203
    Ag_n, 202
    Al_n, 202
    Ar_n, 202, 203
    Au_4, 208, 210
    Au_n, 202, 203
    C_{60}, 203
    fullerene, 203
    point, 203
  internal energy, 207
  internal excitation, 207
  metastable, 207
  orientation, 203
  range, 201
  size, 203, 206, 207
  stable, 207
  yield, 203
clustering probability, 205
cohesive energy, 198, 200, 210, 211
composition
  change, 215
condensed gas, 198
cosmic dust particle, 210
Coulomb explosion, 196, 201
crater, 200, 203, 204, 210, 212, 219
  depth, 202
  formation, 199, 210, 211
    threshold, 211
  length scale, 211
  rim, 203, 204, 206, 208, 211, 213
  size, 210, 211
  structure, 211
  volume, 203, 210

defect, 212
  production, 197, 201, 212
deposited energy, 200
depth of origin, 192, 215
desorption, 216
diffusion, 200, 212
dimer, 196
dimer ejection, 204
dipole moment, 196
displacement energy, 196
dissipation, 189
dissociation, 216, 217
  molecule, 216
  threshold, 207

electrical conduction, 197

electron-atom scattering, 197
electron-phonon coupling, 197
electron-phonon interaction, 197
electronic excitation, 200, 201
electronic sputtering, 192, 196, 200, 211, 216
energy deposition, 193
energy loss, 198
  electronic, 197
    Firsov, 197
    Lindhard-Scharff model, 197
evaporation, 203, 207
excitation, 191, 198
  electronic, 192, 197

fluctuation, 203
fluence, 193, 194, 212, 215, 218
fractal dimension, 204
fractal surface, 204
fragment
  formation, 217
fragmentation
  molecule, 217
  particle-induced, 217
friction, 197, 198

heat conduction, 200

implantation, 212
interaction potential, 190, 191, 193, 194, 210, 217, 219
  AIREBO, 217
  attractive, 205
  embedded-atom-method (EAM), 191
  hydrocarbon (Brenner), 217, 218
  intermolecular, 216, 217
  Lennard-Jones, 200, 216
  Morse, 216
  pair potential, 212
  Stillinger-Weber, 218
interlayer mobility, 212, 213
intra-molecular interaction, 216
ion beam milling, 204
ion beam polishing, 204
ion-beam mixing, 197
ionic bonding, 196
ionic charge transfer, 196
ionization, 191, 198
isotope sputtering, 219

laser ablation
  organic films, 217
lifetime, 197

many-body interaction, 219
matrix isolation spectroscopy, 216
mean-free path, 198
melting, 190, 198, 203, 206, 209, 211, 214
micro-explosion, 209
mixing, 203
molecular dynamics, 189–192, 194, 199, 219
molecule
  fragmentation, 208
  internal excitation, 217
molecule liftoff, 217
molten zone, 210

Newton's equations of motion, 219

organic molecule, 217
outer solar system, 216

partial sputtering yield, 193
preferential sputtering, 194, 195, 215, 219

radical, 217
radioactive waste storage, 196
range
  projectile, 197
reactive ion beam etching (RIBE), 218
recombination, 206, 216
redeposition, 212
reflection, 193, 212
regime
  linear cascade, 192
  linear-cascade, 198
  spike, 199
rotational excitation, 216
RRK transition-state theory, 207

scanning tunnelling microscope, 212
secondary ion mass spectrometry (SIMS), 194, 198, 215, 217
selfsputtering, 209, 215
spike, 198, 199, 201, 211, 219
  elastic collision, 198

lifetime, 200
thermal, 197–199, 202, 210
volume, 200
sputtering of
clusters, 190
molecules, 190
state
excited, 196
metastable, 197
steady, 193
sticking
coefficient, 193
stopping power
electronic, 190, 197, 198, 200, 211
nuclear, 190, 198, 200
surface
composition, 215
defect, 208, 209
erosion, 203
modification, 201
roughness, 190, 204, 211, 215, 218
smoothing, 201, 202, 204, 211, 215
step, 211–213
structure, 211, 212
dot, 203, 215
ripple, 211, 215
tension, 207
vacancy, 208, 213
surface binding energy, 190, 194, 195, 209
surface topography, 190, 191, 209, 211–213, 219

target
alkali halide, 196
alloy, 193
Cu, 205
amorphous hydrogenated carbon, 218
benzene molecular crystal, 217
compound, 193, 196, 203
diatomic molecular solid, 216
frozen gas
H_2O, 216
Ge, 209
hydrocarbon, 216
inorganic material, 216
liquid, 195
metal, 209
model alloy, 194
modification, 202
molecular solid, 200, 216
multicomponent, 194
multilayer film, 217
organic material, 200, 215–218
organic molecule, 216
polyethylene, 217
polymer, 216, 217
single crystal, 191
KCl, 196
LiF, 196
NaCl, 196
structureless, 189
target structure
crystalline, 189
terrace, 213, 214
thermalization, 189, 197
thermodynamic equilibrium, 206
thin film deposition, 201, 215
track, 200, 201, 211, 216
formation, 196
ionisation, 201
trajectory, 198
transmission, 192

vacancy
island, 212
vibrational excitation, 216, 217

Wehner spot, 191, 192

Energy and Angular Distributions of Sputtered Species

Hubert Gnaser

Department of Physics, University of Kaiserslautern,
67663 Kaiserslautern, Germany
gnaser@rhrk.uni-kl.de

Abstract. Energy and angular distributions of sputtered species from a wide variety of target materials (metals, semiconductors, alkali halides, frozen gases, and organic solids) are discussed. Bombardment energies in the range from a few 10 eV to roughly 100 keV are considered, covering irradiation conditions for which nuclear (elastic) collisions dominate the energy dissipation processes. In the linear cascade regime, energy spectra of neutral, excited, and ionized atoms and molecules are presented. The emission characteristics of clusters and large organic molecules are described in considerable detail. In this context, computer simulations can clearly elucidate pertinent ejection mechanisms. Angular distributions from amorphous, polycrystalline, and single-crystal materials illustrate the distinct influence of the sample structure on the spectra. Emission distributions at low impact energies indicate the occurrence of anisotropic cascades and of collision sequences involving only a small number of recoil generations. High-density cascades are examined for cluster-ion bombardment. As compared to atomic irradiation, for cluster impact an additional low-energy component is found in energy spectra. For large cluster projectiles (composed of hundreds of atoms) the angular distributions of sputtered material exhibit a pronounced emission at very oblique polar angles.

1 Introduction

Sputtering of particles from a surface is but one in a wealth of phenomena resulting from the interaction of energetic ions or atoms with condensed matter. The energy dissipation that ensues may lead to atomic relocation, roughly within the ion's range, creating temporary or permanent defects and, eventually, may give rise to the emission of atoms and molecules from the surface. Detailed reviews of essentially all aspects of these processes are available, covering some five decades of extensive research [1–13]. Data specific to sputtering were presented in previous reviews [4, 14–17].

The spectral distributions in terms of the (polar) emission angle and the (kinetic) emission energy of sputtered species reflect, to some degree, the atomistic processes occurring during the dissipation of the projectile's energy in the solid and the sputtering event. Hence, from the energy and angular distributions of sputtered species information about the collisional processes in the solid might be derived. As a consequence, numerous experiments under a wide variety of bombardment conditions were carried out in order to

R. Behrisch, W. Eckstein (Eds.): Sputtering by Particle Bombardment,
Topics Appl. Physics **110**, 231–328 (2007)
© Springer-Verlag Berlin Heidelberg 2007

determine accurately the energy and angular spectra of sputtered atoms and molecules. Already the first measurements of the mean energy [18–20] and of energy spectra [21–24] of sputtered atoms confirmed the *athermal* nature of the sputter ejection process, a very important finding at that time [4].

More detailed results on energy spectra [25] corroborated the concept of sputtering (and damage creation) via collision cascades of target atoms: the dissipation of the projectile's energy proceeds by means of nuclear (elastic) collisions among these atoms and may cause the ejection of atomic or molecular species located at or near the surface. The theoretical concepts describing such processes were adapted [26, 27] to model the sputtering of random targets by medium and heavy ions. For metal and semiconductor targets and projectile energies up to several 10 keV, the dominant energy loss mechanism in this *linear collision-cascade regime* is then due to nuclear atom–atom interactions. However, at very low impact energies (1 keV and below) and for light projectiles like H, D, or He a full collision cascade often does not evolve, but isolated collisions may lead to sputtering (*single knockon regime*). On the other hand, very dense collision cascades with a large number of atoms in motion simultaneously may develop for very heavy projectiles with several tens of keV of energy or for molecular (cluster) bombardment (*high-density cascade* or *spike regime*).

Generally, the sputtered flux is composed of a variety of different species: apart from neutral atoms and molecules, excited atoms and molecules, and ions are found. The energy and angular distributions of sputtered species may depend strongly on the structure of the solid: the ordered arrangement of atoms in a crystalline lattice exerts a distinct influence on the emission characteristics. This observation is well-documented for single-crystal sputtering. In polycrystalline materials, these effects may be less pronounced unless they are strongly textured; the observed spectra are an average due to the emission from many individual crystallites. Only in amorphous specimens such processes would be absent.

In this review, irradiation energies roughly in the range from a few 10 eV to some 100 keV are considered. For metal and semiconductor targets, sputtering is then predominantly due to nuclear collisions. Electronic excitation or ionization of target atoms constitutes an inelastic energy loss mechanism, but is of minor importance for medium and heavy ions in that energy regime. *Electronic* energy loss may become relevant, however, for specific classes of materials such as insulators or ionic crystals. Typical data for alkali halides and condensed gases will be presented, however without discussing the pertinent electronic energy processes in detail.

Although in this chapter primarily experimental data will be presented, selected results from computer simulations are included in order to illustrate specific emission characteristics. The computational methods to obtain them are based either on the principle of (classical) molecular dynamics (MD) or on the binary-collision approximation (such as the TRIM code). Detailed descriptions of both of those approaches are given in the chapter by *Eckstein*,

Urbassek of this volume. This chapter is organized as follows: first a brief overview of theoretical concepts (Sect. 2) and the experimental techniques (Sect. 3) will be given; results of energy and angular distributions in the three sputtering regimes outlined above are presented in Sect. 4–6. A summary and an extensive bibliography conclude the chapter.

2 Theoretical Concepts

2.1 Energy Dissipation, Recoil Generation, and Sputtering

The nuclear stopping of ions creates collision (displacement) cascades in the solid in which a certain fraction of target atoms within the ion range is set in motion (recoil atoms) [8]. Any collision cascade intersecting the surface may cause sputtering of atoms from the surface. A decisive quantity with respect both to defect production within the solid and to sputtering from the surface is the number of atoms participating in such a collision cascade [26–33]; this number is roughly proportional to the fraction of the primary ion's energy E_n spent in nuclear collisions. The average number of atoms in a cascade with an energy E_i recoiling into an energy interval $[E_i,\, \mathrm{d}E_i]$ is then given by [33, 34]

$$F(E_\mathrm{n}, E_i) \approx \Gamma E_\mathrm{n}/E_i^2 \qquad \text{for} \quad \gamma E_\mathrm{n} \gg E_i\,, \tag{1}$$

where $\gamma = 4M_1M_2/(M_1+M_2)^2$ (M_1 and M_2 are the masses of the ion and of the target atom, respectively) and Γ is (weakly) dependent on the atomic interaction ($\Gamma \approx 0.4 - 0.6$) [33]. $F(E_\mathrm{n}, E_i)dE_i$ is the so-called *recoil density* [30,33] and is of great relevance for sputtering as it defines, ultimately, the flux of atoms moving with an energy E_i in the cascade. Those atoms that reach the surface with sufficient energy to overcome the surface binding forces can be sputtered. This indicates that the sputtering yield depends on the energy deposited at or near the surface and that the *internal* energy distribution of atoms is proportional to E_i^{-2}.

Collision cascades leading to sputtering and the ejection events proper have been modeled theoretically by many different concepts [25–27, 33, 35–45]. On the other hand, computer simulations of sputtering [46–53] have contributed enormously to elucidate pertinent processes. An analytical theory for sputtering in the *linear collision-cascade regime* has been proposed by *Sigmund* [26, 27, 30, 33, 35]. According to this approach [33], the sputtering yield Y is predicted to scale linearly with the energy deposited in elastic collisions at the surface, $F_\mathrm{D}(E_0, \theta_0, x=0)$

$$Y(E_0, \theta_0) = \Lambda F_\mathrm{D}(E_0, \theta_0, 0) \tag{2}$$

where Λ is a material-specific constant (see below). $F_\mathrm{D}(E_0, \theta_0, x)$ is the "damage distribution", i.e., the energy deposited by the bombarding ion (energy E_0, incidence angle θ_0 relative to the surface normal) in low-energy

recoils in the depth interval $(x, x + \mathrm{d}x)$. F_D was proposed [26, 27] to scale with the nuclear stopping cross section S_n, $F_\mathrm{D}(E_0, \theta_0, 0) \propto S_\mathrm{n}(E_0)$.

To evaluate Λ, information on the surface potential barrier and the nuclear stopping cross section of (slowly moving) recoil atoms is required. The simplest but not necessarily the only model for the binding of atoms at the surface is a *planar* energy surface barrier U [33, 51]; often the cohesive (or sublimation) energy of the solid is used for U (see Sect. 2.2). Then, the probability $P(E_i, \theta_i)$ for an atom to escape from the surface reads [33]

$$P(E_i, \theta_i) = \begin{cases} 1 & E_i \cos^2\theta_i \geq U \\ 0 & E_i \cos^2\theta_i \leq U \end{cases} . \tag{3}$$

E_i and θ_i are the energy and the angle (relative to the normal) with which the atom approaches the surface from *within* the target. The planar surface potential effects a *refraction* of the atom's path upon passage through the surface. The perpendicular momentum component is reduced by an amount equivalent to the binding force, resulting in an *emission energy* E and a polar *emission angle* θ [54]

$$\begin{aligned} E &= E_i - U \\ E\cos^2\theta &= E_i \cos^2\theta_i - U \, . \end{aligned} \tag{4}$$

Using (3), the recoil density, (1), and the stopping cross section in the power-law form, *Sigmund* derives [26, 27, 33]

$$\Lambda = \frac{\Gamma_m}{8(1-2m)} \frac{1}{N\, C_m\, U^{1-2m}} \tag{5}$$

with N being the atomic density of the sample, Γ_m and C_m depend on the specific cross section chosen to model the energy transfer in nuclear collisions [30, 55–57] and m characterizes the power of the interatomic potential $V(r) \propto r^{-1/m}$ employed to describe atomic collisions. In his original work [26, 27], Sigmund used $m = 0$ with $\Gamma_0 = 6/\pi^2$ and $C_0 = 0.0181\,\mathrm{nm}^2$. Later work [58] established, however, that with this choice the power-law cross sections underestimate nuclear stopping at the energies relevant for atom ejection by roughly a factor of two. It is noted that $\xi_0 = 3/4NC_0$ is a characteristic depth of origin of the sputtered atoms.

While from this approach an analytical expression for the integrated sputtering yield could be derived [26, 27], the differential yields with respect to the kinetic emission energy E and the emission angle θ of the sputtered atom are of particular interest here. *Sigmund* [33] has established the differential yield of atoms sputtered with an emission energy E, into the solid angle Ω around the polar emission angle θ as

$$\frac{\mathrm{d}^3 Y}{\mathrm{d}E\, \mathrm{d}^2\Omega} = F_\mathrm{D}\left(E_0, \theta_0, 0\right) \frac{\Gamma_m}{4\pi} \frac{1-m}{NC_m} \frac{E}{(E+U)^{3-2m}} \cos\theta \, . \tag{6}$$

An essentially identical result had been derived by *Thompson* [25, 41]. Thus, the *monotonously falling* recoil spectrum within the target (1) is transformed into an energy spectrum *peaking* at an energy E_{peak} which depends, in theory, only on the specific sample (via U), but not on the mass and energy of the incident ion

$$E_{\text{peak}} = \frac{U}{2\,(1-m)}\,. \tag{7}$$

Towards high emission energies ($E \gg U$), energy spectra are predicted to fall off as $1/E^{2-2m}$. For many decades, these landmark equations have been used in comparisons with experimental energy spectra, with the aim of assessing the predictions of (6) and (7), in particular with respect to the high-energy falloff proportional to $\approx E^{-2}$ and the peak position at about $\approx U/2$ [59, 60]. Unfortunately, quite often this was done using a simplified, but not necessarily correct form of (6), by assuming $m = 0$

$$\frac{\mathrm{d}Y}{\mathrm{d}E} \propto \frac{E}{(E+U)^3}\,. \tag{8}$$

While even for the low-energy (recoil) flux a value $m = 0$ might not be valid, for the high-energy sputtered flux, that is, in the regime in which the asymptotic E^{-2} falloff is usually investigated, $m > 0$ is conceivable. Often an even more general expression was used in order to compare with the measured spectra:

$$\frac{\mathrm{d}Y}{\mathrm{d}E} \propto \frac{E}{(E+U)^{\alpha+1}}\,. \tag{9}$$

In this case, U or α, or both were treated as a fitting parameter. Such data will be discussed in detail in Sects. 4.1, 4.2, 5.1, and 6.3.

The differential yield expression, (6), predicts a *cosine law* for the polar angular distribution of the sputtered flux from an amorphous solid (For early work on single crystal sputtering see, e. g., [54, 59]). Such a dependence is characteristic of an isotropic flux in the target. Since this simple cosine distribution is often not observed experimentally, in particular at very low or very high energies, measured angular emission distributions were often described by

$$\frac{\mathrm{d}Y}{\mathrm{d}\Omega} \propto \cos^y\theta \tag{10}$$

with y being a fitting parameter, frequently found to be > 1. These observations and possible explanations for deviations from (6) will be discussed in 4.3, 5.2, and 6.4.

The factorization of (6) expressed by (8) to (10) might not generally be correct; in other words, the kinetic energy spectra of sputtered species could

be dependent on the emission angle θ and vice versa. That such an interdependence indeed occurs was illustrated nicely both experimentally [61] and by an MD simulation [62]: the energy-resolved angular distributions of In and Rh atoms sputtered by 5 keV Ar^+ from the elemental samples exhibit a near $\cos\theta$ distribution for low emission energies and a $\cos^2\theta$ spectrum for higher emission energies. Furthermore, the angle-resolved energy distributions show a shift to lower energies as θ is increased from 0° to 75°.

2.2 Surface Binding Energy

Because of its decisive influence on sputtering, the appropriate choice for the surface binding energy U has been discussed extensively in the literature [63–68]. Most often the cohesive (or sublimation) energy [69] has been used. Different authors have argued, however, that the energy required to remove an atom from the surface should be greater by some 30–40 % than that value: at an unperturbed surface an in-surface atom is bound by $U = (2\,Z_{\mathrm{S}}/Z)E_{\mathrm{coh}}$, where Z_{S} and Z are the surface and bulk coordination numbers and E_{coh} is the cohesive energy. This reasoning is based on the application of pairwise interaction potentials. For pair potentials and considering only nearest neighbors, the bond energy is related to E_{coh} by [66, 70–72]

$$E_{\mathrm{coh}} = \frac{Z}{2} E_{\mathrm{bond}} \,, \tag{11}$$

where Z is the bulk coordination number. The surface binding energy of an atom is

$$U = Z_{\mathrm{s}} E_{\mathrm{bond}} = 2\frac{Z_{\mathrm{s}}}{Z} E_{\mathrm{coh}} \,; \tag{12}$$

here Z_{s} is the number of nearest neighbors in the surface. Thus, for the monoatomic case, only one parameter is needed, namely the cohesive energy. For the (100) surface of an fcc crystal ($Z = 12$, $Z_{\mathrm{s}} = 8$) the surface binding energy thus amounts to $U = 1.33E_{\mathrm{coh}}$. Values of U for metals which exceed E_{coh} have been advocated by several studies [63–67, 72–74]. *Gades* and *Urbassek* [67, 72], at the other hand, have stressed the importance of many-body interaction potentials for an adequate description of surface bonding in metals. This is due, largely, to the delocalized nature of metallic bonds. In studies of atomic emission processes and the influence of surface binding energies of alloys, they adopted a tight-binding potential. With this approach they derive for the surface binding energy

$$U = \frac{2Z_{\mathrm{s}}}{Z} E_{\mathrm{coh}} - f \cdot (E_{\mathrm{coh}} - E_{\mathrm{vac}}) \,, \tag{13}$$

where E_{vac} is the energy to form a vacancy in the bulk and f is a factor completely determined by the crystalline structure (e. g., $f \approx 0.28$ for the

(100) surface of an fcc structure). It is noted that for pair potentials $E_{vac} = E_{coh}$ and (13) is identical with (12). Using such potentials to describe atomic emission processes [67], *Gades* and *Urbassek* obtain for metals surface binding energies that are smaller than the values derived for pair potentials. Along these lines they evaluated also the surface binding energies in a binary alloy, both for pair-potential and for many-body interactions. For a more thorough discussion of these features, see [12, 72].

3 Experimental Techniques

This section describes the techniques currently in common use for the determination of energy and angular distributions. The status of such experimental methods has been reviewed, in 1987, by *Thompson* [42] for velocity/energy spectra of sputtered atoms and, with regard to angular and energy measurements, by *Hofer* [59] in 1991 and by *Betz* and *Wien* [60] in 1994. Typically, the majority of the sputtered flux is composed of *neutral* species. Because several of the methods employed for determining energy and angular spectra can be applied only to *charged* species, techniques of *post-ionizing* neutral particles have found an increasingly widespread use in the past. The post-ionization efficiency can be very high (from 1 % to close to 100 %), but it might depend on the neutrals' energy. The typical approaches are therefore described first.

3.1 Post-Ionization of Sputtered Neutrals

To accomplish the *post-ionization* of the neutral atoms and molecules various experimental setups have been devised; in early work, this post-ionization step was achieved by the interaction of the neutral particles with energetic electrons, using either an electron beam [75–78] or the electrons of a low-pressure plasma [79–81]. Hence, ionized species were generated by electron-impact ionization of neutral sputtered species in the gas phase, that is, at some distance from the sample surface. Penning ionization was used as another means for the post-ionization of sputtered neutrals [82–84]. The approach of combining this post-ionization step (either by electrons or by photons, see below) with mass analysis is usually called secondary-neutral mass spectrometry (SNMS) and is applied, like secondary ion mass spectrometry (SIMS) [85, 86] for surface and thin-film characterization [80, 87].

Post-ionization of sputtered neutrals can be accomplished also by absorption of one or more photons from an intense laser field. In these laser SNMS instruments [88], the post-ionizing laser, directed parallel and in close distance to the surface, is fired with a certain temporal delay after an ion pulse has released particles from the specimen, so that the cloud of *neutral* sputtered species can reach the interaction zone. Ions created by this post-ionization process are *accelerated* to an energy much higher than their emission energy

and then injected, for mass selection, into a time-of-flight (ToF) mass spectrometer; quite often this is of the reflectron type, but other spectrometers are also in use [89, 90].

Different photoionization schemes can be employed [91]: A very simple process is *single photon ionization* (SPI) where the absorption of one photon is sufficient to overcome the ionization threshold of the sputtered species. For typical ionization potentials, this requires UV or VUV radiation in order to provide high enough photon energies. If this condition cannot be met, absorption of more than one photon is needed for post-ionization, leading to *multiphoton ionization* (MPI) [92]. MPI schemes can be further distinguished by the way the photons are absorbed: In *resonance enhanced multiphoton ionization* (REMPI) one or more resonant transitions are utilized to excite the sputtered neutral species into a high-lying state from which it is ionized by absorption of another photon [93]. REMPI schemes are extremely efficient due to the large cross sections and very selective with regard to the detected species and its electronic state. *Non-resonant multiphoton ionization* (NRMPI) schemes [94], on the other hand, employ direct multiphoton transitions into the ionization continuum without resonant intermediate steps.

3.2 Methods for the Determination of Energy Spectra

Information about the energy/velocity distributions come from different classes of experiments. Early approaches utilized dynamometric [18–20] or calorimetric [95] techniques to determine the *average* energy or momentum of sputtered species. Very soon also time-of-flight methods were developed [21–23, 96–98] to measure the velocity of sputtered neutrals. The techniques currently in more frequent use are (i) electrostatic energy analysis of charged species, (ii) fluorescence techniques, and (iii) time-of-flight measurements; they are outlined here in more detail [42].

3.2.1 Electrostatic Energy Analysis

In these instruments an electrostatic energy analyzer (e. g., a spherical or cylindrical deflector) is employed to determine the energy-to-charge ratio of *ionized* species. Because ions commonly constitute only a small fraction of the sputtered flux and because the ionization mechanisms depend sensitively on various sample parameters, the analysis of sputtered *neutrals* provides more representative information and post-ionization methods as outlined in Sect. 3.1 are frequently employed. Depending on the specific parameters of the electrostatic analyzer and the ions' pass energy, the energy resolution in such devices may range from a few tenths eV to some eV. These devices are similar to the ones used for electron spectroscopy [99].

Any setup for the determination of energy spectra that includes mass spectrometric capabilities has the distinct advantage of *mass selectivity* and

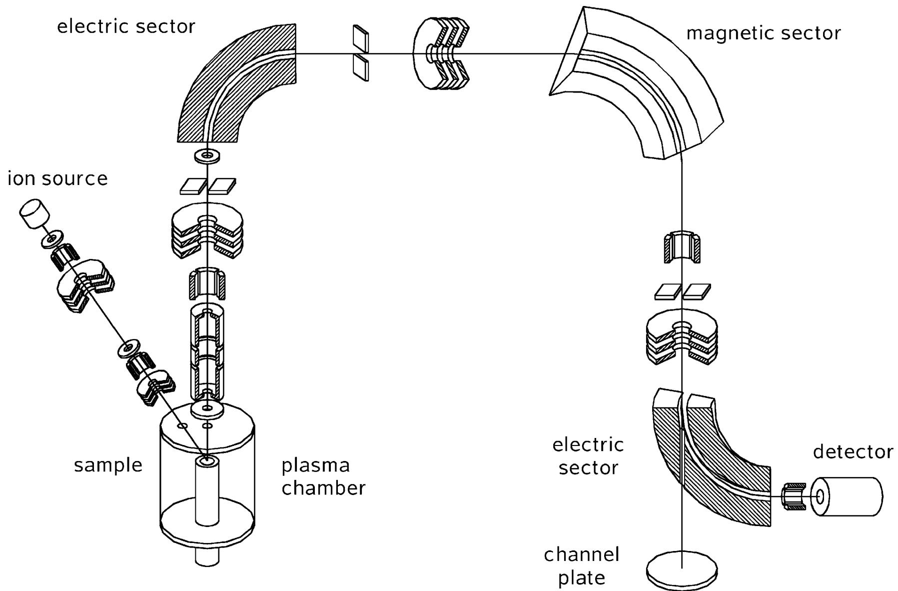

Fig. 1. Schematic layout of a secondary-neutral mass spectrometer. The electrons of a low-density plasma are utilized for post-ionization of sputtered neutral species. The spectrometer consists of an electric and a magnetic condenser with double-focusing properties [81]

often a large dynamic range is achievable. Figure 1 shows such type of an instrument [81, 100] that combines a spherical electrostatic sector with a magnetic sector analyzer (both with 90° deflection) into a truly double-focusing mass spectrometer [85]. In addition, post-ionization of sputtered neutrals is achieved by using the electrons of a low-density plasma. Sputtering is effected either by the plasma ions or by a separate ion source. With this instrument, energy spectra covering five orders of magnitude in the intensity of the sputtered flux were recorded (see Sect. 5.1.1), exemplifying the high sensitivity of such devices. The combination of a plasma with an energy analyzer and a quadrupole mass spectrometer has been extensively used by *Oechsner* and his coworkers [24, 101] to measure the energy spectra of sputtered neutral species. For such systems the overall transmission may be energy dependent; hence, appropriate corrections for these effects are required in order to obtain "true" energy distributions.

3.2.2 Fluorescence Techniques

The photon emission from atoms *excited* in the sputtering process can give information about their velocity by measuring the light intensity as a function of distance from the target surface [102, 103]. Although extensively used in

the past, this light-versus-distance (LvD) technique is limited by the possible occurrence of cascading from higher excited states that can decay into the state under investigation and can also exhibit longer lifetimes than this state. This approach is now rarely used since metastable atoms became accessible to selective laser excitation and post-ionization (see Sect. 3.1).

Of substantial relevance for studying *velocity* distributions of sputtered species were techniques based on laser induced fluorescence (LIF), in particular in a variant that utilizes the Doppler shift of the excitation wavelength to measure the velocity of the sputtered atom, Doppler shift laser fluorescence spectroscopy (DSLFS) [104–109]. For an atom traveling with velocity v directed at an angle φ to the laser beam, its excitation frequency is shifted by an amount

$$\Delta\omega = \frac{v}{c}\omega_0 \cos\varphi \,, \tag{14}$$

where ω_0 is the non-shifted resonance frequency of the atom. By tuning the laser over the Doppler profile of such atoms and simultaneously recording the resulting fluorescence signal, the velocity spectrum is obtained. The excitation cross sections are usually very high and independent of the particle velocity. A velocity resolution down to a few m/s could be achieved, sufficient to resolve the velocity distributions of thermal species. Since this approach is state-selective, ground states and electronic excited states of sputtered atoms can be measured separately. In fact, the first velocity distributions of metastable (long-lived) sputtered neutrals were determined using DSLFS (see Sect. 4.1.1).

3.2.3 Time-of-Flight Measurements

The use of time-of-flight (ToF) measurements for the determination of the velocity distributions of the sputtered flux dates back to the pioneering work by *Thompson* and coworkers in the early 1960s [21]. They used a high-speed spinning rotor for time-resolved registration of particles sputtered by a chopped ion beam. The particle density condensed at the rotor rim reflects the velocity distribution of the sputtered flux. In later versions of that instrument [110–112] the ion beam was chopped electronically and the rotation speed was increased. To detect the deposit, radioactive targets were employed and the radioactivity of the deposited material was determined after sputtering. Most experiments were done with Au specimens because the radioactive isotope ^{198}Au (with the convenient half-life of 2.7 days) could be introduced as tracer into the target by prior neutron irradiation. Thompson and coworkers utilized this ToF instrument extensively in a quest to measure the energy spectra from polycrystalline and single-crystal specimens under various bombarding conditions and to resolve contributions from thermal spike and collisional sputtering processes.

Because these ToF systems are not mass-selective, they detect the velocity distribution of the *total sputtered flux*. To overcome this limitation, ToF

arrangements were combined with a mass analyzer, originally a quadrupole mass filter [97, 113]. The ion beam was pulsed electrically and the sputtered species (mostly neutrals), after passing the drift path, are ionized in an electron impact ionizer and then injected into the quadrupole. In this way, velocity distributions of mass-selected species are obtained. It must be noted, however, that the transmission of quadrupole mass filters often exhibits a velocity dependence which may introduce artifacts in the measured spectra and requires correction procedures.

The above-mentioned laser SNMS instruments constitute an elegant way of combining ToF and mass-selective capabilities, providing the possibility to carry out time-of-flight and mass measurements. The flight time of a sputtered neutral species, from the surface to the ionization region, can be selected by the *time delay* with which the laser is fired; varying this delay, a flight-time distribution is recorded. The photoions are then *accelerated* to an energy of some keV; a subsequent, second time-of-flight path effects mass dispersion (cf. Sect. 3.1). A schematic layout of such an experimental setup is shown in Fig. 2. Of decisive importance in this kind of measurements is the length of the primary ion pulse and the extension of the interaction volume of the sputtered particles with the laser. The details of these timing schemes are rather complex, but can be optimized [91]. Energy (velocity) spectra of sputtered neutral atoms and of molecules/clusters both in the ground-state and in excited states were obtained by combining this ToF technique with laser post-ionization and mass spectrometry (ToF-MS). Such data are presented in Sect. 4.1 for a variety of sputtering conditions and of target materials.

Common to all types of ToF measurements is the feature that the transformation of the measured ToF spectrum $\mathrm{d}Y/\mathrm{d}t$ into the actual energy spectrum $\mathrm{d}Y/\mathrm{d}E$ via

$$\frac{\mathrm{d}Y}{\mathrm{d}E} = -\frac{t^3}{ML^2}\frac{\mathrm{d}Y}{\mathrm{d}t}\,, \tag{15}$$

(where M is the mass of the analyzed species and L is the length of the drift distance), accentuates high-energy features in the ToF spectrum which might appear insignificant in the energy spectrum.

3.3 Methods for Angular Distribution Measurements

A reliable and versatile way [59] of recording simultaneously, for every emission direction, the number of atoms emitted per unit solid angle is the *collector technique*. In this approach, the emitted particles are collected at suitable (hemispherical or semicylindrical) collector foils placed near the target perpendicular to the flux of sputtered particles. Subsequently, the thickness of the deposit thus formed is determined. The sticking of the sputtered atoms on and their potential re-sputtering off the surface by energetic scattered projectiles are critical issues, influencing quantitative measurements. In comparison to angular scans with any kind of particle detector, the large-area

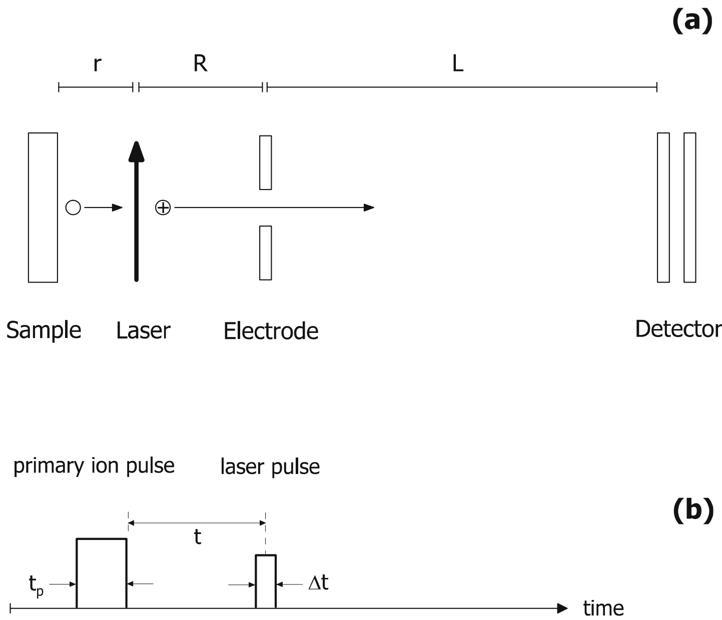

Fig. 2. Schematic principle for velocity distribution measurements by laser post-ionization and time-of-flight mass spectrometry. The diagram in (**a**) shows the experimental setup (not to scale). (**b**) Depicts the timing scheme. An ion pulse (length t_p) striking the sample releases neutral species from the surface which travel the distance r from the surface to the laser interaction region. A laser pulse of length Δt is fired after a delay time t; by varying this delay between the ion pulse striking the sample and the firing of the laser, the velocity of those neutral species can be probed. The photoions created are then accelerated over the distance R to an energy much higher (a few keV) than their emission energy by an electric field between the sample and the electrode. Passing this electrode, the ions start their passage through the field-free region (length L) to the detector. Because the energy of all ions is then essentially identical, this second time-of-flight stage provides mass selectivity

collector method has the important advantage of yielding the angular dependence of the sputtering yield at the same fluence of the bombarding ions. This excludes the influence of possible fluence-dependent transient effects in the sputtered flux on the measured distribution.

A serious problem in angular distribution measurements is the development of surface topography on the target induced by (prolonged) ion irradiation [114, 115]. Such a surface morphology can exhibit widely different length scales, ranging from micrometers (or more) in the case of polycrystalline specimens with individual crystallites oriented differently with respect to the ion beam [7, 114], to nanometers (or less) for ripple structure observed on many semiconductor surfaces [116, 117]. Different transient times (flu-

ences) are usually associated with these different scales; but it is often not clear whether a stationary state in terms of surface topography is actually ever reached. *Littmark* and *Hofer* [118] derived theoretical expressions for the angular dependence of the differential yield from regularly faceted surfaces.

The determination of the thickness profile of the condensate on the collector usually necessitates a suitable technique for thin-film analysis, albeit with some stringent requirements: a sensitivity sufficient for a thickness of the deposit in the range of 0.1–1 of a monolayer, a lateral resolution of the order of 100 µm, and a quantitative evaluation of the deposited material. The quantification of the deposited material should also not be influenced by any possible signal contributions from the collector material, resulting, for example, in a limited detection sensitivity. For the sputtering of multi-element samples, the analytical technique obviously requires an elemental specificity. Of the many techniques that have been used for the analysis of the sputtered deposits [59], two appear to have been favored in current collector experiments: (i) electron-beam induced X-ray emission [119] and (ii) light-ion (Rutherford) backscattering spectroscopy [120]. Other methods often employed were proton-induced X-ray emission [121] and secondary ion mass spectrometry [85].

The collector technique is well suited for recording the angular distribution of the *total* sputtered flux. For the determination of the angular distributions of individual atoms and molecules, *mass spectrometric techniques* are required; however, the necessary variation of the spectrometer's acceptance angle with respect to the specimen can make such a setup fairly complex. In fact, most of the devices employed for the measurement of energy spectra (see Sect. 3.2) contain a mass spectrometer; due to the restricted solid angle of acceptance, these instruments exhibit some angular resolution which, however, is often limited to one specific emission angle.

Winograd and his coworkers [122, 123] have devised an instrument for the detection of sputtered neutral species by combining a time-of-flight mass spectrometer with laser photoionization; the very interesting feature of this setup is the possibility to record the (mass-selected) sputtered flux with respect to both emission angle and kinetic emission energy. This instrument was extensively used for the determination of the angular and energy distributions of mass-selected sputtered species. A very detailed understanding of the respective emission processes resulted from those differential analyses [61, 123–125]; examples from that work are discussed in Sect. 4.3.

A rather special case is the determination of angular distributions from isotopic mixtures, i. e., an elemental material with several isotopes [126]; mass spectrometric techniques are needed in such an experiment.

4 Energy and Angular Distributions in the Linear-Cascade Regime

For the energy dissipation in the linear collision cascade regime it is usually assumed that only a relatively small fraction of the target atoms within the cascade volume is in motion at any given moment and that the low-energy recoil flux is distributed isotropically (however, a residual amount of anisotropy may still exist [127,128]; hence, the influence of the original momentum should be negligible under these conditions. In addition, the presence of the target surface is postulated not to disturb the development of the collision cascade. Clearly, some of these assumptions may often not comply with the situation encountered in real systems. For example, an isotropic movement of recoil atoms within the cascade is not very probable in a specimen that has some crystallographic order, like a single crystal: with an anisotropic arrangement of atoms, the recoil flux may reflect that atomic orientation. This feature was noted already in early experiments by *Wehner* [129,130] who found, in sputtering of single-crystal specimens, a distinct preferential ejection along directions correlated with some crystallographic directions of the respective specimens, an observation termed "Wehner spots" later on. In fact, numerous experiments, theoretical models and computer simulations were devoted to the elucidation of those processes [54,59]. On the other hand, in a system with a random arrangement of atoms (which experimentally might be realized by means of an amorphous or a polycrystalline specimen without texture) the approximation of an isotropic recoil distribution may indeed be an useful one. It is this situation for which (6) might constitute a suitable guideline in terms of the energy and angular distributions of sputtered (atomic) species in the linear collision-cascade regime. The influence of an anisotropy of the momentum recoil density in the collision cascade on the energy and angular distributions of sputtered species was considered in [131]. For the emission of molecules and clusters the situation is more complex: the processes involved in the formation of molecules may have a decisive influence on the ejection characteristics. Similar arguments may apply for sputtered ions; here the ionization process may determine (or even dominate) the emission of the ionized species. To account for these features, energy and angular spectra of *atoms*, *molecules*, and *ions* will be discussed separately in this chapter. The data presented refer to the *linear-cascade* regime; they were obtained from metals and semiconductors, from organic materials, from alkali halides and from frozen gases.

4.1 Energy Spectra from Metals, Semiconductors, and Organic Materials

4.1.1 Energy Spectra of Ground- and Excited-State Atoms, and of Ions

Apart from the measurement of total sputtering yields, the determination of the energy distributions of sputtered species constituted a primary goal already in the early studies of the sputtering phenomena [18–23]. In fact, these and similar investigations established firmly the ballistic nature of the sputtering event. In addition, such experiments indicated the relevance of the surface binding energy both for the total yields as well as for energy spectra. The great interest in energy distributions was also stimulated by the inference that from them the fundamental processes of energy dissipation in the solid ensuing an energetic ion impact might be elucidated. The collision-cascade theory of sputtering advanced by *Sigmund* [17, 26, 27, 33] provided a guideline for that quest. Equations (6) and (8), (9) which result from that theory indicate that energy spectra could procure a direct access to quantities important for sputtering: (i) The surface binding energy U and (ii) the recoil density in the collision cascade via the high-energy falloff of the energy spectrum. As noted, the latter should deviate from the E^{-2} dependence if the parameter m of the power-law cross section is > 0. The importance of this approach is reflected by the enormous number of experiments during the past four decades which recorded the energy distributions of neutral atoms and atomic ions.

a) Energy Spectra of Neutral Ground-State Atoms

From an inspection of the large set of data on energy spectra accumulated in the past [59, 60, 132] the following conclusions emerge: for predominantly nuclear energy loss processes (i. e., for metals and semiconductors at keV energies), the measured energy spectra exhibit very often a high-energy dependence *close* to E^{-2} and a most probable emission energy (i. e., a peak) that corresponds *roughly* with the predictions of (7), applying for U the respective cohesive energy E_{coh}. However, it appears to be not possible to decide presently whether the variations observed in the high-energy slopes and in the peak positions are real (i. e., that they indicate a variance from theory) or result merely from uncertainties of the measurements. In particular, the procedure often applied of fitting the spectra to (8), (9), using U or α or both as fitting parameter(s) may introduce severe ambiguities; these can, of course, be aggravated by a limited range of E in the experiment. A detailed account of these data up to around 1994 is compiled in [60].

Examples of more recent measurements of atomic energy distributions are shown in Fig. 3 which depicts the energy spectra of *neutral* Al [133], Ca [134], and Ag atoms [135] sputtered from the respective metals. Although obtained

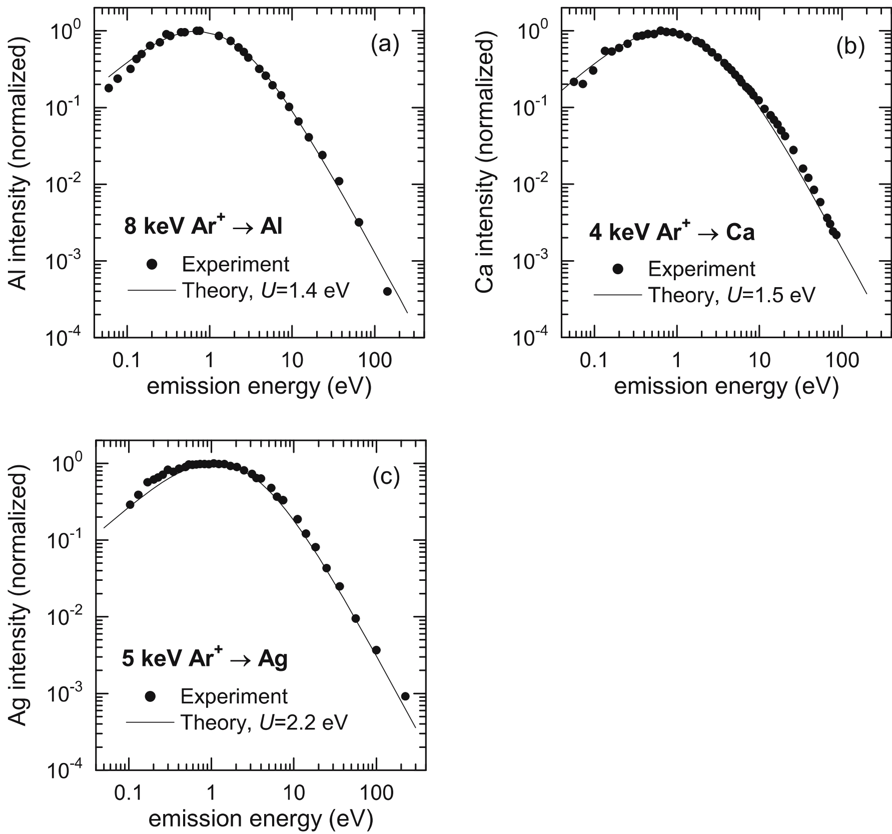

Fig. 3. Energy distributions of neutral (ground-state) atoms: (**a**) Al [133], (**b**) Ca [134], and (**c**) Ag [135] atoms sputtered from the respective elemental specimens. The *solid lines* are fits according to (8) using U as a fitting parameter. The resulting values of U are given

by different groups, the experimental arrangement used was very similar, namely time-of-flight measurements in conjunction with photoionization ToF mass spectrometry (cf. Sect. 3.2.3). The measured data were fitted by (8) and the values derived thereby for U are indicated. While $U = 1.4\,\text{eV}$ for Al is distinctly lower than the cohesive energy of Al ($E_{\text{coh}} = 3.3\,\text{eV}$), the values for the other atoms are moderately lower (by some 10–20 %) than the respective cohesive energies. This finding could be useful to test theoretical predictions of surface binding energies (see Sect. 2.2). The quality of these fits can be somewhat improved by utilizing both U and the high-energy slope α as free parameters. It appears that this procedure would lead to values of α slightly smaller than two, in agreement with $m \neq 0$, cf. (6). Similar data on energy spectra of neutral atoms were published in [136–142].

b) Energy Spectra of Excited Atoms

The flux of sputtered particles contains usually also a (small) fraction of particles (atoms or molecules) which are released in *electronically excited neutral states* [143]. With respect to experimental detection schemes, these can roughly be classified into two categories: (1) *Short-lived* states, on one hand, can easily be detected by the light emission due to their radiative decay closely above the surface. A large number of studies of the population distribution as well as of the kinetic-energy distribution of atoms emitted in such states has been published [143–145]. The interpretation of the acquired data, however, is always complicated by the complex interplay between radiative deexcitation lifetimes and emission velocities as well as by the important role of cascading transitions from higher-lying states. (2) *Metastable* states, on the other hand, are less influenced by transient effects, and are therefore well suited to study the physical mechanisms resulting in the excitation of atoms during the atomic collision cascade leading to their sputter ejection.

During the past decade, a relatively large body of experimental data on sputtered metastable atoms has been compiled using either laser-induced fluorescence (LIF) or resonant photoionization mass spectrometry (see Sect. 3.2.3): Fe [146, 147], Zr [148], Ba [149], In [150], Ti [151, 152], Cr [153], Ca [153], U [154], Rh [155], Ni [156–160], Co [161–163], Ag [164–166], and Cu [167] atoms sputtered in various excited states from the respective clean or oxidized metal surfaces were investigated in detail. A valuable source of information extractable from such experiments is the combination of (i) the *population partition* over different states and (ii) the *kinetic energy* and the *angle of emission* of the sputtered particles. While early experiments have frequently been interpreted in terms of Boltzmann-like population distributions corresponding to certain "temperatures" [144], newer results indicate that the excitation energy alone is not sufficient to characterize the measured population partitions in sputtering. Rather, parameters like the electronic configuration of the departing particle as well as details of the band structure of the bombarded solid surface play a significant role in determining the final probability for the emission of a sputtered particle in a specific electronic state [150].

A particularly interesting case has been reported by *Wucher* and his coworkers for *neutral* Ag atoms sputtered from a polycrystalline silver surface by 5 keV Ar^+. In this case, a sizable fraction of the sputtered atoms is ejected in the first metastable state $4d^9 5s^2(^2D_{5/2})$ of silver with an excitation energy of 3.75 eV [164, 165]. Any quasi-Boltzmann distribution describing the observed population of this state would involve "temperatures" well above 10^4 K, which are absolutely unrealistic. Resonant multiphoton ionization in combination with time-of-flight mass spectrometry was used in order to allow a state-selective detection of the sputtered species [168]. As a result, excited atoms in both states of the metastable multiplet $4d^9 5s^2(^2D_\mathrm{J})$ with excitation energies of 3.75 eV ($^2D_{5/2}$) and 4.30 eV ($^2D_{3/2}$) have been detected. The total

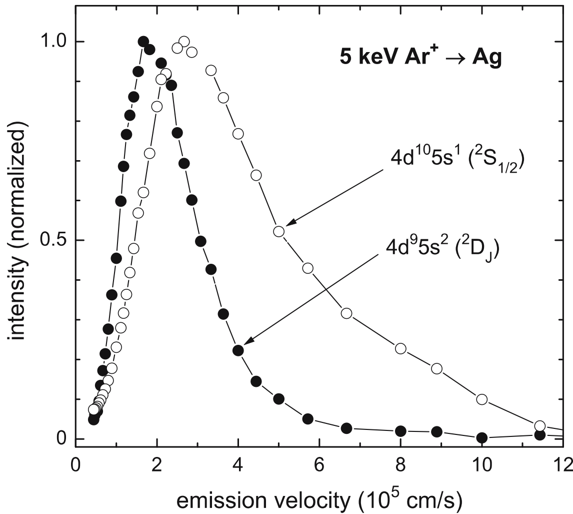

Fig. 4. Emission-velocity distribution of neutral Ag atoms sputtered along the surface normal in the ($^2S_{1/2}$) electronic ground state and the metastable ($^2D_\mathrm{J}$) states, respectively, from an Ag specimen bombarded by 5 keV Ar^+ ions [168]

population of both states is determined to be of the order of 1 %, which is surprisingly high in view of the large excitation energy. The velocity distribution of atoms ejected in both states reveals that the metastable atoms are ejected with *lower* average velocity than those emitted in the electronic ground state, thus indicating a mechanism populating this state which becomes less efficient with increasing emission velocity. Figure 4 exemplifies this finding, showing velocity distributions of neutral Ag atoms sputtered in the electronic ground state ($^2S_{1/2}$) and the metastable state ($^2D_\mathrm{J}$). Originally, the authors [168] discussed these results in terms of a two-step model describing the formation of an excited neutral atom as a combination of collective excitation processes within the collision cascade followed by resonant electron transfer between the surface and the escaping particle. In particular the observation that the velocity distributions of both Ag metastable states are *narrower* than that of the ground state would exclude excitation mechanisms by electron promotion which have been proposed for other sputtered excited-state atoms; these would lead to broader velocity distributions. These authors [169] later modified their concept and assumed that *d* holes are created by energetic collisions which are immediately screened by conduction electrons, thus forming excited atoms. This excitation propagates through the solid and is transferred to a sputtered atom, thereby resulting in a neutral excited Ag atom.

One of the materials studied most extensively in terms of the energy and population distributions of sputtered metastable atoms is nickel. Corresponding data from the Leuven group are presented here. Figure 5 shows the kinetic *energy* distributions of ground-state and metastable-state Ni and Co

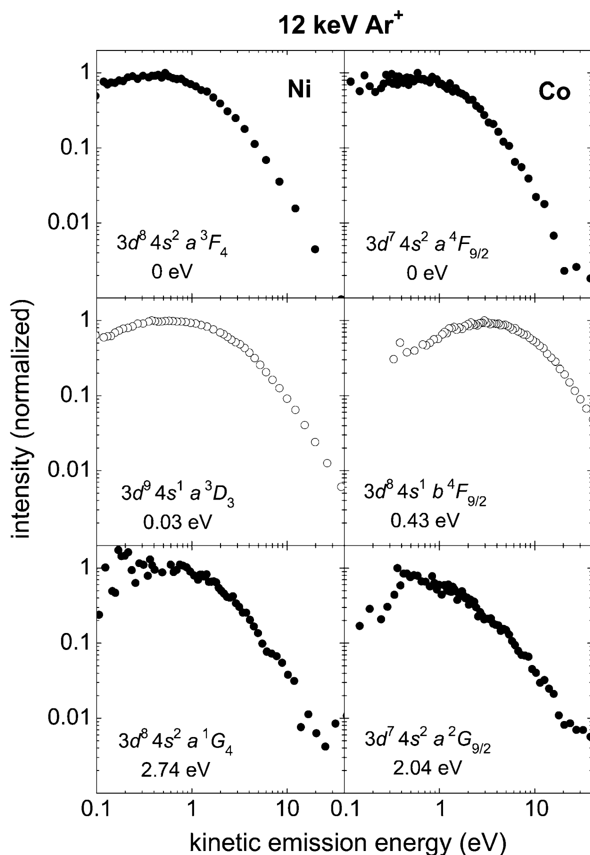

Fig. 5. Selected kinetic energy distributions of neutral Ni atoms (*left panels*) and Co atoms (*right panels*) sputtered in the ground and in low-lying metastable states. Bombardment was by 12 keV Ar^+ ions. The electronic configurations and the excitation energies are given [161]

atoms [159, 161]. For these elements a large variety of electronic configurations could be probed, both with *completely* and with *partially filled* outer shells (represented in Fig. 5 by closed and open symbols, respectively). The spectra reflect the different behavior of the two types of low-lying metastable states: all states with the $3d^x4s^1$ configuration (open symbols in Fig. 5) exhibit energy spectra which fall off *less steeply* and which peak at high energies than those of the $3d^{x-1}4s^2$ states with completely filled outer shells (closed symbols), with $x = 8$ for Co and $x = 9$ for Ni.

Figure 6 shows the *population* distributions of ground-state and metastable-state Ni and Co atoms obtained by sputtering [159, 161]. The distributions show several athermal features. All metastable states with excitation energies up to 2.7 eV are highly populated. The population partition on low-lying

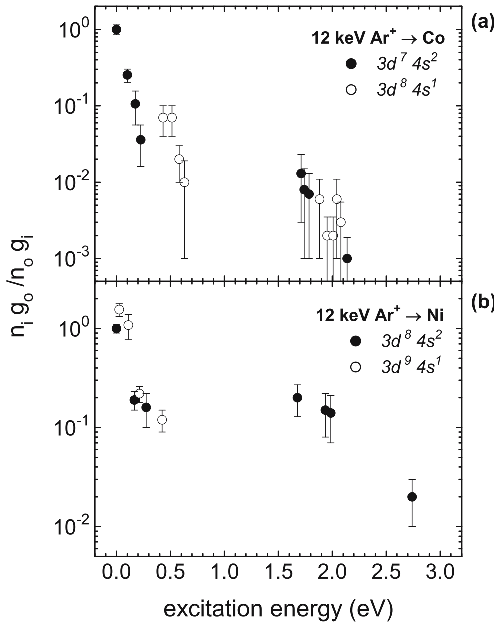

Fig. 6. Population distributions of (**a**) Co and (**b**) Ni metastable-state atoms sputtered by 12 keV Ar^+ ions from polycrystalline foils. The populations n_i are given relative to the population of the ground state and are corrected for the statistical weights g_i. The *open symbols* refer to atomic states with electronic configurations with a partially filled outer shell, the *solid symbols* refer to states with a completely filled outer shell [159]

states with the same electronic configuration of the outer shell follows roughly an exponential dependence as function of the excitation energy. The populations on states with a $3d^x4s^1$ are enhanced with comparison to the states with a $3d^{x-1}4s^2$ configuration. The anomalously high population of high-lying metastable states clearly deviates from a simple extrapolation of the exponential dependence of the population on low-lying metastable states.

The experimental data for metastable atoms sputtered from Ni, Co and other metals lead the authors [159, 160, 163, 166, 167] to the conclusion that the emission of excited atoms is the result of a multichannel resonant electron transfer (RET) process. In this model, a sputtered particle escapes from the surface as a positive ion and becomes neutralized into an atomic state by a resonant transfer of an electron from the valence band of the metal, i. e., a nonadiabatic tunneling of the electron. The velocity-dependent population of a particular state is governed by the correspondence of the electronic configuration of the atomic state with the bulk electronic configuration [170]. A good spatial overlap between the wave functions of the states involved ensures large overlap integrals and thus favors the population of the final state. Both for Co

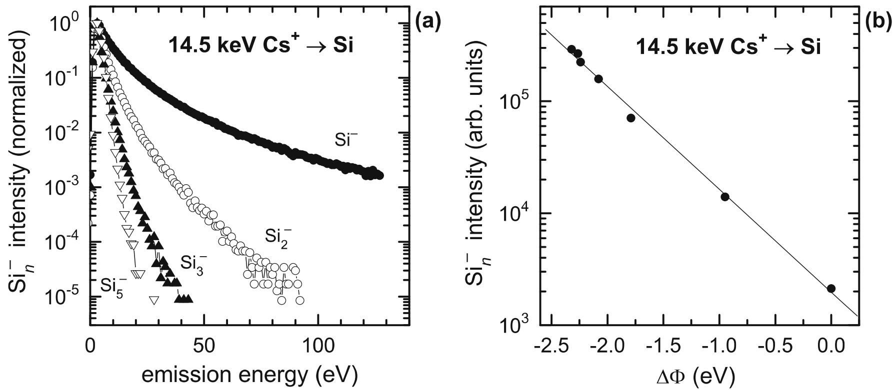

Fig. 7. (**a**) Energy spectra of atomic Si^- and Si_n^- cluster secondary ions sputtered from silicon by 14.5 keV Cs^+ ions. (**b**) The correlation between the Si^- intensity and the work function change $\Delta\Phi$ induced by a gradual increase of the Cs surface concentration. An exponential dependence in agreement with (16) is observed [185]

and Ni, the valence band states have a dominant $3d^x 4s^1$ character [159] which explains an enhanced population on the atomic states with a $3d^x 4s^1$ configuration. Additional evidence for a state-dependent neutralization probability comes from the measured flight-time distributions [159, 160, 162, 163].

RET processes have been invoked also to describe the scattering of atoms from metal surfaces [171] and the yields of sputtered secondary ions [143] (see below); they were used also by *Veje* [172, 173] in the early 1980s to explain the large populations of excited state atoms sputtered from various targets due to bombardment with 80 keV Ar^+ ions.

c) Energy Spectra of Atomic Ions

Energy spectra of *sputtered ions* have been recorded quite frequently in an attempt to elucidate the pertinent ionization processes. They usually indicated some dependence of the ionization probability of sputtered atomic ions on the emission energy [174–178] or emission velocity [179–184] although the respective trends were not clear-cut in all cases (see, e. g., [143]). While in few studies (e. g., [174, 175, 177]) both the distributions of the ion and the neutral species were recorded to derive the energy dependence of the ionization probability, in many cases only the ion spectra were measured and compared with an *assumed* neutral distribution (often of the form given by (8)); the usefulness of such an approach may be limited.

A typical energy distribution of a sputtered ion (Si^-) is shown in Fig. 7a obtained by 14.5 keV Cs^+ bombardment of silicon. Also depicted are the respective spectra of several Si_n^- cluster ions. The formation of *negative* ions in sputtering is known to be strongly enhanced in the presence of alkali

metals at the ions' emission site. This effect is generally ascribed to a lowering of the specimen's work function, Φ. The minimum amount of energy required to transfer an electron from the solid to an atom at infinity to form a negative ion is $\Phi - A$, A being the electron affinity; hence, the ionization probability P^- of sputtered negative ions should depend on this quantity. Several distinct ionization schemes have been proposed [143, 186]: the so-called electron-tunneling model [187] envisages the electronic transition as a resonant electron transfer process between a sputtered atom and the valence band, in close similarity to the RET mechanisms invoked for metastable-state formation. For negatively charged sputtered ions, P^- can be approximated as [143]

$$P^- \propto \exp\left[-\left(\Phi - A\right)/\epsilon_0\right] . \tag{16}$$

It was proposed [188] that ϵ_0 is proportional to the component of the ion's emission velocity perpendicular to the surface. For positive ions an essentially identical relation holds if $\Phi - A$ is replaced by $I - \Phi$, I being the ionization potential of the sputtered ion,

$$P^+ \propto \exp\left[-\left(I - \Phi\right)/\epsilon_0\right] . \tag{17}$$

Equation (16) predicts an exponential dependence of P^- on the work function of the surface. Such a correlation is illustrated in Fig. 7b which depicts the Si^- ion intensity (which is proportional to P^-) as a function of the work function change $\Delta\Phi$, induced by a varying amount of Cs at the surface of the Si specimen [185]. While a distinct work function dependence of P^- could be established in several investigations, studies related to a velocity-dependence (via ϵ_0) produced seemingly conflicting results (see, e. g., [143]). These ambiguities leave some doubt about the actual ionization mechanisms of sputtered ions, because a distinct velocity-dependence probably constitutes the most characteristic signature of an electron-transfer process.

Direct recoils sputtered from the surface in a binary collision with the projectile have been observed in many experiments in the past [25, 189–195]. Apart from neutral atoms, the energy spectra of positively and negatively charged ions were measured. *Eckstein* and coworkers [196–199] studied the charged fraction of these recoil ions for several metals bombarded by rare gas ions of some keV energy. Generally, the charged fraction is lower than 10 %, with singly-charged positive ions constituting the most abundant species [200]. An exponential dependence of the charge state on the component of the ion's emission velocity perpendicular to the surface was found in some cases.

4.1.2 Energy Distributions of Atoms Sputtered from Alloys

The irradiation of multicomponent targets with energetic ions is usually accompanied by composition changes within the near-surface region [12, 70, 71,

201–203]. Preferential sputtering, that is, the preferred ejection of one species in a multicomponent system is an obvious source, but others like collisional mixing, radiation-enhanced diffusion, or recoil implantation may contribute as well to those compositional deviations. Bombardment-induced changes in the surface and near-surface composition have been determined for numerous multicomponent materials [70, 71, 201–203]. While under steady-state sputtering conditions the total sputtered-flux composition is identical with the bulk stoichiometry, any *compositional gradients* existing within the depth of origin of sputtered particles can be expected to have a distinct influence on the energy and angular distributions of sputtered species.

According to (7), energy spectra of a sputtered atom X should peak at $\approx U_X/2$ in the regime of linear cascade sputtering. In several experiments [204–209] values of U_X for the components in binary alloys have been derived from fitting measured distributions by (9), using α and U_X as parameters. The available results suggest that U_X may depend on alloy composition.

Szymonski and coworkers [204–206, 210] have applied that approach extensively; they used ToF measurements combined with a mass spectrometer to obtain mass-selective energy spectra under stationary conditions from a series of binary alloys: Cu–Zn [206], Ag–Au [204], GaAs [205], and HfC [210]. One of the objectives in these investigations was the identification of nonlinear (spike) effects in sputtering by heavy-ion (Xe in this case) impact. The authors observed distinct shifts in the peak positions of the energy spectra in dependence of the alloy composition and established concentration-dependent surface binding energies. For example, in an $Ag_{0.6}Au_{0.4}$ alloy [204] they found $U_{Ag} = 2.1$ eV and $U_{Au} = 3.3$ eV, as compared with the values derived from respective pure-element specimens of $U_{Ag} = 3.1$ eV and $U_{Au} = 3.8$ eV which are very close to these elements' cohesive energies 2.95 and 3.81 eV, respectively. Energy spectra from Ni–W [207] and Cu–Li alloys [208] were evaluated in a similar fashion. Energy distributions from NiW and CuW alloys for very low bombarding energies (from 80 to 700 eV) were recorded [211] by means of SNMS utilizing a low-pressure plasma for post-ionization; some of these data are presented in Sect. 5.1.1.

Vicanek et al. [212] studied, by computations, energy partitioning and particle spectra in multicomponent collision cascades. They investigated a binary Hf_xC_{1-x} compound and observed that, in the zero-fluence limit of the simulations, the particle flux of the lighter species is overstoichiometric, while the flux of the heavy component shows only small deviations from stoichiometry. The energy spectra of sputtered particles, on the other hand, exhibited similar high-energy slopes for Hf and C atoms.

Rather drastic changes in the peak positions of energy spectra were observed in sputtering metals under various amounts of oxygen exposure [153, 209, 213–217] as compared to the respective clean surfaces. Typically, the energy spectra become broader, that is U_X is larger for an oxidized surface and the sputtering yield is reduced [218]. In terms of U_X, an increase by up to a factor of 10 (e.g., for Ba+O_2 and Ca+O_2) was reported (see [66] for a

compilation of pertinent data). In a series of publications, *Kelly* [219–222] has evaluated these energy distributions in terms of surface binding energy differences in metals, metal oxides and related systems; he attempted to correlate that information with available data of ion-bombardment induced compositional changes in those materials.

4.1.3 Energy Spectra of Sputtered Molecules

The sputtered flux from an ion-bombarded solid surface is composed not only of atoms but also of polyatomic molecules and clusters [59, 223, 224]. Following *Urbassek* and *Hofer* [223], the term *cluster* is used here in a broad sense designating any aggregation of identical moieties (atoms or small species like H_2O or CO_2), while *molecule* is reserved for those large atomic aggregations which exhibit strong bonding and may exist as preformed entities in the solid or at the surface. The emission of these species is a rather ubiquitous observation, found for essentially all materials and bombardment conditions. Apart from its inherent importance for understanding energy sharing processes in the solid and the possible transfer of (a part of) this energy to the ejected particles, cluster emission has some relevant applications: Ion-bombardment induced desorption of (large) organic [225, 226] and bio-molecules [227] is utilized in surface mass spectrometry for the characterization of solids. Furthermore, molecular and volatile reaction products may be emitted from a surface bombarded with reactive ions, increasing thereby the erosion rate (reactive ion etching [228] as applied, e. g., in semiconductor device fabrication).

Compared to the emission of atomic species in sputtering, the understanding of the formationand emission of clusters and large molecules under ion irradiation is much more incomplete, despite the fact that a large number of experimental investigations [223, 224, 229–238] and many computer simulations [239–252] over the past four decades have been dedicated to the investigation of cluster emission in sputtering. Both, experiments and computations [253–262] have indicated the importance of fragmentation processes.

Early experiments on the *internal energy* of sputtered clusters and molecules were performed for diatomic species: (i) Various dimers emitted from silicon containing different impurities [230, 263] and from elemental samples bombarded with N_2^+ ions [231, 264]; very broad rotational distributions with pronounced non-Boltzmann character were reported. (ii) S_2 dimers ejected from elemental sulfur and CS_2 specimens [265, 266]; quasithermal vibrational distributions (with a temperature of 1500 K) and strongly athermal rotational populations were found. (iii) Several alkali dimers (Na_2, K_2, Cs_2) [267]; an internal population temperature of 1000 K was deduced. More recently, *Wucher* [268] investigated the internal excitation of sputtered Ag_n clusters by laser spectroscopic methods. For dimers he derived from the spectra vibrational and rotational temperatures around 2700 K and 6700 K, respectively, in very good agreement with corresponding MD simulations [245–247]. For

larger clusters, a large amount of internal energy was inferred from the experiments; for example, around 50 % of the sputtered Ag_6 clusters are formed with internal energies in excess of 0.75 eV. The internal energy scales roughly linearly with the cluster size n [247].

a) Mass Distributions of Neutral Clusters

Some of the unresolved issues in cluster emission concern the size (mass) distribution of the cluster flux and how this depends on the binding energy, the internal energy, and the ionization in the case of charged clusters. The emission mechanisms and the mass distributions of cluster species sputtered from metal and semiconductor targets have been discussed repeatedly in the literature [12, 59, 223]. Most of the early work has been performed using mass spectrometry of sputtered *ions*. Using this technique, *Katakuse* and coworker [269–271] were able to detect sputtered ionized clusters containing more than 200 atoms. Because the ionization processes of those cluster ions are not well understood, it was questioned, however, to what extent their flux is representative of the total flux of the respective species. To circumvent these uncertainties, techniques for the post-ionization of sputtered *neutral* species were devised. Originally, electrons were utilized for that purpose [75, 272–279], but with the application of more powerful laser systems for the photoionization of neutral species, the accessible range of cluster size could be extended dramatically, becoming comparable now [280–282] to that covered by ionized clusters. The *neutral* clusters studied most intensively were Al_n ($n \leq 12$), Ag_n ($n \leq 60$), Cu_n ($n \leq 20$), Ge_n ($n \leq 7$), Ga_n ($n \leq 13$), In_n ($n \leq 200$), Nb_n ($n \leq 10$), and Ta_n ($n \leq 9$) [133–142, 283–289], where n is the number of constituent atoms. Sputtering of the respective elemental targets was typically performed by inert-gas ions with an energy of a few keV. Generally, a strong decay of cluster abundance with n is observed. For homonuclear clusters a falloff of the yield Y_n according to a power dependence on n has been reported in essentially all cases

$$Y_n \propto n^{-\delta} \,. \tag{18}$$

The exponent δ turned out to depend on the bombardment conditions; specifically, an empirical relation of δ with the sputtering yield Y of the target was established: an increasing yield causes a weaker decay of cluster abundances, i. e., results in a larger fraction of larger clusters. The values of δ were found to vary mostly in a range from ≈ 9 to ≈ 4 for cluster sizes $n \leq 30$. However, for larger In_n clusters, $20 \leq n \leq 100$ [282] and for Au_n clusters with $n \geq 500$ [280], a decay exponent $\delta \approx 2$ was found. This transition of δ with cluster size is shown in Fig. 8 for In_n cluster [282]. A value of $\delta \approx 2$ is in agreement with two different theoretical concepts: an approach due to *Bitensky* and *Parilis* [290] treats cluster emission as the result of a shock wave which is initiated by the primary ion impact; it expands inside the solid

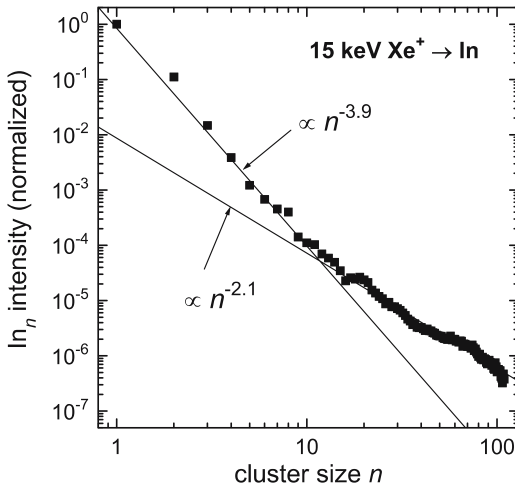

Fig. 8. Relative intensities of neutral In_n clusters sputtered from a polycrystalline indium surface under bombardment with 15 keV Xe^+ ions. The data have been normalized to the intensity of In atoms. Power-law fits according to (18) are shown, indicating the presence of two different exponents δ [282]

and fractures the surface, thus leading to fragmentation and the ejection of clusters into the gas phase. In fact, indications of shock waves have been found in MD simulations of sputtering [291]. The resulting size distribution of ejected species is predicted to be a power law with a fixed decay exponent around $\delta = 2$. The second model, published by *Urbassek* [292, 293], describes the cluster emission process as a thermodynamic expansion of the near-surface irradiated volume through the liquid–gas coexistence regime. Also in this model, a power law size distribution is predicted with a fixed exponent $\delta = 7/3$.

b) Energy Spectra of Neutral Cluster

Sputter experiments at bombarding energies of a few keV and using post-ionization by electron impact [274, 275, 294] produced energy spectra of *small* neutral clusters (dimers and trimers) that qualitatively agree with the predictions of a double-(or multiple-)collision ejection process [229, 273] in which the atoms that will form the cluster are hit individually by target atoms. Energy spectra of neutral Cu_2 and Cu_3 recorded under very low impact energies (< 1 keV) [211] are discussed in Sect. 5.1.1. *Larger* neutral clusters became accessible only with the utilization of photoionization techniques for the detection of neutral species. Detailed studies were carried out for Al_n ($n \leq 6$), Cu_n ($n \leq 6$), Ag_n ($n \leq 7$), In_n ($n \leq 8$), Ge_n ($n \leq 4$) [133, 135–142]. The energy distributions of the large neutral clusters recorded by these means typically showed that the most probable emission energy differs little

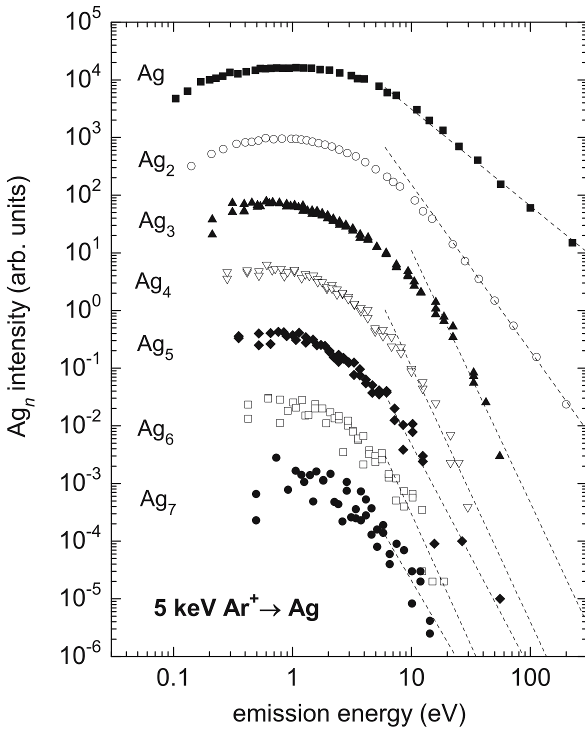

Fig. 9. Kinetic energy distributions of neutral Ag atoms and Ag_n clusters sputtered from a polycrystalline silver sample by 5 keV Ar^+ ion bombardment. (The relative scaling of the different curves is arbitrary.) The *dotted lines* are power-law fits of the asymptotic high-energy dependence of the atom and cluster spectra [135]

for atoms and clusters, while the exponent α in the high-energy decay, $E^{-\alpha}$ (9), is slightly higher for clusters than for the respective atoms, but is largely *independent* of the cluster size. For example, 3.9 keV Ar^+ irradiation of Cu produced $\alpha \approx 2.8$ for Cu-atoms and $\alpha \approx 3.5$ for Cu_n with $2 \leq n \leq 6$. Similar results were reported for other clusters. The respective energy spectra for photoionized neutral Ag_n clusters ($n \leq 7$) [135] are depicted in Fig. 9. The asymptotic exponents derived are: $\alpha \approx 1.7$ for monomers, $\alpha \approx 2.9$ for dimers and $\alpha \approx 4$ for all larger clusters. Although for large clusters these values are somewhat uncertain due to the limited energy range, it is obvious that the measured energy spectra are quite similar for all cluster species.

MD simulations of the energy spectra of Ag_2 dimers are in very good agreement with respective experimental data [244]. Such simulations also show that for keV irradiation sputtered dimers originate with highest probability from nearest-neighbor sites and that a true double-collision mechanism accounts for the majority of emitted dimers. For larger clusters, however, simulations [248] provide rather convincing evidence for an emission mech-

anism in which, due to correlated motion in the collision cascade, a group of neighboring atoms at the surface receives, simultaneously, nearly parallel momenta, effecting the emission of a group of bonded atoms. They indicate, furthermore, that the ejection of (large) clusters occurs at a *late stage* of the particle emission process; the larger the cluster, the later it is ejected. Very probably, cluster emission is correlated with single high-yield events.

c) Energy Spectra of Ionized Cluster

Energy spectra of *cluster ions* have been shown already in Fig. 7a for Si_n^- species. Figure 10 depicts another set of such energy spectra for several negative C_n^- cluster ions sputtered from graphite by 14.5 keV Cs^+ ions [261, 262]. In this graph, the spectra are seen to extend to an *apparent* "negative" emission energy. These negative tails are due to the decay of cluster species during their passage through the accelerating field of the mass spectrometer: the resulting daughter ions carry only a fraction of the full accelerating energy as compared to the intact species that experience the full acceleration. Although the energy spectra of intact cluster fall off rather steeply with increasing (positive) emission energy (cf. Fig. 10), an appreciable number of cluster ions with an energy of ≈ 10 eV is still observed. This finding indicates that, despite the extensive decomposition, these C_n^- cluster ions can be very stable entities. The fragmentation of C_n^- cluster ions has been examined in detail in [261, 262]. Similar energy spectra were reported in [295]. Below such fragmentation processes are discussed more thoroughly.

In related investigations the *ionization probability* of sputtered *negative* cluster ions was studied [296, 297]. For sputtered atomic ions several theoretical concepts were proposed [143, 188, 298] to model the ionization probability P in the ejection event. As discussed in Sect. 4.1.1, quite often, they predict an exponential dependence of P on the work function Φ of the specimen which, for sputtered negative ions, is given by (16). By varying the amount of Cs incorporated into the near-surface region of a graphite specimen [296], the concurrent work-function variations $\Delta\Phi$ and the ionization probabilities P^- of C_n^- cluster ions were found to correlate in agreement with (16). Some of these results are depicted in Fig. 11; they indicate that a resonant electron transfer process is effecting the ionization of those cluster species.

The *ionization probability* of sputtered *positive* Ag_n^+ ($n \leq 40$) and In_n^+ ($n \leq 200$) cluster ions under 15 keV Xe^+ bombardment was studied by *Wucher* and coworkers [282, 289]. They compared the yields of positive cluster ions with those of photoionized neutral cluster measured in the same experimental setup. Generally, the ionization probability is low ($10^{-3} - 10^{-4}$) for small clusters, but increases with cluster size and reaches an almost constant and rather high value for large clusters: $0.05 - 0.1$ for Ag_n^+ [289] and ≈ 0.3 for In_n^+ [282].

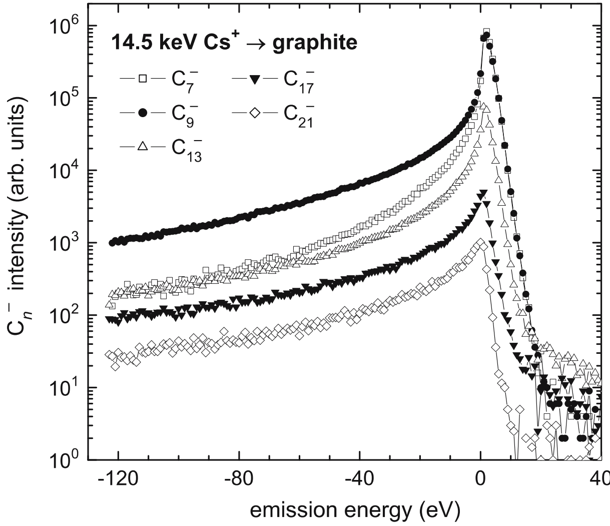

Fig. 10. Emission energy spectra of several C_n^- cluster ions sputtered from graphite by 14.5 keV Cs^+ ion bombardment. The signal at "negative" energies is due to fragment ions [262]

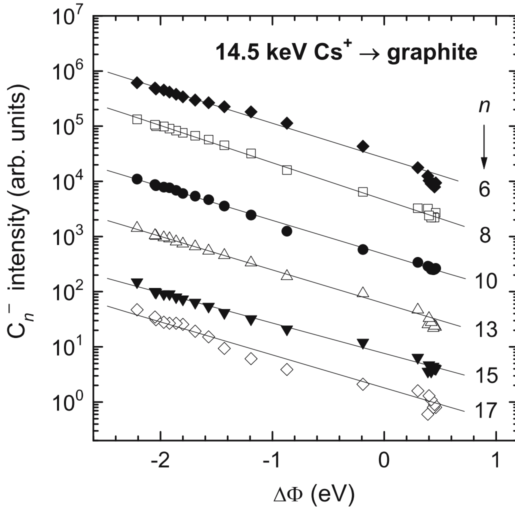

Fig. 11. Emission-energy integrated intensities of several C_n^- cluster ions sputtered from graphite by 14.5-keV Cs^+ ions *versus* the work function change $\Delta\Phi$ induced by Cs incorporation. An exponential dependence of the ionization probability on $\Delta\Phi$ in accordance with (16) is found for all cluster [296]

d) Energy Spectra of Large Organic Molecules

Large molecules sputtered (desorbed) from the surface by keV-particle bombardment [224, 299, 300] are widely used in secondary ion mass spectrometry for the characterization of organic [86, 225, 226] or biological materials [227]. A common way to achieve high yields of large molecular ions in SIMS of organic materials and low molecular weight polymers is the cationization of the sputtered particles by complexation with metal substrate atoms, an approach pioneered by *Cooks* and coworkers [301]. In order to obtain meaningful information, the ejection process should yield molecular species representative of the specimen; ideally, these should be the parent molecule or a distinct pattern of smaller fragment species. Somewhat surprisingly, this goal can be reached for a very broad class of (organic) materials; notwithstanding this success, the understanding of the emission and fragmentation of large molecules is still rather incomplete. The fundamental issue can be condensed probably into the following question: How can molecules comprising hundreds if not thousands of atoms [302] be ejected from the surface of a solid without breaking apart?

There appears to exist now a general consensus that under low- and medium-keV ion bombardment (the energy regime considered in this chapter) collision cascades in the near-surface region of the solid are the primary and necessary initial step for molecule ejection. However, multiple-collision events may play a dominant role [303]. (MeV-ion bombardment [60] and laser irradiation [304–306] constitute other means extensively utilized for the desorption of large molecules.) Several models [272, 274, 275, 307–312] were put forth to describe the sputtering of small clusters or molecules, but concepts for larger molecules remained sparse [224, 313, 314].

Energy spectra of a variety of organic molecules sputtered from different targets were recorded [274, 275, 315–325] to elucidate the pertinent emission processes. In all of these earlier studies *secondary ions* were monitored. Generally, those investigations indicated that the energy spectra of large molecules may peak at low emission energies ($1 - 2\,\mathrm{eV}$), can be very narrow ($< 1\,\mathrm{eV}$) and exhibit a rather steep falloff towards high emission energies. Furthermore, the occurrence of gas-phase decomposition of sputtered species was inferred from the observation of kinetic-energy deficits.

Parent and Fragment Molecular Ions

It was envisaged that from detailed comparisons between experiments and molecular dynamics simulations, progress in the understanding of the emission of molecular parent and fragment species under ion bombardment might be achieved. Using ToF-SIMS, *Bertrand* and *Delcorte* [326–335] carried out extensive investigations into the emission of sputtered molecular *ions* from a variety of targets. They studied in particular ion yields, kinetic energy distributions, disappearance cross sections, and fragmentation processes. In a joint effort with *Garrison's* group, MD simulations developed in this group were

employed [336–341] to elucidate the atomistic processes of molecule emission under keV ion impact and to compared these data with the experimental results. Exemplary results of these (comparative) studies will be outlined here.

The general theme in these investigations is the identification of the mechanisms by which large molecules (and possible fragment species) are sputtered. In the case of polymers and organic adsorbates (typically on a metal such as silver), large characteristic fragments and intact parent ions are detected. Figure 12 illustrates some results from these investigations [337], showing measured and computed kinetic-energy spectra of selected fragments and the parent ion ($M = 474\,\text{amu}$) sputtered from polystyrene tetramers adsorbed on a Ag substrate. The agreement between the experiment (closed symbols in Fig. 12) and the MD simulation (solid lines) is satisfactory. For the larger fragments the high-energy part of the spectra is more intense in the simulation. Excluding, however, all molecules with an internal energy exceeding the threshold for dissociation (dashed lines in Fig. 12), the agreement with the experimental data becomes remarkable for those fragment species [337]. In general, the kinetic energy of the *fragments* decreases with increasing size of the species [326–328], an observation corroborated by MD simulations if dissociation reactions are taken into account [337]. In addition, a correlation between *kinetic* and *internal* energy [337, 342] was found.

The emission of *large parent* and *parent-like ions* is exemplified in Fig. 13 which depicts energy spectra of molecular *ions* ejected from triacontane (TC, $C_{30}H_{62}$, molecular weight MW=422.8), dibenzanthracene (DBA, $C_{22}H_{14}$, MW=278.35), and polystyrene (PS, MW ≈ 700) oligomers adsorbed as thin films on Ag [331, 343]. Sputtering was effected by 15 keV Ga^+ ions. Several quite general observation were drawn from these data: (i) the high-energy tails of the spectra extending even beyond 10 eV clearly support a collisional emission process; (ii) the Ag-cationized molecules are more energetic than the characteristic fragment and parent ions; (iii) the width of the kinetic energy distributions increases with increasing molecular size for these parent-like ions, an effect very distinct for Ag-cationized PS oligomers: the FWHM increases from $\approx 4.5\,\text{eV}$ for $M \approx 600\,\text{amu}$ to $\approx 6\,\text{eV}$ at $M \approx 3000\,\text{amu}$ [343]; (iv) the energy distributions are often broader for the parent (or parent-like) molecules than for fragments. In view of the comparatively high kinetic energy these parent-like ions exhibit, a process involving the *concerted action* of several substrate atoms was suggested to be responsible for the emission of such large organic molecules.

Simulation of Molecule Emission Events

As demonstrated by corresponding MD simulations, several of the abovementioned findings related to parent and fragment ion formation can be explained by specific emission mechanisms. The ejection of characteristic fragments is primarily due to the direct interaction between the primary particle

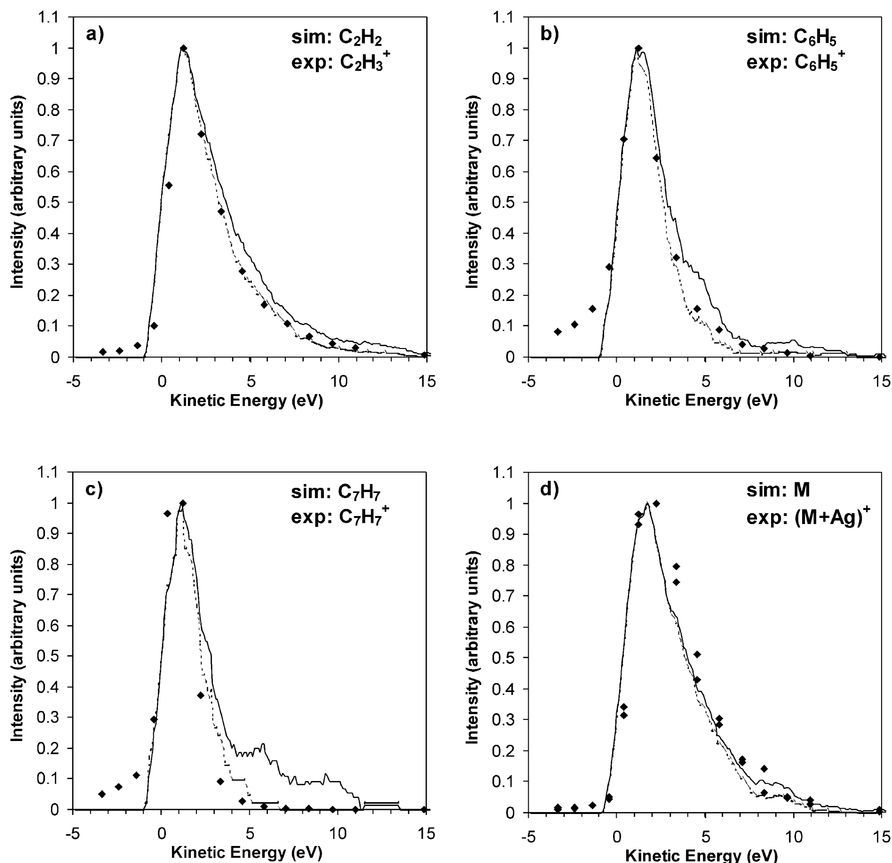

Fig. 12. Comparison of kinetic energy distributions of selected fragments and the parent species ($M = 474\,\text{amu}$) sputtered from polystyrene (PS) tetramers adsorbed on Ag(111) obtained from MD simulations (500 eV Ar bombardment) and experiments (12 keV Ga^+ bombardment). *Full lines* correspond to the computed spectra including all of the fragments with the selected formulas and *dashed lines* to the computed spectra obtained for fragments with internal energies of less than the calculated threshold for dissociation. Experimental distributions are indicated by *black diamonds* [337]

and the organic adsorbate. In contrast, desorption of intact molecules is induced by collision cascades near the sample surface. The emission of energetic intact molecules is best explained by a cooperative uplifting mechanism in which substrate atoms with similar momenta push the molecule upward [337]. Two such events derived from those simulations are shown in Fig. 14 for the sputtering of polystyrene tetramers on Ag(111) by 500 eV Ar. Frame (a) is common to the two considered events and shows a side view of the sample, before starting the action. Frames (b) and (c) show successive time steps of the

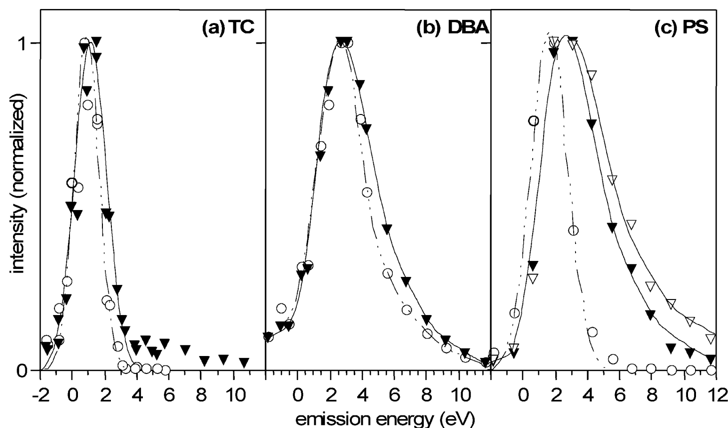

Fig. 13. Kinetic energy distributions of parent-like ions sputtered by 12 keV Ga^+ ion irradiation from triacontane (TC, $C_{30}H_{62}$), dibenzanthracene (DBA, $C_{22}H_{14}$), and polystyrene (PS) oligomers adsorbed on an Ag surface. (**a**) TC: $C_{30}H_{60}^+$ (*open circles*), $[C_{30}H_{60}]Ag^+$ (*closed triangles*); (**b**) DBA: $C_{22}H_{14}{}^+$ (*open circles*), $[C_{22}H_{14}]Ag^+$ (*closed triangles*); (**c**) PS: $C_8H_8{}^+$ (*open circles*), $[C_4H_9(C_8H_8)_nH]Ag^+$ with $n = 4$ (*closed triangles*) and $n = 12$ (*open triangles*) [343]

first trajectory, whereas frames (d)–(f) correspond to the second trajectory. In the first event, frame (b) shows that the molecule is pushed by a single silver atom moving upward at approximately 300 fs. This collision transfers sufficient momentum to eject the molecule. After 1300 fs, the molecule has left the surface and flies toward the vacuum, frame (c). In this case, the shape and orientation of the molecule have been significantly altered by vibrational and rotational motion. The molecule has a *kinetic* energy of 1.9 eV and an *internal* energy of 11.1 eV at the end of the event.

A different scenario unfolds in the second trajectory. Frame (d) of Fig. 14 indicates that the action starts at the approximate time of 200 fs, with the soft collective motion of the silver atoms underneath the PS molecule. Of note is that the fast silver atom leaving at the bottom right of frames (d) and (e) does not impart its momentum to the molecule. At 300 fs, the gentle, cooperative uplifting of the molecule is underway. A corresponding movie indicates that at least five silver atoms act together to lift up the PS tetramer. Frame (f) shows a later view of the ejected molecule with an accompanying silver atom. It is remarkable that the orientation of the molecule in the vacuum is nearly unchanged, suggesting this time that the vibrational and rotational excitations are low. Indeed, the detailed analysis of the sputtered species confirms that this molecule has 6.7 eV of *kinetic* energy and 7.1 eV of *internal* energy at the end of the trajectory. Hence, this mechanism produces a stable molecule with a relatively high kinetic energy.

Although the total energy transferred to the departing molecule is very similar in the two examples illustrated above (13.0 and 13.8 eV, respectively),

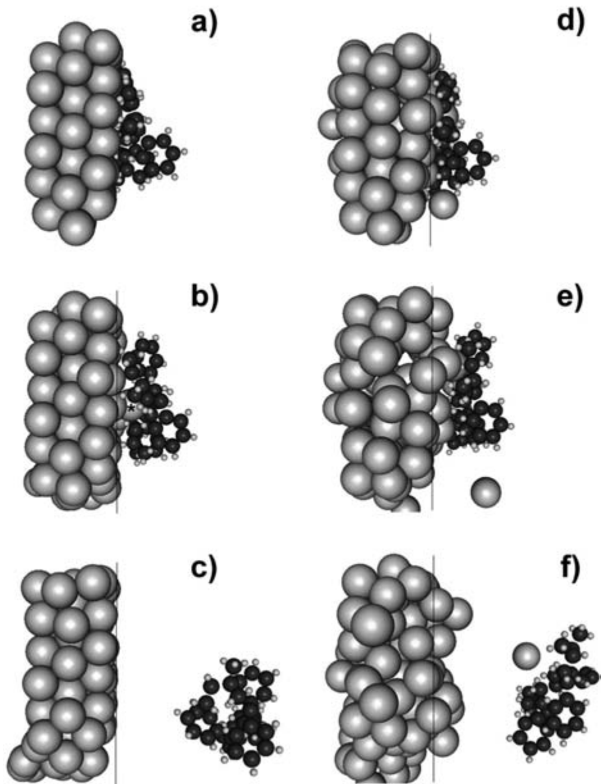

Fig. 14. Two different ejection mechanisms computed for entire PS tetramers. Frames (**b**) and (**c**) correspond to the first event and frames (**d**–**f**) to the second event. Frame (**a**) shows the initial situation of the PS tetramer on the surface, common to both events. The other frames show the time evolution of the two events. First event: (**b**) 300 fs; (**c**) 1300 fs. Second event: (**d**) 200 fs; (**e**) 300 fs; (**f**) 800 fs [337]

the partitioning of this energy in the internal and translational modes is completely different. The first molecule is slow and internally excited, whereas the second is faster but relatively cool.

Related simulations [338] showed that above 1 keV bombarding energy, in addition to trajectories consisting of successive collisions between individual atoms, a significant number of high action trajectories were observed in which several hundreds of substrate atoms are moving simultaneously. These events can generate unusually high emission yields of substrate atoms, clusters, and polystyrene molecules. A detailed examination of the energetic parts of the cascade ("collision trees") shows that high sputtering yields occur when most of the primary particle energy is quickly dissipated among silver (substrate) atoms belonging to the top silver layers [337,338]. In addition, it is shown that high emission events influence not only the yield but also the kinetic energy

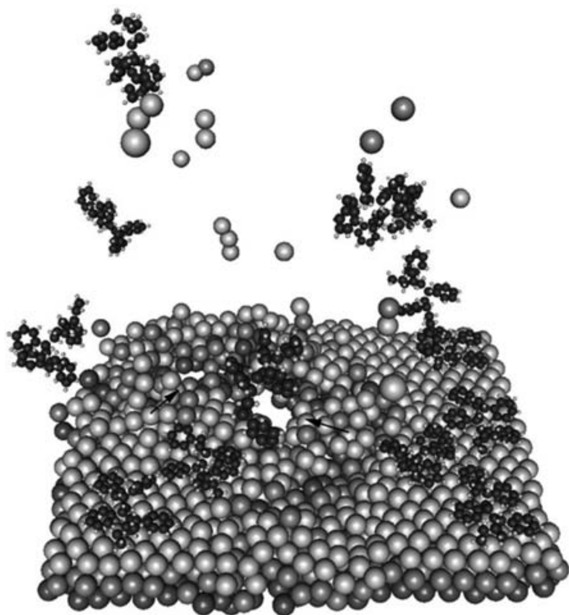

Fig. 15. Mechanistic view of a high-yield sputtering event induced in polystyrene tetramer/Ag(111) sample by a 5 keV Ar atom. The formation of a temporary crater is indicated by *black arrows* [337]

distributions of ejected polystyrene molecules: *high-yield* events can give rise to molecules with *higher* kinetic energy. These results [338] indicate that trajectories falling in the "high yield" category are also capable of desorbing large intact molecules of ≈ 2000 amu. Figure 15 shows a MD snapshot [337] from such a *high-yield* event induced by 5 keV Ar in polystyrene on an Ag substrate. It is interesting to note that no fragments were produced in this event.

Other organic materials studied in such a comparative fashion by ToF-SIMS and by MD simulations include, for example, poly(ethylene terephthalate) (PET) [333] and self-assembled monolayers (SAM) of alkanethiols on gold [335, 344].

Neutral Organic Molecules

The majority of mass spectrometric data obtained for large sputtered molecules utilized *secondary ions*. Although detailed information about the ejection mechanisms could be derived in that way, this situation was not completely satisfying. The uncertainties associated with the, largely unknown, ionization processes in the course of the emission event made measurements based on sputtered *neutral* species highly desirable. The availability of adequate laser systems opened that venue: several groups explored the possi-

bility of detecting sputtered neutral organic molecules via photoionization secondary-neutral mass spectrometry [86]. Of course, also in this approach care has to be taken that the ionization step does not introduce artifacts in the measured signals [345–347].

Winograd's group [348–352] has examined in detail the ion-bombardment induced desorption of physisorbed neutral molecules from metallic single crystals. For example, time-of-flight distributions, angular distributions, and relative sputtering yields of *neutral* benzene molecules (C_6H_6) ejected from submonolayer to multilayer coverage of C_6H_6 on an Ag(111) surface have been measured by 8 keV Ar^+ ion bombardment [349]. Kinetic energy distributions of neutral C_6H_6 molecules sputtered by 8 keV Ar^+ from an Ag surface covered with 0.2 monolayers of C_6H_6 [353] are depicted in Fig. 16. For comparison, molecular dynamics simulations were used to examine the kinetic energy and angular distributions of C_6H_6 molecules from that system, C_6H_6 on Ag(111), and were found to match well with the experimentally measured spectra. Those MD data are also shown in Fig. 16. From the computations, a clear correlation between the *internal* energy and the *kinetic* energy of ejected molecules is derived: The molecules with higher internal energies tend to have higher kinetic energies [353]. If all emitted molecules with an internal *above* 5 eV are discarded from the simulation data (because of their possible fragmentation), the calculated energy spectrum corrected in this way fits the measured spectrum very well, see Fig. 16.

Associated molecular dynamics simulations [352] illustrated the different ejection mechanisms that can lead to ground- and excited-state molecules: a collision between a fast silver monomer and a benzene molecule desorbs a translationally energetic molecule that is internally excited. This type of collision is displayed in Fig. 17A. Such collisions not only impart sufficient kinetic energy to cause the desorption of the molecules, but also stretch bonds, distorting the molecule. Thus, these types of collisions provide a means of internal excitation. Collisions between an adsorbed molecule and several Ag atoms with similar momentum cooperatively lift off internally cool molecules. A rendering of the cooperative process is presented in Fig. 17B. It illustrates that this type of ballistic collision gently pushes the benzene molecule with little or no internal perturbation into the vacuum. Such collision scenarios might be applicable to a broad class of physisorbed molecules.

e) Decomposition of Sputtered Molecules

Metastable decay processes have been mentioned in Sect. 4.1.3 in the context of sputtering of C_n^- clusters; they are found also in the case of (large) organic molecules. Such unimolecular reactions have been monitored in secondary ion mass spectrometers and the decay rates and lifetimes of the parent ions have been determined. For *short* lifetimes, typically in the range 10^{-9}–10^{-7} s, the decomposition occurs in the acceleration region of the mass spectrometer; then, the metastable ions dissociate before having been accelerated to their

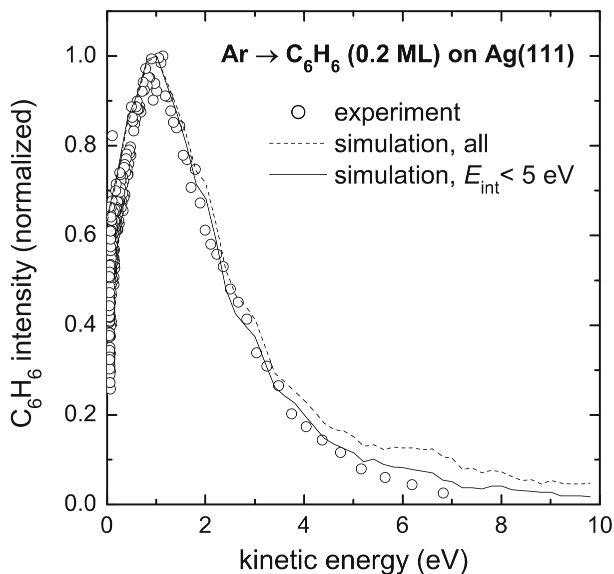

Fig. 16. The experimental kinetic energy distribution of *neutral* C_6H_6 molecules sputtered from a benzene layer (0.2 ML coverage) on Ag(111) by 8 keV Ar^+ ions (*circles*). The calculated kinetic energy distributions for all the ejected C_6H_6 molecules (*broken line*) and for all C_6H_6 molecules with total internal energies less than 5 eV (*solid line*) are given [353]

final energy (usually a few keV). The resulting daughter ions have therefore an energy deficit (as compared to an intact ion of the same mass) and an apparent "negative" energy in the respective energy distributions. For *longer* lifetimes, roughly in the 10^{-6}–10^{-4} s regime, the parent ion may dissociate in a field-free region of the spectrometer; if this happens to occur before the first energy-selective device, the daughter ions of a given reaction have the same energy deficit, which is independent of the decomposition time because they experience no acceleration in this case. Thus, they result in a well-defined peak in the energy spectrum and the mass of the neutral species lost in the reaction can be determined from the energy deficit [332]. According to the theory of unimolecular reactions [354], for a given reaction the number of metastable parent ions Y_p at time t is given by

$$Y_\mathrm{p}(t) = Y_0 \exp(-kt)\,, \tag{19}$$

where Y_0 is the initial number of parent ions and k is the decomposition rate, depending on the internal energy of the fragment. The number of daughter ions at time t follows then from

$$Y_\mathrm{d}(t) = Y_0 - Y_\mathrm{p}(t)\,, \tag{20}$$

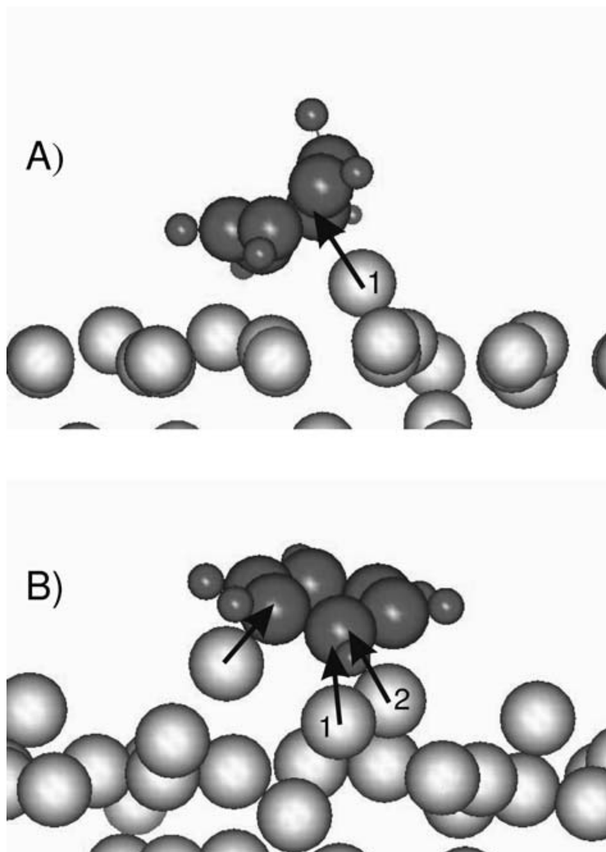

Fig. 17. Illustrations of molecular desorption mechanisms of C_6H_6 molecules from a benzene overlay on an Ag(111) surface by 500 eV Ar. These illustrations represent systems comprised of a monolayer or less of benzene molecules (*dark gray*) physisorbed to a metal surface (*gray*). The emission of internally and translationally hot molecules is depicted in (**A**). The desorption of molecules in the ground state is represented in (**B**) [352]

and its time derivative, that is, the time distribution of daughter ions, can be computed by

$$\frac{\mathrm{d}Y_\mathrm{d}}{\mathrm{d}t} = kY_0 \exp(-kt)\,. \tag{21}$$

In principle, this quite simple expression might be used to derive, from the experimental energy spectra, the values of the decomposition rate k; however, to perform such an evaluation two conditions have to be met: (i) the decay of a given parent ions follows predominantly a single reaction channel; and (ii) the internal energy distribution of the parent species is narrow, thus

corresponding to a specific value of k. Although the validity of these requirements is not certain a priori, this approach was used repeatedly to derive the decay rates and lifetimes of sputtered metastable clusters and large organic molecules (see, e. g., [256–259, 262, 329, 330, 332, 355]).

To illustrate this method, Fig. 18 displays the kinetic energy distribution of various organic molecules sputtered from polystyrene (PS) by 12 keV Ga^+ ions [332, 343]. The main peak in these spectra around zero energy corresponds to an ion sputtered off the surface and staying intact through its flight through the spectrometer. From these peaks a slowly decaying part of the spectra extends to "negative" energies, unto which well-defined peaks are superimposed. The gradual and monotonous falloff is due to a metastable decay of a short-lived parent molecule in the acceleration region of the spectrometer (see Fig. 10 for comparison). By contrast, the distinct peaks are the result of a decay reaction of long-lived metastable parent ions occurring in the field-free drift region of the spectrometer. From the energy deficits of the latter it is possible to assign these peaks to specific decay reactions. In the example shown in Fig. 18 they are formed by the reaction $C_xH_y^+ \rightarrow C_xH_{y-1}^+$ + H [332, 343]. Similar decay reactions have been observed for polyisobutylene [329, 330], but H_2 loss is the dominant decay channel in that case. From these data the half life for the H or H_2 loss reaction was determined to fall in the range from 10 to 100 µs.

4.2 Energy Spectra from Alkali Halides and Condensed Gases

The energy spectra presented in the preceding section were all obtained from materials (metals, semiconductors, and organic samples) for which *nuclear* energy loss is by far the dominant energy loss process for the projectile energy range considered here. By contrast, both for alkali halide specimens and for condensed gases, *electronic* energy loss mechanisms (i. e., excitation and ionization processes) become important or even dominant, even at bombarding energies of only a few keV. This is nicely illustrated by the (frequently carried out) comparison between ion and electron irradiation; for the latter nuclear energy losses are negligible, but still energy and angular emission spectra may be fairly similar to those for ion impact. Hence, under ion bombardment usually nuclear and electron loss processes have to be considered and, quite often, their relative contributions will depend on the ions' impact energy. Because a detailed discussion of sputtering effects induced by electronic processes is beyond the scope of this review, only some pertinent data will be presented. More thorough expositions are given in [60, 356].

4.2.1 Alkali Halides and Related Materials

Alkali halides have attracted considerable interest in the field of particle-surface interactions because of the finding that even under electron and photon irradiation particle emission is observed [357]. From conservation of mo-

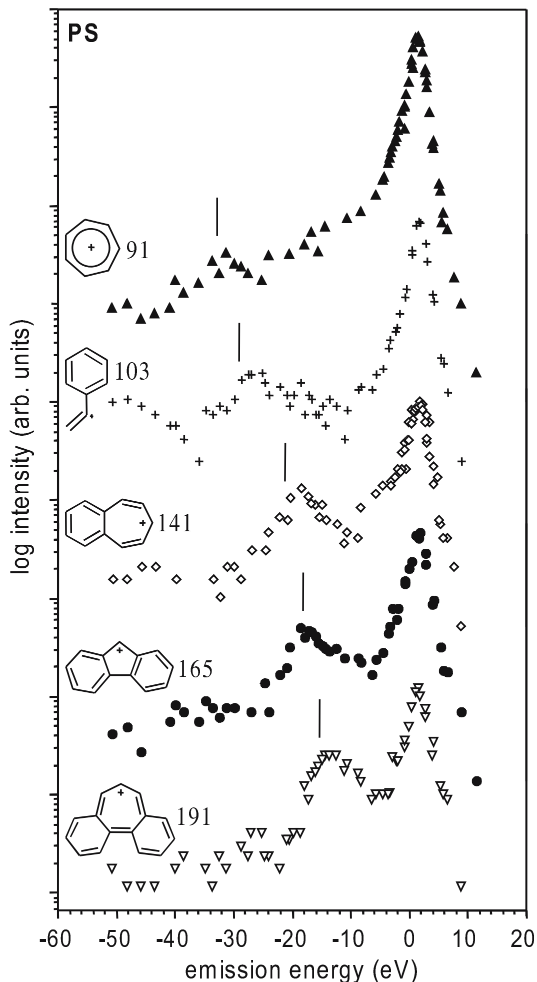

Fig. 18. Kinetic energy spectra of unsaturated molecular ions sputtered from a polystyrene (PS) thin film on a Ag substrate. The *vertical bars* indicate the theoretical energy deficits for the fragmentation reactions $C_xH_y^+ \rightarrow C_xH_{y-1}^+ + H$ [343]

mentum, only inelastic (electronic) energy-loss processes can effect this kind of sputtering. These mechanisms have been investigated in great detail before [357–359] and will not be outlined here. It suffices to say that electronic excitations in alkali halides often are ascribed to the migration of H-centers (an interstitial halogen atom) which leads to the emission of halogen atoms and consequently to the formation of a metal overlay on the surface [357,360–362]. As alkali metals have usually comparatively high vapor pressures, those metal layers may just evaporate thermally [357]; hence, the sample temperature can be a decisive parameter in alkali halide sputtering and a thermal

(low-energy) component in an energy spectrum could be due to such an evaporation of the metal species.

Apart from electronic processes that activate the motion of interstitial halogen atoms (and lead eventually to their release), regular collision cascades will occur under ion bombardment that affect both constituents of the alkali halides, leading to a corresponding sputtered flux. Only the latter processes are relevant in the present context. Several of the early measurements of energy spectra from alkali halides and related compounds [363–365] indicated that two or even three distinct components are required to describe the spectra: (i) a collisional contribution and (ii) one or two contributions of the general form $E\exp(-E/kT)$, where T could be either the actual target temperature or a "spike" temperature which was in the range 1000–2000 K. Later these experimental findings were disputed on the basis that in all of them pressed powders were employed as targets which are prone to oxidize strongly or even to transform into hydroxides; in both cases the results could drastically differ from those obtained from clean surfaces. In fact, in sputtering single crystals of NaCl by 15 keV Ar^+ the velocity distributions were found to be purely *thermal* [366], in clear contrast to previous measurements [365] of that material in powder form. Velocity spectra under electron bombardment were found to be identical to those under ion bombardment for a range of temperatures [367, 368] and the distributions could be fitted by Maxwell-Boltzmann distributions with the respective target temperatures.

Ion bombardment of single-crystal CaF_2 at temperatures up to ≈ 500 K resulted in velocity distributions, determined by DSLFS, which were purely collisional and could be fitted using a surface binding energy of 1.4 eV [367]. For higher temperatures, however, a thermal component started to appear in the energy spectra which, for temperatures above 650 K, became the dominant contribution to the sputtered flux. A tentative explanation for these findings is as follows [60]: inelastic electronic excitations are a prominent energy loss mechanism also for ions, leading to the desorption of the halogen atoms as under electron bombardment. Under ion bombardment, however, any forming residual metal layer will be (partially) removed and an equilibrium between electronic processes leading to halogen loss, thermal evaporation and cascade sputtering of the metal might be established. Thus, while for NaCl even at room temperature thermal evaporation dominates, for CaF_2, owing to the lower vapor pressure, the transition from cascade sputtering to evaporation occurs only at ≈ 650 K. These arguments may explain the observed differences between the velocity distributions for Na from NaCl and Ca from CaF_2 under ion bombardment. However, other explanations have been put forth [368] and the matter appears to be not resolved yet.

4.2.2 Condensed Gases

Energy spectra were recorded for a variety of condensed gases and frozen materials: the rare gases Ne, Ar, Kr, and Xe [369–376], the diatomics O_2,

N_2 and CO [377–383], and several triatomic and polyatomic gases such as H_2O, D_2O [384–387], CO_2 and others. Because the cohesive binding energies of these frozen gases are roughly in the range 0.03–0.5 eV and are therefore by an order of magnitude or more lower than those of metals, the energy deposited into atomic motion is shared among a comparatively large number of atoms. Furthermore, their sputtering yields are much higher than those of metals. Other characteristic features of condensed gases like their very low thermal conductivity and the high electrical resistance may also play important roles in the energy dissipation processes upon ion (or electron) irradiation.

In the regime of collisional sputtering, i. e., when the nuclear stopping cross section S_{n} is higher or similar to the electronic stopping cross section S_{e}, the measured energy spectra from condensed gases often exhibit a high-energy falloff proportional to E^{-2} as found for metals. However, the maximum of the distributions is typically found at an energy considerably lower than half the cohesive energy [373]; in addition, the total sputtering yields are much higher than would be predicted by linear collision cascade theory. Hence, a description of condensed gas sputtering solely in terms of linear collision cascades appears to be not adequate. To resolve these discrepancies, several alternative concepts or modifications of the linear collision cascade approach were proposed [370, 388, 389].

Apart from the purely collisional part additional contributions due to other mechanisms have been frequently noted in the energy distributions from condensed gases. In order to comply with these observations, *Pedrys* [375] deconvoluted the energy spectra of Xe atoms sputtered by Xe^+ ions (0.1–9 keV) from frozen xenon and demonstrated the presence of two different components: one, at short flight times (high emission energies), could be fitted by a collisional spectrum using the correct planar surface potential ($U = 0.16\,\mathrm{eV}$); the remaining second component falls off rapidly at emission energies above $\approx 1\,\mathrm{eV}$, but constitutes a substantial fraction of the total yield. Similar deconvolution procedures were found to work also for other condensed gases [376, 387], the relative magnitude of the two components depending strongly on the bombarding energy: the non-collisional (second) component was found to vary, above certain values of S_{n}, with the second or even the third power of the nuclear stopping cross section, i. e., S_{n}^2 or S_{n}^3. This above-linear dependence was explained by the presence of a high energy density in the collision region, the energy being shared among a large number of atoms which are in motion. Such an "elastic collision spike" might be responsible for the high sputtering yields typically observed for condensed gases. When such a spike volume intersects the surface, atoms or molecules are ejected either by evaporation or hydrodynamically over a time range of $10^{-12} - 10^{-10}$ s during which the spike loses energy to its surrounding. Computer simulations [390] support this notion.

The theoretical models devised to describe the sputtering process from condensed gases have been summarized in [356, 391]. An interesting concept

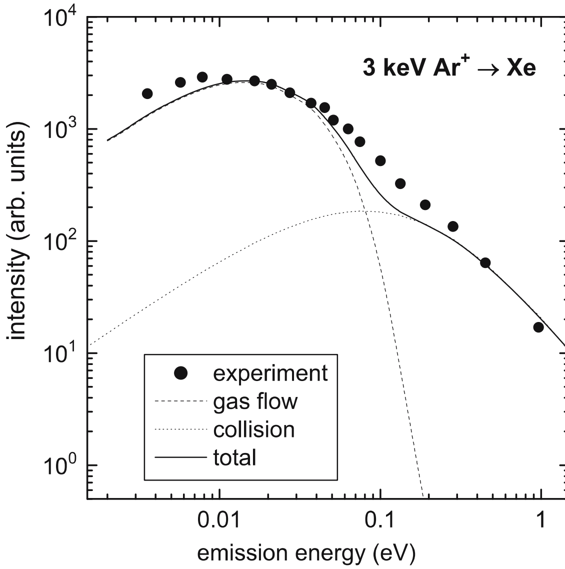

Fig. 19. Energy spectra of Xe atoms sputtered from frozen xenon by 3 keV Ar^+ ions. *Open circles:* experimental results; *dotted line:* collision cascade contribution; *broken line:* gas-flow contribution; *solid line:* sum of gas-flow and collision contributions [311]

is the *gas-flow model* of *Urbassek* and *Michl* [311]; it assumes that within a certain part of the cascade volume the recoiling atoms have received enough energy to bring the solid above the critical point, i. e., into a gaseous state. This volume is free to flow into the vacuum until energy dissipation and recondensation terminate the expansion. The molecular flow was modeled to be collision-free and the required dissipation of energy was simulated by an imaginary force acting on the streaming particles. Figure 19 shows data from that approach, comparing a theoretical energy distribution with an experimental one for 3 keV Ar^+ bombardment of condensed Xe [311]. Two contributions were taken into account: one corresponding to linear cascade sputtering and one determined by gas-flow sputtering. The low-energy portion of the spectrum in Fig. 19 and of similar ones [311] is reproduced quite well by the gas-flow contribution which constitutes a major fraction of the total yield. As a consequence, the typical collision-cascade energy spectra are strongly altered. Whereas the high-energy behavior ($\approx E^{-2}$) remains largely unchanged, the maximum of the energy spectra is shifted to much lower energies. The computations for Ar^+ ions show a slight dip in the energy distributions (cf. Fig. 19), separating the contributions of the cascade and the gas-flow process. These conditions apparently represent a transition regime in which the cascade "temperature" approaches a threshold value and the gas flow is then becoming increasingly restricted.

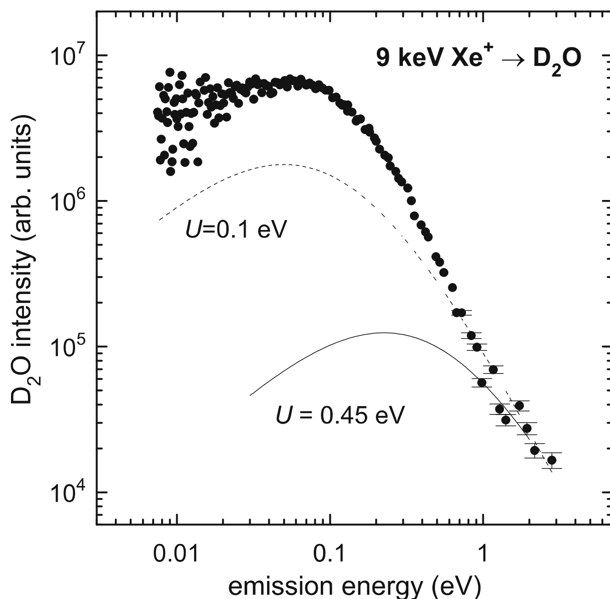

Fig. 20. Kinetic emission energy distributions of D_2O molecules sputtered from water ice (D_2O) by 9 keV Xe^+ ions. The *solid* and *dashed lines* represent energy spectra according to (8) with values of the surface binding energy U of 0.45 and 0.1 eV, respectively [387]

Sputtering from frozen molecular samples is complicated by the fact that the incidence beam often modifies the chemical composition of the irradiated compound. New and sometimes chemically reactive species might be formed in the interaction zone, giving rise to a mass distribution different from the original target composition. Another problem related to molecular specimens is associated with the dissociation of ejected molecules during their passage through the mass spectrometer. An example for the sputtering of a frozen molecular target is presented in Fig. 20. It depicts an energy spectrum obtained from sputtering of water ice by Xe^+ ions [387], detecting D_2O molecules (heavy water was used to reduce background problems). The spectra taken for all impact energies investigated (1–9 keV) exhibit a high-energy slope consistent with (8), i.e., a high-energy slope of E^{-2}, but the peak energy corresponds to a surface binding energy (≈ 0.1 keV) much lower than the sublimation energy of water ice of 0.45 eV. The solid and dashed lines in Fig. 20 present such a collision cascade distribution with surface binding energies of 0.45 and 0.1 eV, respectively, fitted to the high-energy part of the experimental data. The component of the energy distributions due to collision-cascade sputtering was found [387] to decrease with increasing bombarding energy; this observation is similar to the findings for the sputtering of frozen Xe discussed above [375].

4.3 Angular Distribution of Sputtered Species

The angular distribution of sputtered particles recorded, by suitable means, outside of the target reflects, at least to some extent, the directional flux of recoiling atoms *within* the sample. Any anisotropy in this internal flux distribution, caused for example by the anisotropic arrangement of atoms in a crystalline solid or by compositional gradients within the escape depth of sputtered species, is expected to translate into an angular spectrum which may distinctly deviate from that of a random specimen. Hence, in the following sections angular distributions obtained from (i) amorphous and polycrystalline targets (which may, if texture-free, approximate a random solid), (ii) single crystals, and (iii) multicomponent targets will be discussed.

4.3.1 Angular Distributions from Amorphous and Polycrystalline Targets

The differential expression of the sputtering yield, (6), predicts a cosine law for the polar angular distribution of the sputtered flux from an amorphous sample. However, pure cosine distributions are rarely observed. The deviations found at low bombarding energies will be outlined in Sect. 5.2. At higher energies the measured distributions often are found [392–405] to be over-cosine and can be described empirically by $\cos^y\theta$, where y is used as a fitting parameter. Values of y varying between 1.0 and 2.0 have been reported, but in some cases also much larger values have been found. Possible explanations for the over-cosine emission have been based on a surface-induced anisotropy of the recoil flux below the surface and/or anisotropic surface scattering of the flux passing through the surface. *Robinson* [406] suggested that an atom leaving the surface at an oblique angle experiences a net deflection toward the normal because of an asymmetric distribution of scattering atoms. Expressions for y based either on theoretical arguments [36] or on results from computer simulations [407] have been proposed.

The transient from under-cosine (at low energies) to over-cosine distributions is clearly illustrated also in TRIM.SP simulations of Ne^+ bombardment of Ni [68] and of self-sputtering of C, Ni, and W [408]. Increasing the Ne^+ impact energy from 50 eV to 5 keV the change occurred at about 300 eV. On the other hand, the mass of the projectile (H, He, Ne, Ar, and Xe, respectively) appears to have little influence on the distribution for 1-keV bombardment [68].

Figure 21a displays angular spectra obtained from a Ge specimen by 80 keV Ar^+ ion-bombardment at normal incidence [398]. An over-cosine distribution was observed that was fitted by $\cos^y\theta$, with $y = 1.57$. The respective data [398] recorded for impact energies from $\approx$ 1 keV up to 320 keV show y to increase from a value of ≈ 1.3 to ≈ 1.6 between 1 and 80 keV, while decreasing for higher energies to ≈ 1.4 at 320 keV, see Fig. 21b. This energy-dependent variation of the value of y could be reproduced, almost in

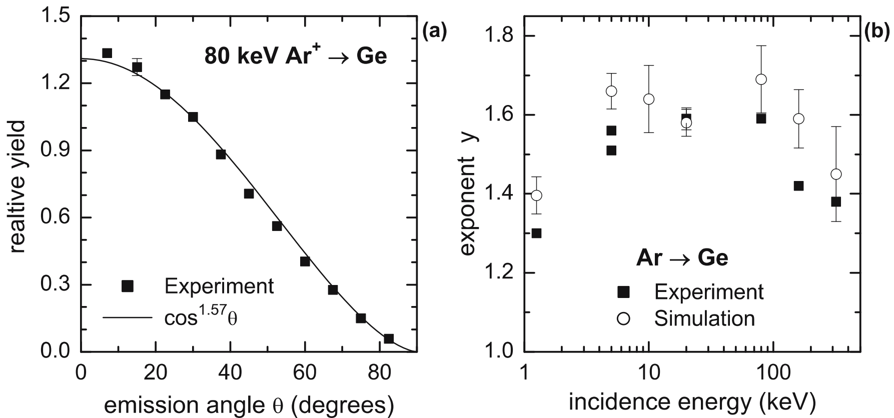

Fig. 21. (**a**) Polar angular distribution of material sputtered from amorphous Ge by 80 keV Ar^+ (*full symbols*) in comparison to a $\cos^{1.57}\theta$ distribution (*solid line*). The data are normalized to correspond to the same absolute yield as that of a pure cosine distribution. (**b**) Exponent y from fits of $\cos^y\theta$ of experimental (*solid squares*) and computed (*open circles*) angular germanium distributions versus Ar^+ ion energy [398, 409]

a quantitative fashion, by Monte-Carlo computer simulations [409]; the respective results are included in Fig. 21b. These calculations found a strongly backward directed recoil flux close to the surface that gives rise to the pronounced over-cosine emission spectra. A non-uniformity in the distribution of the deposited energy at the surface was identified [409] as the most likely cause for that anisotropic recoil flux.

Cosine-type distributions are usually not observed under *oblique ion incidence*. Then, the emission distribution is often peaked at or near the specular direction [410–412]. A correlation between the dominant angle of ejection and the total sputtering yield was reported by *Betz* et al. [413, 414]: the lower Y the more is the emission direction peaked towards the specular direction. In the single knockon regime, this preferred emission is even more pronounced, as demonstrated both experimentally and by simulations for light-ion sputtering (cf. Sect. 5.2). It is emphasized in this context that with an increasing impact angle with respect to the surface normal, the *total* sputtering yield increases because of the higher energy deposition in the vicinity of the surface. Generally, the maximum of the yield occurs between 60° and 80°, while for larger values of θ_0 (approaching 90°) scattering of the incident beam increases and sputtering yields decrease [415–418].

With respect to experimental determinations of angular distributions it is noted that they are usually very sensitive to surface contamination: a continuous surface layer forces atoms from the uppermost *target* layers into pronounced forward emission, resulting in forward-peaked angular spectra [419–421]. The influence of surface roughness on the angular ejection was

simulated by *Yamamura* et al. [422, 423]. The occurrence of such effects results in over-cosine distributions. Because elemental semiconductors readily amorphize under ion irradiation at room temperature [424], little, if any, surface topography is expected to develop on their surface even under prolonged in bombardment. However, also elemental and compound semiconductors exhibit occasionally the formation of ripple-like surface structures surface structures which have been found to influence sputtering and ion yields [116, 117, 425, 426].

4.3.2 Angular Spectra from Single Crystals

In contrast to sputtering from random targets, sputtering processes in crystalline materials are strongly influenced by the crystallographic orientation of the solid relative to the incident beam direction [95, 427, 428] and, for emission-angle-selective experiments, on the position of the detector relative to the crystal axes. Such observations were reported already by several groups in the 1960s [427–436]. Theoretical concepts and experimental data for the sputtering of single crystals have been outlined in reviews by *Robinson* [54] and *Roosendaal* [437]. Angular distributions of particles sputtered from single crystals have been discussed in detail by *Behrisch* [4] and by *Hofer* [59]. The dependence of the *total* sputtering yield on the orientation of the crystal surface sputtered has been examined by several theoretical descriptions [438–443].

Sputtering of crystalline targets results typically in the preferential ejection of atoms (and molecules) in the direction of certain preferred crystal axes (e. g., closed-packed lattice rows). The observation of this effect was first reported by *Wehner* [129, 130, 429] in the 1950s for low energies (some 100 eV and below), but was verified later also for high energies [4, 59]. This preferential emission (often called "Wehner spots") appears to be a general irradiation effect in crystalline solids [4, 59]. While the most prominent preferential ejection directions usually correspond to closed-packed lattice rows (e. g., [110] in fcc and [111] in bcc), some preferentiality was observed also in other lattice directions (e. g., [100] in fcc and [111] in diamond). *Silsbee* [444] and others [445] pointed out the possibility of a lattice influence on the energy dissipation by energetic recoils and demonstrated that momentum focusing along [110] in fcc lattices can be accomplished. These *focusing collision sequences* (also termed "focusons") were widely employed to interpret the observed preferential ejection along closed-packed lattice directions. They have been observed already in several early MD simulations of damage generation [446–448]. In order to explain anisotropic emission distributions observed also at low impact energies when extended focusing collision sequences do not occur, *Lehmann* and *Sigmund* [449] have proposed a quite different mechanism to explain the observed preferential particle emission. They stress the importance of the low-energy fraction of the recoil spectrum and of the regularly ordered *surface* lattice [449, 450].

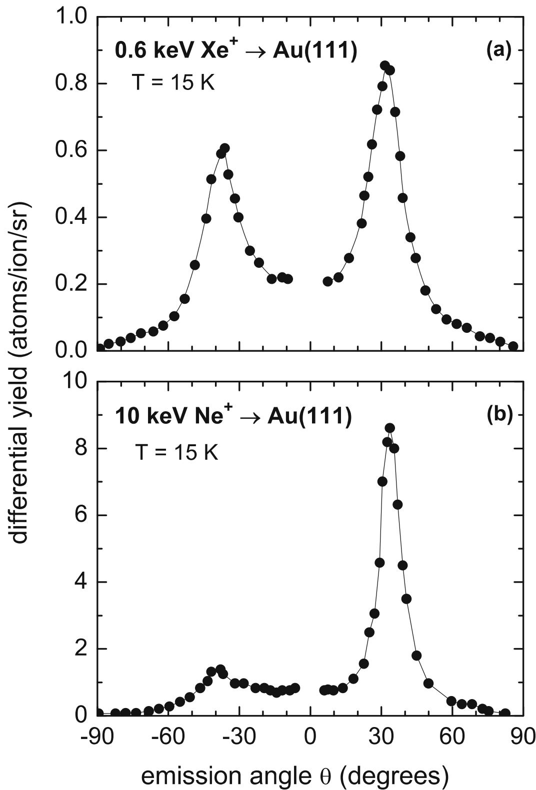

Fig. 22. Polar angular distributions of the differential sputtering yield from an Au(111) single-crystal surface bombarded by normal-incidence ions: (**a**) 0.6 keV Xe^+ and (**b**) 10 keV Ne^+. The measurements were done along the $(1\bar{1}0)$ plane [452]

a) Angular Distributions of the Total Flux

An appreciable number of investigations into the preferential particle ejection from single crystals were performed [4, 59]. *Szymczak* and *Wittmaack* [451, 452] have carried out a rather detailed study covering a wide range of irradiation parameters. They investigated the angular distributions of gold atoms sputtered from an Au(111) crystal as a function of target temperature (15–550 K), ion energy (0.1–270 keV) and ion mass (He, Ne, Xe) using a collector technique in combination with backscattering analysis of the deposits. The distributions produced the well-known [110] and [100] spots superimposed on an apparently random background. Figure 22 shows two examples from those data for 0.6 keV Xe^+ and 10 keV Ne^+ impact [452]. The authors [452] were able to separate the sputtering yields contributing to the spots and to the random background. Surprisingly, no bombardment conditions were found for which anisotropic emission prevails. Rather, the yield due to the random

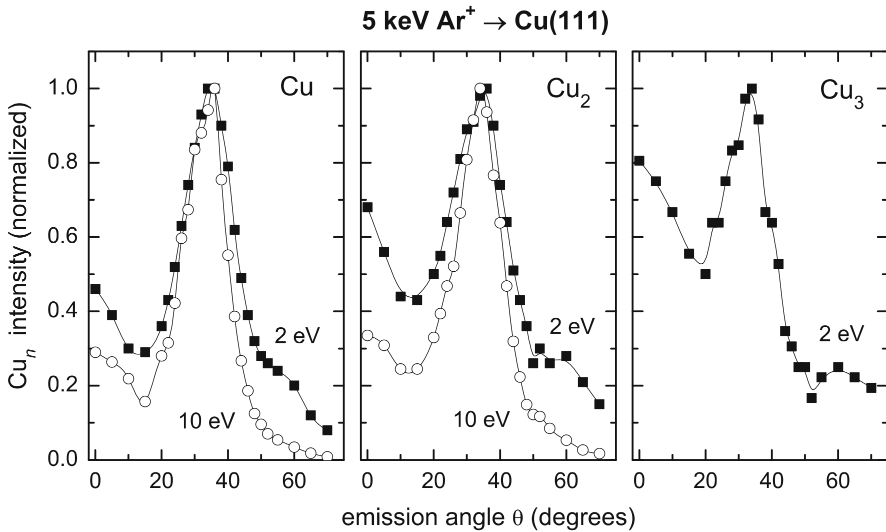

Fig. 23. Polar emission angle dependence of neutral Cu atoms and Cu_n clusters emitted from a Cu(111) surface under 5 keV Ar^+ irradiation. The emission angle θ was varied by rotating the crystal around an axis in the surface and parallel to the $[1\bar{1}0]$ direction; the angle of $\theta = 35°$ corresponds to the [110] lattice direction. Parameter is the emission energy of the ejected species [278, 279]

component dominates, in particular for high energies. At the lowest primary ion energies, the relative contribution of the sputter-emission into the preferred directions to the total sputtering yield amounts to as much as 50 %, but decreases with increasing energy to about 25 % for He and Ne and to 15 % for Xe impact at the highest energies. They suggest that the range of [110] focusing collision sequences may amount to a few nm. While the target temperature has little influence on the total and the partial sputtering yields, the spot width increases with temperature. At 15 K, the half-width of the [110] spot is only 5°, but twice as large at 550 K.

A large number of computer simulations [47, 48, 453–460] has been performed to study the (preferential) ejection from crystalline surfaces, providing a variety of information, some of them inaccessible by experiments.

b) Mass-Selected Angular Emission Spectra

Apart from experiments and computations which determined the preferential ejection of the *total* sputtered flux, several investigations have analyzed the *mass-selected* flux from single crystal surfaces [123, 278, 279, 461–465]. *Gnaser* and *Hofer* [278, 279] have done this using using sputtered-neutral mass spectrometry, post-ionizing the ejected neutral species by electron-impact. Not surprisingly, preferential ejection along low-index directions was found, but

distinct differences were noted depending on particle (cluster) size and emission energy. Figure 23 exemplifies these data, plotting the intensities of *neutral* Cu, Cu_2 and Cu_3 emitted from a Cu(111) crystal surface as a function of the emission angle θ under 5 keV Ar^+ bombardment [279]. Distinct maxima in the yields of all species occur at $\theta \cong 35°$ which corresponds to the [110] direction of this fcc crystal. As a parameter (cf. left and center panel of Fig. 23) the emission energy accepted by the spectrometer was varied; the angular anisotropy is seen to increase at higher energies.

In these experiments [278,279] also energy spectra were recorded for atoms and small clusters sputtered from the (111) surfaces of fcc crystals (Cu and Ni). For monomers and dimers, ejection in the closed-packed direction ($\theta \cong 35°$) shows a broadening of the energy spectra and a distinct shift towards higher energies as compared to the emission at near-normal directions. This finding is in agreement with data of *Thompson* and coworkers [25, 42] who found for the sputtering of Au crystals that energy spectra taken along [110] peak at higher energies as compared to those recorded 15° outside of this preferred ejection direction.

Winograd and coworkers [122,156,461,462,466,467] studied the angular- and energy-selective emission of *ground-state* and *excited-state* Rh atoms from Rh(111) and Rh(100) surfaces by keV-Ar^+ bombardment. Both clean and oxygen-covered surfaces were examined. Because of the sensitivity of the employed technique (cf. Sect. 3.3), the analyses were largely non-destructive, that is, essentially no modification of the atomic arrangement at the surface was induced by ion irradiation. Generally, the experiments were well reproduced by MD simulations [468–470]. The data displayed strong preferential ejection for an emission angle that would correspond to the [110] lattice direction from the (111) surface and an, albeit weaker, emission that might be ascribed to the [100] directions, but somewhat shifted to smaller angles. The authors [461,462,466,467,471] stress, however, that the geometrical structure of the very near-surface region controls the angular anisotropy. The registry of the second-layer atoms with respect to the top layer induces a highly directional momentum transfer in the last collision, leading, in turn, to preferential particle emission in certain crystallographic directions. Similar conclusions were drawn already from early MD simulations of *Harrison* and coworkers [472] and from more recent simulations [466,467,470].

4.3.3 Angular Distributions from Multicomponent Targets

An angular variation of the composition of the sputtered flux from multicomponent specimens was already reported by *Olson* and *Wehner* [473,474]. They observed that sputtering of Ag–Au, Cu–Ni, and Fe–Ni alloys by Hg^+ or Ar^+ ions at energies below 300 eV causes the lighter elements to be ejected preferentially in the direction of the surface normal. The authors suggested that, at these low energies, surface atoms bouncing back from underlying

atoms may contribute significantly to sputter-ejection. With increasing impact energy the enrichment decreases strongly. At 1 keV, preferential emission of Au (from Au–Ag) and of Ni (from both Ni-based alloys) along the surface normal was reported. This can be ascribed to steep concentration gradients at the surface, due to the enrichment of one component at the surface of these alloys.

Compositional gradients within the depth of origin of sputtered atoms may influence the angular distribution of sputtered species, as indicated by *Sigmund* et al. [475, 476]. These authors proposed that the emission patterns should be narrower for those species for which a comparatively larger fraction of sputtered atoms originates from greater depths. This implies that in a binary system the species enriched in the surface layer will have a flatter angular distribution, while that of the depleted element is forward-peaked. In the following, some experiments which examine the validity of this idea will be outlined.

Andersen and coworkers [477–480] recorded angular spectra to determine the presence of segregation at the surface and to identify the segregating species. Specifically, they investigated different alloys (Cu–Pt, Ag–Au, Ni–Pt, Cu_3Au, Ni_5Pd) at various temperatures and bombarding energies; they found [478, 479] preferential forward ejection of one element and ascribed this finding to the Gibbsian segregation of the other (the weaker-bound) component to the surface. The most detailed study was carried out for Cu–Pt [479], with the Ar^+ ion energy covering the range from 1.25 keV to 320 keV. A distinct forward emission of Pt atoms was observed for $E_0 \geq 40$ keV whereas at 10 and 20 keV little angular variation of the yield ratio was found. At the lowest energies, a preferential ejection of Cu atoms at oblique angles dominates while a slightly preferred Pt emission was found for intermediate and near-normal directions. The findings of *Andersen* and coworkers [478, 479] on Cu–Pt are thus in accordance with the composition profiles derived for this system [481, 482]: The Pt-enriched sub-surface region results in a preferential forward emission of Pt atoms in the sputtered flux.

Tombrello and coworkers [483–485] determined the angular distributions of sputtered atoms from a liquid Ga–In eutectic alloy. In this system, Gibbsian segregation gives rise to an outermost layer that is virtually pure In. As expected, their data for Ar^+ bombardment showed that the In atoms had a $\cos^y \theta$ distribution, with $y = 1.80 \pm 0.1$, largely independent of ion energy. By contrast, the angular distribution of Ga was significantly narrower, with $y = 3.2 \pm 0.2$ in the energy range of 15–250 keV, and $y = 4.9 \pm 0.3$ at 3 keV. This increase at low energy was accompanied by an increase in the contribution of the topmost layer to the sputtered flux of atoms. MD simulations on the sputtering of this liquid Ga–In alloy were performed by *Shapiro* et al. [486] for 1.5 and 3 keV Ar bombardment and generally corroborate the corresponding experimental findings [484, 485].

The emission distribution of the sputtered flux from GaAs under 1–3 keV Ar^+ irradiation using a collector technique and analyzing the deposit by

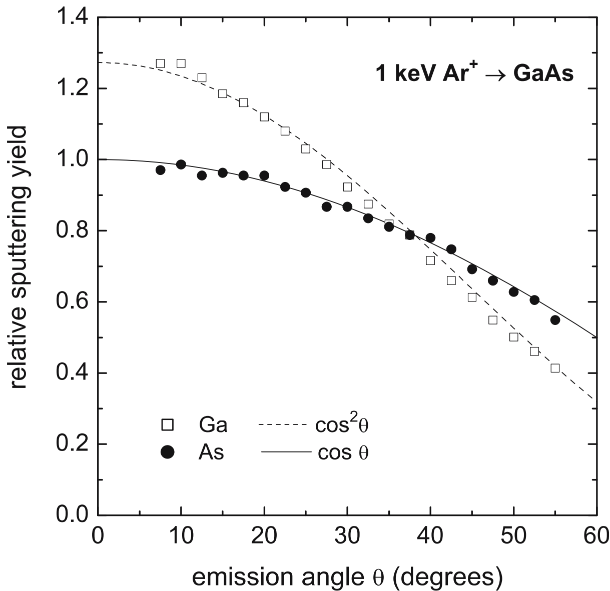

Fig. 24. Polar angular emission distributions of Ga and As atoms sputtered by 1 keV Ar^+ ions from GaAs. The *dotted* and *solid lines* are fits to the respective relative yield data; they are proportional to $\cos^2\theta$ for Ga and to $\cos\theta$ for As. The data refer to stationary state [487]

electron-induced X-ray emission were determined by *Aoyama* et al. [487]. As can be seen in Fig. 24, both the Ga and the As distributions could be fitted with $\cos^y\theta$ distributions, but y was found to be 2.0 for Ga and 1.0 for As at 1 keV; both values slightly increased (to 2.5 and 1.5, respectively) at higher energies. From these findings the authors [487] conclude that the As concentration is higher in the outermost layer, but the subsurface range is (strongly) depleted in As; this would fit the previous observations that the GaAs surface averaged over several monolayers (as seen, e. g., by Auger electron spectroscopy) is depleted of As [12]. Such an oscillatory form of composition profile would indicate that Gibbsian segregation plays an important role for this system. The same group investigated also InP [488] and GaP [489] surfaces using Ar^+ and Xe^+ bombardment at two different energies (1 and 3 keV) and two sample temperatures (153 and 293 K). For theses targets the angular distributions of the two constituents were essentially identical for all experimental conditions. The similar angular distributions of In or Ga and P suggest that the specimen composition is homogeneous within the depth explored and that, contrary to GaAs, no segregation is occurring. (Irradiation-induced composition changes in compound semiconductors are evaluated in [12, 490, 491].)

Angular spectra from many other alloys were studied by experiments: Cu–Ni, Co–Ni, Fe–Ni [492], Au–Cu [493], Ni–Ti [494], Co–Au, Cu–Be, Cu–Zn, and W-Si [495]. Results from TRIM.SP simulations on binary systems are described in [46, 496]. The results discussed here and in other studies [12, 202, 203] provide strong evidence that angular spectra of sputtered species from binary (or multicomponent) systems may be influenced heavily by any *gradients in the surface composition*: typically, the component enriched at the surface will exhibit a flatter angular spectrum, whereas that of the depleted species is more forward-peaked.

Angular distributions of sputtered atoms were also determined [126] for *isotopic mixtures*, that is, for elemental samples with two or more isotopes. Neglecting possible differences in binding energies for two isotopes of an element (an approach perhaps not fully justified [497]), any angular effects can be ascribed then solely to the different isotopic masses. A brief summary of the pertinent findings in terms of angular spectra will be given [12]: these data show that the *lighter* isotope is preferentially sputtered in near-normal emission direction whereas the *heavier* isotope exhibits preferential ejection at oblique directions. For the isotopic pair ^{92}Mo/^{100}Mo the magnitude of this angular shift is in the range from 1 % to 2.5 % for the various projectiles and impact energies investigated. (Under *steady-state* sputtering conditions, the total angle-integrated emitted flux should, of course, reflect the isotopic bulk composition of the specimen.) The experimental data [126] were found to agree quite well with the respective results from computer simulations obtained both with the TRIM.SP code [498] and with an MD code [499].

5 Energy and Angular Distributions in the Single-Knockon Regime

In the single knockon regime, i. e., at low bombarding energies and for light incident ions, the energy and angular distributions of emitted species may change drastically as compared to the linear-cascade case. In addition, sputtering yields generally decrease rapidly with decreasing impact energy. A quantitative theoretical description of sputtering in this regime was found difficult to establish [33, 500], however. For light ions (such as H^+, D^+, and He^+) a large amount of sputtering yield data both from experiments and computer simulations exists [68, 501, 502], primarily due to the importance for thermonuclear fusion research [503]. Because of the limited number of atoms participating in the event, the concept of a linear collision cascade employed in the previous section to describe sputtering may not be adequate for bombardment with very light ions (e. g., H, D, He) and, for heavier ions, at impact energies approaching the *threshold* for sputter ejection. (The occurrence of such a threshold energy E_{th} was inferred from early sputtering experiments [504–506], but is still not a well-defined quantity despite

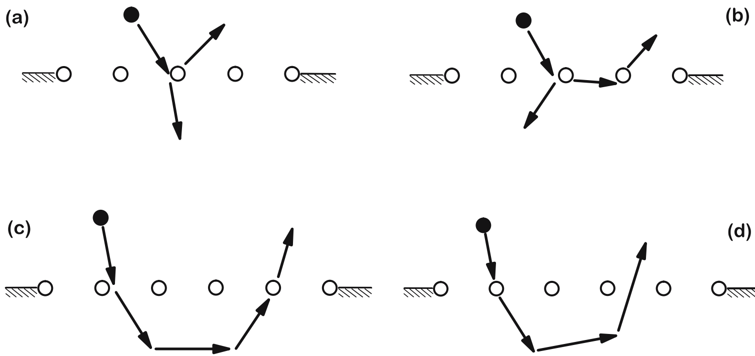

Fig. 25. Illustration of some possible ejection mechanisms in the single-knockon regime: (**a**) A primary recoil is produced in the first collision and ejected directly (or after a further deflection by a target atom); (**b**) a higher order (secondary) recoil is ejected; (**c**) the projectile undergoes multiple collisions, is backscattered and ejects a surface atom in a near-head-on collision; (**d**) a secondary recoil undergoes several collisions (at small scattering angles) that effect reversal of momentum and is ejected directly (or collides with another atom which is ejected) [12]

the long-lasting experimental efforts.) Conversely, rather specific collision sequences may lead to atom ejection [507–512]. Possible scenarios are depicted schematically in Fig. 25; they all illustrate that these collisions sequences may involve only a small number of atoms (i. e., they are short) and a collision cascade does not develop. (It is noted, however, that many small-angle-scattering collisions can also be very efficient for momentum reversal and sputtering at near-threshold energies.) As particle reflection coefficients increase with decreasing energy (and are quite high for light ions), reflective scattering collisions near the target surface contribute increasingly to sputtering. Their importance was noted by *Winters* and *Sigmund* [511] for the sputtering of nitrogen atoms from a tungsten surface.

The relevance of single knockon collisions and of special collision sequences is illustrated impressively by computer simulations [509, 510, 512–516]. Some computations [512] indicate, furthermore, that an optimum number of collisions in those sequences may exist which result in the highest emission energies. For example, *Eckstein* et al. [512, 515–517] simulated near-threshold sputtering and identified distinct collision types leading to sputtering by TRIM.SP. For light ions at normal incidence (e. g., D on Cu), the only process of importance is due to a primary knockon atom generated directly by the projectile on its way back out of the sample after having undergone one (or more) collisions with one (or several) target atoms (see Fig. 25c). For oblique incidence and higher energies the mechanism depicted in Fig. 25a may contribute significantly. For heavier ions (Ar on Cu) two mechanisms are operative: the first involves a primary knockon with the ion moving into the target (Fig. 25a), while in the second a secondary knockon atom cre-

ated by the projectile effects sputtering, possibly after further collisions with other target atoms (Fig. 25d). These mechanisms may change drastically for oblique ion incidence: then, processes like those in Fig. 25a or Fig. 25b can become relevant. Rather detailed accounts of these mechanisms and their importance for near-threshold sputtering are given in [509, 512].

Simple analytical expressions were derived for the maximum emission-energy values in such sputtering events. *Yamamura* and *Bohdansky* [509, 510] established such analytical formulae for a variety of possible collision sequences.

5.1 Energy Spectra and Direct Recoils

While under the conditions of linear collision cascades, energy spectra are typically found to agree roughly with the theoretical predictions as expressed by (6), in particular in terms of the high-energy falloff as E^{-2} for $E \gg U$, such a behavior is not expected at very low impact energies. In other words, reducing the bombarding energy, the prerequisite energy range $E \gg U$ is never established [518, 519]. Energy spectra recorded under such conditions corroborate this anticipation [22, 24, 520–524]: the peak of the energy spectra tends to shift to lower energies and the width of the distribution becomes narrower; in addition, quite often the presence of *direct recoils* in the emission distributions is found.

5.1.1 Normal Incidence Bombardment

Energy spectra of sputtered atoms and molecules at low and near-threshold bombarding energy generally demonstrated that the average energy of sputtered particles decreases with decreasing impact energy of the projectiles [22, 24, 520–522]. More recently, energy spectra at (very) low bombarding energies ($< 100\,\mathrm{eV}$) were investigated for pure Cu and two binary alloys ($Cu_{0.53}W_{0.47}$ and $Ni_{0.92}W_{0.08}$) by electrostatic analysis in the secondary-neutral mass spectrometer displayed in Fig. 1 [211]. Because of the high sensitivity of this technique, a large range both in yields (some five orders of magnitude) and in emission energy (up to several 100 eV) could be studied. Due to a specific sample geometry [525, 526], the total *emission-angle integrated* and *mass-selected flux* of sputtered neutral species was recorded in those measurements, while the Ar^+ ions were impinging perpendicular to the surface. In addition, the experimental data were compared with the respective distributions from TRIM.SP computer simulations. Figure 26 shows the data for the elemental Cu sample and for bombarding energies from 65 eV to ≈ 1000 eV [211]. With decreasing Ar^+ impact energy the emission-energy distributions exhibit a steeper falloff that is related to the *maximum energy* a sputtered Cu atom can receive for a given Ar^+ energy. This falloff is roughly exponential over a wide emission-energy range and the respective slopes in that energy regime show a good agreement between the experimental and the simulation data.

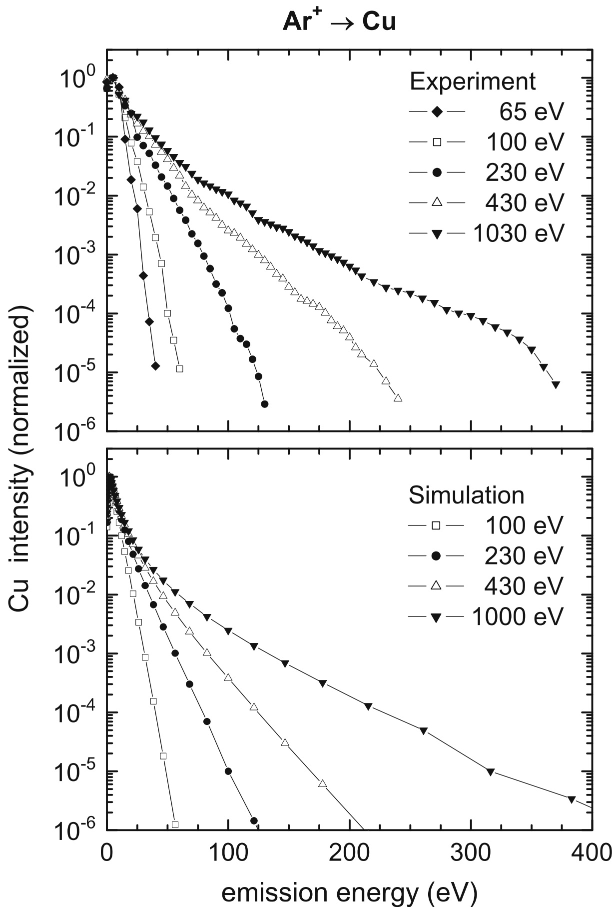

Fig. 26. Emission-angle integrated energy spectra of neutral Cu atoms sputtered from elemental Cu by normal-incidence Ar^+ ions of the indicated energies. Data are from experiments (**a**) and from TRIM.SP simulations (**b**) [211]

Figure 27 depicts the corresponding emission-angle integrated energy spectra for a $Cu_{0.53}W_{0.47}$ alloy [211]. These data (and those for the Ni–W alloy) reveal consistent differences in the spectra for Cu (and Ni) atoms on one hand and for W atoms on the other. The spectra of the former components peak at lower energies, but they extend to higher energies; this gives rise to a crossover of the (normalized) spectra at intermediate emission energies. The different positions of the peak maxima are reasonable in view of the differing surface binding energies for the two components. Although the surface binding energy in these binary systems (Cu–W and Ni–W) are not known, the cohesive energies E_{coh} of the respective pure metals are widely different: $E_{\mathrm{coh}}(\mathrm{Cu}) = 3.52\,\mathrm{eV}$, $E_{\mathrm{coh}}(\mathrm{Ni}) = 4.46\,\mathrm{eV}$ and $E_{\mathrm{coh}}(\mathrm{W}) = 8.68\,\mathrm{eV}$.

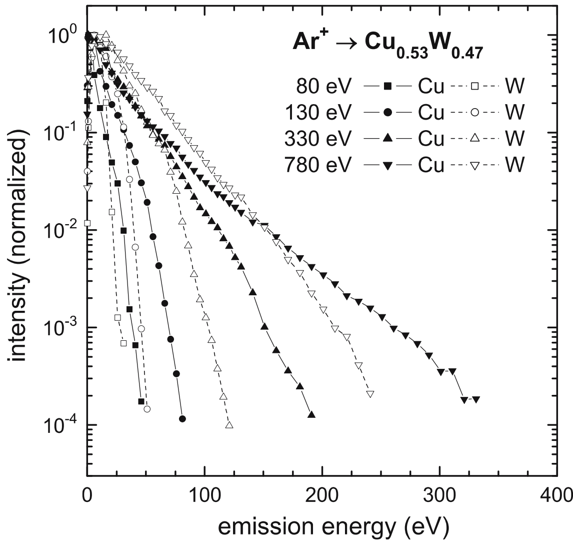

Fig. 27. Experimental emission-angle integrated energy spectra of neutral Cu and W atoms sputtered from $Cu_{0.53}W_{0.47}$ by normal-incidence Ar^+ ions of the indicated energies. Data refer to steady-state sputtering conditions [211]

The more gradual falloff observed for the yields of Cu (and Ni) as compared to W towards higher emission energies can be rationalized by energetic arguments: the primary Ar ions can transfer, in binary collisions, a larger amount of energy to a Cu (or Ni) than to a W atom; hence, the initial Cu (Ni) recoils carry, on average, more energy which they can, in turn, transfer more efficiently in another collision to an atom of like mass (Cu or Ni) than to the heavier W atoms. Similarly, the presence of the heavy W atoms (in Cu–W) facilitates the reversal of the (initially inward directed) momentum and thus results in a higher average energy of Cu atoms sputtered from the Cu–W sample (because less collisions are required) as compared to sputtering from the elemental Cu target [211].

Not surprisingly, the high-energy parts of the spectra of sputtered atoms at these low bombarding energies (see Figs. 26 and 27) cannot be fitted by a power-law E^{-2} as predicted by (8). *Urbassek* [518] has developed a theoretical concept that illustrates the deviations from the power dependence at low impact energies.

Apart from atoms, also energy spectra of small sputtered *neutral clusters* were recorded in the experiment in [211]. Because the yields of metal clusters are small (at most a few percent) at sub-keV bombarding energies [523–527], this generally limits the emission-energy range that can be monitored. Still, for the most abundant cluster observed from the various specimens (the Cu_2 dimer), energy spectra were recorded covering several orders of magnitude in intensity. Such data are shown in Fig. 28. As compared to atomic Cu

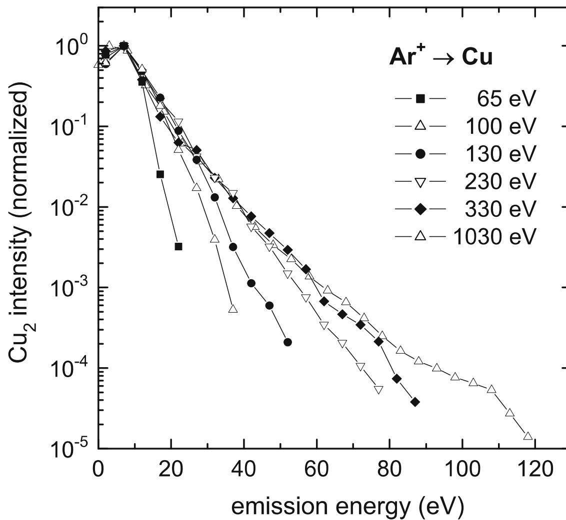

Fig. 28. Experimentally determined emission-angle integrated energy spectra of neutral Cu_2 cluster sputtered from pure Cu by Ar^+ ions of the indicated energies [211]

spectra (cf. Fig. 26), the Cu_2 distributions exhibit a much steeper falloff at high emission energies. In addition, the high-energy decay appears to reach a limiting slope at a bombarding energy of about 300 eV and the major part of the Cu_2 distributions changes little above that impact energy [211].

5.1.2 Oblique Incidence Bombardment

For the case of *oblique ion incidence* an anisotropy of the energy distributions is expected due to contributions of *direct recoils*. Such direct recoils have been investigated extensively by several groups [25, 41, 42, 189–195, 528–532] at (comparatively) high bombarding energies and distinct contributions of direct recoils in the energy spectra of sputtered atoms were observed. However, direct recoils and anisotropic contributions can be observed very clearly also at low impact energies ($<$ 1 keV) as shown recently, in a series of papers, by *Goehlich* and *Döbele* [533–537]. For a certain (limited) range of forward emission angles, a target atom located at or close to the surface may be ejected due to a single collision with the incoming projectile (mass M_1, energy E_0, incidence angle θ_0), see Fig. 25a. The energy T transferred to a target atom (mass M_2) initially at rest is then given by

$$T = \gamma \, E_0 \, \cos^2 \Theta \, , \tag{22}$$

where Θ is the recoil angle of the target atom with respect to the direction of the impinging projectile. Taking into account a planar surface barrier with a magnitude U, the emission energy E^{dr} of a direct recoil results:

$$E^{\mathrm{dr}} = \gamma\, E_0\, \cos^2(\theta_i + \theta_0) - U\,; \tag{23}$$

θ_i is here, as in (3), the angle with which the atom approaches the surface from *within* the target. From this relation the energy of the direct recoil as a function of the emission angle can be computed. For a given incidence angle, *direct recoils* can be observed only above a "critical" emission angle. As discussed in great detail in [200, 533], two energy branches merge at that critical angle of emission. Beyond this angle there are two possible recoil energies corresponding to collisions with different impact parameters, but leading to the same emission angle. Isolated direct recoil peaks are only expected for angles much larger than the critical angle.

Energy spectra from Al, Ti, and W samples under bombardment with Ar^+ and Xe^+ ions of 0.2–5 keV energy were monitored by means of laser induced fluorescence [533–535]; these data illustrated many of the features related to anisotropic collision cascades and the occurrence of direct recoils at low impact energies. Typically, the angular dependence of the energy distribution is much more pronounced at oblique incidence angles, even for comparatively high energies. Figure 29 shows energy spectra of sputtered neutral tungsten atoms for an angle of incidence of $\theta_0 = 50°$ bombarded with 300 eV Ar^+ ions together with results of TRIM.SP simulations (solid lines) and distributions according to (8) as a reference (dotted lines). The latter is not an acceptable approximation under these sputtering conditions. The energy distributions of the sputtered W atoms become substantially broader in forward emission ($\theta = 30°$ and $70°$) as compared to backward emission ($\theta = -30°$) and the peak shifts to higher energies. Cleary evident is the absence of an E^{-2} falloff at high energies. Contributions due to atoms sputtered via direct recoils are seen at $\theta = 70°$ and were observed [533] even more clearly for larger bombarding angles. To exemplify these features, Fig. 30 depicts the energy spectrum of Al atoms sputtered by 500 eV Xe^+ ions at an incidence angle $\theta_0 = 70°$, comparing two emission angles, namely $\theta = -50°$ (backward) and $\theta = 50°$ (forward) [534]. While the former exhibits a shape in good agreement with the theoretical distribution of (8), in the latter a distinct anisotropic contribution to the emitted flux and the occurrence of direct recoils were found, extending the emission energy to considerably higher values.

For *light-ion* (e. g., H and He) sputtering, ejection of surface atoms occurs mostly via primary recoils and by backscattered projectiles. Thus, the primary event, the ion-target atom collision plays a decisive role in the ejection process; this influence of single-collision emission is especially pronounced for oblique incidence and at energies near the sputter threshold. As for heavy projectiles at near-threshold energies, also for light ions the most probable emission energy is no longer directly correlated to the binding energy. Velocity spectra obtained under such conditions for the sputtering with light

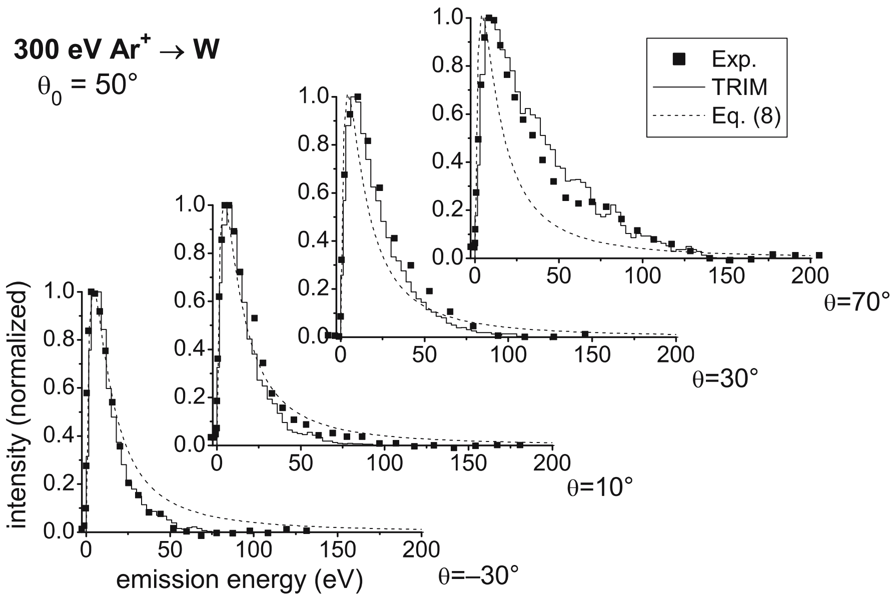

Fig. 29. Energy distributions of neutral tungsten atoms sputtered by 300 eV Ar^+ ions at an oblique incidence angle ($\theta_0 = 50°$) for various emission angles θ, in comparison with simulated data from TRIM.SP calculation (*solid lines*). Distributions according to (8) are added for reference (*dashed lines*) [533]

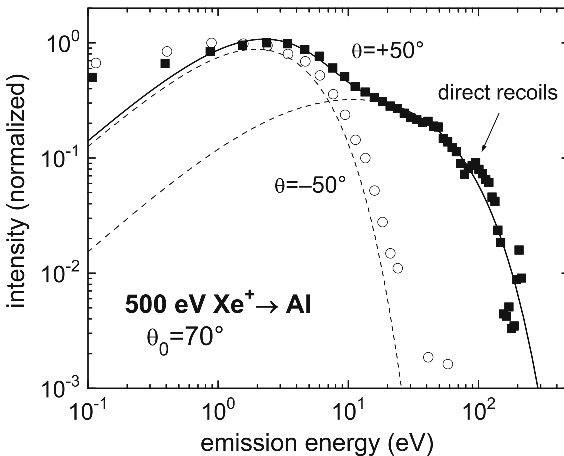

Fig. 30. Energy distributions of neutral Al atoms sputtered by 500 eV Xe^+ bombardment at an oblique incidence angle ($\theta_0 = 70°$). The distributions are detected in forward direction ($\theta = 50°$, *solid squares*) and in backward direction ($\theta = -50°$, *open squares*) [534]

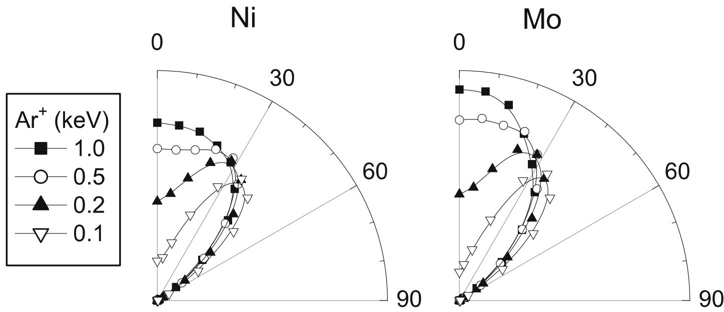

Fig. 31. Polar angular distributions of neutral Ni and Mo atoms sputtered from a Ni-based alloy by Ar^+ ions of different bombarding energy (100 to 1000 eV) [552]

ions [538–541] deviate considerably from those recorded under linear-cascade sputtering and may exhibit distinct features of direct-recoil contributions. A theoretical concept for energy spectra of atoms sputtered by keV light-ion bombardment has been proposed by *Falcone* [542, 543].

5.2 Angular Distributions at Low-Energy Irradiation

The energy spectra of sputtered species at low bombarding energies shown in the previous section emphasized the importance of direct recoils in the ejected flux and illustrated, thereby, the occurrence of a distinct anisotropy in the energy dissipation processes in the solid which lead to particle emission. These mechanisms show up also in the angular distributions of sputtered atoms and molecules. In fact, *Wehner* observed [544], already in 1960, emission distributions which became increasingly "under-cosine" (heart-shaped) when the bombarding energy was reduced below 1 keV: less atoms are ejected normal to the surface and a larger fraction at oblique angles; for the latter, fewer collisions are required to lead to an ejection event. These early findings were later corroborated by other experiments [396, 545–547], by theoretical modeling [548, 549], and by computer simulations [550, 551]. The drastic changes in angular distributions upon a variation of the bombarding energy are illustrated in Fig. 31 which shows the angular emission spectra of *neutral* Ni and Mo atoms sputtered from a polycrystalline Ni-based alloy sample by Ar^+ ions with energies of 0.1, 0.2, 0.5, and 1 keV at normal incidence [552]. A pronounced emission at an oblique angle of $\approx 30°$ is found in all cases for the 100- and 200-eV irradiations; for the higher energies the forward emission becomes more and more prominent.

In sputtering by light ions such as hydrogen or helium, the energy transfer to target atoms is so small that the generation of successive recoils is improbable; therefore, the energy is deposited rather locally [500, 553]. Hence, the direct interaction between the projectile and the target atoms dominates the ejection event. Both experiments and computer simulations indicate that

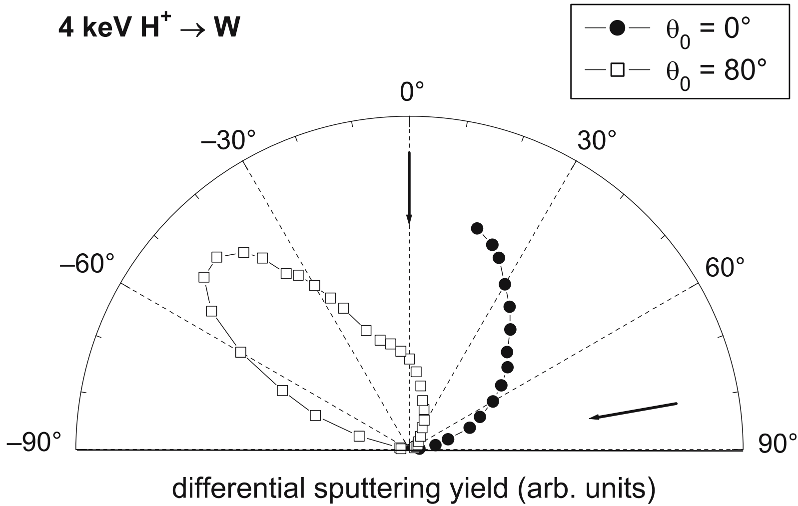

Fig. 32. Polar angular emission distributions of W sputtered by 4 keV H^+ ions at incidence angles of $\theta_0 = 0°$ (*closed symbols*) and $\theta_0 = 80°$ (*open symbols*). The arrows indicate the incidence directions of the H^+ ions. The data for $\theta_0 = 0°$ have been multiplied by a factor of 30 relative to the values at $\theta_0 = 80°$ [555]

the emission of surface atoms by backscattered projectiles is the prevalent sputtering mechanism, see Fig. 25. At perpendicular incidence, the ejection should show then a preferential component normal to the surface, an effect observed in low-energy sputtering of V [554], Ni, and W [555]. Clear over-cosine distributions for H^+ or He^+ irradiation at normal incidence corroborate an emission process induced by backscattered projectile ions. Figure 32 exemplifies such data for the sputtering of a W target by 4 keV H^+ ions at normal incidence. These spectra constitute a distinct contrast to the angular spectra of heavy-ion sputtering at low energies (see Fig. 31) where enhanced oblique emission results in under-cosine distributions.

Even more pronounced for light-ion sputtering is the effect of the primary-ion interaction with surface atoms at oblique incidence [556–558]. Figure 32 illustrates this for 4 keV H^+ ion bombardment of W at an incidence angle $\theta_0 = 80°$ [555]. In this case, the direct ejection of surface atoms by projectiles on their way into the solid is the dominant ejection process. A distinct emission characteristic at polar angles opposite to the ion's incidence direction was found [555], often much more pronounced than the preferred forward emission observed in heavy-ion sputtering under oblique ion bombardment.

6 Energy and Angular Spectra from High-Density Cascades

For bombardment with high-energy heavy ions, sputtering yields are generally observed to be higher than predicted by the analytical expression given by *Sigmund* [26, 27]. The same finding was reported for the irradiation with molecular (or cluster) ions. First clear evidence for an enhanced sputtering yield under cluster bombardment was provided by the experiments of *Andersen* and *Bay* [559–561]. By comparing yields for atomic and dimer ion irradiation, they observed that in the latter case the yield was more than twice as high as the value for monomers of the same velocity. Similar findings were reported by *Thompson* and coworkers [562–567]. These deviations from a linear superposition of atomic yields were interpreted as being caused by *nonlinear* effects in the collision cascade. However, also changes in the effective surface binding energy have been invoked as a possible cause. For the dimer and trimer ions, the observed enhancement factors (defined as the ration of Y for cluster impact to m times the yield for monomers, with m the number of atoms in the cluster) were in the range from ≈ 1 to ≤ 10, for ion energies of some 10 keV/atom. For lower energies or lighter ions the enhancement tends to become fairly small. Apart from enhanced sputtering yields, further evidence for nonlinearities in the collision cascade came from low-energy peaks in the energy spectra of sputtered atoms [568–570] and the formation of extensive craters upon bombardment with heavy ions or molecules [571–573].

Several distinct theoretical models have been proposed to describe those observations of nonlinear collision cascades: they range from shock-wave propagation [574–577] to crater formation and some type of thermal evaporation from high-temperature spikes [21, 578, 579]. These approaches aimed at quantifying this high-density (spike) regime of sputtering in terms of the temporal evolution [580, 581], the energy density [580–583] and the yield enhancement [582, 584, 585]. In this context, also the temperature dependence of the sputtering yield was investigated [586] in order to interpret experimental yield data [587, 588]. Detailed reviews [35, 36, 589, 590] have assessed those concepts. Because of the increasing importance, some aspects of cluster-ion irradiation and the associated yield enhancements will be outlined before discussing the emission characteristics of sputtered species under cluster-ion impact.

6.1 Cluster-Ion Bombardment

Whereas early experimental and theoretical investigations were concerned typically with rather small species (composed of a few atoms), much larger clusters composed of hundreds or even thousands of constituting atoms attracted considerable attention during the past two decades. Several groups [591–605] have used a variety of cluster ions, such as SF_6, ReO_4, Au_n, $(CsI)_nI$,

$(CsI)_nCs$, Ar_n, $(CO_2)_n$ and C_{60} to study impact phenomena at the surface. The reason for this interest was mainly twofold:

(i) The basic mechanisms of ion-solid interactions could be studied for a much wider range of parameters by using cluster-ion impact. For example, the possibility to achieve a high energy-deposition density in the collision cascade was of interest and utilized to explain the enhanced sputtering yields observed in bombardment with small clusters long ago [559–562, 565, 566, 568, 606, 607] and the even more drastic enhancement found later with larger clusters [599–601, 608]. Another feature of interest is the unusual multiple-collision kinematics which might occur in cascades initiated by cluster impact. Many computer simulations [609–630] have provided quantitative information on various important aspects, like the penetration depth and the energy loss of clusters in solids, the energy spectra of transmitted and reflected particles and of target recoils, and the occurrence of cascades within the cluster upon its hitting the surface; these simulations illustrated very impressively the enormously wide spectrum of processes that can occur on and near the surface upon irradiation with large clusters.

(ii) On the other hand, the interest in cluster-ion bombardment was motivated by some pioneering applications, e. g., in thin-film deposition [631–635], enhanced electron and ion yields [591, 592, 594], mass spectrometry [594–597, 636], or surface modifications [598, 608].

In particular, the number of investigations related to the latter two of these applications has increased dramatically in recent years: Because of their distinct advantages in certain analytical modes as compared to the conventionally employed atomic species, cluster ions are used now as primary bombarding species in secondary ion and secondary neutral mass spectrometry [637–658]. Cluster-ion beams have found also a widespread use for surface modifications and materials processing, an area of applications advanced greatly by *Yamada* and his coworkers [659–667] and by many others [668–673].

6.2 Yield Enhancement under Cluster Impact

Bombarding solids by polyatomic projectiles, sputtering and secondary-ion yields are typically (much) *higher* than those induced by the same number of constituents arriving individually. As mentioned above, these *"non-linear" enhancement* effects have been noted already some 30 years ago [559–561]. More recently, rather drastic enhancement effects have been observed employing larger cluster species like Au_m ($m = 1$–13), C_{60}, or Ar_m ($m \approx 3000$). To describe this kind of non-additive sputtering, it is useful to define the following ratio of nonlinearity [596]

$$\epsilon_n^m = \frac{nY_m}{mY_n}\,; \tag{24}$$

Y_m and Y_n being the emission yields induced at identical impact velocities by *projectiles* having m and n constituents, respectively. A ratio larger than 1 implies that the yields obtained with different clusters of the same type are not directly proportional to their size. For gold and silver targets very large sputtering yields induced by Au_m^+ clusters ($m = 1$–13) have been found [674–676]: for example, for an Ag target yield values as high as $\approx 20\,000$ atoms per impact of Au_{13}^+ at 1.2 MeV (92 keV/atom) were measured, whereas only 45 atoms are emitted in the impact of a single Au atom at the same energy per atom. But even for lower impact energies (≈ 30 keV/atom), values of $\epsilon_n^m \approx 10$ were determined. Generally, also *secondary-ion* yields under cluster impact are much higher than under atomic-ion irradiation at the same energy/mass value. This tendency is clearly demonstrated by many data [591, 592, 594, 596, 643, 649, 677–683]. A caveat related to secondary-ion detection is of note: unless determined together with the neutral (total) yields, it might be difficult if not impossible to separate sputtering yield enhancements from effects that are due to an enhanced ion-formation probability under cluster-ion bombardment [684, 685].

For much larger clusters composed of several thousand atoms, *Yamada* and coworkers [608] reported dramatic total-yield enhancements for *cluster* impact as compared to *atomic* ions. The values of Y for several elemental samples under irradiation by 20 keV Ar_m^+ cluster ions ($m \approx 3000$) and by 20 keV Ar^+ ions were determined. The sputtering yield is enhanced drastically (e. g., for Si up to a factor of 30) for cluster ions as compared to atomic ions although the *energy per atom* of the cluster constituents amounts only to about 6.7 eV (for $m \approx 3000$). This value is far below the threshold for single-ion impact sputtering [12].

6.3 Energy Distributions under Cluster Bombardment

The number of experiments that determined emission-energy spectra from surfaces under cluster irradiation appears to be still rather limited, and the majority of these studies measured the energy spectra of selected *secondary-ion* species [679, 686–689]. In addition, data for large clusters (say, more than 10 constituents) are largely lacking. *Belykh* et al. [679, 686] measured the ion yields and the kinetic energy distributions of Ta_n^+ ($n \leq 12$) and Nb_n^+ ($n \leq 16$) secondary cluster *ions* sputtered from the respective metals by Au_m^- ($m = 1$–3) ions with an energy of 6 keV/atom. They found that, for a given secondary ion species, the energy spectra are largely independent of the type of projectile, both in terms of the FWHM of the distributions as well as their high-energy falloff. On the other hand, data for Nb_n^+ and for Ta_n^+ [679] show an enhancement factor (cf. (24)) of the ion yields for cluster bombardment which increases dramatically with the size of the emitted secondary-ion cluster. For example, for Ta^+ a value $\epsilon_1^3 \approx 4$ was observed, whereas $\epsilon_1^3 \approx 900$ was found for Ta_{10}^+. Similarly pronounced non-additive sputtering effects were re-

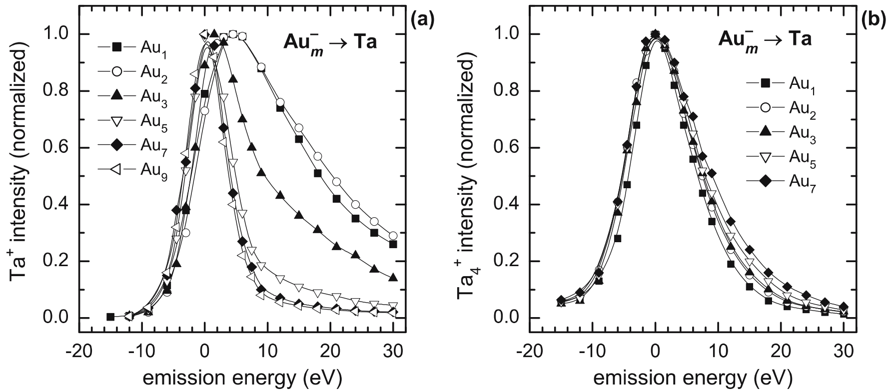

Fig. 33. Normalized energy distributions of atomic Ta^+ ions (**a**) and Ta_4^+ cluster ions (**b**) sputtered by Au_m^- projectiles from a Ta specimen. Bombarding energies were 6 keV/atom for Au_m^- ($m = 1-3$), 18 keV for Au_5^-, and 21 keV both for Au_7^- and Au_9^- [690]

ported by this group also for Nb_n^+ [679], for Si_n^+ ($n \leq 7$) [680], and for Si_nC^+ ($n \leq 12$) [678].

Employing somewhat larger Au_m^- (m = 1–9) projectiles, *Morozov* and *Rasulev* [690] found again distinct non-linear enhancement effects for Ta_n^+ secondary ions. Interestingly, they observe a *narrowing* of the energy spectrum of sputtered Ta^+ ions with *increasing* cluster size. These results are depicted in Fig. 33a. Despite the fact that the yields of secondary-ion *clusters* increase in a non-additive way with increasing cluster size, the shape of their energy distributions remains essentially unchanged. This finding is exemplified, in Fig. 33b, for Ta_4^+ secondary ions sputtered by different Au_m^- projectiles.

Investigations into the emission of sputtered *neutral* species (atoms and clusters) from silver under cluster bombardment were initiated by *Wucher* and his group [691–694]. They reported the abundance distributions of the emitted cluster, but no energy spectra were recorded in these studies. The results reveal that, in contrast to published experiments on sputtered ionic species, the relative abundance of neutral clusters among the sputtered flux is not significantly enhanced with increasing projectile nuclearity. An associated molecular dynamics study [695, 696] of self-sputtering of silver by mono- and poly-atomic projectiles revealed the calculated yields per projectile atom to exhibit a distinct non-linear enhancement when compared to the respective values calculated for monatomic projectiles of the same impact velocity.

Only very few energy spectra of *neutral* species under cluster bombardment have been measured so far [684, 697, 698]. *Winograd's* group [684] has recorded comparative energy spectra of *neutral* Ag and Ag_2 sputtered from polycrystalline silver by 15 keV Ga^+ and C_{60}^+ projectiles. Figure 34 shows

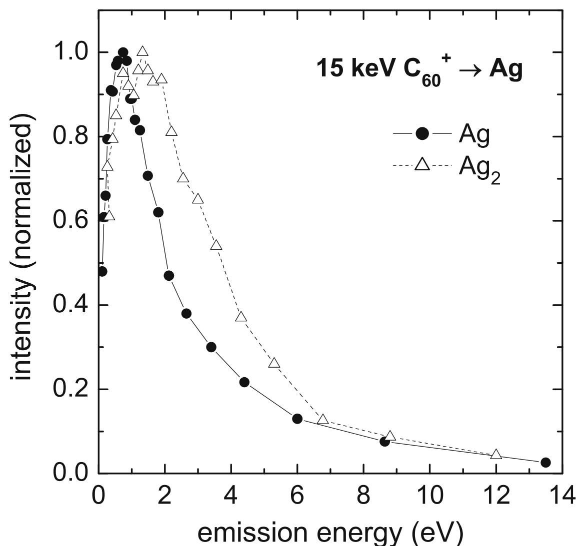

Fig. 34. Kinetic energy distributions of *neutral* Ag atoms and Ag_2 dimers sputtered by 15 keV C_{60}^+ ions from polycrystalline silver [684]

the respective distributions for fullerene ion bombardment. The Ag-atoms sputtered by C_{60}^+ exhibit a most probable emission energy of 0.8 ± 0.1 eV, compared to 1.9 ± 0.4 eV for Ga^+ irradiation. Of special interest is the finding that the most probable energy of the Ag_2 dimer is larger than for the monomer, cf. Fig. 34. This trend is opposite to that found for atomic (Ga^+) bombardment. The authors speculate that the emission mechanisms under cluster impact may resemble an adiabatic expansion from a superheated volume. Then, all particles would leave the surface with similar velocity, thus leading to larger kinetic energies for heavier species.

Similar arguments were invoked by *Wucher* and coworkers [698] to explain their measured energy spectra of neutral In atoms sputtered from indium by 5 and 10 keV Au_m^- (m = 1, 2, and 3) cluster ions. With increasing energy and mass of the cluster, these energy distributions exhibit a distinct low-energy emission component that is superimposed onto the typical spectrum for collision-cascade sputtering. Figure 35 depicts these data and exemplifies that for Au_2^- and Au_3^- irradiation that lower-energy part dominates the energy spectrum of In atoms. The authors demonstrate that this "spike" contribution can be described by the gas-flow model of *Urbassek* and *Michl* [311] which has been mentioned in Sect. 4.2.2. Under these conditions, the emission closely resembles a free expansion of a supercritically heated sub-surface volume. This jet expansion scenario is further corroborated by the observation [698] that the *emission-velocity distributions* of monomers and dimers are essentially identical.

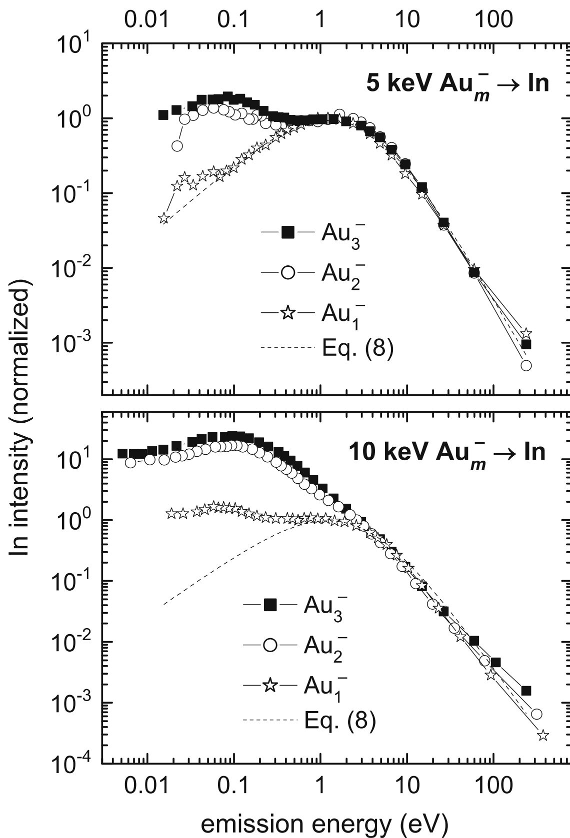

Fig. 35. Emission energy spectra of neutral In atoms sputtered from a polycrystalline In surface by 5 keV and 10 keV Au_m^- ($m = 1 - 3$) projectiles. The *dotted lines* are the predictions of (8) [698]

The effect of the mass and incidence angle of keV energy polyatomic projectiles in silicon sputtering was investigated via molecular dynamics simulations [699]. The kinetic energy distributions of Si atoms under Au and Au_2 bombardment (with an energy of 1.5 keV/atom) were computed both at normal incidence and at 45°. In comparison to Au impact at normal incidence, the spectra for both projectiles incident at 45° are broader with increased low (< 1 eV) and high energy contributions.

6.4 Angular Distributions under Cluster Irradiation

Data on the angular emission characteristics of sputtered species for high-density collision cascades are comparatively rare [400, 700]. The angular distributions of gold self-sputtering at room temperature by 10–30 keV/atom

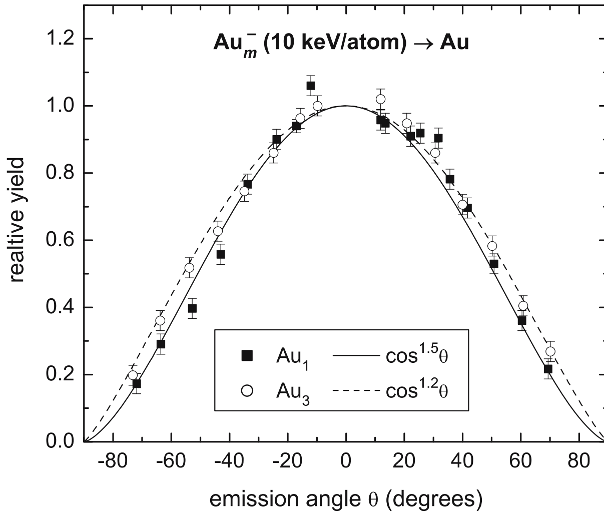

Fig. 36. Polar angular distributions of polycrystalline gold sputtered by Au_1^- and Au_3^- ions (energy 10 keV/atom). The *curves* are fits of the experimental data to $\cos^y\theta$ distributions [700]

Au^-, Au_2^-, and Au_3^- ions have been measured by *Andersen* and coworkers [700]. The sputtered distributions from cluster bombardment of non-textured targets were found to be substantially more isotropic (i.e., cosine like) than the distributions stemming from atomic bombardment. According to the authors, this rules out that the non-linear, presumably spike-produced, component is caused by an outward directed jet of material. Specifically, distributions produced by cluster bombardment could be fitted by $\cos^y\theta$, with $y = 1.2$–1.3; by contrast, for Au irradiation the observed exponents y were substantially larger, $y \geq 1.5$, and were found to increase with impact energy. Figure 36 shows data from that work [700], depicting the relative sputtering yields of Au bombarded by 10 keV/atom Au^- and Au_3^- species. While the distribution resulting from Au_3^- cluster bombardment can be fitted very well by $\cos^{1.2}\theta$, that due to atomic irradiation is best approximated by $\cos^{1.5}\theta$. From measurements on heavily textured samples the authors conclude that the linear and nonlinear components of the yields originate from the same cascades, but are separated in time. The temporal development of sputtered atom distributions from Au targets resulting from 100 keV/atom Au_2 impact was examined by MD simulations [701].

Very pronounced differences in the angular distributions under atomic and cluster bombardment were found for larger clusters by *Yamada*, *Toyoda* and their coworkers [666, 702, 703]: they sputtered a Cu specimen by Ar_{2000} and Ar_{3000} clusters with an energy of 10 and 20 keV and observed angular spectra that are extremely peaked at very oblique emission angles. Figure 37 displays these data in comparison to the distribution obtained by

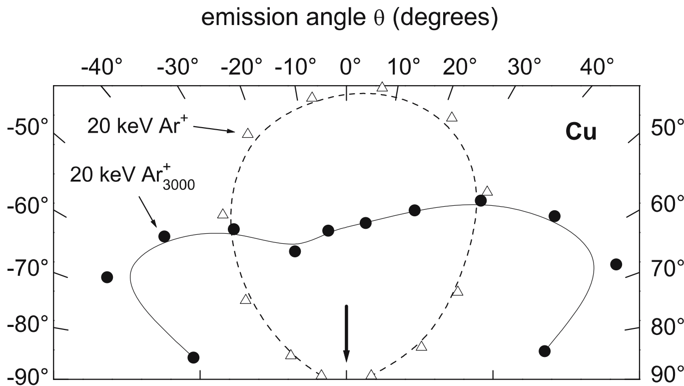

Fig. 37. Polar angular distributions of Cu sputtered by 20 keV Ar^+ monomers (*open triangles*) and by 20 keV Ar^+_{3000} cluster ions (*closed circles*), both at normal incidence. The *lines* are drawn to guide the eye [702]

monomer bombardment (20 keV Ar^+) which is very close to cosine. In associated molecular-dynamics computer simulations the formation of a crater with a distinct rim was noted for Ar cluster impact at normal incidence; the sputtered atoms emitted at oblique angles were found to originate from that crater rim. This kind of sputtering process was termed *"lateral"* sputtering and is probably responsible for surface smoothing as observed in several experimental studies [664–666] and in computer simulations [704].

7 Summary

The energy and angular distributions of sputtered species from a wide variety of target materials (metals, semiconductors, alkali halides, frozen gases, organic solids) are presented, covering irradiation conditions for which nuclear (elastic) collisions constitute the dominant energy loss process, i. e., from about 100 eV to some 100 keV. For the regime of *linear collision cascades*, energy spectra of (neutral) atoms show consistently good agreement with theoretical predictions, while the mechanisms leading to excited/ionized species emerge now more clearly. Emphasis was laid on the emission characteristics of clusters and (large) organic molecules. Computer simulations appear to be extremely valuable to elucidate the pertinent ejection processes. In the *single knockon* regime, energy and angular spectra demonstrate convincingly the (more or less pronounced) presence of an anisotropy in collision cascades and the importance of collision sequences with a small number of recoil generations. In particular, energy distribution data obtained under low (near-threshold) impact energies or oblique incidence angles are well suited to illustrate those features. The occurrence of *high-density collision cascades* is examined for the case of cluster bombardment. Apart from non-linear yield

enhancements, the energy and angle distributions for rather small bombarding species (composed of a few atoms) do not deviate strongly from those obtained for more diluted cascades. However, indications for a possible additional low-energy component were noted in energy spectra under specific bombardment conditions. By contrast, for larger cluster projectiles (with hundreds or thousands of atoms) angular emission distributions exhibit very pronounced differences in that atoms are ejected under very oblique emission angles. It appears that further detailed studies will be required to understand these features in quantitative terms. It is probably justified to think that the investigation of angular and energy distributions of sputtered species will remain a rewarding subject of research in the years to come; such studies can be expected to contribute also substantially to elucidate the energy dissipation processes of energetic ions in solids.

Acknowledgements

I am grateful to the following colleagues for granting the permission to reproduce some of their results and for providing the respective files: H. Andersen, G. Betz, W. Calaway, A. Delcorte, B. Garrison, A. Goehlich, W. Hofer, W. Husinsky, Z. Postawa, R. Pedrys, U. Rasulev, N. Toyoda, H. Urbassek, E. Vandeweert, N. Winograd, and A. Wucher.

References

[1] N. Bohr: K. Dan. Vidensk. Selsk. Mat. Fys. Medd. **18(8)** (1948) 231
[2] G. H. Kinchin, R. S. Pease: Rep. Prog. Phys. **18** (1955) 231
[3] F. Seitz, J. S. Koehler: in F. Seitz, D. Turnbull (Eds.): *Solid State Physics*, vol. 2 (Academic, New York 1956) p. 305 231
[4] R. Behrisch: in S. Flügge, F. Trendelenburg (Eds.): *Ergebnisse der Exakten Naturwissenschaften* (Springer, Berlin, Heidelberg 1964) p. 295 231, 232, 277, 278
[5] M. Kaminsky: *Atomic and Ionic Impact Phenomena on Metal Surfaces* (Springer, Berlin, Heidelberg 1965) 231
[6] G. Leibfried: *Bestrahlungseffekte in Festkörpern* (Teubner, Stuttgart 1965) 231
[7] G. Carter, J. S. Colligon: *Ion Bombardment of Solids* (Heineman, London 1968) 231, 242
[8] M. W. Thompson: *Defects and Radiation Damage in Metals* (Cambridge Univ. Press, Cambridge 1969) 231, 233
[9] C. Lehmann: *Interaction of Radiation with Solids and Elementary Defect Production* (North-Holland, Amsterdam 1977) 231
[10] E. S. Mashkova, V. A. Molchanov: *Medium-Energy Ion Reflection from Solids* (North-Holland, Amsterdam 1985) 231
[11] J. W. Rabalais (Ed.): *Low Energy Ion-Surface Interactions* (Wiley, Chichester 1994) 231

[12] H. Gnaser: *Low-Energy Ion Irradiation of Solid Surfaces* (Springer, Berlin, Heidelberg 1999) 231, 237, 252, 255, 282, 283, 284, 295
[13] P. Sigmund: *Stopping of Heavy Ions* (Springer, Berlin, Heidelberg 2004) 231
[14] R. Behrisch (Ed.): *Sputtering by Particle Bombardment I*, Top. Appl. Phys. **47** (Springer, Berlin, Heidelberg 1981) 231
[15] R. Behrisch (Ed.): *Sputtering by Particle Bombardment II*, Top. Appl. Phys. **52** (Springer, Berlin, Heidelberg 1983) 231
[16] R. Behrisch, K. Wittmaack (Eds.): *Sputtering by Particle Bombardment III*, Top. Appl. Phys. **64** (Springer, Berlin, Heidelberg 1991) 231
[17] P. Sigmund (Ed.): *Fundamental Processes in Sputtering of Atoms and Molecules*, K. Dan. Vidensk. Selsk. Mat. Fys. Medd. **43** (1993) 231, 245
[18] G. K. Wehner: Phys. Rev. **114**, 1270 (1959) 232, 238, 245
[19] G. K. Wehner: J. Appl. Phys. **31**, 1392 (1960) 232, 238, 245
[20] K. Kopitzki, H.-E. Stier: Z. Naturforsch. **17a**, 346 (1962) 232, 238, 245
[21] M. W. Thompson, R. S. Nelson: Philos. Mag. **7**, 2015 (1962) 232, 238, 240, 245, 293
[22] R. V. Stuart, G. K. Wehner: J. Appl. Phys. **35**, 1819 (1964) 232, 238, 245, 285
[23] H. Beuscher, K. Kopitzki: Z. Phys. **184**, 382 (1965) 232, 238, 245
[24] H. Oechsner, L. Reichert: Phys. Lett. **23**, 90 (1966) 232, 239, 285
[25] M. W. Thompson: Philos. Mag. **18**, 377 (1968) 232, 233, 235, 252, 280, 288
[26] P. Sigmund: Phys. Rev. **184**, 383 (1969) 232, 233, 234, 245, 293
[27] P. Sigmund: Phys. Rev. **187**, 768 (1969) 232, 233, 234, 245, 293
[28] M. T. Robinson: Philos. Mag. **12**, 741 (1965) 233
[29] M. T. Robinson: Philos. Mag. **17**, 639 (1968) 233
[30] P. Sigmund: Rev. Roum. Phys. **17**, 823 (1972) 233, 234
[31] P. Sigmund: Rev. Roum. Phys. **17**, 969 (1972) 233
[32] P. Sigmund: Rev. Roum. Phys. **17**, 1079 (1972) 233
[33] P. Sigmund: in R. Behrisch (Ed.): *Sputtering by Particle Bombardment I*, Top. Appl. Phys **47** (Springer, Berlin, Heidelberg 1981) p. 9 233, 234, 245, 283
[34] P. Sigmund: Appl. Phys. Lett. **14**, 114 (1969) 233
[35] P. Sigmund: in N. H. Tolk, J. C. Tully, W. Heiland (Eds.): *Inelastic Ion-Surface Collisions* (Academic, New York 1977) p. 121 233, 293
[36] P. Sigmund: Nucl. Instrum. Methods B **27**, 1 (1987) 233, 275, 293
[37] M. T. Robinson: Philos. Mag. **12**, 145 (1965) 233
[38] W. Brandt, R. Laubert: Nucl. Instrum. Methods **47**, 201 (1967) 233
[39] M. M. R. Williams: Philos. Mag. **34**, 669 (1976) 233
[40] M. M. R. Williams: Philos. Mag. A **43**, 1221 (1981) 233
[41] M. W. Thompson: Phys. Rep. **69**, 335 (1981) 233, 235, 288
[42] M. W. Thompson: Nucl. Instrum. Methods B **18**, 411 (1987) 233, 237, 238, 280, 288
[43] R. Kelly: Radiat. Eff. **80**, 273 (1984) 233
[44] M. W. Thompson: Philos. Trans. R. Soc. Lond. Ser. A **362**, 5 (2004) 233
[45] M. M. Jakas: Philos. Trans. R. Soc. Lond. Ser. A **362**, 139 (2004) 233
[46] W. Eckstein: *Computer Simulation of Ion Solid Interactions*, Ser. Mater. Sci. **10** (Springer, Berlin, Heidelberg 1991) 233, 283
[47] D. E. Harrison, Jr.: Radiat. Eff. **70**, 1 (1983) 233, 279
[48] D. E. Harrison, Jr.: Crit. Rev. Solid State Mater. Sci. **14**, S1 (1988) 233, 279
[49] H. H. Andersen: Nucl. Instrum. Methods **18**, 321 (1987) 233

[50] J. P. Biersack: Nucl. Instrum. Methods B **27**, 21 (1987) 233
[51] M. T. Robinson: K. Dan. Vidensk. Selsk. Mat. Fys. Medd. **43**, 27 (1993) 233, 234
[52] M. H. Shapiro: Radiat. Eff. Def. Solids **142**, 259 (1997) 233
[53] W. Eckstein: Nucl. Instrum. Methods B **232**, 108 (2005) 233
[54] M. T. Robinson: in R. Behrisch (Ed.): *Sputtering by Particle Bombardment I*, Top. Appl. Phys. **47** (Springer, Berlin, Heidelberg 1981) p. 73 234, 235, 244, 277
[55] J. Lindhard, V. Nielsen, M. Scharff: K. Dan. Vidensk. Selsk. Mat. Fys. Medd. **36(10)** (1968) 234
[56] J. Lindhard, M. Scharff, H. E. Schiøtt: K. Dan. Vidensk. Selsk. Mat. Fys. Medd. **33(14)** (1963) 234
[57] K. B. Winterbon, P. Sigmund, J. B. Sanders: K. Dan. Vidensk. Selsk. Mat. Fys. Medd. **37(14)** (1970) 234
[58] M. Vicanek, J. J. Jimenéz-Rodríguez, P. Sigmund: Nucl. Instrum. Methods B **36**, 124 (1989) 234
[59] W. O. Hofer: in R. Behrisch, K. Wittmaack (Eds.): *Sputtering by Particle Bombardment III*, Top. Appl. Phys. **64** (Springer, Berlin, Heidelberg 1991) p. 15 235, 237, 241, 243, 244, 245, 254, 255, 277, 278
[60] G. Betz, K. Wien: Int. J. Mass Spectrom. Ion Proc. **140**, 1 (1994) 235, 237, 245, 260, 269, 271
[61] J. P. Baxter, J. Singh, G. A. Schick, P. H. Kobrin, N. Winograd: Nucl. Instrum. Methods B **17**, 300 (1986) 236, 243
[62] B. J. Garrison: Nucl. Instrum. Methods B **17**, 305 (1986) 236
[63] D. P. Jackson: Radiat. Eff. **18**, 185 (1973) 236
[64] D. P. Jackson: Can. J. Phys. **53**, 1513 (1975) 236
[65] B. J. Garrison, N. Winograd, D. Lo, T. A. Tombrello, M. H. Shapiro, D. E. Harrison: Surf. Sci. **180**, L129 (1987) 236
[66] R. Kelly: Nucl. Instrum. Methods B **18**, 388 (1987) 236, 253
[67] H. Gades, H. M. Urbassek: Nucl. Instrum. Methods B **69**, 232 (1992) 236, 237
[68] J. P. Biersack, W. Eckstein: Appl. Phys. A **34**, 73 (1984) 236, 275, 283
[69] K. A. Gschneidner: in F. Seitz, D. Turnbull (Eds.): *Solid State Physics*, vol. 16 (Academic, New York 1964) p. 275 236
[70] R. Kelly: Nucl. Instrum. Methods **149**, 553 (1978) 236, 252, 253
[71] R. Kelly: Surf. Sci. **100**, 85 (1980) 236, 252, 253
[72] H. Gades, H. M. Urbassek: Nucl. Instrum. Methods B **88**, 218 (1994) 236, 237
[73] M. H. Shapiro, P. K. Haff, T. A. Tombrello, D. E. Harrison, Jr., R. P. Webb: Radiat. Eff. **89**, 234 (1985) 236
[74] A. Oliva, R. Kelly, G. Falcone: Nucl. Instrum. Methods B **19/20**, 101 (1987) 236
[75] R. E. Honig: J. Appl. Phys. **29**, 549 (1958) 237, 255
[76] J. R. Woodyard, C. B. Cooper: J. Appl. Phys. **35**, 1107 (1964) 237
[77] H. Gnaser, J. Fleischhauer, W. O. Hofer: Appl. Phys. A **37**, 211 (1985) 237
[78] D. Lipinsky, R. Jede, O. Ganschow, A. Benninghoven: J. Vac. Sci. Technol. A **3**, 2007 (1985) 237
[79] H. Oechsner, E. Stumpe: Appl. Phys. **14**, 43 (1977) 237

[80] H. Oechsner: in H. Oechsner (Ed.): *Thin Film and Depth Profile Analysis* (Springer, Berlin, Heidelberg 1984) p. 63 237
[81] W. Bieck, H. Gnaser, H. Oechsner: Appl. Phys. Lett. **63**, 845 (1993) 237, 239
[82] J. W. Coburn, E. Kay: Appl. Phys. Lett. **18**, 435 (1971) 237
[83] J. W. Coburn, E. Kay: Appl. Phys. Lett. **19**, 350 (1971) 237
[84] J. W. Coburn, E. W. Eckstein, E. Kay: J. Appl. Phys. **46**, 2828 (1975) 237
[85] A. Benninghoven, F. G. Rüdenauer, H. W. Werner: *Secondary Ion Mass Spectrometry* (Wiley, New York 1987) 237, 239, 243
[86] J. C. Vickerman, D. Briggs (Eds.): *ToF-SIMS: Surface Analysis by Mass Spectrometry* (IM Publications and Surface Spectra, Chichester, Manchester 2000) 237, 260, 266
[87] H. Gnaser: in S. G. Pandalai (Ed.): *Recent Research Developments in Vacuum Science & Technology* (Transworld Research Network, Kerala 2003) p. 111 237
[88] M. J. Pellin, W. F. Calaway, I. V. Veryovkin: in J. C. Vickerman, D. Briggs (Eds.): *ToF-SIMS: Surface Analysis by Mass Spectrometry* (IM Publications and Surface Spectra, Chichester, Manchester 2000) p. 375 237
[89] M. J. Pellin, C. E. Young, W. F. Calaway, J. W. Burnett, B. Jørgensen, E. L. Schweitzer, D. M. Gruen: Nucl. Instrum. Methods B **18**, 446 (1987) 238
[90] B. W. Schueler: in J. C. Vickerman, D. Briggs (Eds.): *ToF-SIMS: Surface Analysis by Mass Spectrometry* (IM Publications and Surface Spectra, Chichester, Manchester 2000) p. 75 238
[91] A. Wucher: in J. C. Vickerman, D. Briggs (Eds.): *ToF-SIMS: Surface Analysis by Mass Spectrometry* (IM Publications and Surface Spectra, Chichester, Manchester 2000) p. 347 238, 241
[92] B. Witzel, C. J. G. J. Uiterwaal, H. Schröder, D. Charalambidis, K.-L. Kompa: Phys. Rev. A **58**, 3836 (1998) 238
[93] M. G. Payne, L. Deng, N. Thonnard: Rev. Sci. Instrum. **65**, 2433 (1994) 238
[94] C. H. Becker, K. T. Gillen: Appl. Phys. Lett. **45**, 1063 (1984) 238
[95] O. Almén, G. Bruce: Nucl. Instrum. Methods **11**, 257 (1961) 238, 277
[96] E. Hulpke, C. Schlier: Z. Phys. **207**, 294 (1967) 238
[97] J. Politiek, J. Kistemaker: Radiat. Eff. **2**, 129 (1969) 238, 241
[98] R. V. Stuart, G. K. Wehner, G. S. Anderson: J. Appl. Phys. **40**, 803 (1969) 238
[99] D. Briggs, M. P. Seah (Eds.): *Auger and X-Ray Photoelectron Spectroscopy*, vol. 1 (Wiley, Chichester 1994) 238
[100] W. Bieck, H. Gnaser, H. Oechsner: J. Vac. Sci. Technol. A **12**, 2537 (1994) 239
[101] A. Wucher, H. Oechsner: Nucl. Instrum. Methods B **18**, 458 (1987) 239
[102] R. B. Wright, D. M. Gruen: J. Chem. Phys. **72**, 147 (1980) 239
[103] I. S. T. Tsong: in E. Taglauer, W. Heiland (Eds.): *Ineleastic Particle-Surface Collisions* (Springer, Berlin, Heidelberg 1982) p. 258 239
[104] D. Hammer, E. Benes, P. Blum, W. Husinsky: Rev. Sci. Instrum. **47**, 1178 (1976) 240
[105] W. Husinsky, R. Bruckmüller, P. Blum, F. Viehböck, D. Hammer, E. Benes: J. Appl. Phys. **48**, 4737 (1977) 240
[106] W. Husinsky: J. Vac. Sci. Technol. B **3**, 1546 (1985) 240
[107] A. Elbern, E. Hintz, B. Schweer: J. Nucl. Mater. **76 & 77**, 143 (1978) 240

[108] H. L. Bay, W. Berres, E. Hintz: Nucl. Instrum. Methods **194**, 555 (1982) 240
[109] R. B. Wright, M. J. Pellin, D. M. Gruen: Surf. Sci. **110**, 151 (1981) 240
[110] M. W. Thompson, B. W. Farmery, P. A. Newson: Philos. Mag. **18**, 361 (1968) 240
[111] G. E. Chapman, B. W. Farmery, M. W. Thompson, I. H. Wilson: Radiat. Eff. **13**, 121 (1972) 240
[112] I. Reid, M. W. Thompson, B. W. Farmery: Radiat. Eff. **46**, 163 (1980) 240
[113] M. Szymonski, A. E. de Vries: Radiat. Eff. **54**, 135 (1981) 241
[114] G. Carter, B. Navinšek, J. L. Whitton: in R. Behrisch (Ed.): *Sputtering by Particle Bombardment II*, Top. Appl. Phys **52** (Springer, Berlin, Heidelberg 1983) p. 231 242
[115] B. M. U. Scherzer: in R. Behrisch (Ed.): *Sputtering by Particle Bombardment II*, Top. Appl. Phys. **52** (Springer, Berlin, Heidelberg 1986) p. 271 242
[116] F. A. Stevie, P. M. Kahora, D. S. Simons, P. Chi: J. Vac. Sci. Technol A **6**, 76 (1988) 242, 277
[117] A. Karen, K. Okuno, F. Soeda, A. Ishitani: J. Vac. Sci. Technol. A **9**, 2247 (1991) 242, 277
[118] U. Littmark, W. O. Hofer: J. Mater. Sci. **13**, 2577 (1978) 243
[119] J. I. Goldstein, D. E. Newbury, P. Echlin, D. C. Joy, C. Fiori, E. Lifshin: *Scanning Electron Microscopy and X-Ray Microanalysis* (Plenum, New York 1984) 243
[120] W. K. Chu, J. W. Mayer, M. A. Nicolet: *Backscattering Spectrometry* (Academic, New York 1978) 243
[121] S. A. E. Johansson, J. L. Campbell, K. G. Malmqvist (Eds.): *Particle-Induced X-Ray Emission Spectrometry (PIXE)* (Wiley, New York 1995) 243
[122] P. H. Kobrin, G. A. Schick, J. P. Baxter, N. Winograd: Rev. Sci. Instrum. **57**, 1354 (1986) 243, 280
[123] J. P. Baxter, G. A. Schick, J. Singh, P. H. Kobrin, N. Winograd: J. Vac. Sci. Technol. A **4**, 1218 (1986) 243, 279
[124] N. Winograd, P. H. Kobrin, G. A. Schick, J. Singh, J. P. Baxter, B. J. Garrison: Surf. Sci. **176**, L817 (1986) 243
[125] C. T. Reimann, K. Walzl, M. El-Maazawi, D. M. Deaven, B. J. Garrison, N. Winograd: J. Chem. Phys. **89**, 539 (1988) 243
[126] D. L. Weathers, S. J. Spicklemire, T. A. Tombrello, I. D. Hutcheon, H. Gnaser: Nucl. Instrum. Methods B **73**, 135 (1993) 243, 283
[127] M. W. Schkerl, P. Sigmund, M. Vicanek: K. Dan. Vidensk. Selsk. Mat. Fys. Medd. **44(3)**, 5 (1996) 244
[128] M. W. Schkerl, M. Vicanek, P. Sigmund: Nucl. Instrum. Methods B **102**, 86 (1995) 244
[129] G. K. Wehner: J. Appl. Phys. **26**, 1056 (1955) 244, 277
[130] G. K. Wehner: Phys. Rev. **102**, 690 (1956) 244, 277
[131] H. E. Roosendaal, J. B. Sanders: Radiat. Eff. **80**, 137 (1980) 244
[132] A. R. Krauss, R. B. Wright: J. Nucl. Mater. **89**, 229 (1980) 245
[133] W. Husinsky, G. Nicolussi, G. Betz: Nucl. Instrum. Methods B **82**, 323 (1993) 245, 246, 255, 256
[134] C. S. Hansen, W. F. Calaway, B. V. King, M. J. Pellin: Surf. Sci. **398**, 211 (1998) 245, 246, 255
[135] M. Wahl, A. Wucher: Nucl. Instrum. Methods B **94**, 36 (1994) 245, 246, 255, 256, 257

[136] S. R. Coon, W. F. Calaway, J. W. Burnett, M. J. Pellin, D. M. Gruen, D. R. Spiegel, J. M. White: Surf. Sci. **259**, 275 (1991) 246, 255, 256
[137] S. R. Coon, W. F. Calaway, M. J. Pellin, J. M. White: Surf. Sci. **298**, 161 (1993) 246, 255, 256
[138] S. R. Coon, W. F. Calaway, M. J. Pellin, G. A. Curlee, J. M. White: Nucl. Instrum. Methods B **82**, 329 (1993) 246, 255, 256
[139] A. Wucher, M. Wahl, H. Oechsner: Nucl. Instrum. Methods B **82**, 337 (1993) 246, 255, 256
[140] A. Wucher, M. Wahl, H. Oechsner: Nucl. Instrum. Methods B **83**, 73 (1993) 246, 255, 256
[141] A. Wucher, M. Wahl: Nucl. Instrum. Methods B **115**, 581 (1996) 246, 255, 256
[142] R. Heinrich, A. Wucher: Nucl. Instrum. Methods B **140**, 27 (1998) 246, 255, 256
[143] M. L. Yu: in R. Behrisch, K. Wittmaack (Eds.): *Sputtering by Particle Bombardment III*, vol. 64, Top. Appl. Phys. (Springer, Berlin, Heidelberg 1991) p. 91 247, 251, 252, 258
[144] D. M. Gruen, M. J. Pellin, C. E. Young, M. H. Mendelsohn: Phys. Scripta **T6**, 42 (1983) 247
[145] G. Betz: Nucl. Instrum. Methods B **27**, 104 (1987) 247
[146] B. Schweer, H. L. Bay: Appl. Phys. A **29**, 53 (1982) 247
[147] C. E. Young, W. F. Calaway, M. J. Pellin, D. M. Gruen: J. Vac. Sci. Technol. A **2**, 693 (1984) 247
[148] M. J. Pellin, R. B. Wright, D. M. Gruen: J. Chem. Phys. **74**, 6448 (1981) 247
[149] M. L. Yu, D. Grischkowsky, A. C. Balant: Phys. Rev. Lett. **48**, 427 (1982) 247
[150] B. I. Craig, J. P. Baxter, J. Singh, G. A. Schick, P. H. Kobrin, B. J. Garrison, N. Winograd: Phys. Rev. Lett. **57**, 1351 (1986) 247
[151] G. Nicolussi, W. Husinsky, D. Gruber, G. Betz: Phys. Rev. B **51**, 8779 (1995) 247
[152] E. Dullni: Appl. Phys. A **38**, 131 (1985) 247
[153] W. Husinsky, G. Betz, I. Girgis: J. Vac. Sci. Technol. A **2**, 698 (1984) 247, 253
[154] R. B. Wright, M. J. Pellin, D. M. Gruen, C. E. Young: Nucl. Instrum. Methods **170**, 295 (1980) 247
[155] Z. Postawa, M. El-Maazawi, R. Maboudian, N. Winograd: Nucl. Instrum. Methods Phys. Res. B **67**, 565 (1992) 247
[156] C. He, Z. Postawa, S. W. Rosencrance, R. Chatterjee, B. J. Garrison, N. Winograd: Phys. Rev. Lett. **75**, 3950 (1995) 247, 280
[157] E. Vandeweert, V. Philipsen, W. Bouwen, P. Thoen, H. Weidele, R. E. Silverans, P. Lievens: Phys. Rev. Lett. **78**, 138 (1997) 247
[158] A. Cortona, W. Husinsky, G. Betz: Phys. Rev. B **59**, 15495 (1999) 247
[159] E. Vandeweert, P. Lievens, V. Philipsen, J. Bastiaansen, R. E. Silverans: Phys. Rev. B **64**, 195417 (2001) 247, 249, 250, 251
[160] J. Bastiaansen, F. Vervaecke, E. Vandeweert, P. Lievens, R. E. Silverans: Spectrochim. Acta B **58**, 1147 (2003) 247, 250, 251
[161] P. Lievens, V. Philipsen, E. Vandeweert, , R. E. Silverans: Nucl. Instrum. Methods B **135**, 471 (1998) 247, 249

[162] E. Vandeweert, J. Bastiaansen, V. Philipsen, P. Lievens, , R. E. Silverans: Nucl. Instrum. Methods B **164–165**, 795 (2000) 247, 251
[163] J. Bastiaansen, F. Vervaecke, E. Vandeweert, P. Lievens, R. E. Silverans: Nucl. Instrum. Methods B **203**, 158 (2003) 247, 250, 251
[164] W. Berthold, A. Wucher: Phys. Rev. Lett. **76**, 2181 (1996) 247
[165] W. Berthold, A. Wucher: Phys. Rev. B **56**, 4251 (1997) 247
[166] R. E. Silverans, J. Bastiaansen, V. Philipsen, E. Vandeweert, P. Lievens: Nucl. Instrum. Methods B **182**, 127 (2001) 247, 250
[167] J. Bastiaansen, V. Philipsen, F. Vervaecke, E. Vandeweert, P. Lievens, R. E. Silverans: Phys. Rev. B **68**, 073409 (2003) 247, 250
[168] C. Staudt, A. Wucher, J. Bastiaansen, V. Philipsen, E. Vandeweert, P. Lievens, R. E. Silverans, Z. Sroubek: Phys. Rev. B **66**, 085415 (2002) 247, 248
[169] Z. Sroubek, F. Sroubek, A. Wucher, J. A. Yarmoff: Phys. Rev. B **68**, 115426 (2003) 248
[170] B. J. Garrison, N. Winograd, R. Chatterjee, Z. Postawa, A. Wucher, E. Vandeweert, P. Lievens, V. Philipsen, R. E. Silverans: Rap. Commun. Mass Spectrom. **12**, 1266 (1998) 250
[171] J. Los, J. J. C. Geerlings: Phys. Rep. **190**, 133 (1990) 251
[172] E. Veje: Phys. Rev. B **28**, 88 (1983) 251
[173] E. Veje: Phys. Rev. B **28**, 5029 (1983) 251
[174] T. R. Lundquist: J. Vac. Sci. Technol. **15**, 684 (1978) 251
[175] T. R. Lundquist: Surf. Sci. **90**, 548 (1979) 251
[176] A. R. Krauss, D. M. Gruen: Surf. Sci. **92**, 14 (1980) 251
[177] A. Wucher, H. Oechsner: Surf. Sci. **199**, 567 (1988) 251
[178] S. N. Schauer, P. Williams: Phys. Rev. B **46**, 15452 (1992) 251
[179] R. F. Garrett, R. J. MacDonald, D. J. O'Connor: Nucl. Instrum. Methods **218**, 333 (1983) 251
[180] M. J. Vasile: Phys. Rev. B **29**, 3785 (1984) 251
[181] P. A. W. van der Heide: Nucl. Instrum. Methods B **86**, 373 (1994) 251
[182] P. A. W. van der Heide: Nucl. Instrum. Methods B **93**, 421 (1994) 251
[183] P. A. W. van der Heide: Surf. Sci. **341**, 150 (1995) 251
[184] P. A. W. van der Heide: Surf. Sci. **365**, 473 (1996) 251
[185] H. Gnaser: Phys. Rev. B **54**, 16456 (1996) 251, 252
[186] P. Williams: Surf. Sci. **90**, 588 (1979) 252
[187] M. L. Yu, N. D. Lang: Phys. Rev. Lett. **50**, 127 (1983) 252
[188] N. D. Lang: Phys. Rev. B **27**, 2019 (1983) 252, 258
[189] S. Datz, C. Snoek: Phys. Rev. **134**, A347 (1964) 252, 288
[190] E. S. Mashkova, V. A. Molchanov: Zh. Tkh. Fiz. **35**, 1321 (1965) [Sov. Phys.-Tech. Phys. **10**, 1024 (1966)] 252, 288
[191] W. F. van der Weg, D. J. Bierman: Physica **38**, 406 (1968) 252, 288
[192] W. F. van der Weg, D. J. Bierman: Physica **44**, 177 (1969) 252, 288
[193] P. J. Schneider, W. Eckstein, H. Verbeek: Nucl. Instrum. Methods **194**, 387 (1982) 252, 288
[194] P. J. Schneider, W. Eckstein, H. Verbeek: Nucl. Instrum. Methods **218**, 713 (1983) 252, 288
[195] J. A. Schultz, P. Kumar, J. W. Rabalais: Chem. Phys. Lett. **100**, 214 (1983) 252, 288
[196] H.-J. Barth, E. Mühling, W. Eckstein: Appl. Surf. Sci. **22/23**, 136 (1985) 252

[197] H.-J. Barth, E. Mühling, W. Eckstein: Surf. Sci. **166**, 458 (1986) 252
[198] W. Eckstein, H.-J. Barth, E. Mühling: Nucl. Instrum. Methods B **14**, 507 (1986) 252
[199] W. Eckstein, E. S. Mashkova: Nucl. Instrum. Methods B **62**, 438 (1992) 252
[200] W. Eckstein: Nucl. Instrum. Methods B **27**, 78 (1987) 252, 289
[201] G. Betz: Surf. Sci. **92**, 283 (1980) 253
[202] G. Betz, G. K. Wehner: in R. Behrisch (Ed.): *Sputtering by Particle Bombardment II*, Top. Appl. Phys. **52** (Springer, Berlin, Heidelberg 1983) p. 11 253, 283
[203] H. H. Andersen: in J. S. Williams, J. M. Poate (Eds.): *Ion Implantation and Beam Processing* (Academic, Sydney 1984) p. 127 253, 283
[204] M. Szymonski, R. S. Bhattacharya, H. Overeijnder, A. E. de Vries: J. Phys. D: Appl. Phys. **11**, 751 (1978) 253
[205] M. Szymonski, R. S. Bhattacharya: Appl. Phys. **20**, 207 (1979) 253
[206] M. Szymonski: Appl. Phys. **23**, 89 (1980) 253
[207] H. Oechsner, J. Bartella: in I. U. Bulgakov, A. F. Tulinov (Eds.): *Proc. 7th Int. Conf. Atomic Collisions in Solids*, vol. II (Moscow State University, Moscow 1981) p. 55 253
[208] R. P. Schorn, M. A. Zaki Ewiss, E. Hintz: Appl. Phys. A **46**, 291 (1988) 253
[209] D. Grischkowsky, M. L. Yu, A. C. Balant: Surf. Sci. **127**, 315 (1983) 253
[210] M. Szymonski: Phys. Lett **82A**, 203 (1981) 253
[211] T. Mousel, W. Eckstein, H. Gnaser: Nucl. Instrum. Methods B **152**, 36 (1999) 253, 256, 285, 286, 287, 288
[212] M. Vicanek, U. Conrad, H. M. Urbassek: Phys. Rev. B **47**, 617 (1993) 253
[213] E. Dullni: Nucl. Instrum. Methods B **2**, 610 (1984) 253
[214] W. Husinsky, G. Betz: Nucl. Instrum. Methods B **15**, 165 (1986) 253
[215] W. Husinsky, P. Wurz, B. Strehl, G. Betz: Nucl. Instrum. Methods B **18**, 452 (1987) 253
[216] M. Saidoh, H. Gnaser, W. O. Hofer: Appl. Phys. A **40**, 197 (1986) 253
[217] H. Gnaser, M. Saidoh, J. von Seggern, W. O. Hofer: Nucl. Instrum. Methods B **15**, 169 (1986) 253
[218] G. P. Chen, J. von Seggern, H. Gnaser, W. O. Hofer: Appl. Phys. A **49**, 711 (1989) 253
[219] R. Kelly: in R. Kelly, M. F. da Silva (Eds.): *Materials Modification by High-Fluence Beams* (Kluwer, Dordrecht 1988) p. 305 254
[220] R. Kelly: Mater. Sci. Engin. A **115**, 11 (1989) 254
[221] R. Kelly: Nucl. Instrum. Methods B **39**, 43 (1989) 254
[222] I. Bertóti, R. Kelly, M. Mohai, A. Tóth: Nucl. Instrum. Methods B **80/81**, 1219 (1993) 254
[223] H. M. Urbassek, W. O. Hofer: K. Dan. Vidensk. Selsk. Mat. Fys. Medd. **43**, 97 (1993) 254, 255
[224] B. U. R. Sundqvist: in R. Behrisch, K. Wittmaack (Eds.): *Sputtering by Particle Bombardment III*, Top. Appl. Phys. **64** (Springer, Berlin, Heidelberg 1991) p. 257 254, 260
[225] L. Van Vaeck, A. Adriaens, R. Gijbels: Mass Spectrom. Rev. **18**, 1 (1999) 254, 260
[226] A. Adriaens, L. Van Vaeck, F. Adams: Mass Spectrom. Rev. **18**, 48 (1999) 254, 260

[227] A. M. Belu, D. J. Graham, D. G. Castner: Biomater. **24**, 3653 (2003) 254, 260
[228] H. F. Winters, J. W. Coburn: Surf. Sci. Rep. **14**, 161 (1992) 254
[229] H. Oechsner: in A. Benninghoven, et al. (Eds.): *Secondary Ion Mass Spectrometry SIMS III* (Springer, Berlin, Heidelberg 1982) p. 106 254, 256
[230] K. J. Snowdon, W. Heiland: Z. Phys. A **318**, 275 (1984) 254
[231] C. M. Loxton, I. S. T. Tsong, D. A. Reed: Nucl. Instrum. Methods B **2**, 465 (1984) 254
[232] K. Snowdon: Nucl. Instrum. Methods B **9**, 132 (1985) 254
[233] H. Oechsner: in M. M. Popovic, P. Krstic (Eds.): *The Physics of Ionized Gases* (World Scientific, Singapore 1985) p. 571 254
[234] P. Sigmund, H. M. Urbassek, D. Matragrano: Nucl. Instrum. Methods B **14**, 495 (1986) 254
[235] H. M. Urbassek: Nucl. Instrum. Methods B **18**, 587 (1987) 254
[236] A. E. de Vries: Nucl. Instrum. Methods B **27**, 173 (1987) 254
[237] H. H. Andersen: Vacuum **39**, 1095 (1989) 254
[238] I. S. Bitensky, E. S. Parilis, I. A. Wojciechowski: Nucl. Instrum. Methods B **67**, 595 (1992) 254
[239] D. E. Harrison, Jr., C. B. Delaplain: J. Appl. Phys. **47**, 2252 (1976) 254
[240] B. J. Garrison, N. Winograd, D. E. Harrison, Jr.: J. Chem. Phys. **69**, 1440 (1978) 254
[241] B. J. Garrison, N. Winograd, D. E. Harrison, Jr.: Phys. Rev. B **18**, 6000 (1978) 254
[242] N. Winograd, K. E. Foley, B. J. Garrison, D. E. Harrison, Jr.: Phys. Lett. **73A**, 253 (1979) 254
[243] F. Karetta, H. M. Urbassek: Appl. Phys. A **55**, 364 (1992) 254
[244] A. Wucher, B. J. Garrison: Phys. Rev. B **46**, 4855 (1992) 254, 257
[245] A. Wucher, B. J. Garrison: Surf. Sci. **260**, 257 (1992) 254
[246] A. Wucher, B. J. Garrison: Nucl. Instrum. Methods B **67**, 518 (1992) 254
[247] A. Wucher, B. J. Garrison: J. Chem. Phys. **105**, 5999 (1996) 254, 255
[248] G. Betz, W. Husinsky: Nucl. Instrum. Methods B **102**, 281 (1995) 254, 257
[249] M. H. Shapiro, T. A. Tombrello: Nucl. Instrum. Methods B **84**, 453 (1994) 254
[250] J. W. Hartman, M. H. Shapiro, T. A. Tombrello: Nucl. Instrum. Methods B **124**, 31 (1997) 254
[251] J. W. Hartman, M. H. Shapiro, T. A. Tombrello: Nucl. Instrum. Methods B **132**, 406 (1997) 254
[252] G. Betz, W. Husinsky: Philos. Trans. R. Soc. Lond. Ser. A **362**, 177 (2004) 254
[253] W. Ens, R. Beavis, K. G. Standing: Phys. Rev. Lett. **50**, 27 (1983) 254
[254] W. Begemann, S. Dreihöfer, K. H. Meiwes-Broer, H. O. Lutz: Z. Phys. D **3**, 183 (1986) 254
[255] W. Begemann, K. H. Meiwes-Broer, H. O. Lutz: Phys. Rev. Lett. **56**, 2248 (1986) 254
[256] N. K. Dzhemilev, A. M. Goldenberg, I. V. Veryovkin, S. V. Verkhoturov: Int. J. Mass Spectrom. Ion Proc. **107**, R19 (1991) 254, 269
[257] N. K. Dzhemilev, A. M. Goldenberg, I. V. Veryovkin, S. V. Verkhoturov: Int. J. Mass Spectrom. Ion Proc. **141**, 209 (1995) 254, 269

[258] N. K. Dzhemilev, A. M. Goldenberg, I. V. Veryovkin, S. V. Verkhoturov: Nucl. Instrum. Methods B **114**, 245 (1996) 254, 269
[259] A. Wucher, A. D. Bekkerman, N. K. Dzhemilev, S. V. Verkhoturov, I. V. Veryovkin: Nucl. Instrum. Methods B **140**, 311 (1998) 254, 269
[260] A. Wucher, N. K. Dzhemilev, I. V. Veryovkin, S. V. Verkhoturov: Nucl. Instrum. Methods B **149**, 285 (1999) 254
[261] H. Gnaser: Nucl. Instrum. Methods B **149**, 38 (1999) 254, 258
[262] H. Gnaser: Nucl. Instrum. Methods B **164-165**, 705 (2000) 254, 258, 259, 269
[263] K. J. Snowdon, W. Heiland, E. Taglauer: Phys. Rev. Lett. **46**, 284 (1981) 254
[264] E. W. Thomas, L. Efstathiou: Nucl. Instrum. Methods B **2**, 479 (1984) 254
[265] R. de Jonge, T. Baller, M. G. Tenner, A. E. de Vries, K. J. Snowdon: Nucl. Instrum. Methods B **17**, 213 (1986) 254
[266] R. de Jonge, T. Baller, M. G. Tenner, A. E. de Vries, K. J. Snowdon: Europhys. Lett. **2**, 449 (1986) 254
[267] P. Fayet, J. P. Wolf, L. Wöste: Phys. Rev. B **33**, 6792 (1986) 254
[268] A. Wucher: Phys. Rev. B **49**, 2012 (1994) 254
[269] I. Katakuse, T. Ichihara, Y. Fujita, T. Matsuo, T. Sakurai, H. Matsuda: Int. J. Mass Spectrom. Ion Proc. **67**, 229 (1985) 255
[270] I. Katakuse, T. Ichihara, Y. Fujita, T. Matsuo, T. Sakurai, H. Matsuda: Int. J. Mass Spectrom. Ion Proc. **74**, 33 (1986) 255
[271] I. Katakuse, T. Ichihara, T. Matsuo, T. Sakurai, H. Matsuda: Int. J. Mass Spectrom. Ion Proc. **91**, 99 (1989) 255
[272] W. Gerhard: Z. Phys. B **22**, 31 (1975) 255, 260
[273] W. Gerhard, H. Oechsner: Z. Phys. B **22**, 41 (1975) 255, 256
[274] G. P. Können, A. Tip, A. E. de Vries: Radiat. Effects **21**, 269 (1974) 255, 256, 260
[275] G. P. Können, A. Tip, A. E. de Vries: Radiat. Effects **26**, 23 (1975) 255, 256, 260
[276] C. B. Cooper, J. R. Woodyard: Phys. Lett. **79A**, 124 (1980) 255
[277] C. B. Cooper, H. A. Hamed: Surf. Sci. **143**, 215 (1984) 255
[278] W. O. Hofer, H. Gnaser: Nucl. Instrum. Methods B **18**, 605 (1987) 255, 279, 280
[279] H. Gnaser, W. O. Hofer: Appl. Phys. A **48**, 261 (1989) 255, 279, 280
[280] L. E. Rehn, R. C. Birtcher, S. E. Donnelly, P. M. Baldo, L. Funk: Phys. Rev. Lett. **87**, 207601 (2001) 255
[281] L. E. Rehn, R. C. Birtcher, P. M. Baldo, A. W. McCormick, L. Funk: Nucl. Instrum. Methods B **212**, 326 (2003) 255
[282] C. Staudt, A. Wucher: Phys. Rev. B **66**, 075419 (2002) 255, 256, 258
[283] S. R. Coon, W. F. Calaway, M. J. Pellin: Nucl. Instrum. Methods B **90**, 518 (1994) 255
[284] Z. Ma, S. R. Coon, W. F. Calaway, M. J. Pellin, D. M. Gruen, E. I. von Nagy-Felsobuki: J. Vac. Sci. Technol. A **12**, 2425 (1994) 255
[285] Z. Ma, W. F. Calaway, M. J. Pellin, E. I. von Nagy-Felsobuki: Nucl. Instrum. Methods B **94**, 197 (1994) 255
[286] T. B. Lill, , W. F. Calaway, M. J. Pellin, D. M. Gruen: Phys. Rev. Lett. **73**, 1719 (1994) 255
[287] T. B. Lill, W. F. Calaway, Z. Ma, M. J. Pellin: Surf. Sci. **322**, 361 (1995) 255

[288] C. S. Hansen, W. F. Calaway, M. J. Pellin, B. V. King, A. Wucher: Surf. Sci. **432**, 199 (1999) 255
[289] C. Staudt, R. Heinrich, A. Wucher: Nucl. Instrum. Methods B **164**–**165**, 677 (2000) 255, 258
[290] I. S. Bitensky, E. S. Parilis: Nucl. Instrum. Methods B **21**, 26 (1987) 255
[291] K. T. Waldeer, H. M. Urbassek: Nucl. Instrum. Methods B **73**, 14 (1993) 256
[292] H. M. Urbassek: Nucl. Instrum. Methods B **31**, 541 (1988) 256
[293] H. M. Urbassek: Radiat. Eff. Def. Solids **109**, 293 (1989) 256
[294] F. Bernhard, H. Oechsner, E. Stumpe: Nucl. Instrum. Methods **132**, 329 (1976) 256
[295] A. D. Bekkerman, N. K. Dzhemilev, S. E. Maksimov, V. V. Solomko, S. V. Verkhoturov, I. V. Veryovkin: Vaccum **47**, 1073 (1996) 258
[296] H. Gnaser: Phys. Rev. B **63**, 045415 (2001) 258, 259
[297] H. Gnaser: Appl. Surf. Sci. **203-204**, 78 (2003) 258
[298] J. K. Nørskov, B. I. Lundqvist: Phys. Rev. B **19**, 5661 (1979) 258
[299] W. Ens: K. Dan. Vidensk. Selsk. Mat. Fys. Medd. **43**, 155 (1993) 260
[300] C. T. Reimann: K. Dan. Vidensk. Selsk. Mat. Fys. Medd. **43**, 351 (1993) 260
[301] H. Grade, N. Winograd, R. G. Cooks: J. Am. Chem. Soc. **99**, 7725 (1977) 260
[302] D. van Leyen, B. Hagenhoff, E. Niehuis, A. Benninghoven, I. V. Bletsos, D. M. Hercules: J. Vac. Sci. Technol. A **7**, 1790 (1989) 260
[303] N. Winograd, B. J. Garrison: in A. W. Czanderna, D. M. Hercules (Eds.): *Ion Spectroscopies for Surface Analysis* (Plenum, New York 1991) p. 45 260
[304] M. Karas: K. Dan. Vidensk. Selsk. Mat. Fys. Medd. **43**, 623 (1993) 260
[305] S. Berkenkamp, C. Menzel, M. Karas, F. Hillenkamp: Rap. Commun. Mass Spectrom. **11**, 1399 (1997) 260
[306] C. Menzel, S. Berkenkamp, F. Hillenkamp: Rap. Commun. Mass Spectrom. **13**, 26 (1999) 260
[307] F. Honda, G. M. Lancaster, Y. Fukuda, J. W. Rabalais: J. Chem. Phys. **69**, 4931 (1978) 260
[308] G. M. Lancaster, F. Honda, Y. Fukuda, J. W. Rabalais: J. Am. Chem. Soc. **101**, 1951 (1979) 260
[309] S. J. Pachuta, R. G. Cooks: Chem. Rev. **87**, 647 (1987) 260
[310] B. V. King, I. S. T. Tsong, S. H. Lin: Int. J. Mass Spectrom. Ion Proc. **78**, 341 (1987) 260
[311] H. M. Urbassek, J. Michl: Nucl. Instrum. Methods B **22**, 480 (1987) 260, 273, 297
[312] R. Galera, J. C. Blais, G. Bolbach: Int. J. Mass Spectrom. Ion Proc. **107**, 531 (1991) 260
[313] A. Benninghoven: in A. Benninghoven (Ed.): *Ion Formation from Organic Solids* (Springer, Berlin, Heidelberg 1983) p. 64 260
[314] P. Williams, B. U. R. Sundqvist: Phys. Rev. Lett. **58**, 1031 (1987) 260
[315] A. W. Kolfschoten, R. A. Haring, A. Haring, A. E. de Vries: J. Appl. Phys. **55**, 3813 (1984) 260
[316] R. Pedrys, D. J. Oostra, R. A. Haring, L. Calcagno, A. Haring, A. E. de Vries: Nucl. Instrum. Methods B **17**, 15 (1986) 260
[317] A. Brown, J. C. Vickerman: Surf. Interf. Anal. **8**, 75 (1986) 260
[318] R. Hoogerbrugge, P. G. Kistemaker: Nucl. Instrum. Methods B **18**, 600 (1987) 260

[319] R. Hoogerbrugge, P. G. Kistemaker: Nucl. Instrum. Methods B **21**, 37 (1987) 260
[320] R. Hoogerbrugge, W. J. van der Zande, P. G. Kistemaker: Int. J. Mass Spectrom. Ion Proc. **76**, 239 (1987) 260
[321] R. A. Haring, H. E. Roosendaal, P. C. Zalm: Nucl. Instrum. Methods B **28**, 205 (1987) 260
[322] G. Gillen: Int. J. Mass Spectrom. Ion Proc. **105**, 215 (1991) 260
[323] G. J. Leggett, J. C. Vickerman: Int. J. Mass Spectrom. Ion Proc. **122**, 281 (1992) 260
[324] I. S. Gilmore, M. P. Seah: Surf. Interface Anal. **23**, 191 (1995) 260
[325] I. S. Gilmore, M. P. Seah: Surf. Interface Anal. **24**, 746 (1996) 260
[326] A. Delcorte, P. Bertrand: Nucl. Instrum. Methods B **115**, 246 (1996) 260, 261
[327] A. Delcorte, P. Bertrand: Nucl. Instrum. Methods B **117**, 235 (1996) 260, 261
[328] A. Delcorte, P. Bertrand: Nucl. Instrum. Methods B **135**, 430 (1998) 260, 261
[329] A. Delcorte, B. G. Segda, P. Bertrand: Surf. Sci. **381**, 18 (1997) 260, 269
[330] A. Delcorte, B. G. Segda, P. Bertrand: Surf. Sci. **389**, 393 (1997) 260, 269
[331] A. Delcorte, P. Bertrand: Surf. Sci. **412/413**, 97 (1998) 260, 261
[332] A. Delcorte, P. Bertrand: Int. J. Mass Spectrom Ion Proc. **184**, 217 (1999) 260, 267, 269
[333] A. Delcorte, X. V. Eynde, P. Bertrand, D. F. Reich: Nucl. Instrum. Methods B **157**, 138 (1999) 260, 265
[334] A. Delcorte, X. V. Eynde, P. Bertrand, D. F. Reich: Int. J. Mass Spectrom. **189**, 133 (1999) 260
[335] B. Arezki, A. Delcorte, , P. Bertrand: Nucl. Instrum. Methods B **193**, 755 (2002) 260, 265
[336] A. Delcorte, B. J. Garrison, P. Bertrand: Nucl. Instrum. Methods B **171**, 277 (2000) 261
[337] A. Delcorte, X. V. Eynde, P. Bertrand, J. C. Vickerman, B. J. Garrison: J. Phys. Chem. B **104**, 2673 (2000) 261, 262, 264, 265
[338] A. Delcorte, B. J. Garrison: J. Phys. Chem. B **104**, 6785 (2000) 261, 264, 265
[339] A. Delcorte, B. J. Garrison: J. Phys. Chem. B **107**, 2297 (2003) 261
[340] A. Delcorte, P. Bertrand, B. J. Garrison: Appl. Surf. Sci. **203-204**, 166 (2003) 261
[341] A. Delcorte, B. Arezki, B. J. Garrison: Nucl. Instrum. Methods B **212**, 414 (2003) 261
[342] B. J. Garrison, K. D. Krantzman, A. Delcorte: Acc. Chem. Res. **33**, 69 (2000) 261
[343] A. Delcorte: *Static Secondary Ion Mass Spectrometry of Thin Organic Layers*, Doctoral thesis, Université Catholique de Louvain (1999) 261, 263, 269, 270
[344] B. Arezki, A. Delcorte, A. C. Chami, B. J. Garrison, P. Bertrand: Nucl. Instrum. Methods B **212**, 369 (2003) 265
[345] M. Terhorst, R. Möllers, E. Niehuis, A. Benninghoven: Surf. Interf. Anal. **18**, 824 (1992) 266
[346] C. L. Brummel, K. F. Willey, J. C. Vickerman, N. Winograd: Intern. J. Mass Spectrom. Ion Proc. **143**, 257 (1995) 266

[347] V. Vorsa, T. Kono, K. F. Willey, N. Winograd: J. Chem. Phys. B **103**, 7889 (1999) 266
[348] R. Chatterjee, D. E. Riederer, Z. Postawa, N. Winograd: Rap. Commun. Mass Spectrom. **12**, 1226 (1998) 266
[349] R. Chatterjee, D. E. Riederer, Z. Postawa, N. Winograd: J. Phys. Chem. B **102**, 4176 (1998) 266
[350] C. A. Meserole, E. Vandeweert, R. Chatterjee, N. Winograd: Appl. Surf. Sci. **141**, 339 (1999) 266
[351] A. Meserole, E. Vandeweert, Z. Postawa, Y. Dou, B. J. Garrison, N. Winograd: Nucl. Instrum. Methods B **180**, 53 (2001) 266
[352] C. A. Meserole, E. Vandeweert, Z. Postawa, B. C. Haynie, N. Winograd: Phys. Chem. B **106**, 12929 (2002) 266, 268
[353] R. Chatterjee, Z. Postawa, N. Winograd, B. J. Garrison: J. Phys. Chem. B **103**, 151 (1999) 266, 267
[354] W. Forst: *Theory of Unimolecular Reactions* (Academic, New York 1973) 267
[355] I. S. Gilmore, M. P. Seah: Appl. Surf. Sci. **144-145**, 26 (1999) 269
[356] R. E. Johnson, J. Schou: K. Dan. Vidensk. Selsk. Mat. Fys. Medd. **43**, 403 (1993) 269, 272
[357] P. D. Townsend: in R. Behrisch (Ed.): *Sputtering by Particle Bombardment II*, Top. Appl. Phys. **52** (Springer, Berlin, Heidelberg 1983) p. 147 269, 270
[358] N. Itoh: Nucl. Instrum. Methods B **27**, 155 (1987) 270
[359] M. Szymonski: K. Dan. Vidensk. Selsk. Mat. Fys. Medd. **43**, 495 (1993) 270
[360] P. D. Townsend: Nucl. Instrum. Methods **198**, 9 (1982) 270
[361] R. T. Williams, K. S. Song, W. L. Faust, C. H. Leung: Phys. Rev. B **33**, 7232 (1986) 270
[362] M. Szymonski: Nucl. Instrum. Methods B **46**, 427 (1990) 270
[363] M. Szymonski, H. Overeijnder, A. E. de Vries: Radiat. Eff. **36**, 189 (1978) 271
[364] H. Overeijnder, R. A. Haring, A. E. de Vries: Radiat. Eff. **37**, 205 (1978) 271
[365] W. Husinsky, R. Bruckmüller: Surf. Sci. **80**, 637 (1979) 271
[366] M. L. Yu, D. Grischkowsky, A. C. Balant: Appl. Phys. Lett. **39**, 703 (1981) 271
[367] G. Betz, W. Husinsky: Nucl. Instrum. Methods B **32**, 331 (1988) 271
[368] M. Szymonski, P. Czuba, T. Dohnalik, L. Jozefowski, A. Karawajczyk, J. Kolodziej, R. Lesniak, Z. Postawa: Nucl. Instrum. Methods B **48**, 534 (1990) 271
[369] R. Pedrys, R. A. Haring, F. W. Saris, A. E. de Vries: Phys. Lett. **82A**, 371 (1981) 271
[370] R. A. Haring, R. Pedrys, A. Haring, A. E. de Vries: Nucl. Instrum. Methods B **4**, 40 (1984) 271, 272
[371] R. Pedrys, D. J. Oostra, A. Haring, A. E. de Vries: Nucl. Instrum. Methods B **33**, 840 (1988) 271
[372] D. J. O'Shaughnessy, J. W. Boring, S. Cui, R. E. Johnson: Phys. Rev. Lett. **61**, 1635 (1988) 271
[373] D. J. O'Shaughnessy, J. W. Boring, J. A. Phipps, R. E. Johnson: Surf. Sci. **203**, 227 (1988) 271, 272
[374] J. W. Boring, R. E. Johnson, D. J. O'Shaughnessy: Phys. Rev. B **39**, 2689 (1989) 271
[375] R. Pedrys: Nucl. Instrum. Methods B **48**, 525 (1990) 271, 272, 274

[376] R. Pedrys, B. Warczak, P. Leskiewicz, J. Schou, O. Ellegaard: Nucl. Instrum. Methods B **157**, 121 (1999) 271, 272
[377] R. A. Haring, R. Pedrys, D. J. Oostra, A. Haring, A. E. de Vries: Nucl. Instrum. Methods B **5**, 476 (1984) 272
[378] R. A. Haring, R. Pedrys, D. J. Oostra, A. Haring, A. E. de Vries: Nucl. Instrum. Methods B **5**, 483 (1984) 272
[379] W. L. Brown, W. M. Augustyniak, K. J. Marcantonio, E. H. Simmons, J. W. Boring, R. E. Johnson, C. T. Reimann: Nucl. Instrum. Methods B **1**, 307 (1984) 272
[380] D. B. Chrisey, W. L. Brown, J. W. Boring: Surf. Sci. **225**, 130 (1990) 272
[381] O. Ellegaard, J. Schou, H. Sørensen, R. Pedrys, B. Warczak: Nucl. Instrum. Methods B **78**, 192 (1993) 272
[382] O. Ellegaard, J. Schou, B. Stenum, H. Sørensen, R. Pedrys, B. Warczak, D. J. Oostra, A. Haring, A. E. de Vries: Surf. Sci. **302**, 371 (1994) 272
[383] J. Schou, R. Pedrys: J. Geophys. Res. **106**, 33309 (2001) 272
[384] R. A. Haring, A. Haring, F. S. Klein, A. C. Kummel, A. E. de Vries: Nucl. Instrum. Methods **211**, 529 (1983) 272
[385] R. A. Haring, A. W. Kolfschoten, A. E. de Vries: Nucl. Instrum. Methods B **2**, 544 (1984) 272
[386] C. T. Reimann, J. W. Boring, R. E. Johnson, J. W. Garrett, K. R. Farmer, W. L. Brown, K. J. Marcantonio, W. M. Augustyniak: Surf. Sci. **147**, 227 (1984) 272
[387] R. Pedrys, F. Krok, P. Leskiewicz, J. Schou, U. Podschaske, B. Cleff: Nucl. Instrum. Methods B **164-165**, 861 (2000) 272, 274
[388] H. E. Roosendaal, R. A. Haring, J. B. Sanders: Nucl. Instrum. Methods **194**, 579 (1982) 272
[389] O. Ellegaard, J. Schou, B. Stenum, H. Sørensen, R. Pedrys: Nucl. Instrum. Methods B **62**, 447 (1992) 272
[390] H. M. Urbassek, K. T. Waldeer: Phys. Rev. Lett. **67**, 105 (1991) 272
[391] J. Schou: Nucl. Instrum. Methods B **27**, 188 (1987) 272
[392] K. Rödelsberger, A. Scharmann: Nucl. Instrum. Methods **132**, 355 (1976) 275
[393] W. Krüger, A. Scharmann, H. Afridi, G. Bräuer: Nucl. Instrum. Methods **168**, 411 (1980) 275
[394] G. Bräuer, D. Hasselkamp, W. Krüger, A. Scharmann: Nucl. Instrum. Methods B **12**, 458 (1985) 275
[395] T. Okutani, M. Shikata, S. Ichimura, R. Shimizu: J. Appl. Phys. **51**, 2884 (1980) 275
[396] H. Tsuge, S. Esho: J. Appl. Phys. **52**, 4391 (1981) 275, 291
[397] H. H. Andersen, J. Chevallier, V. S. Chernysh: Nucl. Instrum. Methods **191**, 241 (1981) 275
[398] H. H. Andersen, B. Stenum, T. Sørensen, H. J. Whitlow: Nucl. Instrum. Methods B **6**, 459 (1985) 275, 276
[399] R. G. Allas, A. R. Knudson, J. M. Lambert, P. A. Treado, G. W. Reynolds: Nucl. Instrum. Methods **194**, 615 (1982) 275
[400] F. R. Vozzo, G. W. Reynolds: Nucl. Instrum. Methods **209/210**, 555 (1983) 275, 298
[401] A. I. Dodonov, I. M. Fayazov, S. D. Fedorovich, E. A. Krylova, E. S. Mashkova, V. A. Molchanov, W. Eckstein: Appl. Phys. A **49**, 299 (1989) 275

[402] T. K. Cini, M. Tanemura, F. Okuyama: Nucl. Instrum. Methodsd B **119**, 387 (1996) 275
[403] V. S. Chernysh, W. Eckstein, A. A. Haidarov, V. S. Kulikauskas, V. A. Kurnaev, E. S. Mashkova, V. A. Molchanov: Nucl. Instrum. Methods B **135**, 285 (1998) 275
[404] V. S. Chernysh, W. Eckstein, A. A. Haidarov, V. S. Kulikauskas, E. S. Mashkova, V. A. Molchanov: Nucl. Instrum. Methods B **160**, 221 (2000) 275
[405] V. S. Chernysh, W. Eckstein, A. A. Haidarov, V. S. Kulikauskas, E. S. Mashkova, V. A. Molchanov: Nucl. Instrum. Methods B **164-165**, 755 (2000) 275
[406] M. T. Robinson: J. Appl. Phys. **40**, 4982 (1969) 275
[407] V. I. Shulga: Nucl. Instrum. Methods B **164-165**, 733 (2000) 275
[408] W. Eckstein, J. P. Biersack: Z. Phys. B **63**, 109 (1986) 275
[409] M. Hautala, H. J. Whitlow: Nucl. Instrum. Methods B **6**, 466 (1985) 276
[410] R. P. Stein, F. C. Hurlbut: Phys. Rev. **123**, 790 (1961) 276
[411] C. Schwebel, C. Pellet, G. Gautherin: Nucl. Instrum. Methods B **18**, 525 (1987) 276
[412] T. J. Whitaker, P. L. Jones, A. Li, R. O. Watts: Rev. Sci. Instrum. **64**, 452 (1993) 276
[413] G. Betz, R. Dobrozemsky, F. P. Viehböck: Ned. Tijdschr. Vacuumtech. **8**, 203 (1970) 276
[414] G. Betz, R. Dobrozemsky, F. P. Viehböck: Int. J. Mass Spectrom. Ion Phys. **6**, 451 (1971) 276
[415] H. H. Andersen, H. L. Bay: in R. Behrisch (Ed.): *Sputtering by Particle Bombardment I*, Top. Appl. Phys. **47** (Springer, Berlin, Heidelberg 1981) p. 145 276
[416] H. Oechsner: Z. Naturf. **21a**, 859 (1966) 276
[417] H. Oechsner: Z. Phys. **261**, 37 (1973) 276
[418] H. Oechsner: Appl. Phys. **8**, 185 (1975) 276
[419] M. Szymonski, W. Huang, J. Onsgaard: Nucl. Instrum. Methods B **14**, 263 (1986) 276
[420] W. Huang: Surf. Sci. **202**, L603 (1988) 276
[421] W. Huang: Phys. Lett. A **134**, 269 (1989) 276
[422] Y. Yamamura, C. Mößner, H. Oechsner: Radiat. Eff. **103**, 25 (1987) 277
[423] Y. Yamamura, C. Mößner, H. Oechsner: Radiat. Eff. **105**, 31 (1987) 277
[424] W. Bock, H. Gnaser, H. Oechsner: Surf. Sci. **282**, 333 (1993) 277
[425] K. Wittmaack: J. Vac. Sci. Technol. A **8**, 2246 (1990) 277
[426] Z. X. Jiang, P. F. A. Alkemade: Appl. Phys. Lett. **73**, 315 (1998) 277
[427] P. K. Rol, J. M. Fluit, F. P. Viehböck, M. de Jong: in N. R. Nilsson (Ed.): *Proc. 4th Int. Conf. Ionization Phenomena in Gases* (North-Holland, Amsterdam 1960) p. 275 277
[428] V. A. Molchanov, V. G. Tel'kovskii, V. M. Chicherov: Sov. Phys.-Doklady **6**, 222 (1961) 277
[429] G. S. Anderson, G. K. Wehner: J. Appl. Phys. **31**, 2305 (1960) 277
[430] V. E. Yurasova: Sov. Phys. - Tech. Phys. **3**, 1806 (1958) 277
[431] M. W. Thompson: Philos. Mag. **4**, 139 (1959) 277
[432] R. S. Nelson, M. W. Thompson: Proc. R. Soc. London A **259**, 458 (1961) 277
[433] R. S. Nelson, M. W. Thompson: Philos. Mag. **7**, 1385 (1962) 277

[434] R. S. Nelson, M. W. Thompson: Philos. Mag. **7**, 1425 (1962) 277
[435] V. E. Yurasova, N. V. Pleshivtsev, I. V. Orfanov: Sov. Phys. JETP **37**, 689 (1960) 277
[436] M. T. Robinson, A. L. Southern: J. Appl. Phys. **38**, 2969 (1967) 277
[437] H. E. Roosendaal: in R. Behrisch (Ed.): *Sputtering by Particle Bombardment I*, Top. Appl. Phys. **47** (Springer, Berlin, Heidelberg 1981) p. 219 277
[438] A. L. Southern, W. R. Willis, M. T. Robinson: J. Appl. Phys. **34**, 153 (1963) 277
[439] J. M. Fluit, P. K. Rol, J. Kistemaker: J. Appl. Phys. **34**, 690 (1963) 277
[440] G. D. Magnuson, C. E. Carlston: J. Appl. Phys. **34**, 3267 (1963) 277
[441] G. D. Odintsov: Sov. Phys. - Solid State **5**, 813 (1963) 277
[442] D. Onderdelinden: Appl. Phys. Lett. **8**, 189 (1966) 277
[443] D. Onderdelinden: Can. J. Phys. **46**, 739 (1968) 277
[444] R. H. Silsbee: J. Appl. Phys. **28**, 1246 (1957) 277
[445] G. Leibfried: J. Appl. Phys. **30**, 1388 (1959) 277
[446] J. B. Gibson, A. N. Goland, M. Milgram, G. H. Vineyard: Phys. Rev. **120**, 1229 (1960) 277
[447] C. Erginsoy, G. H. Vineyard, A. Englert: Phys. Rev. **133**, A595 (1964) 277
[448] C. Erginsoy, G. H. Vineyard, A. Shimizu: Phys. Rev. **139**, A118 (1965) 277
[449] C. Lehmann, P. Sigmund: Phys. Status Solidi **16**, 507 (1966) 277
[450] T. Lenskjaer, F. Nyholm, S. D. Pedersen, N. B. Petersen: Phys. Lett. **47A**, 63 (1974) 277
[451] W. Szymczak, K. Wittmaack: Nucl. Instrum. Methods **194**, 561 (1982) 278
[452] W. Szymczak, K. Wittmaack: Nucl. Instrum. Methods B **82**, 220 (1993) 278
[453] G. Betz, R. Kirchner, W. Husinsky, F. Rüdenauer, H. M. Urbassek: Radiat. Eff. Def. Solids **130/131**, 251 (1994) 279
[454] M. Hou, W. Eckstein: Nucl. Instrum. Methods B **13**, 324 (1986) 279
[455] W. Eckstein, M. Hou: Nucl. Instrum. Methods B **31**, 386 (1988) 279
[456] M. Hou, W. Eckstein: Phys. Rev. B **42**, 5959 (1990) 279
[457] W. Eckstein, M. Hou: Nucl. Instrum. Methods B **53**, 270 (1991) 279
[458] Y. Yamamura, W. Takeuchi: Nucl. Instrum. Methods B **29**, 461 (1987) 279
[459] M. Hautala, J. Likonen: Nucl. Instrum. Methods B **33**, 526 (1988) 279
[460] J. Likonen, M. Hautala: Appl. Phys. A **45**, 137 (1988) 279
[461] R. Maboudian, Z. Postawa, M. El-Maazawi, B. J. Garrison, N. Winograd: Phys. Rev. B **42**, 7311 (1990) 279, 280
[462] M. El-Maazawi, R. Maboudian, Z. Postawa, N. Winograd: Phys. Rev. B **43**, 12078 (1991) 279, 280
[463] A. Wucher, M. Watgen, C. Mößner, H. Oechsner, B. J. Garrison: Nucl. Instrum. Methods B **67**, 531 (1992) 279
[464] B. V. King, C. Zimmermann, D. E. Riederer, S. W. Rosencrance, B. J. Garrison, N. Winograd: Rap. Commun. Mass Spectrom. **12**, 1236 (1998) 279
[465] M. Tan, B. V. King: Appl. Surf. Sci. **203-204**, 248 (2003) 279
[466] S. W. Rosencrance, J. S. Burnham, D. E. Sanders, C. He, B. J. Garrison, N. Winograd, Z. Postawa, A. E. DePristo: Phys. Rev. B **52**, 6006 (1995) 280
[467] S. W. Rosencrance, N. Winograd, B. J. Garrison, Z. Postawa: Phys. Rev. B **53**, 2378 (1996) 280
[468] B. J. Garrison, C. T. Reimann, N. Winograd, D. E. Harrison, Jr.: Phys. Rev. B **36**, 3561 (1987) 280

[469] B. J. Garrison, N. Winograd, D. M. Deaven, C. T. Reimann, D. Y. Lo, T. A. Tombrello, D. E. Harrison, Jr., M. H. Shapiro: Phys. Rev. B **37**, 7197 (1988) 280
[470] D. E. Sanders, K. B. S. Prasad, J. S. Burnham, B. J. Garrison: Phys. Rev. B **50**, 5358 (1994) 280
[471] N. Winograd, M. El-Maazawi, R. Maboudian, Z. Postawa, D. N. Bernardo, B. J. Garrison: J. Chem. Phys. **96**, 6314 (1992) 280
[472] D. E. Harrison, J. P. Johnson, N. S. Levy: Appl. Phys. Lett. **8**, 33 (1966) 280
[473] R. R. Olson, G. K. Wehner: J. Vac. Sci. Technol. **14**, 319 (1977) 280
[474] R. R. Olson, M. E. King, G. K. Wehner: J. Appl. Phys. **50**, 3677 (1979) 280
[475] P. Sigmund, A. Oliva, G. Falcone: Nucl. Instrum. Methods **194**, 541 (1982) 281
[476] P. Sigmund, A. Oliva, G. Falcone: Nucl. Instrum. Methods B **9**, 354 (1985) 281
[477] H. H. Andersen, F. Besenbacher, P. Goddisken: in P. Varga, G. Betz, F. P. Viehböck (Eds.): *Symposium on Sputtering* (Techn. Univ., Vienna 1980) p. 446 281
[478] H. H. Andersen, V. Chernysh, B. Stenum, T. Sørensen, H. J. Whitlow: Surf. Sci. **123**, 39 (1982) 281
[479] H. H. Andersen, B. Stenum, T. Sørensen, H. J. Whitlow: Nucl. Instrum. Methods **209/210**, 487 (1983) 281
[480] H. H. Andersen, B. Stenum, T. Sørensen, H. J. Whitlow: Nucl. Instrum. Methods B **2**, 623 (1984) 281
[481] R. S. Li, C. F. Li, W. L. Zhang: Appl. Phys. A **50**, 169 (1990) 281
[482] R. S. Li, C. F. Li, G. Liu, X. S. Zhang, D. S. Bao: J. Appl. Phys. **70**, 5351 (1991) 281
[483] M. F. Dumke, T. A. Tombrello, R. A. Weller, R. M. Housley, E. H. Cirlin: Surf. Sci. **124**, 407 (1983) 281
[484] K. M. Hubbard, R. A. Weller, D. L. Weathers, T. A. Tombrello: Nucl. Instrum. Methods B **36**, 395 (1989) 281
[485] K. M. Hubbard, R. A. Weller, D. L. Weathers, T. A. Tombrello: Nucl. Instrum. Methods B **40/41**, 278 (1989) 281
[486] M. H. Shapiro, K. R. Bengtson, T. A. Tombrello: Nucl. Instrum. Methods B **103**, 123 (1995) 281
[487] T. Aoyama, M. Tanemura, F. Okuyama: Appl. Surf. Sci. **100/101**, 351 (1996) 282
[488] M. Tanemura, T. Aoyama, A. Otani, M. Ukita, F. Okuyama, T. K. Chini: Surf. Sci. **376**, 163 (1997) 282
[489] M. Tanemura, M. Ukita, F. Okuyama: Surf. Sci. **426**, 141 (1999) 282
[490] J. Malherbe: Crit. Rev. Solid State Mater. Sci. **19**, 55 (1994) 282
[491] J. Malherbe: Crit. Rev. Solid State Mater. Sci. **19**, 129 (1994) 282
[492] S. Ichimura, H. Shimizu, H. Murakami, Y. Ishida: J. Nucl. Mat. **128/129**, 601 (1984) 283
[493] H. J. Kang, Y. Matsuda, R. Shimizu: Surf. Sci. **127**, L179 (1983) 283
[494] V. S. Chernysh, V. S. Tuboltsev, V. S. Kulikauskas: Nucl. Instrum. Methods B **140**, 303 (1998) 283
[495] A. Wucher, W. Reuter: J. Vac. Sci. Technol. A **6**, 2316 (1988) 283
[496] W. Eckstein, J. P. Biersack: Appl. Phys. A **37**, 95 (1985) 283

[497] P. Sigmund, N. Q. Lam: K. Dan. Vidensk. Selsk. Mat. Fys. Medd. **43**, 255 (1993) 283
[498] W. Eckstein, R. Dohmen: Nucl. Instrum. Methods B **129**, 327 (1997) 283
[499] V. I. Shulga, P. Sigmund: Nucl. Instrum. Methods B **119**, 359 (1996) 283
[500] R. Weissmann, P. Sigmund: Radiat. Eff. **19**, 7 (1973) 283, 291
[501] W. Eckstein: Surf. Interf. Anal. **14**, 799 (1989) 283
[502] W. Eckstein: Calculated sputtering, reflection and range values, in *Report IPP 9/132* (MPI für Plasmaphysik, Garching 2002) 283
[503] W. O. Hofer, J. Roth (Eds.): *Physical Processes of the Interaction of Fusion Plasmas with Solids* (Academic, New York 1996) 283
[504] R. V. Stuart, G. K. Wehner: Phys. Rev. Lett. **4**, 409 (1960) 283
[505] R. V. Stuart, G. K. Wehner: Phys. Rev. **33**, 2345 (1962) 283
[506] D. E. Harrison, G. D. Magnuson: Phys. Rev. **122**, 1421 (1961) 283
[507] M. Hou, M. T. Robinson: Appl. Phys. **18**, 381 (1979) 284
[508] R. Behrisch, G. Maderlechner, B. M. U. Scherzer, M. T. Robinson: Appl. Phys. **18**, 391 (1979) 284
[509] Y. Yamamura, J. Bohdansky: Vacuum **35**, 561 (1985) 284, 285
[510] Y. Yamamura, T. Takiguchi, H. Kimura: Nucl. Instrum. Methods B **78**, 337 (1993) 284, 285
[511] H. F. Winters, P. Sigmund: J. Appl. Phys. **45**, 4760 (1974) 284
[512] W. Eckstein, C. García-Rosales, J. Roth, J. László: Nucl. Instrum. Methods B **83**, 95 (1993) 284, 285
[513] R. P. Webb, D. E. Harrison, Jr.: J. Appl. Phys. **53**, 5243 (1982) 284
[514] M. M. Jakas, D. E. Harrison, Jr.: Nucl. Instrum. Methods B **14**, 535 (1986) 284
[515] W. Eckstein, C. Garcia-Rosales, J. Roth, W. Ottenberger: Sputtering data, in *Report IPP 9/82* (MPI für Plasmaphysik, Garching 1993) 284
[516] C. Garcia-Rosales, W. Eckstein, J. Roth: J. Nucl. Mater. **218**, 8 (1994) 284
[517] W. Eckstein, R. Preuss: J. Nucl. Mater. **320**, 209 (2003) 284
[518] M. Urbassek: Nucl. Instrum. Methods B **4**, 356 (1984) 285, 287
[519] W. Eckstein: Nucl. Instrum. Methods B **18**, 344 (1987) 285
[520] H. Oechsner: Phys. Rev. Lett. **24**, 583 (1970) 285
[521] H. Oechsner: Z. Phys. **238**, 433 (1970) 285
[522] J. Dembowski, H. Oechsner, Y. Yamamura, M. Urbassek: Nucl. Instrum. Methods B **18**, 464 (1987) 285
[523] R. A. Brizzolara, C. B. Cooper, T. K. Olson: Nucl. Instrum. Methods B **35**, 36 (1988) 285, 287
[524] R. A. Brizzolara, C. B. Cooper: Nucl. Instrum. Methods B **43**, 136 (1989) 285, 287
[525] H. Gnaser, H. Oechsner: Surf. Sci. **251/252**, 696 (1991) 285, 287
[526] H. Gnaser, H. Oechsner: Nucl. Instrum. Methods B **58**, 438 (1991) 285, 287
[527] H. Gnaser, H. Oechsner: Phys. Rev. B **47**, 14093 (1993) 287
[528] I. Reid, B. W. Farmery, M. W. Thompson: Nucl. Instrum. Methods **132**, 317 (1976) 288
[529] I. Reid, M. W. Thompson, B. W. Farmery: Philos. Mag. **42**, 151 (1980) 288
[530] S. Ahmad, B. W. Farmery, M. W. Thompson: Philos. Mag. **44**, 1383 (1981) 288
[531] S. Ahmad, M. W. Thompson: Philos. Mag. **50**, 299 (1984) 288
[532] M. W. Thompson: Vacuum **66**, 99 (2002) 288

[533] A. Goehlich, N. Niemöller, H. F. Döbele: Phys. Rev. B **62**, 9349 (2000) 288, 289, 290
[534] A. Goehlich, D. Gillmann, H. F. Döbele: Nucl. Instrum. Methods B **164-165**, 834 (2000) 288, 289, 290
[535] A. Goehlich, D. Gillmann, H. F. Döbele: Nucl. Instrum. Methods B **179**, 351 (2001) 288, 289
[536] A. Goehlich: Appl. Phys. A **72**, 523 (2001) 288
[537] D. R. Gillen, W. G. Graham, A. Goehlich: Nucl. Instrum. Methods B **194**, 409 (2002) 288
[538] H. L. Bay, B. Schweer, P. Bogen, E. Hintz: J. Nucl. Mat. **111&112**, 732 (1982) 291
[539] W. Berres, H. L. Bay: Appl. Phys. A **33**, 235 (1984) 291
[540] H. L. Bay, W. Berres: Nucl. Instrum. Methods B **2**, 606 (1984) 291
[541] H. L. Bay: Nucl. Instrum. Methods B **18**, 430 (1987) 291
[542] G. Falcone, A. Oliva: Appl. Phys. A **32**, 201 (1983) 291
[543] G. Falcone: Riv. Nuovo Cimento **19**, 1 (1990) 291
[544] G. K. Wehner, D. Rosenberg: J. Appl. Phys. **31**, 177 (1960) 291
[545] E. Franke, H. Neumann, M. Zeuner, W. Frank, F. Bigl: Surf. Coat. Technol. **97**, 90 (1997) 291
[546] P. C. Smith, D. N. Ruzic: Nucl. Fusion **38**, 673 (1998) 291
[547] P. C. Smith, D. N. Ruzic: J. Vac. Sci. Technol. A **17**, 3443 (1999) 291
[548] M. Stepanova, S. K. Dew: J. Vac. Sci. Technol. A **19**, 2805 (2001) 291
[549] M. Stepanova, S. K. Dew: J. Appl. Phys. **92**, 1699 (2002) 291
[550] V. I. Shulga: Nucl. Instrum. Methods B **155**, 382 (1999) 291
[551] R. Kawakami, J. Kawata, K. Ohya: Jpn. J. Appl. Phys. Part 1, **38**, 6058 (1999) 291
[552] J. Jorzick, J. Lösch, M. Kopnarski, H. Oechsner: Appl. Phys. A **78**, 655 (2004) 291
[553] R. Behrisch, R. Weissmann: Phys. Lett. **30A**, 506 (1969) 291
[554] W. O. Hofer, H. L. Bay, P. J. Martin: J. Nucl. Mater. **76&77**, 156 (1978) 292
[555] H. L. Bay, J. Bohdansky, W. O. Hofer: Appl. Phys. **21**, 327 (1980) 292
[556] J. Bohdansky, G. L. Chen, W. Eckstein, J. Roth, B. M. U. Scherzer, R. Behrisch: J. Nucl. Mater. **111&112**, 717 (1982) 292
[557] J. Roth, J. Bohdansky, W. Eckstein: Nucl. Instrum. Methods **218**, 751 (1983) 292
[558] R. Becerra-Acevedo, J. Bohdansky, W. Eckstein, J. Roth: Nucl. Instrum. Methods B **2**, 631 (1984) 292
[559] H. H. Andersen, H. L. Bay: Radiat. Eff. **19**, 139 (1973) 293, 294
[560] H. H. Andersen, H. L. Bay: J. Appl. Phys. **45**, 953 (1974) 293, 294
[561] H. H. Andersen, H. L. Bay: J. Appl. Phys. **46**, 2416 (1975) 293, 294
[562] D. A. Thompson, S. S. Johar: Appl. Phys. Lett. **34**, 342 (1979) 293, 294
[563] D. A. Thompson, S. S. Johar: Nucl. Instrum. Methods **170**, 281 (1980) 293
[564] D. A. Thompson, S. S. Johar: Radiat. Eff. **55**, 91 (1981) 293
[565] S. S. Johar, D. A. Thompson: Surf. Sci. **90**, 319 (1979) 293, 294
[566] D. A. Thompson: Radiat. Effects **56**, 105 (1981) 293, 294
[567] D. A. Thompson: J. Appl. Phys. **52**, 982 (1981) 293
[568] D. J. Oostra, R. P. van Ingen, A. Haring, A. E. de Vries, F. W. Saris: Phys. Rev. Lett. **61**, 1392 (1988) 293, 294
[569] M. Szymonski, A. E. de Vries: Phys. Lett. **63A**, 359 (1977) 293

[570] S. Ahmad, B. W. Farmery, M. W. Thompson: Nucl. Instrum. Methods **170**, 327 (1980) 293
[571] W. Jäger: J. Microsc. Spectrosc. Electron. **6**, 437 (1981) 293
[572] K. L. Merkle, W. Jäger: Philos. Mag. A **44**, 741 (1981) 293
[573] D. Pramanik, D. N. Seidman: Nucl. Instrum. Methods **209/210**, 453 (1983) 293
[574] G. Carter: Radiat. Eff. Lett. **43**, 193 (1979) 293
[575] G. Carter: Radiat. Eff. Lett. **50**, 105 (1980) 293
[576] Y. Yamamura, Y. Kitazoe: Radiat. Eff. **39**, 251 (1978) 293
[577] J. F. Mahoney, J. Perel, T. D. Lee, P. A. Martino, P. Williams: J. Am. Soc. Mass Spectrom. **3**, 311 (1992) 293
[578] R. Kelly: Radiat. Eff. **32**, 91 (1977) 293
[579] R. Kelly: Surf. Sci. **90**, 280 (1979) 293
[580] P. Sigmund: Appl. Phys. Lett **25**, 169 (1974) 293
[581] P. Sigmund: Appl. Phys. Lett **27**, 52 (1975) 293
[582] P. Sigmund, C. Claussen: J. Appl. Phys. **52**, 990 (1981) 293
[583] M. M. Jakas: Radiat. Eff. Defects Solids **152**, 157 (2000) 293
[584] C. Claussen: Nucl. Instrum. Methods **194**, 567 (1982) 293
[585] M. Urbassek, P. Sigmund: Appl. Phys. A **35**, 19 (1984) 293
[586] P. Sigmund, M. Szymonski: Appl. Phys. A **33**, 141 (1984) 293
[587] K. Besocke, S. Berger, W. O. Hofer, U. Littmark: Radiat. Eff. **66**, 35 (1982) 293
[588] W. O. Hofer, K. Besocke, B. Stritzker: Appl. Phys. A **30**, 83 (1983) 293
[589] H. H. Andersen: K. Dan. Vidensk. Selsk. Mat. Fys. Medd. **43**, 127 (1993) 293
[590] Y. L. Beyec: Int. J. Mass Spectrom. Ion Proc. **174**, 101 (1998) 293
[591] A. D. Appelhans, J. E. Delmore: Anal. Chem. **61**, 1087 (1989) 293, 294, 295
[592] J. F. Mahoney, J. Perel, S. A. Ruatta, P. A. Martino, S. Husain, T. D. Lee: Rap. Commun. Mass Spectrom. **5**, 441 (1991) 293, 294, 295
[593] M. J. van Stipdonk, R. D. Harris, E. A. Schweikert: Rap. Commun. Mass Spectrom. **10**, 1987 (1996) 293
[594] K. Iltgen, C. Bendel, A. Benninghoven, E. Niehuis: J. Vac. Sci. Technol. A **15**, 460 (1997) 293, 294, 295
[595] M. G. Blain, S. Della-Negra, H. Joret, Y. L. Beyec, E. A. Schweikert: Phys. Rev. Lett. **63**, 1625 (1989) 293, 294
[596] M. Benguerba, A. Brunelle, S. Della-Negra, J. Depauw, H. Joret, Y. L. Beyec, M. G. Blain, E. A. Schweikert, G. B. Assayag, P. Saudraud: Nucl. Instrum. Methods B **62**, 8 (1991) 293, 294, 295
[597] K. Boussofiane-Baudin, G. Bolbach, A. Brunelle, S. Della-Negra, P. Håkansson, Y. L. Beyec: Nucl. Instrum. Methods B **88**, 160 (1994) 293, 294
[598] T. Yamaguchi, J. Matsuo, M. Akizuki, C. E. Ascheron, G. H. Takaoka, I. Yamada: Nucl. Instrum. Methods B **99**, 237 (1995) 293, 294
[599] M. W. Matthew, R. J. Beuhler, M. Ledbetter, L. Friedman: Nucl. Instrum. Methods B **14**, 448 (1986) 293, 294
[600] M. W. Matthew, R. J. Beuhler, M. Ledbetter, L. Friedman: J. Phys. Chem. **90**, 3152 (1986) 293, 294
[601] R. Beuhler, L. Friedman: Chem. Rev. **86**, 521 (1986) 293, 294
[602] V. N. Popok, S. V. Prasalovich, E. E. B. Campbell: Surf. Sci. **566-568**, 1179 (2004) 293

[603] R. D. Rickman, S. V. Verkhoturov, E. S. Parilis, E. A. Schweikert: Phys. Rev. Lett. **92**, 047601 (2004) 293

[604] Z. Postawa, B. Czerwinski, N. Winograd, B. J. Garrison: J. Phys. Chem. B **109**, 11973 (2005) 293

[605] A. Novikov, M. Caroff, S. Della-Negra, J. Depauw, M. Fallavier, Y. L. Beyec, M. Pautrat, J. A. Schultz, A. Tempez, A. S. Wood: Rap. Commun. Mass Spectrom. **19**, 1851 (2005) 293

[606] A. R. Oliva-Florio, E. V. Alonso, R. A. Baragiola, J. Ferron, M. M. Jakas: Radiat. Eff. Lett. **50**, 3 (1979) 294

[607] P. C. Zalm, L. J. Beckers: J. Appl. Phys. **56**, 220 (1984) 294

[608] I. Yamada, J. Matsuo, Z. Insepov, D. Takeuchi, M. Akizuki, N. Toyoda: J. Vac. Sci. Technol. A **14**, 781 (1996) 294, 295

[609] P. Sigmund: J. Phys. (Coll. C2) **50**, C2–175 (1989) 294

[610] V. I. Shulga, P. Sigmund: Nucl. Instrum. Methods B **47**, 236 (1990) 294

[611] V. I. Shulga, P. Sigmund: Nucl. Instrum. Methods B **62**, 23 (1991) 294

[612] Z. Pan, P. Sigmund: Nucl. Instrum. Methods B **51**, 344 (1990) 294

[613] P. Sigmund, I. S. Bitensky, J. Jensen: Nucl. Instrum. Methods B **112**, 1 (1996) 294

[614] Z. Postawa, B. Czerwinski, M. Szewczyk, E. J. Smiley, N. Winograd, B. J. Garrison: Anal. Chem. **75**, 4402 (2003) 294

[615] Z. Postawa, B. Czerwinski, M. Szewczyk, E. J. Smiley, N. Winograd, B. J. Garrison: J. Phys. Chem. B **108**, 7831 (2004) 294

[616] Y. Yamamura: Nucl. Instrum. Methods B **33**, 493 (1988) 294

[617] Y. Yamamura: Nucl. Instrum. Methods B **45**, 707 (1990) 294

[618] Y. Yamamura: Nucl. Instrum. Methods B **62**, 181 (1991) 294

[619] Y. Yamamura, T. Muramoto: Nucl. Instrum. Methods B **72**, 331 (1992) 294

[620] M. H. Shapiro, T. A. Tombrello: Phys. Rev. Lett. **65**, 92 (1990) 294

[621] M. H. Shapiro, T. A. Tombrello: Nucl. Instrum. Methods B **58**, 161 (1991) 294

[622] Z. Pan: Nucl. Instrum. Methods B **66**, 325 (1992) 294

[623] H. Hsieh, R. S. Averback, H. Sellers, C. P. Flynn: Phys. Rev. B **45**, 4417 (1992) 294

[624] H. Haberland, Z. Insepov, M. Moseler: Phys. Rev. B **51**, 11061 (1995) 294

[625] T. A. Tombrello: Nucl. Instrum. Methods B **99**, 225 (1995) 294

[626] G. Betz, W. Husinsky: Nucl. Instrum. Methods B **122**, 311 (1997) 294

[627] Z. Y. Pan, Z. Y. Man, Y. K. Ho, J. Xie, Y. Yue: J. Appl. Phys. **83**, 4963 (1998) 294

[628] R. Webb, M. Kerford, A. Way, I. Wilson: Nucl. Instrum. Methods B **153**, 284 (1999) 294

[629] T. J. Colla, H. M. Urbassek: Nucl. Instrum. Methods B **164-165**, 687 (2000) 294

[630] T. J. Colla, R. Aderjan, R. Kissel, H. M. Urbassek: Phys. Rev. B **62**, 8487 (2000) 294

[631] T. Takagi: *Ionized-Cluster Beam Deposition and Epitaxy* (Noyes, Park Ridge 1988) 294

[632] H. Haberland, M. Karrais, M. Mall, Y. Thurner: J. Vac. Sci. Technol. A **10**, 3266 (1992) 294

[633] I. Yamada: Nucl. Instrum. Methods B **99**, 240 (1995) 294

[634] K. Bromann, C. Félix, H. Brune, W. Harbich, R. Monot, K. Kern: Science **274**, 956 (1996) 294
[635] W. Harbich: in K.-H. Meiwes-Broer (Ed.): *Metal Clusters at Surfaces* (Springer, Berlin, Heidelberg 2000) p. 107 294
[636] S. A. Aksyonov, P. Williams: Rap. Commun. Mass Spectrom. **15**, 2001 (2001) 294
[637] M. J. V. Stipdonk, R. D. Harris, E. A. Schweikert: Rap. Commun. Mass Spectrom. **11**, 1796 (1997) 294
[638] G. Gillen, S. Roberson: Rap. Commun. Mass Spectrom. **12**, 1303 (1998) 294
[639] G. Gillen, R. L. King, F. Chmara: J. Vac. Sci. Technol. A **17**, 845 (1999) 294
[640] G. Gillen, R. L. King, B. Freibaum, R. Lareau, J. Bennett, F. Chmara: J. Vac. Sci. Technol. A **19**, 568 (2001) 294
[641] G. Gillen, A. Fahey: Appl. Surf. Sci. **203-204**, 209 (2003) 294
[642] D. Stapel, O. Brox, A. Benninghoven: Appl. Surf. Sci. **140**, 156 (1999) 294
[643] D. Stapel, M. Thiemann, A. Benninghoven: Appl. Surf. Sci. **158**, 362 (2000) 294, 295
[644] L. Hanley, O. Kornienko, E. T. Ada, E. Fuoco, J. L. Trevor: J. Mass Spectrom. **34**, 705 (1999) 294
[645] K. Wittmaack, W. Szymczak, G. Hoheisel, W. Tuszynski: J. Am. Soc. Mass Spectrom. **11**, 544 (2000) 294
[646] R. Loesing, G. M. Guryanov, M. S. Phillips, D. P. Griffis: J. Vac. Sc. Technol. B **20**, 507 (2002) 294
[647] S. V. Verkhoturov, E. A. Schweikert, N. M. Rizkalla: Langmuir **18**, 8836 (2002) 294
[648] N. Toyoda, J. Matsuo, T. Aoki, I. Yamada, D. B. Fenner: Appl. Surf. Sci. **203-204**, 214 (2003) 294
[649] D. Weibel, S. Wong, N. Lockyer, P. Blenkinsopp, R. Hill, J. C. Vickerman: Anal. Chem. **75**, 1754 (2003) 294, 295
[650] S. C. C. Wong, R. Hill, P. Blenkinsopp, N. P. Lockyer, D. E. Weibel, J. C. Vickerman: Appl. Surf. Sci. **203-204**, 219 (2003) 294
[651] N. Davies, D. E. Weibel, P. Blenkinsopp, N. P. Lockyer, R. Hill, J. C. Vickerman: Appl. Surf. Sci. **203-204**, 223 (2003) 294
[652] J. E. Locklear, S. V. Verkhoturov, E. A. Schweikert: Int. J. Mass Spectrom. **238**, 59 (2004) 294
[653] S. Sun, C. Szakal, T. Roll, P. Mazarov, A. Wucher, N. Winograd: Surf. Interf. Anal. **36**, 1367 (2004) 294
[654] J. Xu, C. W. Szakal, S. E. Martin, B. R. Peterson, A. Wucher, N. Winograd: J. Am. Chem. Soc. **126**, 3902 (2004) 294
[655] J. T. Francis, N. S. McIntyre: Surf. Interf. Anal. **37**, 743 (2005) 294
[656] M. S. Wagner: Anal. Chem. **77**, 911 (2005) 294
[657] C. M. Mahoney, J. Yu, J. A. Gardella: Anal. Chem. **77**, 3570 (2005) 294
[658] J. Cheng, N. Winograd: Anal. Chem. **77**, 3651 (2005) 294
[659] I. Yamada, J. Matsuo, N. Toyoda, T. Aoki, E. Jones, Z. Insepov: Mater. Sci. Eng. A **253**, 249 (1998) 294
[660] N. Toyoda, N. Hagiwara, J. Matsuo, I. Yamada: Nucl. Instrum. Methods B **148**, 639 (1999) 294
[661] I. Yamada: Eur. Phys. J. D **9**, 55 (1999) 294
[662] I. Yamada: Nucl. Instrum. Methods B **148**, 1 (1999) 294

[663] I. Yamada, J. Matsuo, Z. Insepov, T. Aoki, T. Seki, N. Toyoda: Nucl. Instrum. Methods B **164-165**, 944 (2000) 294

[664] N. Toyoda, N. Hagiwara, J. Matsuo, I. Yamada: Nucl. Instrum. Methods B **161**, 980 (2000) 294, 300

[665] I. Yamada, J. Matsuo, N. Toyoda, A. Kirkpatrick: Mater. Sci. Eng. R **34**, 231 (2001) 294, 300

[666] N. Toyoda, S. Matsui, I. Yamada: Jpn. J. Appl. Phys. Part 1 **41**, 4287 (2002) 294, 299, 300

[667] I. Yamada, J. Matsuo, N. Toyoda: Nucl. Instrum. Methods B **206**, 820 (2003) 294

[668] S. J. Carroll, S. G. Hall, R. E. Palmer, R. Smith: Phys. Rev. Lett. **81**, 3715 (1998) 294

[669] C. Xirouchaki, R. E. Palmer: Vacuum **66**, 167 (2002) 294

[670] L. Hanley, Y. Choi, E. R. Fuoco, F. A. Akin, M. B. J. Wijesundra, M. Li, A. Tikhonov, M. Schlossman: Nucl. Instrum. Methods B **203**, 116 (2003) 294

[671] J. H. Song, D. K. Choi, W. K. Choi: Nucl. Instrum. Methods B **196**, 268 (2002) 294

[672] J. H. Song, D. K. Choi, W. K. Choi: Nucl. Instrum. Methods B **196**, 275 (2002) 294

[673] J. H. Song, W. K. Choi: J. Korean Phys. Soc. **42**, S606 (2003) 294

[674] H. H. Andersen, A. Brunelle, S. Della-Negra, J. Depauw, D. Jacquet, Y. L. Beyec, J. Chaumont, H. Bernas: Phys. Rev. Lett. **80**, 5433 (1998) 295

[675] S. Bouneau, A. Brunelle, S. Della-Negra, J. Depauw, D. Jacquet, Y. L. Beyec, M. Pautrat, M. Fallavier, J. C. Poizat, H. H. Andersen: Phys. Rev. B **65**, 144106 (2002) 295

[676] A. Brunelle, S. Della-Negra: Nucl. Instrum. Methods B **222**, 68 (2004) 295

[677] C. W. Diehnelt, M. J. V. Stipdonk, E. A. Schweikert: Phys. Rev. A **59**, 4470 (1999) 295

[678] S. F. Belykh, U. K. Rasulev, A. V. Samartsev, L. V. Stroev, A. V. Zinoviev: Vacuum **56**, 257 (2000) 295, 296

[679] S. F. Belykh, B. Habets, U. K. Rasulev, A. V. Samartsev, L. V. Stroev, I. V. Veryovkin: Nucl. Instrum. Methods B **164-165**, 809 (2000) 295, 296

[680] S. F. Belykh, A. P. Kovarsky, V. V. Palitsin, A. Adriaens, F. Adams: Int. J. Mass Spectrom. **209**, 141 (2001) 295, 296

[681] S. F. Belykh, V. V. Palitsin, I. V. Veryovkin, A. Adriaens, F. Adams: Nucl. Instrum. Methods B **203**, 164 (2003) 295

[682] A. Brunelle, S. Della-Negra, J. Depauw, D. Jacquet, Y. L. Beyec, M. Pautrat, K. Baudin, H. H. Andersen: Phys. Rev. A **63**, 022902 (2001) 295

[683] M. Fallavier, R. Kirsch, S. N. Morozov, J. C. Poizat, J. P. Thomas, N. Wehbe: Phys. Rev. B **68**, 140102 (2003) 295

[684] S. Sun, C. Szakal, E. J. Smiley, Z. Postawa, A. Wucher, B. J. Garrison, N. Winograd: Appl. Surf. Sci. **231-232**, 64 (2004) 295, 296, 297

[685] S. Ghalab, A. Wucher: Nucl. Instrum. Methods B **226**, 264 (2004) 295

[686] S. F. Belykh, U. K. Rasulev, A. V. Samartsev, I. V. Veryovkin: Nucl. Instrum. Methods B **136-138**, 773 (1998) 295

[687] I. V. Veryovkin, S. F. Belykh, A. Adriaens, F. Adams: Nucl. Instrum. Methods B **219-220**, 215 (2004) 295

[688] I. V. Veryovkin, S. F. Belykh, A. Adriaens, A. V. Zinovev, F. Adams: Appl. Surf. Sci. **231-232**, 101 (2004) 295

[689] S. Bouneau, S. Della-Negra, D. Jacquet, Y. L. Beyec, M. Pautrat, M. H. Shapiro, T. A. Tombrello: Phys. Rev. B **71**, 174110 (2005) 295
[690] S. N. Morozov, U. K. Rasulev: Nucl. Instrum. Methods B **203**, 192 (2003) 296
[691] R. Heinrich, A. Wucher: Nucl. Instrum. Methods B **164-165**, 720 (2000) 296
[692] S. Ghalab, C. Staudt, S. E. Maksimov, P. Marsarov, V. I. Tugushev, N. K. Dzhemilev, A. Wucher: Nucl. Instrum. Methods B **197**, 43 (2002) 296
[693] R. Heinrich, A. Wucher: Nucl. Instrum. Methods B **193**, 781 (2002) 296
[694] R. Heinrich, A. Wucher: Nucl. Instrum. Methods B **207**, 136 (2003) 296
[695] M. Lindenblatt, R. Heinrich, A. Wucher, B. J. Garrison: J. Chem. Phys. **115**, 8643 (2001) 296
[696] A. Duvenbeck, M. Lindenblatt, A. Wucher: Nucl. Instrum. Methods B **228**, 170 (2005) 296
[697] L. Wang, R. Md Nor, W. G. Graham: J. Phys. D: Appl. Phys. **30**, 2379 (1997) 296
[698] A. V. Samartsev, A. Duvenbeck, A. Wucher: Phys. Rev. B **72**, 115417 (2005) 296, 297, 298
[699] M. Medvedeva, I. Wojciechowski, B. J. Garrison: Surf. Sci. **505**, 349 (2002) 298
[700] H. H. Andersen, A. Johansen, V. S. Touboltsev: Nucl. Instrum. Methods B **164-165**, 727 (2000) 298, 299
[701] M. H. Shapiro, T. A. Tombrello: Nucl. Instrum. Methods B **217**, 253 (2004) 299
[702] N. Toyoda, H. Kitani, N. Hagiwara, T. Aoki, J. Matsuo, I. Yamada: Mater. Chem. Phys. **54**, 262 (1998) 299, 300
[703] N. Toyoda, J. Matsuo, I. Yamada: Nucl. Instrum. Methods B **216**, 379 (2004) 299
[704] Z. Insepov, I. Yamada, M. Sosnowski: Mater. Chem. Phys. **54**, 234 (1998) 300

Index

absorption, 237, 238
angular distribution
  cosine, 235, 275, 276
  Mo, 291
  Ni, 291
  over-cosine, 275, 276, 291
  under-cosine, 275, 290, 291
  W, 292

band structure, 247
BCA program
  TRIM, 232
  TRIM.SP, 275, 281, 283, 286, 288, 289
binary collision approximation (BCA), 232
bulk
  composition, 282
  coordination number, 236

cluster
  Ag_n^+, 258
  C_n^-, 257, 258, 267
  Cu_n, 256
  dimer, 255
  emission, 254, 255
    Ag_n, 255
    Ag_6, 254
    Al_n, 255
    Au_n, 255
    benzene, 265, 266
    Cu_n, 255
    Ga_n, 255
    Ge_n, 255
    In_n, 255
    In_n^+, 258
    metal, 286
    metastable, 268
    Nb_n, 255
    Si_n^-, 251, 257
    Ta_n, 255
  energy spectra
    Ag_n, 256
    Al_n, 256
    Cu_n, 256
    Cu_2, 256
    Cu_3, 256
    Ge_n, 256
    In_n, 256
    Si_n^-, 251
  formation, 254
  homonuclear, 255
  impact, 231, 292–296, 298
    $(CO_2)_n$, 293
    $(CsI)_nCs$, 293
    $(CsI)_nI$, 293
    Ar_n, 293
    Ar_{3000}^+, 299
    Au_n, 293
    C_{60}, 293
    ReO_4, 293
    SF_6, 293
  secondary ion, 295
  size, 254–256, 259, 295
  species, 254, 294
  trimer, 255, 292
cohesive energy, 234, 236, 245, 253, 271, 285
collisional mixing, 252
composition
  change, 252, 253, 281
  gradient, 252, 274, 280
  profile, 281
condensed gas, 271, 272
crater
  formation, 292, 298
  rim, 298
cross section
  excitation, 240
  nuclear stopping, 271, 272
cylindrical deflector, 238

damage distribution, 233
decay rate, 267, 268
decomposition, 258, 267
  rate, 268
  time, 268
defect, 231
  production, 233
deposited energy, 233, 275
depth of origin, 234, 252, 280
desorption, 254, 262, 265, 266, 271
detection technique
  collector, 241, 243, 277, 281

foil, 241
differential yield, 234, 235
dimer, 254, 292, 296
Ag_2, 256
Cs_2, 254
Cu_2, 286
K_2, 254
Na_2, 254
S_2, 254
disappearance cross section, 260
dissipation, 231
dissociation, 273
threshold, 260
Doppler profile, 240
Doppler shift laser fluorescence spectroscopy (DSLFS), 240, 271
dynamic range, 238

electrical resistivity, 271
electron affinity, 251
electron impact ionizer, 240
electron promotion, 248
electron spectroscopy, 238
electron-induced X-ray emission, 243, 281
electron-tunneling model, 251
electronic configuration, 247, 248, 250
electrostatic energy analysis, 238
energy deposition, 275
energy dissipation, 231, 232, 243, 271, 272, 277
energy loss, 270
electronic, 232, 270
nuclear, 245, 270
energy resolution, 238
energy spectra
Ag, 296
Ag_2, 296
Al, 290
Cu_2, 287
In, 297
Si^-, 251
Ta^+, 295
Ta_4^+, 295
W, 289
escape depth, 274
evaporation, 270–272, 292
excitation, 270
electronic, 232, 270, 271
energy, 247, 249
frequency, 240
rotational, 264
vibrational, 264

fluence, 242
fluorescence, 238
focusing collision sequence, 277
fragment, 262, 264
ion formation, 262
species, 260
fragmentation, 254, 255, 260
C_n^-, 258
large molecule, 259
species, 260

Gibbsian segregation, 280, 281

interaction potential, 234
many-body, 236
pair potential, 236
tight-binding, 236
internal energy, 254, 263–266
ionization, 232, 244, 255, 264, 270
continuum, 238
electron impact, 237
low density plasma, 239
multiphoton (MPI), 238
non-resonant multiphoton (NRMPI), 238
Penning, 237
potential, 238
probability, 251, 258
resonance enhanced multiphoton (REMPI), 238
single photon (SPI), 238
threshold, 238

laser excitation, 239
laser induced fluorescence (LIF), 240, 247, 288
lifetime, 267, 268
radiative deexcitation, 246
light-versus-distance (LvD) technique, 239

mass selectivity, 238
mass spectrometer, 238, 253, 257
double focusing, 238
quadrupole, 239

secondary-neutral, 239
time-of-flight, 237, 243
mass spectrometry, 254, 293
material processing, 293
Maxwell-Boltzmann distribution, 271
metallic bond, 236
molecular dynamics, 232
molecule
emission, 254
formation, 244, 254
organic, 265
orientation, 263
shape, 263
momentum focusing, 277
multilayer coverage, 265

neutralization probability, 250
neutron activation, 240

oligomer, 261, 262
organic adsorbate, 260, 262
organic material, 259, 264

photoionization, 238, 265
laser, 243
photon emission, 239
planar surface potential, 234, 288
polymer, 260
population distribution, 247
population temperature, 254
post-ionization, 237–239, 255
electron impact, 255, 278
laser, 241, 242
plasma, 239, 253
preferential sputtering, 252
proton-induced X-ray emission, 243

quadrupole mass filter, 240

radiation-enhanced diffusion, 252
radiative decay, 246
recoil
density, 233, 234, 244, 245
direct, 252, 284, 288, 289
flux, 243, 275
generation, 233
implantation, 252
isotropic distribution, 244
primary, 289
spectrum, 235, 277
recondensation, 272
reflectron, 237
refraction, 234
regime
high-density collision cascade, 300
linear cascade, 231–233, 243, 244
single knockon, 232, 300
spike, 232, 292
relocation, 231
resonant electron transfer (RET), 249, 251
resonant photoionization mass spectrometry, 247
rotational population, 254
Rutherford backscattering spectroscopy (RBS), 243

secondary ion mass spectrometry (SIMS), 237, 243, 259, 267, 293
secondary neutral mass spectrometry (SNMS), 237, 253, 265, 293
laser, 241
segregation, 280
selfsputtering, 275, 298
shock wave, 255
spherical deflector, 238
spherical electrostatic sector, 238
spike, 253, 272
elastic collision, 272
temperature, 270
thermal, 240
volume, 272
sputtering of
molecules, 259
state
charge, 252
excited, 239, 240, 246, 247, 250
Ag, 247
Ba, 247
Ca, 247
Co, 247
Cr, 247
Cu, 247
Fe, 247
In, 247
Ni, 247
Rh, 247, 279
Ti, 247

U, 247
Zr, 247
ground, 240, 247
Ag, 246, 248
Al, 246
Ca, 246
Co, 248, 249
Ni, 248, 249
Rh, 279
metastable, 239, 246
Ag, 247, 248
Co, 248–250
formation, 251
high-lying, 249
low-lying, 248
Ni, 248–250
short-lived, 246
steady, 252, 282, 287
valence band
Co, 250
Ni, 250
sticking, 241
stoichiometry, 252, 253
stopping power
electronic, 271
nuclear, 234
sublimation energy, 234, 236, 273
surface
composition, 282
modification, 293
morphology, 242
roughness, 276
smoothing, 298
structure
ripple, 242, 276
surface binding energy, 236, 237, 244, 245, 253, 271, 273, 285, 292
surface contamination, 276
surface potential barrier, 234
surface topography, 242, 276

target
alkali halide, 231, 232, 244, 270, 299
alkali metal, 270
alkanethiol, 264
alloy, 252
$Ag_{0.6}Au_{0.4}$, 253
Ag–Au, 253, 280
Au–Cu, 281
Co–Au, 281
Co–Ni, 281
$Cu_{0.53}W_{0.47}$, 285
Cu_3Au, 280
Cu–Be, 281
Cu–Ni, 280, 281
Cu–Pt, 280
Cu–Zn, 253, 281
Cu-Li, 253
Fe–Ni, 280, 281
Ga–In, 281
$Ni_{0.92}W_{0.08}$, 285
Ni_5Pd, 280
Ni–Pt, 280
Ni–Ti, 281
Ni–W, 253
W-Si, 281
amorphous, 232, 275
biological material, 259
composition, 273
compound
GaAs, 253
$Hf_xC_{(1-x)}$, 253
HfC, 253
condensed gas, 232, 270, 271
crystalline, 276
dibenzanthracene, 261
frozen gas, 231, 244, 299
Ar, 271
CO, 271
CO_2, 271
D_2O, 271
H_2O, 271
Kr, 271
N_2, 271
Ne, 271
O_2, 271
Xe, 271, 272, 274
insulator, 232
ionic crystal, 232
isotopic mixture, 243, 282
metal, 231, 232, 244, 253, 254, 269, 299
multicomponent, 252, 274, 280
organic material, 231, 244, 269, 299
oxide, 253
polycrystalline, 232
polyethyleneterephthalate (PET), 264

polyisobutylene, 269
polystyrene, 264
polystyrene (PS), 260, 261, 263, 264, 268
radioactive, 240
semiconductor, 231, 232, 244, 254, 269, 276, 299
single crystal, 232, 240, 274, 276
CaF_2, 271
NaCl, 270
triacontane, 261
target structure
amorphous, 231, 235, 274
crystalline, 231, 236, 274
polycrystalline, 231, 240, 274
thermal conductivity, 271
time-of-flight (ToF), 238, 240, 253
time-of-flight mass spectrometry, 241, 242, 247
ToF-SIMS, 260, 264
trajectory, 263, 264

vapor pressure, 270
vibrational distribution, 254

Wehner spot, 244, 277
work function, 251, 252, 258

Chemical Sputtering

Wolfgang Jacob and Joachim Roth

Max-Planck-Institut für Plasmaphysik, EURATOM Association,
Boltzmannstr. 2, 85748 Garching, Germany
Wolfgang.Jacob@ipp.mpg.de
Joachim.Roth@ipp.mpg.de

Abstract. If a target is bombarded with chemically reactive species, chemical effects have to be taken into account. Two converse effects can occur. Chemical reactions between target and projectile atoms may form species which are more loosely bound to the surface and more easily sputtered. This causes an increase of the sputtering yield. This process is usually subsumed under the expression chemical sputtering. Otherwise, newly formed compounds may posses an enhanced bond strength to the target atoms and, consequently, a higher surface binding energy. This causes a decrease of the sputtering yield compared with the original target.

In this chapter the emphasis is put on sputtering of carbon with hydrogen ions because it is the best studied system. The process of chemical sputtering is defined. The experimental methods to measure it and the available experimental data are discussed. Model conceptions of the basic, microscopic mechanisms developed for chemical sputtering of carbon by hydrogen are reviewed. Finally, several additional species that cause chemical sputtering of carbon materials are presented.

1 Introduction

In 1912, at a time when the basic mechanisms of the erosion of the cathode in a gas discharge were under active discussion, *Kohlschütter* [1] proposed a process in which volatile radicals are formed in the interaction of the bombarding ions with the target atoms. This model was, however, soon abandoned because cathode erosion was also found in noble gas discharges. In 1926 it was observed [2] that the deposition patterns of sputtered material for some combinations of discharge gas and cathode materials, such as H^+ on C, Bi, Sb, As, and Te were very different from the ones expected and found for non-reactive materials (Fig. 1). For most metals the deposited amount decreases with increasing distance from the cathode as expected. However, for C, Bi, Sb, As, and Te the thickness of the deposits did not decrease, but rather increased with increasing distance from the cathode. This was attributed to the formation of volatile hydrides at the cathode and subsequent cracking by electron impact in the discharge. From this observation *Güntherschulze* [2] concluded that chemical reactions must have contributed to the erosion. Since then the expression *chemical sputtering* has been used in the literature for

R. Behrisch, W. Eckstein (Eds.): Sputtering by Particle Bombardment,
Topics Appl. Physics **110**, 329–400 (2007)
© Springer-Verlag Berlin Heidelberg 2007

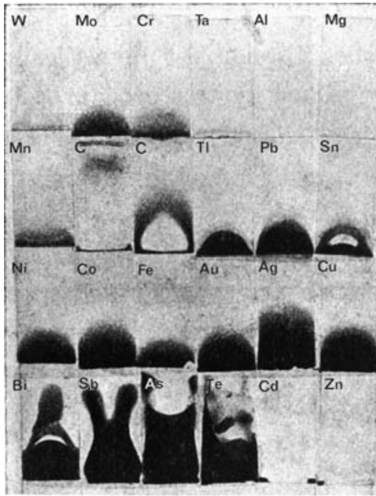

Fig. 1. Deposition of material sputtered from different cathode plates in a hydrogen discharge on a glass plate perpendicular to the cathode surface (from [2])

the different aspects of the chemical interactions of the projectile and target atoms during sputtering.

About 30 years ago, the chemical aspects of sputtering found renewed interest. In semiconductor technology the strong selectivity of the chemical erosion process depending on the ion–target–atom combination enabled new techniques for etching and structuring of surface patterns [3, 4] and for the first time the details of surface reactions leading to volatile molecule formation were investigated for the Si–F system [5].

In fusion research the use of graphite or carbon-fibre composites as plasma-facing material led to large carbon erosion and strong plasma contamination due to the interaction of hydrogen and oxygen ions from the plasma with carbon surfaces [6]. In 1976 the first controlled investigations of carbon erosion due to hydrogen bombardment using ion beams were reported [7–9] and the first atomistic interpretations were proposed [7, 8, 10]. While in semiconductor technology ion-beam etching has become the basic process for surface structuring [11–13], the improved understanding of the chemical erosion processes of carbon in fusion devices has led to ways of reducing its influence [14–19].

2 Chemical Effects in Sputtering

Energetic ions bombarding a solid are partly backscattered and partly penetrate the surface. They are slowed down and may come to rest near the surface of the material. Bombardment of a solid with ions which react chemi-

cally with the atoms of the solid surface may lead to the formation of surface molecules with different binding energies to the surface.

The development of such an altered surface layer has also been found for bombardment by non-reactive ions in a reactive gas atmosphere. If the number of reactive atoms arriving at the surface is comparable or larger than the number of atoms removed by sputtering, a compound layer can be formed which was found to spread over a thickness equivalent to the range of the bombarding ions. This may be formed by recoil implantation and cascade mixing [20–22] or diffusion [23, 24] of the atoms implanted in the near-surface layer. The build-up of the altered surface layer generally leads to a different sputtering behaviour than for the original surface. The sputtering yield can be decreased or increased and the composition and the distributions of the sputtered species will be different. Causes of these changes may be divided into two groups:

– Presence of trapped ions: The incident ions may be implanted and chemically bound, forming an altered surface layer. The altered surface layer will modify the spread of the collision cascade, especially if the mass of the trapped ions is very different from the mass of the target atoms, thus decreasing the sputtering yield of the original target atoms [23–31].
– Changes of the binding energies: The compound formed in the surface layer and on the surface will generally lead to formation of molecules with a binding energy to surface atoms which is different from that of the original solid. A lower binding energy will result in an increase of the sputtering yield and a higher binding energy in a decrease of the sputtering yield. For sufficiently low binding energies, thermal desorption of compound molecules can lead to additional erosion. This thermal release will be best observable if the yields from collisional effects are low such as at low bombarding energies.

In addition to their fundamental interest, these effects are of significant importance in a number of technical processes. For example, metal oxides, carbides, and nitrides are produced by reactive sputtering. In reactive sputtering, metal atoms are sputtered from a solid target using typically an argon plasma. A small admixture of an appropriate reactive gas leads to the deposition of the desired layers on the substrate. However, chemical processes occurring at the target surface can also cause an altered surface layer forming a compound that has a higher surface binding energy and thus a lower sputtering yield. This is a major problem for a reliable control of reactive sputtering processes and has recently been discussed by *Sproul* et al. [32]. On the other hand, the enhancement of sputtering yields due to chemical effects, i.e., chemical sputtering, plays an important role in a variety of modern plasma etching [33] processes for fabrication of memory and logic chips in the microelectronics industry [12]. Plasma etching in the semiconductor industry is generally called "dry etching" in contrast to "wet etching" using liquid chemical substances.

Although the involved chemistries for dry etching processes in semiconductor technology and chemical sputtering in the interaction of fusion plasmas with carbon-based plasma-facing materials are largely different, the general mechanisms are similar. We will focus in this chapter on the erosion of carbon in the interaction with hydrogen ions because the basic processes in the C-H system as a whole are more comprehensively studied. Since we will touch upon silicon etching only marginally, we refer the interested reader here to some reviews in that field: A survey of phenomena and basic processes occurring in reactive etching in microelectronics, fusion, and space technologies was compiled by *Auciello* and coauthors [34]. The basics of plasma etching are presented in the textbook by *Manos* and *Flamm* [33]. The surface sciences aspects of etching reactions on semiconductor materials have been reviewed by *Winters* and *Coburn* [35].

3 Definitions

Chemical sputtering was investigated in very different fields, such as dry etching of semiconductor materials in microelectronics and erosion of carbon in the thermonuclear fusion community, and by a large number of different groups. As a consequence of this diversity many different names were coined to describe identical processes and different authors have used and still use identical phrases to denote different processes. Actually, many authors have used in the past the phrase chemical erosion synonymously with chemical sputtering. This has led and can still lead to some confusion. In addition, a large number of alternative names has been used for what we call chemical sputtering: chemically enhanced (physical) sputtering [36, 37], ion-assisted chemical erosion [38], ion-assisted etching [39], and reactive ion sputtering or reactive ion etching [11–13]. The important phrases with relevance to chemical sputtering which will be used throughout this chapter are defined in this section.

3.1 Physical Sputtering

Physical sputtering is caused by momentum transfer from the impinging projectiles to target atoms. It takes place for all target materials and incident particles with an energy above a threshold energy in the range of about 100 eV. Physical sputtering is reasonably well understood as presented in the Chap. by *Eckstein*.

Sputtered particles originate predominantly from the topmost surface layer with only small contributions from the second and third atomic layer. In general, they are monoatomic and have mean energies in the eV range, i.e., their kinetic energy is much higher than that of thermally released species.

3.2 Chemical Erosion

Chemical erosion is the process initiated by chemical reactions between neutral, thermal species from the gas phase with surface atoms. For carbon materials chemical effects are of paramount importance for hydrogen, oxygen, and fluorine projectiles, but chemical effects are also known for other impinging species (e.g. nitrogen).

3.3 Chemical Sputtering

Chemical sputtering is defined as "a process whereby ion bombardment causes or allows a chemical reaction to occur which produces a particle that is weakly bound to the surface and hence easily desorbed into the gas phase" [35]. The erosion process depends on both the kinetic energy and the chemical reactivity of the impinging species. The main effect of ion bombardment is to promote the chemical reaction. The release will mostly be thermally driven.

The occurrence of chemical sputtering may be inferred from a number of different experimental observations.

- Molecules are formed between projectile and target atoms.
- The process varies strongly with the projectile target combination.
- The sputtering yields are significantly higher compared with physical sputtering predictions from computer simulations. In contrast, data for sputtering with noble gases or selfsputtering are, in general, in excellent agreement with such predictions.
- The threshold energy is substantially lower than for physical sputtering.
- The sputtering yield shows a pronounced temperature dependence.
- The energy distribution of the released species should be close to the target surface temperature.

The clearest proof for identification of chemical sputtering is the detection of chemical compounds formed between target and projectile atoms. Newly formed species at the surface can have a lower surface binding energy and are consequently more easily sputtered such that the sputtering yield increases. This is a possible indication for chemical sputtering and, in fact, it was frequently used in the literature [25]. On the other hand, newly formed compounds can have a higher surface binding energy than the corresponding unreacted surfaces and, as a consequence, the sputtering yield decreases. This is, for example, the case for oxygen, carbon, or nitrogen bombardment of various metals where metal oxides (Al_2O_3, SiO_2, TiO_2, etc.), carbides (TiC, WC, SiC, etc.), and nitrides (TiN) are formed.

Physical sputtering shows a negligible temperature dependence if the temperature is well below the melting point of the material [40–42]. For carbon, however, a strong increase of the sputtering yield close to the sublimation temperature was reported for all bombarding ions. This process was named

radiation-enhanced sublimation (RES) [43–46]. In contrast, chemical sputtering shows a strong temperature dependence significantly below melting or sublimation temperatures. This has been observed in systems where chemical interactions between target and projectile atoms play a significant role. A prominent, but not unique, example which has been thoroughly investigated is the interaction of hydrogen with carbon. Such a temperature dependence can in principle be caused by activation of chemical reactions and/or by activation of diffusion of species produced in deeper layers.

A significant deviation of the energy distribution of released species from that of physically sputtered particles is also an indication of chemical sputtering. While physically sputtered species have mean energies of a few eV, chemically sputtered species which are released by a thermal desorption process after a chemical reaction at the surface have an energy distribution which is determined by the surface temperature. In the case of hydrogen ions impinging on carbon surfaces at a temperature of 800 K the dominant fraction of released molecules has a thermal energy distribution corresponding to the surface temperature [47]. On the other hand, for bombardment at room temperature the emitted CH_3 radicals have a significant suprathermal component which is, however, also different from a distribution of species produced by physical sputtering [47].

A further indication of chemical sputtering can be deduced from the redeposition pattern. Indeed, the first experimental observation of chemical sputtering by *Güntherschulze* [2] (see Fig. 1) was based on the observation of differences in the deposition pattern. Physical sputtering leads to deposition almost exclusively at surfaces which are in line of sight of the particle source. However, chemically released radical species, which can survive several wall collisions can also be transported to remote areas which are not in line of sight. A method to investigate this effect is presented in Sect. 4.5.

A new sputtering mechanism named: "Swift Chemical Sputtering" was discovered in molecular dynamics simulations [48–53]. Swift chemical sputtering leads to the release of hydrocarbon radicals (including single C atoms) down to energies of about 2 eV by a kinetic emission process. The "Swift Chemical Sputtering" process has recently been shown to occur also for bombardment with helium ions [54]. It is a new process which differs from usual physical sputtering and from chemical sputtering.

4 Experimental Methods

To achieve a relatively complete picture of the underlying physical and chemical processes, two or more experimental methods have to be combined. In laboratory experiments, the most frequently applied methods to determine the total erosion yields are weight loss measurement, ellipsometry, and mass spectrometry. The latter is also applied for identification of released species.

In plasma experiments, optical emission spectroscopy of different excited hydrocarbon fragments is employed to determine chemical sputtering yields.

4.1 Weight Loss

The total erosion yield can be obtained from the weight loss of the sample after bombardment with a certain ion fluence. Weight loss measurements can be performed using vacuum micro-balances with sensitivities of the order of 1 µg [55, 56] or quartz oscillators, where the frequency shift due to the mass loss of a deposited layer is determined (see, e.g., [57–59]). By proper calibration sensitivities of the order of sub-monolayers can be achieved using quartz microbalances [57–59]. Quartz microbalance measurements require preparation of thin film systems while vacuum balance measurements can be applied to bulk samples. Weight loss measurements have the advantage to integrate over all possible mass loss processes and all types of species. In contrast to mass spectrometry, different sensitivities for different eroded molecules do not play a role. The main disadvantage of the weight loss method arises in cases where the incident particles accumulate in the target and give rise to uncontrolled weight increases [60]. For hydrogen on carbon, as for most metals, the amount of retained hydrogen can be neglected compared with the weight loss due to erosion provided the ion fluence is sufficiently high [61]. The need to accumulate high fluences until measurable weight changes are obtained, makes the method unsuited for investigating fluence dependences of the erosion yield [62]. Consequently, weight loss measurements determine in general the steady-state value of the sputtering yield. The precision of the measured yields increases with increasing total weight change. Therefore, at sufficiently long measuring times, weight loss measurements in steady state produce the most precise sputtering yields.

4.2 Mass Spectrometry

Identification of released species using a remote mass spectrometer in the sputtering chamber is a very useful method to verify chemical sputtering. However, the species measured in the remote mass spectrometer may also be formed on other wall areas by reflected projectiles. Indeed, extensive production of CH_4 on the walls of the sputtering chamber by atomic hydrogen reflected from the substrate led to a higher CH_4 signal than the reaction at the sample surface and thus hampered these early attempts to measure the interaction of atomic hydrogen with carbon surfaces [63–65]. But the wall may act not only as particle source but also as sink. Reactive species or long chain hydrocarbons which may be produced in the interaction with the sample may stick to the chamber walls [66] or be converted to other species. In any case, if a remote mass spectrometer is used, species reach the ionizer only after many wall collisions and, in general, only stable or so-called recycling

species contribute to the signal. Thus, in practise, a remote mass spectrometer merely measures the partial pressure of stable molecules that builds up in the vacuum chamber. In general, it cannot measure species with a high sticking probability.

A big advantage of mass spectrometry is that it produces real-time data and allows measuring parameter variations in much shorter times than weight loss measurements. However, the determination of total chemical sputtering yields by mass spectrometry requires extensive data evaluation and interpretation. Firstly, the sensitivity of the mass spectrometer has to be properly calibrated for each eroded species. For many species this can be achieved by appropriate calibration procedures with stable gases [67, 68], but for reactive species, such as hydrocarbon radicals, this method fails. Secondly, if the eroded particle flux comprises more than one species and their cracking patterns produced by the ionisation process in the ion source of the mass spectrometer overlap, then the measured mass spectra have to be decomposed into the individual contributions. In most cases the cracking pattern cannot be determined for all species in the mixture, and the inverse problem is therefore ill posed. Routines used for the decomposition of multi-component mass spectra like the recursive method [69] or least square fits [70] provide only poor and sometimes nonphysical results such as negative concentrations [69]. Recently, advanced analysis techniques were developed using Bayesian probability theory [71, 72] and a generalized maximum entropy approach [73].

A frequently used method for quantifying mass spectrometry data is measuring the intensity of a certain mass signal and relating this to the flux of a released species. In simple cases in particular, if the number of produced species is small, such a signal can be attributed to one species only and by comparison to other methods, e.g., to weight loss data, it can possibly be quantified. But this works reliably only in few favorable cases. What can be measured in this case is the production rate of one or a few released species. Whether or not this production rate is proportional to the total sputtering yield has to be thoroughly checked. Unfortunately, the erosion of carbon materials by hydrogen suffers from several problems: Firstly, depending on experimental conditions, the product spectrum of released species can be very rich [74–79]. Secondly, the product spectrum of released species changes as a function of experimental parameters. E.g., for the chemical sputtering of metal-doped carbon materials it was shown that the methane yield increases with dopant concentration while the total yield decreases strongly [19]. Under such conditions the quantification of total sputtering yields is very challenging. Due to the mentioned inherent problems in the quantification of mass spectrometric data for the chemical sputtering of carbon by hydrogen, there has always been a systematic disagreement with weight loss data [80, 81]. Weight loss resulted in most cases in higher chemical sputtering yields than mass spectrometric investigations. The disagreement decreased with the consideration of higher hydrocarbons, but it did not vanish completely.

A possibility to circumvent or reduce the contribution of species produced at the chamber walls to the measured signal is using a line-of-sight mass spectrometry setup. But even if the mass spectrometer has a line of sight to the surface of interest, the signal is in most cases dominated by recycling species. This shall be explained by the following sample calculation. Let us assume that we have a flow of stable species leaving the surface. The ionizer of the mass spectrometer is in line of sight with the sample in a direction perpendicular to the sample surface and has a distance x from the surface. Species that go directly to the ionizer of the mass spectrometer contribute to the beam component of the signal, species that go to other chamber wall areas are reflected and contribute to the background pressure in the chamber. The mass spectrometer signal is determined by the particle density in the ionizer of the mass spectrometer. As a consequence, the beam-to-background ratio of the mass spectrometer signal, R_{bb}, is given by the ratio of the particle densities due to the directed beam, n_{beam}, and the background density, $n_{\mathrm{background}}$ [82]. The background pressure and therewith the background density are determined by the effective pumping speed, S_{eff}, of the pumping system. If we neglect all other possible background contributions R_{bb} is given by [82]

$$R_{\mathrm{bb}} = \frac{n_{\mathrm{beam}}}{n_{\mathrm{background}}} = \frac{S_{\mathrm{eff}}}{\pi x^2 \overline{v}_{\mathrm{beam}}} \,. \tag{1}$$

Here $\overline{v}_{\mathrm{beam}}$ is the average velocity of the beam particles. The denominator πx^2 accounts for the reduction in the flux density for a cosine distribution in a distance x [83]. Equation (1) demonstrates that the beam-to-background ratio depends critically on two parameters: the effective pumping speed, S_{eff}, of the chamber and the distance of the ionizer of the mass spectrometer from the particles' origin. A typical value for the effective pumping speed of a vacuum system is 100 l/s. Let us for simplicity assume that the distance is 10 cm (in real cases the distance is often larger). If we then assume that the species is a methane molecule and leaves the sample surface with a mean velocity according to a room temperature distribution, we can calculate R_{bb}. This yields a value of about 5×10^{-3} (for CH_4). It is obvious that under such conditions it is virtually impossible to discriminate beam particles from background. Even if the distance x is reduced to 1 cm, which is practically impossible, R_{bb} increases only to 0.5. The preceding estimate is still rather optimistic because all other contributions to the background signal are neglected. In addition, R_{bb} will further decrease if the particles leave the surface with a temperature higher than 300 K or if they are even emitted with some kinetic energy, such as, for example, in physical sputtering where the sputtered particles have energies in the eV range.

The preceding discussion has shown that a line-of-sight setup is necessary but not sufficient to detect reactive species and that significant effort has to be spent to reduce the signal contribution of recycling species. This can be achieved by putting the mass spectrometer in a separate vacuum chamber which is differentially pumped. Such a measurement geometry is often named

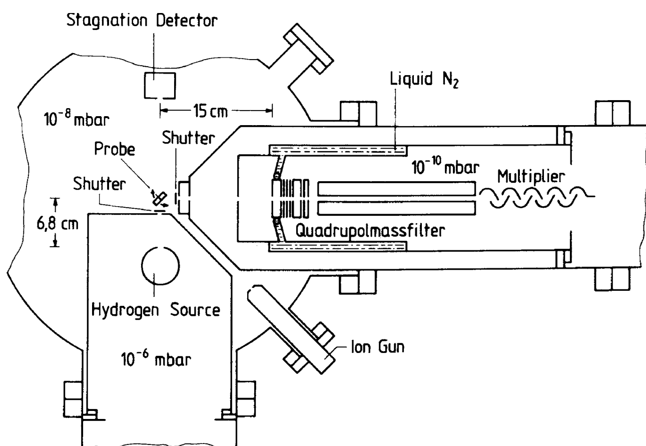

Fig. 2. Experimental setup of *Vietzke* et al. [77, 85]

molecular beam mass spectrometry (MBMS). Furthermore, for quantification of the species fluxes it is not sufficient to reduce the contribution from the isotropic background, but in addition its magnitude has to be determined. This can be done with a simple flag or with a continuous chopper connected with lock-in data acquisition. The flag or chopper has to be placed directly in front of the ionizer in the last pumping stage. If the flag or chopper is situated in one of the differential pumping stages, or even in the sample chamber, care has to be taken to account for the modulation of the background in the ionizer. The direct background measurement is then only possible when the chopping period is shorter than the residence time of the species [84].

Vietzke and colleagues used a line-of-sight setup such that any reaction product or sputtered species is detected directly without hitting a wall [77, 85]. The experimental setup of Vietzke et al. is shown in Fig. 2. Surface-scattered species and reaction products are detected in a two-stage differentially pumped quadrupole mass spectrometer positioned perpendicular to the hydrogen-beam direction. The housing around the QMS and part of its ionizer is cooled by liquid nitrogen to reduce background signals in the QMS chamber. Background signals from the main chamber are subtracted from the measured signal by chopping the particle flux inside the reaction chamber. However, this chopping in the reaction chamber can cause a modulation of the background signal and thus hamper a correct analysis. The sensitivity of the QMS is determined by a Knudsen cell placed at the position of the target. This setup is able to detect about 10^{10} product molecules per second.

4.3 Ellipsometry

Ellipsometry is an optical method that measures the change of polarization upon reflection from a surface. It is applicable to thin transparent films on a reflecting surface. Where it is applicable, it has significant advantages over other methods. Its biggest advantage is its very high sensitivity, which allows detection of changes at the surface of less than a monolayer.

The physical quantities that can be extracted from ellipsometry measurements are the complex refractive index of a thin film and its thickness. Since ellipsometry measures only the thickness change during an experiment, the density of the material has to be known from other measurements to convert the thickness change into the number of sputtered atoms. Details of ellipsometry can be found in the textbook of *Azzam* and *Bashara* [86]. Its application to the investigation of thin carbon layers is described in [38] and [87].

Owing to its very high sensitivity, only a few monolayers of material have to be removed to get reliable results. Thus, it is orders of magnitude faster than weight loss measurements and transient changes in the sputtering yield can be followed. Moreover, ellipsometry is sensitive to changes of the optical properties of thin overlayers which may be caused by ion bombardment [38, 87–90]. This enables very detailed studies of the interaction of ions with surfaces. Among other effects ellipsometry is sensitive to surface roughness.

4.4 Optical Emission Spectroscopy

In a plasma environment, species released from the surface can be detected by optical emission spectroscopy (OES). Hydrocarbon molecules and radicals formed at the surface by chemical erosion or chemical sputtering penetrate the edge plasma after being released from the surface. By collisions with plasma electrons they may become ionized, dissociated, or excited. The released amount of carbon can be quantified from the analysis of the radiation emitted from these molecular species. However, this requires a rather detailed modelling of the hydrocarbon dissociation chain and knowledge about the excitation mechanisms of the individual species and of their possible sticking to surfaces. Many studies in very different experimental environments such as edge plasmas of tokamak devices [91–103], plasma generators (PISCES [104], PSI-1 [105]), and laboratory plasmas [106–109] have been performed.

The determination of particle fluxes from spectroscopy measurements in a plasma was thoroughly discussed by *Behringer* et al. [110] for the case of atom and ion fluxes. The analysis for molecular species is in principle very similar, but in addition to the ionization, the dissociation of the molecules has to be modelled, which adds further uncertainties. Important spectroscopic quantities that have to be determined from calibration measurements and/or theoretical models are the S/XB and D/XB ratios ("inverse photon efficiencies" for ionisation and dissociation, respectively) that link measured photon fluxes of break-up products to the corresponding particle fluxes [110, 111].

The related problems were discussed by *Brezinsek* et al. [112]. For the time being, these spectroscopic quantities which depend on the actual plasma conditions are a matter of ongoing discussion [93, 95, 104, 112, 113]. As a consequence, OES data are relatively simple to measure, but hard to quantify and relate to the initially sputtered species. In that sense, they are similar to the problems encountered in mass spectrometry. An advantage of OES is that it delivers real-time data and allows online measurements in a plasma environment such as in the boundary layers of fusion devices where particle fluxes are very high. Measurements at these high, fusion-relevant fluxes are only possible with OES.

4.5 Cavity Probes

A further method for investigating properties of released species is determining the redeposition pattern. In general, physical sputtering produces species with some kinetic energy which have a high sticking probability. As a consequence, these species can only be deposited in line of sight from their place of origin. On the other hand, chemical sputtering produces thermal species with largely varying sticking probabilities. Such species can survive many wall collisions and therefore be transported also to areas which have no direct line of sight to the sputtered surface. These two different sputtering processes lead to very different redeposition patterns [2].

The effective surface loss probability of released species can be determined by measuring the deposition pattern in a well-defined geometry, e.g., using cavity probes [114–120]. This method has recently been applied to investigate the redeposition of species produced during chemical sputtering of graphite with hydrogen ions [66]. Clearly, the determination of surface loss probabilities with cavity probes does not allow determining the species spectrum, but it is a relativly simple, qualitative method to discriminate between physical and chemical sputtering.

4.6 Dedicated Multiple Beam Experiments

Most experiments for chemical sputtering have been carried out using a single ion beam. But a number of different groups investigated chemical sputtering processes applying dedicated multiple beam setups using, e.g., an atom beam and an ion beam. A big advantage of multiple beam setups compared with single beam setups is that they can provide a much better insight into the underlying microscopic processes and phenomena.

Vietzke and coworkers investigated the simultaneous interaction of beams of atomic hydrogen and argon ions using a molecular beam mass spectrometer (MBMS) setup [47, 77, 121] which was briefly described in Sect. 4.2. It allows the independent control of atomic hydrogen flux and ion flux and an identification of the released species. Due to the MBMS configuration not

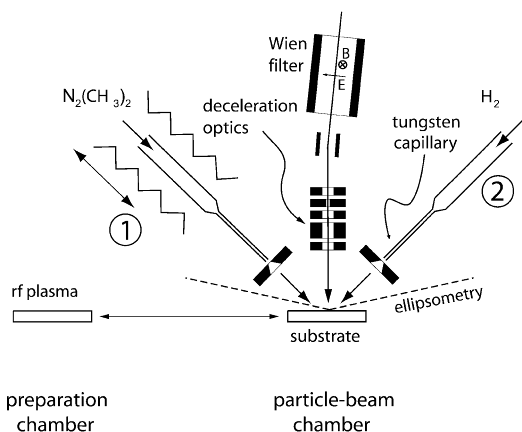

Fig. 3. Sketch of the MAJESTIX setup. The main components in the particle-beam chamber are the ion gun system, two radical beam sources, and a line of sight for the in-situ ellipsometry diagnostic. Each radical source can either be run with H_2 or D_2 to produce atomic H and D, respectively

only stable molecules, but also radical species can be measured and quantified. A later upgrade to a time-of-flight mass spectrometer [47] also enabled the determination of the energy distribution of the released species.

Dual beam experiments were also carried out at the university of Toronto. This dual beam accelerator experiment [122] comprises two independent ion beam sources and was applied to study a variety of simultaneous irradiation phenomena with two different ion beams. They studied the simultaneous irradiation of graphite with C^+ and H^+ ions [123], noble gas ions (He^+, Ne^+, Ar^+) and H^+ ions [122, 124, 125], D^+ and H^+ ions [126–128], O^+ and H^+ ions [129–133], and tungsten erosion due to low energy O^+ and D^+ impact [134]. For detection of released species they used a remote mass spectrometer.

Winters and *Coburn* studied the etching of silicon due to irradiation with fluorine and argon ions [35]. Etch products, recombination products or reflected incident species were detected by the modulated-beam line-of-sight mass spectrometric detection system. There are four stages of differential pumping between the sample and the mass spectrometer. A mechanical chopper inside the reaction chamber modulates the flux of surface-scattered species and reaction products. Sample surface conditions are periodically monitored by an Auger electron spectrometer.

A variety of particle-beam experiments were performed in the MAJESTIX device at IPP Garching [135–142]. A sketch of the experimental setup is shown in Fig. 3. MAJESTIX is an UHV-based particle-beam experiment comprising two radical beam sources and one source for low energy ions [143]. As a diagnostic tool, real-time in-situ ellipsometry is implemented. The fluxes of the radical beam sources are absolutely quantified for production of hydro-

gen atoms and methyl radicals [144, 145]. The ion source can produce a wide variety of ionic species, e.g. He^+, Ne^+, Ar^+, H^+, H_2^+, H_3^+, N_2^+, and CH_3^+. Ion energies from above 1 keV down to 1 eV are achievable. The setup allows to investigate heterogeneous surface processes of one single species or the simultaneous interaction of up to three different, individually-controllable species with a surface of interest. Running one of the radical sources to produce atomic hydrogen and the ion source with the mentioned ions, microscopic surface processes such as chemical sputtering, can be studied in great detail.

5 Chemical Erosion of Carbon by Atomic Hydrogen

5.1 Thermal Process

Chemical erosion of carbon by hydrogen is a thermally activated process which does not require energetic species. Chemical erosion of graphite due to thermal atomic hydrogen has been studied in great detail using a variety of diagnostics for the surface hydrogen content, the hybridisation of carbon atoms in the surface layer, and the emitted species [10, 16, 63–65, 74–78, 85, 146–158].

The first quantitative investigations originate from 1975 from modulated atomic-hydrogen-beam experiments by *Balooch* and *Olander* [10]. Atomic hydrogen was produced in an oven at a temperature of 2000 K and impinged onto pyrolytic graphite samples. The reaction probability was measured by determining the intensity of emitted hydrocarbons in a quadrupole mass spectrometer as a function of the surface temperature. Below about 800 K, CH_4 was the dominant reaction product, whereas C_2H_2 evolved at temperatures above 1200 K. The results were explained by a detailed atomistic model assuming an atomic hydrogen gas in thermal and chemical equilibrium with the solid surface. However, agreement with the data could only be obtained assuming that atomic hydrogen and methane molecules only partly reach equilibrium at the carbon surface, the equilibration probability decreasing strongly with increasing temperature.

Around 1995 the individual steps in the erosion process have been elucidated and quantitatively described by cross sections and activation energies [155]. The atomistic steps of the chemical reaction of thermal atomic hydrogen with a thin amorphous hydrogenated carbon layer (a–C:H) on platinum were investigated in detail for atom fluxes of about $10^{17}\,m^{-2} \cdot s^{-1}$ [151, 155, 156]. The hybridisation stages of the involved carbon atoms from graphitic sp^2 to hydrogenated sp^3 were analysed using high resolution electron energy loss spectroscopy (HREELS), while the hydrogen and hydrocarbon content of the layer were determined by thermal desorption spectroscopy (TDS). Together with isotope exchange experiments between hydrogen and deuterium, this resulted in a description of the reaction scheme

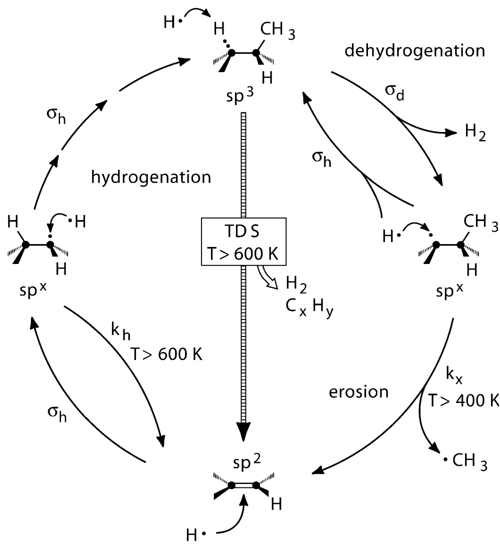

Fig. 4. Chemical erosion cycle of graphite in the interaction with thermal atomic hydrogen [155, 157]

by four individual processes shown schematically in Fig. 4 and summarised here:

Even at low temperatures sp^2 carbon atoms at the edges of graphitic planes or with broken bonds are hydrogenised to sp^3 hydrocarbon complexes via an intermediate radical stage sp^x (left-hand side of Fig. 4). The hydrogenation is not thermally activated, but proportional to a cross section σ_h for the subsequent addition of hydrogen. Further irradiation with thermal atomic hydrogen will also lead to hydrogen molecule formation and desorption with a cross section, σ_d, leaving a radical stage sp^x with a broken bond in the a–C:H network (right-side of Fig. 4). Due to the much larger value of σ_h compared with σ_d the sp^x concentration will only be about 2-4% of the sp^3 concentration.

With increasing temperature, different thermally activated processes will become possible: at temperatures around 400 K chemical erosion can occur. Hydrocarbon complexes attached to the a–C:H network in the neighbourhood of sp^x radicals (right-side of Fig. 4) can be desorbed with a rate constant k_x by simultaneously joining the neighbouring free bond to a double bond, thus returning to the basic graphitic sp^2 configuration. On a fully hydrogenated surface the last step of radical sp^x formation is rate limiting for erosion. With further increasing temperature, however, incoming hydrogen atoms may recombine with adsorbed atoms above 600 K with a rate constant k_h (left-hand side of Fig. 4), thus interrupting the hydrogenation process and, therefore,

Table 1. Model parameters for calculating the chemical erosion yield according to (6) [155]

σ_d (m^2)	σ_h (m^2)	A (s^{-1})	B (s^{-1})	E_therm (eV)	E_rel (eV)
0.05×10^{-20}	4.5×10^{-20}	1×10^{13}	1×10^{13}	1.61	1.73

reducing the sp^3 concentration and subsequent chemical erosion. Thus, the erosion rate will exhibit a maximum at intermediate temperatures. For the given experimental parameters [151, 155, 156] this maximum occurs around 600 K. If the hydrogen irradiation is stopped, already available hydrocarbon complexes can be desorbed above 600 K (indicated by the central arrow in Fig. 4).

For each hybridisation state of carbon, i.e. sp^2, sp^x and sp^3 a balance equation can be formulated in steady state. The equations can be solved for the concentration of sp^3 complexes [155, 159].

$$c^{\mathrm{sp}^3} = \frac{\sigma_\mathrm{h}\Phi + k_\mathrm{x}}{\sigma_\mathrm{h}\Phi + \left(1+\frac{\sigma_\mathrm{d}}{\sigma_\mathrm{h}^2}\frac{k_\mathrm{h}}{\Phi}\right)k_\mathrm{x}}\,, \tag{2}$$

$$k_\mathrm{x} = A\cdot\exp(-E_\mathrm{therm}/kT)\,, \tag{3}$$

$$k_\mathrm{h} = B\cdot\exp(-E_\mathrm{rel}/kT)\,. \tag{4}$$

k_x and k_h are the thermally activated rate coefficients, as described above, with the activation energies E_therm and E_rel and the pre-exponential factors A and B. All necessary model parameters, i.e., σ_h, σ_d, k_x, k_h, A, and B were quantitatively determined from experiments [151, 155, 156].

In contrast to earlier assumptions made by *Erents* et al. [8] and *Busharov* et al. [9] the erosion yield related to an incident atomic hydrogen flux Φ is not dependent on the hydrogen concentration but on the concentration of hydrogenated sp^x centres. In steady state the erosion rate is given by the product of c^{sp^x} with k_x and n_0, n_0 being the total number density of carbon surface sites per unit area (for graphite, $n_0 = 2.3\times10^{19}\ \mathrm{m}^{-2}$). c^{sp^x} is given by

$$c^{\mathrm{sp}^x} = c^{\mathrm{sp}^3}\frac{\sigma_\mathrm{d}\Phi}{\sigma_\mathrm{h}\Phi + k_\mathrm{x}}\,. \tag{5}$$

The corresponding erosion yield Y_therm is given by the erosion rate divided by the flux

$$Y_\mathrm{therm} = \frac{n_0\,c^{sp^x}k_\mathrm{x}}{\Phi} = \frac{n_0\,c^{\mathrm{sp}^3}k_\mathrm{x}}{\Phi}\frac{\sigma_\mathrm{d}\Phi}{\sigma_\mathrm{h}\Phi + k_\mathrm{x}} = \frac{n_0\,\sigma_\mathrm{d}k_\mathrm{x}}{\sigma_\mathrm{h}\Phi + \left(1+\frac{\sigma_\mathrm{d}}{\sigma_\mathrm{h}^2}\frac{k_\mathrm{h}}{\Phi}\right)k_\mathrm{x}}\,. \tag{6}$$

The model parameters are given in Table 1. The resulting erosion yield is shown in Fig. 5 as a function of temperature, together with the erosion data

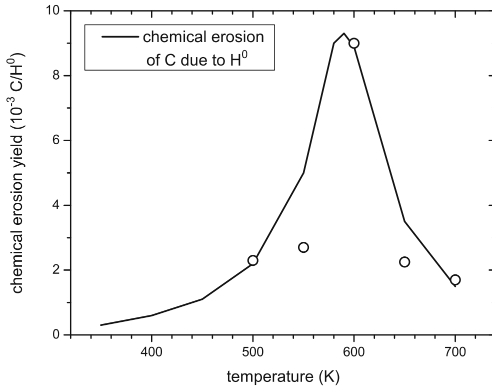

Fig. 5. Model results for chemical erosion of amorphous hydrocarbon layers due to interaction with thermal atomic hydrogen (atom flux about $10^{17}\,\mathrm{m}^{-2}\cdot\mathrm{s}^{-1}$) [155]. The *circles* show experimental data from *Horn* et al. [155]

for thermal atomic hydrogen [155]. At room temperature chemical erosion is negligible, and above 600 K the erosion decreases due to the recombinative release of hydrogen molecules. The maximum yield at 600 K is about 9×10^{-3} C atoms per H atom.

The reaction of atomic hydrogen with different grades of graphite [160] was also investigated. It was found that the scatter of the data between different samples of the same grade of up to a factor of 2 is of similar magnitude as the scatter between different graphites. From this fact, they concluded that there is no significant influence of the type of graphite on the reaction of atomic hydrogen. On the other hand, experiments by *Vietzke* et al. have shown that the reactivity of graphite towards atomic hydrogen is greatly enhanced – by more than one order of magnitude – if the surface is irradiated by energetic ions prior to the experiment [77, 79]. It was concluded that the chemical attack of hydrogen on graphite requires active surface sites (dangling bonds) which are in this experiment produced by the preceding ion bombardment. This is in accordance with the conclusions made by *Küppers* and coworkers [157] who have shown that undisturbed graphitic planes are essentially unreactive towards atomic hydrogen. Hydrogen can react only with the edges of graphitic planes. Ion bombardment of well-ordered graphitic regions produces plenty of additional reaction centres. This causes a significant increase of the reaction yield. The deposition of impurities (e.g., nickel [160]) significantly reduces the reactivity at the surface.

5.2 Species Released by Chemical Erosion

According to the reaction scheme elaborated by *Küppers* and coworkers, the primary erosion product of the thermally driven chemical erosion process is CH_3 [157]. This was indeed measured by *Vietzke* and coworkers [85] who have

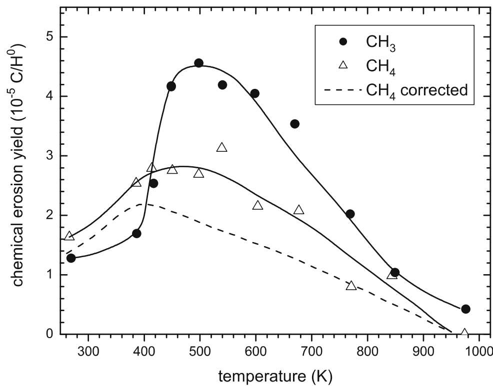

Fig. 6. Temperature dependence of the production yield of CH_3 and CH_4 for chemical erosion of graphite with thermal atomic hydrogen ($1.6 \times 10^{20}\,m^{-2} \cdot s^{-1}$) [85]. The *dashed line* (CH_4 corrected) is obtained by correcting the measured CH_4 signal with the CH_4 signal originating from recombination of CH_3 at the chamber walls

shown that in the reaction of atomic hydrogen with graphite CH_3 dominates over CH_4 (Fig. 6). The maximum yield in their experiments was found to be around 500 K. No significant influence of the type of graphite on the reaction of atomic hydrogen with graphite has been found [77, 160]. The reaction probability is below 10^{-4}, i.e., it is much lower than the yield determined by *Horn* et al. [155] (see Fig. 5). Horn et al. investigated carbon layers with a thickness of only a few monolayers deposited on a Pt substrate. For this model system all carbon atoms can be assumed to be available for hydrogen attachment and the model agrees reasonably well with the experimental data without a free fit parameter. For the application to chemical erosion of graphitic materials the only available sites for hydrogen bonding and chemical erosion are edge atoms of graphitic planes or damage sites due to ion bombardment [157]. To account for that, an additional scaling parameter C was introduced which defines the height of the peak maximum [80]. A comparison of Figs. 5 and 6 suggests that this scaling parameter has to be of the order of 10^{-2} for chemical erosion of graphite. A further improvement of (6) first suggested by *Horn* et al. [155] and later introduced by *Roth* [80] was: instead of using a fixed value for the activation energy E_{therm} for CH_3 release, a Gaussian distribution of activation energies with a standard deviation of 0.3 eV was used. This broadens the chemical erosion peak and leads to a better agreement with experimental data.

In addition to CH_3 and CH_4 formation, C_2H_y species were also detected [77]. Quantitative studies by *Davis* et al. [161], who used a remote mass spectrometer to measure stable species, have shown that the chemical erosion by thermal hydrogen atoms is clearly dominated by C_2 and C_3 hydrocarbons. The production of CH_4 accounts for only 5–10 % of the the total erosion yield.

In addition to graphite, the erosion of amorphous hydrogenated carbon (a–C:H) films by thermal atomic hydrogen was investigated by *Vietzke* et al. [78, 148, 162]. a–C:H layers are a model system for a graphite surface being irradiated by hydrogen ions (this point will be discussed in more detail in Sect. 6.1). The main reaction product is the radical CH_3. It is accompanied by a wide variety of other hydrocarbons including other radicals. CH_3, C_2H_y, and C_3H_y species are formed with a relative proportion of 1:0.8:0.5. The temperature maxima for the different products occur at different temperatures. The maximum for CH_3 production is at 750 K, that for C_2H_y at 650 K, and that for C_3H_y at 520 K. The total chemical erosion yield as well as the product spectrum depend strongly on the a–C:H structure. The yield is much higher than for graphite. The total chemical erosion yield at 520 K for hard a–C:H films is about 0.014 and for soft, polymer-like films it increases to 0.05 and even to 0.16 depending on the actual film structure. In contrast, the yield for graphite is of the order of 10^{-4}. The reaction of deuterium with hard a–C:H films leads predominantly to fully deuterated hydrocarbon species. The hydrogen from the layers is released as HD. This means that the isotope exchange with the layer is much faster than the chemical erosion process. This finding is again in excellent agreement with the reaction scheme proposed by *Küppers* et al. which was discussed in Sect. 5.1.

The product distribution of chemical erosion of thin, hard a–C:H layers was studied in detail by *Zecho* et al. [74, 75]. If a thin a–C:H film is exposed to a flux of atomic hydrogen (a flux of about 10^{20} H $m^{-2} \cdot s^{-1}$ was used in these experiments), C_1 and C_2 hydrocarbons are the main products, but contributions of higher hydrocarbons (C_3 to C_8) were detected as minority species. C_1 and C_2 hydrocarbons exhibit an erosion maximum around 750 K, while C_3 to C_5 hydrocarbons show a maximum around 650 K. The quantitative analysis of the data demonstrates that the hydrogen-induced chemical erosion of a–C:H films is dominated by formation of C_2 hydrocarbons (see Fig. 7). About 50% of the eroded carbon atoms appear in this channel. The maximum erosion yield at around 750 K is 0.1 C/H. The product distribution found by Zecho et al. is in good agreement with the earlier work of *Davis* et al. [161] who investigated graphite instead of a–C:H layers. But the absolute yields are, as earlier found by *Vietzke* et al. [78, 148, 162], much higher for a–C:H compared with graphite. Although the yield of Zecho et al. is in accordance with that of Vietzke et al., the product distributions differ somewhat. This can be attributed to a difference in the structure of the a–C:H layers investigated by both groups. It was shown by *Vietzke* et al. [78, 148, 162] that the film structure has a great influence on the total yield, so it can be assumed that it also influences the product distribution.

Zecho et al. [75] also investigated the influence of thermally induced structural changes of a–C:H films on the chemical erosion. Annealing of the films at 1100 K leads to a partial regraphitization, but hydrogen atoms rapidly rehydrogenate the surface even at temperatures of up to 800 K. Consequently, this annealing does not change the erosion yield; however, it influences the

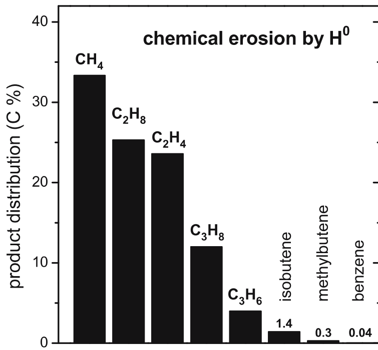

Fig. 7. Product distribution of the H-atom-induced chemical erosion of a thin, hard amorphous hydrocarbon layer (16 nm thick) from a temperature programmed erosion experiment in the temperature range 300 to 1000 K (heating rate 0.5 K/s) [74]. Shown is the fraction of the total number of carbon atoms eroded via the respective channel [74]

product distribution and the temperature dependence. The erosion of annealed a–C:H films is dominated by formation of C_2 hydrocarbons followed by C_1 and C_3 species; C_4 and C_5 occur as minority species.

6 Chemical Sputtering

As defined in Sect. 3 we subsume under the phrase chemical sputtering all processes where the erosion process depends on both the kinetic energy and the chemical reactivity of the impinging species. In experiments this can appear in two different cases: i) bombardment with reactive ions (e.g., H^+) where the ion carries the kinetic energy and is chemically reactive and ii) combined bombardment by noble gas ions and reactive thermal species where the energy is supplied by the noble gas ion and the chemically active species has only thermal energy. These two different cases are discussed in the two following subsections. In addition, more complicated cases are possible if instead of noble gas ions reactive ions are used (e.g., H_2^+ and atomic H). In chemical sputtering experiments all three basic erosion mechanisms – chemical erosion, physical sputtering, and chemical sputtering – may be active. To what extent they influence the measured effects depends on the experimental parameters, particularly on the energy of the ions and the temperature of the sample.

An early review of chemical sputtering in general was compiled by *Roth* in a chapter in a preceding volume of this series [36]. Over the years, several review articles summarized the status of knowledge of the interaction of hydrogen atoms and ions with carbon surfaces. *Auciello* et al. reviewed the synergism in materials erosion due to multispecies impact in 1985 [163]. The erosion of graphite due to particle impact was reviewed by *Roth, Vietzke*, and

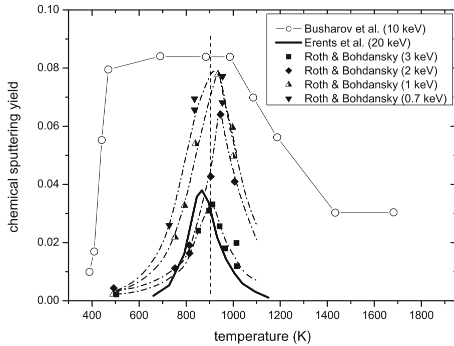

Fig. 8. Compilation of the early results from 1976 by *Roth* et al. [7], *Erents* et al. [8, 165], and *Busharov* et al. [9] showing the temperature dependence of chemical sputtering of graphite due to bombardment with hydrogen ions at different energies. Note that the value and position of the maximum depend on ion flux and energy

Haasz in 1991 [164] and later on by *Vietzke* and *Haasz* in 1996 [16]. In that period most of the experiments in this field were motivated by thermonuclear fusion research. The fuel for a fusion plasma are hydrogen isotopes and large areas of the plasma-facing components are made of carbon materials so that the interaction of energetic and atomic hydrogen species with carbon surfaces is a very important plasma-surface-interaction process. The majority of these experiments was carried out using beams of hydrogen ions at energies between several ten eV up to some keV.

6.1 Chemical Sputtering with Reactive Ions

The chemical sputtering of graphite by hydrogen ions is a complex process depending on surface temperature, ion flux, surface state of the material, and energy of the incident particles. Although these various experimental parameters show strong interdependences, we discuss them in the following separate subsections.

6.1.1 Temperature Dependence

Initially discovered by *Günterschulze* [2] in 1926, chemical sputtering of carbon due to bombardment by hydrogen ions found renewed interest in 1976. The first systematic investigations of chemical sputtering were carried out simultaneously by several groups (*Roth* et al. [7], *Erents* et al. [8, 165], and *Busharov* et al. [9]). All of these early experiments studied the temperature dependence of the CH_4 production rate during bombardment of different carbon grades with hydrogen ions using a remote mass spectrometer. Ion energies in the range from 100 eV up to 30 keV were used.

The results are summarized in Fig. 8. The common observation of all these experiments is that the CH_4 production yield increases with increasing target temperature, reaches a maximum in the range of about 900 K, and decreases for further increasing temperature. In this view, already the first experiments proved two mandatory requirements for a chemical sputtering process: i) the erosion process produces molecules comprising target and projectile atoms and ii) the process shows a pronounced temperature dependence. Soon thereafter, *Yamada* et al. 1980 [166] published similar results with a maximum yield at $T_{\max} = 800\,\mathrm{K}$. We will see later that this temperature value depends on the ion flux. Following investigations corroborated these early findings and extended the experimental data base [76, 79, 85, 148, 167–169]. This early work has been reviewed by *Roth* et al. [164] in 1991 and by *Vietzke* and *Haasz* [16] in 1996.

The occurrence of a maximum yield for chemical sputtering with energetic hydrogen ions at the temperature $T_{\max}$ was assumed to result from the competition of an exponential increase of the reaction rate between carbon and hydrogen with an even stronger decrease of the hydrogen concentration in the surface at temperatures exceeding 800 K. At lower temperatures the lattice concentration of hydrogen saturates and the reaction rate increases with increasing temperature, while at higher temperatures the recombinative hydrogen release decreases the hydrogen content so that the reaction rate decreases [8, 9].

Details of the temperature dependence and the value of the maximum erosion yield depend on ion flux and energy as will be discussed in the following subsections.

6.1.2 Energy Dependence

Already the first published results about chemical sputtering of carbon by hydrogen isotopes as presented in Fig. 8 [7, 8] have shown that the maximum chemical sputtering yield depends strongly on the ion energy. In the following years, different aspects of the energy dependence were studied in great detail [44, 81, 159, 166, 169–180]. However, in the initial publications, only the methane production yield was determined and it was implicitly assumed that this is equivalent to the total chemical sputtering yield. This assumption is, however, not valid, as will be further discussed in Sect. 6.1.5.

Over the years, the energy and temperature dependence of the methane production yield due to high energy ($> 300\,\mathrm{eV}$) hydrogen ion bombardment of graphite have been investigated by several groups producing relatively consistent results [7–9, 44, 148, 160, 165, 166, 170, 173]. A typical set of methane production yields as a function of temperature for different ion energies is shown in Fig. 9 [170]. In this experiment pyrolytic graphite samples were bombarded with H_3^+ ions of different energies. The methane production was measured by residual gas analysis using a remote mass spectrometer. Between ion energies of 300 and 3000 eV (per H^+, i.e., 900 to 9000 eV per H_3^+ ion)

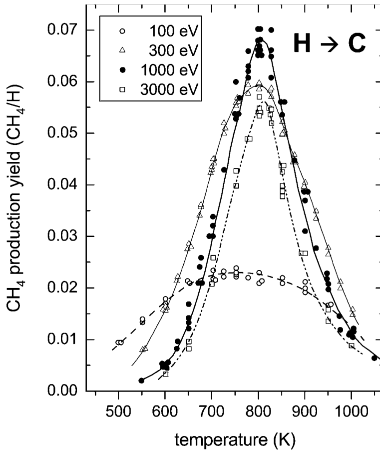

Fig. 9. Methane production yield as a function of substrate temperature for hydrogen ions with different energies impinging on pyrolytic graphite [170]. H_3^+ ions with three times the indicated energy have been used in this experiment. The ion flux density was $\approx 1 \times 10^{20}\,\mathrm{m}^{-2} \cdot \mathrm{s}^{-1}$ and beam at normal incidence. The production yield is, as in all comparable following figures, normalized to the number of hydrogen atoms in the used molecular ion

methane production peaks at a temperature of 800 K ($T_{\max} = 800$ K). At lower ion energy (100 eV/H^+) the peak broadens and the maximum shifts to slightly lower temperatures such that below about 600 K the methane production yield is even higher than for bombardment with high energy ions. The energy dependence of the data from Fig. 9 is presented in Fig. 10. The maximum yield peaks at about 600 eV per H^+ with a value of about 0.085 CH_4/H (flux $= 2 \times 10^{18}\,\mathrm{m}^{-2} \cdot \mathrm{s}^{-1}$) [170]. We note that the yield shows a slight flux dependence (Sect. 6.1.4).

Yamada et al. measured the methane production yields of various types of carbon in the energy range from 100 to 6000 eV [166]. The curves have a distinct maximum around 1 keV (see Fig. 11). For higher energies the yield decreases. This general behaviour is the same for all investigated temperatures ranging from 620 to 870 K. They found the highest yield of about 0.07 methane molecules per impinging H^+ ion for an energy of 1 keV ($T_{\max} =$ 800 K). *Roth* et al. have shown in total weight loss measurements that the maximum of the energy dependence shifts to lower energy with decreasing temperature. The maximum measured at 300 K is at about 300 eV [44], while measurements at $T_{\max}$ result in an energy of maximum yield of about 1 keV in agreement with *Yamada* et al. [166]. Because the shape of the energy dependence was found to be strikingly similar to physical sputtering, the influence of similar knock-on effects was assumed to be responsible. *Mech* et al. [175, 176] extended the energy range down to 10 eV and indeed found a

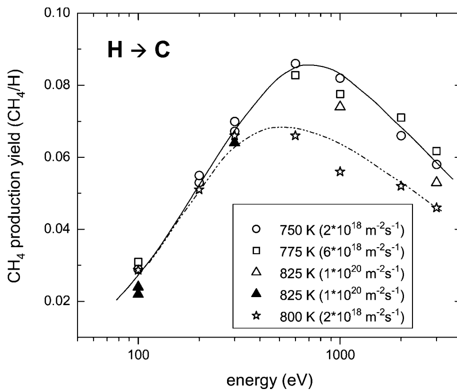

Fig. 10. Methane production yield as a function of ion energy for hydrogen ions impinging on pyrolytic graphite [170]. The *solid line* shows the yields determined from data similar to those presented in Fig. 9 at the individual temperature maximum for each energy value. The *dashed line* shows the corresponding yield determined for a fixed temperature of 800 K. Different symbols correspond to different applied ion fluxes. The experimental parameters (target temperature and ion flux) are given in the legend

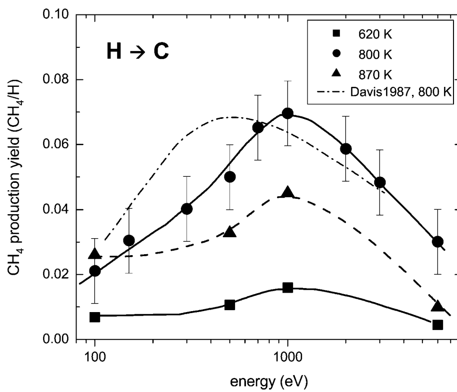

Fig. 11. Methane production yield as a function of ion energy for hydrogen ions impinging on pyrolytic graphite measured at different sample temperatures [166]. The ion flux density was $\approx (3 \text{ to } 12) \times 10^{18}\,\text{m}^{-2} \cdot \text{s}^{-1}$ and beam at normal incidence. For comparison, the data from Fig. 10 (measured at 800 K and $2 \times 10^{18}\,\text{m}^{-2} \cdot \text{s}^{-1}$) are also shown

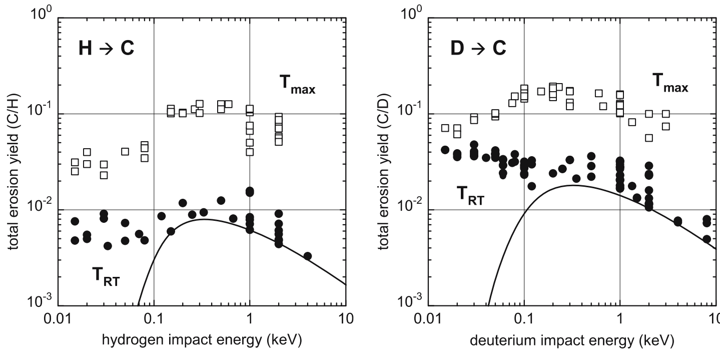

Fig. 12. Energy dependence of the erosion yield of a variety of different carbon materials due to bombardment with H^+ and D^+ ions at room temperature and at $T_{\max}$ for the respective energy ($T_{\max} = 570 - 920\,\mathrm{K}$) [81]. The *solid line* shows the result of the "Eckstein–Preuss fit formula" which describes physical sputtering (see also Fig. 8 in Chap. by *Eckstein*)

decrease of the maximum chemical sputtering yield indicating a threshold at energies around a few eV.

Experimental results for the sputtering of carbon by hydrogen and deuterium ions determined by weight loss measurements are shown in Fig. 12 for sample temperatures of 300 K and $T_{\max}$. The solid line in Fig. 12 shows the result of the "Eckstein–Preuss fit formula" (see Chap. by Eckstein) which is based on TRIM.SP calculations and provides a good quantitative description of physical sputtering. At sample temperatures of 300 K and ion energies exceeding $\sim$ 200 eV the observed rates are in reasonable agreement with the theoretical data (Fig. 12) and can thus to a large extent be explained by physical sputtering. However, the experimental values in this range are consistently higher than the results of the analytic description. *Küstner* et al. [181] have shown that this difference is partially due to the roughness of the real graphite surface. On the other hand, chemical sputtering may still contribute to the total erosion in this energy range, so it is not surprising that the measured data lie above the theoretical data for pure physical sputtering.

At energies below 100 eV the measured yields do not decrease as anticipated for physical sputtering when approaching the threshold energy, but they remain constant [81, 159]. It was even found that the yield remains constant down to temperatures of about 100 K [18, 182]. A prominent isotope effect is observed with yields for deuterium being higher by a factor of 5 to 7. For higher energies ($>$ 100 eV) the isotope effect is only a factor of 2 to 3. The energy dependence at $T_{\max}$ shows higher yields than at 300 K, the increase being more pronounced at energies above 100 eV. In this energy range increased damage formation enhances the chemical reactivity throughout the implantation range.

6.1.3 Dependence on the Type of Graphite

Chemical sputtering of carbon by hydrogen ions shows a significant dependence of the initial sputtering yield on the type or grade of graphite used for the experiment [166]. With increasing ion fluence strong transient effects occur, but the energy and temperature dependences of the steady-state yields are not affected by the structure of the different types of carbon. This was attributed to the amorphisation of the sample surface due to the ion bombardment. The dependence of the yield on structural properties is particularly high at very low energy or for reaction with atomic hydrogen [183], where no amorphisation occurs. In general, steady-state yields were obtained after the target was bombarded with proton fluences of more than 1×10^{22} H^+ m^{-1} [160, 166, 169]. The methane production yield for amorphous hydrogenated carbon (a–C:H) layers is, in general, significantly higher than for graphite [78, 148, 162, 168].

The fact that the steady-state yields of chemical sputtering of graphite due to hydrogen ion bombardment are relatively insensitive to the type of graphite is explained by the following: If graphite is bombarded with energetic hydrogen isotopes (ions), the unreflected fraction of the isotopes is implanted into the graphite and initially retained to 100 % [76, 184–193]. Concomitantly, radiation damage is produced within this range. With increasing ion fluence, the local concentration of hydrogen increases and an increasing fraction of the implanted hydrogen is reemitted. The saturation concentration of hydrogen in carbon at 300 K is about 30 % (H/C $\approx$ 0.4) ([167, 186, 187, 189]) and it decreases with increasing temperature. When the local concentration exceeds the saturation limit, 100 % of the locally implanted hydrogen are reemitted [194] mainly in form of H_2 molecules [190, 192, 193], but also in form of hydrocarbons [85, 125–127, 195]. These hydrogen and hydrocarbon molecules are formed at the end of the ion range [85, 125–127, 190, 192, 195]. With further increasing fluence, the saturated region increases until it reaches the surface. Then steady state is reached and the whole implantation range is saturated with hydrogen. Any further implanted hydrogen ion is reemitted. The fluence required to reach this saturation is naturally dependent on the ion energy and substrate temperature. For typical energies used for the investigation of chemical sputtering, i.e., in the low keV range, this saturation fluence at room temperature is in the 10^{21} m^{-2} to 10^{22} m^{-2} range [76, 166]. After such a fluence, an altered amorphous layer with a significant hydrogen content has developed at the graphite surface [196–198]. The material that is formed at the surface is comparable to "hard" a–C:H layers produced by plasma deposition from methane low-pressure gas discharges as, e.g., in laboratory studies [38, 199] or during carbonisation of fusion devices [6, 200]. While considerable variation exists in the structural characteristics of these films, mostly depending on ion energies and impinging species fluxes during deposition [38], the hydrogen content of "hard" a–C:H layers is similar to that of hydrogen implanted graphite, i.e., H/C $\approx$ 0.4 at 300 K. Within this

altered surface layer the different properties of different types of graphite have disappeared.

6.1.4 Flux Dependence

The position of the temperature maximum of the chemical sputtering yield increases with increasing ion flux [44, 159]. At fluxes above $10^{21} m^{-2} \cdot s^{-1}$ as reached in plasma-wall interaction in nuclear fusion experiments, the temperature maximum, T_{max}, reaches values of about 1000 K. At these elevated temperatures, the thermodynamic equilibrium of the H/C system shifts from CH_4 formation to H_2 release [201] and the erosion yield is expected to decrease with ion flux. Additionally, the onset of graphitisation will lead to the annealing of radiation damage resulting in the suppression of reactivity of the carbon material. The coupling of the flux dependence with the temperature dependence leads to conditions where emission of hydrogen molecules prevents the chemical erosion. This has lead to the prediction that at such high fluxes the yield at T_{max} decreases.

Efforts to determine a flux dependence in ion beam experiments [170, 202] in the flux range of 10^{19}–10^{20} D^+ $m^{-2} \cdot s^{-1}$ did not yield conclusive results within the scatter of the data. Actually, measuring the erosion yield at fixed temperature, rather than at T_{max}, resulted in slowly increasing yields at low fluxes and decreasing yields at higher fluxes, as T_{max} passed across the temperature of the measurements [170]. The first indication for a decrease of the yield at high ion fluxes came from measurements on hydrocarbon production at the limiter in the DITE tokamak [203] where hardly any CH A-X band intensity, indicative for methane production, could be detected spectroscopically above the background. Later, the use of plasma simulators and edge plasmas in tokamaks has widely increased the data basis and measured chemical erosion yield data are available from the plasma simulators PSI-1 in Berlin [105, 204], PISCES B in San Diego [104], and from plasma edge and divertor measurements in fusion facilities, such as JET [93], Tore Supra [205, 206], TEXTOR [207], ASDEX Upgrade [102, 208], and JT-60 U [209]. However, until 1998 [80] the flux dependence at high fluxes could not be clarified within the scatter of the available data due to the differing conditions of ion energy and surface temperature.

In 2004, an attempt was made to normalise all data to the same conditions, such as particle energy and surface temperature [210]. From ion beams and plasma simulators most of the data were obtained at 30 eV, and all data from tokamaks were subsequently normalised to these conditions using the known dependences on ion energy and substrate temperature.

After this re-evaluation and normalisation of the data, a consistent set of high flux data for methane production at T_{max} is available (see Fig. 13). The data are for deuterium ions, normalised to an incident ion energy of 30 eV and taken at or near T_{max}. While individual data sets in a narrow range of fluxes cannot distinguish clearly flux dependences, the ensemble of data

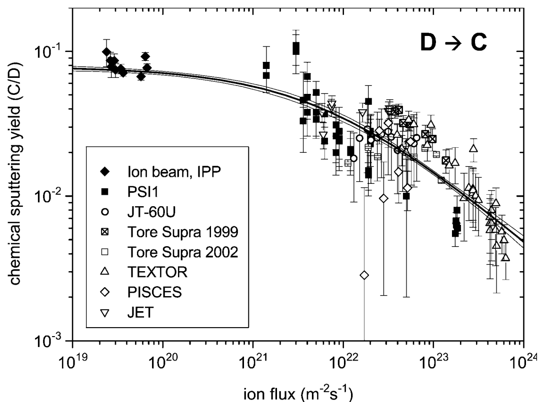

Fig. 13. Flux dependence of the chemical sputtering yield for deuterium at $T_{\max}$ and an ion energy of 30 eV determined from ion beam experiments and spectroscopic measurements in different fusion devices and plasma simulators [210]. The *solid lines* are a fit using Bayesian probability theory and its confidence intervals [212]. The experimental data are from the following sources: ion beam experiments (IPP) [81], linear plasma devices PSI-1 [105, 204] and PISCES B [104], plasma edge and divertor measurements in the fusion experiments JET [93], Tore Supra [205, 206], TEXTOR [207], and JT-60 U [209]

points suggests a decrease of the erosion yield with ion flux starting at fluxes of about $10^{21}\,\mathrm{m}^{-2}\cdot\mathrm{s}^{-1}$. The model for the functional dependence was

$$Y(E,T,\Phi) = Y_{\mathrm{low}}(E,T)/(1+(\Phi/\Phi_0)^z) \tag{7}$$

where $Y_{\mathrm{low}}(E,T) = 0.08$ is given by low flux data from ion beams, Φ_0 is the flux where the transition to a flux dependence occurs, and z is the power of the decrease at high fluxes. Bayesian probability theory was employed to determine the free parameters of the model function [211]. The resulting fit indicates a decrease of the yield at high fluxes with $z = 0.54$ and $\Phi_0 = 6\times10^{21}\,\mathrm{m}^{-2}\cdot\mathrm{s}^{-1}$ [212]. The thin solid lines in the figure give the confidence interval of the resulting fit, predicting a yield of $(5\pm0.5)\times10^{-3}$ at a flux of $10^{24}\ \mathrm{m}^{-2}\cdot\mathrm{s}^{-1}$, in contrast to previous conservative estimates of 3×10^{-2} [80].

The flux dependence, as given in (7) for the erosion yield at $T_{\max}$ seems also to apply at room temperature as obtained from data measured in the fusion experiment ASDEX Upgrade [102]. Therefore, it can be assumed that at all temperatures the same flux dependence occurs.

6.1.5 Identification of Species Released by Chemical Sputtering

While the first investigations of chemical sputtering concentrated on the detection of CH_4 molecules, later work also included measurement of higher hydrocarbons (C_xH_y, $x \geq 2$) [161, 169, 172, 175, 176, 183, 213].

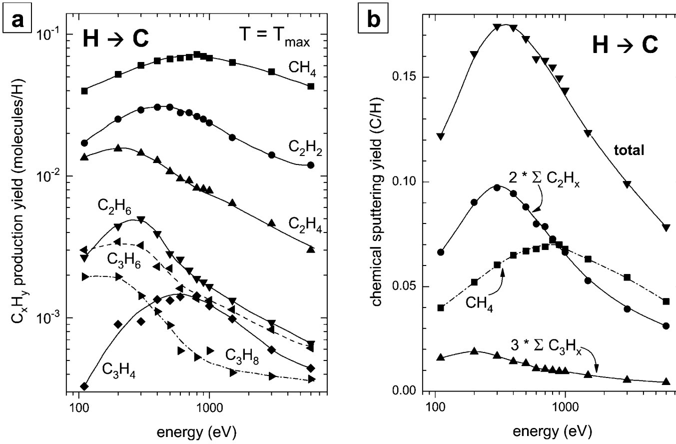

Fig. 14. **a** Production yields for C_1, C_2, and C_3 hydrocarbons as a function of ion energy measured at the individual, energy-dependent maximum temperature $T_{\max}$ [172]. (**b**) chemical sputtering yields, calculated from the data in (a) by multiplying the production yields with the number of carbon atoms in the corresponding hydrocarbon species. The contributions of C_1, C_2, and C_3 hydrocarbons are shown separately together with the total yield calculated from the sum of these three components

Investigating the contributions of higher hydrocarbon species (C_xH_y, $x \geq 2$) to the chemical sputtering of graphite [172, 213] an unexpected finding was made: The product spectrum changes dramatically with ion energy. In addition, the temperature maxima for different species behave differently for different ion energies, so that a sound determination of the total sputtering yield by mass spectrometric methods becomes a rather laborious task. Bombarding a graphite surface with hydrogen ions between 0.1 and 6 keV the maximum of the CH_4 production was found around 750 K. The corresponding maxima for C_2 and C_3 species are shifted to somewhat lower temperatures. The shifts are larger for higher hydrocarbons and for lower energies. For example, the peak for C_3H_6 at 400 eV ion energy is at about 650 K.

The hydrocarbon production yields as a function of ion energy are displayed in Fig. 14. For energies higher than about 1 keV the chemical sputtering yield is still dominated by CH_4 production. However, at energies below about 1 keV the contribution of C_2 species to the total erosion yield dominates. The contribution of C_3 species remains small in the whole energy range, although the relative contribution increases strongly with decreasing energy. Figure 14b clearly demonstrates that the maximum of the total carbon erosion yield at about 350 eV differs significantly from the maximum of CH_4 production at about 800 eV.

Experiments by *Davis* et al. [161, 169] yielded very similar results with the exception of the contributions of C_2 hydrocarbons (Fig. 15). The C_2 pro-

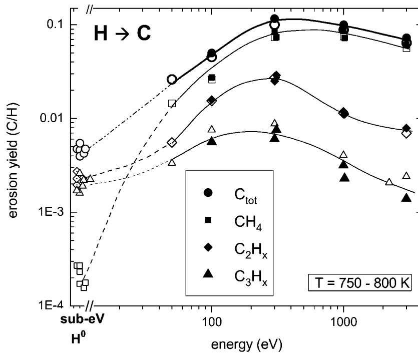

Fig. 15. Production yields for C_1, C_2, and C_3 hydrocarbons as a function of ion energy measured at T = 750 to 800 K [169]. In addition to ion beam data also erosion yields for thermal H^0 (sub-eV H^0) are shown. *Lines* are only a guide to the eye. *Open* and *closed symbols* belong to different experimental campaigns

duction yields of *Davis* et al. are in general a factor of 3-4 lower than those of *Yamada* [172] (Fig. 14). The reason for this discrepancy was attributed to a fluence dependence of C_2 hydrocarbon formation [214], but remains unresolved quantitatively. As a consequence, the total chemical sputtering yield is in the experiments by *Davis* et al. in the whole investigated energy range (50 to 3000 eV) dominated by CH_4 production. The relative contribution of C_2 and C_3 species increases, as in Yamada's experiments, with decreasing ion energy, but remains below 50 % in all cases. An extrapolation of ion beam results to thermal energies [169] suggests that the contribution of C_2 and C_3 species should dominate at energies below about 30 eV (Fig. 15). In later experiments at very low energies it was indeed found to dominate at energies below about 50 eV [175, 176] (Fig. 16).

Due to the fact that the hydrocarbon product spectrum changes as a function of ion energy and substrate temperature, the total chemical sputtering yield shows a different behaviour than the methane production yield (see Figs. 14 to 16). This can even lead to the fact that the methane production stays constant or increases at low ion energies while the total chemical sputtering yield, which is dominated by heavier hydrocarbons, decreases [18, 19, 182].

One point that has to be addressed here is a critical comparison of mass spectrometry and weight loss measurements. There has always been a significant difference between chemical sputtering yields determined by mass spectrometry and those determined by weight loss measurements. For the first investigations, this was due to the fact that only methane production yields have been measured by mass spectrometry. The discussion in this section has clearly shown that methane is not the only hydrocarbon species produced. In a certain parameter range, the chemical sputtering yield may be dominated by methane production, but in many cases the yield is domi-

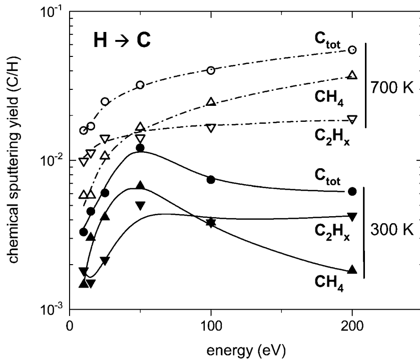

Fig. 16. Energy dependence and product distribution of chemical sputtering of graphite due to bombardment with hydrogen ions measured at T = 350 and 700 K [176]

nated by the sum of the contributions of higher hydrocarbons (see Figs. 7, 14, 15, and 16). The consideration of the contributions of C_1, C_2, and C_3 hydrocarbon has significantly reduced the difference between the yields measured by mass spectrometry and weight loss, but still a systematic difference remains. It has been shown that this is not due to experimental uncertainties if comparing results from different experiments, but this difference occurs also for measurements in the same experiment [80, 81]. The reason is, that some of the species released by chemical sputtering are highly reactive and stick to the chamber walls [66, 81]. As a consequence, total chemical sputtering yields and correct particle flux distributions for the interaction of hydrogen with carbon surfaces can only be measured by molecular-beam mass spectrometry (see Sect. 4.2). A remote mass spectrometer or a simple line-of-sight setup is not sufficient for that purpose. What can be reliably measured by mass spectrometry are production yields of stable molecules which are not lost or transformed at the chamber walls.

6.2 Combined Irradiation with Noble Gas Ions and Hydrogen Atoms

Chemical sputtering has also been investigated with two independent particle beams, namely thermal hydrogen atoms and argon ions [77, 85]. The fundamental advantage of this approach is that the chemical and physical interactions of the species with the surface can be controlled independently. In these experiments, a graphite target was exposed to a flux of thermal hydrogen atoms ($1.6 \times 10^{20}\,\mathrm{m^{-2} \cdot s^{-1}}$). An additional simultaneous flux of 5 keV argon ions ($1.1 \times 10^{17}\,\mathrm{m^{-2} \cdot s^{-1}}$) caused a synergistic enhancement of the hydrocarbon production yield from about 6×10^{-5} C/H^0, measured for atomic hydrogen irradiation alone (Fig. 6), to about 6×10^{-3} C/H^0 (Fig. 17). The enhancement factor depends on the type of ion, the ion energy, and the

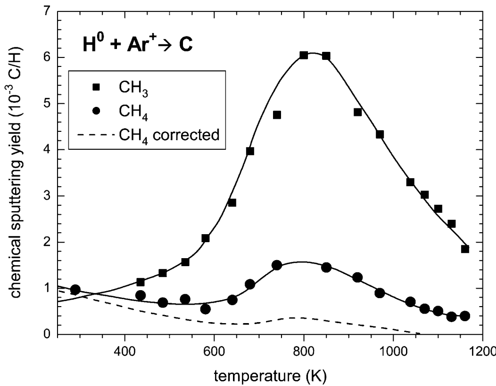

Fig. 17. Temperature dependence of the production yield of CH_3 and CH_4 for chemical sputtering of graphite due to combined irradiation with thermal atomic hydrogen ($1.6 \times 10^{20}\,\mathrm{m^{-2} \cdot s^{-1}}$) and argon ions ($1.1 \times 10^{17}\,\mathrm{m^{-2} \cdot s^{-1}}$, 5 keV) [85]. The *dashed line* (CH_4 corrected) is obtained by correcting the measured CH_4 signal with the CH_4 signal originating from recombination of CH_3 at the chamber walls

H-atom-to-ion flux ratio. The temperature dependence is very similar to the case of bombardment with hydrogen ions only and shows a maximum of the yield at 800 K. On the other hand, no enhancement was found when using molecular hydrogen instead of atomic hydrogen. Obviously, a new mechanism was active that requires the simultaneous interaction of energetic ions and atomic hydrogen. This mechanism is chemical sputtering as defined in Sect. 3. It is important to mention that *Vietzke* et al. determined the sputtering yield by mass spectrometry using an MBMS setup (see Sect. 4.2). Therefore, they were also able to detect radical species. They found that CH_3 is the dominantly released species under these experimental conditions, but CH_4 and higher hydrocarbons are also produced [77, 85].

An important finding of this seminal work by *Vietzke* et al. was that their results were not in agreement with the earlier model by *Erents* et al. [8]. As a consequence, this model had to be discarded. *Vietzke* et al. concluded that the collisional energy transfer from the energetic ions to the carbon lattice must be responsible for the drastic enhancement of the yield. A substantial contribution of electronic excitation was excluded due to the results of co-bombardment of graphite with energetic electrons and atomic hydrogen, which did not show a significant enhancement of the sputtering yield [63, 64, 77]. The basic explanation for the strong synergistic effect is a competition between annealing of defects which are produced by the ions and reaction of atomic hydrogen with these defects. Later *Vietzke* and coworkers also investigated chemical erosion due to exposure to thermal atomic hydrogen of carbon pre-irradiated by different ion species [79]. They found that the erosion yield exceeds that of atomic hydrogen alone by more than one order of magnitude and that the amount of hydrogen bonded in the surface

is less important than the damage produced during the ion bombardment. This supports the earlier assumption of the importance of nuclear damage due to the ion bombardment.

Different aspects of chemical sputtering by co-bombardment with ions and hydrogen atoms were investigated using a variety of different ion species. Haasz and coworkers investigated chemical sputtering of graphite using hydrogen [161, 215, 216] and carbon ions [37]. Initially they focused their work on the determination of the methane production rate by mass spectrometry [215, 216]. Later they also measured the production rate of larger hydrocarbons (Fig. 18) [161]. The synergistic methane yield shows a distinct temperature dependence similar to irradiation by hydrogen atoms only. The methane production yield increases with increasing temperature, shows a maximum between 750 and 800 K [161, 215, 216], and then decreases again. With decreasing ion energy, a noticeable broadening of the peak shape occurs [216]. The methane production yield depends on the ion energy and the atom-to-ion flux ratio [161, 215]. As for the ions-only case, the product spectrum changes with ion energy. The relative contribution of higher hydrocarbons increases significantly with decreasing ion energy and varies also with the atom-to-ion flux ratio [161]. In contrast to the ions-only case, where methane is the dominant product in most of the energy range, the synergistic erosion due to ion and hydrogen atom co-bombardment is dominated by the sum of higher hydrocarbons (C_2 and C_3) in the whole energy range (50 eV to 3 keV) [161] (Fig. 18b). Due to the contribution of higher hydrocarbons, the total chemical sputtering yield exhibits a temperature maximum at about 650 K [161], which is substantially lower than the maximum of the methane production yield of 800 K (Fig. 18b) [161, 215, 216]. The product spectrum for chemical sputtering due to combined irradiation of graphite with H^0 and H^+ (Fig. 18b) also differs significantly from that of chemical erosion due to atomic hydrogen (Fig. 18a). For the latter, CH_4 is a minority species in the whole temperature range.

In contrast to *Haasz* and coworkers and *Vietzke* and coworkers, who measured hydrocarbon production yields by mass spectrometry [161, 215, 216] and molecular beam mass spectrometry [77, 79, 85], respectively (for description of the experimental setups see Sect. 4.2), *Hopf* and coworkers investigated the chemical sputtering of a–C:H films using in-situ real-time ellipsometry [141, 142, 217–219] (Sect. 4.3). This approach directly yields the total chemical sputtering yields but no information on the released species. In this view, it provides complementary information to the mass spectrometric investigations.

Hopf et al. [141, 142, 217, 218] investigated erosion of amorphous hydrogenated carbon (a–C:H) films due to combined Ar^+ ion and thermal atomic hydrogen atom impact in the low-temperature, low-energy regime. As discussed in Sect. 6.1.3, hard a–C:H films are a good model system for a graphite surface bombarded by hydrogen ions or a combination by arbitrary ions and atomic hydrogen. Hard a–C:H films were exposed to either one of the beams

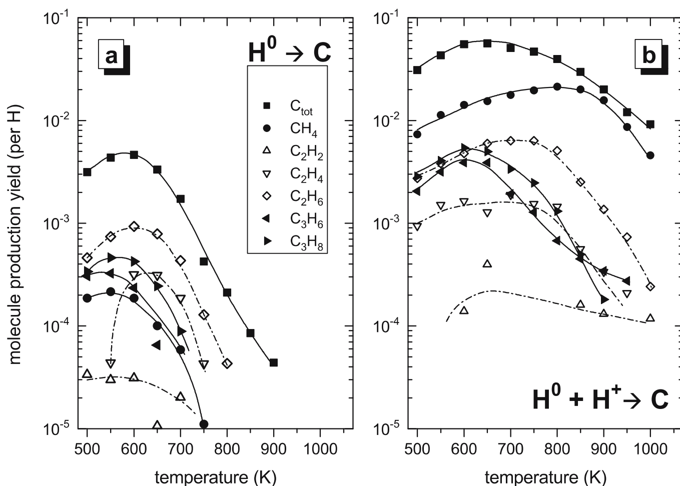

Fig. 18. Molecule production yields and total erosion yields as a function of temperature for bombardment of graphite with (**a**) atomic hydrogen alone ($1.1 \times 10^{19}\,\mathrm{m}^{-2} \cdot \mathrm{s}^{-1}$) and (**b**) combined with hydrogen ions (H^0: $1.8 \times 10^{19}\,\mathrm{m}^{-2} \cdot \mathrm{s}^{-1}$; H^+ (900 eV H_3^+): 2.1×10^{18} $H^+\,\mathrm{m}^{-2} \cdot \mathrm{s}^{-1}$) [161]

alone or to the combined Ar^+ ion and hydrogen atom beams. The experiments were performed at a surface temperature of about 340 K. The ion flux density was between 3 and $4 \times 10^{16}\,\mathrm{m}^{-2} \cdot \mathrm{s}^{-1}$ and the hydrogen atom flux was $\sim 1.4 \times 10^{19}\,\mathrm{m}^{-2} \cdot \mathrm{s}^{-1}$.

Figure 19 shows the erosion yield (per argon ion) as a function of ion energy. As all experiments involving ions were performed at approximately constant ion flux density, the yields on the left hand scale correspond roughly to the rates given on the right hand scale. The squares show the erosion by ions only. Physical sputtering is observed at energies of 200 eV and above. Below these energies the resulting rates are too low to be reliably detected in the experiment. For comparison, TRIM.SP [220] calculations were performed for a–C:H films with an H/(H+C) ratio of 0.3 using a surface binding energy of $E_{\mathrm{sb}} = 2.8\,\mathrm{eV}$. This is shown as dash-dotted line. It is in good agreement with the experimental results.

The erosion rate caused by the atomic hydrogen beam alone is shown as the dashed horizontal line in Fig. 19. Since in the absence of ion bombardment it makes no sense to define an erosion yield (per ion) we can not compare the erosion yields, but we can compare the erosion rates (right-hand scale). For the used hydrogen atom flux the measured erosion rate of $\sim 5 \times 10^{15}\,\mathrm{m}^{-2} \cdot \mathrm{s}^{-1}$ results in an erosion yield per hydrogen atom (not per argon ion as the other yields in Fig. 19) of 6.4×10^{-4}.

If both beams interact simultaneously with the film the resulting erosion rate greatly exceeds the sum of physical sputtering and thermal chemical erosion; clearly a synergistic mechanism is active – *chemical sputtering*. The

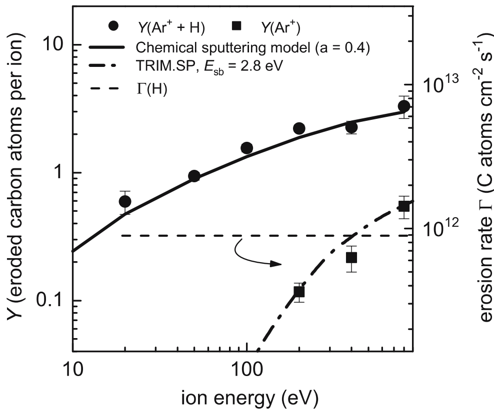

Fig. 19. Energy dependence of the erosion yield $Y(\mathrm{Ar}^+)$ of physical sputtering of an a–C:H film by Ar^+ ions (*squares*) and the yield $Y(\mathrm{Ar}^+ + \mathrm{H})$ for chemical sputtering by a simultaneous flux of Ar^+ ions and hydrogen atoms (*circles*). The *dash-dotted line* shows the carbon physical sputtering yields as calculated by TRIM.SP [220] for sputtering by argon ions using a carbon surface-binding energy of $E_{\mathrm{sb}} = 2.8$ eV. The *solid line* is the result of the chemical sputtering model by *Hopf* et al. [141]. The *dashed line* shows the absolute erosion rate (*right-hand scale*) by the applied flux of hydrogen atoms only. The surface temperature was about 340 K

chemical sputtering yield decreases with decreasing energy. At the lowest energy being used, 20 eV, the measured rate is still a factor of 3 higher than the rate for pure chemical erosion by the hydrogen flux alone. For the case of simultaneous bombardment (hydrogen atoms and Ar^+ ions at 200 eV) the yield per hydrogen atom increases from 3.5×10^{-4} (no ions) to 3.5×10^{-3}. It can thus be concluded that the reactivity of the surfaces with atomic hydrogen is increased by a factor of 10, which is in good agreement with the findings of *Vietzke* et al. [77, 85] and *Haasz* et al. [161, 215, 216]. This general result resembles that of erosion experiments applying energetic hydrogen isotopes [81], but, in contrast to these data, a clear decrease of the yield with decreasing ion energy is observed here. This is most probably due to the use of two separate beams and the fact that the atomic hydrogen flux is much higher than the ion flux. Based on these data, *Hopf* et al. suggested a microscopic model of chemical sputtering and devised a mathematical description of the energy dependence for this process. The model takes into account the damage produced by the impinging ions and the reaction of atomic hydrogen with this damage. The ion-induced damage is calculated with TRIM.SP. The model is explained in detail in Sect. 7.2. The solid line in Fig. 19, which represents the result of this model, is in excellent agreement with the data.

The identical experiment was also performed for co-bombardment with neon ions and atomic hydrogen. The results are presented in Fig. 20 [219]. Remarkably, the model for chemical sputtering, which was developed for and

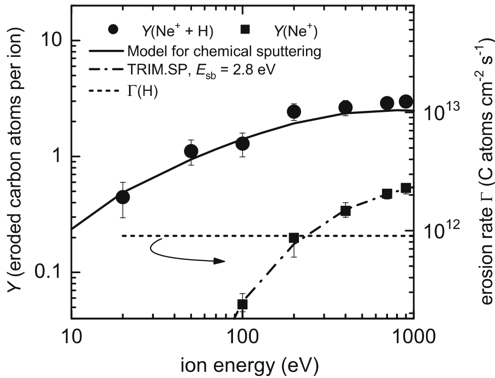

Fig. 20. Same as Fig. 19, but for neon ions

fitted to the argon-hydrogen data, leads to a perfect description also of the neon-hydrogen data without any adjusted parameter.

6.3 Effect of Doping

The multi-step process of chemical erosion depends on a critical combination of hydrogen attachment and desorption and the thermal release of reaction products (Sect. 5.1). As the activation energies for the different processes are similar, small changes in the activation energies for hydrogen desorption and hydrocarbon radical release can strongly influence the resulting erosion yield.

It was observed already in the early years of research on chemical sputtering that additions of small quantities of impurity atoms to graphites can reduce the erosion yield. Dopants such as Fe, Ni, Ti, Mo, Si [221] and Ni [160] were shown to be effective, but most prominently boron additions almost completely suppressed chemical sputtering [221–223]. Even small amounts of B, for example 0.5 at %, lead to a decrease of the temperature of hydrogen desorption [224] and, consequently, to a drastic reduction of chemical sputtering at elevated temperatures. As the activation energy for hydrogen desorption decreases below the activation energy for hydrocarbon radical emission, the reaction chain leading to erosion is interrupted [80, 225].

Once the thermal chemical erosion is suppressed, other emission processes, which do not require elevated temperatures, are more readily distinguished. Fig. 21 shows the chemical sputtering yield of a 15 at % boron-doped pyrolytic graphite, USB15, as a function of temperature for different ion energies in comparison with high purity pyrolytic graphite [226]. At 1 keV, the chemical sputtering yield with a maximum at 800 K is almost completely suppressed, while for decreasing energy a low temperature process emerges which is active up to the temperature for hydrogen desorption. The activation energy for hydrogen desorption from USB15 was determined to about 1.2 eV. In contrast, pure graphite has an activation energy of 1.8 eV [80]. Chemical sputtering is

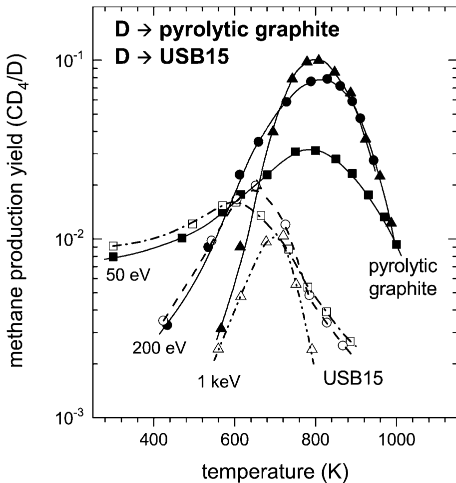

Fig. 21. Temperature dependence of the CD_4 production yield due to deuterium bombardment of pyrolytic graphite (*solid symbols*) and USB15 (*open symbols*) at different energies [226]

possible up to temperatures where thermal release of hydrogen molecules sets in. The total chemical sputtering yield due to this low temperature process for deuterium ions at room temperature and 30 eV is about 3 at %. It remains constant down to 150 K [18, 19, 182].

The decrease of the chemical sputtering yield with boron doping has led to attempts to produce new graphitic materials with low erosion yield. Dopants, such as Si, Ti, V, Zr and W were added as carbide grains to carbon powder in the production process of fine grain graphites [17, 227] and the chemical sputtering yield was studied using deuterium ions for 30 eV and 1 keV as a function of temperature, ion fluence, and grain size [228]. The effect of the dopants increased with decreasing carbide particle size. Finally, the addition of metallic dopants, such as titanium, vanadium, or tungsten, in atomic form by simultaneous sputter deposition of carbon and metal atoms, leads to doped carbon material with similar erosion behaviour as for boron doping [19, 182]. For example, 3 at % W reduces the thermal erosion process as efficiently as 15 at % B [182]. For high ion fluences the preferential sputtering of carbon and the simultaneous enrichment of dopant particles leads to a development of a pronounced column-like surface structure and to an almost complete suppression of erosion below the threshold energy for sputtering of dopant atoms [228].

6.4 Chemical Sputtering with Molecular Ions at Low Energies

In recent years, much attention has been paid to determining chemical sputtering yields at room temperature and at very low energy. To achieve suffi-

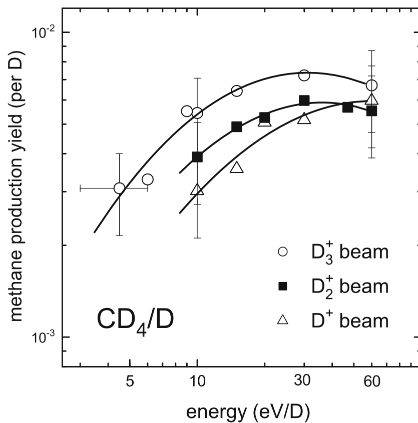

Fig. 22. Energy dependence of the methane production yield for sputtering of carbon with deuterium at room temperature [180]. Plotted is the yield per D atom for bombardment with D^+, D_2^+, and D_3^+ ions. For energies below 60 eV/D the measured yields start to deviate from each other. The *lines* are only a guide to the eye

ciently high ion fluxes most researchers used molecular ion beams, i.e. H_2^+ and H_3^+ and the corresponding deuterated ions. The general assumption used in the evaluation of measured data is that a molecular ion is identical to the corresponding number of individual atoms impinging at the same velocity. This means that the energy is shared evenly between the constituents of the molecular ion, in other words, an H_2^+ ion is equivalent to two H^+ ions at half the energy and an H_3^+ ion equivalent to three H^+ ions at one third of the energy. This concept holds at high energies (E $>$ about 100 eV), but it breaks down at lower energies. This has been demonstrated by *Yao* et al. who investigated the physical sputtering of gold by N_2^+ and O_2^+ ions [229]. An enhancement of the measured sputtering yield per atom for N_2^+ compared to N^+ was observed for energies below 500 eV per projectile (i.e. 250 eV per atom). The difference increased with decreasing ion energy. At 50 eV per atom the N_2^+ yield is about a factor of 4 higher than the N^+ yield. For O_2^+ they found similar enhancements over O^+ for energies below 100 eV per atom.

For the chemical sputtering of carbon by D^+, D_2^+, and D_3^+ ions and energies below 60 eV per deuteron the methane production yields per deuteron for the three different ion species start to deviate (Fig. 22) [177–180]. The difference between these yields increases with decreasing energy per deuteron. The yield for D_2^+ is always higher than that for D^+, and that for D_3^+ higher than that for D_2^+. At the energy of 10 eV/D the D_3^+ yield is a factor of two higher than the D^+ yield. This effect has to be taken into account if experimental results at low ion energies are compared and different ion species have been used.

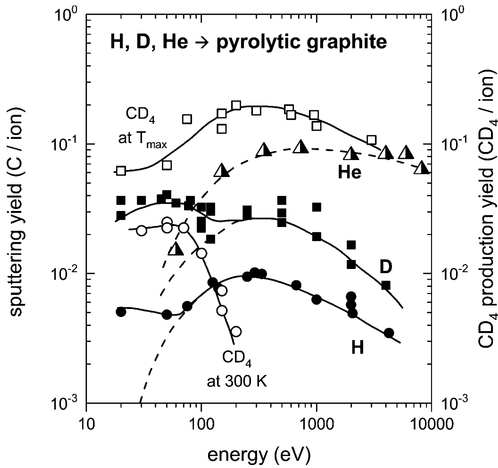

Fig. 23. Sputtering of carbon (pyrolytic graphite) with hydrogen, deuterium, and helium ions [173]. Comparison of weight loss data and CD_4 production. The *dashed lines* are predictions from an empirical formula for physical sputtering (see [173]). *Solid lines* are only a guide to the eye

6.5 Summary of Experimental Results

Chemical sputtering depends on a variety of experimental parameters such as type of carbon material, sample temperature, ion energy, and ion flux. These various parameters show strong, nonlinear interdependences so that a compact presentation of the physical and chemical dependences can be confusing at first glance. All relevant erosion processes (as defined in Sect. 3), i.e., physical sputtering, chemical erosion, and chemical sputtering can occur simultaneously. Which of them dominates the results depends on the experimental conditions. Strong interdependences exist between these processes. Furthermore, direct comparison of different experiments is difficult because in most cases more than one parameter is different. Nevertheless, the existing data base allows a rather advanced description of the physical and chemical processes and development of microscopic models for their interpretation. Before we start with a presentation of different models describing chemical sputtering, we want to make a critical assessment of the data, compare results from different methods, and summarize the most important points.

The energy dependence of sputtering of carbon materials with hydrogen ions differs from physical sputtering. The yield remains high at low energies, even below the threshold for physical sputtering (Figs. 12 and 23). The yield shows a strong isotope dependence (Figs. 12 and 23). At energies above about 100 eV yields for deuterium ions are a factor of 2–3 higher than those for hydrogen. The difference increases to about 5 to 7 for decreasing energies (below 100 eV). This is a proof that momentum transfer from the projectile ions to the target atoms, i.e., physical effects, plays an important role in this

process. The difference between physical sputtering and chemical sputtering is nicely summarized in Fig. 23. Sputtering by helium ions leads to physical sputtering. The measured weight loss data are in good agreement with an analytical prediction of physical sputtering shown by the line through the data points [173]. With decreasing energy the physical sputtering yield decreases strongly. For energies above about 100 eV the data for hydrogen and deuterium can also be well described by physical sputtering, but, in contrast to helium, their yields do not decrease with decreasing energy as anticipated for physical sputtering. They rather remain at relatively high values compared with physical sputtering. For the case of deuterium bombardment, the CD_4 production at 300 K, measured by a remote mass spectrometer, is also shown. Two points are remarkable: Firstly, at low energies, the yield is significantly lower than the weight loss data. This is due to the fact that CD_4 is not the only produced species. This point was discussed in Sect. 6.1.5. It underlines the fact that weight loss measurements provide the most reliable data for total sputtering yields. Secondly, at energies above about 80 eV the CH_4 production yield decreases strongly with increasing energy. This is in part due to the change of the product spectrum of released species which was also thoroughly discussed in Sect. 6.1.5. It is an indication that the dominant erosion processes below and above about 100 eV are different.

Fig. 23 also shows the enhanced CD_4 production yield at $T_{\mathrm{max}} = 820\,\mathrm{K}$. At energies below about 100 eV the CD_4 production yield at 820 K is a factor of 3 higher than at 300 K and it is even higher than the weight loss measurements at 300 K. This higher chemical sputtering yield at T_{max} was also shown by weight loss data (see Fig. 12) and it is due to the temperature dependence of chemical sputtering (Sect. 6.1.1). The chemical sputtering yield increases with increasing temperature, shows a maximum around 800 K, and decreases for higher temperatures (Figs. 8 and 9). The exact position of the temperature maximum of the chemical sputtering yield depends on the ion flux (Sect. 6.1.4) and the ion energy (Sect. 6.1.2).

The chemical sputtering yield also shows a distinct flux dependence for ion fluxes higher than $10^{21}\ \mathrm{m}^{-2} \cdot \mathrm{s}^{-1}$ (Sect. 6.1.4, Fig. 13). At these high fluxes, the maximum of chemical sputtering shifts to temperatures beyond 1000 K (see (6)). Since at such high temperatures the dominant process is hydrogen release the hydrocarbon yield is reduced.

Use of molecular ions at low energies leads to systematically different yields for different types of ions. The chemical sputtering yields per impinging D atom at the same energy per atom for bombardment with D^+, D_2^+, and D_3^+ start to depend on incident species below energies of about 60 eV per atom (Sect. 6.4, Fig. 22).

7 Mechanisms and Modelling for Chemical Sputtering

For the interaction of energetic hydrogen ions with carbon, it was found that the chemical reaction occurs after slowing down at the end of the range of the ions [85, 125–127, 195] impinging energetic hydrogen ions we can thus use the following simple concept: As long as the projectiles are fast, chemical interactions with the target atoms are negligible and interaction with the target is dominated by kinetic processes, i.e., displacement of target atoms and physical sputtering. At the end of range, when the energetic particles are finally thermalised, they interact chemically with the target atoms. This chemical reaction at the end of the ion range can be described by the chemical erosion of carbon due to thermal hydrogen atoms. The first kinematic models of the reaction of atomic hydrogen with a carbon surface were proposed in the 1970s [10, 230]. The most current and detailed one by *Küppers* et al. [155, 157] was outlined in Sect. 5. The corresponding chemical erosion yield, Y_{therm}, is quantitatively described by (6). But, in addition to chemical erosion, effects due to the energetic ion impact have to be taken into account. These additional effects cause an enhancement of the yield due to

- radiation damage in the graphite lattice
- low temperature near-surface emission processes.

Further processes, which were shown to play a role in chemical sputtering by energetic ions are:

- diffusion of hydrocarbons from the end of range to the surface [124, 125]
- the balance of formation and decomposition of hydrocarbons during irradiation [124, 125] leading to transient effects at the start of the ion irradiation or after changing the temperature [44, 124, 125, 231].

7.1 Empirical Analytic Description

Based on the just described simple concept of chemical sputtering, *Roth* and *García-Rosales* [159] suggested an empirical, analytical description which is capable of reproducing a variety of experimental observations. In particular, it describes the temperature, energy, flux, and isotope dependence of chemical sputtering.

7.1.1 Radiation Damage

Well-ordered graphitic structures provide only a very limited number of reaction sites for attack of atomic hydrogen. Although hydrogen atoms can form stable bonds with lattice atoms [232], chemical reactions occur only at edge atoms of graphitic planes [157]. Radiation damage (broken C–C bonds) provides additional reaction sites for hydrogen atoms, thus enhancing the

chemical erosion yield. Radiation damage is created by kinetic-energy transfer from incident ions to lattice atoms (nuclear energy loss). It is responsible for the dependence of the chemical sputtering yield on ion energy and hydrogen isotope. To break a C–C bond a minimum energy has to be transferred to carbon lattice atoms. Therefore, this yield enhancement is characterized by a threshold energy for damage production, E_{dam}. With increasing ion energy the total energy deposited in the target by nuclear collisions increases monotonically. However, the total energy deposited by nuclear collisions near the surface increases, reaches a maximum between 300 eV and 2 keV, and then decreases again. The chemical sputtering yield shows a similar energy dependence (see Figs. 10, 11, 14, and 15) as the energy deposited in the near-surface region. Thus it was concluded that the chemical sputtering yield is proportional to the energy deposited by nuclear collisions near the surface. The decrease of the chemical sputtering yield at higher energies indicates that energy deposition at large depths, typically beyond 200 nm, does not efficiently contribute to chemical sputtering. The effect of the damage production process is assumed to be similar to the physical sputtering process, but with a different threshold energy, E_{dam}. From a comparison of cross sections for damage production obtained by *Mech* et al. [233] with the analytic description of these processes analogous to physical sputtering (10), a value of 15 eV for E_{dam}, both for hydrogen and deuterium ions, was deduced.

Hence, this damage effect can be described by a multiplicative term to the basic chemical erosion yield, Y_{therm} (6), that includes a radiation damage yield, Y_{dam},

$$Y_{\mathrm{therm}}^{\mathrm{damage}} = Y_{\mathrm{therm}}(1 + D \cdot Y_{\mathrm{dam}})\,, \tag{8}$$

where D is a constant depending on the isotope mass of the bombarding particles. The numerical values for D are given in Tab. 2 (Sect. 7.1.3).

Below the threshold for damage production, the basic thermal reaction depends strongly on the crystalline perfection of the carbon material, with maximum yields between 10^{-4} for well annealed pyrolytic graphite and 10^{-1} for amorphous a–C:D layers [148]. At energies where radiation damage amorphises the graphite lattice, the dependence on the material structure disappears [78, 148, 162, 166, 168].

7.1.2 Low-temperature Near-surface Process, Y_{surf}

The mechanism for the low-temperature near-surface process, Y_{surf}, was deduced [159, 176] by comparing the measured sputtering yields of carbon at room temperature due to H^+ and D^+ bombardment as a function of incident energy (see Fig. 12). The measured yields close to and below the threshold of physical sputtering (solid line in Fig. 12) are due to hydrocarbon formation. This formation cannot be explained by the reactions of the Küppers model, where a thermal activation at temperatures higher than 600 K is necessary for chemical erosion. Moreover, whereas the elementary reactions of

the Küppers model do not show any isotope effect, a remarkable isotope effect (see Sect. 7.4) can be observed in the data plotted in Fig. 12. Based on this observation it was suggested that physical sputtering of weakly bound sp^3 CH_n groups from the surface is an explanation for Y_{surf}. The concentration of these groups at the surface is high at room temperature under hydrogen bombardment, as demonstrated by *Küppers* and co-workers [157, 158].

7.1.3 Empirical Roth–García-Rosales Formula

The total sputtering yield, Y_{tot}, for bombardment of a graphite surface with hydrogenic ions is given by the sum of physical sputtering, Y_{phys}, the chemical erosion enhanced by damage production, Y^{damage}_{therm} (8), and the near-surface process, Y_{surf}.

$$Y_{tot} = Y_{phys} + Y_{therm}(1 + D\,Y_{dam}) + Y_{surf}\,, \tag{9}$$

where D is a parameter depending on the hydrogen isotope. For the physical sputtering yield for ions with energy E_0 the description by *Bohdansky* [234] is used

$$Y_{phys}(E_0) = QS_n(E_0)\left[1 - \left(\frac{E_{th}}{E_0}\right)^{2/3}\right]\left(1 - \frac{E_{th}}{E_0}\right)^2, \tag{10}$$

with

$$S_n(E_0) = \frac{0.5\ln\left[1 + 1.2288\,(E_0/E_{TF})\right]}{E_0/E_{TF} + 0.1728\sqrt{E_0/E_{TF}} + 0.008\,(E_0/E_{TF})^{0.1504}}\,. \tag{11}$$

Improvements included in the more recent description of physical sputtering by Eckstein and Preuss (see Chap. by *Eckstein*) are not significant in the context of chemical sputtering.

The thermal erosion yield at an ion flux, Φ, is obtained from

$$Y_{therm} = c^{sp^3}\,\frac{0.033\exp(-E_{therm}/kT)}{2\times10^{-32}\,\Phi + \exp(-E_{therm}/kT)}\,, \tag{12}$$

with

$$c^{sp^3} = \frac{C\left(2\times10^{-32}\Phi + \exp(-E_{therm}/kT)\right)}{2\times10^{-32}\,\Phi + \left[1 + \dfrac{2\times10^{29}}{\Phi}\exp(-E_{rel}/kT)\right]\exp(-E_{therm}/kT)}\,. \tag{13}$$

The factor C,

$$C = \frac{1}{1 + (\Phi/6\times10^{21})^{0.54}}\,, \tag{14}$$

Table 2. Parameters for the empirical Roth–García-Rosales formula for the description of chemical sputtering by different hydrogen isotopes

Parameter	Hydrogen	Deuterium	Tritium
E_{TF}	415 eV	447 eV	479 eV
Q	0.035	0.1	0.12
E_{th}	31 eV	27 eV	29 eV
E_{dam}	15 eV	15 eV	15 eV
E_{des}	2 eV	2 eV	2 eV
D	250	125	83
E_{rel}	1.8 eV for pure carbon, 1.5 eV for Si, Ti, W doped carbon, 1.2 eV for B doped carbon		
E_{therm}	Gauss distribution of activation energies around 1.7 eV, $\sigma = 0.3$ eV		

includes the dependence on ion flux, reducing the yield at fluxes above $6 \times 10^{21}\,\mathrm{m}^{-2} \cdot \mathrm{s}^{-1}$. The chemical erosion at elevated temperature is enhanced by damage production given by

$$Y_{\mathrm{dam}}(E_0) = Q S_n(E_0) \left[1 - \left(\frac{E_{\mathrm{dam}}}{E_0}\right)^{2/3}\right] \left(1 - \frac{E_{\mathrm{dam}}}{E_0}\right)^2 \tag{15}$$

with $S_{\mathrm{n}}(E_0)$ given by (11).

The surface erosion process is given by

$$Y_{\mathrm{surf}}(E_0, T) = c^{\mathrm{sp}^3} \frac{Y_{\mathrm{des}}(E_0)}{\left(1 + e^{\frac{E_0 - 65\,\mathrm{eV}}{40\,\mathrm{eV}}}\right)} \tag{16}$$

with

$$Y_{\mathrm{des}}(E_0) = Q S_{\mathrm{n}}(E_0) \left[1 - \left(\frac{E_{\mathrm{des}}}{E_0}\right)^{2/3}\right] \left(1 - \frac{E_{\mathrm{des}}}{E_0}\right)^2 . \tag{17}$$

Although the detailed mechanism of the near-surface process is still under discussion, it is here assumed to scale as a physical sputtering term, but with reduced threshold energy, E_{des}. The denominator in (16) restricts the process to low energies, i.e., processes near the surface.

The parameters Q, E_{therm}, E_{th}, E_{dam}, E_{des}, E_{rel}, E_{TF} and D are given in Table 2 for the different hydrogen isotopes. Changes in the numerical values in (14) and (16) compared to [80,159] are introduced to smoothen the transition between different processes.

7.1.4 Comparison with Erosion Data

Fig. 24 shows the combined energy dependence of physical sputtering, chemical erosion, and chemical sputtering together with the analytic description

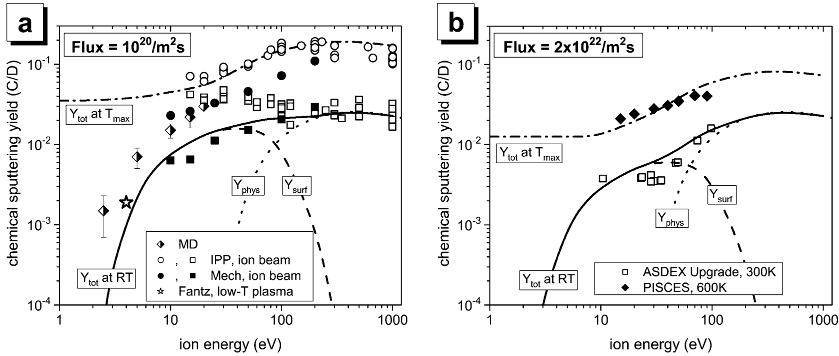

Fig. 24. Experimental data for the energy dependence of the erosion of graphite under D^+ bombardment as a function of energy compared to MD calculations and the analytical model [159, 235]: (**a**) for a flux of $10^{20}\,\mathrm{m}^{-2}\cdot\mathrm{s}^{-1}$, (**b**) for a flux of $2\times10^{22}\,\mathrm{m}^{-2}\cdot\mathrm{s}^{-1}$. The data are from the following sources: MD [49], IPP [81], Mech [176], Fantz [106], ASDEX Upgrade [91], PISCES [104]. *Open symbols* are for weight loss and spectroscopic data, *solid symbols* for mass spectrometry

developed on the basis of the results by *Küppers* et al. [155, 157] for thermal hydrogen atoms and the inclusion of damage production and chemical sputtering by energetic ions [80, 159]. The analytic description adequately describes the chemical erosion in its energy and temperature dependence.

As shown in Fig. 24a for deuterium, the formula leads to a good agreement with the available laboratory data (obtained for ion fluxes of the order of $10^{20}\,\mathrm{m}^{-2}\cdot\mathrm{s}^{-1}$) for the energy dependence of the chemical sputtering yield at room temperature and close to $T_{\max}$. The contributions of Y_{phys} and Y_{surf} are plotted separately. The experimental data shown are total sputtering yields obtained by weight loss measurements (open symbols) and mass spectrometry including higher hydrocarbons (solid symbols). Data at room temperatures and below 20 eV were obtained by MD simulations [49].

In Fig. 24b the analytical description is compared to the limited amount of data at an ion flux of about $10^{22}\,\mathrm{m}^{-2}\cdot\mathrm{s}^{-1}$. The observed general decrease of the chemical sputtering yield is well reproduced by the flux dependence of the model.

7.1.5 Extrapolation to Thermal Energies

The experimental data for energetic ions extends only down to energies of 10 eV and has to be extrapolated to lower energies. At $T_{\max}$ the yield for chemical erosion due to exposure to thermal hydrogen depends strongly on the surface state of the material: for well annealed graphite surfaces exposed to H^0, $Y_{\max}$ is of the order of 10^{-4}, while for the case of a–C:H layers or pre-irradiated graphite exposed to H^0 the erosion yields can reach 10^{-1}. For graphite irradiated simultaneously with H^0 and energetic ions (see Figs. 17

and 18) this yield is equivalent to the one for a–C:H layers [77–79, 148, 168] (see Sect. 6.1.3). For carbon surfaces in interaction with hydrogen plasmas, as e.g. in fusion applications, one has to assume that due to simultaneously incident energetic particles the plasma-facing surfaces are always amorphised and activated, such that the proposed equation predicts high, energy independent erosion yields Y_{therm} at T_{max}. In Fig. 24 it can be seen that using the analytical description for extrapolation of the chemical sputtering yield at T_{max} towards very low energies leads to values above 10^{-2}. For undamaged surfaces Y_{therm} may be an order of magnitude lower.

At room temperature measurements of chemical erosion due to exposure to thermal hydrogen show very low or no chemical erosion, depending on the actual structure of the carbon material. Therefore, the dominant erosion yield at low energies is Y_{surf} with a threshold energy around 2 eV and negligible yields at lower energies.

7.2 Chemical Sputtering Model by Hopf

Hopf et al. recently suggested a microscopic model for chemical sputtering of graphite with hydrogen ions at room temperature [141]. According to this concept, the key mechanisms are:

- Impinging ions break carbon-carbon bonds at the surface and within the ion penetration range.
- Locally available hydrogen reacts with these broken bonds forming C–H bonds.
- Consecutive C–C bond breaking and C–H bond formation processes lead to the production of stable, volatile hydrocarbon molecules at and below the surface (within the ion penetration range).
- Finally, the formed volatile hydrocarbon molecules diffuse to the surface and desorb. At room temperature, subsurface hydrocarbon species can desorb only from a limited near-surface layer.

Based on this microscopic concept, they devised a mathematical description of the energy dependence of chemical sputtering [236]. The impinging hydrogen ions provide both the damage (broken C–C bonds) and the chemically reactive species. The depth distributions of the broken C–C bonds, $y_{\mathrm{bb}}^{C}(x, E)$, and the implanted species, $n(x, E)$, are calculated with TRIM.SP. The limitation of the out-diffusion of the molecules to a near-surface region is modelled by an exponentially decaying, depth-dependent probability for the outdiffusion, $\exp(-x/\lambda)$. The resulting contribution to the chemical sputtering yield due to formation of hydrocarbon species at room temperature, Y_{CH}, is given by the integral of the product of these three functions,

$$Y_{\mathrm{CH}} = a \int y_{\mathrm{bb}}^{\mathrm{C}}(x, E) n(x, E) \exp(-x/\lambda) \, \mathrm{d}x \,. \tag{18}$$

The parameter a is simply a scaling parameter. $y_{\mathrm{bb}}^{C}(x,E)$ and $n(x,E)$ are both dependent on the ion energy and the mass of the impinging ions. The decay length of the out-diffusion probability is chosen as $\lambda = 0.4\,\mathrm{nm}$ [236]. The energy required to break a C–C bond, E_{bb}, was chosen as 5 eV being a typical C–C bond energy. E_{bb} is an input parameter used for the TRIM.SP simulations. The surface binding energy of the hydrogen projectiles on graphite was approximated with the desorption energy of hydrogen from a fully hydrogen-covered graphite (0001) surface [237]. It becomes important at low energies because the projectile energy is increased by this amount when approaching the surface. The surface binding energy of carbon atoms was set to 7.4 eV [220]. Using these parameters, the chemical sputtering yield was calculated. The total sputtering yield, Y_{tot}, is given by the sum of the physical sputtering yield, Y_{phys}, and the contribution due to formation of hydrocarbons, Y_{CH},

$$Y_{\mathrm{tot}} = Y_{\mathrm{phys}} + Y_{\mathrm{CH}}\,. \tag{19}$$

Y_{phys} is also calculated with TRIM.SP. Y_{tot} and the individual contributions of Y_{phys} and Y_{CH} (with a = 1) are shown in Fig. 25 together with experimental data from [81] for chemical sputtering at 300 K, which were already shown in Fig. 12. Considering the simplicity of the model, the agreement with the data is excellent. The model correctly describes the magnitude of the yield and the obvious isotope effect. It even reproduces details of the isotope effect (i.e., the ratio of the D^+ and H^+ yields). The hydrogen yield decreases slightly from 100 down to 15 eV while the deuterium yield actually increases in this range. This is reproduced by the model as well as the absolute difference between hydrogen and deuterium yields. The isotope effect and the fact that it is more pronounced at lower energies is discussed in Sect. 7.4.

This microscopic concept of the processes during chemical sputtering has some similarity to an earlier model where the chemical sputtering yield was scaled with the total nuclear energy deposition, i.e., the total energy transferred in projectile-target and target-target elastic collisions, in a near-surface layer [190]. But the observed large isotope effect at low energies requires that the term describing damage production must be associated with a process that has an threshold energy. If the total nuclear energy deposition instead of y_{bb}^{C} is used to describe the ion-induced damage in (18) a very different threshold behaviour occurs [236]. At energies above about 50 eV the choice of either total nuclear energy deposition or y_{bb}^{C} produces practically indistinguishable results, but below 50 eV y_{bb}^{C} leads to the decrease with decreasing energy as shown in Fig. 25, while the total nuclear energy deposition results in a monotonically increasing chemical sputtering yield with decreasing energy for both hydrogen isotopes [236].

The model by *Hopf* and coworkers [141] was originally developed for the combined irradiation of a–C:H films by energetic argon ions and thermal, atomic hydrogen (Sect. 6.2) [141, 142, 217–219] and had to be adapted to

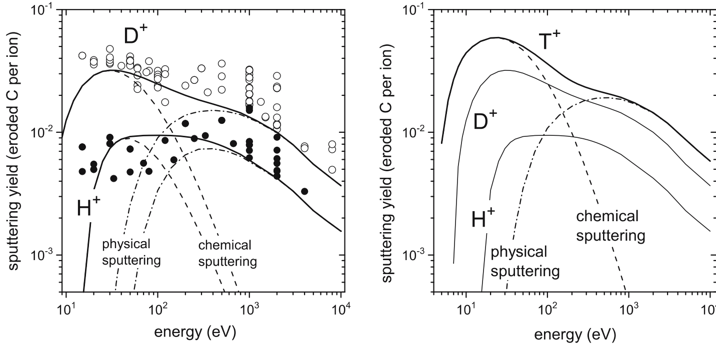

Fig. 25. *Left-hand side:* Total sputtering yield of graphite bombarded with hydrogen or deuterium ions at room temperature as a function of ion energy. The *open* and *solid symbols* are measured yields taken from [81] for D^+ and H^+ bombardment, respectively. The *lines* show the physical sputtering yield calculated with TRIM.SP (*dash-dotted*), the chemical sputtering yield according to (18) (*dashed*), and the sum of chemical and physical sputtering (*solid*). *Right-hand side:* physical sputtering yield calculated with TRIM.SP (*dash-dotted*), chemical sputtering yield (18) (*dashed*), and total sputtering yield (19) (*solid*) for tritium. For comparison the total sputtering yields for hydrogen and deuterium from the *left side* are reproduced

the case of bombardment of graphite with hydrogenic ions [236]. The main difference between the two cases is not the involved microscopic processes, but the source of the available hydrogen atoms. While for the hydrogen ion case, the projectile provides both damage and reactive species, for the co-bombardment case damage is produce by the argon ions and hydrogen is provided by the impinging atomic hydrogen flux. This leads to different depth distributions of the damage, $y_{\mathrm{bb}}^{C}(x,E)$ and hydrogen densities.

For the hydrogen atom distribution in the target surface it was assumed that the density of hydrogen, and accordingly the probability that a reaction with a dangling bond occurs, decreases with increasing distance from the surface. This decay was described by an exponentially decaying function $\exp(-x/\lambda)$. The decay length was chosen to $\lambda = 0.4\,\mathrm{nm}$ resulting in a maximum range of $\sim 2\,\mathrm{nm}$ as found experimentally [89, 238]. The chemical sputtering yield for the co-bombardment case is described by

$$Y_{\mathrm{CH}} = a \int y_{\mathrm{bb}}^{\mathrm{C}}(x) \exp(-x/\lambda)\,\mathrm{d}x, \tag{20}$$

where a is a scaling factor. The difference between (20) and (18) is that in (20) the term $n(x,E)$ is missing and the interpretation of $\exp(-x/\lambda)$ is different. However, the interpretation of $\exp(-x/\lambda)$ as penetration for atomic hydrogen is, although intuitive, not unique. This was pointed out already in [141]. In light of the adaptation of this model to the hydrogen ion case it seems more appropriate to interpret $\exp(-x/\lambda)$ as the depth-dependent probability for

out-diffusion of the formed volatile species. The model curves according to (20) are presented in Fig. 19 for Ar^+ + H and in Fig. 20 for Ne^+ + H as solid lines using $a = 0.4$ as scaling factor. Obviously the agreement with the data is very satisfying.

For the co-bombardment case, the chemical sputtering yield depends also on the incident atom-to-ion flux ratio. The flux dependence was investigated and discussed by *Hopf* et al. [141]. It was shown that a much higher atomic hydrogen flux compared with the ion flux is required to achieve maximal yields. In the Ar^+ + H experiment the ratio of neutral hydrogen to argon ions was 400 [141,217] and even higher flux ratios are required for saturation of the process. A simple rate equation model to fit the experimentally observed flux dependence results in a saturation value for the chemical sputtering yield of about 3 (for Ar^+ ions at 200 eV) which is reached for flux ratios above 1000 [141]. This need for excess supply of atomic hydrogen can be understood taking into account that the dominant ion-induced process is displacement of bonded hydrogen [38]. This ion-induced depletion of hydrogen in the surface layer has to be balanced by the much higher influx of atomic hydrogen to keep the hydrogen concentration in the surface region high. *Hopf* et al. hypothesize that the flux ratio influences the fitting parameter a in (20), but this was not yet investigated in detail.

7.3 Molecular Dynamics Simulations

The chemical sputtering of carbon by hydrogen was also investigated in MD simulations in some detail by the Helsinki group [48–54, 239–244]. *Salonen* et al. [239] studied the erosion of carbon by bombardment with hydrogen atoms at low energies (1 and 10 eV) but at high hydrogen fluxes. Atoms with 1 eV cause no carbon erosion, but at 10 eV some carbon erosion was observed. They also found that at very high fluxes carbon erosion is suppressed. They interpreted this effect as indicating that at high-flux hydrogen bombardment temporary supersaturation of hydrogen occurs at the surface. The high hydrogen content leads to the shielding of carbon atoms from new incoming hydrogen atoms, and thus a decrease of roughly one order of magnitude in the carbon erosion yield. They also found ejection of small hydrocarbon species (CH_y and C_2H_y). C_2H_y species contribute about 46 % to the carbon removal rate.

In following investigations they identified a new sputtering mechanism which they named: “Swift Chemical Sputtering” [48–53]. Swift chemical sputtering leads to the release of hydrocarbon radicals (including single C atoms) down to energies of 2 eV. Room temperature bombardment of an a–C:H sample at 10 eV caused an erosion yield of 5×10^{-3}. With increasing temperature the yield increases, has a peak of about 0.02 at 900 K, and then decreases again [48]. This behaviour compares well with experimental results (see Sect. 6.1.1). The emitted species spectrum is dominated by CH_y and C_2H_y with a higher C_2H_y contribution at 900 K as compared to 300 K [49].

The energy dependence was studied in the interval from 1-35 eV [48, 49]. The simulated yields for hydrogen, deuterium, and tritium are about a factor of 10 higher than the corresponding physical sputtering yields calculated by TRIM.SP. Furthermore, the simulations show a clear isotope effect increasing towards the threshold for chemical sputtering [49, 51]. The yields for bombardment with tritium ions are consistently higher than those for deuterium, which in turn are higher than those for protium. These observations clearly support the picture that for chemical sputtering in this parameter range, i.e., 300 K and low energies (1-35 eV), chemical and physical interactions are of relevance.

The carbon erosion mechanism underlying the “Swift Chemical Sputtering” process is the breaking of C–C bonds of surface hydrocarbon entities bonded to the network. These entities can be single carbon atoms or larger hydrocarbon groups. Since at these low energies the impinging atoms have not enough kinetic energy to physically sputter a carbon atom or a hydrocarbon group, the bond breaking takes place in a different manner. To break these bonds, ions penetrate the region directly between carbon atoms, i.e., they directly attack the covalent bond. The carbon atoms are then forced apart by the strong repulsive part of the potential energy function. This repulsion occurs very fast so that the surrounding carbon network does not have time to relax to a new equilibrium. The momentum transfer to the carbon atoms of the attacked covalent bond depends on the time the hydrogen atom spends between them. As a consequence, swift chemical sputtering can occur only in a certain incident energy range, so that it does not only have a low energy limit, but also a high energy limit. This is distinctly different than for the case of physical sputtering where only a low-energy limit (threshold energy) exists. This dependence on the interaction time offers also an explanation for the isotope dependence. As the velocity of different hydrogen isotopes changes according to the mass of the isotope, deuterium and tritium spend at the same incident energy more time between the carbon atoms than hydrogen. MD simulation have shown that the larger the mass of the hydrogen isotope, the larger the energy range where the bond breaking can occur is [52, 53]. The “Swift Chemical Sputtering” process, originally discovered for hydrogen bombardment of carbon, has recently been shown to occur also for bombardment with helium ions [54]. “Swift Chemical Sputtering” is a new process which differs from usual physical sputtering and from chemical sputtering.

Recent simulations by *Krstić, Stuart* and *Reinhold* [245–248] have stressed the importance of preparing model surfaces by particle bombardment consistently with sputtering beam experiments. Self-consistent preparation of carbon surfaces [245, 248] by cumulative bombardment with the species (D, D_2, D_3), energy, and rovibrational-state-resolved projectiles led to improved agreement with measurements at 300 K [180] across the whole simulated energy range (7.5-30 eV/D), even at the level of partial hydrocarbon yields (methane, acetylene). Furthermore, it was shown [246] that chemical sputtering yields for molecular projectiles at impact energies below 15 eV/D exhibit a

strong dependence on their initial, preimpact vibrational state. In fact, it was argued that resonant neutralization of the D_2^+ ions used in experiments above the surface is expected to result in vibrationally excited D_2. Calculations using this assumption are found to be in better agreement with experiments for sputtering of methane [180] and acetylene [179] by D_2^+ impact.

The atomistic nature of the MD modelling allows to identify the sputtered hydrocarbon species. The factor determining which type of hydrocarbon molecule is released is the depth of the broken C–C bond. The hydrocarbon chain above the broken bond leaves the surface. The predominantly eroded species are small hydrocarbons CH_y and C_2H_y, in agreement with experiments. Only a small fraction of heavier hydrocarbons are seen [49, 241]. The composition of the released hydrocarbon flux changes with the structure of the a–C:H sample, with the incident energy, and with the type of hydrogen isotope. These changes are largest at very low energies ($< 15\,\mathrm{eV}$). Details can be found in [241]. Differences in the structure of the a–C:H sample can also lead to considerable differences in the total carbon erosion yield. The crucial factor is how many C–C bonds to the bulk and hydrocarbon groups an entity at the surface has. An entity with only one C–C bond to the surface erodes much easier than one with several bonds [48–50].

For low impact energies ($< 15\,\mathrm{eV/D}$) CD_y and C_2D_y were found to be the dominant species [247]. The role of heavier hydrocarbons increases with energy, leading to substantial contributions of C_4D_y and C_5D_y at $30\,\mathrm{eV/D}$ impact energies. Energy spectra of the sputtered particles were found to be nearly independent of the mass of the sputtered particles or the impact energy: The average energy of the sputtered hydrocarbons is about $0.5\,\mathrm{eV}$, indicating a kinetic desorption process [247].

To rule out a possible dependence of the MD results on the choice of the potential, MD simulations were conducted by the Helsinki group for three varieties of the empirical Brenner potential as well as in a tight-binding quantum-mechanical framework which is completely independent of the classical simulations [52, 53]. It was shown that simulations with a quantum-mechanical treatment of the atomic system validate the bond breaking (and subsequently, erosion) mechanism, though the carbon sputtering yields given by the empirical and tight-binding models differ quantitatively.

MD at its present level is only capable of simulating a very short time after the impact, typical durations are of the order of a few picoseconds, but some simulations have been performed up to a few nanoseconds. This seems to be satisfactory at low impact energies ($< 30\,\mathrm{eV/D}$), where the penetration depth of the impact particle is small enough ($< 1\,\mathrm{nm}$) to allow sputtered particles to reach the surface through pores in the surface. For larger impact energies and accordingly deeper penetration of the projectiles, MD cannot describe any process that requires much longer time scales. Experiments by *Vietzke* et al. have, however, shown that a large fraction of the species is released with thermal energies and on a timescale of miliseconds [47]. In particular, MD

can not describe the postulated processes of chemical sputtering as described in Sect. 7.2.

The characteristic time scale of the swift chemical sputtering process is of the order of 10 fs. The swift chemical sputtering process found in MD simulations and described above might be a good microscopic description of the surface process, Y_{surf}, postulated by *Roth* et al. [159] (see Sect. 7.1.2).

7.4 Isotope Effect

In the preceding discussion of mechanisms of chemical sputtering in many instances the isotope effect was mentioned. The importance of the isotope effect, i.e., the yield ratio Y_D/Y_H, for the understanding of the dominating mechanism is outlined in the following.

On the one hand, the chemical interaction of hydrogen isotopes with carbon is only weakly dependent on the isotope mass. Activation energies for hydrogen and deuterium desorption have been found to differ by less than 0.1 eV [155] and consequences for the thermally activated term of the chemical erosion yield, Y_{therm}, can, therefore, be neglected in (6). On the other hand, radiation damage and physical sputtering are certainly dependent on ion mass. The latter can be clearly seen in the experimental data on physical sputtering of carbon by H^+ and D^+, where typically yields a factor of 2 higher are found for D^+ ions [81] (see solid lines in Fig. 12). Using TRIM.SP the physical sputtering yield has been calculated for T^+. It turns out that the increase of physical sputtering from D^+ to T^+ is only small compared to the increase from H^+ to D^+ (Fig. 25b).

This leads to the expectation that also the chemical sputtering at elevated temperature and energies above 100 eV does not increase strongly from D^+ to T^+. These expectations are corroborated by the first direct measurements of chemical sputtering with T^+ [249]. In fact, the chemical sputtering yield for tritium is the same as for deuterium within the uncertainties of the data.

The surface process Y_{surf} requires a bond-breaking process, both to form hydrocarbon reaction sites [141] and to release CH_n groups from the surface [49]. In this case, however, the damage production must occur within the first few monolayers of the solid and energies well below 100 eV play the dominant role. At energies close to the threshold for damage production, much stronger isotope effects must be expected. The simulation of the kinetic bond breaking process in MD calculations [49, 245, 247] indicates a threshold energy around 2 eV for D^+. These predictions agree well with recent experimental data for CD_4 emission [177–180]. Also, *Salonen* et al. [49] found strong isotope effects in MD simulations in going from hydrogen to deuterium and tritium, increasing with decreasing energy.

The isotope effect and the fact that it is more pronounced at lower energies can, according to the Hopf model (Sect. 7.2), be explained by the following dependences:

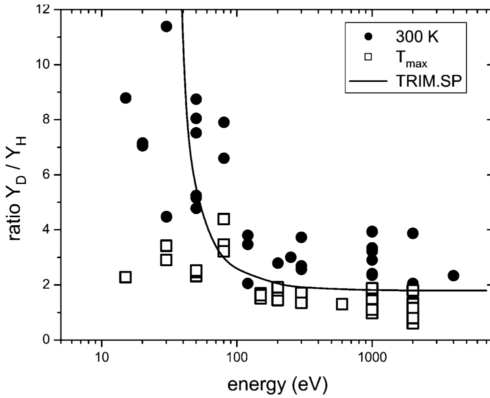

Fig. 26. Ratio of the chemical sputtering yield of graphite due to bombardment by D^+ and H^+ as a function of ion energy. Shown are the yields for bombardment at 300 K and at T_{max} (about 700 to 800 K) and results from TRIM.SP simulations of physical sputtering. The data are from [81]

(i) The collisional energy transfer is different for different projectile masses. The maximum transferrable energy in a head-on collision is given by the kinematic factor $\gamma(M_1, M_2) = 4M_1M_2/(M_1 + M_2)^2$ where M_1 and M_2 are the projectile and target masses. For collisions with carbon the ratio of the kinematic factors for deuterium and protium projectiles is $\gamma(M_D, M_C)/\gamma(M_H, M_C) \approx 1.7$. Indeed, both in the experiment and in the TRIM.SP calculations a ratio $Y_{phys}(D)/Y_{phys}(H) \approx 2$ is found.

(ii) Due to the need to transfer a certain minimum amount of energy to a carbon atom to break a bond, $E_{bb} = 5$ eV in this case, there is an energy threshold $E_{th} = E_{bb}/\gamma(M_1, M_C)$ below which the chemical sputtering yield becomes zero. Small differences in the threshold energy between hydrogen, deuterium, and tritium will result in large isotope effects close to the threshold energy, as is observed for physical sputtering. This threshold is lower for D^+ than for H^+. Consequently, the isotope effect increases when approaching the threshold from the high-energy side and becomes infinite below the threshold for protons.

Figure 26 shows a compilation of experimental data for the ratio of Y_{D^+}/Y_{H^+} for sputtering at room temperature and at T_{max} as a function of ion energy taking the total sputtering yield from weight loss data [81]. The thermal chemical erosion yield at T_{max} shows an isotope effect of the order of a factor of 2, as predicted by the ratio of radiation damage production at high energies. In contrast, Y_{surf} measured at room temperature increases strongly towards low energies and a comparison with the isotope effect of physical sputtering, as obtained from TRIM.SP calculations, shows reasonable agreement. This comparison indicates that the threshold energies for hydrogen and deuterium, although being similar around 2 eV, differ clearly

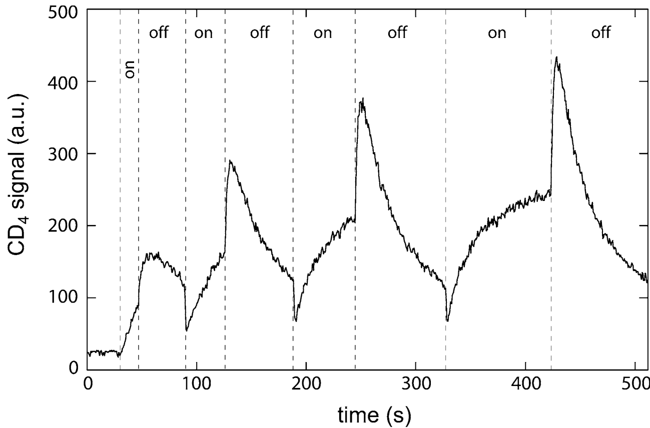

Fig. 27. Transient changes of the CD_4 signal of a remote mass spectrometer during chemical sputtering of graphite at $T_{\rm max}$ using 8 keV D^+ when switching on and off the incident ion beam [251]

with slightly higher values for hydrogen. It can be expected that the threshold for tritium is even lower (see Fig. 25b) resulting in even higher isotope ratios Y_{T^+}/Y_{H^+}.

It is interesting to note that such high isotope ratios are not observed by residual gas analysis of the emitted stable hydrocarbons [250]. For stable hydrocarbons, which amount only to part of the total yield [81,245,247] ratios of the order of 2 were reported, similar to thermal hydrogen erosion. It may be speculated that stable hydrocarbons result from thermal emission, while the kinetic bond breaking processes result predominantly in the emission of radicals [49]. More investigations on the isotope effect, both experimentally and in MD simulations, will give valuable information of the underlying physical and chemical emission processes.

7.5 Effects due to Out-diffusion of Hydrocarbons

The fact that chemical erosion at elevated temperatures occurs at the end of the ion range requires that volatile reaction products diffuse to the surface, either through the crystalline lattice or along grain boundaries. The diffusion of reaction products has been inferred from transient effects after rapidly switching on or off the ion beam at constant surface temperature [124, 125, 251].

Figure 27 shows the CD_4 signal of a remote mass spectrometer during chemical sputtering of graphite at $T_{\rm max}$ using 8 keV D^+ as a function of time. When the beam is switched off, a sudden increase of the emission of hydrocarbons occurs before the mass spectroscopic signal decreases. In contrast, when the beam is switched back on during the decrease of the signal a transient drop of the signal is observed before the steady state emission is

re-established [124]. The transients are more pronounced the higher the ion energy is between 8 keV D^+ and 100 keV D^+ [251]. These effects have been interpreted as the decomposition of reaction products by the incident ions during their diffusion to the surface, which reduces the hydrocarbon emission in steady state, but ends when the beam is turned off. Immediately after turning off the beam, a higher hydrocarbon emission results. From more detailed studies [124, 125] a multi-region model for intra-granular diffusion and diffusion along grain boundaries was developed. Similar transients occur upon rapid changes in temperature and ion flux [44, 231]. The study and interpretation of these transients can give more detailed insight into the chemical erosion process.

7.6 Summary

The different modelling approaches presented in this chapter serve different purposes. The empirical description (Roth–García-Rosales formula) was developed to provide an easy tool for predicting erosion rates in fusion devices. It allows to estimate erosion for a variety of parameters, such as temperature, energy of the impinging ions, ion flux, and isotope mass without detailed understanding of processes such as the flux dependence and near-surface emission.

The model by *Hopf* et al. (Sect. 7.2) [141] specialises on chemical sputtering at room temperature. It provides a microscopic explanation of the near-surface process Y_{surf} and, based on this, a mathematical model describing the energy dependence at room temperature. The Hopf model takes into account the depth distributions of the implanted hydrogen atoms and the radiation damage and the depth-dependent out-diffusion of the produced stable hydrocarbon species. It provides a deeper insight into the processes subsumed under the near-surface process, Y_{surf}, postulated in the empirical (Roth–García-Rosales formula). A key point of the Hopf model is that at room temperature out diffusion of produced hydrocarbon species is limited to a near-surface layer with a thickness of about 2 nm and it involves an energy threshold of about 5 eV given by the minimum energy required to break a carbon–carbon bond.

Even more basic physical understanding can be gained from MD simulations. Many elementary reaction and emission processes can be investigated in great detail. Due to technical restrictions in computing power, for the time being, only such processes which proceed on time scales below 1 ns can be evaluated. Thus MD simulations concentrate on kinetic emission processes, while thermal processes including particle diffusion cannot be accessed. The MD simulation suggest a threshold energy of about 2 eV for the near-surface process. Such a threshold is in accordance with recent experimental data for the energy dependence of the process down to 5 eV [177–180].

8 Chemical Sputtering with Other Reactive Species

8.1 Oxygen

Oxygen as a highly reactive chemical species interacts strongly with carbon and carbonaceous materials. Molecular oxygen forms the gaseous products CO and CO_2 at elevated temperature, i. e., above ≈ 500–800 K, depending on the specific carbon material [252–256]. The CO/CO_2 ratio increases substantially at higher temperatures and lower pressures [257]. More recently, *Stanmore* et al. [258] reviewed the gasification of carbon and the chemistry of combustion. They also report that the reaction rates are strongly influenced by the presence of impurities which, for example, may act as catalysts. Furthermore, the rates are influenced by the structure of the carbon material as was investigated in detail by *Müller* et al. [256] and *Balden* et al. [254]. For different graphites the yields typically range between 10^{-6} and 10^{-3} C/O_2 at 1000 K and at pressures between ≈ 10^{-5} mbar and atmospheric pressure [254, 259]. At 2000 K yields of up to 10^{-2} have been measured [259]. In the case of thermal atomic oxygen the yields are substantially higher, as reported by *Rosner* and *Allendorf* [260]. The reaction yield increases with increasing temperature. It is about 0.08 at 700 K and reaches its maximum of about 0.6 around 1600 K.

If energetic oxygen ions impinge on carbon materials, the impinging oxygen is trapped or reemitted in the form of CO and CO_2 [261, 262], while reemitted O and O_2 has not been found. At room temperature the saturation concentration of oxygen in graphite is 0.25 O/C [261, 262]. It decreases with increasing temperature. For energies higher than 50 eV, the chemical sputtering yield at room temperature is around 0.7 removed C atoms per impinging O atom [261–263]. In the energy range from 50 eV to 10 keV, the energy dependence of the total carbon sputtering yield is rather weak [56, 263–265]. The yield increases slightly with increasing energy. For energies higher than 500 eV, it is higher than 1 due to the increasing contribution of physical sputtering [56, 261, 263]. The maximum of the yield occurs at about 3 keV [56]. For energies lower than 50 eV, the yield decreases significantly.

Vietzke et al. [261] have also shown that the reactivity of thermal O_2 on graphite is enhanced by simultaneous argon ion bombardment at 5 keV. Furthermore, the ion bombardment makes the graphite surface reactive to O_2 even at room temperature. This interaction was recently also studied for a–C:H films in the low energy regime (20-800 eV) [266] using the MAJESTIX setup (see Sect. 4). While the physical sputtering yield for argon ions at 400 eV is about 0.3 (see Fig. 19), the chemical sputtering yield in the presence of molecular oxygen is about 3 removed carbon atoms per argon ion at room temperature (Fig. 28). The flux densities toward the sample surface in the experiment were approximately 4×10^{12} Ar^+ cm^{-2} s^{-1} and 1×10^{16} O_2 cm^{-2} s^{-1}. Obviously, the energy deposited by the incident ions causes reactions between oxygen and carbon. With increasing target temperature the yield increases

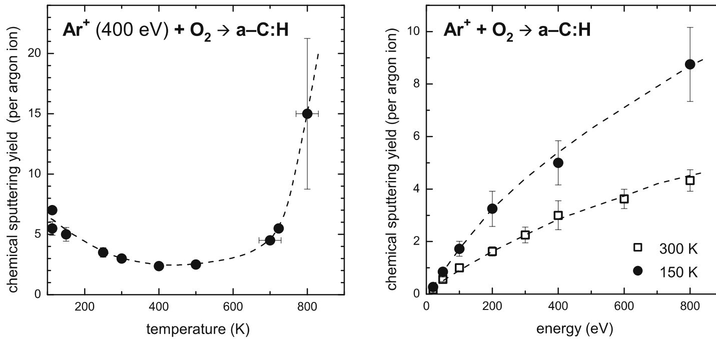

Fig. 28. Chemical sputtering of a–C:H films due to combined irradiation with Ar^+ ions and molecular oxygen as a function of temperature (at a fixed ion energy of 400 eV) and ion energy (at 150 and 300 K) [266, 267]. The *lines* are only a guide to the eye

to about 15 at 800 K due to an increasing contribution of thermally activated oxidation. Surprisingly, it also increases if the target temperature is decreased from room temperature to 110 K [266, 267]. The latter observation can tentatively be explained as follows: Oxygen adsorbs at the surface into a weakly bound state. Incident ions cause chemical reactions of the adsorbed oxygen due to local heating and damage production, which lead to the formation of carbon oxides. With increasing temperature the desorption rate of the adsorbed oxygen increases, whereby the steady-state oxygen coverage decreases and, hence, the average number of oxides formed per incident ion decreases. The right-hand side of Fig. 28 shows the energy dependence. The chemical sputtering yield increases with increasing ion energy. This can be explained by increased energy deposition and damage production at the surface with increasing ion energy.

Besides these experiments with ion beams, a number of groups investigated the erosion of carbon and carbon films using oxygen-containing low-temperature plasmas [268–271]. In addition, several studies of plasma erosion of carbon films in fusion devices were conducted [272–277]. The interpretation of such experiments is complicated by the fact that many different species – O^+, O_2^+, O_3^+ ions, O atoms, O_2, and O_3 molecules and possibly other plasma ingredients – interact simultaneously with the surface. So far, not much is known about possible synergistic interactions, but the discussed particle-beam experiments for the co-bombardment with argon ions and molecular oxygen indicate that the ion–O_2 synergism may play a significant role in these plasma-erosion experiments. All of these experiments show consistently that very high erosion yields can be achieved with oxygen-containing plasmas. In fact, for the time being this is the most effective method for removing carbon and hydrocarbon layers. Furthermore, oxygen plasmas are used in the micro-

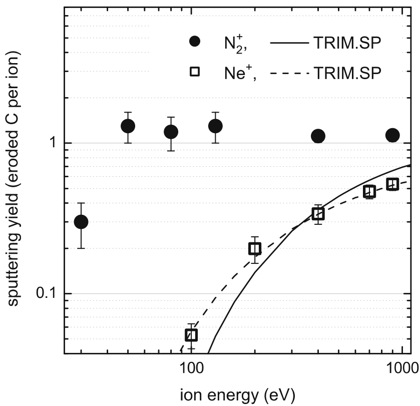

Fig. 29. Chemical sputtering of a–C:H films due to bombardment with N_2^+ compared with physical sputtering by Ne^+ ions [280] ($T = 340\,\mathrm{K}$)

electronics industry for the ashing of photoresist [278] and the patterning of polymers [279].

8.2 Nitrogen

The erosion of carbon layers due to bombardment with nitrogen ions was investigated in a few ion beam experiments [280–283]. Sputtering of plasma-deposited, tetrahedrally coordinated amorphous carbon films (ta–C, a very dense and hard form of amorphous carbon) with N_2^+ ions at an energy of 1.5 keV gave yields between 0.54 (at 450 K) and 0.75 (at 1070 K) carbon atoms per nitrogen atom [281, 282]. Furthermore, production of C_2N_2 was confirmed using a remote mass spectrometer [281, 282]. Chemical sputtering of sputter-deposited amorphous carbon layers using 150 eV N_2^+ ions [283] resulted in a sputtering yield of ~ 0.5 per N_2^+ and the formation of C_2N_2 species by mass spectrometry was also observed. At this low energy, the physical sputtering calculated by TRIM.SP is well below 10^{-2} (see [280] and Fig. 3.9 in Chap. by *Eckstein*), so that chemical sputtering is the dominant erosion mechanism. The chemical sputtering yield of a–C:H layers by N_2^+ ion bombardment in the energy range between 50 and 900 eV is nearly constant at about 1 carbon per N_2^+ ion (Fig. 29) [280]. This value agrees well with the result of *Grigull* et al. [282], who found 0.5 C per N atom (which is equivalent to 1 per N_2^+ ion) for sputtering of ta–C films.

Chemical sputtering yields of hydrocarbon films due to combined irradiation with hydrogen atoms and N_2^+ ions [284] are shown in Fig. 30 together with the data for N_2^+ ions alone. The additional flux of hydrogen atoms causes a strong increase of the chemical sputtering yield. This is the highest yield per ion observed so far for such experiments. This can be attributed to three causes: i) two nitrogen atoms at half the ion energy arrive at the surface per N_2^+ ion, ii) due to the similar mass of nitrogen and carbon the energy transfer from nitrogen to carbon is very efficient. Both causes lead to a high density

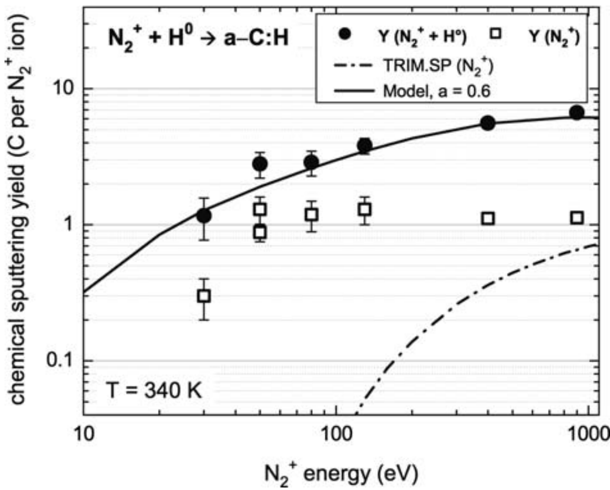

Fig. 30. Chemical sputtering of a–C:H films due to combined irradiation with hydrogen atoms and N_2^+ ions as a function of ion energy [284]. For comparison, the data for bombardment by N_2^+ ions alone are also shown. The *dash-dotted line* shows the prediction for physical sputtering due to N_2^+ ions alone, the *solid line* is the result of the chemical sputtering model with $a = 0.6$ (see (20) in Sect. 7.2)

of broken bonds at or very close to the surface. iii) nitrogen alone shows already chemical sputtering (Fig. 29). This enhances the erosion additionally as compared with noble gas ions. The yield remains relatively constant if the sample is cooled from 340 K down to 120 K [284]. This shows that at these temperatures thermal activation does not play a big role.

Besides these ion-beam experiments a number of investigations were carried out using nitrogen-containing plasmas for deposition of a–C:N:H films [285–293]. Trying to understand measured growth rates all authors came to the conclusion that chemical sputtering during deposition is an important effect. In optical emission spectroscopy and mass spectrometry investigations of the gas phase in such plasmas, C–N species, predominantly C_2N_2, were found [288–290, 292].

Deposition of thin carbon nitride films was investigated by cathodic arc evaporation of a graphite cathode under simultaneous bombardment of the growing film by a nitrogen ion beam produced with a Kaufman-type ion source [286]. A reduction of the net carbon-deposition rate as a function of the energy of the additional nitrogen ion beam and as a function of increasing substrate temperature was found. This was interpreted as an additional chemical erosion mechanism and is obviously due to chemical sputtering by nitrogen ions [280]. *Hong* and *Turban* investigated the erosion of a–C:H films in nitrogen plasmas [288]. The erosion rate increases with increasing ion energy which is in reasonable agreement with the dual beam experiments [280, 284]. They detected HCN and C_2N_2 by OES and mass spectrometry. With X-ray

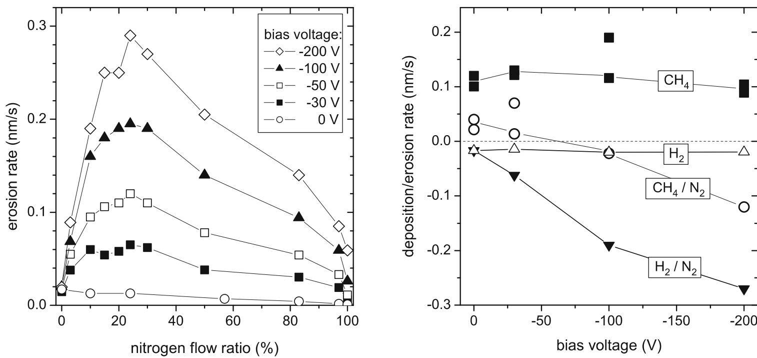

Fig. 31. Erosion and deposition of a–C:H layers in nitrogen containing plasmas. *Left-hand side:* Erosion rates of a–C:H layers in plasmas using H_2/N_2 gas mixtures as a function of the N_2 addition for different bias voltages (the bias voltage defines the ion energy). *Right-hand side:* Deposition and erosion rates of a–C:H layers in plasmas using different gas mixtures as a function of the substrate bias voltage [293]. The nitrogen admixture to H_2 and CH_4 was 30 %. *Lines* are only a guide to the eye

photoelectron spectroscopy they found the presence of 15–17 % N in the near surface region after nitrogen plasma exposure.

The deposition and erosion of a–C:H layers was investigated in low-temperature plasmas using methane and hydrogen, respectively, with varying nitrogen addition [293]. The results are shown in Fig. 31. Already small additions of nitrogen to hydrogen cause a dramatic increase of the erosion rate if the ion energy, which is in this experiment defined by the substrate bias voltage, is higher than 30 eV. The erosion rate has a distinct maximum for a nitrogen addition of about 25 % and decreases again for higher nitrogen fractions. In the whole mixture range the erosion rate is higher than in pure hydrogen or pure nitrogen plasmas. Because this effect strongly depends on the ion energy it has to be due to surface processes and cannot be explained by gas-phase reactions in the plasma. This enhancement of the erosion rate for hydrogen/nitrogen mixtures is due to the strong enhancement of the chemical sputtering yield for the combined interaction of atomic hydrogen and nitrogen ions that was observed in dual beam experiments (Fig. 30).

The right-hand side of Fig. 31 shows deposition and erosion rates of a–C:H layers in plasmas using different gas mixtures as a function of the substrate bias voltage, which is almost equivalent to the ion energy in this case. Methane (CH_4) leads to a relatively constant deposition rate of about 0.1 nm/s and hydrogen to a nearly constant erosion rate of about 0.02 nm/s in the whole investigated bias voltage range. The curve for H_2/N_2 (30 % N_2 addition) shows a monotonic increase of the erosion rate with increasing bias voltage. The CH_4/N_2 (30 % N_2 addition) mixture leads at low bias voltage to deposition which decreases with increasing bias voltage and then turns into

erosion. The slope is similar to that of the H_2/N_2 curve. This change over from deposition to erosion is caused by the increasing chemical sputtering yield with increasing bias voltage.

8.3 Fluorine

Etching of carbon layers by fluorine atoms is an important process in microelectronics. The plasma chemistry in the etching of silicon and silicon oxide is controlled in such a way that polymeric fluoro-carbon layers are deposited on the side walls of the etched features. These deposits have to be removed in the following processing step. Therefore, the related plasma-surface-interaction processes have been studied in great detail [294–299]. On the other hand, if carbon or hydrocarbon films are etched in fluorine-containing plasmas, a CF surface layer is built up at the very surface, so that the aforementioned processes are also relevant for the etching (chemical sputtering) of carbon.

References

[1] V. Kohlschütter: Jahrb. Radioakt. **9**, 355 (1912) 329
[2] A. Güntherschulze: Z. Phys. **36**, 563 (1926) 329, 330, 334, 340, 349
[3] W. Hauffe: in R. Behrisch, K. Wittmaack (Eds.): *Sputtering by Particle Bombardment III*, Top. Appl. Phys. **64** (Springer, Berlin, Heidelberg 1991) russ. translation: (MIR, Moscow 1998) 330
[4] J. W. Coburn, H. F. Winters: J. Vac. Sci. Technol. **16**, 391 (1979) 330
[5] H. F. Winters, J. W. Coburn: Appl. Phys. Lett. **34**, 70 (1979) 330
[6] J. Winter: J. Nucl. Mater. **161**, 265 (1989) 330, 354
[7] J. Roth, J. Bohdansky, W. Poschenrieder, M. K. Sinha: J. Nucl. Mater. **63**, 222 (1976) 330, 349, 350
[8] S. K. Erents, C. M. Braganza, G. M. McCracken: J. Nucl. Mater. **63**, 399 (1976) 330, 344, 349, 350, 360
[9] N. P. Busharov, E. A. Gorbatov, V. M. Gusev, M. I. Guseva, Y. V. Martynenko: J. Nucl. Mater. **63**, 230 (1976) 330, 344, 349, 350
[10] M. Balooch, D. R. Olander: J. Chem. Phys. **63**, 4772 (1975) 330, 342, 369
[11] L. Zielinski, G. C. Schwartz: in , Electrochem. Soc. Abstracts **75** (1975) p. 117 330, 332
[12] M. Armacost, P. D. Hoh, R. Wise, W. Yan, J. J. Brown, J. H. Keller, G. A. Kaplita, S. D. Halle, K. P. Muller, M. D. Naeem, S. Srinivasan, H. Y. Ng, M. Gutsche, A. Gutmann, B. Spuler: IBM J. Res. Dev. **43**, 39 (1999) 330, 331, 332
[13] J. P. Chang, J. W. Coburn: J. Vac. Sci. Technol. **21**, 145 (2003) 330, 332
[14] T. A. Burtseva, O. K. Chugunov, E. F. Dovguchits, V. L. Komarov, I. V. Mazul, A. A. Mitrofansky, M. I. Persin, Y. G. Prokofiev, V. A. Sokolov, E. I. Trofimchuk, L. P. Zav'jalsky: J. Nucl. Mater. **191–194**, 309 (1992) 330
[15] C. García-Rosales, W. Eckstein, J. Roth: J. Nucl. Mater. **218**, 8 (1994) 330

[16] E. Vietzke, A. A. Haasz: in W. O. Hofer, J. Roth (Eds.): *Physical Processes of the Interaction of Fusion Plasmas with Solids* (Academic, New York 1996) p. 135 330, 342, 349, 350
[17] C. García-Rosales, M. Balden: J. Nucl. Mater. **290**–**291**, 173 (2001) 330, 365
[18] E. de Juan Pardo, M. Balden, B. Cieciwa, C. García-Rosales, J. Roth: Phys. Scripta **T111**, 62 (2005) 330, 353, 358, 365
[19] M. Balden, C. Adelhelm, E. de Juan Pardo, J. Roth: J. Nucl. Mater. **363**–**365**, 1173 (2007) 330, 336, 358, 365
[20] P. Sigmund, A. Gras-Marti: Nucl. Instrum. Meth. **168**, 389 (1980) 331
[21] A. Gras-Marti, P. Sigmund: in P. Varga, G. Betz, E. P. Viehböck (Eds.): *Proc. Symp. on Sputtering (SOS)* (Techn. Univ. Wien, Vienna 1980) p. 512 331
[22] U. Littmark, W. O. Hofer: Nucl. Instrum. Meth. **168**, 329 (1980) 331
[23] K. Schmid, J. Roth, W. Eckstein: J. Nucl. Mater. **290**–**293**, 148 (2001) 331
[24] K. Schmid, J. Roth: J. Nucl. Mater. **302**, 96 (2002) 331
[25] O. Almén, G. Bruce: Nucl. Instrum. Meth. **11**, 279 (1961) 331, 333
[26] R. A. Zuhr, J. Roth, W. Eckstein, von Toussaint, U., J. Luthin: J. Nucl. Mater. **290**–**293**, 162 (2001) 331
[27] K. Schmid, J. Roth: Surf. Coat. Technol. **158**, 81 (2002) 331
[28] K. Schmid, J. Roth: J. Nucl. Mater. **313**–**316**, 302 (2003) 331
[29] C. Linsmeier, J. Roth, K. Schmid: Atomic and Plasma-Material Interaction Data for Fusion **12**, 79 (2003) 331
[30] K. Schmid, M. Baldwin, R. Doerner: J. Nucl. Mater. **337**–**339**, 862 (2005) 331
[31] M. J. Baldwin, R. P. Doerner, D. Nishijima, K. Schmid, D. G. Whyte, J. G. Kulpin, G. Wright: J. Nucl. Mater. **358**, 96 (2006) 331
[32] W. D. Sproul, D. J. Christie, D. C. Carter: Thin Solid Films **491**, 1 (2005) 331
[33] D. M. Manos, D. L. Flamm (Eds.): *Plasma Etching: An Introduction* (Academic, San Diego 1989) 331, 332
[34] O. Auciello, D. E. Ibbotson, D. L. Flamm: Nucl. Instrum. Meth. B **23**, 419 (1987) 332
[35] H. F. Winters, J. W. Coburn: Surf. Sci. Rep. **14**, 161 (1992) 332, 333, 341
[36] J. Roth: in R. Behrisch (Ed.): *Sputtering by Particle Bombardment II*, Top. Appl. Phys. **52** (Springer, Berlin, Heidelberg 1981) p. 91, russ. translation: (MIR, Moscow 1986) 332, 348
[37] J. W. Davis, A. A. Haasz: Appl. Phys. Lett. **57**, 1976 (1990) 332, 361
[38] W. Jacob: Thin Solid Films **326**, 1 (1998) 332, 339, 354, 377
[39] J. W. Coburn, H. F. Winters: J. Appl. Phys. **50**, 3189 (1979) 332
[40] E. P. Vaulin, N. E. Georgieva, T. P. Martynenko, L. V. Feoktistov: Sov. J. Plasma Phys. **7**, 23 (1981) 333
[41] R. P. Doerner, S. I. Krasheninnikov, K. Schmid: J. Appl. Phys. **95**, 4471 (2004) 333
[42] K. Schmid, M. Baldwin, R. Doerner: J. Nucl. Mater. **348**, 294 (2006) 333
[43] J. Roth: J. Nucl. Mater. **103**, 291 (1982) 334
[44] J. Roth, J. Bohdansky, K. L. Wilson: J. Nucl. Mater. **111**–**112**, 775 (1982) 334, 350, 351, 355, 369, 383
[45] V. Philipps, K. Flaskamp, E. Vietzke: J. Nucl. Mater. **111**–**112**, 781 (1982) 334
[46] J. Roth, W. Möller: Nucl. Instrum. Meth. B **7**–**8**, 788 (1985) 334

[47] E. Vietzke: J. Nucl. Mater. **290–293**, 158 (2001) 334, 340, 341, 379
[48] E. Salonen, K. Nordlund, J. Keinonen, C. Wu: Europhys. Lett. **52**, 504 (2000) 334, 377, 378, 379
[49] E. Salonen, K. Nordlund, J. Keinonen, C. Wu: Phys. Rev. B **63**, 195415 (2001) 334, 373, 377, 378, 379, 380, 382
[50] E. Salonen, K. Nordlund, J. Keinonen, C. Wu: J. Nucl. Mater. **290–293**, 144 (2001) 334, 377, 379
[51] K. Nordlund, E. Salonen, J. Keinonen, C. Wu: Nucl. Instrum. Meth. B **180**, 77 (2001) 334, 377, 378
[52] A. Krasheninnikov, E. Salonen, K. Nordlund, J. Keinonen, C. Wu: Contrib. Plasma Phys. **42**, 451 (2002) 334, 377, 378, 379
[53] A. Krasheninnikov, K. Nordlund, E. Salonen, J. Keinonen, C. Wu: Computational Mater. Sci. **25**, 427 (2002) 334, 377, 378, 379
[54] K. Nordlund: Nucl. Instrum. Meth. B **218**, 9 (2004) 334, 377, 378
[55] J. Roth, J. Bohdansky, A. P. Martinelli: Radiat. Eff. Def. Sol. **48**, 213 (1980) 335
[56] E. Hechtl, J. Bohdansky, J. Roth: J. Nucl. Mater. **103**, 333 (1981) 335, 384
[57] G. Sauerbrey: Zeitschrift für Physik **155**, 206 (1959) 335
[58] M. C. Chuang, J. W. Coburn: J. Vac. Sci. Technol. A **8**, 1969 (1990) 335
[59] G. Hayderer, M. Schmid, P. Varga, H. Winter, F. Aumayr: Rev. Sci. Instrum. **70**, 3696 (1999) 335
[60] J. Bohdansky, J. Roth, M. K. Sinha, W. Ottenberger: J. Nucl. Mater. **63**, 115 (1976) 335
[61] H. L. Bay, J. Roth, J. Bohdansky: J. Appl. Phys. **48**, 4722 (1977) 335
[62] R. Behrisch, J. Roth, J. Bohdansky, A. Martinelli, B. Schweer, D. Rusbüldt, E. Hintz: J. Nucl. Mater. **93–94**, 645 (1980) 335
[63] A. A. Haasz, P. C. Stangeby, O. Auciello: J. Nucl. Mater. **111–112**, 757 (1982) 335, 342, 360
[64] O. Auciello, A. A. Haasz, P. C. Stangeby: Phys. Rev. Lett. **50**, 783 (1983) 335, 342, 360
[65] P. C. Stangeby, O. Auciello, A. A. Haasz: J. Vac. Sci. Technol. A **1**, 1425 (1983) 335, 342
[66] J. Roth, C. Hopf: J. Nucl. Mater. **334**, 97 (2004) 335, 340, 359
[67] A. Nerken, L. C. Beavis, K. Bhagwan Das, R. Grande, D. H. Holekeboer, J. E. McRea, D. Patterson, E. Stroebelt, P. Varadi: J. Vac. Sci. Technol. **9**, 1260 (1972) 336
[68] J. A. Basford, M. D. Boeckmann, R. E. Ellefson: J. Vac. Sci. Technol. A **11**, 22 (1993) 336
[69] D. J. Dagel, C. M. Mallouris, J. R. Doyle: J. Appl. Phys. **79**, 8735 (1996) 336
[70] R. Dobrozemsky: J. Vac. Sci. Technol. **9**, 220 (1972) 336
[71] T. Schwarz-Selinger, R. Preuss, V. Dose, W. Linden: J. Mass Spectrom. **36**, 866 (2001) 336
[72] H. D. Kang, R. Preuss, T. Schwarz-Selinger, V. Dose: J. Mass Spectrom. **37**, 748 (2002) 336
[73] von Toussaint, U., V. Dose, A. Golan: J. Vac. Sci. Technol. A **56**, 401 (2004) 336
[74] T. Zecho, B. D. Brandner, J. Biener, J. Küppers: J. Phys. Chem. B **105**, 6194 (2001) 336, 342, 347, 348

[75] T. Zecho, B. D. Brandner, J. Biener, J. Küppers: J. Phys. Chem. B **106**, 610 (2002) 336, 342, 347
[76] V. Philipps, E. Vietzke, M. Erdweg, A. Flaskamp: J. Nucl. Mater. **145–147**, 292 (1987) 336, 342, 350, 354
[77] E. Vietzke, K. Flaskamp, V. Philipps: J. Nucl. Mater. **111–112**, 763 (1982) 336, 338, 340, 342, 345, 346, 359, 360, 361, 363, 374
[78] E. Vietzke, V. Philipps, K. Flaskamp, C. Wild: in P. Koidl, P. Oelhafen (Eds.): *Amorphous hydrogenated carbon films* (Les Éditions de Physique, Les Ulis 1987) 336, 342, 347, 354, 370, 374
[79] E. Vietzke, V. Philipps, K. Flaskamp: J. Nucl. Mater. **162–164**, 898 (1989) 336, 345, 350, 360, 361, 374
[80] J. Roth: J. Nucl. Mater. **266–269**, 51 (1999) 336, 346, 355, 356, 359, 364, 372, 373
[81] M. Balden, J. Roth: J. Nucl. Mater. **280**, 39 (2000) 336, 350, 353, 356, 359, 363, 373, 375, 376, 380, 381, 382
[82] T. Schwarz-Selinger: to be published 337
[83] W. Walcher: Z. Physik **122**, 62 (1944) 337
[84] J. Benedikt, S. Agarwal, D. J. Eijkman, W. Vandamme, M. Creatore, M. C. M. van de Sanden: J. Vac. Sci. Technol. A **23**, 1400 (2005) 338
[85] E. Vietzke, K. Flaskamp, V. Philipps: J. Nucl. Mater. **128–129**, 545 (1984) 338, 342, 345, 346, 350, 354, 359, 360, 361, 363, 369
[86] R. M. A. Azzam, N. M. Bashara: *Ellipsometry and Polarized Light* (Elsevier, Amsterdam 1977) 339
[87] R. W. Collins: Materials Science Forum **52/53**, 341 (1989) 339
[88] A. von Keudell, W. Jacob, W. Fukarek: Appl. Phys. Lett. **66**, 1322 (1995) 339
[89] A. von Keudell, W. Jacob: J. Appl. Phys. **79**, 1092 (1996) 339, 376
[90] A. von Keudell, W. Jacob: J. Appl. Phys. **81**, 1531 (1997) 339
[91] A. Kallenbach, A. Thoma, A. Bard, K. H. Behringer, K. Schmidtmann, M. Weinlich, ASDEX Upgrade Team: Nucl. Fusion **38**, 1097 (1998) 339, 373
[92] A. Kallenbach, A. Bard, A. Carlson, R. Dux, the ASDEX Upgrade Team: Phys. Scripta **T81**, 43 (1999) 339
[93] M. F. Stamp, S. K. Erents, W. Fundamenski, G. F. Matthews, R. D. Monk: Phys. Scripta **T91**, 13 (2001) 339, 340, 355, 356
[94] M. F. Stamp, S. K. Erents, W. Fundamenski, G. F. Matthews, R. D. Monk: J. Nucl. Mater. **290–293**, 321 (2001) 339
[95] D. G. Whyte, W. P. West, C. P. C. Wong, R. Bastasz, J. N. Brooks, W. R. Wampler, N. H. Brooks, J. W. Davis, R. P. Doerner, A. A. Haasz, R. C. Isler, G. L. Jackson, R. G. Macaulay-Newcombe, M. R. Wade: Nucl. Fusion **41**, 1243 (2001) 339, 340
[96] S. Brezinsek, P. T. Greenland, P. Mertens, A. Pospieszczyk, D. Reiter, U. Samm, B. Schweer, G. Sergienko: J. Nucl. Mater. **313–316**, 967 (2003) 339
[97] S. Brezinsek, P. Mertens, A. Pospieszczyk, G. Sergienko, U. Samm: Phys. Scr. **T103**, 51 (2003) 339
[98] S. Brezinsek, A. Huber, S. Jachmich, A. Pospieszczyk, B. Schweer, G. Sergienko: Fusion Sci. Technol. **47**, 209 (2005) 339

[99] S. Brezinsek, A. Pospieszczyk, M. F. Stamp, A. Meigs, A. Kirschner, A. Huber, P. Mertens: J. Nucl. Mater. **337–339**, 1058 (2005) 339
[100] S. Brezinsek, G. Sergienko, A. Pospieszczyk, P. Mertens, U. Samm, P. T. Greenland: Plasma Phys. Contr. Fusion **47**, 615 (2005) 339
[101] M. F. Stamp, P. Andrew, S. Brezinsek, A. Huber: J. Nucl. Mater. **337–339**, 1038 (2005) 339
[102] R. Pugno, K. Krieger, A. Kirschner, A. Kallenbach, D. Coster, R. Dux, U. Fantz, J. Likonen, H. W. Müller, J. Neuhauser, V. Rohde, E. Vainonen-Ahlgren, ASDEX Upgrade Team: J. Nucl. Mater. **337–339**, 985 (2005) 339, 355, 356
[103] U. Fantz, S. Meir, ASDEX Upgrade Team: J. Nucl. Mater. **337–339**, 1087 (2005) 339
[104] D. Whyte, G. Tynan, R. Doerner, J. Brooks: Nucl. Fusion **41**, 47 (2001) 339, 340, 355, 356, 373
[105] H. Grote, W. Bohmeyer, P. Kornejew, H. D. Reiner, G. Fussmann, R. Schlögl, G. Weinberg, C. H. Wu: J. Nucl. Mater. **266–269**, 1059 (1999) 339, 355, 356
[106] U. Fantz, H. Paulin: Phys. Scr. **T91**, 25 (2001) 339, 373
[107] U. Fantz: Contrib. Plasma Phys. **44**, 508 (2004) 339
[108] U. Fantz: *Nuclear Fusion Research – Understanding Plasma–Surface Interaction*, Springer Ser. Chem. Phys. (Springer, Berlin, Heidelberg 2005) p. 99 339
[109] P. Starke, U. Fantz, M. Balden: J. Nucl. Mater. **337–339**, 1005 (2005) 339
[110] K. Behringer, H. P. Summers, B. Denne, M. Forrest, M. Stamp: Plasma Phys. Contr. Fusion **31**, 2059 (1989) 339
[111] A. Pospieszczyk, Y. Ra, Y. Hirooka, R. W. Conn, D. M. Goebel, B. LaBombard, R. E. Nygren: *Spectroscopic Studies of Carbon Containing Molecules and their Break-up in Pisces-A*, Technical report, UCLA Report PPG-1251 (1989) 339
[112] S. Brezinsek, A. Pospieszczyk, A. Kirschner, G. Sergienko, A. Huber, V. Philipps, P. Mertens, U. Samm, M. F. Stamp, A. Meigs, P. T. Greenland, JET-EFDA contributors: Phys. Scr. **T111**, 42 (2004) 340
[113] V. Philipps, M. Stamp, A. Pospieszczyk, A. Huber, A. Kirschner, E. Vietzke: J. Nucl. Mater. **313–316**, 354 (2003) 340
[114] J. Perrin, Y. Takeda, N. Hirano, Y. Takeuchi, A. Matsuda: Surf. Sci. **210**, 114 (1989) 340
[115] A. Matsuda, K. Nomoto, Y. Takeuchi, A. Suzuki, Y. Yuuki, J. Perrin: Surf. Sci. **227**, 50 (1990) 340
[116] D. A. Doughty, J. R. Doyle, G. H. Lin, A. Gallagher: J. Appl. Phys. **67**, 6220 (1990) 340
[117] A. Nuruddin, J. R. Doyle, J. R. Abelson: J. Appl. Phys. **76**, 3123 (1994) 340
[118] C. Hopf, K. Letourneur, W. Jacob, T. Schwarz-Selinger, A. von Keudell: Appl. Phys. Lett. **74**, 3800 (1999) 340
[119] C. Hopf, T. Schwarz-Selinger, W. Jacob, A. von Keudell: J. Appl. Phys. **87**, 2719 (2000) 340
[120] W. Jacob, C. Hopf, A. von Keudell, T. Schwarz-Selinger: in C. H. W. and (Ed.): *Hydrogen Recycling at Plasma Facing Materials* (Kluwer, Dordrecht 2000) p. 331 340
[121] E. Vietzke, K. Flaskamp, M. Hennes, V. Philipps: Nucl. Instrum. Meth. B **2**, 617 (1984) 340

[122] A. A. Haasz, J. W. Davis: Nucl. Instrum. Meth. B **83**, 117 (1993) 341
[123] J. W. Davis, A. A. Haasz, C. H. Wu: J. Nucl. Mater. **196–198**, 581 (1992) 341
[124] S. Chiu, A. A. Haasz, P. Franzen: J. Nucl. Mater. **218**, 319 (1995) 341, 369, 382, 383
[125] A. Haasz, S. Chiu, P. Franzen: J. Nucl. Mater. **220–222**, 815 (1995) 341, 354, 369, 382, 383
[126] S. Chiu, A. A. Haasz: J. Nucl. Mater. **196–198**, 972 (1992) 341, 354, 369
[127] S. Chiu, A. A. Haasz: J. Nucl. Mater. **208**, 282 (1994) 341, 354, 369
[128] S. Chiu, A. A. Haasz: J. Nucl. Mater. **210**, 34 (1994) 341
[129] A. A. Haasz, A. Y. K. Chen, J. W. Davis, E. Vietzke: J. Nucl. Mater. **248**, 19 (1997) 341
[130] A. Y. K. Chen, J. W. Davis, A. A. Haasz: J. Nucl. Mater. **266–269**, 399 (1999) 341
[131] A. Y. K. Chen, J. W. Davis, A. A. Haasz: J. Nucl. Mater. **290–293**, 61 (2002) 341
[132] A. Y. K. Chen, J. W. Davis, A. A. Haasz: J. Nucl. Mater. **312**, 16 (2003) 341
[133] A. Y. K. Chen, A. A. Haasz, J. W. Davis: J. Appl. Phys. **94**, 1617 (2003) 341
[134] R. G. Macaulay-Newcombe, A. A. Haasz, C. H. Wu, J. W. Davis: J. Nucl. Mater. **327**, 114 (2004) 341
[135] A. von Keudell, T. Schwarz-Selinger, W. Jacob: J. Appl. Phys. **89**, 2979 (2001) 341
[136] A. von Keudell: Thin Solid Films **402**, 1 (2002) 341
[137] A. von Keudell, W. Jacob: Prog. Surf. Sci. **76**, 21 (2004) 341
[138] M. Meier, A. von Keudell: J. Appl. Phys. **90**, 3585 (2001) 341
[139] M. Meier, A. von Keudell: J. Chem. Phys. **116**, 5125 (2002) 341
[140] C. Hopf, A. von Keudell, W. Jacob: J. Appl. Phys. **93**, 3352 (2003) 341
[141] C. Hopf, A. von Keudell, W. Jacob: J. Appl. Phys. **94**, 2373 (2003) 341, 361, 363, 374, 375, 376, 377, 380, 383
[142] C. Hopf, W. Jacob, A. von Keudell: J. Appl. Phys. **97**, 094904–1 (2005) 341, 361, 375
[143] W. Jacob, C. Hopf, A. von Keudell, M. Meier, T. Schwarz-Selinger: Rev. Sci. Instrum. **74**, 5123 (2003) 341
[144] T. Schwarz-Selinger, A. von Keudell, W. Jacob: J. Vac. Sci. Technol. A **18**, 995 (2000) 342
[145] T. Schwarz-Selinger, V. Dose, W. Jacob, A. von Keudell: J. Vac. Sci. Technol. A **19**, 101 (2001) 342
[146] C. S. Pitcher, O. Auciello, A. A. Haasz, P. C. Stangeby: J. Nucl. Mater. **128–129**, 597 (1984) 342
[147] A. A. Haasz, O. Auciello, P. C. Stangeby: J. Vac. Sci. Technol. A **4**, 1179 (1986) 342
[148] E. Vietzke, K. Flaskamp, V. Philipps, G. Esser, P. Wienhold, J. Winter: J. Nucl. Mater. **145–147**, 443 (1987) 342, 347, 350, 354, 370, 374
[149] A. Schenk, J. Biener, B. Winter, C. Lutterloh, U. Schubert, J. Küppers: Appl. Phys. Lett. **61**, 2414 (1992) 342
[150] J. Biener, U. Schubert, A. Schenk, B. Winter, C. Lutterloh, J. Küppers: Advan. Mater. **5**, 639 (1993) 342
[151] J. Biener, U. Schubert, A. Schenk, B. Winter, C. Lutterloh, J. Küppers: J. Chem. Phys. **99**, 3125 (1993) 342, 344

[152] J. Biener, A. Schenk, B. Winter, J. Küppers: J. Electr. Spectr. Rel. Phen. **64/65**, 331 (1993) 342
[153] J. Biener, A. Schenk, B. Winter, U. Schubert, C. Lutterloh, J. Küppers: Phys. Rev. B **49**, 17307 (1994) 342
[154] J. Biener, A. Schenk, B. Winter, C. Lutterloh, U. Schubert, J. Küppers: Surf. Sci. **307–309**, 228 (1994) 342
[155] A. Horn, A. Schenk, J. Biener, B. Winter, C. Lutterloh, M. Wittmann, J. Küppers: Chem. Phys. Lett. **231**, 193 (1994) 342, 343, 344, 345, 346, 369, 373, 380
[156] A. Schenk, B. Winter, J. Biener, C. Lutterloh, U. Schubert, J. Küppers: J. Appl. Phys. **77**, 2462 (1995) 342, 344
[157] J. Küppers: Surf. Sci. Rep. **22**, 249 (1995) 342, 343, 345, 346, 369, 371, 373
[158] M. Wittmann, J. Küppers: J. Nucl. Mater. **227**, 186 (1996) 342, 371
[159] J. Roth, C. García-Rosales: Nucl. Fusion **36**, 1647 (1996) see also corrigendum by J. Roth, C. García-Rosales: Nucl. Fusion **37**, 897 (1997). 344, 350, 353, 355, 369, 370, 372, 373, 380
[160] V. Philipps, K. Flaskamp, E. Vietzke: J. Nucl. Mater. **122–123**, 1440 (1984) 345, 346, 350, 354, 364
[161] J. W. Davis, A. A. Haasz, P. C. Stangeby: J. Nucl. Mater. **155–157**, 234 (1988) 346, 347, 356, 357, 361, 362, 363
[162] E. Vietzke, V. Philipps, K. Flaskamp, P. Koidl, C. Wild: Surf. Coat. Technol. **47**, 156 (1991) 347, 354, 370
[163] O. Auciello, A. A. Haasz, P. C. Stangeby: Radiat. Eff. **89**, 63 (1985) 348
[164] J. Roth, E. Vietzke, A. A. Haasz: in *Atomic and Plasma-Material Interaction Data for Fusion*, Suppl. Nucl. Fusion **1** (1991) p. 63 349, 350
[165] C. M. Braganza, S. K. Erents, G. M. McCracken: J. Nucl. Mater. **75**, 209 (1978) 349, 350
[166] R. Yamada, K. Nakamura, K. Sone, M. Saidoh: J. Nucl. Mater. **95**, 278 (1980) 350, 351, 352, 354, 370
[167] E. Vietzke, V. Philipps: Nucl. Instrum. Meth. B **23**, 449 (1987) 350, 354
[168] J. W. Davis, A. A. Haasz: J. Nucl. Mater. **149**, 349 (1987) 350, 354, 370, 374
[169] A. A. Haasz, J. W. Davis: J. Nucl. Mater. **175**, 84 (1990) 350, 354, 356, 357, 358
[170] J. W. Davis, A. A. Haasz, P. C. Stangeby: J. Nucl. Mater. **145–147**, 417 (1987) 350, 351, 352, 355
[171] R. Yamada, K. Sone: J. Nucl. Mater. **116**, 200 (1983) 350
[172] R. Yamada: J. Nucl. Mater. **145–147**, 359 (1987) 350, 356, 357, 358
[173] J. Roth, J. Bohdansky: Nucl. Instrum. Meth. B **23**, 549 (1987) 350, 367, 368
[174] A. A. Haasz, B. V. Mech, J. D. Davis: J. Nucl. Mater. **231**, 170 (1996) 350
[175] B. V. Mech, A. A. Haasz, J. W. Davis: J. Nucl. Mater. **241–243**, 1147 (1997) 350, 351, 356, 358
[176] B. V. Mech, A. A. Haasz, J. W. Davis: J. Nucl. Mater. **255**, 153 (1998) 350, 351, 356, 358, 359, 370, 373
[177] L. I. Vergara, F. W. Meyer, H. F. Krause: J. Nucl. Mater. **347**, 118 (2005) 350, 366, 380, 383
[178] F. W. Meyer, H. F. Krause, L. I. Vergara: J. Nucl. Mater. **337–339**, 922 (2005) 350, 366, 380, 383
[179] F. W. Meyer, L. I. Vergara, H. F. Krause: Phys. Scr. **T124**, 44 (2006) 350, 366, 379, 380, 383

[180] L. I. Vergara, F. W. Meyer, H. F. Krause, P. Träskelin, K. Nordlund, E. Salonen: J. Nucl. Mater. **357**, 9 (2006) 350, 366, 378, 379, 380, 383
[181] M. Küstner, W. Eckstein, V. Dose, J. Roth: Nucl. Instrum. Meth. B **145**, 320 (1998) 353
[182] M. Balden, de Juan Pardo, E., I. Quintana, B. Cieciwa, J. Roth: J. Nucl. Mater. **337**–**339**, 980 (2005) 353, 358, 365
[183] E. Vietzke, V. Philipps: Fusion Technol. **15**, 108 (1989) 354, 356
[184] B. M. U. Scherzer, R. Behrisch, W. Eckstein, U. Littmark, J. Roth, M. K. Sinha: J. Nucl. Mater. **63**, 100 (1976) 354
[185] G. Staudenmaier, J. Roth, R. Behrisch, J. Bohdansky, W. Eckstein, P. Staib, S. Matteson, S. K. Erents: J. Nucl. Mater. **84**, 149 (1979) 354
[186] J. Roth, B. M. U. Scherzer, R. S. Blewer, D. K. Brice, S. T. Picraux, W. R. Wampler: J. Nucl. Mater. **93**–**94**, 601 (1980) 354
[187] W. R. Wampler, D. K. Brice, C. W. Magee: J. Nucl. Mater. **102**, 304 (1981) 354
[188] B. M. U. Scherzer, R. A. Langley, W. Möller, J. Roth, R. Schulz: Nucl. Instrum. Meth. **194**, 497 (1982) 354
[189] M. Braun, B. Emmoth: J. Nucl. Mater. **128**–**129**, 657 (1984) 354
[190] W. Möller, B. M. U. Scherzer: Appl. Phys. Lett. **50**, 1870 (1987) 354, 375
[191] B. M. U. Scherzer, M. Wielunski, W. Möller, A. Turos, J. Roth: Nucl. Instrum. Meth. B **33**, 714 (1988) 354
[192] W. Möller, B. M. U. Scherzer: J. Appl. Phys. **64**, 4860 (1988) 354
[193] W. Möller: J. Nucl. Mater. **162**–**164**, 138 (1989) 354
[194] B. L. Doyle, P. S. Peercy: Appl. Phys. Lett. **34**, 811 (1979) 354
[195] J. Roth, J. Bohdansky: Appl. Phys. Lett. **51**, 964 (1987) 354, 369
[196] J. Roth, R. A. Zuhr, S. P. Withrow, W. P. Eatherly: J. Appl. Phys. **63**, 2603 (1988) 354
[197] K. Niwase, M. Sugimoto, T. Tanabe, F. E. Fujita: J. Nucl. Mater. **155**–**157**, 303 (1988) 354
[198] R. Siegele, J. Roth, B. M. U. Scherzer, S. J. Pennycook: J. Appl. Phys. **73**, 2225 (1993) 354
[199] T. Schwarz-Selinger, A. von Keudell, W. Jacob: J. Appl. Phys. **86**, 3988 (1999) 354
[200] J. Winter, H. G. Esser, P. Wienhold, V. Philipps, E. Vietzke, K. H. Besocke, W. Möller, B. Emmoth: Nucl. Instrum. Meth. B **23**, 538 (1987) 354
[201] B. Lersmacher, H. Lydtin, W. F. Knippenberg, A. W. Moore: Carbon **5**, 205 (1967) 355
[202] J. Roth: in R. K. Janev, H. W. Drawin (Eds.): *Atomic and Plasma-Material Interaction Processes in Controlled Thermonuclear Fusion* (Elsevier, Amsterdam 1993) p. 381 355
[203] C. S. Pitcher, G. M. McCracken, D. H. J. Goodall, A. A. Haasz, G. F. Matthews, P. C. Stangeby: Nucl. Fusion **26**, 1641 (1986) 355
[204] P. Kornejew, W. Bohmeyer, H. D. Reiner: Phys. Scr. **T81**, 40 (1990) 355, 356
[205] R. Ruggiéri, E. Gauthier, J. Hogan, J. M. Layet, T. Loarer: J. Nucl. Mater. **266**–**269**, 660 (1999) 355, 356
[206] A. Cambe, E. Gauthier, J. Hogan, J. M. Layet: J. Nucl. Mater. **313**–**316**, 364 (2003) 355, 356

[207] A. Pospiescczyk, V. Philipps, A. Huber, A. Kirschner, B. Schweer, E. Vietzke: Phys. Scr. **T81**, 48 (1999) 355, 356
[208] A. Kallenbach, A. Bard, D. Coster, R. Dux, C. Fuchs, J. Gafert, A. Herrmann, R. Schneider, ASDEX Upgrade Team: J. Nucl. Mater. **266–269**, 343 (1999) 355
[209] T. Nakano, H. Kubo, S. Higashijima, N. Asakura, H. Takenaga, T. Sugie, K. Itami: Nucl. Fusion **42**, 689 (2002) 355, 356
[210] J. Roth, R. Preuss, W. Bohmeyer, S. Brezinsek, A. Cambe, E. Casarotto, R. Doerner, E. Gauthier, G. Federici, S. Higashijima, J. Hogan, A. Kallenbach, A. Kirschner, H. Kubo, J. Layet, T. Nakano, V. Philipps, A. Pospieszczyk, R. Pugno, R. Ruggieri, B. Schweer, G. Sergienko, M. Stamp: Nucl. Fusion **44**, L21 (2004) 355, 356
[211] V. Dose: Rep. Prog. Phys. **66**, 1421 (2003) 356
[212] V. Dose, R. Preuss, J. Roth: J. Nucl. Mater. **288**, 153 (2001) 356
[213] R. Yamada: J. Vac. Sci. Technol. A **5**, 305 (1987) 356, 357
[214] R. Yamada: J. Nucl. Mater. **174**, 118 (1990) 358
[215] A. A. Haasz, O. Auciello, P. C. Stangeby, I. S. Youle: J. Nucl. Mater. **128–129**, 593 (1984) 361, 363
[216] A. A. Haasz, J. W. Davis, O. Auciello, P. Stangeby, E. Vietzke, K. Flaskamp, V. Philipps: J. Nucl. Mater. **145–147**, 412 (1987) 361, 363
[217] C. Hopf, A. von Keudell, W. Jacob: Nucl. Fusion **42**, L27 (2002) 361, 375, 377
[218] W. Jacob, C. Hopf, M. Meier, T. Schwarz-Selinger: in *Nuclear Fusion Research – Understanding Plasma–Surface Interaction*, 1st ed., Springer Ser. Chem. Phys. (Springer, Berlin, Heidelberg 2005) p. 249 361, 375
[219] W. Jacob, C. Hopf, M. Schlüter: Phys. Scr. **T124**, 32 (2006) 361, 363, 375
[220] W. Eckstein: *Computer Simulation of Ion Solid Interactions*, Springer Ser. Mater. Sci. (Springer, Berlin, Heidelberg 1991) russ. translation: (MIR, Moscow 1995) 362, 363, 375
[221] J. Roth, J. Bohdansky, J. B. Roberto: J. Nucl. Mater. **128–129**, 534 (1984) 364
[222] J. Roth, C. García-Rosales, R. Behrisch, W. Eckstein: J. Nucl. Mater. **191**, 45 (1992) 364
[223] R. Schwörer, H. Plank, J. Roth: J. Nucl. Mater. **241–243**, 1156 (1997) 364
[224] V. K. Alimov, R. Schwörer, B. M. U. Scherzer, J. Roth: J. Nucl. Mater. **187**, 191 (1992) 364
[225] R. Schwörer, J. Roth: J. Appl. Phys. **77**, 3812 (1995) 364
[226] C. García-Rosales, J. Roth: J. Nucl. Mater. **196–198**, 573 (1992) 364, 365
[227] C. García-Rosales, J. Roth, R. Behrisch: J. Nucl. Mater. **212–215**, 1211 (1994) 365
[228] M. Balden, C. García-Rosales, R. Behrisch, J. Roth, P. Paz, J. Etxeberria: J. Nucl. Mater. **290–293**, 52 (2001) 365
[229] Y. Yao, Z. Hargitai, M. Albert, R. G. Albridge, A. V. Barnes, J. M. Gilligan, B. P. Ferguson, G. Lüpke, V. D. Gordon, N. H. Tolk, J. C. Tully, G. Betz, W. Husinsky: Phys. Rev. Lett. **81**, 550 (1998) 366
[230] R. K. Gould: J. Chem. Phys. **63**, 1825 (1975) 369
[231] M. Balden, J. Roth, E. D. Pardo, A. Wiltner: J. Nucl. Mater. **313–316**, 348 (2003) 369, 383

[232] T. Zecho, A. Güttler, X. Sha, B. Jackson, J. Küppers: J. Chem. Phys. **117**, 8486 (2002) 369
[233] B. V. Mech, A. A. Haasz, J. W. Davis: J. Appl. Phys. **84**, 1655 (1998) 370
[234] J. Bohdansky, J. Roth, H. Bay: J. Appl. Phys. **51**, 2861 (1980) 371
[235] J. Roth: Phys. Scr. **T124**, 37 (2005) 373
[236] C. Hopf, W. Jacob: J. Nucl. Mater. **342**, 141 (2005) 374, 375, 376
[237] E. Ghio, L. Mattera, C. Salvo, F. Tommasini, U. Valbusa: J. Chem. Phys. **73**, 556 (1980) 375
[238] J. Pillath, J. Winter, F. Waelbroek: in P. Koidl, P. Oelhafen (Eds.): *Amorphous hydrogenated carbon films* (Les Éditions de Physique, Les Ulis 1987) p. 449 376
[239] E. Salonen, K. Nordlund, J. Tarus, T. Ahlgren, J. Keinonen, C. Wu: Phys. Rev. B **60**, R14 005–1–4 (1999) 377
[240] E. Salonen, K. Nordlund, J. Keinonen, N. Runeberg, C. Wu: J. Appl. Phys. **92**, 2216 (2002) 377
[241] E. Salonen, K. Nordlund, J. Keinonen, C. Wu: Contrib. Plasma Phys. **42**, 458 (2002) 377, 379
[242] E. Salonen, K. Nordlund, J. Keinonen, C. Wu: J. Nucl. Mater. **313–316**, 404 (2003) 377
[243] P. Träskelin, K. Nordlund, J. Keinonen: Nucl. Instrum. Meth. B **228**, 319 (2005) 377
[244] K. Nordlund: Phys. Scr. **T124**, 53 (2006) 377
[245] S. J. Stuart, P. S. Krstić, T. A. Embry, C. O. Reinhold: Nucl. Instrum. Meth. B **255**, 202 (2007) 378, 380, 382
[246] P. S. Krstić, C. O. Reinhold, S. J. Stuart: Europhys. Lett. **77**, 33002 (2007) 378
[247] P. S. Krstić, S. J. Stuart, C. O. Reinhold: AIP Proc. **876**, 201 (2006) 378, 379, 380, 382
[248] C. O. Reinhold, P. S. Krstić, S. J. Stuart: Nucl. Instrum. Meth. B **258**, 274 (2007) 378
[249] R. G. Macaulay-Newcombe, A. A. Haasz, J. W. Davis: J. Nucl. Mater. **337–339**, 857 (2005) 380
[250] A. A. Haasz, J. W. Davis: Fus. Sci. Technol. **50**, 58 (2006) 382
[251] P. Franzen: *Report IPP 9/92* (MPG, Garching 1993) 382, 383
[252] K. Maruyama, W. Jacob, J. Roth: J. Nucl. Mater. **264**, 56 (1999) 384
[253] W. M. Wang, J. Roth, W. Eckstein, R. Schwörer, H. Plank, M. Du: Nucl. Instrum. Meth. B **129**, 210 (1997) 384
[254] M. Balden, K. U. Klages, W. Jacob, J. Roth: J. Nucl. Mater. **341**, 31 (2005) 384
[255] C. Li, T. C. Brown: Carbon **39**, 725 (2001) 384
[256] J. O. Müller, D. S. Su, R. E. Jentoft, J. Kröhnert, F. C. Jentoft, R. Schlögl: Catalysis Today **102–103**, 259 (2005) 384
[257] H. Marsh, K. Kuo: in H. Marsh (Ed.): *Introduction to Carbon Science* (Butterworths, London 1989) p. 107 384
[258] B. R. Stanmore, J. F. Brilhac, P. Gilot: Carbon **39**, 2247 (2001) 384
[259] J. W. Davis, C. G. Hamilton, A. A. Haasz: J. Nucl. Mater. **288**, 148 (2001) 384

[260] D. E. Rosner, H. D. Allendorf: *Kinetics of the Attack of Refractory Materials by Dissociated Gases* (Plenum, New York 1970) see also references therein 384
[261] E. Vietzke, T. Tanabe, V. Philipps, M. Erdweg, K. Flaskamp: J. Nucl. Mater. **145**–**147**, 425 (1987) 384
[262] A. Refke, V. Philipps, E. Vietzke: J. Nucl. Mater. **250**, 13 (1997) 384
[263] E. Vietzke, A. A. Haasz: in W. O. Hofer, J. Roth (Eds.): *Physical Processes of the Interaction of Fusion Plasmas with Solids* (Academic, New York 1996) p. 135 384
[264] E. Hechtl, J. Bohdansky: J. Nucl. Mater. **141**–**143**, 139 (1986) 384
[265] E. Hechtl, J. Bohdansky: J. Nucl. Mater. **154**, 201 (1988) 384
[266] C. Hopf, M. Schlüter, W. Jacob: J. Appl. Phys. (2007) to be published 384, 385
[267] C. Hopf, M. Schlüter, W. Jacob: Appl. Phys. Lett. **90**, 224106 (2007) 385
[268] B. Landkammer, von Keudell, A., W. Jacob: J. Nucl. Mater. **264**, 48 (1999) 385
[269] G. Adamopoulos, C. Godet, B. Drévillon, Y. Sato, D. N. Batchelder, A. Grosman, C. Ortega: Diamond Relat. Mater. **12**, 983 (2003) 385
[270] A. M. Baranov, V. V. Sleptsov, A. A. Nefedov, A. E. Varfolomeev, L. Calliari: Diamond Relat. Mater. **13**, 1356 (2004) 385
[271] K. K. Hirakuri, K. Kuwashima, K. Tatsuta, K. Sato: Diamond Relat. Mater. **14**, 1067 (2005) 385
[272] W. L. Hsu: J. Vac. Sci. Technol A **7**, 1047 (1989) 385
[273] D. Mueller, W. Blanchard, J. Collins, J. Hosea, J. Kamperschroer, P. H. LaMarche, A. Nagy, D. K. Owens, C. H. Skinner: J. Nucl. Mater. **241**–**243**, 897 (1997) 385
[274] W. Jacob, B. Landkammer, C. Wu: J. Nucl. Mater. **266**–**269**, 552 (1999) 385
[275] J. S. Hu, J. G. Li, X. M. Wang, the HT-7 team: Plasma Phys. Control. Fusion **47**, 1271 (2005) 385
[276] J. S. Hu, J. G. Li, X. M. Wang: J. Nucl. Mater. **350**, 9 (2006) 385
[277] C. Hopf, V. Rohde, W. Jacob, A. Herrmann, R. Neu, J. Roth, the ASDEX Upgrade Team: J. Nucl. Mater. **363**–**365**, 882 (2007) 385
[278] S. Fujimura, K. Shinagawa, M. T. Suzuki, M. Nakamura: J. Vac. Sci. Technol. B **9**, 357 (1991) 386
[279] T. E. F. M. Standaert, P. J. Matsuo, X. Li, G. S. Oehrlein, T. M. Lu, R. Gutmann, C. T. Rosenmayer, J. W. Bartz, J. G. Langan, W. R. Entley: J. Vac. Sci. Technol. A **19**, 435 (2001) 386
[280] W. Jacob, C. Hopf, M. Schlüter: Appl. Phys. Lett. **86**, 204103 (2005) 386, 387
[281] S. Grigull, W. Jacob, D. Henke, C. Spaeth, L. Sümmchen, W. Sigle: J. Appl. Phys. **83**, 5185 (1998) 386
[282] S. Grigull, R. Behrisch, S. Parascandola: J. Nucl. Mater. **275**, 158 (1999) 386
[283] P. Hammer, W. Gissler: Diamond Relat. Mater. **5**, 1152 (1996) 386
[284] M. Schlüter, C. Hopf, T. Schwarz-Selinger, W. Jacob: J. Appl. Phys. (2007) to be published 386, 387
[285] K. J. Clay, S. P. Speakman, G. A. J. Amaratunga, S. R. P. Silva: J. Appl. Phys. **79**, 7227 (1996) 387
[286] C. Spaeth, U. Kreissig, F. Richter: Thin Solid Films **355**–**356**, 64 (1999) 387

[287] S. E. Rodil, N. A. Morrison, J. Robertson, W. I. Milne: Phys. Stat. Solidi (A) **174**, 25 (1999) 387
[288] J. Hong, G. Turban: Diamond Relat. Mater. **8**, 572 (1999) 387
[289] J. Hong, A. Granier, A. Goullet, G. Turban: Diamond Relat. Mater. **9**, 573 (2000) 387
[290] N. Hellgren, M. P. Johansson, B. Hjörvarsson, E. Broitman, M. Östblom, B. Liedberg, L. Hultman, J. E. Sundgren: J. Vac. Sci. Technol. A **18**, 2349 (2000) 387
[291] N. Hellgren, M. P. Johansson, E. Broitman, P. Sandström, L. Hultman, J. E. Sundgren: Thin Solid Films **382**, 146 (2001) 387
[292] N. A. Morrison, S. E. Rodil, J. Robertson, W. I. Milne: J. Appl. Phys. **89**, 5754 (2001) 387
[293] T. Schwarz-Selinger, C. Hopf, C. Sun, W. Jacob: J. Nucl. Mater. **363–365**, 174 (2007) 387, 388
[294] J. W. Butterbaugh, D. C. Gray, H. H. Sawin: J. Vac. Sci. Technol. B **9**, 1461 (1991) 389
[295] G. S. Oehrlein, D. Zhang, D. Vender, M. Haverlag: J. Vac. Sci. Technol. A **12**, 323 (1994) 389
[296] G. S. Oehrlein, D. Zhang, D. Vender, O. Joubert: J. Vac. Sci. Technol. A **12**, 333 (1994) 389
[297] T. E. F. M. Standaert, M. Schaepkens, P. G. M. Sebel, N. R. Rueger, G. S. Oehrlein: J. Vac. Sci. Technol. A **16**, 239 (1998) 389
[298] T. Standaert, C. Hedlund, E. A. Joseph, G. S. Oehrlein, T. J. Dalton: J. Vac. Sci. Technol. A **22**, 53 (2004) 389
[299] D. Humbird, D. B. Graves, X. F. Hua, G. S. Oehrlein: Appl. Phys. Lett. **84**, 1073 (2004) 389

Index

activation energy
  desorption, 380
  Gaussian distribution, 346
  hydrocarbon release, 364
  hydrogen desorption, 364
amorphisation, 354
annealing, 360

Bayesian theory, 336, 355
bond breaking, 374, 380, 386

cascade mixing, 331
catalyst, 383
cavity probe, 340
chemical erosion, 333, 342
  released species, 345, 347
chemical sputtering, 333, 340, 342
  combined irradiation, 348, 360, 386
  doping, 363
  energy dependence, 351
  flux dependence, 354, 355
  model, 374
  modelling, 368
  molecular ion, 365
  reactive species, 383
  released species, 356
  temperature dependence, 349

damage formation, 353
decomposition
  hydrocarbon, 369
desorption, 342, 374, 380, 384
diffusion, 369, 376, 382
dissociation
  hydrocarbon, 339
  molecule, 339

electron high energy loss spectroscopy(HREELS), 342
ellipsometry, 334, 338, 339, 341, 362
etching
  dry, 331
  ion-assisted, 332
  plasma, 331
  reactive ion, 332
  wet, 331
excitation
  electronic, 360

flux dependence, 356

graphitization, 347, 355

hybridisation, 342, 344
hydrogenation, 342, 343

implantation range, 354
interaction potential
  hydrocarbon (Brenner), 379
ionization, 339
isotope effect, 353, 375, 381
isotope exchange, 347
isotpe sputtering, 379

mass spectrometer
  background signal, 337
  line-of-sight, 337
  quadrupole, 338
  remote, 335, 346
  sensitivity, 336
  time-of-flight, 340
mass spectrometry, 334, 336, 361, 373, 386
  molecular beam (MBMS), 338, 340, 362
molecular dynamics, 377
molecule
  formation, 330, 333, 342
  hydrocarbon, 339

optical emission spectroscopy, 339, 386

production rate
  methane, 361
production yield
  C_2, 358
  hydrocarbon, 362
  methane, 351, 361

radiation damage, 354, 355, 369, 380, 381
radiation-enhanced sublimation (RES), 334
radical
  hydrocarbon, 336, 339
  methyl, 341
  species, 360
  suprathermal, 334
  volatile, 329
range, 376, 382
reaction rate, 383
reaction yield, 384
recoil implantation, 331

selfsputtering, 333
simultaneous bombardment, 341, 386
sputtering of
  carbides, 331
  nitrides, 331
  oxides, 331
sticking
  probability, 336, 340
sublimation temperature, 333
surface
  altered layer, 331
  roughness, 339
surface binding energy, 331, 333, 375
surface topography, 365
swift chemical sputtering, 334
synergistic effect, 360

target
  a–C:H layer, 386
    hard, 347, 354
    soft, 347
  graphite
    grade, 344, 353
    pre-irradiated, 373
    type, 353
  metal-doped carbon, 336
  pyrolytic graphite, 342
thermal desorption, 331, 334
thermal desorption spectrocopy (TDS), 342
threshold energy, 332, 333, 353, 380

weight loss, 335

Electronic Sputtering with Swift Heavy Ions

Walter Assmann[1], Marcel Toulemonde[2], and Christina Trautmann[3]

[1] Department für Physik, Ludwig-Maximilians-Universität,
Maier-Leibnitz-Laboratorium, Am Coulombwall 6, 85748 Garching, Germany
Walter.Assmann@Physik.Uni-Muenchen.de

[2] Centre Interdisciplinaire de Recherches Ions Laser (CIRIL),
CEA-CNRS-ISMRA, BP 5133, 14070 Caen-Cedex 05, France
toulemonde@ganil.fr

[3] Gesellschaft für Schwerionenforschung (GSI),
Planckstraße 1, 64129 Darmstadt, Germany
c.trautmann@gsi.de

Abstract. Swift heavy ions of energies where electronic processes dominate the slowing down process in matter induce sputtering mainly by inelastic effects, and not by elastic collision cascades. Given by the high energy input per incident ion, the measurements of sputtering yields include specific problems and require different techniques than for nuclear sputtering. Electronic sputtering shows a strong dependence on material properties, therefore experimental results are presented for metals, oxides, and ionic crystals separately. The sputtering yields vary by more than four orders of magnitude and the shape of the angular distribution can be almost isotropic or exhibit a jet-like contribution. In a general accepted picture for damage creation induced by swift heavy ions, the projectiles create hot zones of molten or even vaporized material resulting in the ejection of surface atoms. The inelastic thermal spike model based on this picture reproduces quantitatively the measured sputtering yields in oxides, and indicates a synergetic effect between nuclear and electronic energy loss for metals and a non-thermal mechanism for ionic crystals.

1 Introduction

The sputtering of solids caused by bombardment with heavy ions having a specific energy around or above of 1 MeV per nucleon (MeV/u) is generally larger - sometimes orders of magnitude – than would be expected from purely collisional processes, indeed it is sometimes entirely governed by the electronic energy loss mechanism (electronic sputtering). At such high energies, the slowing down of projectiles is principally caused by electronic excitation and ionization of target atoms (electronic energy loss) rather than by elastic collisions (nuclear energy loss) which contribute only 1% at most to the total energy loss. The electronic energy loss as a function of projectile energy reaches a maximum (termed the *Bragg peak*) around a few MeV/u. Figure 1 displays the energy loss of ^{197}Au ions in a titanium target. The Bragg peak lies at around 1 GeV (5 MeV/u), the electronic energy loss $(dE/dx)_{\mathrm{e}}$ is here

R. Behrisch, W. Eckstein (Eds.): Sputtering by Particle Bombardment,
Topics Appl. Physics **110**, 401–450 (2007)
© Springer-Verlag Berlin Heidelberg 2007

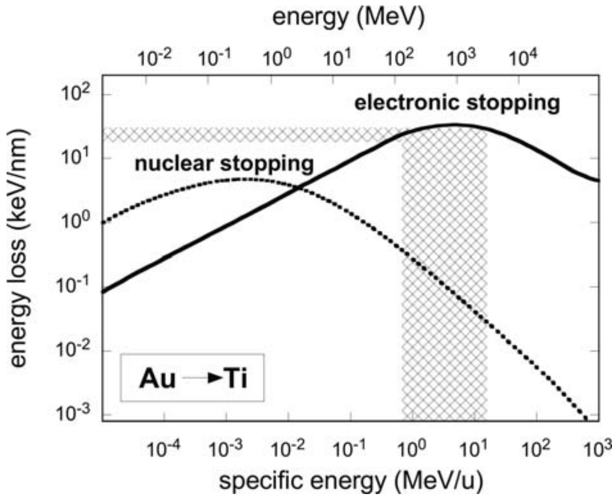

Fig. 1. Energy loss as a function of specific and total projectile energy for gold ions in a titanium target. For energies below 10 MeV, the energy loss is governed by elastic collisions (nuclear energy loss), whereas for higher energies, electronic excitation and ionization (electronic energy loss) become the dominant processes. Most sputtering experiments in the electronic energy loss regime have been performed in the energy and energy loss range indicated by the *hatched zone* around the so-called *Bragg Peak*

about 40 keV/nm, whereas the nuclear energy loss $(dE/dx)_n$ contributes only 0.06 keV/nm.

Energetic ions can have the same nominal electronic energy loss on both the left and right hand sides of the Bragg maximum. Under these circumstances, the specific energies (velocities) and the nuclear energy-loss contributions of the projectiles are different. The unequal beam velocity has a direct influence on the spatial range of the electron cascade, leading to lower deposited energy densities for larger projectile velocities [1, 2] and corresponding effects on sputtering (velocity effect). Another important parameter is the charge state of the ion. In matter, the projectile will lose all outer electrons with orbital velocities smaller than the projectile velocity. This velocity-dependent equilibrium charge state Z_{eff} enters the formula of the electronic energy loss and thus affects electronic sputtering.

In many solids, the enormous local energy deposition of swift heavy ions leads to severe material modifications along the ion trajectory including the formation of "nuclear tracks" [3–5]. They consist of narrow but extended cylindrical zones with a high concentration of defects. The diameter of ion tracks is typically 5–20 nm and their length depends on the ion energy and may range from a few µm up to cm for GeV ions. Within the track volume, the crystalline order of the host structure may be completely amorphized as illustrated by electron microscopy of ion-irradiated high-T_c superconductors

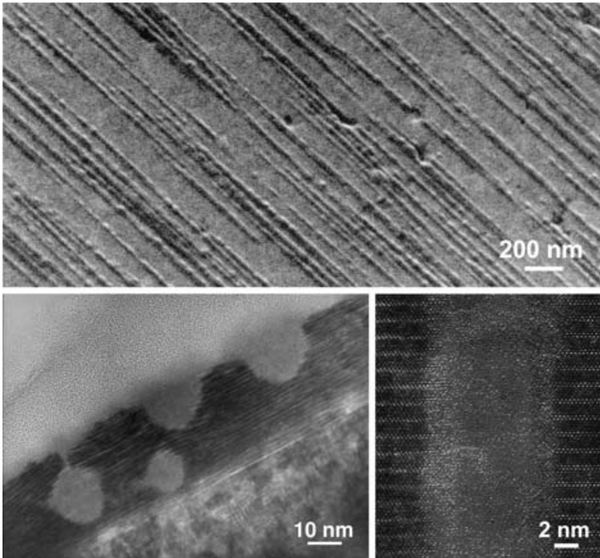

Fig. 2. Scanning electron microscopy (*top*) and cross-section transmission electron microscopy image (*bottom left*) of ion tracks produced by 275 MeV Au ions under almost parallel incidence with respect to the surface of single crystalline $YBa_2Cu_3O_7$ grown on MgO substrate [8]. High-resolution electron microscopy image (*bottom right*) of an amorphous track zone produced along the trajectory of a single 1.4 GeV Au ion in crystalline $Bi_2Sr_2CaCu_2O_8$ [9]

in Fig. 2. In various materials, in particular in insulators, the track zone can be preferentially attacked by a suitable chemical etchant. Track etching allows the controlled fabrication of cylindrical nanopores or other nanostructures suitable for applications in many different fields [5–7].

Since track formation was initially observed only in insulating materials and could not be explained quantitatively by nuclear collision cascades, a *Coulomb explosion* mechanism was proposed in 1965 as summarized by *Fleischer* et al. [5]. In this model, target atoms along the ion path are highly ionized; taken the resulting repulsion of the charged atoms of the solid leads directly to the observed damage. It was early pointed out that even surface atoms could be ejected by this mechanism, and, that there should exist a strong relation between track formation and sputtering, i.e. between bulk and surface phenomena [10]. In the 1970s this prediction initiated a series of sputtering experiments on insulators with MeV heavy ions, for example 20 MeV ^{35}Cl ions [11]. In some cases, the yields measured were orders of magnitude above the yields calculated for collisional sputtering [12] and consequently were attributed to electronic sputtering. Reviews of these experiments can be found in [13–17], and are most detailed in the proceedings of the SPUT92-Symposium [18].

Later, large accelerator facilities such as GANIL/Caen (France) or GSI/ Darmstadt and ISL/Berlin (both Germany) provided swift heavy ions with energies up to GeV for materials research, extending the energy loss to above e.g. 80 keV/nm for Au ions in Au targets. Given these possibilities, several groups began systematic investigations of irradiation effects and radiation damage for a wide range of different materials. At such high energy densities amorphous tracks, phase transformations, or specific defect aggregates could now be observed not only in insulators but in almost any type of material [1, 19–32] (see also SHIM-Conference proceedings, e.g. [33]).

The material response is quite specific and depends on electrical, thermal, and structural properties of the solid. In insulators such as silicates (e.g., SiO_2 quartz [21] or mica [23]) and garnets [19, 34] tracks consist of amorphized zones. However, there also exists track formation in a number of non-amorphizable, rather radiation-resistant insulators such as UO_2 [35, 36], Al_2O_3 [37], zirconia or hafnia [38, 39], and in the class of alkaline-earth and alkaline halides (e.g. LiF, NaCl, CaF_2, etc.) [28, 40–49] which are known to be very sensitive to electronic excitation but difficult to amorphize because of the strong binding character. Of particular importance was the observation of ion tracks in conductive materials, which earlier had been assumed to be insensitive to electronic energy-loss effects. It was argued that the high electron mobility in metals could lead to rapid screening of ionized atoms and then Coulomb explosion could not develop.

In attempting to describe the new findings, the original thermal-spike concept of *Seitz* and *Koehler* [50] (which – interestingly enough – already predicted electronic effect for transition metals) was re-examined and developed into the inelastic thermal spike model (i-TS). Here, the ion energy is first deposited in the electron subsystem of the target and then via electron-phonon coupling transferred to the target atoms, creating a transient increase of temperature around the ion trajectory. This model was used to reproduce quantitatively the observed energy threshold for track formation and the track radii as a function of the electronic energy loss [51, 52].

In contrast to track formation, sputtering in the electronic energy loss regime has been studied less extensively. Recent investigations concentrated on systematic sputtering experiments with swift heavy ions and different material classes [53–56]. Such data are important because the existing knowledge of collisional sputtering cannot be applied to electronic sputtering. The difference is related to the fact that swift heavy ions interact with target electrons whereas projectiles in the nuclear energy loss regime transfer their energy via elastic collisions to the target atoms, initiating a collision cascade which can eventually lead to the direct ejection of surface atoms. If the energy density in the cascade is sufficiently high, collisional sputtering is enhanced by thermal evaporation [57]. This temperature effect was described by the elastic thermal spike model by *Sigmund* and *Claussen* [58]. In the electronic energy loss regime, the scenario is more complex because the projectile energy is first deposited into the electronic subsystem ($\sim 10^{-16} - 10^{-14}$ s) and only at a later

stage transferred to the lattice atoms ($\sim 10^{-14} - 10^{-11}$ s). Particle emission in the early electronic excitation phase could be based on Coulomb explosion, whereas sputtering arising from thermalization of the lattice atoms may stem from a pressure spike and/or from a thermal spike induced evaporation process [59] which leads to the so-called electronic sputtering.

Although $(dE/dx)_{\mathrm{n}}$ is rather small in the electronic energy loss regime, one has to keep in mind that collisional sputtering results from a direct and thus effective energy transfer to the target atoms. Whereas for electronic sputtering the transfer efficiency of $(dE/dx)_{\mathrm{e}}$ is controlled by the strength of the electron-phonon coupling of a given material. The different contributions of the nuclear and electronic sputtering process are not easy to separate experimentally. However, trends can be deduced from characteristic fingerprints given for example by the yield dependence on the specific energy, mass, and charge of the ions, by the angular distributions being affected by the emission kinetics, by the kinetic energy of the ejected particles which are linked to the emission temperature, and last but not least by the stoichiometry and size of the sputtered species.

Hitherto, most sputtering experiments in the electronic energy loss regime have relied on the analysis of emitted *ionized* species because it is much easier to measure ions rather than neutrals using techniques such as time-of-flight or quadrupole mass spectrometry. Ionized particles, however, contribute at most a few percent to the total yield [60]. Moreover, the characteristics of sputtered ions may differ strongly from those of neutral atoms. It is unclear whether sputtering data deduced for ions are representative of the overall sputtering process.

Various experiments mainly performed in the 1980s, provided *total* yields of electronic sputtering [14,60–66]. More recent measurements with ion beams around the Bragg peak concentrated on those materials for which track data had already been recorded including metals such as Ti, Zr, and Au [53, 54, 56, 67] and insulators for example yttrium iron garnet [68, 69], SiO_2, and various fluoride crystals [55, 56]. They now offer a useful basis for thermal spike model calculations testing if the same set of parameters can describe track formation as well as surface sputtering.

The following sections present electronic sputtering phenomena with medium and heavy ion beams of energies close to the Bragg peak ($\sim 1\,\mathrm{MeV/u}$). We deliberately exclude sputtering with electrons or photons (in literature also referred to as electronic sputtering) and with slow highly-charged ions and molecular or cluster beams; they are reviewed in references such as [57, 70–73]. Section 2 focuses on the special demands and problems of sputtering experiments in the electronic energy loss regime and describes the experimental methods and representative apparatus. Section 3 gives a summary of recent experimental results subject to the incidence angle and the charge state of the ion beam, and to angular distributions and total yields for different materials such as metals, oxides and ionic crystals. Section 4 briefly describes some theoretical approaches to the sputtering mechanism,

but mainly concentrates on the inelastic thermal spike model, being at present the only quantitative model which describes track formation and sputtering for a large number of materials. A summary of the most prominent signatures of electronic sputtering and an outlook listing urgent needs for future efforts finally concludes the chapter.

2 Sputtering Experiments

2.1 Special Problems in High-Energy Sputtering

In sputtering experiments with heavy ions in the electronic energy loss regime several specific problems have to be considered. To avoid excessive heating, melting, or even evaporation of the sample, the incident ion flux has to be kept sufficiently low. On a thick target, for example, a millimeter-focused beam of 100 MeV I ions of 1 μA current can deposit the enormous power density of 1 kW/cm^2. Practical experience suggests that the beam current density should not exceed, say, nA/cm^2 corresponding to about 10^{10} ions/cm$^2 \cdot$s. Such limited beam currents (in combination with restricted beamtimes) have two major consequences: 1. the target surface does not undergo self-cleaning during the sputtering experiments, and 2. the detection technique has to be extremely sensitive because of the small number of sputtered particles.

Since sputtered atoms originate from the outermost target layers, contamination or oxidation of the surface can play an important role. Even a monolayer of oxide may seriously affect the experimental results. A dynamically clean surface can only be maintained if the sputtering rate is much larger than the adsorption rate of contaminants. A rule of thumb gives an adsorption rate of 10^{15} particles/cm$^2 \cdot$s in a vacuum of 10^{-6} mbar. Taking into account the flux limitation and a sputtering yield of $\sim$ 10 atoms/ion, even after some hours of beam exposure only one monolayer at most will be removed by sputtering.

The low number of sputtered particles also demands a very sensitive detection technique. Using a beam spot size of about 1 mm^2, the total number of particles sputtered from a monolayer is around 10^{13}. This low number rules out the usual methods such as weight loss or thickness change measurements and makes the catcher technique in combination with ion-beam analysis the method of choice, particularly when angular distribution measurements are envisaged. The sensitivity problem, however, is then transferred to the analysis of the catcher. A more complex alternative of comparable sensitivity could be based on the use of lasers, which allows element-selective detection and offers the additional opportunity to measure the velocity and hence the energy distribution of the sputtered particles (see also Chap. by *Gnaser*).

Sputtering is not only sensitive to surface contamination but also to the structural and morphological properties of the target surface. Energetic ions can roughen and deform surfaces [74], crystalline samples can be amorphized,

and preferential sputtering can change significantly the composition of materials with more than one component. In most cases, however, such effects can be minimized by limiting the total fluence within a given beam spot on the target.

Sputtering yields were observed to depend on the grain size of a polycrystalline sample and on the thickness of a film if smaller than several nm [13,75–79]. These effects are attributed to a change of the deposited energy density related to the energy confinement in such a small sample volume and to modified heat transport properties.

For electronic sputtering, channeling of high-energy projectiles in single-crystalline samples is a minor problem because the critical angles are in the range of tenths of a degree.

With respect to beam properties, the charge state of the projectiles plays an important role. Particles delivered, for example, by a tandem accelerator are usually far from their equilibrium charge state in matter. Figure 3 shows the charge state evolution of 1 MeV/u Ni ions penetrating into a carbon target as deduced from Classical–Trajectory Monte Carlo (CTMC) simulations taking into account the interaction of all target and projectile electrons along the ion path [80]. When entering the solid, the projectiles lose or pick up electrons until they reach the equilibrium charge state. At 1 MeV/u, this occurs within a path length of about 10 nm, in agreement with experimental observations [81]. Close to the surface, the energy loss strongly changes with depth [82] and may evolve for different incoming charge states as shown in Fig. 3. In this context it should be noted that energy-loss tables in general list values of ions in the equilibrium charge state.

In sputter experiments, the equilibrium charge state can be adjusted by mounting a thin carbon foil in front of the target [83–85]). Behind such a stripper foil, however, ions do not have a single fixed charge state but a charge state distribution. We emphasize that beams of equilibrium charge state should be used, whenever well-defined energy loss values are required, for example, when comparing different experimental data, or data with model calculations.

2.2 Measuring Techniques for Sputtering Yields

In the past, several measuring techniques have been developed for sputtering experiments with keV projectiles accessing parameters such as total yield, angular and mass distribution, velocity, energy or even the excited state of the sputtered species. In this section, we will concentrate on those methods which are also suitable for MeV-ion beams and which measure *all* sputtered particles, not only *ionized* species.

Several methods are based on the rather complex laser-induced excitation or ionization of the sputtered particles [86], see also the Chap. by *Gnaser*. Resonance processes can achieve high selectivity. Level schemes for ground-state excitation are available for almost all elements. Absolute sputtering yields

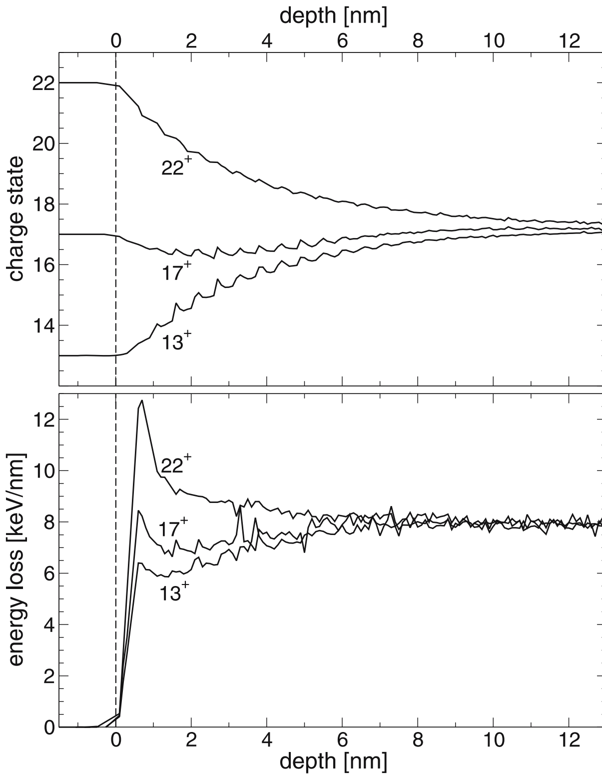

Fig. 3. Charge state (*top*) and corresponding energy loss (*bottom*) as a function of penetration depth of 1 MeV/u Ni ions entering into a carbon target. The data shown are calculated for initial charge states below (13^+), around (17^+), and above (22^+) the equilibrium charge state [80]

can be determined if excitation or ionization efficiencies reach nearly 100 %. In laser-induced fluorescence (LIF), for example, the laser is tuned to a resonance transition and spontaneously emitted fluorescence radiation can be detected with photon counting techniques. The analysis of the velocity distributions of sputtered atoms is based on Doppler shift LIF [87,88]. The angular dependence of the Doppler shift can even be used to deduce the angular distribution. Laser-induced resonance ionization spectroscopy (RIS) is based on two or three resonance steps with the last ionizing photon tuned to an autoionizing level above the ionization potential [89, 90]. The large laser powers which are available nowadays allow non-resonant (non-linear) multi-photon processes for the final ionization step [91]. Recent high-energy sputtering experiments employed a completely non-resonant multi-photon ionization process [92]. The energy and mass distribution of the post-ionization particles are analysed by means of time-of-flight technique and mass spectrometry. With non-resonant processes all sputtered species can be ionized simultaneously fa-

cilitating quantitative yield measurements. Selectivity, however, is then lost and UHV conditions are required to minimize background particles.

A less complicated, common approach to quantify sputtering yields is the collection of the sputtered particles (ions, atoms, molecules, clusters) on a catcher irrespective of their charge and mass. Angular distributions are also easily measured with an arc-shaped catcher. Any high purity material (e.g., Al, Si, or Cu) is suitable as catcher. For angular distribution measurements, the catcher foils should be thin but stable enough to be mounted on an arc-shaped holder. After sputtering, this foil is removed, stretched out flat, and analyzed step by step along its full length. The species and the number of sputtered particles of each position is then correlated to the emission angle θ.

Quantitative analysis of the catchers is typically carried out by means of ion-beam techniques such as Rutherford backscattering spectroscopy (RBS) [93] or elastic recoil detection analysis (ERDA) [82, 94, 95]. Both methods have a high sensitivity, are selective for different elements, and give absolute particle numbers. To avoid interference effects, the catcher material should be composed of an element lighter than the sputtered species for RBS and vice versa for ERDA. Because of the risk of being stripped off the catcher during the RBS and ERDA analysis, the sputtered particles should be protected by a thin evaporated layer of high-purity material (e.g., 50 nm Cu layer). If needed, the detection sensitivity can be increased by using single-crystalline catchers (e.g. Si wafers) and performing the analysis in channeling conditions. The detection of the extremely low number of $10^{12}\,\text{cm}^{-2}$ sputtered Ti particles was demonstrated with 1.5 MeV ^{12}C ions and channeling RBS [67].

The catcher technique is quite universal but inapplicable to quantitative analysis of collected oxygen particles (e.g. emitted from oxide targets) because of unavoidable surface oxidation of the catcher. For the special case of uranium compounds (UF_4 [62], UO_2 [96]), the sputtered U particles can be counted quantitatively by exposing the catcher to neutrons which induce fission of ^{235}U. To determine the number of fission fragments, the catcher is covered with a sheet of mica as track detector. Collecting the U particles on a rotating catcher wheel and pulsing (chopping) the bombarding projectiles even gives access to the velocity distribution of the sputtered uranium [62].

An inherent problem of the catcher method is the unknown collection efficiency (i.e. sticking coefficient) of the different sputtered species. This directly influences the uncertainty of the total yield. Accurate measurements of the sticking probability are scarce [97, 98]. One possibility is the calibration of the catcher collection-efficiency based on sputtering yields known from experiments in the nuclear energy loss regime and apply the same sticking coefficient at high beam energies [99]. In another approach the number of particles collected on the catcher is compared with the thickness decrease of the target monitored simultaneously by online-ERDA. The sputtering yield is extracted from the thickness decrease as a function of the ion fluence. Independent sputtering yield measurements by online-ERDA have been obtained for SiO_2 films of thicknesses down to a few nm. This was possible because

of the high sensitivity of ERDA for the light oxygen particles [75, 77]. Using thin bilayers of isotopically labelled $Si^{16}O_2$ and $Si^{18}O_2$ one can estimate the depth of origin of the sputtered species [75].

Finally the microbalance technique should be mentioned, which allows extremely sensitive yield measurements of thin films deposited on a quartz crystal [100]. This method is not suitable for bulk materials or for angular distribution measurements. Moreover, irradiations with swift heavy ions damage the quartz crystal, and for materials with low sputtering yields, the mass increase due to projectile implantation may become comparable to sputtering-induced mass losses [101].

2.3 Angular Distribution, Total Yield, and Fluence Effect

Measurement of angular distributions (e.g., by RBS or ERDA of the catcher) gives the particle number $N_Y(\theta, \varphi)$ per unit area for a certain catcher position, where θ and φ are the respective polar and azimuthal emission angles of the sputtered particles. Taking into account the geometrical conditions (see Fig. 4), $N_Y(\theta, \varphi)$ is related to the differential yield $Y_{\text{diff}}(\theta, \varphi)$ expressed in steradian by

$$Y_{\text{diff}}(\theta, \varphi) = N_Y(\theta, \varphi)\frac{d^2}{I}\,, \tag{1}$$

where d is the distance between catcher and target, and I denotes the total number of incident ions. In most experiments, sputtered particles are recorded as a function of the polar angle whereas the azimuthal symmetry is only cross checked by rotating the arc position around φ.

From the full angular distribution the total yield Y_{tot} is derived by integrating Y_{diff} over the solid angle. Based on several measurements of angular distributions and assuming azimuthal sputtering symmetry, the integration gives

$$Y_{\text{tot}} = \iint Y_{\text{diff}} \sin\theta \, \mathrm{d}\theta \, \mathrm{d}\varphi = 2\pi \int_0^{\pi/2} Y_{\text{diff}} \sin\theta \, \mathrm{d}\theta\,. \tag{2}$$

If the angular distribution is isotropic ($Y_{\text{diff}} \sim \cos\theta$) or follows an over-cosine law ($Y_{\text{diff}} \sim \cos^y\theta$), the total yield is equal to

$$Y_{\text{tot}} = 2\pi \int_0^{\pi/2} Y_{\text{diff}}(0^\circ)(\cos\theta)^y \sin\theta \, \mathrm{d}\theta = 2\pi \frac{Y_{\text{diff}}(0^\circ)}{y+1}\,, \tag{3}$$

where $Y_{\text{diff}}(0^\circ)$ is the differential yield measured at the catcher position opposite to the beam spot on the target.

The specific shape of the angular distribution does not only depend on the target material itself but is also influenced by the surface topography. Figure 5 shows a flat and a rough surface of an irradiated LiF crystal together with the respective angular distributions. Sputtering from the flat surface produces a

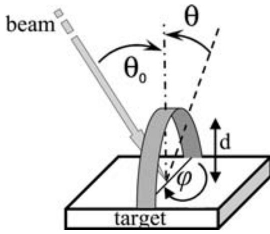

Fig. 4. Scheme of angular distribution measurements with an arc-shaped catcher mounted above the target: θ_0 denotes the incidence angle of the beam with respect to the surface normal, and θ and φ are the respective polar and azimuthal emission angles of the sputtered particles

highly anisotropic distribution with a jet-like component peaked around the surface normal (for more details see Sect. 3.5). If the beam intensity applied to the target is too high, the surface becomes corrugated and the angular distribution is almost isotropic (Fig. 5). Despite this significant change, the total yield is the same for both cases. Surface roughness can also shift the maximum of the angular distribution with respect to beam incidence as seen in sputtering experiments exposing Ti targets to 230 MeV Au ions [54]. For reliable angular distribution measurements, it is therefore essential to control the surface topography and avoid surface corrugation by excessive beam exposure. Moreover, a large fluence may influence the sputtering yield by amorphizing a crystalline sample (see Sect. 3.4.1).

2.4 Experimental Arrangements

A standard equipment for sputtering experiments with the catcher technique in combination with ERDA is shown in Fig. 6. To determine sputtering yields, the number of incoming ions has to be known accurately. A direct measurement of the beam current, for example on the sample holder, requires proper suppression of secondary electrons. Alternatively, the current can be determined from ions scattered from the sample itself or from a thin foil in front of the sample. In the arrangement presented in Fig. 6, the carbon foil mounted in front of the target serves as beam monitor and simultaneously as electron stripper to adjust the equilibrium charge state of the projectiles. In this situation, the signal needs to be calibrated by measuring the absolute current of the beam with defined charge state using a Faraday cup (here FC1). Comparing the current of two cups, before and behind the stripper foil (FC1 and FC2), gives the mean ion charge state after stripping.

The target together with the catcher is mounted on a special arc-shaped holder which allows one to move the sample under the fixed catcher if a fresh surface is needed (Fig. 7, left). Two catcher arcs are mounted for experimental checks of the azimuthal symmetry (Fig. 7, right).

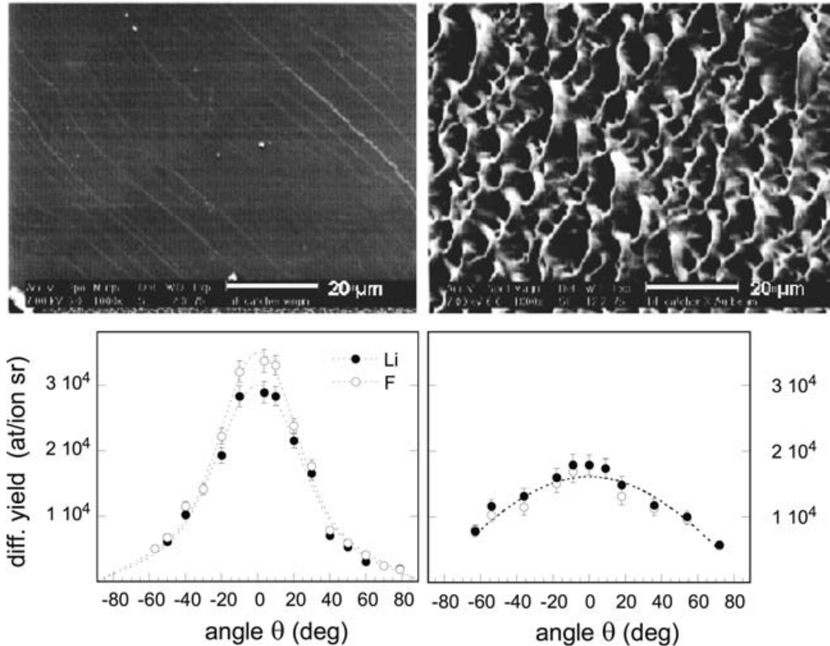

Fig. 5. *Top:* Scanning electron micrograph of LiF crystal irradiated with 210 MeV Au ions of different fluence and (*bottom*) corresponding angular distributions. *Left:* Under low-fluence irradiation with 2×10^{12} ions/cm^2 on 9 different target spots, the surface remains flat and the angular distribution exhibits a non-isotropic jet-like component, whereas (*right*) at a high fluence of 8×10^{13} ions/cm^2 applied on one single spot, the surface is corrugated and the angular distribution is isotropically smeared out

After the sputtering experiment, the catcher foils are analyzed in the same chamber using, if possible, even the same ion beam. The thin catcher film with the sputtered particles is removed from the arc, stretched out on a flat substrate, covered by a thin ultra-clean Cu layer, and remounted into the chamber. ERDA records the energy loss ΔE in coincidence with the remaining energy E_{rest} of the recoil target atoms. The $\Delta E - E_{\mathrm{rest}}$ spectrum can be analysed quantitatively for the different species in particular for light elements. Figure 8 shows a representative ERDA spectrum from a sputtering experiment on LiF in combination with an Al catcher. Signals of sputtered Li and F particles are well separated.

In the case of metallic targets, reliable sputtering experiments need more effort because UHV conditions are mandatory. The problem is caused by the general tendency of metals to oxidize and thus form insulating compounds on the surface. An operating vacuum below $\sim 10^{-10}$ mbar requires bake-out procedures (at $\sim 250\,^{\circ}$C) and *in-situ* cleaning of the target surface. Figure 9 shows the apparatus used in Munich which satisfies both conditions [67].

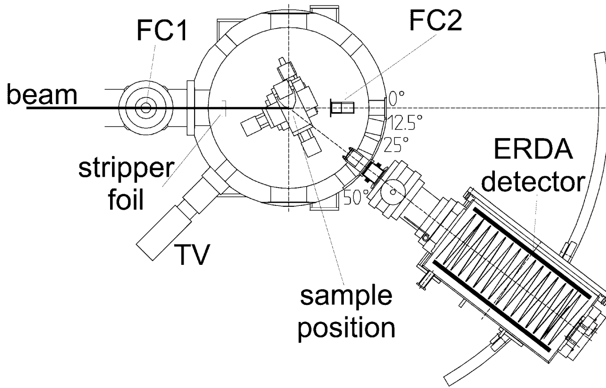

Fig. 6. Scheme of experimental arrangement for sputtering experiments in combination with high-energy ERD analysis at the tandem accelerator in Munich [102,103]. FC1 and FC2 are Faraday cups for beam current measurements. The beam spot position can be checked by a TV-camera. The carbon foil serves simultaneously as electron stripper and beam flux monitor. The sample is mounted on a computer-controlled 5-axis positioning system in the centre of the chamber. The ERDA detector consists of a position-sensitive transversal field ionization counter with a subdivided anode to record the energy loss (ΔE) and remaining stopping energy (E_{rest}) of the recoils

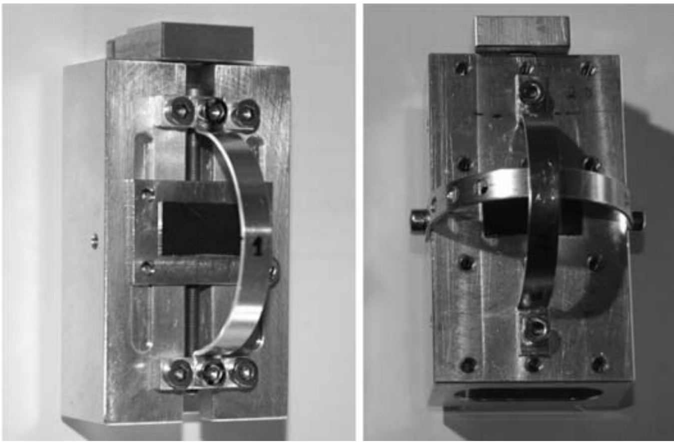

Fig. 7. *Left:* Target holder with arc-shaped catcher mounted perpendicular to the incident ion beam, and movable sample position. *Right:* Double arc configuration for checks of the azimuthal symmetry. After the sputtering experiment, the catcher foil is dismounted, covered by a ~ 50 nm thick Cu layer and analyzed with ERDA

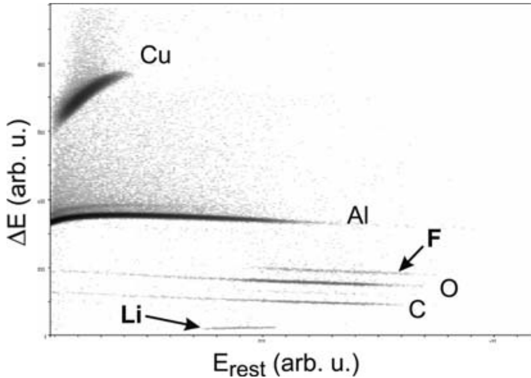

Fig. 8. Typical 2-dim ERDA spectrum (ΔE: energy loss, $E_{\rm rest}$: remaining stopping energy, from which the recoil nuclear charge and depth of origin can be extracted) of Al catcher with particles sputtered from a LiF target. In particular, light elements such as Li and F can be detected with high sensitivity [94]. The Cu signal originates from a thin protective layer deposited on the catcher surface. C and O are omnipresent contaminations especially in the absence of UHV conditions

The UHV chamber is decoupled from the beam line vacuum by a two-stage differential pumping system with two cryo-pumps and a cryo-baffle. By means of quadrupole mass spectrometry the vacuum composition of the chamber can be monitored. To avoid cross contamination, a baffle plate divides the chamber in a lower level for *in-situ* sputter cleaning and an upper level for sample irradiation. A vacuum manipulator moves the targets between the two sections.

Under UHV-conditions, monitoring of the surface contamination during the irradiation is an essential feature which is as important as surface cleaning. Provided that the scattering geometry is suitable, i.e. the beam incidence is sufficiently oblique, ERDA permits simultaneous control of the surface composition. In the apparatus described, a UHV-compatible detector telescope, mounted at a scattering angle of 35°, consists of a gas ionization chamber for ΔE and a solid state detector for $E_{\rm rest}$ detection. The angular variation of the recoil energy can be removed by measuring the scattering angle of the recoils using the position sensitivity of the ΔE unit [103] (kinematic correction). The depth resolution is then sufficient to separate surface and bulk contamination. Surface contaminations as low as $\sim 10^{12}$ at/cm^2 (corresponding to about 10^{-3} of a monolayer) can be identified (Fig. 10). With the careful surface control thus provided, reproducibility of sputtering yields within 15 % has been demonstrated [53, 67].

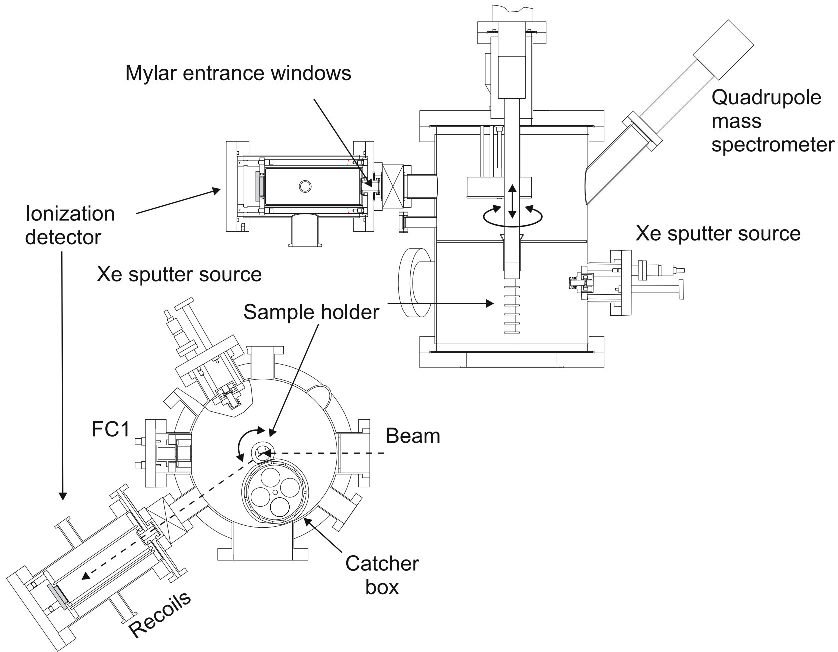

Fig. 9. UHV chamber for sputtering of metallic targets. For in-situ surface cleaning, the samples can be moved into the lower chamber containing a 8 keV Xe sputter gun. Beam exposure and collection of the sputtered particles take place in the upper position. During the experiment the sample surface is monitored by means of ERDA which detects target-specific recoils in a UHV-compatible ionization chamber with a differentially pumped two foil entrance window

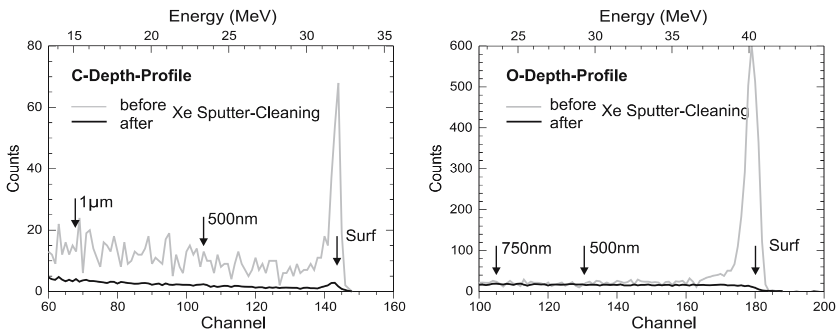

Fig. 10. Surface depth profiles of carbon (*left*) and oxygen (*right*) contamination of a Ti target measured in-situ during 3 h of sputtering with a beam of 230 MeV Au ions before and after sputter cleaning with 8 keV Xe ions. Spectra are normalized to the same ion fluence. The carbon surface peak corresponds to 1 monolayer (ML) before and 0.05 ML after sputter cleaning, respectively to 20 MLs and 0.002 ML of oxygen

3 Experimental Results

This chapter reports experimental results of particles sputtered from surfaces of several materials when irradiated with swift heavy ions. Since the response to high electronic excitations strongly depends on the material class, the angular distributions of sputtered particles and total sputtering yields are grouped according to metals, oxides, and ionic crystals. Before describing the specific details, we shortly discuss phenomena linked to the charge state of the incoming ion and to the dependence of the angle of beam incidence which follow similar trends for all different materials. The experimental errors throughout this chapter are typically 25 % unless stated otherwise.

3.1 Dependence of Sputtering Yield on Charge State of Incoming Ions

The first study with projectiles of different charge states was performed by *Meins* et al. [104] who analyzed the sputtering yield of U particles emitted from a UF_4 surface. Later *Arnoldbik* et al. [77] examined vitreous SiO_2 and *Mieskes* et al. [54] carried out a series of measurements with different materials using ions of equilibrium (eq) charge state or of nonequilibrium (neq) charge state as delivered by the accelerator. Table 1 lists the irradiation parameters and the experimental sputtering yields of these experiments.

Except for Au as target, the sputtering yield becomes significantly larger with increasing charge state of the incoming projectile. For insulators the sensitivity to the electronic energy loss is known and thus the charge dependence is expected. More surprising is the increased sputtering for the two metallic targets Ti and Zr for which sputtering is obviously also influenced by the electronic energy loss.

3.2 Dependence of Sputtering Yield on Angle of Beam Incidence

The total sputtering yield Y_{tot} increases steadily as a function of the incidence angle θ_0 (Fig. 11) without having a maximum around 80° as found for collisional sputtering (see Chap. by *Eckstein*). For the insulators as well as for the Au target, the dependence of Y_{tot} on the angle of beam incidence is well described by

$$Y_{\mathrm{tot}}(\theta_0) = Y_{\mathrm{tot}}(0°)(\cos\theta_0)^{-x} . \tag{4}$$

The exponent x of the data shown scatters between 1.4 and 1.9 with a mean value of $x = 1.7 \pm 0.2$ which is in agreement with experimental results for frozen oxygen [65] and predictions of MD simulations by *Bringa* et al. [106]. The yield enhancement ($x > 1$) is obviously stronger than expected from geometrical considerations, probably because under more grazing incidence the deposited energy becomes more confined in near-surface layers. Equation (4) permits us to normalize and compare total yield values measured at different angles of beam incidence.

Table 1. Sputtering yields and irradiation parameters for different targets and ion beams of various charge states. The angle of beam incidence θ_0 is given with respect to the normal of the sample surface. In some of the experiments, the ions passed through a stripper foil and thus were in equilibrium charge state with a mean charge $\langle q \rangle$. The yield Y_{tot} denotes the total number of sputtered particles per incoming ion (note: only underlined components of compounds are analysed)

Target	Ions	Energy	θ_0	Non-equilibrium (neq)		Equilibrium (eq)		Ref.
		MeV		low charge	Y_{tot}	high charge	Y_{tot}	
Au	Au	230	72°	16^+	10.6	$\langle 29^+ \rangle$	11.8	[54]
Zr	Au	230	72°	16^+	1.7	$\langle 29^+ \rangle$	2.9	[54]
	Au	109	72°	11^+	3.6	$\langle 26^+ \rangle$	5.5	[54]
$\underline{U}F_4$	F	4.8	0°	2^+	7.4	6^+	11.9	[104]
	F	19	0°	4^+	2.1	8^+	7.3	[104]
	F	28.5	0°	5^+	1.1	9^+	8.8	[104]
$\underline{CsI}$	Au	230	72°	16^+	9 100	$\langle 29^+ \rangle$	12 580	[53]
$\underline{Y}_3\underline{Fe}_5O_{12}$	Au	230	72°	16^+	12.4	$\langle 29^+ \rangle$	20.6	[53]
Ge	Au	275	72°	18^+	1.7	$\langle 29^+ \rangle$	2.6	[53]
Ti	Au	275	72°	18^+	3.5	$\langle 29^+ \rangle$	6.5	[54]
	Au	230	72°	16^+	3.7	$\langle 29^+ \rangle$	7.4	[54]
$\underline{LiF}$	Au	230	70°	15^+	21 830	$\langle 29^+ \rangle$	36 090	[105]
a-Si$\underline{O}_2$	Cu	50	75°	8^+	~ 260	$\langle 16^+ \rangle$	~ 425	[77]

3.3 Metallic Materials

The number of electronic sputtering experiments conducted on metallic materials is rather scarce because UHV conditions are necessary as discussed in detail in section 2.4. A first attempt was performed by *O'Connor* et al. [64, 107] using Nb as target. Sputtering yields for irradiations with 100 keV Br^{1+} ions (nuclear energy loss) as well as with neq 70 MeV Br^{7+} ions (electronic energy loss) scale with the nuclear energy loss and follow simulations with the TRIM-CASCADE (TC) code [108]. These observations indicate that sputtering of Nb is not influenced by electronic excitations, at least not for beam parameters as used in this experiment. Later, the approach of *Mieskes* et al. was more systematic by considering several metals of different sensitivity versus swift heavy ion effects [53, 54, 67]. From studies of bulk modifications it is known that only a limited number of pure metals such as Ti, Co, Zr [109], Fe [110], Bi [111]) and some special alloys (e.g., $NiZr_2$ [20], Ni_3B [112], TiNi [113], or metallic glasses [114–116]) can indeed record ion tracks or show modifications in the electronic energy loss regime [20]. If bulk modifications and sputtering follows the same sensitivity pattern, Zr and Ti target were expected to respond by increased electronic sputtering, whereas Au should be an insensitive target material.

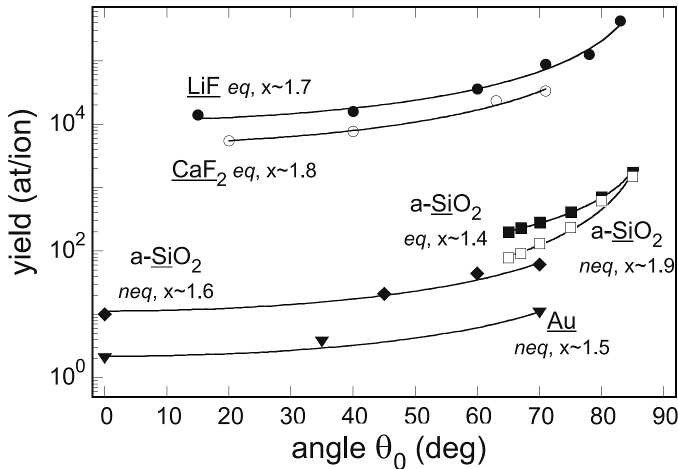

Fig. 11. Total sputtering yield as a function of angle of beam incidence θ_0 with respect to the surface normal for various targets. Irradiations with ions of equilibrium charge states and below equilibrium charge state are denoted by eq and neq, respectively (see also Table 1). The *fitted lines* follow a $(\cos\theta_0)^{-x}$ law. LiF and CaF_2 were irradiated with 210 MeV Au (eq) [55, 105]. Amorphous silica (a-SiO_2) was studied by two groups using (1) 50 MeV Cu ions of charge state 8^+ (neq) or $\langle 16^+ \rangle$ (eq) for θ_0 between 65° and 85° [77] and (2) 30 MeV Cl^{6+} ions (neq) for θ_0 between 0° and 70° [75]. The experiment with the Au target was performed with 230 MeV Au^{16+} ions (neq) [54]. Only underlined components are analysed

3.3.1 Angular Distribution of Sputtered Particles for Metallic Targets

Figure 12 shows the angular distribution of sputtered particles for four different metallic targets. The Nb data are well described by a nearly isotropic $(\cos\theta)^{1.5}$ distribution, in agreement with nuclear collision sputtering where the exponent is in general below 2 [64, 117]. In contrast to Nb, the irradiation of Zr, Ti, and Au targets with 230 MeV Au^{16+} ions produces angular distributions which clearly deviate from isotropy [54]. They can be fitted by a $(\cos\theta)^y$ function with an exponent of $y = 2.5$ for Ti, $y = 3.2$ for Zr, and $y = 3.5$ for the Au target.

3.3.2 Total Sputtering Yields for Metallic Targets

The total yield is obtained by integrating differential sputtering yields of angular distribution measurements using (3) and assuming azimuthal symmetry. The experimental results in combination with nuclear sputtering yields calculated with the TRIM-CASCADE code [108] are summarized in Table 2 for Au, in Table 3 for Zr, and in Fig. 13 for Ti. The stopping powers of the

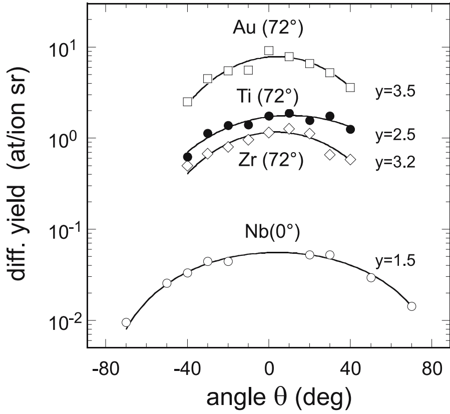

Fig. 12. Angular distributions for different metallic targets following a $(\cos\theta)^y$ law (*solid lines*). The angle of beam incidence with respect to the surface normal and the fitted values for y are indicated. The irradiation of Nb was performed with 70 MeV Br^{7+} ions (neq), whereas the Zr, Ti, and Au targets were exposed to 230 MeV Au^{16+} ions (neq) [54]

Table 2. Irradiation parameters and sputtering yields for Au targets exposed to Au and I ions under beam incidence of $\theta_0 = 72°$. The ions were either in equilibrium mean charge state $\langle q \rangle$ or had a well defined but lower charge state q. $(dE/dx)_\mathrm{e}$ for ions in equilibrium charge state and $(dE/dx)_\mathrm{n}$ are deduced from the TRIM code [118]. The sputtering yield caused by elastic collisions (Y_TC) is calculated with the TRIM-CASCADE code [108]

projectile	charge state	$(dE/dx)_\mathrm{e}$ keV/nm	$(dE/dx)_\mathrm{n}$ keV/nm	Y_TC at/ion	Y_exp at/ion
Au	$\langle 29^+ \rangle$				11.8 ± 1.4
		55.4	0.62	3.0	
230 MeV	16^+				10.6 ± 1.1
I	$\langle 21^+ \rangle$				8.3 ± 1.1
		22.7	0.63	4.1	
55 MeV	7^+				10.3 ± 1.3

different ion beams are deduced from the TRIM code [118]. Note that projectiles of non-equilibrium charge state have a different electronic energy loss which is in general not well defined (cf. Fig. 3).

Although the results for the Au targets are rather limited, there is no obvious evidence for electronic stopping effects such as charge state dependence of the yield or increased sputtering for larger electronic stopping values. However, we note that the experimental yields are significantly larger than the ones expected from collisional sputtering.

Table 3. Irradiation parameters and sputtering yields for Zr targets exposed to Au and I ions under beam incidence of $\theta_0 = 72°$. The ions were either in equilibrium mean charge state $\langle q \rangle$ or had a well defined but lower charge state q. $(dE/dx)_n$ and $(dE/dx)_e$ for ions in equilibrium charge state are deduced from the TRIM code [118]. The sputtering yield caused by elastic collisions (Y_{TC}) is calculated with the TRIM-CASCADE code [108]

projectile	charge state	$(dE/dx)_e$ keV/nm	$(dE/dx)_n$ keV/nm	Y_{TC} at/ion	Y_{exp} at/ion
Au	$\langle 29^+ \rangle$				2.9 ± 0.3
		30	0.27	1.07	
230 MeV	16^+				1.9 ± 0.2
Au	$\langle 29^+ \rangle$				5.5 ± 0.7
		22	0.47	1.93	
109 MeV	11^+				3.6 ± 0.4
I	$\langle 28^+ \rangle$				0.8 ± 0.1
		24	0.10	0.50	
210 MeV	15^+				0.5 ± 0.1
I	$\langle 21^+ \rangle$				1.7 ± 0.2
		15	0.26	1.39	
59 MeV	8^+				1.3 ± 0.2

In contrast, sputtering of Zr (see Table 3) and Ti (see Fig. 13) show several indications of being influenced although not dominated by the electronic energy loss: 1. For a fixed beam energy, higher charge states corresponding to higher electronic energy losses result in larger sputtering yields. 2. For ions with equilibrium charge state and fixed nuclear energy loss, the sputtering yield increases with electronic energy loss (cf. 230 MeV $Au^{\langle 29+ \rangle}$ ions and 59 MeV $I^{\langle 21+ \rangle}$). 3. Sputtering experiments with similar electronic but different nuclear energy loss (cf. 109 MeV $Au^{\langle 26+ \rangle}$ and 210 MeV $I^{\langle 28+ \rangle}$ ions) give larger sputtering yields at higher nuclear energy losses; the difference may be additionally enhanced by the velocity effect. 4. In particular for high electronic energy losses, the yields of sputtered Zr and Ti particles calculated with the TC code [108] are smaller than the experimental yields.

Another example is shown in Fig. 13 for titanium irradiated with eq Au ions of different energies between 100 MeV and almost 300 MeV. For increasing beam energy, the sputtering rate remains nearly constant although the electronic energy loss increases by a factor 1.4 while the nuclear energy loss decreases by a factor of 2. These results can not be explained assuming exclusively nuclear or electronic effects. To separate the contributions quantitatively is difficult at that stage, in particular in view of the very small absolute yield values.

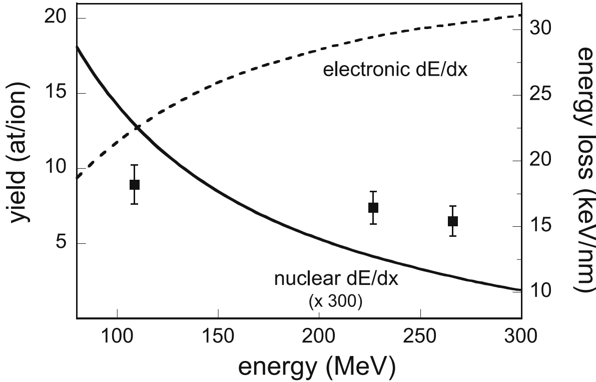

Fig. 13. Experimental sputtering yield as a function of the beam energy for a Ti target exposed to Au ions. The *lines* are the nuclear (multiplied by a factor of 300) and the electronic energy losses according to [118]

3.4 Insulating Oxides

3.4.1 Angular Distributions of Sputtered Particles for Oxides

Sputtering experiments with insulating materials are easier because the yields are much larger and there is no risk of surface oxidation such as for metals. However, as mentioned above, reliable quantification of sputtered oxygen is difficult, therefore most experimental results are limited to the non-oxide component of the target. Figure 14 presents angular distributions of three different crystalline oxides: non-amorphizable UO_2 [119], and two materials that easily amorphize $Y_3Fe_5O_{12}$ [53] and SiO_2 quartz [55].

Sputtered Si particles from crystalline as well as from amorphous SiO_2 exhibit a slightly over-cosine distribution with an exponent of around 1.3. The yield of amorphous SiO_2 is about twice as large as for crystalline quartz. This is in good agreement with track observations in bulk material where amorphous SiO_2 is more sensitive [120] than is SiO_2 in its crystalline phase [121]. The yields observed for UO_2 and $Y_3Fe_5O_{12}$ are 1-2 orders of magnitude lower. In contrast to the isotropic cosine distribution of SiO_2, the particle emission of UO_2 and $Y_3Fe_5O_{12}$ shows an enhanced peak indicating preferential sputtering normal to the sample surface. The data cannot be fitted to a simple $(\cos\theta)^y$ equation, but a second Gaussian shaped component is needed (see (5)). For $Y_3Fe_5O_{12}$ the relative composition of the sputtered Y and Fe atoms is not preserved at large theta angles. *Matsunami* et al. performed special experiments with carbon catchers [122, 123] and find indications for stoichiometric sputtering of oxides such as SiO_2, $SrCeO_3$, $SrTiO_3$, but not of $YBa_2Cu_3O_{7-\delta}$ [99].

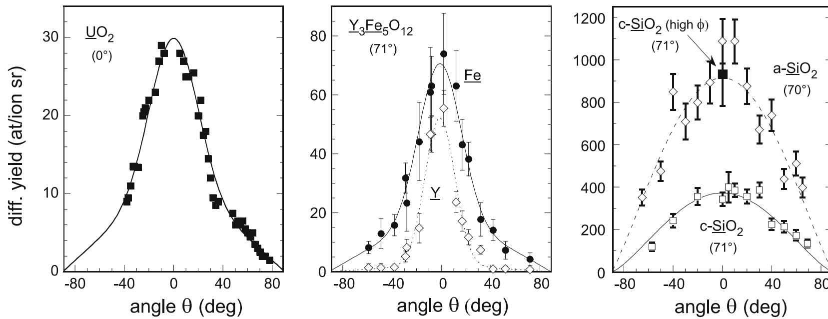

Fig. 14. Differential sputtering yields as a function of the azimuthal angle for different oxides (the angle of beam incidence θ_0 is indicated, analyzed components are *underlined*): (*left*) UO_2 irradiated with 980 MeV Xe ions, (*center*) $Y_3Fe_5O_{12}$ irradiated with 200 MeV Au ions, and (*right*) amorphous (a-SiO_2) and crystalline SiO_2 (c-SiO_2) irradiated with 200 MeV Au ions. The single data point (*full square*) results from a high-fluence irradiation of crystalline SiO_2 where severe track overlap leads to amorphization

3.4.2 Total Sputtering Yields for Oxides

Most early sputtering experiments recording total yields used flat catchers (e.g., Eu_2O_3 [60], $YBa_2Cu_3O_{7-\delta}$ [99], Al_2O_3 [123,124], UO_2 [62], $LiNbO_3$ [124], SiO_2, $SrCeO_3$, $SrTiO_3$, MgO, TiO_2, and ZnO [122, 123]). More recent investigations concentrated on the angular distribution of the sputtered particles by collecting them on arc-shaped catchers (e.g., SiO_2 [55] and UO_2 [119]). In case of an isotropic distribution (or close to isotropic), the total yield is deduced by integrating the differential yield according to (2), otherwise (e.g., UO_2 and $Y_3Fe_5O_{12}$) a two component equation has to be used as discussed in more detail in Sect. 3.5.1. The evolution of the total sputtering yield versus electronic energy loss is clearly influenced by the material itself (Fig. 15). The power laws fitted to the different solids have an exponent between approximately 1.5 and 4.

Data presented on the right graph of Fig. 15 were obtained with low irradiation fluences avoiding amorphization of the sample structure. In contrast, experimental results shown in Fig. 15 (left) were produced with fluences leading to overlapping of amorphized track zones. In this situation the solid is probably no longer in its crystalline state. This is a crucial point because amorphous solids can have a higher sputtering yield than crystals as demonstrated for vitreous and crystalline SiO_2 (Fig. 14, right). Sputtering yields deduced from high-fluence irradiations have to consider this effect. In some cases such as for example high-T_c superconductors, the situation is even more dramatic because, in the course of irradiation, amorphization transforms this metal into an insulator.

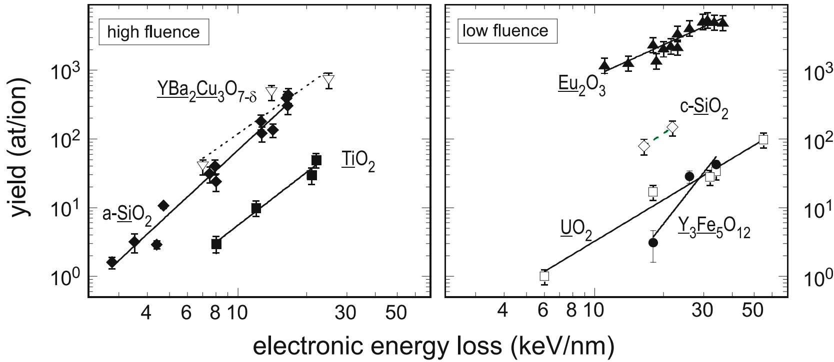

Fig. 15. Total sputtering yield as a function of energy loss for different oxides, $YBa_2Cu_3O_{7-\delta}$ [99], vitreous (a-SiO_2) (deduced either from Si yield [105, 122] or from O yield measurements [75, 77]) and crystalline quartz (c-SiO_2) [55], TiO_2 [122, 123], Eu_2O_3 [60], $Y_3Fe_5O_{12}$ [68] and UO_2 [119] (analyzed components are *underlined*, data are corrected by angle of beam incidence). The sputtering experiments were performed (*right*) at low ion fluences in the single track regime (i.e., below $\sim 2 \times 10^{12}$ ions/cm^2) and (*left*) at high fluence with significant track overlapping and thus amorphization. The yield as a function of electronic energy loss is fitted by a power law $((\mathrm{d}E/\mathrm{d}x)_\mathrm{e})^p$ (*lines*), for all materials the exponent is close to 2 ± 0.5 except for a-SiO_2 ($p = 3.1$) and for $Y_3Fe_5O_{12}$ ($p = 4.2$)

3.5 Ionic Insulators

3.5.1 Angular Distributions of Sputtered Particles for Ionic Crystals

The first sputtering experiments in the electronic energy loss regime which aimed to measure neutral particles in combination with the arc-catcher technique were performed in the 1980s for a UF_4 target irradiated with O, F, and Cl ions of energies around the Bragg peak [11,62,104]. The measured velocity of the emitted U atoms was close to a Boltzmann distribution, and the angular distribution followed a cosine law of $(\cos\theta)^{\sim 0.85}$. By applying a similar arc-catcher technique, more recent experiments for other non-amorphizable targets (e.g., LiF, CaF_2, NaCl) revealed angular distributions which are not purely isotropic but exhibit an additional jet-like component [55,105] as illustrated in Figs. 16 and 17. Depending on the beam parameters, this component is more or less pronounced, but it always appears normal to the surface for all angles of beam incidence.

A fit to the observed angular distributions can be accomplished by a two-component equation (see Fig. 16):

$$Y_\mathrm{diff}(\theta) = A_\theta \cos\theta + B_\theta \exp^{-\theta^2/2\sigma^2} , \quad (5)$$

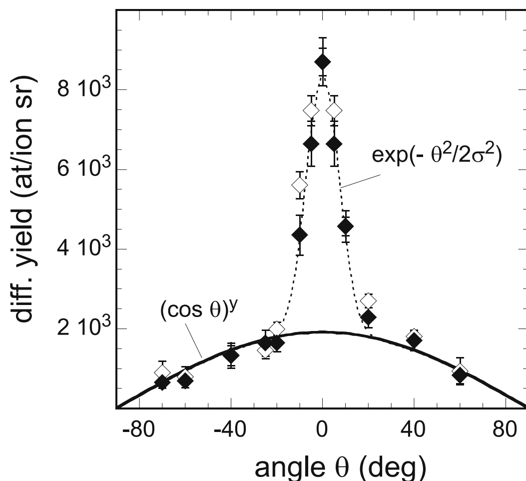

Fig. 16. Angular distribution of Li (*full symbol*) and F (*open symbol*) sputtered from the (100) surface of a single LiF crystal irradiated with 210 MeV Au ions under beam incidence of $\theta_0 = 20^\circ$ with respect to the surface normal. Mathematically the distribution is described by a broad cosine (*bold line*) superimposed by a sharp Gaussian curve (*dashed line*) as given by (5)

where the first component is broad and characterizes the isotropic contribution, and the second Gaussian part describes the "jet-like" peak of width σ (in rad); A_θ and B_θ denote the respective contributions of the two components.

Within the experimental errors, sputtering of Li and F is stoichiometric. The total yield of LiF reaches values of several thousands of sputtered particles per incident ion, almost two orders of magnitude larger than for SiO_2. This huge yield is well beyond collisional cascade sputtering expectations and rules out any crystalline orientation effect such as Wehner spots [125].

The angular distributions for various ion species and energies are illustrated in Fig. 17 showing the results for two different angles of beam incidence ($\theta_0 = 20$–25° (left) and 71° (right)). The projectiles between Ni and Au ($\sim 1\,\text{MeV/u}$) cover an electronic energy loss regime from 5–22 keV/nm. For a given energy loss, the sputtering yield increases with decreasing angle of beam incidence, in agreement with (4).

The width of the jet component depends on the angle of incidence and on the energy loss of the projectile (Fig. 18). Under flat incidence ($\theta_0 = 71^\circ$), the jet width gets broader for larger energy losses in contrast to the narrowing at smaller angles of incidence ($\theta_0 = 20$–25°). For Au and I ions the contribution of the jet component to the total sputtering yield follows the same trend. A similar characteristic also appears for other ionic crystals such as CaF_2 and NaCl.

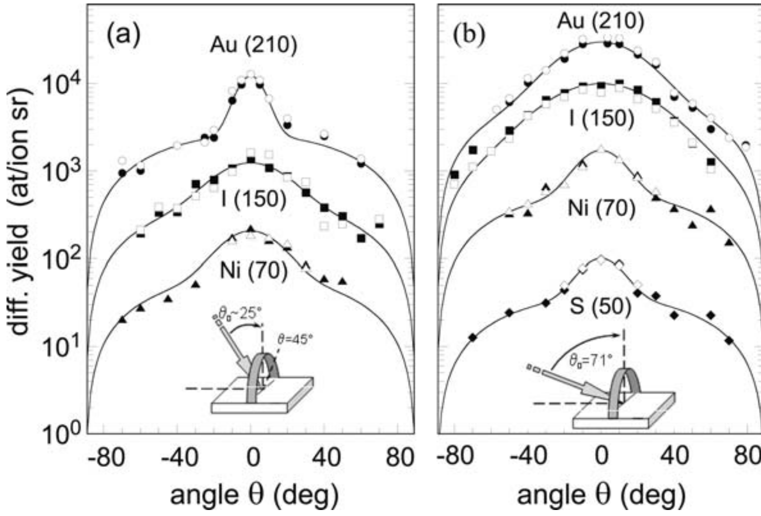

Fig. 17. Angular distributions of the Li (*full symbols*) and F (*open symbols*) sputtered from cleaved (100)-LiF crystals. The irradiations were performed under $\theta_0 = 20$–$25°$ (*left*) and $\theta_0 = 71°$(*right*) using different ions of equilibrium charge state. The energy of the beam is indicated in MeV [55]

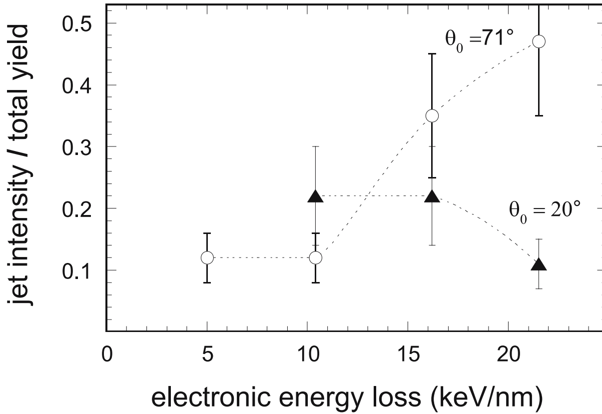

Fig. 18. LiF irradiated with various ions under $\theta_0 = 71°$ and 20°. The relative intensity of the jet component (deduced from angular distribution data using (5)) as a function of the electronic energy loss strongly depends on the angle of beam incidence (*lines* are guides to the eye)

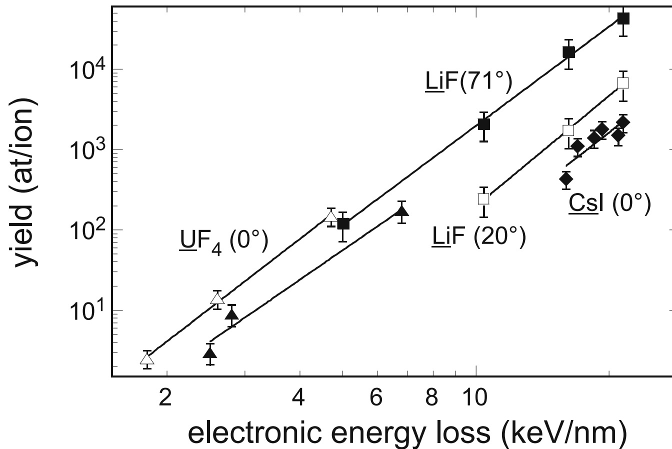

Fig. 19. Total sputtering yield as a function of electronic energy loss for CsI (*diamonds*) [60], UF_4 (*open triangles* for 0.25 MeV/u beam, *full triangles* for 1 MeV/u beam) [104], and LiF (*squares*) [55] (only *underlined* components are presented). The angle of beam incidence is given with respect to the sample surface. *Lines* are fits based on a dE/dx power law with an exponent of 4 ± 0.4

3.5.2 Total Sputtering Yields for Ionic Crystals

When determining the total yield of the sputtering process by integrating the differential yield over 2π solid angle, it is evident that the shape of the distribution plays an important role. Several experiments with double catchers mounted parallel *and* perpendicular to the incoming beam have shown that the jet component exhibits approximately azimuthal symmetry. The integration of (5) gives the total sputtering yield Y_{tot}

$$Y_{\mathrm{tot}} = 2\pi \int_0^{\pi/2} (A_\theta \cos\theta + B_\theta \exp^{-\theta^2/2\sigma^2}) \sin\theta \, \mathrm{d}\theta = \pi(A_\theta + 2B_\theta\sigma^2) \,. \quad (6)$$

Figure 19 presents total yields of CsI, UF_4, and LiF as a function of the electronic energy loss. Fitting these data by a power law (solid lines) leads to an exponent of about 4 ± 0.4 independent of material and beam incidence. The significant yield difference between the two UF_4 data sets is ascribed to the projectile velocities.

3.6 Summary of Experimental Sputtering Data of Different Materials

In the electronic energy loss regime, metals, oxides, and ionic crystals differ significantly concerning total sputtering yields as well as angular distributions of the sputtered particles (Fig. 20). The electronic sputtering yields of insulators are several orders of magnitude larger than those of metals. Among

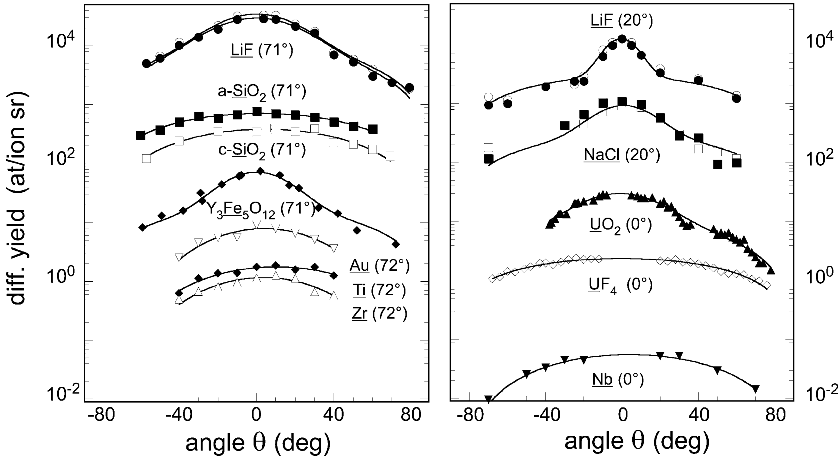

Fig. 20. Angular distributions of particles emitted from different metallic and insulating targets: (*left*) rather flat beam incidence ($\theta_0 \sim 71$–$72°$) and (*right*) close to normal incidence ($\theta_0 \sim 0$–$20°$). Only yields of underlined sputtering components are presented (LiF [55], SiO_2 [55], $Y_3Fe_5O_{12}$ [105], Au, Ti, Zr [54], NaCl [105], UO_2 [119], UF_4 [62], and Nb [64])

insulators, ionic crystals reveal much larger sputtering yields than oxides. This trend follows the sensitivity of these materials known for bulk modifications under swift heavy ion irradiation. For all materials investigated so far, the total yield increases for larger grazing beam incidence by a $(\cos\theta_0)^{-x}$ law, with x between 1.4 and 1.9.

Electronic sputtering is demonstrated for metals such as Ti and Zr. The total yield is low, but reaches values typically one order of magnitude larger than expected for nuclear sputtering. Electronic contributions to the sputtering process are also apparent by the fact that the yield of Ti and Zr depends on the charge state of the incident ions and thus scales with the electronic energy loss. Although $(\mathrm{d}E/\mathrm{d}x)_\mathrm{n}$ is rather small in the electronic energy loss regime, one has to keep in mind that collisional sputtering results from a direct and thus effective energy transfer to the target atoms. Whereas for electronic sputtering the transfer efficiency of $(dE/dx)_\mathrm{e}$ is controlled by the strength of the electron-phonon coupling of a given material and amounts to 1 % typically. The Ti and Zr angular distributions exhibit a slightly overcosine shape. Finally we should emphasize that the observation of electronic sputtering is consistent with the fact that Ti as well as Zr is one of the few track recording metals.

For insulators, electronic sputtering yields are orders of magnitude larger than typical yields in the nuclear energy loss regime. Crystalline targets exhibit lower sputtering yields than the same material in its amorphous state. To avoid structural changes the total applied fluence within a given beamspot area has therefore to be limited.

Concerning the angular distribution of insulators two major trends were observed: several oxides (e.g., SiO_2) have a slightly overcosine distribution, whereas sputtering of ionic crystals (e.g., LiF, CaF_2, NaCl, etc.) and some oxides (e.g., $Y_3Fe_5O_{12}$) is characterized by a jet component superposed on the isotropic cosine distribution. The jet component is a new phenomenon, irrespective of the incoming beam it appears normal to the target surface and seems to exhibit azimuthal symmetry. The relative intensity of the jet component varies with the angle of beam incidence and electronic energy loss.

4 Calculations Based on the Inelastic Thermal Spike Model

In the past, Monte-Carlo codes such as TRIM.SP [126] or TRIM-CASCADE [108] and Molecular Dynamics (MD) computer simulations (see Chaps. by *Eckstein* and *Urbassek* and by *Urbassek*) have greatly contributed to the quantitative understanding of sputtering caused by collisional cascades in the nuclear stopping regime. For high-energy ions, TRIM-based codes include electronic stopping (tabulated values) between two elastic collisions, but they do not take into account that the energy of the incident ion is in fact first given to the electrons and only partially transferred to the atoms. Because of this limitation, sputtering at energies where the dominant stopping process is based on electron interactions cannot be simulated by these standard codes. Most existing MD calculations describe effects resulting from elastic collisions and only a few simulations are committed to the electronic energy loss regime mainly concentrating on the size and cylindrical geometry of the energy deposition [106, 127–131]. An exploratory effort has been made to simulate sputtering when the energy deposited in the electronic subsystem is gradually transferred to the lattice system [132]. These calculations give strong indications for a non-linear dependence of the sputtering yield on the energy of the incident ions in agreement with experimental observations [55, 66, 133].

Besides these microscopic descriptions of sputtering, there exists also a thermodynamic approach to the problem. The energy input by the projectile acts as a heat source and the diffusion of the deposited energy is followed in space and time by the classical heat transport equation. In the nuclear energy loss regime, thermal-spike models (e.g. elastic collision spike [58]) were developed to explain non-linear sputtering by thermal effects. In the electronic energy loss regime, however, the ion energy is first deposited to the electrons on a time scale of $\sim 10^{-16}$ to $\sim 10^{-14}$ s. Since this is much faster than the characteristic time of electron-phonon relaxation ($\sim 10^{-14}$ to $\sim 10^{-11}$ s), the energy is first shared and thermalized between the electrons (within $\sim 10^{-15}$ s), and with some time delay, the electrons finally transfer energy to the lattice atoms producing a local thermal spike. The term "thermal spike" originally proposed by *Seitz* and *Koehler* [50] and analytically elaborated by *Lifshitz* et

al. [134] considers the short time scale on which these processes take place. Later, it has also been applied to describe electron and lattice temperatures in targets exposed to ps- or fs-laser pulses [135]. In the following section, we are presenting a model based on such a transient thermal process that successfully describes ion track formation in many materials and was recently extended to surface sputtering [54, 55, 136].

This model, denoted as *inelastic* thermal-spike (i-TS), gives a quantitative description of experimental threshold values for track formation, the evolution of track radii as a function of electronic stopping for many metals [51, 111] and insulators [52, 137], and thermally activated defect annealing in metals [138–140]. The temperature evolution of the electronic and atomic subsystems is described by two non-linear differential heat-flow equations (7 and 8) with mutual energy exchange. The heat source $A(r,t)$ is provided by the energy deposition of the projectile to the electronic subsystem [2, 141, 142]. Since the trajectory of the projectiles can be regarded as straight, the equations are expressed in cylindrical geometry with r being the radial distance from the ion trajectory and t the time:

$$C_{\mathrm{e}}(T_{\mathrm{e}}(r,t))\frac{\partial T_{\mathrm{e}}(r,t)}{\partial t} = \frac{1}{r}\frac{\partial}{\partial r}\left[rK_{\mathrm{e}}[T_{\mathrm{e}}(r,t)]\frac{\partial T_{\mathrm{e}}(r,t)}{\partial r}\right] - g(T_{\mathrm{e}}(r,t) - T_{\mathrm{a}}(r,t)) + A(r,t) \quad (7)$$

$$C_{\mathrm{a}}(T_{\mathrm{a}}(r,t))\frac{\partial T_{\mathrm{a}}(r,t)}{\partial t} = \frac{1}{r}\frac{\partial}{\partial r}\left[rK_{\mathrm{a}}[T_{\mathrm{a}}(r,t)]\frac{\partial T_{\mathrm{a}}(r,t)}{\partial r}\right] + g(T_{\mathrm{e}}(r,t) - T_{\mathrm{a}}(r,t)) \quad (8)$$

T, C, and K are the respective temperature, specific heat coefficient and thermal conductivity of the electronic (index e) and atomic system (index a). The energy exchange between the two subsystems is taken into account by the product of the coupling constant g and the temperature difference of the two systems. In the initial phase, the temperature of the electronic system is higher than the lattice temperature, and energy is transferred from the electrons to the atoms. At the end of the thermal spike process, the situation can be inverted ($T_{\mathrm{e}} < T_{\mathrm{a}}$), and electron-phonon coupling may have the reverse effect acting for example in metals as a cooler for the lattice. $A(r,t)$ denotes the spatiotemporal energy deposition of the projectile to the electron subsystem described by a Gaussian time distribution and a radial distribution $F(r)$ of the delta electrons according to the Katz model [2, 141]

$$A(r,t) = b(dE/dx)_{\mathrm{e}} \exp^{-(t-t_0)^2/2t_0^2} F(r)\,, \quad (9)$$

where t_0 corresponds to the time, the electrons take to reach thermal equilibrium [142]. The majority of the electrons deposit their energy close to the ion path within $t_0 = 10^{-15}$ s. In the calculation, the energy deposition extends over a time period of 4×10^{-15} s. The factor b ensures that the integration of A(r,t) in space and time is equal to the total electronic energy loss $(dE/dx)_{\mathrm{e}}$ [111].

The thermal parameters C_e and K_e in (7) and (8) strongly depend on the material properties. For noble metals, the thermal parameters are well described by the quasi-free-electron gas theory. At low temperature, the specific heat C_e is given by a linear function of T_e

$$C_\mathrm{e} = \gamma T_\mathrm{e} = (\pi^2 k_B^2 n_\mathrm{e}/2E_\mathrm{F})T_\mathrm{e} \quad \text{and} \quad E_\mathrm{F} = (\hbar/2m_\mathrm{e})(3\pi^2 n_\mathrm{e})^{2/3}\,, \tag{10}$$

where E_F is the Fermi energy, m_e is the electron mass, n_e is the electron density, and k_B and $\hbar$ are the Boltzmann and Planck constants, respectively. C_e values follow this linear law up to the Fermi temperature $T_\mathrm{F} = E_\mathrm{F}/k_\mathrm{B}$ and then remain constant ($C_\mathrm{e} = 1.5k_\mathrm{B}n_\mathrm{e}$) at higher temperatures. The thermal conductivity $K_\mathrm{e}(T_\mathrm{e})$ is determined from $K_\mathrm{e}(T_\mathrm{e}) = C_\mathrm{e}(T_\mathrm{e})D_\mathrm{e}(T_\mathrm{e})$, where D_e denotes the temperature dependent thermal diffusivity of the electrons. Since in a noble metal (such as Au, Ag, or Cu) the thermal conductivity is mainly controlled by the electrons, the temperature dependence of D_e can be deduced from conductivity measurements in combination with the quasifree electron-gas model. According to this approach, D_e decreases with the electron temperature (approximately by T_e^{-1}) and finally reaches a constant value (D_min) around the Fermi temperature. This behavior agrees well with the universal curve for the electron mean free path as a function of the electron energy [143]. In the i-TS simulations, a value of $D_\mathrm{e}(300\,\mathrm{K}) = 150\,\mathrm{cm}^2\cdot\mathrm{s}^{-1}$ and $D_\mathrm{min} = 2\,\mathrm{cm}^2\cdot\mathrm{s}^{-1}$ is supposed for all metallic targets [111, 144].

The electron-phonon coupling parameter g describes the relaxation between the electrons and the atoms of the lattice. For a metal characterized by the quasifree electron gas model, g can be expressed according to *Kaganov* et al. [145] by

$$g = \frac{\pi^4 (k_\mathrm{B} n_\mathrm{e} \nu)^2}{18K(T_\mathrm{a})} \quad \text{with} \quad \nu = \frac{k_\mathrm{B} T_D}{\hbar(6\pi^2 N)^{1/3}}\,, \tag{11}$$

where ν is the speed of sound, T_D is the Debye temperature, and N denotes the atomic density. Here $K(T_\mathrm{a})$ is the measured thermal conductivity of the irradiated metal. According to this equation, the electron-phonon coupling is large for metals, which have a large Debye temperature and a small thermal conductivity.

The thermodynamical parameters of the lattice subsystem such as specific heat, enthalpy of fusion, and sublimation energy can be measured. Rather delicate is the thermal conductivity of the lattice because in metals it is dominated by the transport properties of electrons, and thus electron and phonon effects cannot be separated experimentally. On the other hand, metals are cooled down within $\sim 3\times10^{-13}$ s via electron-phonon coupling. In this short time period, the energy transport on the atoms is negligible and thus the exact knowledge of the thermal conductivity of the lattice is of minor relevance.

For insulators the electronic parameters are more problematic mainly because the evolution of C_e and D_e as a function of temperature is not known.

According to *Baranov* et al. [13], hot electrons in the conduction band of an insulator are expected to behave like hot electrons in a metal. At high electron temperatures, the i-TS model therefore assumes that C_e and D_e are constant and equal to $1\,\mathrm{J \cdot cm^{-3} \cdot K^{-1}}$ and $2\,\mathrm{cm^2 \cdot s^{-1}}$, respectively [52]. The electron-phonon coupling of insulators is linked to the electron-phonon mean free path λ by the relation $\lambda^2 = C_e D_e / g$. When the electronic temperature has cooled down below T_a, electrons are supposed to be trapped in the lattice and consequently the lattice cooling by cold free electrons is inhibited. The thermodynamical lattice parameters of insulators, including the thermal conductivity, are experimental data from literature.

In the i-TS model calculations, g (metal) and λ (insulator) is the respective free parameter which is fitted to the experimental track radius of a given ion and corresponding energy loss. The two differential equations (7) and (8) are solved numerically as a function of space and time [21,51,52,111]. Within the time interval $\mathrm{d}t$, the energy deposited in the electronic system spreads as a function of the radius according to the thermal conductivity. Using the specific heat, this energy is converted into a temperature of the electrons. The difference in temperature between the electron and lattice subsystems $[T_e(r,t) - T_a(r, t - \mathrm{d}t)]$ multiplied by $(g \cdot \mathrm{d}t)$ gives that part of the energy that is transferred to the atomic subsystem during $\mathrm{d}t$. Subsequently, the energy is dissipated in the lattice subsystem providing the energy per atom $E_a(r,t)$ and respective lattice temperature $T_a(r,t)$.

For metals and amorphisable insulators, track formation has been linked to the criteria of local melting. The track size is therefore defined by the radial zone which contains sufficient energy for melting, e.g. the energy to reach the melting temperature plus the latent heat of fusion [51, 52, 137]. During the temperature increase, the latent heat of the solid-liquid or liquid-gas transition could in principle be taken into account. However, given the rapid heating of the lattice, superheating (SH) seems to be a more adequate scenario and thus is assumed in most i-TS calculations [54,55,146]. During the cooling process, the molten cylinder is quenched resulting in an amorphous or otherwise defective track zone.

Figure 21 shows the result of thermal spike calculations for a 200 MeV Au ion in SiO_2 quartz. In the electron subsystem (left), a cylindrical zone of $\sim 8\,\mathrm{nm}$ heats up within several $10^{-15}\,\mathrm{s}$ to more than 1000 K, meanwhile the atomic subsystem (right) is still cold. The temperature of the atoms increases with a time delay of about $10^{-14}\,\mathrm{s}$. According to the model calculation (assuming super heating), the temperature at a distance of 0.5 nm to the ion path can reach almost 8000 K.

In Fig. 22, the thermal-spike temperatures of metallic Ti and insulating SiO_2 quartz are compared. For both materials, the enthalpy of fusion (melting) and the sublimation energy are surpassed. Compared to quartz, the temperature of Ti cools down about two orders of magnitude faster because cooling of the lattice is strongly enhanced.

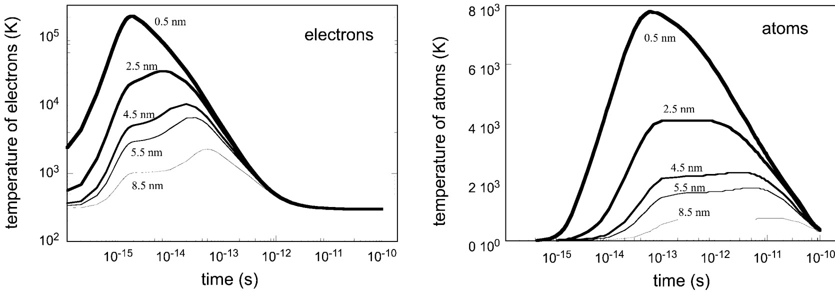

Fig. 21. Thermal-spike model calculations, describing the energy dissipation of a 200 MeV Au ion in SiO_2 quartz: temperature of the electron (*left*) and atomic (*right*) subsystem as a function of time. The *curves* represent different radial distances from the ion path

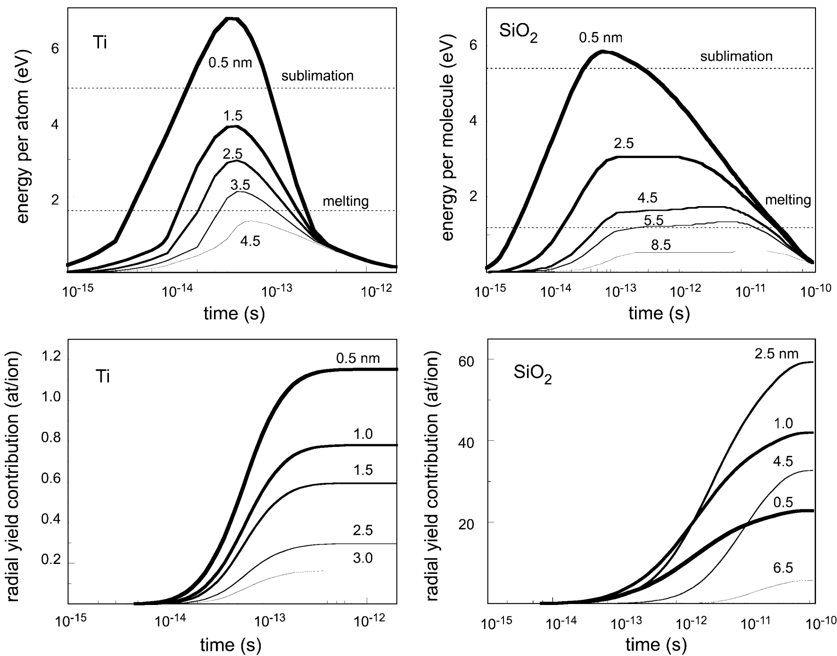

Fig. 22. Thermal-spike calculations for metallic Ti (*left*) and insulating SiO_2 quartz (*right*) irradiated with Au ions of 275 and 200 MeV, respectively. Note the different time scales for the two materials. *Top:* Energy per atom in the lattice system as a function of time. The different *curves* correspond to different cylinder shells around the ion path in nm (shell width 0.5 nm). Fits to experimental track radii yield $g = 10^{13}\,\mathrm{W \cdot K^{-1} cm^{-3}}$ for Ti [51] and $\lambda = 3.8\,\mathrm{nm}$ for SiO_2 quartz [147]. *Bottom:* Time integrated number of Ti atoms and SiO_2 molecules sputtered from different cylinder shells (width 0.5 nm) around the ion impact

The g values fitted to experimental track radii of various metals [51] are in good agreement with results derived from electrical conductivity measurements or femto-second laser experiments [148]. For insulators a direct comparison with values deduced by other techniques is not available, but plotting the fitted λ values for different insulators points to a direct relation to the inverse of the band gap energy [52, 137]. This is not unexpected when considering that cooling of hot electrons occurs via excitation of peripheral cold electrons from the valence to the conduction band which is directly linked to the band gap [149].

To describe electronic sputtering, the i-TS model calculations were extended in such a way that the thermal evaporation rate can be computed as a function of the local energy $E_\mathrm{a}(r,t)$ of the atoms. According to the Sigmund model [58], the sputtering process can be described by statistical thermodynamics and the Maxwell-Boltzmann equation with an evaporation rate $\varPhi$ of

$$\varPhi[E_\mathrm{a}(r,t)] = N\sqrt{\frac{E_\mathrm{a}(r,t)}{2\pi M}}\,\exp^{-U/E_\mathrm{a}(r,t)}\,, \tag{12}$$

where N is the atomic density and M is the molecular mass of the target. U denotes the sublimation energy per evaporated atom or molecule which is assumed equal to the surface binding energy. For temperatures above vaporization, the thermal diffusivity of the lattice increases with the square root of the temperature [150, 151]. The total sputtering yield Y_tot is obtained from the time and space integral of $\varPhi(r,t)$

$$Y_\mathrm{tot} = \int_0^\infty \mathrm{d}t \int_0^\infty \varPhi(E_\mathrm{a}(r,t))2\pi r\,\mathrm{d}r\,. \tag{13}$$

Large sputtering yields are obtained if the sublimation energy is small and if the duration of increased lattice temperature is large.

The numerical calculations are performed in cylindrical geometry, and projectiles are assumed to be in an equilibrium charge state, i.e., the energy loss along the ion trajectory does not change. Because of the short time of sputtering, radiative losses at the surface are neglected. Also the kinetic energy removed by the emitted atoms is not taken into account. The ion impact occurs under normal incidence to avoid geometrical effects (e.g., reduced cooling under grazing incidence given by the proximity of the free surface). When comparing with sputtering yields from tilted beam experiments, the data have therefore to be angle corrected by $(\cos\theta_0)^{-x}$. According to experimental findings, we apply the value $x = 1.5$ for metals [53], $x = 1.6$ for SiO_2 [75, 77], and $x = 1.8$ for LiF as target [55].

The two lower plots of Fig. 22 present evaporated particles accumulated as a function of time based on i-TS calculations. The particles originate from different cylinder shells around the ion impact point. For Ti the sputtering process ceases after about 3×10^{-13} s leading to a small total yield, in contrast to quartz where sputtering persists beyond 10^{-11} s due to limited cooling.

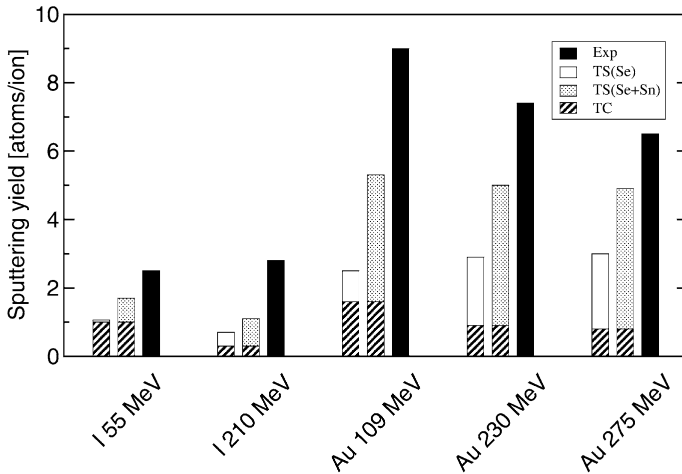

Fig. 23. Sputtering yields for Ti irradiated with I and Au ions of different nuclear and electronic energy loss. *Exp* denotes experimental data, and *TC* corresponds to collisional sputtering as deduced from the TRIM-CASCADE code. Additional contributions to TC from pure electronic *TS(Se)* and from a combination of the nuclear and electronic heating *TS(Se + Sn)* are calculated with the i-TS model

This leads to much higher sputtering yields although in both lattice systems the deposited energy contents are of the same order of magnitude.

4.1 Application to Metals

Experiments in the electronic energy loss regime show that sputtering yields of metallic Ti and Zr targets are significantly larger than pure nuclear sputtering due to collisional cascades (see TC values in Fig. 23). Comparing the different data of Fig. 13 suggests that the electronic energy loss does not play a predominant role. Simulations with the i-TS model demonstrate that sputtering yields can be strongly influenced by synergetic effects of the nuclear and the electronic energy loss. The calculations use the electron-phonon coupling as deduced from best fits to experimental track radii; otherwise there is no free parameter included. For Ti as target ($g = 10^{13}\,\mathrm{W \cdot K^{-1} \cdot s^{-3}}$ [51] and $U = 4.9\,\mathrm{eV}$), Fig. 23 shows that calculated sputtering yields assuming exclusively electronic energy loss heating (cf. TS(Se) values) are much smaller than the experimental results. For Zr which has a smaller electron-phonon coupling ($g = 2.6 \times 10^{12}\,\mathrm{W \cdot K^{-1} \cdot s^{-3}}$) and a larger sublimation energy ($U = 6.3\,\mathrm{eV}$) than Ti, the discrepancy is even more striking, because the i-TS model calculations predict no sputtering caused by electronic energy loss.

When the nuclear energy loss is included into the heat diffusion equation of the atomic subsystem (8) as an additional energy source term, the sputtering yields increase, i.e., getting closer the experimental data. In analogy to the

electronic energy density $A(r,t)$ described by (9), the nuclear energy density $B(r,t)$ is given by

$$B(r,t) = b_{\mathrm{n}}(dE/dx)_{\mathrm{n}} \exp(-t/\tau)\,(1/r)\exp(-r/R_0)\,, \tag{14}$$

where b_{n} is the normalization factor to ensure that the integration of $B(r,t)$ in space and time gives $(\mathrm{d}E/\,\mathrm{d}x)_{\mathrm{n}}$. The deposition time τ is equal to the slowing down of the recoil atoms [150, 151], and R_0 denotes the range of the recoils, i.e. the cylinder radius in which the recoil energy is deposited [58, 152]. The precise value of τ is not very crucial because a variation between 5×10^{-14} and 2×10^{-13} s leads only to a change of about 10 % in the sputtering yield. More important seems to be the range of the recoils because a 30 % change of R_0 from 1.5 to 2 nm decreases the sputtering yield by a factor of two. An accurate estimation of R_0 requires therefore realistic values for the mean recoil energy based on known nuclear cross sections [54,56]. The synergy effect is illustrated for a Zr target in Fig. 24, showing separate calculations for pure nuclear energy loss, for pure electronic energy loss, and for a combination of the two.

The situation seems to be different for Au targets. In the nuclear energy loss regime, the experimental sputtering yields [57, 153] of a Au target irradiated with Au ions of up to 3 MeV are much larger than predicted by TC calculations. To explain this effect, Sigmund proposed the collision spike model [58]. Later *Flynn* et al. [154] and *Tappin* et al. [155] considered a possible contribution by electron-phonon coupling which was finally included in MD calculations by *Finnis* et al. [156] mainly to investigate the quench rate of the cascade. Using the i-TS program, the influence of electron-phonon coupling can easily be tested: the calculation without electron-phonon coupling ($g = 0$) gives much higher yield values than the experimental data (Fig. 25). However, if electron-phonon coupling is activated, the lattice system is additionally cooled by energy transfer from the lattice to the electron system and the sputtering rate decreases in the entire energy regime (solid line). As electron-phonon coupling we used a value of $g = 2.3\times10^{10}\,\mathrm{W\cdot K^{-1}\cdot s^{-3}}$ as deduced from fs-laser experiments [148].

To test different systems, this thermal spike approach has also been applied for a Pt target where TC calculations (see Chap. by *Eckstein*) give good agreement with experimental sputtering yields. In contrast to the Au target, the thermal-spike contribution leads only to a small increase of the sputtering yield. This is a direct consequence of the higher sublimation energy of Pt ($U = 5.8$ eV) compared with Au ($U = 3.8$ eV). Table 4 illustrates the additional sputtering yields from thermal spike calculations (i-TS) for both systems exposed to 45 keV Xe. The sum of collisional sputtering (TC) and thermal-spike contributions give better agreement with experimental data.

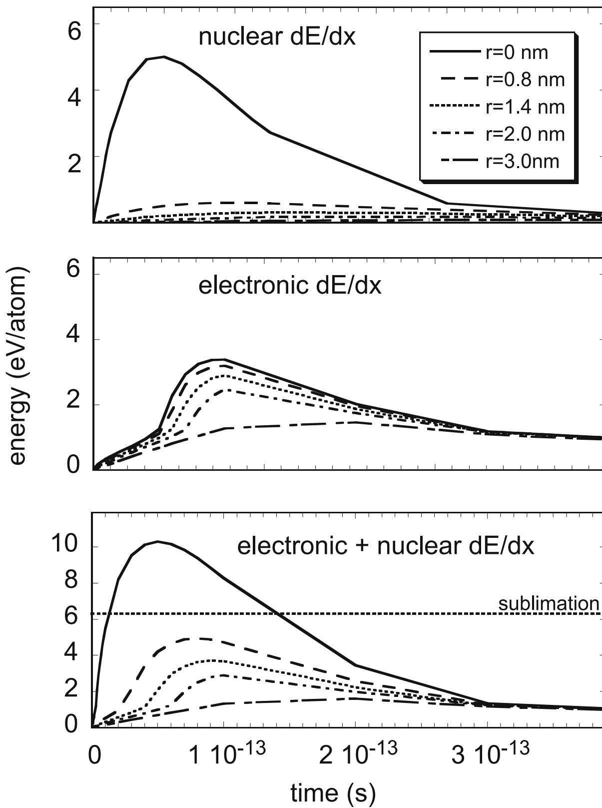

Fig. 24. Thermal spike calculations for a Zr target irradiated with 230 MeV Au ions: energy per atom as a function of time for various radii around the ion path. The sublimation energy of 6.3 eV can only be exceeded if the nuclear and the electronic energy loss contribute to the thermal spike

Table 4. Sputtering yields in the nuclear energy loss regime exposing Au and Pt targets to 45 keV Xe ions. U denotes the sublimation energy. Experimental data from the Chap. by *Eckstein* are compared with calculations based on pure collisional sputtering (TC) and on i-TS calculations with an electron-phonon coupling constant g

target	U (eV)	g ($\mathrm{W \cdot K^{-1} \cdot cm^{-3}}$)	i-TS	TC	i-TS + TC	exp. yield
Au	3.8	2.3×10^{10}	17	~ 14	~ 31	~ 40
Pt	5.8	1×10^{11}	5	~ 12	~ 17	~ 16

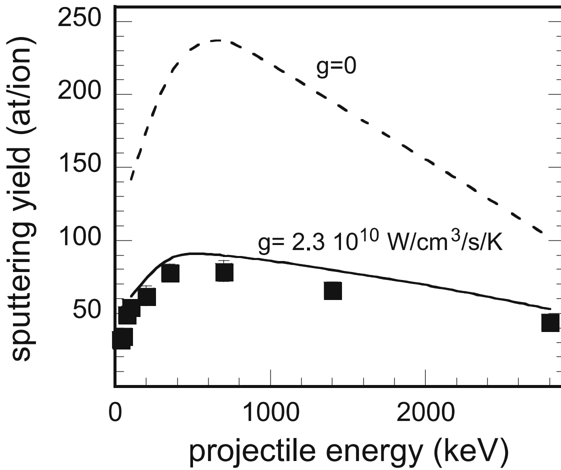

Fig. 25. Sputtering yields as a function of the projectile energy for Au targets irradiated with Au ions in the nuclear energy loss regime [57]. If electron-phonon coupling is inactivated (g = 0) and thus the nuclear energy loss is the only heating source of the atomic system, the sputtering yields deduced by i-TS simulations are largely overestimated (*dashed line*). In contrast, electron-phonon coupling of $g = 2.3 \times 10^{10}\,\mathrm{W \cdot K^{-1} \cdot s^{-3}}$ [148] (*solid line*) gives good agreement with experimental data

4.2 Application to Insulators

For crystalline and vitreous SiO_2, the experimental data of track radii and sputtering yields as a function of the electronic energy loss are shown in Fig. 26. The thermal spike calculations give best agreement with the experimental track radii for a chosen electron mean free path λ of 3.8 nm for crystalline SiO_2 and 3.0 nm for vitreous SiO_2 (dashed lines) [52]. The different λ values reflect the fact that the electron mean free path is smaller in a disordered lattice and thus leads to higher track temperatures than in a crystalline lattice. The λ value together with the respective sublimation energy (c-SiO_2: $U = 5.4\,\mathrm{eV}$, a-SiO_2: $U = 5.3$ eV) gives us calculated sputtering yields (full lines) of the same order of magnitude as the experimental results.

Figure 27 shows the experimental and calculated sputtering yields of LiF as a function of the electronic energy loss. The model calculations are performed with a selected electron mean free path of $\lambda = 3.8\,\mathrm{nm}$ and a sublimation energy of 2.8 eV per LiF molecule. The steep yield increase evolving with $(dE/dx)^4$ is rather well reproduced (solid line), but the absolute yield is underestimated by at least one order of magnitude. A reasonable fit to the data can only be obtained if a much smaller sublimation energy of $U = 1.3\,\mathrm{eV}$ is inserted [55].

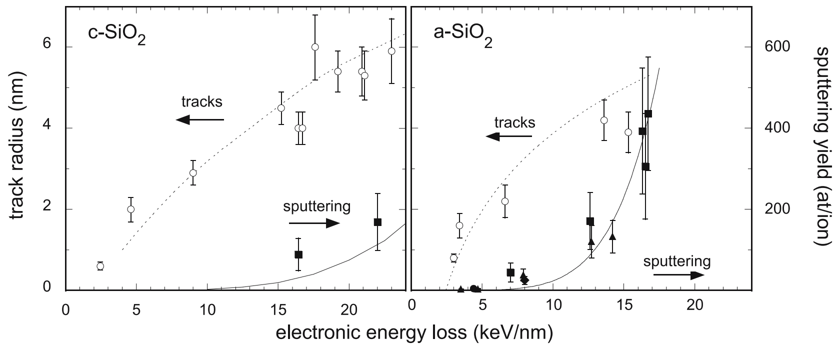

Fig. 26. Experimental track radii [21, 55] and sputtering yields as a function of the electronic energy loss for (*left*) crystalline and (*right*) vitreous SiO_2 (data normalized to perpendicular beam incidence by $(\cos\theta_0)^{-1.7}$). The thermal-spike calculations include melting as criteria for track formation and sublimation for sputtering together with superheating

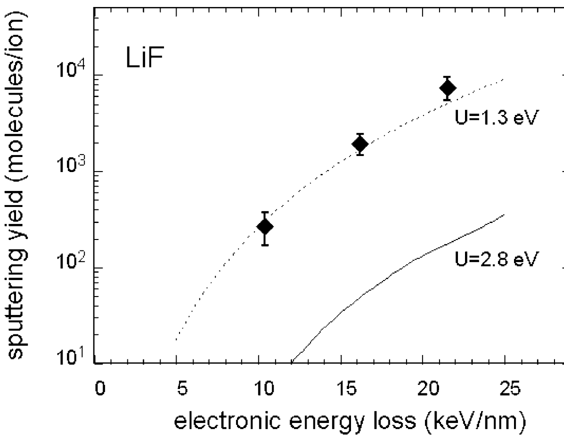

Fig. 27. Experimental sputtering yields as a function of energy loss for LiF molecules under beam incidence of $\theta_0 = 20°$ [55, 56]. Thermal-spike based calculations assume superheating and use an electron mean free path of $\lambda = 3.8$ nm [55]. To obtain good agreement with experimental results, the value for the sublimation energy in the simulation has to be reduced from 2.8 eV (*solid line*) to 1.3 eV (*dotted line*)

4.3 Thermal Spike Conclusion

In summary, we can state that the thermal spike concept seems to give a satisfactory description of sputtering for a number of metals and insulators. The calculations of the sputtering yields apply the same material parameters as used for the thermal spike description of track formation in the bulk, indicating a close relation between the two processes.

The sputtering process is governed by the dissipation of the deposited energy and the duration of the cooling phase. Given by the electron-phonon coupling, the thermal spike duration in metals is less than 10^{-12} s. A special property of metals is that the electron and the atom subsystem can exchange energy in both directions, and synergetic effects may have a significant influence in the nuclear as well as in the electronic energy loss regime.

For insulators the situation is more complicated mainly because of missing knowledge of the electron-phonon coupling. For the calculations, the coupling constant is replaced by the electron-phonon mean free path. Details are probably not very crucial because – in contrast to metals – insulators cool down predominantly via phonon-phonon interaction typically on a much slower time scale of 10^{-11} s and more. The thermal spike gives a consistent description of track radii in many amorphisable insulators and of sputtering yields as demonstrated for crystalline and vitreous SiO_2.

The situation is less satisfactory for ionic crystals. Although the overall evolution of the total sputtering yield as a function of electronic energy loss is well described, the thermal spike approach can explain neither the huge experimental sputtering yields nor the centrally directed enhanced sputtering normal to the surface. The reason why we cannot model such high sputtering yields may have several explanations. Exciton-based processes as commonly observed for low-energy projectiles [157] are less likely because fluorine is preferentially sputtered whereas electronic sputtering follows the stoichiometry of the target. However, high ionization and excitation densities as induced by the ion projectiles are known to soften the interatomic bonds [158–162]. Also sputtering of larger clusters would not involve the full sublimation energy applicable to species in thermodynamic equilibrium because only bonds at the cluster surface would be involved in bond breakage. Concerning the jet component, the directed emission normal to the surface is more characteristic of a hydrodynamic process [163, 164]. In particular for cleavable crystals, a directional cluster emission is just conceivable. The directed emission is probably related to high pressure developed in the track interior. In bulk material, effects due to pressure in the order of GPa are known [165–167] and also found in MD simulations [127–129, 132].

5 Concluding Remarks and Outlook

Electronic sputtering processes reveal several peculiar signatures and phenomena which differ considerably from elastic sputtering in the nuclear stopping regime. The most prominent characteristics are:

- The strong dependence on the *metallic* or *insulating* character of the target. Sputtering yields of insulators are by several orders of magnitude larger than yields of metallic targets.
- Among insulators, *ionic crystals* exhibit highest sputtering yields with a significant part of the atoms being emitted in a *jet-like* manner normal to the surface.
- The *structure* of the target has a strong influence on electronic sputtering: the yield of an amorphous material is larger than that of a crystal.
- The yield depends on the projectile *charge state*.
- Sputtering occurs above a material dependent energy loss *threshold*. There is strong evidence that for a given material the sputtering threshold is in general larger than the critical energy loss required for track formation.

Electronic sputtering is dominated by the primary stopping process in which the energy of swift heavy ions is mainly transferred to the electrons. For the energy dissipation, the mean free path of the electrons is the crucial parameter and thus plays an important role for the sputtering efficiency.

Thermal spike calculations show that electronic sputtering processes can be described fairly well by heat diffusion processes in the electronic and atomic subsystem using the thermal properties of a given target material. The good agreement, obtained when applying parameters deduced from ion tracks in the bulk, is a strong indication that these two processes are closely related. The thermal spike concept is sometimes heavily disputed because the conversion of energy into temperature of the lattice atoms takes place far from thermodynamical equilibrium. However, model calculations show considerable success in describing and predicting electronic sputtering observations quantitatively.

Finally, we like to conclude this contribution with a list of open problems to be investigated in order to reach a better understanding of the physical processes involved: There is a substantial need for more systematic data covering all material classes. At present, electronic sputtering of semiconductors is hardly investigated. Concerning the dependence of the total sputtering yield on the electronic energy loss, it is of interest to use cluster ion beams which have even higher energy loss values than mono-atomic ion beams. Another important point is the charge state dependence of the electronic energy loss. Using projectiles in and out of equilibrium charge state (accompanied by nN-CTMC simulations [80]), one can shift the energy loss maximum (hot spot) from the surface to larger depths [168] and study the effect on the total yield as well as on the angular distribution. A first test measurement using

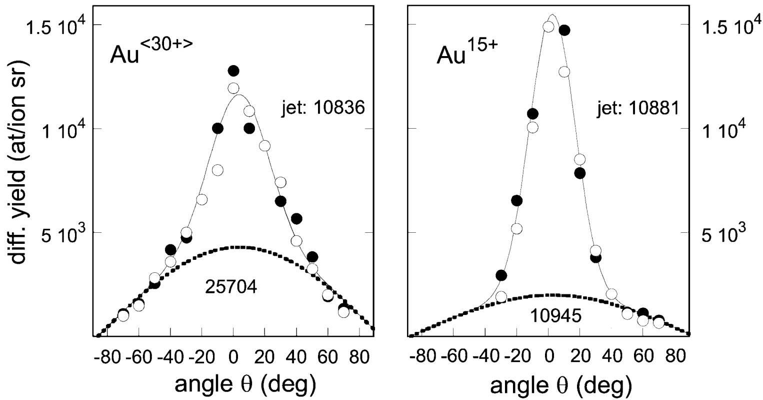

Fig. 28. Angular distribution of Li (*full symbol*) and F (*open symbol*) atoms sputtered from the (100) surface of a single LiF crystal irradiated with 210 MeV Au ions of mean charge state $\langle 30^+ \rangle$ (*left*) and of nonequilibrium charge state $q = 15^+$ (*right*) under beam incidence of $\theta_0 = 60°$ [105]. The *numbers* in the graph indicate the respective jet and isotropic components based on analysis using (5)

Au projectiles of two different charge states indicates a significant decrease of the isotropic sputtering yield for a lower incident charge state, whereas the jet contribution remains approximately constant together with a reduced width of the peak component (Fig. 28).

Additional information is needed about the energy and velocity distribution of sputtered particles. Laser-induced post-ionization of neutral sputtered particles, for example, would greatly help to better understand the dependence of the angular distribution and the jet component in particular.

At large sputtering yields, the emission of clusters may play a substantial role. A first attempt to identify and analyze the size of sputtered clusters is shown on the transmission electron microscopy image of Fig. 29 [169]. In this experiment, the catcher is a thin carbon foil supported by a Cu grid as typically used for TEM. With this technique, cluster formation has already been found for collisional sputtering [170, 171].

From the theoretical side, it would be extremely important to develop more sophisticated microscopic and macroscopic models. Hydrodynamic processes, i.e. pressure spike and Coulomb explosion, should be included as well as a time dependent energy source term as introduced in [132]. MD calculations should be performed for materials and under conditions closer to the experimental situation; it would be a significant improvement if the internal structure and binding character of different target materials such as metals, oxides, or ionic crystals could be taken into account.

A solid theoretical description with predictive character is also of practical interest as sputtering, for instance, can severely limit elastic recoil detection analysis with swift heavy ions [95]. It could additionally help to understand

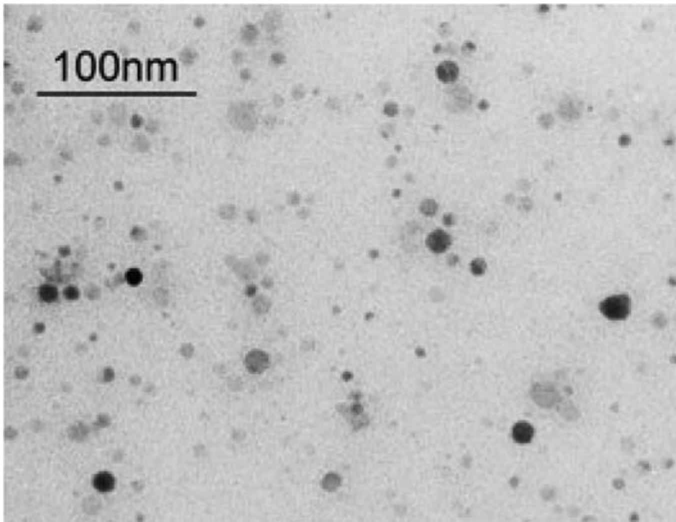

Fig. 29. Transmission electron microscopy image of sputtered nanoclusters collected on a carbon-coated grid. The sputtering experiment was performed by irradiating a cleaved (111) surface of a CaF_2 single crystal with 210 MeV Au ions. The grid was mounted at $\theta = 0^\circ$

and reduce beam-induced desorption and related vacuum problems at large accelerator facilities [172, 173].

Acknowledgements

The authors gratefully acknowledge many helpful suggestions and remarks by R. Behrisch, G. Dollinger, W. Eckstein, and D. A. Young, and M. Schubert for his assistance with the figures.

References

[1] A. Meftah, F. Brisard, J. M. Costantini, M. Hage-Ali, J. P. Stoquert, F. Studer, M. Toulemonde: Phys. Rev. B **48**, 920 (1993) 402, 404
[2] R. Katz, E. J. Kobetich: Phys. Rev. **186**, 344 (1969) 402, 429
[3] E. C. H. Silk, R. S. Barnes: Phil. Mag. **4**, 970 (1959) 402
[4] D. A. Young: Nature **183**, 375 (1958) 402
[5] R. L. Fleischer, P. B. Price, R. M. Walker: *Nuclear Tracks in Solids. Principles and Applications* (University of California Press, Berkeley 1975) 402, 403
[6] R. Spohr: *Ion Tracks and Microtechnology, Basic Principles and Applications* (Vieweg, Braunschweig 1990) 403
[7] M. Toulemonde, C. Trautmann, E. Balanzat, K. Hjort, A. Weidinger: Nucl. Instrum. Methods B **216**, 1 (2004) 403

[8] H. Walter, W. Prusseit, R. Semerad, H. Kinder, W. Assmann, H. Huber, H. Burkhardt, D. Rainer, J. A. Sauls: Phys. Rev. Lett. **80**, 3598 (1998) 403
[9] J. Wiesner: Ph.D. thesis, Univ. Darmstadt (1994) 403
[10] P. K. Haff: Appl. Phys. Lett. **29**, 473 (1976) 403
[11] L. E. Seiberling, C. K. Meins, B. H. Cooper, J. E. Griffith, M. H. Mendenhall, T. A. Tombrello: Nucl. Instrum. Methods **198**, 17 (1982) 403, 423
[12] P. Sigmund: Phys. Rev. **184**, 383 (1969) 403
[13] I. A. Baranov, Yu. V. Martynenko, S. O. Tsepelevich, Yu. N. Yavlinskii: Sov. Phys. Usp. **31**, 1015 (1988) 403, 407, 431
[14] T. A. Tombrello: Nucl. Instrum. Methods B **2**, 555 (1984) 403, 405
[15] K. Wien: Radiat. Eff. and Def. Sol. **109**, 137 (1989) 403
[16] N. Itoh, A. M. Stoneham: *Materials Modifications by Electronic Excitation* (Cambridge Univ. Press, Cambridge 2001) 403
[17] R. A. Baragiola: Phil. Trans. R. Soc. A **362**, 29 (2004) 403
[18] P. Sigmund (Ed.): K. Dan. Videns. Selsk. Mat. Fys. Medd. **43** (1993) 403
[19] C. Houpert, F. Studer, D. Groult, M. Toulemonde: Nucl. Instrum. Methods B **39**, 720 (1989) 404
[20] A. Barbu, A. Dunlop, D. Lesueur, R. S. Averback: Europhys. Lett. **15**, 426 (1991) 404, 417
[21] A. Meftah, F. Brisard, J. M. Costantini, E. Dooryhée, M. Hage-Ali, M. Hervieu, J. P. Stoquert, F. Studer, M. Toulemonde: Phys. Rev. B **49**, 12457 (1994) 404, 431, 438
[22] A. Dunlop, H. Dammak, D. Lesueur: Nucl. Instrum. Methods B **112**, 23 (1996) 404
[23] J. Vetter, R. Scholz, D. Dobrev, L. Nistor: Nucl. Instrum. Methods B **141**, 747 (1998) 404
[24] B. Canut, N. Bonardi, S. M. M. Ramos, S. Della-Negra: Nucl. Instrum. Methods B **146**, 296 (1998) 404
[25] A. Dunlop, G. Jaskierowicz, S. Della-Negra: Nucl. Instrum. Methods B **146**, 302 (1998) 404
[26] A. Colder, O. Marty, B. Canut, M. Levalois, P. Marie, X. Portier, S. M. M. Ramos, M. Toulemonde: Nucl. Instrum. Methods B **174**, 491 (2001) 404
[27] P. I. Gaiduk, A. Nylandsted-Larsen, J. Lundsgaard Hansen, C. Trautmann, M. Toulemonde: Appl. Phys. Lett. **83**, 1746 (2003) 404
[28] K. Schwartz, C. Trautmann, T. Steckenreiter, O. Geiss, M. Krämer: Phys. Rev. B **58**, 11232 (1998) see also C. Trautmann and M. Toulemonde and J. M. Costantini and J. J. Grob and K. Schwartz: Phys. Rev. B 62, 13 (2000) 404
[29] F. Studer, Ch. Houpert, D. Groult, J. Y. Fan, A. Meftah, M. Toulemonde: Nucl. Instrum. Methods B **82**, 91 (1993) 404
[30] M. Toulemonde, G. Fuchs, N. Nguyen, F. Studer, D. Groult: Phys. Rev. B **35**, 6560 (1987) 404
[31] S. Ghosh, D. K. Avasthi, A. Tripathi, D. Kabiraj, S. Singh, D. S. Misra: Nucl. Instrum. Methods B **219/220**, 973 (2004) 404
[32] Y. Zhu, Z. X. Cai, R. C. Budhani, M. Suenaga, D. O. Welch: Phys. Rev. B **48**, 6436 (1993) 404
[33] R. Neumann, P. Apel, M. Toulemonde, C. Trautmann, (Eds.): Nucl. Instrum. Methods B **245** (2005) 404

[34] J. M. Costantini, F. Ravel, F. Brisard, M. Caput, C. Cluzeau: Nucl. Instrum. Methods B **80/81**, 1249 (1993) 404
[35] T. Wiss, H. Matzke, C. Trautmann, M. Toulemonde, S. Klaumünzer: Nucl. Instrum. Methods B **122**, 583 (1997) 404
[36] H. Matzke, P. G. Lucuta, T. Wiss: Nucl. Instrum. Methods B **166–167**, 920 (2000) 404
[37] B. Canut, A. Benyagoub, G. Marest, A. Meftah, N. Moncoffre, S. M. M. Ramos, F. Studer, P. Thevenard, M. Toulemonde: Phys. Rev. B **51**, 12194 (1995) 404
[38] A. Benyagoub, F. Levesque, F. Couvreur, C. Gibert-Mougel, Ch. Dufour, E. Paumier: Appl. Phys. Lett. **77**, 3197 (2000) 404
[39] A. Benyagoub: Nucl. Instrum. Methods B **225**, 88 (2004) 404
[40] K. Schwartz, C. Trautmann, A. S. El-Said, R. Neumann, M. Toulemonde, W. Knolle: Phys. Rev. B **70**, 184104 (2004) 404
[41] I. Manika, J. Maniks, K. Schwartz, M. Toulemonde, C. Trautmann: Nucl. Instrum. Methods B **209**, 93 (2003) 404
[42] M. Enculescu, K. Schwartz, C. Trautmann, M. Toulemonde: Nucl. Instrum. Methods B **229**, 397 (2005) 404
[43] N. Khalfaoui, C. C. Rotaru, S. Bouffard, M. Toulemonde, J. P. Stoquert, F. Haas, C. Trautmann, J. Jensen, A. Dunlop: Nucl. Instrum. Methods B **240**, 819 (2005) 404
[44] K. Schwartz, C. Trautmann, R. Neumann: Nucl. Instrum. Methods B **209**, 73 (2003) 404
[45] C. Müller, A. Benyagoub, M. Lang, R. Neumann, K. Schwartz, M. Toulemonde, C. Trautmann: Nucl. Instrum. Methods B **209**, 175 (2003) 404
[46] T. Davidson, K. Schwartz, J. D. Comins, A. G. Kozakiewicz, M. Toulemonde, C. Trautmann: Phys. Rev. B **66**, 214102 (2002) 404
[47] C. Trautmann, M. Boccanfuso, A. Benyagoub, S. Klaumünzer, K. Schwartz, M. Toulemonde: Nucl. Instrum. Methods B **191**, 144 (2002) 404
[48] M. Boccanfuso, A. Benyagoub, K. Schwartz, M. Toulemonde, C. Trautmann: Prog. Nuc. Energy **38**, 271 (2001) 404
[49] M. Boccanfuso, A. Benyagoub, M. Toulemonde, C. Trautmann, K. Schwartz, Ch. Dufour: Nucl. Instrum. Methods B **175–177**, 590 (2001) 404
[50] F. Seitz, J. S. Koehler: in F. Seitz, D. Turnbull (Eds.): *Solid. State Physics*, vol. 2 (Academic, New York 1956) p. 305 404, 428
[51] Z. G. Wang, Ch. Dufour, E. Paumier, M. Toulemonde: J. Phys.: Condens. Matter **6**, 6733 (1994) 404, 429, 431, 432, 433, 434
[52] M. Toulemonde, Ch. Dufour, A. Meftah, E. Paumier: Nucl. Instrum. Methods B **166–167**, 903 (2000) 404, 429, 431, 433, 437
[53] H. D. Mieskes: Ph.D. thesis, Univ. München (1999) 404, 405, 414, 417, 421, 433
[54] H. D. Mieskes, W. Assmann, F. Grüner, H. Kucal, Z. G. Wang, M. Toulemonde: Phys. Rev. B **67**, 155414 (2003) 404, 405, 411, 416, 417, 418, 419, 427, 429, 431, 435
[55] M. Toulemonde, W. Assmann, F. Grüner, C. Trautmann: Phys. Rev. Lett. **88**, 057602 (2002) 404, 405, 418, 421, 422, 423, 425, 426, 427, 428, 429, 431, 433, 437, 438

[56] M. Toulemonde, W. Assmann, C. Trautmann, F. Grüner, H. D. Mieskes, H. Kucal, Z. G. Wang: Nucl. Instrum. Methods B **212**, 346 (2003) 404, 405, 435, 438
[57] H. H. Andersen, A. Brunelle, S. Della-Negra, J. Depauw, D. Jacquet, Y. Le Beyec, J. Chaumont, H. Bernas: Phys. Rev. Lett. **80**, 5433 (1998) 404, 405, 435, 437
[58] P. Sigmund, C. Claussen: J. Appl. Phys. **52**, 990 (1981) 404, 428, 433, 435
[59] E. M. Bringa, R. E. Johnson: Phys. Rev. Lett. **88**, 165501 (2002) 405
[60] W. Guthier: in A. Benninghoven (Ed.): *Proceedings of the 3rd International Workshop on Ion Formation from Organic Solids*, Springer Proc. Phys. **9** (Springer, Berlin, Heidelberg 1986) 405, 422, 423, 426
[61] W. L. Brown, L. J. Lanzerotti, J. M. Poate, W. M. Angustyniak: Phys. Rev. Lett. **40**, 1027 (1978) 405
[62] J. E. Griffith, R. A. Weller, L. E. Seiberling, T. A. Tombrello: Radiat. Eff. and Def. **51**, 223 (1980) 405, 409, 422, 423, 427
[63] L. E. Seiberling, J. E. Griffith, T. A. Tombrello: Radiat. Eff. and Def. **52**, 201 (1980) 405
[64] J. P. O'Connor, L. M. Baumel, P. G. Blauner, K. M. Hubbard, M. R. Weller, R. A. Weller: Nucl. Instrum. Methods B **13**, 365 (1986) 405, 417, 418, 427
[65] K. M. Gibbs, W. L. Brown, R. E. Johnson: Phys. Rev. B **38**, 11001 (1988) 405, 416
[66] R. E. Johnson, M. Pospieszalska, W. L. Brown: Phys. Rev. B **44**, 7263 (1991) 405, 428
[67] H. D. Mieskes, W. Assmann, M. Brodale, M. Dobler, H. Glückler, P. Hartung, P. Stenzel: Nucl. Instrum. Methods B **146**, 162 (1998) 405, 409, 412, 414, 417
[68] A. Meftah, M. Djebara, J. P. Stoquert, F. Studer, M. Toulemonde: Nucl. Instrum. Methods B **107**, 242 (1996) 405, 423
[69] N. Khalfaoui, M. Beuve, S. Bouffard, M. Caron, H. Rothard, S. Schlutig, J. P. Stoquert, M. Toulemonde: Nucl. Instrum. Methods B **209**, 304 (2003) 405
[70] T. Schenkel, M. A. Briere, H. Schmidt-Böcking, K. Bethge, D. H. Schneider: Phys. Rev. Lett. **78**, 2481 (1997) 405
[71] T. Schenkel, A. V. Barnes, A. V. Hamza, D. H. Schneider, J. C. Banks, B. L. Doyle: Phys. Rev. Lett. **80**, 4325 (1998) 405
[72] A. Brunelle, S. Della-Negra, J. Depauw, D. Jacquet, Y. Le Beyec, M. Pautrat, Ch. Schoppmann: Nucl. Instrum. Methods B **125**, 207 (1997) 405
[73] I. A. Baranov, S. Della-Negra, M. Fallavier, S. Kirillov, Y. Le Beyec, A. Novikov, V. Obnorskii, K. Wien, S. Yarmiychuk: Nucl. Instrum. Methods B **245**, 184 (2006) 405
[74] A. Gutzmann, S. Klaumünzer, P. Meier: Phys. Rev. Lett. **74**, 2256 (1995) 406
[75] S. Sugden, C. J. Sofield, M. P. Murrell: Nucl. Instrum. Methods B **67**, 569 (1992) 407, 410, 418, 423, 433
[76] A. Gupta, D. K. Avasthi: Phys. Rev. B **64**, 155407 (2001) 407
[77] W. M. Arnoldbik, N. Tomozeiu, F. H. P. M. Habraken: Nucl. Instrum. Methods B **203**, 151 (2003) 407, 410, 416, 417, 418, 423, 433
[78] K. L. Merkle: Phys. Rev. Lett. **9**, 150 (1962) 407

[79] A. Berthelot, S. Hémon, F. Gourbilleau, Ch. Dufour, E. Dooryhée, E. Paumier: Nucl. Instrum. Methods B **146**, 437 (1998) 407
[80] F. Grüner, F. Bell: Phys. Rev. A **72**, 024902 (2005) 407, 408, 440
[81] C. M. Frey, G. Dollinger, A. Bergmaier, T. Faestermann, P. Maier-Komor: Nucl. Instrum. Methods B **107**, 31 (1996) 407
[82] G. Dollinger, C. M. Frey, A. Bergmaier, T. Faestermann: Nucl. Instrum. Methods B **136–138**, 603 (1998) 407, 409
[83] E. Baron, B. Delaunay: Phys. Rev. A **12**, 40 (1975) 407
[84] E. Baron, M. Bajard, Ch. Ricaud: Nucl. Instrum. Methods A **328**, 177 (1993) 407
[85] A. Leon, S. Melki, D. Lisfi, J. P. Grandin, P. Jardin, M. G. Suraud, A. Cassimi: Atomic Data and Nucl. Data Tables **69**, 217 (1998) 407
[86] D. M. Gruen, M. J. Pellin, C. E. Young, W. F. Calaway: J. Vac. Sci. Technol. A **4**, 1779 (1986) 407
[87] W. Husinsky, R. Bruckmüller, P. Blum: Nucl. Instrum. Methods **170**, 287 (1980) 408
[88] R. B. Wright, M. J. Pellin, D. M. Gruen, C. E. Young: Nucl. Instrum. Methods **170**, 295 (1980) 408
[89] D. M. Gruen, W. F. Calaway, M. J. Pellin, C. E. Young, D. R. Spiegel, R. N. Clayton, A. M. Davis, J. D. Blum: Nucl. Instrum. Methods B **58**, 505 (1991) 408
[90] H. F. Arlinghaus, M. T. Spaar, T. Tanigaki, A. W. McMahon, P. H. Holloway: J. Vac. Sci. Technol. B **12**, 263 (1994) 408
[91] F. M. Kimock, J. P. Baxter, N. Winograd: Nucl. Instrum. Methods Phys. Res. **218**, 287 (1983) 408
[92] M. Roth, B. Walz, G. Schiwietz, B. Schattat: in *ISL Annual Report* (HMI, Berlin 2004) p. 13 408
[93] W.-K. Chu, J. W. Mayer, M.-A. Nicolet: *Backscattering Spectrometry* (Academic, New York 1978) 409
[94] W. Assmann, J. A. Davies, G. Dollinger, J. S. Forster, H. Huber, T. Reichelt, R. Siegele: Nucl. Instrum. Methods B **118**, 242 (1996) 409, 414
[95] G. Dollinger, M. Boulouednine, A. Bergmaier, T. Faestermann, C. M. Frey: Nucl. Instrum. Methods B **118**, 291 (1996) 409, 441
[96] S. Bouffard, J. P. Duraud, M. Mosbah, S. Schlutig: Nucl. Instrum. Methods B **141**, 372 (1998) 409
[97] K. G. Libbrecht, J. E. Griffith, R. A. Weller, T. A. Tombrello: Rad. Eff. and Def. **49**, 195 (1980) 409
[98] M. R. Weller, T. A. Tombrello: Radiat. Eff. and Def. **49**, 239 (1980) 409
[99] N. Matsunami, M. Sataka, A. Iwase: Nucl. Instrum. Methods B **175–177**, 56 (2001) 409, 421, 422, 423
[100] G. Hayderer, M. Schmid, P. Varga, H. P. Winter, F. Aumayr: Rev. Sci. Instrum. **70**, 3696 (1999) 410
[101] S. Ninomiya, C. Imada, M. Nagai, Y. Nakata, T. Aoki, J. Matsuo, N. Imanishi: Nucl. Instrum. Methods B **230**, 483 (2003) 410
[102] W. Assmann, P. Hartung, H. Huber, P. Staat, H. Steffens, Ch. Steinhausen: Nucl. Instrum. Methods B **85**, 726 (1994) 413
[103] W. Assmann, H. Huber, Ch. Steinhausen, M. Dobler, H. Glückler, A. Weidinger: Nucl. Instrum. Methods B **89**, 131 (1994) 413, 414

[104] C. K. Meins, J. E. Griffith, Y. Qiu, M. H. Mendenhall, L. E. Seiberling, T. A. Tombrello: Radiat. Eff. and Def. **71**, 13 (1983) 416, 417, 423, 426
[105] W. Assmann, M. Toulemonde, C. Trautmann, K.-O. Voss: unpublished data 417, 418, 423, 427, 441
[106] E. M. Bringa, R. E. Johnson: Surf. Sci. **451**, 108 (2000) 416, 428
[107] J. P. O'Connor, P. G. Blauner, R. A. Weller: Nucl. Instrum. Methods **218**, 293 (1983) 417
[108] J. P. Biersack: Nucl. Instrum. Methods B **27**, 21 (1987) 417, 418, 419, 420, 428
[109] H. Dammak, D. Lesueur, A. Dunlop, P. Legrand, J. Morillo: Radiat. Eff. Def. Solids **126**, 111 (1993) 417
[110] A. Dunlop, D. Lesueur, J. Morillo, J. Dural, R. Spohr, J. Vetter: Nucl. Instrum. Methods B **48**, 419 (1990) 417
[111] Ch. Dufour, A. Audouard, F. Beuneu, J. Dural, J. P. Girard, A. Hairie, M. Levalois, E. Paumier, M. Toulemonde: J. of Phys.: Condens. Matt. **5**, 4573 (1993) 417, 429, 430, 431
[112] A. Audouard, E. Balanzat, S. Bouffard, J. C. Jousset, A. Chamberod, A. Dunlop, D. Lesueur, G. Fuchs, R. Spohr, J. Vetter, L. Thomé: Phys. Rev. Lett. **65**, 875 (1990) 417
[113] A. Barbu, A. Dunlop, A. Hardouin-Duparc, G. Jaskierowicz, N. Lorenzelli: Nucl. Instrum. Methods B **145**, 354 (1998) 417
[114] S. Klaumünzer, M.-D. Hou, G. Schumacher: Phys. Rev. Lett. **57**, 850 (1986) 417
[115] M.-D. Hou, S. Klaumünzer, G. Schumacher: Phys. Rev. B **41**, 1144 (1990) 417
[116] A. Audouard, E. Balanzat, J. C. Jousset, A. Chamberod, G. Fuchs, D. Lesueur, L. Thomé: Philos. Mag. B **63**, 727 (1991) 417
[117] H. H. Andersen, A. Johansen, V. S. Touboltsev: Nucl. Instrum. Methods B **164–165**, 727 (2000) 418
[118] J. F. Ziegler, J. P. Biersack, U. Littmark: The stopping and ranges of ions in matter, in *The Stopping and Range of Ions in Solids*, vol. 1 (Pergamon, New York 1985) 419, 420, 421
[119] S. Schlutig: Ph.D. thesis, Univ. Caen (2001) URL: `http://tel.archives-ouvertes.fr/tel-00002110` 421, 422, 423, 427
[120] T. van Dillen, E. Snoeks, W. Fukarek, C. M. van Kats, K. P. Velikov, A. van Blaaderen, A. Polman: Nucl. Instrum. Methods B **175–177**, 350 (2001) 421
[121] M. Toulemonde, S. M. M. Ramos, H. Bernas, C. Clerc, B. Canut, J. Chaumont, C. Trautmann: Nucl. Instrum. Methods B **178**, 331 (2001) 421
[122] N. Matsunami, M. Sataka, A. Iwase: Nucl. Instrum. Methods B **193**, 830 (2002) 421, 422, 423
[123] N. Matsunami, M. Sataka, A. Iwase, S. Okayasu: Nucl. Instrum. Methods B **209**, 288 (2003) 421, 422, 423
[124] Y. Qiu, J. E. Griffith, T. A. Tombrello: Rad. Eff. and Def. **1**, 111 (1982) 422
[125] G. K. Wehner: J. Appl. Phys. **26**, 1056 (1955) 424
[126] J. P. Biersack, W. Eckstein: Appl. Phys. **34**, 73 (1984) 428
[127] H. M. Urbassek, H. Kafeman, R. E. Johnson: Phys. Rev. B **49**, 786 (1994) 428, 439
[128] D. A. Young: Nucl. Instrum. Methods B **225**, 231 (2004) 428, 439
[129] D. A. Young: Nucl. Instrum. Methods B **252**, 175 (2006) 428, 439

[130] E. M. Bringa, R. E. Johnson, L. Dutkiewicz: Nucl. Instrum. Methods B **152**, 267 (1999) 428
[131] E. M. Bringa, R. E. Johnson: Nucl. Instrum. Methods B **180**, 99 (2001) 428
[132] M. Beuve, N. Stolterfoht, M. Toulemonde, C. Trautmann, H. M. Urbassek: Phys. Rev. B **68**, 125423 (2003) 428, 439, 441
[133] R. E. Johnson, R. Evatt: Rad. Eff. and Def. **52**, 187 (1980) 428
[134] I. M. Lifshitz, M. I. Kaganov, L. V. Tanatarov: J. Nucl. Energy A **12**, 69 (1960) 429
[135] S. I. Anisimov, B. L. Kapeliovich, T. L. Perel'man: Sov. Phys. JETP **39**, 375 (1974) 429
[136] A. Meftah, M. Djebara, N. Khalfaoui, M. Toulemonde: Nucl. Instrum. Methods B **146**, 431 (1998) 429
[137] A. Meftah, J. M. Costantini, N. Khalfaoui, S. Boudjadar, J. P. Stoquert, F. Studer, M. Toulemonde: Nucl. Instrum. Methods B **237**, 563 (2005) 429, 431, 433
[138] Z. G. Wang, Ch. Dufour, E. Paumier, M. Toulemonde: Nucl. Instrum. Methods B **115**, 577 (1996) 429
[139] Ch. Dufour, Z. G. Wang, E. Paumier, M. Toulemonde: Bull. Mater. Sci. **22**, 671 (1999) 429
[140] G. H. Vineyard: Rad. Eff. and Def. **29**, 245 (1976) 429
[141] M. P. R. Waligorski, R. N. Hamm, R. Katz: Nucl. Tracks Radiat. Meas. **11**, 309 (1986) 429
[142] B. Gervais, S. Bouffard: Nucl. Instrum. Methods B **88**, 355 (1994) 429
[143] G. Somorjai: *Chemistry in Two Dimensions: Surfaces* (Cornell Univ. Press, Ithaca 1981) 430
[144] Yu. V. Martynenko, Yu. N. Yavlinskii: Sov. Phys. Dokl. **28**, 391 (1983) 430
[145] M. I. Kaganov, I. M. Lifshitz, L. V. Tanatarov: Zh. Tekh. Fiz. **31**, 237 (1956) 430
[146] P. Hermes, B. Danielzik, N. Fabricius, D. von der Linde, J. Kuhl, J. Huppner, B. Stritzker, A. Pospieszcyk: Appl. Phys. A **39**, 9 (1986) 431
[147] M. Toulemonde, Ch. Dufour, Z. G. Wang, E. Paumier: Nucl. Instrum. Methods B **112**, 126 (1996) 432
[148] S. D. Brorson, A. Kazeroonian, J. S. Moodera, D. W. Face, T. K. Cheng, E. P. Ippen, M. S. Dresselhaus, G. Dresselhaus: Phys. Rev. Lett. **64**, 2172 (1990) 433, 435, 437
[149] R. F. Haglund, R. Kelly: Mat. Fys. Medd. **43**, 527 (1992) 433
[150] P. Sigmund: Appl. Phys. Lett. **25**, 169 (1974) 433, 435
[151] P. Sigmund: Appl. Phys. Lett. **27**, 52 (1975) 433, 435
[152] P. Sigmund: Nucl. Instrum. Methods B **164–165**, 401 (2000) 435
[153] H. L. Bay, H. H. Andersen, W. O. Hofer, O. Nielsen: Nucl. Instrum. Methods **132**, 301 (1976) 435
[154] C. P. Flynn, R. S. Averback: Phys. Rev. B **38**, 7118 (1988) 435
[155] D. K. Tappin, I. M. Robertson, M. A. Kirk: Phil. Mag. A **70**, 463 (1994) 435
[156] M. W. Finnis, P. Agnew, A. J. E. Foreman: Phys. Rev. B **44**, 567 (1991) 435
[157] J. A. M. Pereira, E. F. da Silveira: Nucl. Instrum. Methods B **127–128**, 157 (1997) 439
[158] J. Bok: J. Phys. C Paris **5**, 3 (1983) 439
[159] G. S. Khoo, C. K. Ong, N. Itoh: J. Phys.: Condens. Matter **5**, 1187 (1993) 439

[160] P. Stampfli, K. H. Benneman: Appl. Phys. A **60**, 191 (1995) 439
[161] N. Itoh, A. M. Stoneham: Nucl. Instrum. Methods B **146**, 362 (1998) 439
[162] N. Itoh: Nucl. Instrum. Methods B **135**, 175 (1998) 439
[163] R. E. Johnson, B. U. R. Sundqvist, S. Hedin, D. Fenyö: Phys. Rev. B **40**, 49 (1989) 439
[164] M. M. Jakas, E. M. Bringa: Phys. Rev. B **62**, 824 (2000) 439
[165] A. Berthelot, S. Hémon, F. Gourbilleau, Ch. Dufour, B. Domenges, E. Paumier: Phil. Mag. A **80**, 2257 (2000) 439
[166] A. Berthelot: Ph.D. thesis, Univ. Caen (2000) 439
[167] Ch. Dufour, S. Hémon, F. Gourbilleau, E. Paumier, E. Dooryhée: Mater. Sci. Forum **248–249**, 21 (1997) 439
[168] J. P. Rozet, C. Stephan, D. Vernhet: Nucl. Instrum. Methods B **107**, 67 (1996) 440
[169] W. Assmann, R. Grüner, M. Schubert, M. Toulemonde, G. Miehe, C. Trautmann, K.-O. Voss: in *MLL Annual Report* (Univ. of Munich, Accelerator Laboratory, Garching 2002) 441
[170] R. C. Birtcher, S. E. Donnelly, S. Schlutig: Phys. Rev. Lett. **85**, 4968 (2000) 441
[171] R. C. Birtcher, S. E. Donnelly, S. Schlutig: Nucl. Instrum. Methods B **215**, 69 (2004) 441
[172] E. Mahner, J. Hansen, J.-M. Laurent, N. Madsen: Phys. Rev. ST-AB **6**, 013201 (2003) 442
[173] H. Kollmus, M. Bender, M. C. Bellachioma, E. Mahner, L. Westerberg, E. Hedlund, O. B. Malyshev, A. Krämer, H. Reich-Sprenger: AIP Proc. **773**, 207 (2005) 442

Index

amorphization, 423
angular dependence of the sputtering yield, 416
angular distribution, 410, 418, 421–423, 425–427
  cosine, 421, 428
  isotropic, 411
  jet-like, 411, 412, 424
  over-cosine, 410, 421

band gap energy, 433
BCA program
  Monte Carlo (MC), 407, 428
  TRIM-CASCADE, 417, 418, 420
beam monitor, 411
Bragg peak, 401, 402

channeling, 407, 409
cluster
  size, 440
conduction band, 433
Coulomb explosion, 403–405

Debye temperature, 430
defect
  annealing, 429
delta electron, 429
deposited energy, 428
depth
  resolution, 414
depth of origin, 410
desorption, 442
detection technique
  catcher, 406, 409, 411
  element selective, 406
differential yield, 410, 418
diffusion, 428

elastic recoil detection analysis (ERDA), 409, 411, 412, 414, 442
electron-phonon coupling, 404, 405, 427, 429, 430, 434, 436, 438
electron-phonon relaxation, 428
electronic sputtering, 401, 403, 407
energy deposition, 402, 429
energy loss
  electronic, 402, 404, 405, 416, 417, 420, 421, 423, 426–428, 434, 435, 437, 438
  nuclear, 402, 409, 417, 420, 434–436
enthalpy of fusion, 430
evaporation, 406
  rate, 433
excitation, 407, 439
  electronic, 405, 417

Fermi energy, 430
Fermi temperature, 430
fragment
  fission, 409

heat-flow equation, 429

inelastic thermal spike model (i-TS), 404, 406, 428, 429, 431, 433, 434
insulator, 437
ionization, 407, 439

Katz model, 429

laser induced fluorescence (LIF), 408
laser induced resonance ionization spectroscopy (RIS), 408

mass spectrometry, 405, 408
material modification, 402
Maxwell-Boltzmann distribution, 423
melting, 406
microbalance, 410
molecular dynamics, 416, 428, 436, 439

phase transformation, 404
post-ionization, 440
preferential sputtering, 421

quench rate, 436

range
  recoil, 435
Rutherford backscattering spectroscopy (RBS), 409

specific heat coefficient, 429
spike
  elastic collision, 436
  thermal, 404, 405, 428, 431, 436–440
state
  charge, 402, 405, 416, 419
  equilibrium charge, 407, 411, 418, 425, 440
  excited, 407
sticking
  coefficient, 409
  probability, 409
sublimation energy, 430, 433, 436–438
surface
  composition, 414
  contamination, 414
  corrugation, 411
  roughness, 411
surface binding energy, 433
surface topography, 410, 411

target
  alkali halide, 404
  alkaline earth, 404
  alloy
    Ni_3B, 417
    Ni-Zr, 417
    Ti-Ni, 417
  amorphous
    SiO_2, 421
  compound
    CsI, 417
    LiF, 417
    SiO_2, 416
    UF_4, 416
    $Y_3Fe_5O_{12}$, 417
  frozen gas
    O_2, 416
  insulator, 403, 412, 423, 427, 438
    garnet, 404
    mica, 404
    oxide, 421
    quartz, 404, 421
    radiation-resistant, 404
    silicate, 404

ionic crystal, 416, 426
metal, 412, 416, 418, 427, 434, 438
metallic glass, 417
oxide, 416, 427
single crystal, 427
target structure
crystalline, 407, 411
thermal conductivity, 429–431
thermal diffusivity, 430, 433
thermodynamic equilibrium, 439
threshold energy, 439
time-of-flight (ToF), 405, 408
track, 404, 423, 427, 439
amorphous, 404
detector, 409
diameter, 402
formation, 403, 404, 429, 431, 437, 438
ion, 417
radius, 431, 437, 439
size, 431
volume, 402
zone, 403, 431
trajectory, 429

valence band, 433
vaporization, 433
velocity effect, 402

Wehner spot, 424

Index

absorption, 237, 238
adatom, 100, 209, 210, 212
  island, 209, 212, 215
  production, 209
adsorption of
  oxygen, 34
  water, 34
amorphization, 198, 215, 423
  dose, 196
angular dependence of the sputtering yield, 416
  Ag, 119
  Al, 105
  Au, 122–124
  Be, 103
  C, 103–105
  Cu, 110–114, 127
  Fe, 106
  Mo, 116–118
  Nb, 115
  Ni, 107–109
  Pd, 120
  Si, 105
  Ta, 120
  Ti, 106
  W, 121
  Zr, 115
angular distribution, 3, 4, 25, 410, 418, 421–423, 425–427
  cosine, 4, 235, 275, 276, 421, 428
  isotropic, 411
  jet-like, 411, 412, 424
  Mo, 291
  Ni, 291
  over-cosine, 275–277, 292, 410, 421
  under-cosine, 275, 291, 292
  W, 292
annealing, 132, 196
asymptotic trajectory, 24

backscattering, 24, 25, 35
band gap energy, 433
band structure, 26, 247
Bayesian statistics, 39
BCA program
  ACAT, 8, 35, 133
  MARLOWE, 8, 21, 22, 126, 133
  Monte Carlo (MC), 22, 124, 131, 132, 189, 190, 215, 219, 407, 428
  SDTrimSP, 25
  TRIDYN, 8, 25, 37, 128, 129
  TRIM, 8, 21, 133, 232
  TRIM-CASCADE, 8, 417, 418, 420
  TRIM.SP, 8, 21, 22, 24, 25, 35, 101, 133, 275, 283, 284, 286, 289, 290
beam monitor, 411
binary collision approximation (BCA), 8, 21, 23–25, 35, 189, 232
blistering, 5
Boltzmann transport equation, 21
boundary condition, 27, 191, 219
  free, 28
  periodic, 27
Bragg peak, 401, 402
breathing sphere approach, 217
bulk
  composition, 283
  coordination number, 236
  vacancy, 209

catcher foils, 35
channeling, 3, 28, 40, 132, 196, 407, 409
chemical sputtering, 203, 218
cluster, 2, 3, 9, 11, 189, 201, 207
  abundance distribution, 206
  Ag_n^+, 258
  C_n^-, 258, 266

Cu_n, 257
deposition, 201
dimer, 204, 205, 256
emission, 206, 219, 254–256
$(H_2O)_n$, 216
Ag_n, 255
Ag_{60}, 205
Ag_6, 255
Al_n, 255
Au_n, 206, 255
benzene, 266
Cu_n, 255
Ga_n, 255
Ge_n, 255
In_n, 255
In_n^+, 258
In_{200}, 205
metal, 287
metastable, 269
Nb_n, 255
Si_n^-, 251, 258
Ta_n, 255
energy, 206
energy spectra
Ag_n, 256, 257
Al_n, 256
Cu_n, 256
Cu_2, 256
Cu_3, 256
Ge_n, 256
In_n, 256
Si_n^-, 251
formation, 204, 206, 207, 254
fragmentation, 207, 208
homonuclear, 255
impact, 200–204, 206, 211, 212, 219, 231, 293–295, 297, 299, 300
$(CO_2)_n$, 294
$(CO)_2$, 203
$(CsI)_nCs$, 294
$(CsI)_nI$, 294
Ag_n, 202
Al_n, 202
Ar_n, 202, 203, 294
Ar_{3000}^+, 300
Au_4, 208, 210
Au_n, 202, 203, 294
C_{60}, 203, 294
fullerene, 3, 203
point, 203
ReO_4, 294
SF_6, 294
internal energy, 208
internal excitation, 207
metastable, 207
orientation, 203
range, 201
secondary ion, 295, 296
size, 203, 206, 208, 255, 257, 258, 296, 441
species, 255, 294
stable, 207
trimer, 256, 293
yield, 203
clustering probability, 205
cohesive energy, 198, 200, 211, 234, 236, 245, 246, 253, 272, 286
collision cascade, 1, 10, 21, 26
collisional mixing, 253
composition, 24
change, 37, 126, 215, 252, 254, 282
gradient, 253, 275, 281
profile, 281, 282
compound formation, 126
compound target, 24
condensed gas, 198, 272
conduction band, 433
cosmic dust particle, 210
Coulomb explosion, 196, 201, 403–405
crater, 200, 203, 204, 210, 212, 219
depth, 34, 202
formation, 199, 210, 211, 293, 300
threshold, 211
length scale, 211
rim, 203, 204, 207, 209, 211, 215, 300
size, 211
structure, 211
volume, 203, 211
cross section
excitation, 240
nuclear stopping, 272
cylindrical deflector, 238

damage distribution, 233
Debye temperature, 430
decay rate, 266, 269
decomposition, 258, 266
rate, 268

time, 267
defect, 212, 231
annealing, 429
production, 197, 201, 213, 233
delta electron, 429
deposited energy, 200, 233, 276, 428
depth
distribution, 128, 129
resolution, 414
depth of origin, 133, 192, 215, 234, 253, 281, 410
depth resolution, 11
desorption, 216, 254, 262, 266, 271, 441
detection technique
catcher, 406, 409, 411
collector, 241, 243, 278, 281
foil, 241
element selective, 406
differential yield, 234, 235, 410, 418
diffusion, 10, 126, 129, 132, 200, 212, 428
dimer, 196, 254, 293, 297
Ag_2, 257
Cs_2, 254
Cu_2, 287
K_2, 254
Na_2, 254
S_2, 254
dimer ejection, 204
dipole moment, 196
Dirac-Hartree-Fock-Slater (DHFS), 23
disappearance cross section, 260
displacement energy, 2, 26, 196
dissipation, 189, 231
dissociation, 216, 217, 274
molecule, 216
threshold, 207, 261
Doppler profile, 240
Doppler shift laser fluorescence spectroscopy (DSLFS), 240, 271
dynamic range, 239

elastic recoil detection analysis (ERDA), 409, 411, 412, 414, 441
electrical conduction, 197
electrical resistivity, 34, 272
electron affinity, 252
electron impact ionizer, 241
electron microprobe, 34
electron microscopy, 11
electron promotion, 248
electron spectroscopy, 238
electron-atom coupling, 28
electron-atom interaction, 26, 28
electron-atom scattering, 197
electron-induced X-ray emission, 243, 282
electron-phonon coupling, 197, 404, 405, 427, 429, 430, 434, 435, 437, 439
electron-phonon interaction, 26, 197
electron-phonon relaxation, 428
electron-tunneling model, 252
electronic configuration, 247, 249, 250
electronic excitation, 200, 201
electronic sputtering, 192, 196, 200, 211, 216, 401, 403, 407
electrostatic energy analysis, 238
energy dependence of the sputtering yield
Ag, 35, 36, 78, 79
Al, 48, 49
Au, 94, 95
B, 44
Be, 42, 43
Bi, 96
C, 45, 46
Ca, 51
Cd, 80
Co, 60, 61
Cr, 56, 57
Cs, 82
Cu, 64, 65
Fe, 58, 59
Ga, 66
Ge, 66, 67
Hf, 84
Hg, 96
In, 80
Ir, 91, 93
Li, 41
Mg, 47
Mn, 57
Mo, 39, 72, 73
Nb, 70, 71
Ni, 37, 62, 63
Os, 90
Pb, 97

Pd, 76, 77
Pt, 92, 93
Re, 89
Rh, 75
Ru, 74
Sb, 82
Sc, 51
Se, 69
Si, 50
Sm, 83
Sn, 81
Ta, 85, 86
Tb, 83
Te, 82
Th, 98
Ti, 52, 53
Tl, 96
Tm, 83
U, 99, 100
V, 54, 55
W, 87, 88
Zr, 68, 69
energy deposition, 193, 276, 402, 429
energy dissipation, 231, 232, 244, 272, 273, 277
energy loss, 24, 198, 269
electronic, 7, 21, 23, 36, 38, 100, 197, 232, 269, 270, 402, 404, 405, 416, 417, 420, 421, 423, 426–428, 434–436, 438, 439
Firsov, 197
Lindhard-Scharff model, 23, 36, 197
Oen-Robinson model, 23, 36
nuclear, 23, 245, 269, 402, 409, 417, 420, 434–437
energy resolution, 238
energy spectra, 24, 25
Ag, 297
Ag_2, 297
Al, 290
Cu_2, 288
In, 298
Si^-, 251
Ta^+, 296
Ta_4^+, 296
W, 290
enthalpy of fusion, 430
escape depth, 275
escape time, 133
evaporation, 2, 132, 203, 208, 271, 272, 293, 406
rate, 433
excitation, 191, 198, 269, 408, 439
electronic, 192, 197, 232, 270, 271, 405, 417
energy, 247, 248, 250
frequency, 240
rotational, 263
vibrational, 263

Fermi energy, 430
Fermi temperature, 430
field ion microscopy (FIM), 11, 35
finite-element-method, 27
fluctuation, 132, 203
fluence, 5, 6, 37, 38, 126–130, 193, 194, 212, 215, 218, 243
fluorescence, 238
focusing collision sequence, 3, 277, 279
fractal dimension, 204
fractal surface, 204
fractionation, 130, 131
fragment, 261, 265
fission, 409
formation, 217
ion formation, 261
species, 260
fragmentation, 254, 256, 260, 261
C_n^-, 258
large molecule, 260
molecule, 217
particle-induced, 218
species, 261
friction, 23, 197, 198

Gibbsian segregation, 281, 282

Hartree-Fock-Slater (HFS), 23
heat conduction, 200
heat of sublimation, 2, 7, 24, 35, 125, 131
heat-flow equation, 429

impact parameter, 22
implantation, 11, 128, 129, 213
inelastic thermal spike model (i-TS), 404, 406, 428, 429, 431, 433, 434
insulator, 3, 437

interaction potential, 22, 25, 26, 28, 35, 36, 38, 100, 132, 190, 191, 193, 194, 211, 217, 219, 234
AIREBO, 217, 218
attractive, 205
Coulomb, 23
embedded-atom-method (EAM), 26, 191
hydrocarbon (Brenner), 217, 218
intermolecular, 216, 217
Lennard-Jones, 26, 200, 216
many-body, 236
Morse, 216
Nakagawa-Yamamura, 35
pair potential, 212, 236
power, 131, 132
screened Coulomb, 22, 23
KrC (WHB), 23, 35, 38
Molière, 23, 35
ZBL, 23, 35
screening function, 23
Stillinger-Weber, 218
three-body, 26
tight-binding, 236
interlayer mobility, 213
internal energy, 254, 263, 266
intra-molecular interaction, 216
ion beam milling, 204
ion beam polishing, 204
ion-beam mixing, 197
ion-solid interaction, 25
ionic bonding, 196
ionic charge transfer, 196
ionization, 191, 198, 232, 244, 255, 265, 269, 408, 439
continuum, 238
electron impact, 237
low density plasma, 239
multiphoton (MPI), 238
non-resonant multiphoton (NRMPI), 238
Penning, 237
potential, 238
probability, 251, 252, 258
resonance enhanced multiphoton (REMPI), 238
single photon (SPI), 238
threshold, 238
isotope sputtering, 130, 131, 220
isotropic surface potential, 24

Katz model, 429

Langevin dynamics, 27
laser ablation
organic films, 217
laser excitation, 240
laser induced fluorescence (LIF), 240, 247, 289, 408
laser induced resonance ionization spectroscopy (RIS), 408
lattice code, 22
lattice vibration, 131
lifetime, 197, 266, 269
radiative deexcitation, 247
light-versus-distance (LvD) technique, 240
low energy electron (LEED), 11

many-body interaction, 219
mass change, 34
mass selectivity, 238
mass spectrometer, 239, 253, 258
double focusing, 239
quadrupole, 239
secondary-neutral, 239
time-of-flight, 238, 243
mass spectrometry, 254, 255, 294, 405, 408
material modification, 402
material processing, 294
matrix isolation spectroscopy, 216
Maxwell-Boltzmann distribution, 271, 423
mean-free path, 198
melting, 190, 198, 203, 206, 209, 211, 214, 406
metallic bond, 236
micro-explosion, 209
microbalance, 410
mixing, 203
molecular dynamics, 21, 25–28, 131, 189–192, 194, 199, 219, 232, 416, 428, 435, 439
molecule, 2, 3
emission, 254
formation, 244, 254
fragmentation, 208

internal excitation, 217
organic, 266
orientation, 263
shape, 263
molecule liftoff, 217
molten zone, 209
momentum focusing, 277
multilayer coverage, 266

negative binomial distribution, 132
neutralization probability, 251
neutron activation, 35, 240
neutron sputtering, 3
Newton's equations of motion, 25, 219

oligomer, 261
organic adsorbate, 261, 262
organic material, 260, 265
organic molecule, 217
oscillations, 129
outer solar system, 216

partial sputtering yield, 126, 193
phase transformation, 404
photoionization, 238, 266
laser, 243
photon emission, 239
planar surface potential, 24, 234, 289
planetary science, 131
Poisson distribution, 132
polymer, 261
population distribution, 247
population temperature, 254
post-ionization, 237–240, 255, 441
electron impact, 256, 279
laser, 241, 242
plasma, 239, 253
preferential sputtering, 129, 130, 194, 195, 215, 219, 253, 421
projectile binding energy, 102
proton-induced X-ray emission, 243

quadrupole mass filter, 241
quench rate, 435

radiation damage, 1, 2, 25, 26
radiation-enhanced diffusion, 253
radiative decay, 247
radical, 217
radioactive waste storage, 196
range
projectile, 197
recoil, 435
reactive ion beam etching (RIBE), 218
recoil
angle, 22
atom, 2, 8
density, 233, 234, 244, 245
direct, 252, 285, 288, 289, 291
flux, 244, 275, 276
generation, 233
implantation, 253
isotropic distribution, 244
primary, 289
spectrum, 235, 277
recombination, 206, 216
recondensation, 273
redeposition, 212
reduced energy, 38
reflection, 193, 213
reflection coefficient, 25, 126, 127
reflectron, 238
refraction, 24, 101, 234
regime
deposition, 127
erosion, 127–129
high-density collision cascade, 300
linear cascade, 2, 7, 192, 231–233, 244
linear-cascade, 198
single knockon, 2, 232, 300
spike, 2, 199, 232, 293
relocation, 231
resonant electron transfer (RET), 250, 252
resonant photoionization mass spectrometry, 247
rotational excitation, 216
rotational population, 254
RRK transition-state theory, 207
Rutherford backscattering spectroscopy (RBS), 243, 409

scanning tunnelling microscope, 212
scattering angle, 22, 23
screening length, 23, 35, 38

secondary ion mass spectrometry (SIMS), 4, 194, 198, 216, 217, 237, 243, 260, 266, 294
secondary neutral mass spectrometry (SNMS), 237, 253, 266, 294
  laser, 241
segregation, 126, 129, 132, 281
selfsputtering, 3, 24, 101, 102, 128, 209, 215, 275, 298
sheath potential, 130
shock wave, 255
simultaneous bombardment, 130
simultaneous weak collision, 24
solid–liquid transition, 131
specific heat coefficient, 429
spherical deflector, 238
spherical electrostatic sector, 239
spike, 198, 199, 201, 211, 219, 253, 272
  elastic collision, 101, 198, 272, 435
  lifetime, 200
  temperature, 271
  thermal, 27, 28, 197–199, 202, 210, 240, 404, 405, 428, 431, 435, 437, 439, 440
  volume, 200, 272
sputtering of
  clusters, 190
  molecules, 190, 260
sputtering yield, 3, 5, 7–10, 34–36
sputtering yield oscillations, 128
state
  charge, 4, 130, 252, 402, 405, 416, 419
  equilibrium charge, 407, 411, 418, 425, 440
  excited, 196, 240, 247, 251, 407
    Ag, 247
    Ba, 247
    Ca, 247
    Co, 247
    Cr, 247
    Cu, 247
    Fe, 247
    In, 247
    Ni, 247
    Rh, 247, 280
    Ti, 247
    U, 247
    Zr, 247
  ferromagnetic, 132
  ground, 4, 9, 240, 248
    Ag, 246, 248
    Al, 246
    Ca, 246
    Co, 248, 249
    Ni, 248, 249
    Rh, 280
  magnetic, 132
  metastable, 197, 240, 247
    Ag, 247, 248
    Co, 249, 250
    formation, 252
    high-lying, 250
    low-lying, 249
    Ni, 248–250
  paramagnetic, 132
  short-lived, 247
  steady, 33, 126–130, 193, 253, 283, 287
  valence band
    Co, 250
    Ni, 251
sticking, 35, 241
  coefficient, 193, 409
  probability, 409
stoichiometry, 129, 253
stopping power
  electronic, 190, 197, 198, 200, 211, 272
  nuclear, 38, 190, 198, 200, 234
sublimation energy, 234, 236, 274, 430, 433, 435, 437
surface
  composition, 215, 283, 414
  contamination, 414
  corrugation, 411
  defect, 208, 209
  erosion, 203
  modification, 201, 294
  morphology, 242
  roughening, 5
  roughness, 34, 38, 100, 124, 126, 132, 190, 204, 211, 215, 219, 276, 411
  smoothing, 5, 201, 202, 204, 212, 215, 300
  step, 211–213
  structure, 212
    dot, 203, 215
    ripple, 211, 215, 242, 277

  tension, 207
  vacancy, 209, 215
surface binding energy, 2, 7, 22, 24, 28, 35, 100, 125, 130, 131, 190, 194, 195, 209, 236, 237, 245, 246, 253, 254, 271, 274, 286, 293, 433
surface contamination, 276
surface potential barrier, 234
surface topography, 4–6, 190, 191, 209, 211–213, 215, 219, 220, 242, 243, 277, 410, 411

target
  alkali halide, 196, 231, 232, 244, 269, 271, 300, 404
  alkali metal, 270
  alkaline earth, 404
  alkanethiol, 265
  alloy, 10, 193, 253
    $Ag_{0.6}Au_{0.4}$, 253
    Ag–Au, 253, 280, 281
    Au–Cu, 283
    Co–Au, 283
    Co–Ni, 283
    Cu, 205
    $Cu_{0.53}W_{0.47}$, 285, 286
    Cu_3Au, 281
    Cu–Be, 283
    Cu–Ni, 280, 283
    Cu–Pt, 281
    Cu–Zn, 253, 283
    Cu-Li, 253
    Fe–Ni, 280, 283
    Ga–In, 281
    Ni_3B, 417
    $Ni_{0.92}W_{0.08}$, 285
    Ni_5Pd, 281
    Ni–Pt, 281
    Ni–Ti, 283
    Ni–W, 253
    Ni-Zr, 417
    Ti-Ni, 417
    W-Si, 283
  amorphous, 35, 40, 232, 275
    SiO_2, 421
  amorphous hydrogenated carbon, 218
  benzene molecular crystal, 217
  biological material, 260
  composition, 130, 274
  compound, 4, 10, 129, 130, 193, 196, 203
    CsI, 417
    GaAs, 253
    $Hf_xC_{(1-x)}$, 253
    HfC, 253
    LiF, 417
    SiO_2, 416
    UF_4, 416
    $Y_3Fe_5O_{12}$, 417
  condensed gas, 232, 269, 271
  crystalline, 277
  diatomic molecular solid, 216
  dibenzanthracene, 261
  frozen gas, 231, 244, 300
    Ar, 271
    CO, 272
    CO_2, 272
    D_2O, 272
    H_2O, 216
    H_2O, 272
    Kr, 271
    N_2, 272
    Ne, 271
    O_2, 416
    O_2, 271
    Xe, 271, 272, 274
  Ge, 209
  glass, 5
  hydrocarbon, 217
  inorganic material, 216
  insulator, 232, 403, 412, 423, 427, 439
    garnet, 404
    mica, 404
    oxide, 421
    quartz, 404, 421
    radiation-resistant, 404
    silicate, 404
  ionic crystal, 232, 416, 426
  isotopic mixture, 243, 283
  liquid, 25, 195
  metal, 209, 231, 232, 244, 254, 255, 269, 300, 412, 416, 418, 427, 434, 439
  metallic glass, 417
  model alloy, 194
  modification, 202
  molecular solid, 200, 216

multicomponent, 24, 126, 132, 194, 252, 253, 275, 280
multilayer film, 217
organic material, 200, 216–218, 231, 244, 269, 300
organic molecule, 217
oxide, 254, 416, 427
polycrystalline, 35, 40, 232
polyethylene, 218
polyethyleneterephthalate (PET), 265
polyisobutylene, 269
polymer, 217
polystyrene, 263
polystyrene (PS), 261–265, 269
radioactive, 240
randomized, 131
semiconductor, 5, 231, 232, 244, 255, 269, 277, 300
InAs, 5
InP, 5
InSb, 5
single crystal, 4, 9, 35, 40, 127, 132, 191, 232, 240, 275, 277, 427
CaF_2, 271
KCl, 196
LiF, 196
NaCl, 196, 271
structureless, 189
triacontane, 261
target structure
amorphous, 22, 33, 231, 235, 275
crystalline, 3, 22, 27, 33, 189, 231, 236, 275, 407, 411
polycrystalline, 22, 33, 231, 240, 275
target temperature, 9, 10
terrace, 213, 214
thermal conductivity, 272, 429–431
thermal diffusivity, 430, 433
thermal equilibrium, 1
thermalization, 189, 197
thermodynamic equilibrium, 206, 439
thin film deposition, 11, 201, 215
threshold energy, 2, 4, 8, 9, 39, 102, 125, 126, 440
time-of-flight (ToF), 238, 240, 253, 405, 408
time-of-flight mass spectrometry, 241, 242, 247
ToF-SIMS, 260, 265
track, 200, 201, 211, 217, 404, 423, 427, 439
amorphous, 404
detector, 409
diameter, 402
formation, 196, 403, 404, 429, 431, 438, 439
ion, 417
ionisation, 201
radius, 431, 437, 439
size, 431
volume, 402
zone, 403, 431
trajectory, 22, 198, 263, 264, 429
transmission, 25, 192
tunneling microscope, 124

vacancy
island, 212
valence band, 433
vapor pressure, 270
vaporization, 131, 433
velocity effect, 402
vibrational distribution, 254
vibrational excitation, 216, 218

Wehner spot, 132, 191, 192, 244, 277, 424
work function, 252, 258

x-ray analysis, 34

Author Index

The reference number before the point gives the chapter:
Behrisch, Eckstein [1.], Eckstein, Urbassek [2.], Eckstein [3.], Urbassek [4.], Gnaser [5.], Jacob, Roth [6.], Assmann, Toulemonde, Trautmann [7.]

Abe, T. [3.195]
Abelson, J.R. [6.117]
Abrams, C.F. [4.37, 4.38, 4.40, 4.244]
Ada, E.T. [5.644]
Adamopoulos, G. [6.269]
Adamov, G.V. [1.146, 3.312]
Adams, F. [5.226, 5.680, 5.681, 5.687, 5.688]
Adelhelm, C. [6.19]
Aderjan, R. [4.145, 4.179, 5.630]
Adriaens, A. [5.225, 5.226, 5.680, 5.681, 5.687, 5.688]
Afridi, H. [3.257, 5.393]
Agarwal, S. [6.84]
Agnew, P. [2.46, 4.86, 7.156]
Ahlgren, T. [6.239]
Ahmad, S. [5.530, 5.531, 5.570]
Akaishi, K. [3.169, 3.170]
Akiba, M. [3.266, 3.297, 3.489]
Akin, F.A. [5.670]
Akizuki, M. [4.141, 5.598, 5.608]
Aksyonov, S.A. [5.636]
Albe, K. [4.206]
Albert, M. [6.229]
Albridge, R.G. [6.229]
Alder, B.J. [2.26, 4.10]
Aleksandrov, L.N. [4.192]
Alekseev, V.I. [3.405]
Alimov, V.K. [6.224]
Alkemade, P.F.A. [5.426]
Allain, J.P. [3.46, 3.137, 3.330, 3.393, 3.486]
Allas, R.G. [3.100, 3.139, 5.399]
Alldred, J.C. [3.167]
Allen, M.P. [2.28, 2.30]

Allendorf, H.D. [6.260]
Almén, O. [1.52, 1.60, 3.79, 3.90, 3.402, 5.95, 6.25]
Alonso, E.V. [3.174, 5.606]
Alton, G.D. [3.154]
Amaratunga, G.A.J. [6.285]
Andersen, H.H. [1.84 - 1.86, 1.89 - 1.92, 1.128, 2.22, 3.2, 3.114, 3.162, 3.214, 3.229, 3.236, 3.238, 3.291, 3.410, 4.11, 4.93, 4.94, 5.49, 5.203, 5.237, 5.397, 5.398, 5.415, 5.477 - 5.480, 5.559 - 5.561, 5.589, 5.674, 5.675, 5.682, 5.700, 7.57, 7.117, 7.153]
Andersen, N. [3.298]
Anderson, G.S. [1.51, 1.61, 5.98, 5.429]
Andreadis, T.D. [3.353, 3.354, 3.358, 3.490]
Andrew, P. [6.101]
Anisimov, S.I. [7.135]
Aoki, T. [3.360, 4.127, 4.143, 4.245, 4.246, 5.648, 5.659, 5.663, 5.702, 7.101]
Aoyama, T. [5.487, 5.488]
Apel, P. [7.33]
Appelhans, A.D. [5.591]
Appelt, J. [3.131]
Appleton, B.R. [3.348]
Arezki, B. [5.335, 5.341, 5.344]
Arlinghaus, H.F. [7.90]
Armacost, M. [6.12]
Arminen, E. [3.151]
Arnoldbik, W.M. [7.77]
Asakura, N. [6.209]
Ascheron, C.E. [5.598]
Aschke, L. [1.196]
Ashkenazy, Y. [4.206]
Ashley, J.C. [4.72]
Askerov, S.G. [3.407]
Assmann, W. [7.6, 7.54 - 7.56, 7.67, 7.94, 7.102, 7.103, 7.105, 7.169]
Ato, Y. [3.65, 3.171]
Atwater, H.A. [4.239]
Auciello, O. [6.34, 6.63 - 6.65, 6.146, 6.147, 6.163, 6.215, 6.216]
Audouard, A. [7.111, 7.112, 7.116]
Augustyniak, W.M. [3.123, 5.379, 5.386, 7.61]
Aumayr, F. [1.69, 3.129, 3.475, 6.59, 7.100]
Avasthi, D.K. [7.31, 7.76]
Averback, R.S. [2.44, 4.76, 4.85, 4.95, 4.117, 4.118, 4.120, 4.121, 4.124, 4.125, 4.175, 4.206, 5.623, 7.20, 7.154]
Azzam, R.M.A. [6.86]
Baba, S. [3.232]
Bach, H. [1.191 - 1.193]
Bachurin, V.I. [3.457]
Bacon, D.J. [4.75]
Bader, M. [3.148]
Bailón, L.A. [4.26, 4.204]
Bajard, M. [7.84]
Balant, A.C. [5.149, 5.209, 5.366]

Balanzat, E. [7.9, 7.112, 7.116]
Balden, M. [1.66, 1.148, 1.149, 1.162, 3.74, 3.112, 6.17 - 6.19, 6.81, 6.109, 6.182, 6.228, 6.231, 6.254]
Baldo, P.M. [4.162, 5.280, 5.281]
Baldwin, M.J. [3.315, 6.30, 6.31, 6.42]
Baller, T. [5.265, 5.266]
Balooch, M. [6.10]
Bandourko, V. [3.266, 3.297]
Banerjee, S. [4.214 - 4.216]
Banks, J.C. [1.68, 7.71]
Bao, D.S. [5.482]
Baragiola, R.A. [3.174, 5.606, 7.17]
Baranov, A.M. [6.270]
Baranov, I.A. [7.13, 7.73]
Barbolla, J. [4.26, 4.203, 4.204]
Barbu, A. [7.20, 7.113]
Bard, A. [6.91, 6.92, 6.208]
Baretzky, B. [3.483, 3.484]
Barna, A. [3.340, 3.368]
Barnes, A.V. [1.68, 6.229, 7.71]
Barnes, R.S. [7.3]
Baron, E. [7.83, 7.84]
Barone, M.E. [4.240 - 4.242]
Barskaya, A.Ya. [3.172]
Bartella, J. [5.207]
Barth, H.-J. [3.380, 5.196 - 5.198]
Bartz, J.W. [6.279]
Barucki, K. [1.214]
Basford, J.A. [6.68]
Bashara, N.M. [6.86]
Baskes, M. [2.37]
Bastasz, R. [3.487, 6.95]
Bastiaansen, J. [5.159, 5.160, 5.162, 5.163, 5.166 - 5.168]
Basu, D. [3.177]
Batchelder, D.N. [6.269]
Baudin, K. [5.682]
Baumann, H. [3.118]
Baumel, L.M. [3.192, 7.64]
Baxter, J.P. [5.61, 5.122 - 5.124, 5.150, 7.91]
Bay, H.L. [1.84, 1.85, 1.86, 1.89 - 1.91, 1.128, 3.2, 3.72, 3.114, 3.134, 3.153, 3.155, 3.157, 3.162, 3.194, 3.214, 3.229, 3.236, 3.259, 3.265, 4.35, 4.36, 4.93, 5.108, 5.146, 5.415, 5.538 - 5.541, 5.554, 5.555, 5.559 - 5.561, 6.61, 6.234, 7.153]
Beardmore, K. [4.149, 4.228]
Beavis, L.C. [6.67]
Beavis, R. [5.253]
Becerra-Acevedo, R. [3.371, 5.558]
Becker, C.H. [5.94]
Beckers, L.J. [3.126, 3.127, 5.607]
Bedrossian, P. [4.193]

Beeler, J.R.,Jr. [2.34]
Begemann, W. [5.254, 5.255]
Behringer, K.H. [6.91, 6.110]
Behrisch, R. [1.43, 1.45 - 1.47, 1.65, 1.97, 1.142, 1.156, 1.163, 1.174, 1.176, 1.177, 1.179, 1.183, 1.186, 1.187, 3.1, 3.9, 3.10, 3.68, 3.92, 3.135, 3.160, 3.183, 3.207, 3.241, 3.247, 3.270, 3.307, 3.364, 3.481, 4.1 - 4.3, 4.55, 5.4, 5.14 - 5.16, 5.553, 5.556, 6.62, 6.184, 6.185, 6.222, 6.227, 6.228, 6.282]
Bekkerman, A.D. [5.259, 5.295]
Bell, F. [7.80]
Bellachioma, M.C. [7.173]
Belu, A.M. [5.227]
Belykh, S.F. [5.678 - 5.681, 5.686 - 5.688]
Ben Assayag, G. [5.596]
Benazeth-Colombie, N. [3.122]
Bendel, C. [5.594]
Bender, M. [7.173]
Benedek, R. [4.117]
Benedikt, J. [6.84 Benes, E. [5.104, 5.105]
Bengtson, K.R. [5.486]
Benguerba, M. [5.596]
Benneman, K.H. [7.160]
Bennett, J. [5.640]
Benninghoven, A. [1.200 - 1.202, 3.209, 5.78, 5.85, 5.302, 5.313, 5.345, 5.594, 5.642, 5.643]
Benyagoub, A. [7.37 - 7.39, 7.45, 7.47 - 7.49]
Berg, S. [3.287, 3.288, 3.342]
Berger, S. [5.587]
Bergmaier, A. [7.81, 7.82, 7.95]
Bergsaker, H. [3.82, 3.86]
Berkenkamp, S. [5.305, 5.306]
Bernardo, D.N. [4.81, 5.471]
Bernas, H. [5.674, 7.57, 7.121]
Bernhard, F. [5.294]
Berres, W. [5.108, 5.539, 5.540]
Bert, N.A. [3.485]
Bertóti, I. [5.221]
Berthold, W. [5.164, 5.165]
Bertholot, A. [7.79, 7.165, 7.166]
Bertrand, P. [4.229, 5.326 - 5.337, 5.340, 5.344]
Besenbacher, F. [5.477]
Besocke, K.H. [5.587, 5.588, 6.200]
Bethe, H.A. [2.20]
Bethge, K. [1.67, 3.118, 7.70]
Betz, G. [1.157, 1.181, 3.89, 3.281, 3.339, 3.466, 4.23, 4.144, 4.159, 4.168, 4.191, 5.60, 5.133, 5.145, 5.151, 5.153, 5.158, 5.201, 5.202, 5.214, 5.215, 5.248, 5.252, 5.367, 5.413, 5.414, 5.453, 5.626, 6.229]
Beuhler, R.J. [5.599 - 5.601]
Beuneu, F. [7.111]
Beuscher, H. [5.23]

Beuve, M. [4.114, 7.69, 7.132]
Bhagwan Das, K. [6.67]
Bhattacharjee, S. [3.204]
Bhattacharya, R.S. [3.216, 5.204, 5.205]
Bieck, W. [5.81, 5.100]
Biener, J. [6.74, 6.75, 6.149 - 6.156]
Bierman, D.J. [5.191, 5.192]
Biersack, J.P. [1.34, 1.39, 1.82, 1.101, 1.134, 1.135, 2.9, 2.10, 2.13, 2.14, 2.24, 3.28, 3.31, 3.35, 3.186, 3.245, 3.246, 3.287, 3.293, 3.332, 3.360, 3.365, 3.372, 3.373, 3.390, 3.468, 4.6, 4.8, 5.50, 5.68, 5.408, 5.496, 7.108, 7.118, 7.126]
Bigl, F. [1.110, 5.545]
Birtcher, R.C. [2.54, 4.162, 4.183 - 4.185, 5.280, 5.281, 7.170, 7.171]
Birukov, A. Yu. [3.59]
Bischoff, A. [3.378]
Bitensky, I.S. [4.158, 4.163, 5.238, 5.290, 5.613]
Blaaderen, A. van [7.120]
Blain, M.G. [5.595, 5.596]
Blais, J.C. [5.312]
Blanchard, W. [6.273]
Blank, P. [3.130]
Blauner, P.G. [3.192, 7.64, 7.107]
Blenkinsopp, P. [5.649 - 5.651]
Bletsos, I.V. [5.302]
Blewer, R.S. [3.50, 6.186]
Bloch, F. [2.21]
Blum, P. [5.104, 5.105, 7.87, 7.89]
Bobek, T. [1.118]
Boccanfuso, M. [7.47 - 7.49]
Bock, W. [5.424]
Boeckmann, M.D. [6.68]
Bogdanov, Z. [3.474]
Bogen, P. [5.538]
Bohdansky, J. [1.129, 1.141, 1.175, 1.183, 3.37, 3.48, 3.50 - 3.52, 3.68, 3.69, 3.72, 3.78, 3.80, 3.83, 3.85, 3.87, 3.111, 3.131, 3.135, 3.145, 3.153, 3.155, 3.157, 3.159, 3.179, 3.194, 3.208, 3.241, 3.252, 3.254, 3.258, 3.259, 3.262, 3.265, 3.371, 3.473, 3.483, 5.509, 5.555 - 5.558, 6.7, 6.44, 6.55, 6.56, 6.60 - 6.62, 6.173, 6.185, 6.195, 6.221, 6.234, 6.264, 6.265]
Bohmeyer, W. [6.105, 6.204, 6.210]
Bohr, N. [1.40, 5.1]
Boivin, R. [3.56, 3.57]
Bok, J. [7.158]
Bolbach, G. [5.312, 5.597]
Bonardi, N. [7.24]
Borders, J.A. [3.75, 3.478]
Boring, J.W. [5.372 - 5.374, 5.379, 5.380, 5.386]
Borisov, A.M. [3.93]
Boudjadar, S. [7.137]
Bouffard, S. [7.43, 7.69, 7.96, 7.112, 7.142]
Boulouednine, M. [7.95]

Bouneau, S. [5.675, 5.689]
Boussofiane-Baudin, K. [5.597]
Bouwen, W. [5.157]
Bräuer, G. [3.180, 3.257, 5.393, 5.394]
Bradley, R.M. [1.115]
Braganza, C.M. [6.8, 6.165]
Bramham, R.W. [3.228]
Brandner, B.D. [6.74, 6.75]
Brandt, W. [5.38]
Braun, M. [3.102, 3.189, 3.201, 3.482, 6.189]
Bredov, M.M. [2.4]
Brenner, D.W. [2.41, 4.211, 4.221, 4.222, 4.231]
Bresnock, F.J. [3.125]
Brezinsek, S. [6.96 - 6.101, 6.112, 6.210]
Brice, D.K. [6.186, 6.187]
Briehl, B. [2.53]
Briere, M.A. [1.67, 7.70]
Briggs, D. [1.159, 5.86, 5.99]
Brilhac, J.F. [6.258]
Bringa, E.M. [2.49, 4.57, 4.105 - 4.110, 4.112, 4.178, 4.186, 4.187, 7.59, 7.106, 7.130, 7.131, 7.164]
Brisard, F. [7.1, 7.21, 7.34]
Brizzolara, R.A. [5.523, 5.524]
Brock, J.D. [4.201, 4.202]
Brodale, M. [7.67]
Brodzinski, R.L. [3.183]
Broitman, E. [6.290, 6.292]
Bromann, K. [5.634]
Brooks, J.N. [6.95, 6.104]
Brooks, N.H. [6.95]
Broomfield, K. [3.450, 4.28]
Brorson, S.D. [7.148]
Brossa, F. [3.473]
Brown, A. [5.317]
Brown, J.J. [6.12]
Brown, T.C. [6.255]
Brown, W.L. [3.123, 5.379, 5.380, 5.386, 7.61, 7.65, 7.66]
Brox, O. [5.642]
Bruce, G. [1.52, 1.60, 3.79, 3.90, 5.95, 6.25]
Bruckmüller, R. [5.105, 5.365, 7.87]
Brummel, C.L. [4.172, 5.346]
Brune, H. [5.634]
Brunelle, A. [3.238, 5.596, 5.597, 5.674 - 5.676, 5.682, 7.57, 7.72]
Buchanov, W.M. [1.79]
Buchta, R. [3.102]
Budhani, R.C. [7.32]
Burkhardt, H. [7.6]
Burnett, J.W. [4.191, 5.89, 5.125]
Burnham, J.S. [4.21, 5.466, 5.470]

Burtseva, T.A. [1.64, 6.14]
Busharov, N.P. [6.9] Busse, C. [4.177]
Busza, P. [3.196]
Butterbaugh, J.W. [6.294]
Buzhinskij, O.I. [3.416]
Börner, H.G. [2.42]
Cai, Z.X. [7.32]
Calaway, W.F. [5.88, 5.89, 5.134, 5.136 - 5.138, 5.147, 5.283 - 5.288, 7.86, 7.89]
Calcagno, L. [5.316]
Calliari, L. [6.270]
Cambe, A. [6.206, 6.210]
Campbell, E.E.B. [5.602]
Campbell, J.L. [1.25, 5.121]
Canut, B. [7.24, 7.26, 7.37, 7.121]
Caput, M. [7.34]
Carlson, A. [6.92]
Carlston, C.E. [3.103, 5.440]
Caro, A. [2.45, 2.48, 4.73, 4.74, 4.88]
Caroff, M. [5.605]
Caron, M. [7.69]
Carroll, S.J. [5.668]
Carter, D.C. [6.32]
Carter, G. [1.26, 1.152, 3.3, 5.7, 5.114, 5.574, 5.575]
Carter, W.A. [4.238]
Casarotto, E. [6.210]
Cassimi, A. [7.85]
Castaing, R. [1.203]
Castner, D.G. [5.227]
Cecchi, J. [1.196]
Cernusca, S. [1.69, 3.475]
Chakarov, I.R. [3.323]
Chamberod, A. [7.112, 7.116]
Chami, A.C. [5.344]
Chang, J.P. [6.13]
Chapman, G.E. [5.111]
Charalambidis, D. [5.92]
Chatterjee, R. [4.227, 5.156, 5.170, 5.348 - 5.350, 5.352]
Chaumont, J. [5.674, 7.57, 7.121]
Chen, A.Y.K. [6.129 - 6.133]
Chen, G.L. [3.135, 3.258, 5.556]
Chen, G.P. [5.218]
Cheney, K.B. [3.168]
Cheng, J. [5.658]
Cheng, T.K. [7.148]
Chernysh, V.S. [1.145, 3.427, 5.397, 5.403 - 5.405, 5.478, 5.494]
Chevallier, J. [5.397]
Chi, P. [5.116]
Chiba, S. [3.360, 4.245]
Chicherov, V.M. [1.59, 3.275, 5.428, 5.435]

Chini, T.K. [5.488]
Chiu, S. [6.124 - 6.128]
Chmara, F. [5.639, 5.640]
Choi, D.K. [5.671, 5.672]
Choi, W.K. [5.671 - 5.673]
Choi, Y. [5.670]
Chou, P.S. [3.337, 3.374]
Chrisey, D.B. [5.380]
Christie, D.J. [6.32]
Chu, W.K. [3.418, 5.120, 7.93]
Chuang, M.C. [6.58]
Chuang, T.J. [3.119]
Chugunov, O.K. [1.64, 6.14]
Chuong, Pham van [3.104]
Cieciwa, B. [1.148, 6.18, 6.182]
Cini, T.K. [5.402]
Cirlin, E.H. [1.207, 5.483]
Clark, R.E.H. [3.41]
Clary, D.C. [3.448, 3.450, 4.28]
Claussen, C. [5.582, 5.584, 7.58]
Clay, K.J. [6.285]
Clayton, R.N. [7.89]
Cleff, B. [5.387]
Clerc, C. [7.121]
Cluzeau, C. [7.34]
Cobic, B. [3.166]
Coburn, J.W. [3.113, 3.119, 5.82 - 5.84, 5.228, 6.4, 6.5, 6.13, 6.35, 6.39, 6.58]
Colder, A. [7.26]
Colla, T.J. [2.53, 4.30, 4.145, 4.146, 4.168, 4.190, 5.629, 5.630]
Colligon, D.S. [3.375, 3.388]
Colligon, J.S. [1.152, 3.228, 3.234, 3.454, 5.7]
Collins, J. [6.273]
Collins, R.W. [6.87]
Colombie, N. [3.104, 3.175]
Comeaux, A. [3.103]
Comins, J.D. [7.46]
Comsa, G. [1.107]
Conn, R.W. [3.315, 6.111]
Conrad, U. [3.303, 3.320, 5.212]
Cooks, R.G. [5.301, 5.309]
Coon, S.R. [5.136 - 5.138, 5.283, 5.284]
Cooper, B.H. [4.196, 4.201, 4.202, 7.11]
Cooper, C.B. [5.76, 5.276. 5.277, 5.523, 5.524]
Coronell, D.G. [3.451, 4.34]
Cortona, A. [5.158]
Costantini, J.M. [7.1, 7.21, 7.34, 7.137]
Coster, D. [6.102, 6.208]
Coudray, C. [3.385]
Coufal, H. [4.35, 4.36]

Couture, A. [4.201, 4.202]
Couvreur, F. [7.38]
Coventry, M.D. [3.316, 3.330, 3.393]
Coveyou, R.R. [2.5, 3.381]
Craig, B.I. [5.150]
Creatore, M. [6.84]
Cui, S. [4.213, 4.215, 5.372]
Cummings, P.T. [4.215]
Cuomo, J.J. [3.125, 3.223]
Curlee, G.A. [5.127]
Czanderna, W. [5.276]
Czerwinski, B. [4.150, 5.604, 5.614, 5.615]
Czuba, P. [5.368]
Dagel, D.J. [6.69]
Dahlgren, S.D. [3.152]
Dairaku, M. [3.489]
Dale, C.J. [3.418]
Dalton, T.J. [6.298]
Daly, N.R. [3.185, 3.193]
Dammak, H. [7.22, 7.109]
Dandachi, C. [4.168]
Daneljan, L. S. [3.59]
Daniel, G.S. [3.144]
Danielzik, B. [7.146]
Das, S.K. [3.183, 3.196]
Datz, S. [5.189]
Davarya, F. [3.353, 3.354, 3.358]
David, D.E. [4.101]
Davidson, T. [7.46]
Davies, J.A. [7.94]
Davies, N. [5.651]
Davis, A.M. [7.89]
Davis, J.W. [3.41, 3.73, 6.37, 6.95, 6.122, 6.123, 6.129 - 6.134, 6.161, 6.168 - 6.170, 6.174 - 6.176, 6.216, 6.233, 6.249, 6.250, 6.259]
Daw, M.S. [2.37]
Dawson, J. [3.133]
DePristo, A.E. [4.18, 4.19, 4.21, 5.466]
Dearnaley, G. [1.12, 1.115]
Deaven, D.M. [5.125, 5.469]
Dekorsky, T. [1.116, 1.118]
Delaplain, C.B. [5.239]
Delaunay, B. [7.83]
Delcorte, A. [4.217, 4.226, 4.229, 5.326 - 5.344]
Delgass, W.N. [3.436]
Della-Negra, S. [3.238, 5.595 - 5.597, 5.605, 5.674 - 5.676, 5.682, 5.689, 7.24, 7.25, 7.57, 7.72, 7.73]
Delmore, J.E. [5.591]
Dembowski, J. [5.522]
Deng, L. [5.93]

Denne, B. [6.110]
Depauw, J. [3.238, 5.596, 5.605, 5.674, 5.675, 5.682, 7.57, 7.72]
Devienne, F.-M. [3.217]
Dew, S.K. [5.548, 5.549]
Diaz de la Rubia, T. [4.74, 4.117]
Diehnelt, C.W. [5.677]
Dieleman, J. [4.236]
Diesing, D. [4.79]
Dillen, T. van [7.120]
Dimitrijevic, D.S. [3.230]
Djebara, M. [7.68, 7.136]
Djordjević, Z. [3.474]
Dobler, M. [7.67, 7.103]
Dobrev, D. [7.23]
Dobrozemsky, R. [3.89, 3.339, 5.413, 5.414, 6.70]
Dodonov, A.I. [5.401]
Döbele, H.F. [5.533 - 5.535]
Doerner, R.P. [3.18, 3.315, 3.328, 6.30, 6.31, 6.41, 6.42, 6.95, 6.104, 6.210]
Dohmen, R. [2.25, 3.271, 3.285, 5.498]
Dohnalik, T. [5.368]
Dollinger, G. [7.81, 7.82, 7.94, 7.95]
Domenges, B. [7.165]
Donnelly, S.E. [2.54, 4.162, 4.183 - 4.185, 5.280, 7.170, 7.171]
Dooryhée, E. [7.21, 7.79, 7.167]
Dose, V. [3.262, 3.267, 6.71 - 6.73, 6.145, 6.181, 6.211, 6.212]
Dou, Y. [4.58, 5.351]
Doughty, D.A. [6.116]
Dovguchits, E.F. [1.64, 6.14]
Doyle, B.L. [1.68, 6.194, 7.71]
Doyle, J.R. [6.69, 6.116, 6.117]
Dreihöfer, S. [5.254]
Dresselhaus, G. [7.148]
Dresselhaus, M.S. [7.148]
Drévillon, B. [6.269]
Du, M. [6.253]
Dufour, Ch. [7.38, 7.49, 7.51, 7.52, 7.79, 7.111, 7.138, 7.139, 7.147, 7.165, 7.167]
Dullni, E. [5.152, 5.213]
Dumke, M.F. [5.483]
Dunlop, A. [7.20, 7.22, 7.25, 7.43, 7.109, 7.110, 7.112, 7.113]
Dupp, G. [3.163]
Dural, J. [7.110, 7.111]
Duraud, J.P. [7.96]
Dutkiewicz, L. [1.93, 4.98, 4.106, 4.212]
Duvenbeck, A. [4.92, 5.696, 5.698]
Dux, R. [6.92, 6.102, 6.208]
Dvurechenskii, A.V. [4.192]
Dybkjaer, G. [3.291]
Dzhemilev, N.Kh. [4.170, 5.256 - 5.260, 5.295, 5.638]
Eatherly, W.P. [6.196]

Echenique, P.M. [4.72]
Echlin, P. [5.119]
Ecke, G. [3.349]
Eckstein, W. [1.10, 1.34, 1.38, 1.39, 1.94 - 1.96, 1.101, 1.102, 1.130, 1.131, 1.142, 1.160, 1.161, 1.178, 2.2, 2.10, 2.24, 2.25, 3.27 - 3.29, 3.32, 3.34 - 3.41, 3.43, 3.44, 3.47, 3.60, 3.64, 3.66, 3.80, 3.93, 3.135, 3.187, 3.188, 3.225, 3.252, 3.255, 3.256, 3.258, 3.261, 3.267 - 3.269, 3.271, 3.272, 3.279, 3.283 - 3.286, 3.289, 3.290, 3.293 - 3.296, 3.307, 3.308, 3.318, 3.319, 3.325 - 3.327, 3.329, 3.331, 3.332, 3.334, 3.338, 3.351, 3.371, 3.373, 3.380, 3.392, 3.412, 3.467, 3.483, 3.484, 3.487, 3.488, 4.6, 4.8, 4.29, 4.35, 4.36, 5.46, 5.53, 5.68, 5.84, 5.193, 5.194, 5.196 - 5.200, 5.211, 5.401, 5.403 - 5.405, 5.408, 5.454 - 5.457, 5.496, 5.498, 5.501, 5.502, 5.512, 5.515 - 5.517, 5.519, 5.556 - 5.558, 6.15, 6.23, 6.26, 6.181, 6.184, 6.185, 6.220, 6.222, 6.253, 7.126]
Economou, D.J. [4.41]
Eernisse, E.P. [3.8, 3.120, 3.227]
Effron, H.M. [3.432]
Efstathiou, L. [5.264]
Eijkman, D.J. [6.84]
El Khakani, M.A. [3.408]
El-Maazawi, M. [4.20, 5.125, 5.155, 5.461, 5.462, 5.471]
El-Said, A.S. [7.40]
Elbern, A. [5.107]
Ellefson, R.E. [6.68]
Ellegaard, O. [5.376, 5.381, 5.382, 5.389]
Elovikov, S.S. [3.416, 3.428, 3.469 - 3.472]
Eltekov, V.A. [3.367, 3.416, 3.420, 3.423, 3.424, 3.438, 3.441, 3.454]
Embry, T.A. [6.245]
Emmoth, B. [3.82, 3.86, 3.102, 3.189, 3.201, 3.482, 6.189, 6.200]
Enculescu, M. [7.42]
Engelmann, F. [1.184]
Engin, C. [4.177]
Englert, A. [5.447]
Ens, W. [5.253, 5.299]
Entley, W.R. [6.279]
Erdweg, M. [6.76, 6.261]
Erents, S.K. [6.8, 6.93, 6.94, 6.165, 6.185]
Erginsoy, C. [5.447, 5.448]
Esho, S. [5.396]
Esser, G. [6.148, 6.200]
Etxeberria, J. [6.228]
Evatt, R. [7.133]
Ezato, K. [3.489]
Fabricius, N. [7.146]
Face, D.W. [7.148]
Facsko, S. [1.113, 1.114, 1.116, 1.118]
Faestermann, T. [7.81, 7.82, 7.95]
Fagot, B. [3.104]
Fahey, A. [5.641]
Fahland, M. [1.215]
Falcone, G. [5.74, 5.475, 5.476, 5.542, 5.543]

Fallavier, M. [5.605, 5.675, 5.683, 7.73]
Fan, J.Y. [7.29]
Fantz, U. [1.149, 6.102, 6.103, 6.106 - 6.109]
Farmer, K.R. [5.386]
Farmery, B.W. [3.14, 5.110 - 5.112, 5.528 - 5.530, 5.570]
Faust, W.L. [5.361]
Fayazov, I.M. [3.256, 5.401]
Fayet, P. [5.267]
Fechner, R. [1.194, 1.197, 1.213]
Federici, G. [1.186, 3.247, 6.210]
Fedorovich, S.D. [5.401]
Feil, H. [4.236, 4.237]
Feldermann, H. [1.112]
Félix, C. [5.634]
Fenner, D.B. [5.648]
Fenyö, D. [4.102, 4.103, 7.163]
Feoktistov, L.V. [6.40]
Ferguson, B.P. [6.229]
Fermi, E. [2.18]
Ferron, J. [3.174, 5.606]
Fert, C. [3.104]
Fetz, H. [3.11, 3.55]
Filiks, J. [3.292]
Fine, J. [4.80, 4.82]
Finfgeld, C.R. [3.149, 3.226]
Fink, D. [1.82, 3.245, 3.246]
Finnis, M.W. [2.36, 2.46, 4.86, 7.156]
Fiori, C. [5.119]
Firsov, O.B. [2.19, 4.70]
Fitch, R.K. [3.231]
Flamm, D. [1.194, 1.197]
Flamm, D.L. [6.33, 6.34]
Flaskamp, K. [6.45, 6.76 - 6.79, 6.85, 6.121, 6.148, 6.160, 6.162, 6.216, 6.261]
Fleisch, T. [3.436]
Fleischer, R.L. [7.5]
Fleischhauer, J. [5.77]
Fluit, J.M. [1.54, 1.58, 3.263, 3.274, 5.427, 5.439]
Flynn, C.P. [2.44, 4.85, 4.118, 5.623, 7.154]
Foiles, S.M. [2.37, 2.38]
Foley, K.E. [3.437, 3.439, 5.242]
Fontell, A. [3.151]
Foreman, A.J.E. [2.46, 4.86, 7.156]
Forrest, M. [6.110]
Forst, W. [5.354]
Forster, J.S. [7.94]
Fotric, Z.B. [3.230]
Frach, F. [1.146, 1.215]
Francis, J.T. [5.655]
Frank, W. [1.197, 5.545]

Franke, E. [5.545]
Franzen, P. [6.124, 6.125, 6.251]
Freeman, J.H. [1.12, 1.115]
Freeman, N.J. [3.185, 3.193]
Freibaum, B. [5.640]
Frenkel, D. [2.33]
Frey, C.M. [7.81, 7.82, 7.95]
Fricke, B. [3.351]
Fried, Th. [3.201, 3.482]
Friedman, L. [5.599 - 5.601]
Friedrich, A. [3.459, 4.198, 4.199]
Fritzsch, B. [3.480]
Frölich, O. [3.118]
Frost, F. [1.108, 1.110, 1.111, 1.117, 1.194, 1.197, 1.214]
Fruit, M. [1.195]
Fuchs, C. [6.208]
Fuchs, G. [7.30, 7.112, 7.116]
Fujimura, S. [6.278]
Fujita, F.E. [6.197]
Fujita, Y. [5.269, 5.270]
Fukarek, W. [6.88, 7.120]
Fukuda, Y. [5.307, 5.308]
Fundamenski, W. [6.93, 6.94]
Funk, L. [4.162, 5.280, 5.281]
Fuoco, E. [5.644, 5.670]
Furr, A.K. [3.226]
Fussmann, G. [6.105]
Gades, H. [4.25, 4.48, 4.155, 4.176, 5.67, 5.72]
Gafert, J. [6.208]
Gaiduk, P.I. [7.27]
Galera, R. [5.312]
Gallagher, A. [6.116]
Ganschow, O. [5.78]
García-Rosales, C. [1.65, 1.66, 1.130, 1.148, 1.161 - 1.164, 3.27, 3.43, 3.66, 3.76, 3.272, 5.512, 5.515, 5.516, 6.15, 6.17, 6.18, 6.159, 6.222, 6.226 - 6.228]
Gardella, J.A. [5.657]
Garrett, J.W. [5.386]
Garrett, R.F. [5.179]
Garrison, B.J. [3.425, 3.434 - 3.437, 3.439, 3.444, 4.20, 4.21, 4.24, 4.27, 4.58, 4.81, 4.83, 4.135, 4.150, 4.165, 4.168, 4.171, 4.172, 4.211, 4.217 - 4.220, 4.224 - 4.227, 4.229, 4.230, 4.235, 4.236, 5.62, 5.65, 5.124, 5.125, 5.150, 5.156, 5.170, 5.240 - 5.242, 5.244 - 5.247, 5.303, 5.336 - 5.342, 5.344, 5.351, 5.353, 5.461, 5.463, 5.464, 5.466 - 5.471, 5.603, 5.614, 5.615, 5.684, 5.695, 5.699]
Gassiot, J.P. [1.3]
Gautherin, G. [5.411]
Gauthier, E. [3.255, 3.334, 3.467, 6.205, 6.206, 6.210]
Geerlings, J.J.C. [5.171]
Geiss, O. [7.28]
Georgieva, N.E. [6.40]

Gerhard, W. [5.272, 5.273]
Gerlach-Meyer, U. [3.113]
Gerthsen, Ch. [1.21]
Gervais, B. [1.20, 7.142]
Geyer, U. [1.112]
Ghalab, S. [5.685, 5.692]
Ghaly, M. [4.95, 4.120, 4.121, 4.175]
Ghio, E. [6.237]
Ghoniem, N.M. [3.337, 3.374]
Ghose, D. [3.177]
Ghosh, S. [7.31]
Gibbs, K.M. [7.65]
Gibert-Mougel, C. [7.38]
Gibson, J.B. [2.27, 4.9, 5.446]
Gijbels, R. [5.225]
Gillen, D.R. [5.537]
Gillen, G. [5.322, 5.638 - 5.641]
Gillen, K.T. [5.94]
Gilligan, J.M. [6.229]
Gillmann, D. [5.534, 5.535]
Gilmore, I.S. [5.324, 5.325, 5.355]
Gilot, P. [6.259]
Girard, J.P. [7.111]
Girgis, I. [5.153]
Gissler, W. [6.283]
Glöß, D. [1.146, 1.215]
Glückler, H. [7.67, 7.103]
Gnaser, H. [3.301, 4.47, 5.12, 5.77, 5.81, 5.87, 5.100, 5.126, 5.188, 5.211, 5.216 - 5.218, 5.261, 5.262, 5.278, 5.279, 5.296, 5.297, 5.424 - 5.527]
Gnehr, W.M. [1.215]
Goddisken, P. [5.477]
Godet, C. [6.269]
Goebel, D.M. [3.18, 6.111]
Gödeke, K. [1.215]
Goedicke, K. [1.210]
Goehlich, A. [5.533 - 5.537]
Goktepe, O.F. [3.353, 3.354, 3.358, 3.490]
Golan, A. [6.73]
Goland, A.N. [2.27, 4.9, 5.446]
Goldenberg, A.M. [5.256 - 5.258]
Goldman, D.T. [2.5, 3.381]
Goldstein, E. [1.172, 1.173]
Goldstein, H. [2.11]
Goldstein, J.I. [5.119]
Golse, W. [1.112]
Goodall, D.H.J. [6.203]
Gorbatov, E.A. [6.9]
Gordon, V.D. [6.229]
Gotoh, T. [3.169. 3.170]

Gould, R.K. [6.230]
Goullet, A. [6.289]
Gourbilleau, F. [7.79, 7.165, 7.167]
Grønlund, F. [3.205]
Grade, H. [5.301]
Graham, D.J. [5.227]
Graham, W.G. [5.537, 5.697]
Grande, R. [6.67]
Grandin, J.P. [7.85]
Granier, A. [6.289]
Gras-Marti, A. [4.149, 6.20, 6.21]
Graves, D.B. [4.37, 4.38, 4.40, 4.240 - 4.242, 4.244, 6.299]
Gray, D.C. [6.294]
Greenland, P.T. [6.96, 6.100, 6.112]
Grefte, H.A.M. de [3.242, 3.343]
Gregg, R. [3.239]
Griffis, D.P. [5.646]
Griffith, J.E. [3.491, 7.11, 7.62, 7.63, 7.97, 7.104, 7.124]
Grigull, S. [3.91, 3.92, 6.281, 6.282]
Grischkowsky, D. [5.149, 5.209, 5.366]
Grosman, A. [6.269]
Grossman, A. [3.315, 3.328]
Grote, H. [6.105]
Groult, D. [7.19, 7.29, 7.30]
Grove, W.R. [1.1, 1.2]
Gruber, D. [5.151]
Gruen, D.M. [3.133, 4.191, 5.89, 5.102, 5.109, 5.125, 5.144, 5.147, 5.148, 5.154, 5.176, 5.284, 5.286, 7.86, 7.88, 7.89]
Grüner, F. [7.54 - 7.56, 7.80, 7.169]
Gschneidner, K.A. [5.69]
Gspann, J. [4.148, 4.181]
Güntherschulze, A. [1.16, 1.30, 1.105, 3.399, 6.2]
Güttler, A. [6.232]
Güvenc, Z.B. [3.426, 4.43]
Guinan, M.W. [4.74]
Gupta, A. [7.76]
Gureev, V.M. [3.58, 3.59, 3.61, 3.62, 3.313]
Gurmin, B.M. [3.181]
Guryanov, G.M. [5.646]
Gusev, V.M. [6.9]
Guseva, M.I. [3.16, 3.17, 3.47, 3.58, 3.59, 3.61, 3.62, 3.140, 3.161, 3.220, 3.313, 6.9]
Guthier, W. [7.60]
Gutmann, A. [6.12]
Gutmann, R. [6.279]
Gutsche, M. [6.12]
Gutzmann, A. [7.74]
Gvosdover, R.S. [3.428, 3.471]
Haas, F. [7.43]
Haasz, A.A. [3.41, 3.73, 6.16, 6.37, 6.63 - 6.65, 6.95, 6.122 - 6.134, 6.146, 6.147,

6.161, 6.163, 6.164, 6.168 - 6.170, 6.174 - 6.176, 6.203, 6.215, 6.216, 6.233, 6.249, 6.250, 6.259, 6.263]
Habenicht, S. [1.112]
Haberland, H. [2.51, 2.52, 4.123, 4.126, 4.132, 5.624, 5.632]
Habets, B. [5.679]
Habraken, F.H.P.M. [7.77]
Hackel, S. [3.351]
Haddeman, E.F.C. [3.419, 4.205]
Hänsel, T. [1.111, 1.195, 1.196, 1.215]
Haff, P.K. [3.386, 3.447, 4.49, 5.73, 7.10]
Hage-Ali, M. [7.1, 7.21]
Hagenhoff, B. [5.302]
Haggmark, L.G. [1.134, 2.9, 2.13, 3.31, 3.336, 3.365, 3.372]
Hagiwara, N. [5.660, 5.664, 5.702]
Haglund, R.F. [7.149]
Hagstrum, H.D. [1.17]
Haidarov, A.A. [5.403 - 5.405]
Haijeck, D.J. [1.123]
Haile, J.M. [2.29]
Hairie, A. [7.111]
Håkansson, P. [5.597]
Hall, E. [4.187]
Hall, S.G. [5.668]
Halle, S.D. [6.12]
Hamed, H.A. [5.277]
Hamilton, C.G. [6.259]
Hamm, R.N. [7.141]
Hammer, D. [5.104, 5.105]
Hammer, P. [6.283]
Hamza, A.V. [1.68, 7.71]
Hanley, L. [5.644, 5.670]
Hansen, C.S. [5.134, 5.288]
Hansen, H. [4.177, 4.199]
Hansen, J. [7.172]
Hanson, D.E. [3.345, 3.451, 4.34, 4.207]
Harada, A. [4.133]
Harbich, W. [5.634, 5.635]
Hardouin-Duparc, A. [7.113]
Hargitai, Z. [6.229]
Haring, A. [5.315, 5.316, 5.370, 5.371, 5.377, 5.378, 5.382, 5.384, 5.568, 5.584]
Haring, R.A. [3.246, 5.315, 5.316, 5.321, 5.364, 5.369 - 5.371, 5.377, 5.378, 5.384, 5.385, 5.388]
Harling, O.K. [3.183]
Harper, J.M.E. [1.115, 3.125]
Harris, R.D. [5.593, 5.637]
Harrison, D.E., Jr. [1.35 - 1.37, 2.1, 2.5, 3.22, 3.108, 3.347, 3.381 - 3.383, 3.430 - 3.437, 3.440, 3.447, 3.463, 4.12, 4.27, 4.49, 4.50, 4.89, 4.173, 4.174, 5.47, 5.48, 5.65, 5.73, 5.239 - 5.242, 5.468, 5.469, 5.472, 5.506, 5.513, 5.514]
Harrison, J.A. [4.223, 4.224]

Hartman, J.W. [4.166, 4.167, 5.250, 5.251]
Hartnagel, H.L. [1.116]
Hartung, P. [7.67, 7.102]
Hassanein, A.M. [3.363]
Hasselkamp, D. [3.180, 5.394]
Hauffe, W. [1.28, 1.106, 1.121, 6.3]
Hautala, M. [3.387, 3.443, 4.87, 5.409, 5.459, 5.460]
Haverlag, M. [6.295]
Hayderer, G. [1.69, 3.475, 6.59, 7.100]
Haymann, P. [1.120]
Haynie, B.C. [5.352]
Hayward, W.H. [3.101]
He, C. [4.21, 5.156, 5.466]
Hechtl, E. [1.141, 3.60, 3.64, 3.66, 3.78, 3.85, 3.87, 3.155, 3.157, 3.208, 3.221, 3.225, 3.261, 3.268, 6.56, 6.264, 6.265]
Hedin, S. [7.163]
Hedlund, C. [6.298]
Hedlund, E. [7.173]
Heide, P.A.W. van der [5.181 - 5.184]
Heiland, W. [1.14, 1.22, 1.156, 1.158, 5.230, 5.263]
Heinemann, D. [3.351]
Heinig, K.H. [2.42, 4.192]
Heinrich, R. [4.135, 4.160, 4.168, 5.142, 5.289, 5.691, 5.693 - 5.695]
Heldt, L. [3.210]
Hellgren, N. [6.290, 6.292]
Hémon, S. [7.79, 7.165, 7.167]
Hendricks, M.R. [3.46, 3.137, 3.486]
Henke, D. [3.91, 6.281]
Henkel, M. [4.129]
Hennes, M. [6.121]
Henriksson, K.O.E. [4.182]
Herbots, N. [3.348]
Hercules, D.M. [5.302]
Hereć, J. [3.292]
Hermes, P. [7.146]
Herr, W. [1.168, 3.429]
Herrmann, A. [6.208, 6.277]
Hervieu, M. [7.21]
Higashijima, S. [6.209, 6.210]
Hill, C.C. [4.202]
Hill, R. [5.649 - 5.651]
Hillenkamp, F. [5.305, 5.306]
Hintz, E. [1.183, 3.145, 3.241, 3.483, 5.107, 5.108, 5.208, 5.538, 6.62]
Hippler, R. [3.426, 4.43]
Hirakuri, K.K. [6.271]
Hirano, N. [6.114]
Hirooka, Y. [3.41, 3.56, 3.57, 6.111]
Hirotami, N. [4.133]
Hirsch, D. [1.214]

Hjort, K. [7.9]
Hjörvarsson, B. [6.290]
Ho, Y.K. [5.627]
Hochhold, M. [3.465]
Höche, T. [1.117]
Hofer, W.O. [1.91, 1.98, 1.138, 3.134, 3.236, 3.265, 4.93, 4.152, 4.189, 5.59, 5.77, 5.118, 5.216 - 5.218, 5.223, 5.278, 5.279, 5.503, 5.554, 5.555, 5.587, 5.588, 6.22, 6.263, 7.153]
Hoffmann, V. [1.69, 3.475]
Hofsäss, H. [1.112]
Hogan, J. [6.205, 6.206, 6.210]
Hoh, P.D. [6.12]
Hoheisel, G. [5.645]
Holcombe, H.T. [3.433]
Holekeboer, D.H. [6.67]
Holloway, P.H. [3.143, 7.90]
Holmén, G. [3.178, 3.402]
Holmes, D.K. [2.7]
Homer, R. [3.123]
Honda, F. [5.307, 5.308]
Hong, J. [6.288, 6.289]
Honig, R.E. [1.199, 5.75]
Hoogerbrugge, R. [5.318 - 5.320]
Hopf, C. [6.66, 6.118 - 6.120, 6.140 - 6.143, 6.217 - 6.219, 6.236, 6.266, 6.267, 6.277, 6.280, 6.284, 6.293]
Horn, A. [6.155]
Horne, D. [3.224]
Hosaka, K. [3.42]
Hosea, J. [6.273]
Hou, M. [3.279, 3.284, 3.326, 3.384, 3.462, 4.122, 5.454 - 5.457, 5.507]
Hou, M.-D. [7.114, 7.115]
Houpert, C. [7.19, 7.29]
Housley, R.M. [5.483]
Hsieh, H. [4.117, 4.118, 4.124, 4.125, 5.623]
Hsu, W.L. [6.272]
Hu, J.S. [6.275, 6.276]
Hua, X.F. [6.299]
Huang, W. [5.419 - 5.421]
Hubbard, K.M. [3.192, 5.484, 5.485, 7.64]
Huber, A. [6.98, 6.99, 6.101, 6.112, 6.113, 6.207]
Huber, A.M. [1.202]
Huber, H. [7.6, 7.94, 7.102, 7.103]
Hulpke, E. [5.96]
Hultman, L. [6.290, 6.291]
Humbird, D. [6.299]
Hundur, Y. [3.426, 4.43]
Huppner, Y. [7.146]
Hurlbut, F.C. [5.410]
Husain, S. [5.592]

Husinsky, W. [3.466, 4.23, 4.144, 4.159, 5.104 - 5.106, 5.133, 5.151, 5.153, 5.158, 5.214, 5.215, 5.248, 5.252, 5.365, 5.367, 5.453, 5.626, 6.229, 7.87]
Hutcheon, I.D. [3.301, 5.126]
Iamada, C. [7.101]
Ibbotson, D.E. [6.34]
Ichihara, T. [5.269 - 5.271]
Ichimura, S. [5.395, 5.492]
Iltgen, K. [5.594]
Ilyinsky, L. [3.86]
Imanishi, N. [7.101]
Inami, T. [3.414]
Ingen, R.P. van [3.128, 5.568]
Inoue, K. [3.479]
Insepov, Z. [2.52, 4.123, 4.126 - 4.128, 4.131, 4.140 - 4.143, 5.608, 5.624, 5.663, 5.704]
Ippen, E.P. [7.148]
Ishida, Y. [5.492]
Ishitani, A. [5.117]
Ishitani, T. [3.359]
Isler, R.C. [6.95]
Ismail, H. [3.403]
Itabasi, K. [4.133]
Itami, K. [6.209]
Itikawa, Y. [3.251]
Ito, Y. [3.67]
Itoh, N. [3.251, 5.358, 7.16, 7.159, 7.161, 7.162]
Iwanov, I.N. [3.452]
Iwase, A. [3.414, 7.99, 7.122, 7.123]
Jachmich, S. [6.98]
Jackson, B. [6.232]
Jackson, D.P. [5.56]
Jackson, G.L. [6.95]
Jacob, W. [3.91, 6.38, 6.88 - 6.90, 6.118 - 6.120, 6.135, 6.137, 6.140 - 6.145, 6.199, 6.217 - 6.219, 6.236, 6.252, 6.254, 6.266 - 6.268, 6.274, 6.277, 6.280, 6.281, 6.284, 6.293]
Jacobsen, J. [4.196, 4.201, 4.202]
Jacquet, D. [3.238, 5.674, 5.675, 5.682, 5.689, 7.57, 7.72]
Jäger, W. [5.571, 5.572]
Jaffrezic, H. [3.408]
Jakas, M.M. [3.174, 3.347, 3.382, 3.383, 3.430, 3.463, 4.89, 4.108, 4.110 - 4.113, 5.45, 5.514, 5.583, 5.606, 7.164]
Janev, R.K. [3.42]
Jaraíz, M. [4.26, 4.203, 4.204]
Jardin, P. [7.85]
Jaskierowicz, G. [7.25, 7.113]
Jede, R. [5.78]
Jenkins, L.H. [3.183]
Jensen, J. [5.613, 7.43]
Jentoft, F.C. [6.256]
Jentoft, R.E. [6.256]

Jentschel, M. [2.42]
Jiang, W. [4.61]
Jiang, Z.X. [5.426]
Jimbou, R. [3.266, 3.297]
Jimenéz-Rodríguez, J.J. [5.58]
Johannessen, K. [4.22, 4.52, 4.134]
Johansen, A. [3.291, 5.700, 7.117]
Johansson, M.P. [6.290, 6.291]
Johansson, S.A.E. [1.25, 5.121]
Johar, S.S. [5.562 - 5.565]
Johnson, E. [3.291]
Johnson, J.P. [3.432, 5.472]
Johnson, R.E. [4.31, 4.32, 4.57, 4.102 - 4.109, 4.112, 4.186, 4.187, 4.212 - 4.216, 5.356, 5.372 - 5.374, 5.379, 5.386, 7.59, 7.65, 7.66, 7.106, 7.127, 7.130, 7.131, 7.133, 7.163]
Jolie, J. [2.42]
Jones, E. [5.659]
Jones, P.L. [5.412]
Jong, M. de [1.58, 3.274, 5.427]
Jonge, R. de [5.265, 5.266]
Joret, H. [5.595, 5.596]
Jørgensen, B. [5.89]
Jorzick, J. [5.552]
Joseph, E.A. [6.298]
Joubert, O. [6.296]
Jousset, J.C. [7.112, 7.116]
Joy, D.C. [5.119]
Jozefowski, L. [5.368]
Juan Pardo, E. de [1.148 - 1.150, 6.18, 6.19, 6.182, 6.231]
Kabeya, Z. [3.169, 3.170]
Kabiraj, D [7.31]
Kaczerowski, W. [3.390]
Kafemann, H. [4.104, 4.210, 7.127]
Kaganov, M.I. [7.134, 7.145]
Kahora, P.M. [5.116]
Kallenbach, A. 6.91, 6.92, 6.102, 6.208, 6.210]
Kamada, K. [3.331]
Kaminsky, M. [1.151, 3.95, 3.132, 3.183, 3.196, 3.477, 5.5]
Kamperschroer, J. [6.273]
Kang, H.D. [6.72]
Kang, H.J. [3.233, 5.493]
Kang, S.T. [3.124]
Kapeliovich, B.L. [7.135]
Kapinos, V.G. [4.75]
Kaplita, G.A. [6.12]
Karas, M. [5.304, 5.305]
Karawajczyk, A. [5.368]
Karen, A. [5.117]
Karetta, F. [4.153, 5.243]

Karlsson, B.R. [4.102]
Karmohapatro, S.B. [3.177]
Karolewski, M.A. [2.56, 3.464, 4.200, 4.209]
Karpuzov, D.S. [3.323, 3.324, 3.346]
Karrais, M. [5.632]
Katakuse, I. [5.269 - 5.271]
Katardjiev, I.V. [3.288, 3.342]
Kats, C.M. van [7.120]
Katz, R. [7.2, 7.141]
Kaufman, H.R. [3.125]
Kawakami, R. [5.551]
Kawamoto, J. [3.355]
Kawamura, T. [3.33, 3.248]
Kawano, A. [3.355]
Kawata, J. [5.551]
Kawatoh, E. [3.233]
Kay, E. [3.113, 5.82 - 5.84]
Kazeroonian, A. [7.147]
Kegeler, J. [1.196]
Keinonen, J. [2.49, 2.53, 3.394, 4.147, 4.178, 4.182, 4.183, 4.208, 4.232 - 4.234, 6.48 - 6.53, 6.239 - 6.243]
Keller, J.H. [6.12]
Kelly, P.W. [3.434]
Kelly, R. [3.109, 5.43, 5.66, 5.70, 5.71, 5.74, 5.219 - 5.222, 5.578, 5.579, 7.149]
Kenknight, C.E. [1.166, 3.49]
Kenmotsu, T. [3.42]
Kenny, D.J. [4.130]
Kenny, S.D. [4.62]
Kerford, M. [5.628]
Kern, K. [5.634]
Kessler, E.G. [2.42]
Keudell, A. von [6.88 - 6.90, 6.118 - 6.120, 6.135 - 6.145, 6.199, 6.217, 6.268]
Keywell, F. [1.31, 3.165]
Khalfaoui, N. [7.43, 7.69. 7.136, 7.137]
Khanh, N.Q. [3.368]
Kharlamochkin, E.S. [3.457]
Kharmalov, V. [3.349]
Khirnov, I.V. [3.377]
Khoo, K.S. [7.159]
Khripunov, B.I. [3.313]
Kido, Y. [3.355]
Kimock, F.M. [7.91]
Kimura, H. [5.510]
Kinbara, A. [3.232]
Kinchin, G.H. [1.41, 5.2]
Kinder, H. [7.6]
King, B.V. [5.134, 5.288, 5.310, 5.464, 5.465]
King, M.E. [5.474]
King, R.L. [5.639, 5.640]

Kirchhoff, V. [1.210, 1.211, 1.213]
Kirchner, R. [4.23, 4.149, 5.453]
Kirilov, S. [7.73]
Kirk, M.A. [7.155]
Kirkpatrick, A. [5.665]
Kirsch, R. [5.683]
Kirschner, A. [6.99, 6.102, 6.112, 6.113, 6.207, 6.210]
Kishidaka, H. [3.158]
Kissel, R. [4.145, 5.630]
Kistemaker, J. [1.54, 3.263, 5.97, 5.439]
Kistemaker, P.G. [5.318 - 5.320]
Kitani, H. [5.702]
Kitazoe, Y. [3.396, 5.577]
Kiyahara, A. [3.169, 3.170]
Klages, K.U. [6.254]
Klaumünzer, S. [7.35, 7.47, 7.74, 7.114, 7.115]
Klein, F.S. [5.384]
Klein, P. [4.33]
Klitsner, T. [4.193]
Knapp, K. [1.196]
Kneff, D.W. [3.141, 3.184]
Knippenberg, W.F. [6.201]
Knolle, W. [7.40]
Knudsen, P. [3.150]
Knudson, A.R. [3.100, 3.139, 5.399]
Kobetich, E.J. [7.2]
Kobiyama, M. [3.414]
Kobrin, P.H. [5.61, 5.122, 5.124, 5.138]
Kodali, P.B.S. [4.219]
Koedam, M. [1.75 - 1.77, 3.212]
Koehler, J.S. [1.42, 5.3, 7.50]
Können, G.P. [4.156, 4.157, 5.274, 5.275]
Koert, C. [1.116]
Kohlschütter, V. [1.7, 1.208, 6.1]
Koidl, P. [6.162]
Kolbasov, B.N. [3.313]
Kolesnikov, A.S. [3.417, 4.151]
Kolfschoten, A.W. [5.315, 5.385]
Kollmus, H. [7.173]
Kolodziej, J. [5.368]
Koma, A. [3.198]
Komarov, V.L. [1.64, 6.14]
Komizo, M. [3.169, 3.170]
Kompa, K.-L. [5.92]
Kono, T. [5.347]
Konov, D.A. [1.146, 3.312, 3.428]
Kopitzki, K. [5.20, 5.23]
Kopnarski, M. [5.552]
Koponen, I. [2.47, 4.77, 4.78, 4.87]

Kopte, T. [1.210, 1.211]
Kornejew, P. [6.105, 6.204]
Kornienko, O. [5.644]
Korshunov, S.N. [3.16, 3.17, 3.58, 3.59, 3.61, 3.62, 3.313]
Koshkin, V.K. [3.147]
Kosiba, R. [3.349]
Kotis, L. [3.340]
Kovacs, Gy.J. [3.340]
Kovarsky, A.P. [5.680]
Kozakiewicz, A.G. [7.46]
Krämer, A. [7.173]
Krämer, M. [7.28]
Kräutle, H. [3.237]
Krantzman, K.D. [4.217, 4.224, 4.225, 5.342]
Krasheninnikov, A. [6.52, 6.53]
Krasheninnikov, S.I. [6.41]
Kraus, J.S. [1.23]
Krause, H.F. [6.177 - 6.180]
Krauss, A.R. [5.132, 5.176]
Krebs, K.H. [1.18, 3.94]
Kreissig, U. [6.286]
Kremer, K. [1.93, 4.98]
Kress, J.D. [3.345, 3.451, 4.34, 4.207]
Krieger, K. [3.413, 6.102]
Kröhnert, J. [6.256]
Krok, F. [5.387]
Krstić, P.S. [6.245 - 6.248]
Krüger, W. [3.180, 3.257, 5.393, 5.394]
Krutenat, R.C. [3.218]
Krylova, E.A. [5.401]
Kubo, H. [6.209, 6.210]
Kubota, A. [4.41]
Kucal, H. [7.54, 7.56]
Kudriavtsev, Yu.A. [3.485]
Külzer, H. [1.168, 3.429]
Küppers, J. [6.74, 6.75, 6.149 - 6.158, 6.232]
Küstner, M. [3.267, 3.268, 6.181]
Kuhl, J. [7.146]
Kukushkin, A. [1.186, 3.247]
Kulikauskas, V.S. [3.59, 5.403 - 5.405, 5.494]
Kulpin, J.G. [6.31]
Kumar, P. [5.195]
Kummel, A.C. [5.384]
Kunz, H. [1.116]
Kuo, K. [6.257]
Kuratomi, Y. [3.99]
Kurbatov, O.V. [3.138]
Kuriki, S. [3.67]
Kurnaev, V.A. [5.403]

Kurz, H. [1.118]
Kuvakin, M.V. [1.145, 3.427, 3.457]
Kuwajima, S. [3.415]
Kuwashima, K. [6.271]
LaBombard, B. [6.111]
Laegreid, N. [1.209, 3.63]
Lam, N.Q. [1.180, 4.45, 4.52, 5.497]
Lam, S.K. [3.95]
LaMarche, P.H. [6.273]
Lambert, J.M. [3.100, 3.139, 5.399]
Lancaster, G.M. [5.307, 5.308]
Landkammer, B. [6.268, 6.274]
Lang, I.G. [2.4]
Lang, M. [7.45]
Lang, N.D. [5.186, 5.187]
Langan, J.G. [6.279]
Langley, R.A. [3.75, 3.80, 6.188]
Lanzerotti, L.J. [7.61]
Lareau, R. [5.640]
László, J. [3.255, 3.329, 3.334, 3.392, 3.467, 5.512]
Laubert, R. [5.38]
Laurent, J.-M. [7.172]
Layet, J.M. [6.205, 6.206, 6.210]
Layton, J.K. [3.70, 3.71]
Lazarev, N.E. [3.16, 3.17]
Le Beyec, Y. [3.238, 5.590, 5.595 - 5.597, 5.605, 5.674, 5.675, 5.682, 5.689, 7.57, 7.72]
Leach, A.R. [2.32]
Leary, P.A. [3.125]
Ledbetter, M. [5.599, 5.600]
Ledyakin, D.W. [3.452]
Lee, T.D. [5.577, 5.592]
Leggett, G.J. [5.323]
Legrand, P. [7.109]
Lehmann, Ch. [1.80, 5.9, 5.450]
Leibfried, G. [1.74, 1.80, 1.126, 5.6, 5.445]
Lenskjaer, T. [5.450]
Leon, A. [7.85]
Lersmacher, B. [6.201]
Leskiewicz, P. [5.376, 5.387]
Lesniak, R. [5.368]
Lesueur, D. [7.20, 7.22, 7.109, 7.110, 7.112, 7.116]
Letourneur, K. [6.118]
Leung, C.H. [5.361]
Levalois, M. [7.26, 7.111]
Levesque, F. [7.38]
Levy, N.S. [3.432, 5.472]
Leyen, D. van [5.302]
Li, A. [5.412]

Li, C. [6.255]
Li, C.F. [5.481, 5.482]
Li, J.G. [6.275, 6.276]
Li, M. [5.670]
Li, R.S. [5.481, 5.482]
Li, X. [6.279]
Libbrecht, K.G. [7.97]
Libiseller, G. [3.129]
Lieb, K.-P. [3.110]
Lieb, K.L. [1.112]
Liebl, H. [1.204, 1.205, 3.262]
Liedberg, B. [6.290]
Lievens, P. [5.157, 5.159 - 5.163, 5.166 - 5.168, 5.170]
Lifshin, E. [5.119]
Lifshits, I.M. [7.134, 7.145]
Likonen, J. [3.387, 3.443, 5.459, 5.460, 6.102]
Lill, T.B. [5.286, 5.287]
Lin, G.H. [6.116]
Lin, S.H. [5.310]
Linde, D. von der [7.146]
Linden, W. von der [6.71]
Lindenblatt, M. [4.135, 5.695, 5.696]
Lindhard, J. [1.70, 1.124, 1.125, 2.16, 3.45, 4.69, 5.55, 5.56]
Lindner, A. [3.206]
Lindner, H. [1.141, 3.208]
Linke, U. [4.177]
Linsmeier, C. [6.29]
Lipinsky, D. [5.78]
Lisfi, D. [7.85]
Littmark, U. [2.14, 4.189, 5.118, 5.539, 6.22, 6.184, 7.118]
Liu, C. [4.60]
Liu, C.L. [3.451, 4.34]
Liu, G. [5.482]
Liu, M. [4.32, 4.216]
Liu, X.Y. [3.451, 4.34]
Lo, D.Y. [3.302, 3.386, 4.51, 5.57, 5.469]
Loarer, T. [6.205]
Locklear, J.E. [5.652]
Lockyer, N. [5.649 - 5.651]
Lösch, J. [5.552]
Loesing, R. [5.646]
Logan, C.M. [3.183]
Lorenzelli, N. [7.113]
Los, J. [5.171]
Loxton, C.M. [5.231]
Lu, H.F. [3.461]
Lu, T.M. [6.279]
Luckhardt, S.C. [3.315, 3.328]
Lucuta, P.G. [7.36]

Ludwig, K. [4.225]
Lüpke, G.L. [6.229]
Lundquist, T.R. [5.174, 5.175]
Lundqvist, B.I. [5.298]
Lundsgaard-Hansen, J. [7.27]
Lunev, A.V. [3.485]
Luthin, J. [3.290, 6.26]
Lutovich, A.S. [3.350]
Lutterloh, C. [6.149 - 6.151, 6.153 - 6.156]
Lutz, H.O. [5.254, 5.255]
Lydtin, H. [6.201]
Ma, Z. [5.284, 5.285, 5.287]
Maboudian, R. [4.20, 5.155, 5.461, 5.462, 5.471]
MacDonald, J.W. [1.68]
MacDonald, R.J. [5.179]
Macaulay-Newcombe, R.G. [6.95, 6.134, 6.249]
Machicoane, T.A. [1.68]
Maderlechner, G. [3.270, 3.364, 5.508]
Madsen, N. [7.172]
Magee, C.W. [6.187]
Magnuson, G.D. [3.103, 5.440, 5.506]
Mahavedan, P. [3.103]
Mahmoud, E.A. [3.231]
Mahner, E. [7.172, 7.173]
Mahoney, C.M. [5.657]
Mahoney, J.F. [5.577, 5.592]
Maier, H. [1.149]
Maier-Komor, P. [7.81]
Maissel, L. [1.212]
Maksimov, S.E. [5.295, 5.692]
Malherbe, J.B. [5.490, 5.491]
Mall, M. [5.632]
Mallouris, C.M. [6.69]
Malmqvist, K.G. [5.121]
Malyshev, O.B. [7.173]
Man, Z.Y. [5.627]
Manika, I. [7.41]
Maniks, J. [7.41]
Mann, F.M. [3.141, 3.184]
Manos, D.M. [6.33]
Marcantonio, K.J. [5.379, 5.386]
Marconi, M. [1.138]
Marest, G. [3.408, 7.37]
Marie, P. [7.26]
Marqués, L.A. [4.26, 4.203, 4.204]
Marsarov, P. [5.692]
Marsh, H. [6.257]
Martin, P.J. [3.134, 5.513]
Martin, S.E. [5.654]

Martinelli, A.P. [1.141, 1.183, 3.111, 3.145, 3.208, 3.241, 6.55, 6.62]
Martino, P.A. [5.577, 5.592]
Marty, O. [7.26]
Martynenko, T.P. [3.378, 3.400, 3.406, 6.40]
Martynenko, Yu.V. [3.59, 3.140, 3.313, 6.9, 7.13, 7.144]
Maruyama, K. [6.252]
Mashkova, E.S. [1.8, 1.9, 1.11, 1.143, 1.144, 3.38, 3.93, 3.121, 3.256, 3.260, 3.269, 5.10, 5.190, 5.199, 5.401, 5.403 - 5.405]
Matragrano, D. [5.234]
Matsuda, A. [6.114, 6.115]
Matsuda, H. [5.269 - 5.271]
Matsuda, Y. [5.493]
Matsunami, N. [3.414, 7.99, 7.122. 7.123]
Matsui, S. [5.666]
Matsuo, J. [3.360, 4.127, 4.141, 4.143, 4.245, 4.246, 5.598, 5.608, 5.648, 5.659, 5.660, 5.663 - 5.665, 5.667, 5.702, 5.703, 7.101]
Matsuo, P.J. [6.279]
Matsuo, T. [5.269 - 5.271]
Mattera, L. [6.237]
Matteson, S. [6.185]
Matthew, M.W. [5.599, 5.600]
Matthews, G.F. [6.93, 6.94, 6.203]
Matzke, Hj. [7.35, 7.36]
Mayer, J.W. [3.123, 5.120, 7.93]
Mayer, T.M. [3.418]
Mayerhofer, U. [3.81]
Mazanec, A. [3.66, 3.261]
Mazarov, P. [5.653]
Mazey, D.J. [1.103]
Mazul, I.V. [1.64, 6.14]
Mazzone, A.M. [4.194, 4.195]
McClanahan, E.D. [1.209, 3.152]
McCormick, A.W. [5.281]
McCown, D. [3.7]
McCracken, G.M. [1.13, 1.116, 3.5, 6.8, 6.165, 6.203]
McIntyre, N.S. [5.655]
McKoewn, D. [1.170]
McMahon, A.W. [7.90]
McRea, J.E. [6.67]
Md Nor, R. [5.697]
Mech, B.V. [6.174 - 6.176, 6.233]
Medved, D.B. [3.213]
Medvedeva, M. [4.136, 5.699]
Meftah, A. [7.1, 7.21, 7.29, 7.37, 7.52, 7.68, 7.136, 7.137]
Meier, M. [6.138, 6.139, 6.143, 6.218]
Meier, P. [7.74]
Meigs, A. [6.99, 6.112]
Meins, C.K. [7.11, 7.104]
Meir, S. [6.103]

Meisenheimer, R. [3.183]
Meiwes-Broer, K.H. [5.254, 5.255]
Melki, S. [7.85]
Mendelsohn, M.H. [5.144]
Mendenhall, M.H. [7.11, 7.104]
Menyhard, M. [3.340, 3.368]
Menzel, C. [5.305, 5.306]
Merkle, K.L. [3.235, 5.572, 7.78]
Mertens, P. [6.96, 6.97, 6.99, 6.100, 6.112]
Meserole, C.A. [5.350 - 5.352]
Meyer, C.H., Jr. [3.70, 3.71, 3.197]
Meyer, F.W. [6.177 - 6.180]
Meyer, S. [4.79]
Meyer, V.K. [3.399]
Michely, T. [1.107, 3.458, 4.177, 4.199]
Michl, J. [4.100, 4.101, 5.311]
Miehe, G. [7.169]
Mieskes, H.D. [7.53, 7.54, 7.56, 7.67]
Mika, K. [1.126]
Milgram, M. [2.27, 4.9, 5.446]
Milić, M. [3.474]
Milne, W.I. [6.287, 6.292]
Mioduszewski, P. [3.80]
Misra, D.S. [7.31]
Mitrofansky, A.A. [1.64, 6.14]
Miyagawa, S. [3.65]
Miyagi, S. [3.199]
Miyake, K. [3.115]
Miyazaki, K. [3.99]
Mizuno, Y. [3.369, 3.370]
Mizutani, T. [3.418]
Möller, W. [1.38, 1.39, 1.102, 2.24, 3.34, 3.35, 3.294, 3.488, 6.46, 6.188, 6.191 - 6.193, 6.200]
Möllers, R. [5.345]
Mössner, C. [3.356, 3.357, 5.422, 5.423, 5.463]
Mohai, M. [5.221]
Molchanov, V.A. [1.8, 1.9, 1.11, 1.53, 1.59, 1.143, 1.144, 3.38, 3.121, 3.256, 3.260, 3.264, 3.269, 3.275, 5.10, 5.190, 5.401, 5.403 - 5.405, 5.428, 5.435]
Molière, G. [2.12]
Moncoffre, N. [7.37]
Monk, R.D. [6.93, 6.94]
Monot, R. [5.634]
Montcoffre, N. [3.408]
Montgomery, H. [1.78]
Moodera, J.S. [7.148]
Moore, A.W. [6.201]
Moore, J.L. [3.154]
Moore, W.J. [3.205, 3.206, 3.210]
Moore, W.L., Jr, [3.433]

Morgan, A.E. [3.242, 3.343]
Morillo, J. [7.109, 7.110]
Moriya, Y. [3.65]
Morozov, S.N. [5.683, 5.690]
Morris, R.C. [1.23]
Morrison, N.A. [6.287, 6.292]
Mosbah, M. [7.96]
Moseler, M. [2.51, 2.52, 4.123, 4.126, 4.132, 5.624]
Moskovkin, P.S. [3.59]
Mosunov, A.S. [1.146, 3.311, 3.312, 3.375, 3.376, 3.388, 3.454, 3.470 - 3.472]
Motaweh, H.A. [3.424]
Mousel, T. [5.211]
Mühling, E. [3.380, 5.196 - 5.198]
Müller, C. [7.45]
Mueller, D. [6.273]
Müller, H.W. [6.102]
Müller, J.O. [6.256]
Muller, K.P. [6.12]
Murakami, H. [5.492]
Muramoto, T. [4.133, 4.169, 5.619]
Muraoka, K. [3.366]
Murrell, M.P. [7.75]
Murty, M.V.R. [4.239]
Mutzke, A. [2.25]
Naeem, M.D. [6.12]
Nagai, M. [7.101]
Nagata, S. [3.82, 3.86]
Nagel, W. [3.271]
Nagy, A. [6.273]
Nagy-Felsobuki, E.I. von [5.284, 5.285]
Nakagawa, S.T. [2.15, 3.30]
Nakamura, K. [3.266, 3.297, 6.166]
Nakamura, M. [6.278]
Nakano, T. [6.209, 6.210]
Nakata, Y. [7.101]
Narasinham, N.A. [3.167]
Nate, T. [3.199]
Naujoks, D. [1.188, 3.295, 3.296]
Navinšek, B. [1.26, 5.114]
Nefedov, A.A. [6.270]
Negrebetskaya, N.N. [3.416, 3.420]
Neidhart, T. [3.129, 3.465]
Nelson, G.C. [3.478]
Nelson, R.S. [1.12, 1.78, 1.103, 1.140, 1.154, 3.14, 3.310, 5.21, 5.432 - 5.434]
Nenadović, T.M. [3.230, 3.474]
Nender, C. [3.287]
Nerken, A. [6.67]
Neu, R. [6.277]
Neuhauser, J. [6.102]

Neumann, H. [1.214, 5.545]
Neumann, R. [7.33, 7.40, 7.44, 7.45]
Neumoin, V.E. [3.56 - 3.58, 3.61, 3.62]
Newbury, D.E. [5.119]
Newman, M.W. [1.68]
Newson, P.A. [5.110]
Ney, J. [3.186]
Ng, H.Y. [6.12]
Nguyen, N. [7.30]
Nickel, A. [1.111, 1.214]
Nicolet, M.A. [5.120, 7.93]
Nicolussi, G. [5.133, 5.151]
Niedermayr, T.R. [1.68]
Niehuis, E. [5.302, 5.345, 5.594]
Nielsen, O. [1.91, 3.236, 4.93, 7.153]
Nielsen, R. [3.477]
Nielsen, V. [1.125, 3.45, 5.55]
Niemöller, N. [5.533]
Niemann, D. [1.69, 3.475]
Nieminen, R.M. [1.137, 2.43, 4.14, 4.72]
Nikiforov, V.I. [3.377]
Ninomiya, S. [7.101]
Nishijima, D. [6.31]
Nishikawa, M. [3.67]
Nistor, L. [7.23]
Niwase, K. [6.197]
Nizam, J. [3.122]
Noggle, T.S. [3.348]
Noll, A. [1.142, 1.206]
Nomoto, K. [6.115]
Nordiek, J. [2.51, 4.132]
Nordlund, K. [2.49, 2.53, 3.394, 4.59, 4.76, 4.147, 4.175, 4.178, 4.180, 4.182, 4.183, 4.208, 4.232 - 4.234, 6.48 - 6.54, 6.180, 6.239 - 6.244]
Normand, C.E. [3.108]
Nørskov, J.K. [5.298]
Novikov, A. [5.605, 7.73]
Nunogaki, M. [3.99]
Nuruddin, A. [6.117]
Nuver, T.T. [3.455]
Nygren, R.E. [6.111]
Nyholm, F. [5.450]
Nylansted-Larsen, A. [7.27]
O'Briain, C.D. [3.197]
O'Connor, D.J. [5.179]
O'Connor, J.P. [3.192, 7.64, 7.107]
Obnorskii, V. [7.73]
Odintsov, G.D. [5.441]
Oechsner, H. [1.44, 3.55, 3.105, 3.191, 3.200, 3.356, 3.357, 5.24, 5.79 - 5.81, 5.100, 5.101, 5.139, 5.140, 5.177, 5.207, 5.229, 5.233, 5.273, 5.294, 5.416 - 5.418, 5.422 -

5.424, 5.463, 5.520 - 5.522, 5.525 - 5.527, 5.552]
Oehrlein, G.S. [6.279, 6.295 - 6.299]
Oen, O.S. [2.7, 2.8, 2.17, 3.476]
Östblom, M. [6.290]
Oetjen, G.H. [3.68, 3.467]
Ogilvie, G.J. [1.107, 3.273]
Ohashi, Y. [3.158]
Ohsaka, T. [3.415]
Ohtsuka, H. [3.195]
Ohya, K. [3.344, 5.551]
Okai, M. [4.169]
Okajima, Y. [3.106]
Okayasu, S. [7.123]
Okumura, Y. [3.297]
Okuneva, N.M. [2.4]
Okuno, K. [5.117]
Okutani, T. [3.124, 5.395]
Okuyama, F. [5.402, 5.487 - 5.489]
Olander, D.R. [6.10]
Oliphant, M.E.L. [1.15]
Oliva, A. [5.74, 5.475, 5.476, 5.542]
Oliva-Florio, A. [3.174, 5.606]
Ollerhead, R.W. [3.141, 3.184]
Olsen, M. [3.291]
Olson, R.R. [5.473, 5.474]
Olson, T.K. [5.523]
Onderdelinden, D. [1.71, 3.280, 5.442, 5.443]
Ong, C.K. [7.159]
Ono, T. [3.248]
Onsgaard, J. [5.419]
Oostra, D.J. [3.128, 5.316, 5.371, 5.377, 5.378, 5.382, 5.568]
Opimach, I.V. [3.416]
Orfanov, I.V. [5.434]
Ortega, C. [6.269]
O'Shaughnessy, D.J. [5.372 - 5.374]
Otani, A. [5.488]
Ottenberger, W. [3.27, 3.48, 3.50, 3.51, 3.72, 3.83, 5.515, 6.60]
Overeijnder, H. [3.216, 5.204, 5.363, 5.364]
Owens, D.K. [6.273]
Pachuta, S.J. [5.309]
Palenius, H.P. [3.189]
Palitsin, V.V. [5.680, 5.681]
Palmer, R.E. [4.130, 5.668, 5.669]
Pan, J. [3.156, 3.215]
Pan, Z. [4.119, 5.612, 5.622]
Pan, Z.Y. [4.122, 5.627]
Panjan, P. [3.340, 3.368]
Panzera, C. [3.218]
Papaleo, R. [4.186, 4.187]

Parascandola, S. [3.92, 6.282]
Parilis, E.S. [4.158, 4.163, 5.238, 5.290, 5.603]
Park, S.C. [3.448]
Patel, M.H. [3.234]
Pattersen, H. [3.15]
Patterson, D. [6.67]
Paulin, H. [6.106]
Paumier, E. [7.38, 7.51, 7.52, 7.111, 7.138, 7.139, 7.147, 7.165, 7.167]
Pautrat, M. [5.605, 5.675, 5.682, 5.689, 7.72]
Pavlenko, V.I. [3.377]
Pavlov, P.V. [3.405]
Payne, M.G. [5.93]
Paz, P. [6.228]
Pease, R.S. [1.41, 5.2]
Pedersen, S.D. [5.450]
Pedrys, R. [1.93, 4.98, 4.212, 5.316, 5.369 - 5.371, 5.375 - 5.378, 5.381 - 5.383, 5.387, 5.389]
Peercy, P.S. [6.194]
Pelaz, L. [4.203]
Pellet, C. [5.411]
Pellin, M.J. [4.191, 5.88, 5.89, 5.109, 5.134, 5.136 - 5.138, 5.144, 5.147, 5.148, 5.154, 5.283 - 5.288, 7.86, 7.88, 7.89]
Peltola, J. [4.208]
Pennycook, S.J. [3.348, 6.198]
Pereira, J.A.M. [7.157]
Perel'man, T.L. [7.135]
Perel, J. [5.577, 5.592]
Perović, B. [3.166]
Perraillon, B. [3.474]
Perrin, J. [6.114, 6.115]
Persin, M.I. [1.64, 6.14]
Petersen, N.B. [5.450]
Peterson, B.R. [5.654]
Petrov, V.B. [3.313]
Pezoldt, J. [3.349]
Philipps, V. [6.45, 6.76 - 6.79, 6.85, 6.112, 6.113, 6.121, 6.148, 6.160, 6.162, 6.167, 6.182, 6.200, 6.207, 6.210, 6.216, 6.261, 6.262]
Philipsen, V. [5.157, 5.159, 5.161, 5.162, 5.166 - 5.168, 5.170]
Phillips, A.H. [3.367, 3.423]
Phillips, M.S. [5.646]
Phipps, J.A. [5.373]
Piaskowy, J. [4.225]
Picraux, S.T. [6.186]
Pillath, J. [6.238]
Pitcher, C.S. [6.146, 6.203]
Pitkin, E.T. [3.168]
Plank, H. [6.223, 6.253]
Pleshivtsev, N.V. [1.153, 5.435]
Plessis, J. du [3.219]

Poate, J.M. [3.123, 7.61]
Podschaske, U. [5.387]
Poizat, J.C. [5.675, 5.683]
Poker, D.B. [3.117]
Politiek, J. [5.97]
Polman, A. [7.120]
Polop, C. [4.199]
Pomeroy, J.M. [4.201, 4.202]
Popok, V.N. [5.602]
Poppa, H. [3.213]
Portier, X. [7.26]
Poschenrieder, W. [1.156, 6.7]
Pospieszalska, M. [7.66]
Pospieszcyk, B. [7.146]
Pospieszczyk, A. [6.96 - 6.100, 6.111 - 6.113, 6.207, 6.210]
Postawa, Z. [4.20, 4.21, 4.24, 4.150, 4.224, 4.225, 4.227, 5.155, 5.156, 5.170, 5.348, 5.349, 5.351 - 5.353, 5.368, 5.461, 5.462, 5.466, 5.467, 5.471, 5.604, 5.614, 5.615, 5.684]
Postnikov, S.A. [3.375]
Pramanik, D. [5.573]
Prasad, K.B.S. [5.470]
Prasalovich, S.V. [5.602]
Pratontep, S. [4.130]
Preuss, R. [1.131, 3.44, 5.517, 6.71, 6.72, 6.210, 6.211]
Price, P.B. [7.5]
Prokofiev, Yu.G. [1.61, 6.14]
Promokhov, A.A. [3.311, 3.454, 3.469, 3.470]
Pronko, P.P. [3.235]
Prusseit, W. [7.6]
Prönnecke, S. [4.74]
Pugacheva, T.S. [3.350]
Pugno, R. [6.102, 6.210]
Qiu, Y. [7.104, 7.124]
Quintana, I. [6.182]
Ra, Y. [6.111]
Raabe, D. [2.31]
Rabalais, J.W. [5.11, 5.195, 5.307, 5.308]
Radnoczi, G. [3.340]
Raeker, T.J. [4.18, 4.19]
Rainer, D. [7.6]
Ralchenko, Yu.V. [3.42]
Ramasavmy, D. [4.62]
Ramer, C.E. [3.167]
Ramos, S.M.M. [7.24, 7.26, 7.121]
Ranjan, R. [3.137]
Rasulev, U.K. [5.678, 5.679, 5.686, 5.690]
Rattunde, O. [4.132]
Rau, C. [1.23]
Rauschenbach, B. [1.108, 1.111, 1.117]

Ravel, F. [7.34]
Ray, P.K. [3.204]
Razvina, L.P. [3.438]
Reed, D.A. [5.231]
Refke, A. [6.262]
Rehn, L.E. [4.162, 5.280, 5.281]
Reich, D.F. [5.333, 5.334]
Reich-Sprenger, H. [7.173]
Reichelt, Th. [7.94]
Reichert, L. [5.24]
Reid, I. [5.112, 5.528, 5.529]
Reimann, C.T. [5.125, 5.300, 5.379, 5.386, 5.468, 5.469]
Reiner, H.D. [6.105, 6.204]
Reinhold, C.O. [6.245 - 6.248]
Reiter, D. [1.186, 3.247, 6.96]
Reuter, W. [5.495]
Reynolds, G.W. [3.100, 3.139, 5.399, 5.400]
Reynolds, H.K. [3.167]
Ricaud, Ch. [7.84]
Riccato, A. [3.186, 3.390]
Richter, F. [6.286]
Rickman, R.D. [5.603]
Ridge, M.J. [1.107, 3.273]
Riederer, D.E. [5.348, 5.349, 5.464]
Ritchie, R.H. [4.72]
Rizkalla, N.M. [5.647]
Roberson, S. [5.638]
Roberto, J.B. [3.154, 6.221]
Robertson, I.M. [7.155]
Robertson, J. [6.287, 6.292]
Robinson, D.E. [3.96]
Robinson, J.E. [3.183]
Robinson, M.T. [1.49, 1.62, 1.132, 1.133, 2.6 - 2.8, 2.17, 3.23, 3.107, 3.146, 3.270, 3.300, 3.321, 3.326, 3.364, 3.384, 3.398, 3.476, 4.7, 4.13, 5.28, 5.29, 5.37, 5.51, 5.54, 5.406, 5.436, 5.438, 5.507, 5.508]
Roccaforte, F. [1.112]
Rodil, S.E. [6.287, 6.292]
Rödelsberger, K. [5.392]
Rohde, V. [6.102, 6.277]
Rol, P.K. [1.54, 1.58, 3.164, 3.263, 3.274, 5.427, 5.439]
Roll, T. [5.653]
Roosendaal, H.E. [1.55, 3.276, 5.131, 5.321, 5.388, 5.437]
Rosenberg, D. [1.29, 1.166, 3.13, 3.54, 5.544]
Rosencrance, S.W. [4.21, 4.24, 5.156, 5.464, 5.466, 5.467]
Rosenmayer, C.T. [6.279]
Rosner, D.E. [6.260]
Rotaru, C.C. [7.43]
Roth, J. [1.65, 1.130, 1.141, 1.147, 1.148, 1.163 - 1.165, 1.176, 1.179, 1.183, 3.27, 3.37, 3.43, 3.47, 3.48, 3.50 - 3.53, 3.60, 3.66, 3.68, 3.69, 3.74, 3.76, 3.78, 3.80, 3.83,

3.111, 3.112, 3.131, 3.135, 3.145, 3.153, 3.179, 3.194, 3.208, 3.223, 3.241, 3.252 - 3.255, 3.258, 3.261, 3.262, 3.265, 3.267, 3.268, 3.271, 3.272, 3.290, 3.308, 3.309, 3.314, 3.334, 3.371, 3.412, 3.413, 3.467, 3.473, 3.483, 5.503, 5.512, 5.515, 5.516, 5.556 - 5.558, 6.7, 6.15, 6.18, 6.19, 6.23, 6.24, 6.26 - 6.29, 6.36, 6.43, 6.44, 6.46, 6.55, 6.56, 6.60 - 6.62, 6.66, 6.80, 6.81, 6.159, 6.164, 6.173, 6.181, 6.182, 6.184 - 6.186, 6.188, 6.195, 6.196, 6.198, 6.202, 6.210, 6.212, 6.221 - 6.228, 6.231, 6.234, 6.235, 6.252 - 6.254, 6.277]
Roth, M. [7.92]
Rothard, H. [1.20, 7.69]
Roush, M.L. [3.353, 3.354, 3.358, 3.490]
Roustan, A. [3.217]
Rozet, J.P. [7.168]
Ruatta, S.A. [5.592]
Rubio, J.E. [4.26, 4.203, 4.204]
Rüdenauer, F.G. [4.23, 5.85, 5.453]
Rueger, N.R. [6.297]
Ruggiéri, R. [6.205, 6.210]
Runeberg, N. [6.240]
Rusbüldt, D. [1.183, 3.145, 3.241, 6.62]
Ruzic, D.N. [3.46, 3.137, 3.330, 3.333, 3.335, 3.393, 3.486, 5.546, 5.547]
Ryazantseva, O. [3.172]
Rylov, S.V. [3.58]
Ryzhov, Yu.A. [3.376, 3.388]
Sagara, A. [3.331]
Saidoh, M. [3.67, 3.195, 3.202, 3.203, 5.216, 5.217, 6.166]
Saidov, M.S. [3.350]
Saiki, K. [3.198]
Sakisaka, M. [3.199]
Sakurai, T. [5.269 - 5.271]
Salonen, E. [3.394, 4.147, 4.232 - 4.234, 6.48 - 6.53, 6.180, 6.239 - 6.242]
Saltmarsh, M.J. [3.183]
Salvo, C. [6.237]
Samartsev, A.V. [5.678, 5.679, 5.686, 5.698]
Samm, U. [6.96, 6.97, 6.100, 6.112]
Samoylov, V.M. [3.367, 3.423, 3.424, 3.441, 3.480]
Sanden, M.C.M. van de [6.84]
Sanders, D.E. [4.19, 4.21, 5.466, 5.470]
Sanders, F.H.M. [3.126]
Sanders, J.B. [1.127, 5.57, 5.131, 5.388]
Sandström, P. [6.291]
Santaniello, A. [3.131]
Sanz-Navarro, C.F. [4.130]
Saravanan, C. [3.345, 4.207]
Sarholt, L. [3.291]
Saris, F.W. [5.369, 5.568]
Sassmannshausen, U. [1.168, 3.429]
Sataka, M. [3.414, 7.99, 7.122, 7.123]
Sato, K. [3.489, 6.271]
Sato, Y. [6.269]

Saudraud, P. [5.596]
Sauerbrey, G. [3.6, 6.57]
Sauls, J.A. [7.6]
Sawin, H.H. [6.294]
Schaepkens, M. [6.297]
Scharff, M. [1.124, 1.125, 2.16, 3.45, 4.69, 5.55, 5.56]
Scharmann, A. [3.163, 3.180, 3.257, 5.392 - 5.394]
Schattat, B. [7.92]
Schauer, S.N. [5.178]
Schenk, A. [6.149 - 6.156]
Schenkel, T. [1.67, 1.68, 7.69 - 7.71]
Scherzer, B.M.U. [1.27, 3.4, 3.10, 3.135, 3.187, 3.270, 3.364, 3.481, 5.115, 5.508, 5.556, 6.184, 6.186, 6.188, 6.190 - 6.192, 6.198, 6.224]
Schick, G.A. [5.61, 5.122 - 5.124, 5.150]
Schiewitz, G. [7.92]
Schiller, S. [1.210, 1.211]
Schilling, G. [3.68]
Schindler, A. [1.110, 1.111, 1.194 - 1.197, 1.214]
Schiøtt, H.E. [5.56]
Schirrwitz, H. [1.182, 3.88]
Schkerl, M.W. [5.127, 5.128]
Schlögl, R. [6.105, 6.256]
Schlüter, M. [6.219, 6.266, 6.267, 6.280, 6.284]
Schlaug, R.N. [3.389]
Schlier, C. [5.96]
Schlossman, M. [5.670]
Schlutig, S. [7.69, 7.96, 7.119, 7.170, 7.171]
Schmid, K. [3.309, 3.314, 6.23, 6.24, 6.27 - 6.31, 6.41, 6.42]
Schmid, M. [1.69, 3.129, 3.465, 3.475, 6.59, 7.100]
Schmidl, H. [3.10, 3.481]
Schmidt-Böcking, H. [1.67, 7.70]
Schmidtmann, K. [6.91]
Schneider, D.H. [1.67, 7.70, 7.71]
Schneider, P.J. [5.193, 5.194]
Schneider, R. [2.25, 6.208]
Scholz, R. [7.23]
Schoolcraft, T.A. [4.235]
Schoppmann, Ch. [7.72]
Schorn, R.P. [3.483, 3.484, 5.208]
Schou, J. [1.93, 4.31, 4.98, 4.99, 5.356, 5.376, 5.381 - 5.383, 5.387, 5.389, 5.391]
Schröder, H. [5.92]
Schubert, F. [1.196]
Schubert, M. [7.169]
Schubert, U. [6.149 - 6.151, 6.153, 6.154, 6.156]
Schueler, B.W. [5.90]
Schultz, J.A. [5.195, 5.605]
Schulz, R. [6.188]
Schulze, M. [1.211]
Schwabe, R. [1.214]

Schwartz, G.C. [6.11]
Schwartz, K. [7.28, 7.40 - 7.42, 7.44 - 7.49]
Schwarz-Selinger, T. [6.71, 6.72, 6.82, 6.118 - 6.120, 6.135, 6.143 - 6.145, 6.199, 6.218, 6.284, 6.293]
Schwebel, C. [5.411]
Schweer, B. [1.183, 3.145, 3.241, 5.107, 5.146, 5.538, 6.62, 6.96, 6.98, 6.207, 6.210]
Schweikert, E.A. [5.593, 5.595, 5.596, 5.603, 5.637, 5.647, 5.652, 5.677]
Schweitzer, E.L. [5.89]
Schwoerer, R. [6.223 - 6.225, 6.253]
Scott, H.G. [3.12]
Seah, M.P. [1.159, 5.99, 5.324, 5.325, 5.355]
Sebel, P.G.M. [6.297]
Seefeld, H. von [3.10, 3.481]
Segda, B.G. [5.329, 5.330]
Seggern, J. von [5.217, 5.218]
Seiberling, L.E. [3.491, 7.62, 7.63, 7.11, 7.104]
Seidenkranz, G. [1.214]
Seidman, D.N. [5.573]
Seifert, N. [3.466]
Seitz, F. [1.42, 5.3, 7.50]
Seki, T. [4.143, 5.663]
Sellers, H. [4.118, 5.623]
Semenov, A.A. [3.388, 3.472]
Semerad, R. [7.8]
Semyonov, A.A. [3.376]
Sena, L.A. [3.172, 3.407]
Seraydarian, R. [3.315]
Sergienko, G. [6.96 - 6.98, 6.100, 6.112, 6.210]
Sethna, J.P. [4.196, 4.201, 4.202]
Sha, X. [6.232]
Shaarschmidt, G. [3.378]
Shapiro, M.H. [3.302, 3.386, 3.447, 3.449, 3.456, 4.42, 4.49 - 4.51, 4.65 - 4.68, 4.80, 4.82, 4.137 - 4.139, 4.154, 4.166, 4.167, 4.197, 5.52, 5.65, 5.73, 5.249 - 5.251, 5.486, 5.620, 5.621, 5.689, 5.701]
Shelyakin, L.B. [1.145, 1.146, 3.312, 3.378, 3.427, 3.428]
Shikata, M. [5.395]
Shimizu, A. [5.448]
Shimizu, H. 5.492]
Shimizu, R. [3.124, 3.233, 3.359, 5.395, 5.493]
Shimotomai, M. [3.183]
Shinagawa, K. [6.278]
Shivaparan, N.R. [3.204]
Shkarban, I.I. [3.376, 3.388, 3.416, 3.472]
Shulga, V.I. [3.249, 3.250, 3.284, 3.304, 3.305, 3.308, 3.395, 3.442, 3.445, 3.446, 4.29, 4.53, 4.54, 4.115, 4.116, 5.407, 5.499, 5.550, 5.610, 5.611]
Shumacher, G. [7.114, 7.115]
Shutthanandan, V. [3.204]
Siderov, A.V. [3.256]
Siegele, R. [6.198, 7.94]

Sielanko, J. [3.292, 3.352, 3.361]
Sigle, W. [3.91, 6.282]
Sigmund, P. [1.19, 1.32, 1.33, 1.48, 1.63, 1.87, 1.88, 1.127, 1.169, 1.180, 3.20, 3.21, 3.298, 3.299, 3.304, 3.305, 3.317, 4.4, 4.5, 4.45, 4.46, 4.53, 4.54, 4.115, 4.116, 4.188, 5.13, 5.17, 5.26, 5.27, 5.30 - 5.36, 5.57, 5.58, 5.127, 5.128, 5.234, 5.450, 5.475, 5.476, 5.497, 5.499, 5.500, 5.511, 5.580 - 5.582, 5.585, 5.586, 5.609 - 5.613, 6.20, 6.21, 7.12, 7.18, 7.58, 7.49, 7.150 - 7.152]
Silk, E.C.H. [7.3]
Silsbee, R.H. [1.73, 5.444]
Silva, E.F. da [7.157]
Silva, S.R.P. [6.285]
Silverans, R.E. [5.157, 5.159 - 5.163, 5.166 - 5.168, 5.170]
Simmons, E.H. [5.379]
Simons, D.S. [5.116]
Singh, J. [5.61, 5.123, 5.124, 5.150]
Singh, S. [7.31]
Sinha, M.K. [3.69, 3.179, 6.7, 6.60, 6.184]
Sizmann, R. [1.171]
Skinner, C.H. [6.273]
Slabopitskii, R.P. [3.377]
Sleptsov, V.V. [6.270]
Sletten, G. [3.150]
Slodzian, G. [1.203, 3.385]
Smentkowski, V.S. [1.160]
Smiley, E.J. [4.150, 5.614, 5.615, 5.684]
Smit, B. [2.33]
Smith, D.L. [3.363]
Smith, G.J. [3.183]
Smith, H.J. [3.173, 3.176, 3.411]
Smith, J.N., Jr. [3.70, 3.71, 3.190, 3.197]
Smith, P.C. [3.333, 5.546, 5.547]
Smith, R. [2.35, 4.16, 4.27, 4.62, 4.130, 4.149, 4.228, 5.668]
Smith, R.J. [3.204]
Snoek, C. [5.189]
Snoeks, E. [7.120]
Snouse, T.W. [3.148]
Snowdon, K.J. [5.230, 5.232, 5.263, 5.265, 5.266]
Soeda, F. [5.117]
Sofield, C.J. [7.75]
Sokolov, V.A. [1.61, 6.14]
Sokolov, Yu.A. [3.58, 3.59]
Solomko, V.V. [5.295]
Somerjai, G. [7.143]
Sommerfeldt, H. [1.143, 1.144, 3.121]
Sone, K. [3.195, 3.202, 3.203, 6.166, 6.171]
Song, J.H. [5.671 - 5.673]
Song, K.S. [5.361]
Sørensen, H. [5.381, 5.382, 5.389]
Sørensen, T. [5.398, 5.478 - 5.480]

Soshnikov, I.P. [3.485]
Sosnowski, M. [4.131, 5.704]
Sotnikov, V.M. [3.269, 3.391]
Southern, A.L. [1.62, 3.107, 3.146, 5.436, 5.438]
Spaar, M.T. [7.90]
Spaeth, C. [3.91, 6.281, 6.286]
Speakman, S.P. [6.285]
Spicklemire, S.J. [3.301, 5.126]
Spiegel, D.R. [5.125, 7.89]
Spohr, R. [7.6, 7.110, 7.112]
Sporn, M. [3.129]
Sproul, W.D. [6.32]
Spuler, B. [6.12]
Srinivasan, S. [6.12]
Srivastava, D. [4.230]
Sroubek, F. [4.84, 4.92, 5.169]
Sroubek, Z. [4.84, 4.90 - 4.92, 5.168, 5.169]
Staat, P. [7.102]
Städele, M. [3.246]
Stahl, A. [1.118]
Staib, Ph. [1.156, 3.10, 6.185]
Stamp, M.F. [6.93, 6.94, 6.99, 6.101, 6.110, 6.112, 6.113, 6.210]
Stampfli, P. [7.160]
Standaert, T.E.F.M. [6.279, 6.297, 6.298]
Standing, K.G. [5.253]
Stangeby, P.C. [6.63 - 6.65, 6.146, 6.147, 6.161, 6.163, 6.170, 6.203, 6.215, 6.216]
Stanmore, B.R. [6.258]
Stansfield, R.A. [3.448, 3.450, 4.28]
Stapel, D. [5.642, 5.643]
Stark, J. [1.5, 1.6, 1.57]
Starke, P. [1.149, 6.109]
Staudenmaier, G. [6.185]
Staudt, C. [4.160, 4.161, 4.168, 5.168, 5.282, 5.289, 5.692]
Stave, M.S. [4.19]
Steckenreiter, T. [7.28]
Steffens, H. [7.102]
Stein, R.P. [5.410]
Steinbrüchel, C. [3.133, 4.39]
Steinhausen, Ch. [7.102, 7.103]
Stenum, B. [5.382, 5.389, 5.398, 5.478 - 5.480]
Stenzel, P. [7.67]
Stepanova, M. [5.548, 5.549]
Stephan, C. [7.168]
Stephen, J. [1.12, 1.115]
Stephens, B.C. [3.345, 4.207]
Stephens, J.A. [3.41]
Stevie, F.A. [5.116]
Stewart, A.D.G. [1.122]
Stier, H.-E. [5.20]

Stillinger, F.H. [2.39, 4.243]
Stipdonk, M.J. van [5.593, 5.637, 5.677]
Stock, D. [4.192]
Stolterfoht, N. [1.69, 3.475, 4.114, 7.132]
Stolyarova, V.G. [3.58, 3.59, 3.61, 3.62]
Stoneham, A.M. [7.16, 7.161]
Stoquert, J.P. [7.1, 7.21, 7.43, 7.68, 7.69, 7.137]
Strehl, B. [5.215]
Stritzker, B. [5.588, 7.146]
Stroebelt, E. [6.67]
Stroev, L.V. [5.678, 5.679]
Strunnikov, V.M. [3.58]
Stuart, R.V. [3.136, 3.142, 3.182, 4.44, 5.22, 5.98, 5.504, 5.505]
Stuart, S.J. [4.223, 4.224, 6.245 - 6.248]
Studer, F. [7.1, 7.19, 7.21, 7.29, 7.30, 7.68, 7.137]
Stumpe, E. [5.70, 5.294]
Su, D.S. [6.256]
Sümmchen, L. [3.91, 6.281]
Suenaga, M. [7.32]
Sugden, S. [7.75]
Sugie, T. [6.209]
Sugimoto, M. [6.197]
Summa, G.M. [3.125]
Summers, A.J. [3.185, 3.193]
Summers, H.P. [3.19, 6.110]
Sun, C. [6.293]
Sun, S. [5.653, 5.684]
Sundgren, J.E. [6.290, 6.291]
Sundqvist, B.U.R. [4.102, 5.224, 5.314, 7.163]
Suraud, M.G. [7.85]
Sushkova, J.V. [3.416]
Suvorov, A.L. [3.16, 3.17]
Suzuki, A. [6.115]
Suzuki, M.T. [6.278]
Suzuki, T. [3.158]
Switkowski, Z.E. [3.141, 3.184]
Szakal, C. [5.653, 5.654, 5.684]
Sze, D. [3.56, 3.57]
Szewczyk, M. [4.150, 5.614, 5.615]
Szymczak, W. [5.449, 5.452, 5.645]
Szymonski, M. [3.216, 4.56, 5.113, 5.204 - 5.206, 5.210, 5.359, 5.362, 5.363, 5.368, 5.419, 5.569, 5.586]
Szyszko, W. [3.352, 3.361]
Tachi, S. [3.115]
Taga, Y. [3.479]
Taglauer, E. [1.14, 1.158, 1.189, 1.190, 3.80, 3.219, 3.483, 5.263]
Takagi, T. [5.631]
Takaoka, G.H. [5.598]
Takeda, Y. [6.114]

Takenaga, H. [6.209]
Takeuchi, D. [4.141, 5.608]
Takeuchi, W. [1.136, 3.26, 3.33, 3.278, 5.458]
Takeuchi, Y. [6.114, 6.115]
Takiguchi, T. [5.510]
Tan, M. [5.465]
Tanabe, T. [6.197, 6.261]
Tanaka, H. [3.198]
Tanaka, S. [3.198]
Tanatarov, L.V. [7.134, 7.145]
Tanemura, M. [5.402, 5.487 - 5.489]
Tanigaki, T. [7.90]
Taniguchi, M. [3.489]
Tao, Z. [3.156, 3.215]
Tappin, D.K. [7.155]
Tarus, J. [2.54, 4.183, 6.239]
Tatsuta, K. [6.271]
Tawara, H. [3.24, 3.25]
Taylor, R.S. [4.171, 4.172]
Teichert, Ch. [3.458]
Tel'kovskii, V.G. [1.53, 1.59, 3.264, 3.275, 5.428, 5.435]
Teller, E. [2.18]
Tempez, A. [5.605]
Tenner, M.G. [5.265, 5.266]
Terhorst, M. [5.345]
Tersoff, J. [2.40]
Tetel'baum, D.I. [3.405]
Thacker, G.R. [3.186]
Thevenard, P. [7.37]
Thevuthasan, S. [4.61]
Thiel, K. [1.168, 3.429]
Thiemann, M. [5.643]
Thijsse, B.J. [3.419, 4.205]
Thoen, P. [5.157]
Thoma, A. [6.91]
Thomas, E.W. [3.80, 5.264]
Thomas, H.-J. [1.214]
Thomas, J.P. [5.683]
Thomas, M.T. [3.183]
Thompsen, P.V. [1.125]
Thompson, D.A. [3.183, 5.562 - 5.567]
Thompson, M.W. [1.78, 1.83, 1.155, 3.14, 5.8, 5.21, 5.25, 5.41, 5.42, 5.44, 5.110 - 5.112, 5.431 - 5.434, 5.528 - 5.532, 5.570]
Thomé, L. [7.112, 7.116]
Thonnard, N. [5.93]
Thurner, Y. [5.632]
Tikhonov, A. [5.670]
Tildesley, D.J. [2.28, 2.30]
Tilinin, I.S. [4.71]

Tip, A. [4.156, 4.157, 5.274, 5.275]
Tjan, K. [3.246]
Todorov, S.S. [3.323]
Tokuyama, T. [3.115]
Tolk, N.H. [1.22, 1.23, 3.466, 6.229]
Tolle, H.J. [3.343]
Tolmachev, A.I. [3.38, 3.256]
Tolmien, W. [1.105]
Tombrello, T.A. [1.167, 1.169, 3.141, 3.184, 3.239, 3.301, 3.302, 3.306, 3.386, 3.447, 3.449, 3.456, 3.491, 4.42, 4.49 - 4.51, 4.65 - 4.68, 4.82, 4.137 - 4.139, 4.154, 4.166, 4.167, 4.197, 5.65, 5.73, 5.126, 5.249 - 5.251, 5.469, 5.483 - 5.486, 5.620, 5.621, 5.625, 5.689, 5.701, 7.11, 7.14, 7.62, 7.63, 7.97, 7.98, 7.104, 7.124]
Tomita, M. [3.199]
Tomlin, D.H. [3.15]
Tommasini, F. [6.237]
Tomozeiu, N. [7.77]
Torrens, I.M. [1.132, 2.6, 4.7]
Tóth, A. [5.221]
Toth, Z. [3.465]
Touboltsev, V.S. [3.291, 5.700, 7.117]
Tougard, S. [1.19]
Toulemonde, M. [3.244, 4.114, 7.1, 7.9, 7.19, 7.21, 7.26, 7.27, 7.29, 7.30, 7.33, 7.35, 7.37, 7.40 - 7.43, 7.45 - 7.49, 7.51, 7.52, 7.54 - 7.56, 7.68, 7.69, 7.105, 7.111, 7.121, 7.132, 7.136 - 7.139, 7.147, 7.169]
Toussaint, U. von [3.290, 6.26, 6.73]
Tousset, J. [3.408]
Townsend, P.D. [1.81, 5.357, 5.360]
Toyoda, N. [1.198, 4.141, 4.143, 5.608, 5.648, 5.659, 5.660, 5.663 - 5.667, 5.702, 5.703]
Träskelin, P. [6.180, 6.243]
Tracy, J.G. [3.240]
Trappe, C. [1.116]
Trautmann, C. [4.114, 7.7, 7.27, 7.28, 7.33, 7.35, 7.40 - 7.49, 7.55, 7.56, 7.105, 7.121, 7.132, 7.169]
Trbojevic, D. [3.139, 3.144]
Treado, P.A. [3.100, 3.139, 3.144, 5.399]
Treichel, O. [1.213]
Trevor, J.L. [5.644]
Tripathi, A. [7.31]
Trofimchuk, E.I. [1.61, 6.14]
Trovato, E. [4.42]
Trushin, Y. [3.349]
Tsepelevich, S.O. [7.13]
Tsong, I.S.T. [1.24, 5.103, 5.231, 5.310]
Tsuge, H. [5.396]
Tsunoyama, K. [3.158]
Tu, K.N. [3.123]
Tuboltsev, V.S. [5.494]
Tugushev, V.I. [5.638]

Tully, J.C. [1.22, 1.23, 6.229]
Turban, G. [6.288, 6.289]
Turos, A. [6.191]
Tuszynski, W. [5.645]
Tutein, A.B. [4.223]
Tynan, G. [3.315, 6.104]
Uchida, M. [3.99]
Uecker, H. [3.186]
Ueda, S. [3.415]
Uiterwaal, C.J.G.J. [5.92]
Ukita, M. [5.488, 5.489]
Urazgil'din, I.F. [3.452, 3.453]
Urbassek, H.M. [1.138, 1.139, 2.3, 2.23, 2.50, 2.53, 2.55, 3.303, 3.320, 3.459, 4.15, 4.23, 4.25, 4.30, 4.33, 4.48, 4.96, 4.97, 4.100, 4.104, 4.114, 4.129, 4.145, 4.146, 4.152, 4.153, 4.155, 4.164, 4.168, 4.176, 4.177, 4.179, 4.190, 4.198, 4.199, 4.210, 5.67, 5.72, 5.212, 5.223, 5.234, 5.235, 5.243, 5.291 - 5.293, 5.311, 5.390, 5.453, 5.518, 5.522, 5.585, 5.629, 5.630, 7.127, 7.132]
Vainonen-Ahlgren, E. [6.102]
Valbusa, U. [6.237]
Vaeck, L. van [5.225, 5.226]
Vandamme, W. [6.84]
Vanden Eynde, X. [5.333, 5.334, 5.337]
Vandeweert, E. [5.157, 5.159 - 5.163, 5.166 - 5.168, 5.170, 5.350 - 5.352]
Varadi, P. [6.67]
Varfolomeev, A.E. [6.270]
Varga, P. [1.69, 1.157, 3.129, 3.465, 3.475, 6.59, 7.100]
Varshavskii, S.P. [3.172]
Vasichkina, N.G. [3.420]
Vasile, M.J. [5.180]
Vasiliev, V.I. [3.58]
Vaulin, E.P. [6.40]
Veen, G.N.A. van [3.128]
Veje, E. [5.172, 5.173]
Velikov, K.P. [7.120]
Vender, D. [6.295, 6.296]
Verbeek, H. [1.10, 1.156, 3.68, 3.80, 3.187, 5.193, 5.194]
Vergara, L. I. [6.177 - 6.180]
Verkhoturov, S.V. [4.170, 5.256 - 5.260, 5.295, 5.603, 5.647, 5.652]
Vernhet, D. [7.168]
Vertes, A. [4.212]
Vervaecke, F. [5.160, 5.163, 5.167]
Veryovkin, I.V. [4.170, 5.88, 5.256 - 5.260, 5.295, 5.679, 5.681, 5.686 - 5.688]
Vetter, J. [7.23, 7.110, 7.112]
Vicanek, M. [4.32, 4.115, 5.58, 5.127, 5.128, 5.212]
Vichev, R.G. [3.324, 3.325, 3.327]
Vickerman, J.C. [4.172, 5.86, 5.317, 5.323, 5.337, 5.346, 5.649 - 5.651]
Victoria, M. [2.45, 4.74, 4.88]
Viehböck, F.P. [1.58, 1.157, 3.89, 3.274, 3.339, 5.105, 5.413, 5.414, 5.427]
Vietzke, E. [3.41, 6.16, 6.45, 6.47, 6.76 - 6.79, 6.85, 6.113, 6.121, 6.129, 6.148, 6.160,

6.162, 6.164, 6.167, 6.183, 6.200, 6.207, 6.216, 6.261 - 6.263]
Viljoen, E.C. [3.219]
Vineyard, G.H. [2.27, 4.9, 5.446 - 5.448, 7.140]
Vogt, A. [1.116]
Vorsa, V. [5.347]
Voss, K.O. [7.105, 7.169]
Voter, A.F. [3.451, 4.34]
Vozzo, F.R. [3.139, 5.400]
Vries, A.E. de [3.128, 3.216, 3.246, 4.156, 4.157, 5.113, 5.204, 5.236, 5.265, 5.266, 5.274, 5.275, 5.315, 5.316, 5.363, 5.364, 5.369 - 5.371, 5.377, 5.378, 5.382, 5.384, 5.385, 5.568, 5.569]
Wach, W. [3.282]
Wade, M.R. [6.95]
Waelbroeck, F. [3.482, 6.238]
Wagner, M.S. [5.656]
Wahl, M. [5.135, 5.139 - 5.141]
Wainwright, T.E. [2.26, 4.10]
Walcher, W. [6.83]
Waldeer, K.T. [2.50, 4.96, 4.97, 5.291, 5.390]
Waligorski, M.P.R. [7.141]
Walker, R.M. [7.5]
Walter, H. [7.6]
Walz, B. [7.92]
Walzl, K. [5.125]
Wampler, W.R. [6.186, 6.187]
Wang, L. [5.697]
Wang, W.M. [1.179, 6.253]
Wang, X.M. [6.275, 6.276]
Wang, Z.G. [7.51, 7.54, 7.56, 7.138, 7.139, 7.147]
Wang, Z. [3.156, 3.215]
Warczak, B. [5.376, 5.381, 5.382]
Warmoltz, N. [3.242]
Watgen, M. [5.463]
Watts, R.O. [5.412]
Way, A. [5.628]
Weakliem, P.C. [4.238]
Weathers, D.L. [3.301, 5.126, 5.485]
Webb, R.P. [3.447, 4.149, 4.173, 4.174, 5.64, 5.513, 5.628]
Weber, T. [3.110]
Weber, T.A. [2.39, 4.243]
Weber, W.J. [4.61]
Wedelking, J.F. [3.183]
Weg, W.F. van der [3.123, 5.191, 5.192]
Wehbe, N. [5.683]
Wehner, G.K. [1.29, 1.50, 1.51, 1.61, 1.72, 1.119, 1.123, 1.166, 1.181, 3.13, 3.49, 3.54, 3.63, 3.84, 3.136, 3.142, 3.182, 3.211, 3.277, 3.401, 3.404, 3.409, 4.44, 5.18, 5.19, 5.22, 5.98, 5.129, 5.130, 5.202, 5.429, 5.473, 5.474, 5.504, 5.505, 5.544, 7.125]
Wei, L. [4.76]
Weibel, D. [5.649 - 5.651]

Weidele, H. [5.157]
Weidinger, A. [7.9, 7.103]
Weijsenfeld, C.H. [3.98]
Weinberg, G. [6.105]
Weinlich, M. [6.91]
Weiss, A. [3.210]
Weissmann, R. [3.9, 3.160, 5.500, 5.553]
Welch, D.O. [7.32]
Weller, M.R. [3.192, 7.64, 7.98]
Weller, R.A. [3.192, 3.491, 5.484, 5.485, 7.62, 7.64, 7.97, 7.107]
Wendt, G. [1.57]
Werner, H.A. [3.242]
Werner, H.W. [1.202, 5.85]
West, W.P. [6.95]
Westerberg, L. [7.173]
Westmoreland, J.E. [3.317]
Whitaker, T.J. [5.412]
White, C.W. [1.22]
White, J.M. [5.125, 5.126, 5.127]
Whitlow, H.J. [3.422, 5.398, 5.409, 5.478 - 5.480]
Whitton, J.L. [1.26, 5.114]
Whyte, D.G. [3.18, 3.315, 6.31, 6.95, 6.104]
Wielunski, [6.191]
Wien, K. [5.60, 7.15, 7.73]
Wienhold, P. [3.482, 6.148, 6.200]
Wiesner, J. [7.7]
Wijesundra, M.B.J. [5.670]
Wild, C. [6.78, 6.162]
Willey, K.F. [5.346, 5.347]
Williams, M.M.R. [5.39, 5.40]
Williams, P. [5.178, 5.185, 5.314, 5.577, 5.636]
Williams, R.T. [5.361]
Willis, W.R [1.62, 3.146, 5.438]
Wilson, I.H. [1.104, 5.111, 5.628]
Wilson, K.L. [3.75, 3.80, 3.254, 6.44]
Wilson, W.D. [2.13, 3.31, 3.336]
Wiltner, A. [1.165, 6.231]
Winograd, N. [1.56, 3.434 - 3.437, 3.444, 4.17, 4.20, 4.21, 4.24, 4.58, 4.150, 4.172, 4.224, 4.225, 4.227, 5.61, 5.65, 5.122 - 5.125, 5.150, 5.155, 5.156, 5.170, 5.240 - 5.242, 5.301, 5.303, 5.346 - 5.353, 5.461, 5.462, 5.464, 5.466 - 5.469, 5.471, 5.604, 5.614, 5.615, 5.653, 5.654, 5.658, 5.684, 7.91]
Winter, B. [6.149 - 6.156]
Winter, H.P. [1.69, 3.129, 3.475, 6.59, 7.100]
Winter, J. [3.482, 6.6, 6.148, 6.200, 6.238]
Winterbon, K.B. [1.127, 5.57]
Winters, H.F. [3.119, 3.224, 4.35, 4.36, 5.228, 5.511, 6.4, 6.5, 6.35, 6.39]
Wise, R. [6.12]
Wiss, T. [7.35, 7.36]
Withrow, S.P. [6.196]

Witteborn, F.C. [3.148]
Wittmaack, K. [1.100, 1.159, 3.117, 3.130, 3.222, 3.282, 3.362, 5.16, 5.425, 5.449, 5.452, 5.645]
Wittmann, M. [6.155, 6.158]
Witzel, B. [5.92]
Wöste, L. [5.267]
Wojciechowski, I. [4.83, 4.136, 4.158, 5.238, 5.645]
Wolf, J.P. [5.267]
Wolsky, S.P. [3.421]
Wolter, A.R. [3.101]
Won, J. [3.56, 3.57]
Wong, C.P.C. [6.95]
Wong, S. [5.649, 5.650]
Wood, A.S. [5.605]
Woodyard, J.R. [5.76, 5.276]
Wottke, H. [3.89]
Wright, G. [6.31]
Wright, R.B. [5.102, 5.109, 5.132, 5.148, 5.154, 7.88]
Wu, C.H. [3.60, 3.64, 3.73, 3.225, 3.394, 4.232 - 4.234, 6.48 - 6.53, 6.105, 6.123, 6.134, 6.239 - 6.242, 6.274]
Wu, C.J. [4.238]
Wu, K.J. [1.68]
Wucher, A. [4.79, 4.84, 4.91, 4.92, 4.135, 4.160, 4.161, 4.165, 4.168, 4.170, 5.91, 5.101, 5.135, 5.139 - 5.142, 5.164, 5.165, 5.168 - 5.170, 5.177, 5.244 - 5.247, 5.259, 5.260, 5.268, 5.282, 5.288, 5.289, 5.463, 5.495, 5.653, 5.654, 5.684, 5.685, 5.691 - 5.696, 5.698]
Wurz, P. [5.215]
Xiao, Z. [3.422]
Xie, J. [5.627]
Xirouchaki, C. [5.669]
Xu, J. [5.654]
Yamada, I. [1.198, 3.360, 4.127, 4.128, 4.131, 4.140 - 4.143, 4.246, 5.598, 5.608, 5.633, 5.648, 5.659 - 5.667, 5.702 - 5.704]
Yamada, R. [3.195, 6.166, 6.171, 6.172, 6.213, 6.214]
Yamaguchi, T. [5.598]
Yamaguchi, Y. [4.148]
Yamamura, Y. [1.136, 2.15, 3.24 - 3.26, 3.30, 3.33, 3.248, 3.251, 3.278, 3.322, 3.341, 3.356, 3.357, 3.357, 3.369, 3.370, 3.396, 3.397, 4.133, 4.169, 5.422, 5.423, 5.458, 5.509, 5.510, 5.522, 5.576, 5.616 - 5.619]
Yamashita, M. [3.77, 3.232]
Yamashita, Y. [4.169]
Yan, Q. [3.466]
Yan, W. [6.12]
Yang, H.R. [3.64, 3.225]
Yao, Y. [6.229]
Yarmiychuk, S. [7.73]
Yarmoff, J.A. [4.84, 5.169]
Yavlinskii, Yu.N. [7.13, 7.144]
Ye, Z.-Y. [3.460]

Yokoyama, K. [3.489]
Yonts, O.C. [3.96. 3.97, 3.108]
Yorizane, K. [4.169]
Youle, I.S. [6.215]
Young, C.E. [5.89, 5.144, 5.147, 5.154, 7.86, 7.88, 7.89]
Young, D.A. [4.63, 4.64, 7.4, 7.128, 7.129]
Yu, J. [5.657]
Yu, M.L. [1.99, 5.143, 5.149, 5.187, 5.209, 5.366]
Yue, Y. [5.627]
Yurasova, V.E. [1.79, 1.145, 1.146, 3.311, 3.312, 3.367, 3.375, 3.376, 3.378, 3.379, 3.388, 3.416, 3.420, 3.423, 3.424, 3.427, 3.428, 3.438, 3.441, 3.452 - 3.454, 3.457, 3.469 - 3.472, 5.430, 5.435]
Yuuki, Y. [6.115]
Zaki Ewiss, M.A. [5.208]
Zalar, A. [1.206, 3.340, 3.368]
Zalm, P.C. [3.116, 3.126, 3.127, 3.243, 5.321, 5.607]
Zande, W.J. van der [5.320]
Zatekin, V.V. [3.59]
Zav'jalsky, L.P. [1.61, 6.14]
Zdanuk, E.J. [3.421]
Zecho, T. [6.74, 6.75, 6.232]
Zehe, A. [3.480]
Zeuner, M. [5.545]
Zhang, C. [3.461]
Zhang, D. [6.295, 6.296]
Zhang, J. [3.156, 3.215]
Zhang, Q.-Y. [3.460, 3.461]
Zhang, T. [3.422]
Zhang, W.L. [5.481]
Zhang, X.S. [5.482]
Zhang, Y. [3.422]
Zhigilei, L.V. [4.58, 4.219, 4.220]
Zhong, Y. [4.76, 4.206]
Zhu, H. [4.121]
Zhu, Y. [7.32]
Zhukova, E.Yu. [3.375, 3.469, 3.471, 3.472]
Zhurkin, E.E. [3.417, 4.151]
Ziberi, B. [1.117, 1.194, 1.197]
Ziegler, J.F. [2.14, 2.22, 2.23, 3.223, 7.118]
Zielinski, L. [6.11]
Zimmermann, C. [5.464]
Zimmermann, S. [2.55]
Zinovev, A.V. [5.678, 5.688]
Zinovyev, V.A. [4.192]
Zorin, E.I. [3.405]
Zschack, P. [3.477]
Zsolt, G. [3.368]
Zuhr, R.A. [3.154, 3.290, 3.348, 6.26, 6.196]
Zykova, E.Yu. [3.375, 3.469, 3.471, 3.472]

Topics in Applied Physics

94 **Silicon Photonics**
By L. Pavesi, D.J. Lockwood (Eds.) 2004, 262 Figs. XVI, 397 pages

95 **Few-Cycle Laser Pulse Generation and Its Applications**
By Franz X. Kärtner (Ed.) 2004, 209 Figs. XIV, 448 pages

96 **Femtsosecond Technology for Technical and Medical Applications**
By F. Dausinger, F. Lichtner, H. Lubatschowski (Eds.) 2004, 224 Figs. XIII 326 pages

97 **Terahertz Optoelectronics**
By K. Sakai (Ed.) 2005, 270 Figs. XIII, 387 pages

98 **Ferroelectric Thin Films**
Basic Properies and Device Physics for Memory Applications
By M. Okuyama, Y. Ishibashi (Eds.) 2005, 172 Figs. XIII, 244 pages

99 **Cryogenic Particle Detection**
By Ch. Enss (Ed.) 2005, 238 Figs. XVI, 509 pages

100 **Carbon**
The Future Material for Advanced Technology Applications
By G. Messina, S. Santangelo (Eds.) 2006, 245 Figs. XXII, 529 pages

101 **Spin Dynamics in Confined Magnetic Structures III**
By B. Hillebrands, A. Thiaville (Eds.) 2006, 164 Figs. XIV, 345 pages

102 **Quantum Computation and Information**
From Theory to Experiment
By H. Imai, M. Hayashi (Eds.) 2006, 49 Figs. XV, 281 pages

103 **Surface-Enhanced Raman Scattering**
Physics and Applications
By K. Kneipp, M. Moskovits, H. Kneipp (Eds.) 2006, 221 Figs. XVIII, 464 pages

104 **Theory of Defects in Semiconductors**
By D. A. Drabold, S. K. Estreicher (Eds.) 2007, 60 Figs. XIII, 297 pages

105 **Physics of Ferroelectrics**
A Modern Perspective
By K. Rabe, Ch. H. Ahn, J.-M. Triscone (Eds.) 2007, 129 Figs. XII, 390 pages

106 **Rare Earth Oxide Thin Films**
Growth, Characterization, and Applications
By M. Fanciulli, G. Scarel (Eds.) 2007, 210 Figs. XVI, 426 pages

107 **Microscale and Nanoscale Heat Transfer**
By S. Volz (Ed.) 2007, 144 Figs. XIV, 370 pages

108 **Light Scattering in Solids IX**
Novel Materials and Techniques
By M. Cardona, R. Merlin (Eds.) 2007, 215 Figs. XIV, 432 pages

109 **Molecular Building Blocks for Nanotechnology**
From Diamondoids to Nanoscale Materials and Applications
By G.A. Mansoori, Th.F. George, L. Assoufid, G. Zang (Eds.) 2007, 229 Figs. XIV, 440 pages

110 **Sputtering by Particle Bombardment**
Experiments and Computer Calculations from Treshold to MeV Energies
By R. Behrisch, W. Eckstein (Eds.) 2007, 201 Figs. XIV, 470 pages